

รายงานวิจัยฉบับสมบูรณ์

โครงการส่งเสริมกลุ่มวิจัย (เมธิวิจัยอาวุโส)

การวิจัยและพัฒนาใหม่ ๆ ของวัสดุพอลิเมอร์สีเขียวและประโยชน์ใช้งาน

โดย

ศาสตราจารย์ ดร. สุดา เกียรติกำจรวงศ์

รายงานวิจัยฉบับสมบูรณ์

โครงการส่งเสริมกลุ่มวิจัย (เมธีวิจัยอาวุโส)

การวิจัยและพัฒนาใหม่ ๆ ของวัสดุพอลิเมอร์สีเขียวและประโยชน์ใช้งาน

ศาสตราจารย์ ดร. สุดา เกียรติกำจรวงศ์ ภาควิชาวิทยาศาสตร์ทางภาพถ่ายและเทคโนโลยีทางการพิมพ์ คณะวิทยาศาสตร์ จุฬาลงกรณ์มหาวิทยาลัย

สนับสนุนโดยสำนักงานกองทุนสนับสนุนการวิจัย

(ความเห็นในรายงานนี้เป็นของผู้วิจัย สกว. ไม่จำเป็นต้องเห็นด้วยเสมอไป)

กิตติกรรมประกาศ

รายงานวิจัยฉบับนี้ เป็นผลงานจากโครงการเมธีวิจัยอาวุโส ระยะที่ 2 หรือ โครงการส่งเสริมกลุ่ม วิจัย ประจำปี 2550 – 2553 ได้รับการสนับสนุนจากสำนักงานกองทุนสนับสนุนการวิจัย (สกว.) และ สำนักงานคณะกรรมการการอุดมศึกษา (สกอ.) เรื่อง การวิจัยและพัฒนาใหม่ ๆ ของวัสดุพอลิเมอร์สี เขียวและประโยชน์ใช้งาน (Novel Research and Development in Green Polymer Materials and Their Applications)

ด้วยปรารถนาของหัวหน้าโครงการวิจัยที่จะรวบรวมผลงานต่าง ๆ ให้สมบูรณ์ที่สุด จึงได้ขยาย เวลาวิจัยจากปกติใช้เวลา 3 ปี มาเป็นเวลา 4 ปี (พ.ศ. 2554) หัวหน้าโครงการซาบซึ้งในการสนับสนุน อย่างเต็มที่ของสำนักงาน สกว. ทั้งในช่วงเวลาปกติ และช่วงที่ขยายเวลาออกไปอีก 1 ปี ทำให้สามารถ ผลิตนิสิตระดับบัณฑิตศึกษาได้อีก 3 คน พร้อมบทความที่จะเกิดขึ้นอีกจำนวนหนึ่ง ในฐานะหัวหน้า โครงการเมธิวิจัยอาวุโส ระยะที่ 2 ขอกราบขอบพระคุณสำนักงานกองทุนสนับสนุนการวิจัย โดยเฉพาะ อย่างยิ่ง อดีตผู้อำนวยการผ่ายวิชาการ (ศาสตราจารย์ ดร. วิชัย บุญแสง) ที่ให้กำลังใจมาตลอดเวลา 3 ปี ที่ท่านอยู่ในตำแหน่ง โดยท่านให้ความกรุณามาเปิดงานประชุมวิชาการประจำปีทุกปีอย่างสม่ำเสมอ ให้ ข้อแนะนำ ให้กำลังใจ และช่วยเสนอวิธีแก้ปัญหามาตลอด ขอขอบพระคุณท่านรักษาการผู้อำนวยการ ฝ่ายวิชาการคนใหม่ (ศาสตราจารย์ ดร. สวัสดิ์ ตันตระรัตน์) ที่ให้การสนับสนุนอย่างดีเช่นกันใน 1 ปี ที่ ผ่านมา

นอกจากนี้ คณะวิจัยขอบพระคุณหน่วยงานเจ้าสังกัดของนักวิจัยทุกท่านที่อนุเคราะห์สถานที่ และให้ใช้อุปกรณ์ประกอบการวิจัย เป็นอย่างดีตลอดมา ขอขอบคุณบริษัทและโรงงานผู้ผลิตที่เอื้อเพื้อ สารเคมีบางประเภทที่ได้กล่าวไว้ในรายงานความก้าวหน้าการวิจัยและในบทความที่พิมพ์เผยแพร่ใน วารสารวิชาการ อย่างไรก็ตาม หัวหน้าโครงการนี้จะขอกราบขอบพระคุณอีกครั้งหนึ่งสำหรับทุกสิ่งทุก อย่างที่ท่านได้ให้การสนับสนุนทั้งที่มีการกล่าวถึงและไม่ได้กล่าวถึง

ศาสตราจารย์ ดร. สุดา เกียรติกำจรวงศ์

หัวหน้าโครงการเมธิวิจัยอาวุโส ระยะที่ 2

พ.ศ. 2550 - 2554

การวิจัยและพัฒนาใหม่ ๆ ของวัสดุพอลิเมอร์สีเขียวและประโยชน์ใช้งาน

Novel Research and Development in Green Polymer Materials and Their Applications

บทคัดย่อ

บทน้ำ

โครงการนี้เป็นโครงการเมธีวิจัยอาวุโสระยะที่สอง ประจำปี พ.ศ. 2550 – พ.ศ. 2553 มีโครงการ ย่อยในโครงการหลักนี้ 10 โครงการย่อย ระยะเวลาวิจัยแต่ละโครงการตั้งแต่ 1 ปี ถึง 3 ปี เนื่องจากมี โครงการย่อยจำนวนมากและครอบคลุมสาระวิชาหลายแขนง จึงทำให้ทำวิจัยไม่เสร็จทันเวลาที่กำหนด ด้วยความกรุณาของผู้อำนวยการฝ่ายวิชาการ จึงได้รับการอนุมัติให้ขยายเวลาวิจัยออกไปอีก 1 ปี สิ้นสุดโครงการวันที่ 31 กรกฎาคม 2554 เพื่อให้โครงการสมบูรณ์และผู้ช่วยวิจัยสามารถทำวิจัยเสร็จและ สำเร็จการศึกษาจำนวนหนึ่ง โครงการย่อยทั้งหมดมีดังนี้

โครงการวิจัยย่อยที่ 1

Reactive Blending of Cassava Starch and Acrylamide and Its Application in Thermoplastic Vulcanizates of NR/PP blends

รีแอ็กที่ฟเบลนดิงของแป้งมันสำปะหลังกับอะคริลาไมด์และเทอร์โมพลาสติกวัลคะในเซตส์ของยาง ธรรมชาติกับพอลิโพรไพลีนเบลนด์

โครงการวิจัยย่อยที่ 2

Biomedical Applications of Surface-Charged Chitosan Particles and Assembled Thin Film of Charged Derivatives of Chitosan

การประยุกต์ทางชีวการแพทย์ของอนุภาคไคโทซานที่พื้นผิวมีประจุและฟิล์มประกอบแบบบางของ อนุพันธ์ที่มีประจุของไคโตซาน

โครงการวิจัยย่อยที่ 3

- 3.1 Synthesis and Performance of Grafted Chitosan/Mica Nanocomposite for Antibacterial Activities การสังเคราะห์และสมรรถนะของใคโทซานกราฟต์/ไมกานาโนคอมพอสิตสำหรับต้านเชื้อแบคทีเรีย
- 3.2 Synthesis and Characterization of Controlled Release NPK Fertilizer Hydrogel การสังเคราะห์และการตรวจสอบเอกลักษณ์ของปุ๋ยไฮโดรเจลเอ็นพีเคที่ควบคุมการปลดปล่อย

โครงการวิจัยย่อยที่ 4

Microencapsulation via Glass Membrane Emulsification and Controlled Release of Menthol ไมโครเอนแคปซูเลชันของเมนทอลโดยกลาสเมมเบรนอิมัลซิฟิเคชันและการปลดปล่อยแบบควบคุม

โครงการวิจัยย่อยที่ 5

Synthesis of Acrylamide-Based Copolymeric Superabsorbents with Thermal Stability and Flame Retardant Properties

การสังเคราะห์ซูเปอร์แอบซอร์แบนต์นาโนคอมพอสิตที่มีสมบัติความเสถียรทางความร้อนและหน่วงการติดไฟ

โครงการวิจัยย่อยที่ 6

Surface Modification of Electrospun Chitosan Nanofibers for Antibacterial Activity การดัดแปรผิวของไคโทซานนาโนไฟเบอร์จาการปั่นเส้นใยเพื่อต้านฤทธิ์เชื้อแบคทีเรีย

โครงการวิจัยย่อยที่ 7

Synthesis of Hydrogel from Collagen การสังเคราะห์ไฮโดรเจลจากคอลลาเจน

โครงการวิจัยย่อยที่ 8

Pretreatment of Kapok Fiber for Pulping and Papermaking การปรับสภาพเส้นใยนุ่นเพื่อการผลิตเยื่อและกระดาษ

โครงการวิจัยย่อยที่ 9

- 9.1 Simulation of Printed Images on Silk Fabric by Ink Jet Printer การจำลองภาพพิมพ์บนผ้าไหมด้วยเครื่องพิมพ์อิงก์เจ็ต
- 9.2 Textile Fabric Pretreatment and Pretreated Fabric Ink-jet Ink Printing การปรับผิวเส้นใยผ้าและการพิมพ์ผ้าที่ปรับผิวแล้วด้วยหมึกพิมพ์อิงก์เจ็ต

โครงการวิจัยย่อยที่ 10

Reinforcement of Dipped Natural Rubber Film by *In Situ* Generated Silica การเสริมแรงฟิล์มยางธรรมชาติแบบจุ่มด้วยซิลิกาที่เกิดขึ้นภายใน ณ จุดเกิดปฏิกิริยา

เนื่องจากครงการวิจัยนี้มีโครงการย่อยจำนวนมากที่ใช้สารตั้งต้น หรือวัตถุประสงค์ปลายทางคล้าย กัน จึงเห็นว่า ควรนำมารวมกลุ่มงานวิจัยได้ 7 กลุ่มโครงการวิจัยที่มีวัตถุประสงค์ตรงกัน เพื่อให้เห็น ภาพของงานวิจัยได้ชัดเจนขึ้น ง่ายต่อการอ่านและด้านนำไปใช้งานได้ชัดเจนขึ้นในอนาคต ดังนี้

กลุ่มโครงการวิจัยที่ 1 ยางธรรมชาติและการดัดแปรคุณลักษณะของยางธรรมชาติ มีงานวิจัย 4 เรื่อง ดังนี้

- 1.1 Preparation of Cassava Starch-Graft-Polyacrylamide Superabsorbent Polymers and Associated Superabsorbent Polymer Composites by Reactive Blending
- 1.2 Synthesis and Characterization of Water Swellable Natural Rubber Composites
- 1.3 Reinforcement of Dipped Natural Rubber Film by In Situ Generated Silica
- 1.4 Silica Formation inside Natural Rubber Grafted with Methyl Methacrylate/
 Methacryloxypropyl Trimethoxysilane

กลุ่มโครงการวิจัยที่ 2 ไคโทซานและการพัฒนาไคโทซานสำหรับการใช้งานทางชีวการแพทย์ มี 2 เรื่องหลัก 5 หัวข้อย่อย ดังนี้

- 2.1 Biomedical Applications of Surface-Charged Chitosan Particles and Assembled
 Thin Film of Charged Derivatives of Chitosan มี 2 เรื่องย่อย
 - 2.1.1 Surface-quaternized Chitosan Particles as Alternative and Effective Organic Antibacterial Fillers
 - 2.1.2 Multilayer Thin Films Assembled from Charged Derivatives of Chitosan:
 Formation and Biological Responses
- 2.2 Syntheses, Characterization and Antibacterial Activity of Chitosan Grafted Hydrogels and Associated Mica Containing Nanocomposite Hydrogels
 - 2.3 Surface Modification of Electrospun Chitosan Nanofibers for Antibacterial Activity

กลุ่มโครงการวิจัยที่ 3 ไฮโดรเจลสำหรับสิ่งแวดล้อม มีงานวิจัย 3 เรื่อง

- 3.1 Synthesis of Acrylamide/Acrylic Acid-Based Aluminum Flocculant for Dye Reduction and Textile Wastewater Treatment
- 3.2 Photocatalytic Efficiency of TiO₂/Poly[Acrylamide-co-(Acrylic Acid)] Composite for Textile Dye Degradation

3.3 Acrylamide-Based Composite Hydrogel Initiated by TiO₂ Photocatalyst for Dye and Hydrogel Degradation

กลุ่มโครงการวิจัยที่ 4 ไฮโดรเจลกับการใช้งานเฉพาะทาง มี 5 เรื่อง

- 4.1 Gel Strength and Swelling of Acrylamide-Protic Acid Superabsorbent Copolymers
- 4.2 Acrylamide–Itaconic Acid Superabsorbent Polymers and Superabsorbent Polymer/Mica Nanocomposites
- 4.3 Synthesis of Acrylamide-co-(Itaconic Acid) Superabsorbent Polymers and Associated Silica Superabsorbent Polymer Composites
- 4.4 Acrylamide/2-acrylamido-2-methylpropane Sulfonic Acid and Associated Sodium Salt Superabsorbent Copolymers with Mica Nanocomposites as Fire Retardants
- 4.5 Effect of Fire Retardant on Flammability of Acrylamide and 2-Acrylamido-2-Methylpropane Sodium Sulfonate Copolymer Composites
- 4.6 Swelling Properties and Strength of Poly[Acrylamide-co-(Itaconic Acid)] Gel and Clay-Modified Poly[Acrylamide-co-(Itaconic Acid)] Gel

กลุ่มโครงการวิจัยที่ 5 ไมโครเอนแคปซูเลชันและการควบคุมการปล่อยของวัสดุอนินทรีย์/อินทรีย์ มีงานวิจัย 4 เรื่อง

- 5.1 Microencapsulation of Menthol via Glass Membrane Emulsification and Controlled Release
- 5.2 Synthesis of Microcapsules of Eucalyptus Oil via Shirasu Porous Glass Membrane Emulsification and Controlled Release
- 5.3 Synthesis and Characterization of Controlled Release Compound NPK Fertilizer Hydrogel
- 5.4 Synthesis and Characterization of Hydrogel for Insulin Released from Collagen Grafted Poly[(Acrylic Acid)-co-(Methacrylic Acid)]

กลุ่มโครงการวิจัยที่ 6 การผลิตเส้นใยและกระดาษจากนุ่น มีงานวิจัย 3 เรื่อง

6.1 Kapok I: Properties Investigation of Kapok Fiber as a Potential Pulp Source for Papermaking

- 6.2 Kapok II: Pretreatment of Kapok Fibers for Pulping and Papermaking
- 6.3 Kapok III: Use of Kapok Pulp to Improve Properties of Recycled Paper

กลุ่มโครงการวิจัยที่ 7 การปรับผิวผ้าและการพิมพ์ผ้าด้วยหมึกพิมพ์อิงก์เจ็ต

- 7.1 Modified Chitosan Pretreatment of Polyester Fabric for Printing by Ink Jet Ink
- 7.2 Anionically Surface-Modified Pigment/Binder Ink Jet Inks for Silk Fabric Printing
- 7.3 Simulation of Printed Images on Silk Fabric by Ink Jet Printer
- 7.4 Effects of Chitosan and Glycine Pretreatment on Polyester Fabric Printed by Ink Jet Ink
- 7.5 Effects of Ink Formulation Containing Surface-Modified Pigmented Jet Inks on Jettability

ดังนั้น จึงขอรายงานบทคัดย่อของงานวิจัยนี้ตามลำดับเนื้องานวิจัยดังกล่าวข้างต้น

กลุ่มโครงการวิจัยที่ 1 ยางธรรมชาติและการดัดแปรคุณลักษณะของยางธรรมชาติ

1.1 Preparation of Cassava Starch-Graft-Polyacrylamide Superabsorbent Polymers and Associated Superabsorbent Polymer Composites by Reactive Blending

Cassava starch-*g*-polyacrylamide (PAM) was successfully prepared by a reactive batch processing using a specially designed batch reactor resulting in a superabsorbent polymer (SAP) with water absorption of 605 g/g being obtained under the optimized reaction conditions. The occurrence of a graft copolymer was confirmed by FT-IR spectra, where it was found to exhibit all characteristic bands of both starch and acrylamide (AM) units. SEM micrographs of the starch granules showed an irregular shape and varied particle sizes with a smooth surface, while the graft copolymers had a coarse porous structure and broad network. Various types of inorganic filler were added to the graft copolymer to prepare the SAP composites (SAPC). It was found that the SAPC with bentonite clay exhibited the highest water absorption of approximately 730 g/g. Conversely, the incorporation of silica to the graft copolymer gave a significantly lower water absorption capability than the copolymer alone.

Key words: Acrylamide, Batch reactor, Cassava starch, Superabsorbent polymer composite

การเตรียมพอลิเมอร์ซูเปอร์แอบซอร์เบนต์ของแป้งมันสำปะหลังกราฟต์พอลิอะคริลาไมด์และ คอมพอสิตแอบซอร์เบนต์ที่สอดคล้องกัน

โครงการนี้ได้เตรียมแป้งมันสำปะหลังกราฟต์พอลิอะคริลาไมด์ (พีเอเอ็ม หรือ PAM) ด้วยวิธีรีแอก ที่ฟแบบกะในปฏิกรณ์ที่ออกแบบพิเศษ ทำให้ได้พอลิเมอร์ซูเปอร์แอบซอร์เบนต์ (เอสเอพี หรือ SAP) ที่ มีค่าการดูดซึมน้ำ 605 กรัมต่อกรัมของสารแห้ง ภายใต้ภาวะของปฏิกิริยาที่ควบคุมให้เหมาะสม เทคนิค FTIR ตรวจพบลักษณะเฉพาะของพีกหรือแบนด์ทั้งในแป้งและพอลิอะคริลไมด์ (PAM) ภาพอิเล็กตรอน ไมโครกราฟแสดงเม็ดแป้งที่มีขนาดไม่แน่นอน แต่มีผิวเรียบ ในขณะที่ภาพของกราฟต์โคพอลิเมอร์มี โครงสร้างหยาบ พร้อมรูพรุนและโครงข่ายกว้าง ได้ใส่สารเติมแต่งอนินทรีย์หลายชนิดให้แก่กราฟต์โคพอลิเมอร์เพื่อเตรียมพอลิเมอร์ซูเปอร์แอบซอร์เบนต์คอมพอสิต (SAPC) พบว่า SAPC ที่ผสมแร่ดินเบน โทในต์ มีค่าการดูดซึมน้ำมากสุด 730 กรัมต่อกรัมของสารแห้ง ในทางตรงกันข้าม การใส่ผงซิลิกาใน กราฟต์โคพอลิเมอร์ลดค่าการดูดซึมน้ำลงมากอย่างมีนัยสำคัญเมื่อเปรียบเทียบกับโคพอลิเมอร์ที่ไม่เดิม ผงซิลิกา

คำสำคัญ: อะคริลาไมด์, ปฏิกิริยาแบบกะ, แป้งมันสำปะหลัง, ซูเปอร์แอบซอร์เบนต์พอลิเมอร์คอมพอสิต

1.2 Synthesis and Characterization of Water Swellable Natural Rubber Composites

Superabsorbent polymer (SAP) based on cassava starch-g-polyacrylamide was prepared by a reactive batch processing using a specially designed batch reactor. The SAP composites (SAPCs) were prepared by blending with 20 phr of bentonite clay. The clay was used to increase water absorbency of the SAP from 605 g/g to SAPC of 730 g/g. Water swellable natural rubber (WSNR) was then prepared by blending high ammonia natural rubber (HANR) latex, and dry blending of epoxidized natural rubber (ENR), and maleated natural rubber (MNR) with SAPC, poly(ethylene oxide) (PEO) and trimethylol propane trimethacrylate coupling agent (TMPTMA). Curing, mechanical, morphological properties and water absorbency of WSNRs were characterized. The WSNR with PEO and TMPTMA gave higher mechanical strength and water absorbency. Increasing PEO loadings rendered higher absorbency with lower mechanical strength at its contents higher than 10 phr. A higher scorch time, cure time with a low crosslinking density, and cure rate index were found in the MNR base WSNRs compared with those of the unmodified NR and ENR base WSNRs. The ENR base WSNR exhibited the highest water absorbency with lower mechanical strength compared with the unmodified NR base WSNR.

Key words: Coupling agent, Poly(ethylene oxide), Superabsorbent polymer, Superabsorbent polymer composite, Trimethylol propane trimethacrylate, Water swellable natural rubber.

การสังเคราะห์และการตรวจลักษณะเฉพาะของยางธรรมชาติคอมพอสิตบวมน้ำ

ได้เตรียมพอลิเมอร์ซูเปอร์แอบซอร์เบนต์ (SAP) ของแป้งมันสำปะหลังกราฟต์พอลิอะคริลาไมด์ โดยทำปฏิกิริยาในปฏิกรณ์แบบกะที่ออกแบบพิเศษ และเตรียมพอลิเมอร์ซูเปอร์แอบซอร์เบนต์คอมพอ สิต (SAPC) โดยผสมแร่ดินเบนโทในต์ 20 พีเอชอาร์ การใช้แร่ดินก็เพื่อเพิ่มความแข็งแรงและค่าการดูด ซึมน้ำของ SAP จาก 605 กรัมต่อกรัมของสารแห้ง เป็นค่า 730 กรัมต่อกรัมของสารแห้งใน SAPC เตรียมยางธรรรมชาติบวมน้ำจากการผสมเลเท็กซ์ของยางธรรมชาติที่มีความเข้มขันของแอมโมเนียมาก และผลิตยางธรรมชาติดัดแปรบวมน้ำมากอีก 2 ประเภท คือ ยางธรรมชาติอิพอกซิไดส์ (ENR) และยาง ธรรมชาติมาลิเอต (MNR) ผสมยางธรรมชาติแต่ละประเภทด้วย SAPC พอลิเอทิลีนออกไซด์ (PEO)

และสารคู่ควบไทรเมทิลอลโพรเพนไทรเมทาคริเลต (TMPTMA) ตรวจคุณลักษณะด้านการบ่ม ด้าน สัณฐานวิทยา สมบัติเชิงกล และค่าการดูดซึมน้ำ พบว่า ยางธรรมชาติไม่ดัดแปรที่มี PEO และ TMPTMA ให้ค่าสมบัติเชิงกลและค่าการดูดซึมน้ำดีขึ้น เมื่อเติม PEO 10 พีเอชอาร์ ทำให้ยางธรรมชาติ บวมน้ำมีค่าการดูดซึมมากขึ้นแต่ความแข็งแรงเชิงกลลดลง และใช้เวลาทำให้ยางสุกและเกรียมนานขึ้น แต่ยังมีค่าความหนาแน่นของการเชื่อมขวางต่ำลง ในยางธรรมชาติบวมน้ำมาลิเอกมีค่าดัชนีของอัตรา การบ่มสูงขึ้นเมื่อเทียบกับยางธรรมชาติบวมน้ำที่ไม่มีการดัดแปรโครงสร้างของยางและยางธรรมชาติ บวมน้ำอีพอกซิไดส์ให้ค่าการดูดซึมน้ำมากกว่าและมี ค่าสมบัติเชิงกลต่ำลงกว่ายางธรรมชาติบวมน้ำที่ไม่ดัดแปรโครงสร้าง

คำสำคัญ: สารคู่ควบ, พอลิเอทิลีนออกไซด์, พอลิเมอร์ซูเปอร์แอบซอร์เบนต์, พอลิเมอร์ซูเปอร์แอบซอร์ เบนต์คอมพอสิต, ไทรเมทิลอลโพรเพนไทรเมทาคริเลต, ยางธรรมชาติบวมน้ำ

1.3 Reinforcement of Dipped Natural Rubber Film by In Situ Generated Silica

A method for preparing silica-reinforced rubber thin film by latex dipping process was established. The latex used in the dipping step was pre-mixed with alkoxysilane precursor and sulfur curing agents. By one heating step, both *in situ* silica formation and rubber curing took place successfully in the rubber thin films. This work focused on the use of two alkoxysilane precursors that contained one vinyl group, i.e., vinyl triethoxysilane (VTOS), and methacryloxypropyl trimethoxysilane (MPS). Both were able to covalently link to the double bonds in NR chains via sulfur or radical crosslinking. Therefore, the size and distribution of *in situ* silica as well as its reinforcement capability on the NR vulcanizates were investigated as a function of the type and amount of added alkoxysilanes.

Key words: Particle-reinforcement, Mechanical properties, Sol-gel process.

การเสริมแรงฟิล์มยางธรรมชาติแบบจุ่มด้วยซิลิกาที่เกิดขึ้นภายใน ณ จุดเกิดปฏิกิริยา

งานวิจัยได้ศึกษากรรมวิธีการเตรียมฟิล์มบางของลาเท็กซ์ยางธรรมชาติแบบจุ่ม เลเท็กซ์นี้ต้องผสม กับแอลคอกซิไซเลนพรีเคอร์เซอร์และสารบ่มซัลเฟอร์ก่อน แค่ให้ความร้อนเพียงขั้นเดียวก็ทำให้เกิดผงซิ ลิกาจากสารพรีเคอร์เซอร์พร้อมกับเกิดการบ่มฟิล์มยางอย่างสมบูรณ์ งานวิจัยนี้เน้นการใช้แอลคอกซิไซ เลนพรีเคอร์เซอร์ที่มีหมู่ไวนิลเพียง 1 หมู่ 2 ชนิด คือ ไวนิลไทรเอทอกซิไซเลน (VTOS) และเมทาคริลอ ชิโพรพิลไทรเมทอกซิไซเลน (MPS) สารทั้งสองนี้สามารถเกิดพันธะโควาเลนต์กับพันธะคู่ในสายโซ่ของ ยางธรรมชาติผ่านซัลเฟอร์ หรือการเชื่อมขวางด้วยอนุมูลอิสระ ดังนั้น จึงศึกษาขนาดและการกระจาย ขนาดของผงซิลิกาที่เกิดขึ้นระหว่างการบ่มกับความสามารถในการเสริมแรงของยางวัลคะในเซตส์ ซึ่ง เป็นตัวแปรของชนิดและปริมาณของแอลคอกซีไซเลนที่เติมลงไป

คำสำคัญ: การเสริมแสงด้วยอนุภาค สมบัติเชิงกล, กระบวนการโซล-เจล

1.4 Silica Formation inside Natural Rubber Grafted with Methyl Methacrylate/Gamma-Methacryloxypropyl Trimethoxysilane

Methyl methacrylate (MMA) and γ -methacryloxypropyl trimethoxysilane (γ -MPS) were both grafted onto isoprene units of natural rubber (NR) with the aim to prepare rubber-silica hybrid. The methoxy silane units of γ -MPS were allowed to undergo hydrolysis and condensation reaction by heating the cast film of the grafted latex at 50°C to form silica particles within the rubber matrix. The formation of this rubber-silica hybrid was confirmed by ATR-FTIR, TEM and SEM. The γ -MPS coupling agent could also transform into silica inside the rubber. The addition of tetraethoxysilane (TEOS) resulted in an increase of *in situ* silica of up to 6 phr. The grafting efficiency of MMA onto rubber was around 80%, while that of γ -MPS was about 48%. The final composition of the hybrid rubber was 86:12:2.0 (by weight) of NR: MMA: γ -MPS.

Key words: In situ silica, Methyl methacrylate, γ -methacryloxypropyl trimethoxysilane, Natural rubber

การเกิดซิลิกาภายในยางธรรมชาติกราฟต์ด้วยเมทิลเมทาคริเลต / เมทาคริลอกซีโพรพิลไทร เมทอกซีไซเลน

โครงการนี้ได้เตรียมยางธรรมชาติผสมผงซิลิกาโดยกราฟต์เมทิลเมทาคริเลต (MMA) และแกมมา-เมทอะคริลอกซีโพรพิลไทรเมทอกซิไซเลน (γ-MPS) บนหน่วยไอโซพรินของยางธรรมชาติ หน่วยเม ทอกซีไซเลนของ γ-MPS เกิดไฮโดรไลซิสและปฏิกิริยาควบแน่นได้โดยให้ความร้อน 50 องศาเซลเซียส แก่ฟิล์มจุ่มของเลเท็กซ์กราฟต์เพื่อให้เกิดอนุภาคซิลิกา ณ จุดเกิดปฏิกิริยาแก่เมทริกซ์ของยาง ยืนยัน เอกลักษณ์และการเกิดผงซิลิกาในยางผสมซิลิกาด้วยเทคนิค ATR-FTIR, TEM และ SEM สารคู่ควบ γMPS นี้สามารถเปลี่ยนรูปและเกิดซิลิกา ณ จุดเกิดปฏิกิริยาอยู่ภายในยางธรรมชาติด้วย การเติมเททระ เอทอกซีไซเลน (TEOS) ทำให้เพิ่มปริมาณซิลิกาที่เกิด ณ จุดเกิดปฏิกิริยาเพิ่มขึ้นถึง 6 phr ประสิทธิ์ ภาพการกราฟต์ของ MMA บนยางธรรมชาติอยู่ที่ร้อยละ 80 ในขณะที่การกราฟต์ด้วย γ-MPS มี ประสิทธิ์ภาพเพียงร้อยละ 48 องค์ประกอบสุดท้ายของยางผสมผงซิลิกามีสัดส่วนของยางธรรมชาติ : MMA : γ--MPS เป็น 86:12:2

คำสำคัญ: ซิลิกาที่เกิด ณ จุดเกิดปฏิกิริยา, เมทิลเมทาคริเลต, แกมมา-เมทอะคริโลซีโพรพิลไทรเมทอกซิ ไชเลน, ยางธรรมชาติ

กลุ่มโครงการวิจัยที่ 2 ไคโทซานและการพัฒนาไคโทซานสำหรับการใช้งานทางชีวการแพทย์

2. Biomedical Applications of Surface-Charged Chitosan Particles and Assembled Thin Film of Charged Derivatives of Chitosan

Chitosan is a partially deacetylated form of chitin, a natural substance found abundantly in the exoskeletons of insects, shells of crustaceans, and fungal cell walls. Because of its favorable physicochemical and biological properties such as biocompatible, non-toxic, antibacterial, chitosan is considered as an attractive material that can be potentially used in many biomedical-related applications. The repeating units of chitosan constitute a large number of hydroxyl and amino groups. These two functional groups offer several possibilities for derivatization and immobilization of biologically active species. Taking advantages of functional group availability for chemical reactions of chitosan and the diversified bioactivity of chitosan and its charged derivatives, this research aimed to explore the applicability of chargefunctionalized chitosan. The research was divided into two parts. The first part concentrated on the formation of multilayer films from charged derivatives of chitosan via layer-by-layer adsorption. The charged derivatives that were of our interest are N-sulfofurfuryl chitosan (SFC), N-succinyl chitosan (SCC), and N-[(2-hydroxyl-3-trimethylammonium)propyl] chitosan chloride (HTACC). The assembly process and viscoelastic properties were monitored by quartz crystal microbalance (QCM). Stratification of the multilayer film was demonstrated by water contact angle analysis. The coverage of the assembled films was characterized by atomic force microscopy and ATR-FTIR spectroscopy. Biological responses of the selected assembled films were assessed in term of in vitro cell adhesion and proliferation of fibroblasts, antibacterial activity, and platelet adhesion.

Keywords: Chitosan, Charged derivative, Multilayer film, Biocompatibility, Particles, Antibacterial activity, Biosensor, DNA, PNA, Ion exchanger

ไคโทซานได้จากการกำจัดหมู่แอซิทิลบางส่วนของไคทิน สารธรรมชาติที่พบมากในเปลือกของ แมลง สัตว์มีกระดอง และผนังเซลล์ของเห็ดและราบางขนิด เนื่องจากสมบัติทางกายภาพ เคมี และ ชีวภาพที่น่าสนใจของไคโทซาน เช่น เข้ากันได้กับสิ่งมีชีวิต ไม่เป็นพิษ และด้านแบคทีเรีย ทำให้ไคโท ชานเป็นวัสดุที่น่าสนใจและมีศักยภาพในการพัฒนาเพื่อการประยุกต์ในงานที่เกี่ยวข้องกับชีวการแพทย์ หน่วยซ้ำของไคโทซานประกอบด้วยหมู่ไฮดรอกซิลและหมู่แอมิโนที่สามารถนำไปใช้ในเปลี่ยนเป็น อนุพันธ์ต่างๆ หรือการตรึงสารที่ไวทางชีวภาพได้ ใช้ประโยชน์จากการมีหมู่ฟังก์ชันที่สามารถนำไปใช้ใน การดัดแปรทางเคมีของไคโทซานและสมบัติทางชีวภาพที่หลากหลายของอนุพันธ์ที่มีประจุของไคโท ซาน งานวิจัยนี้มีเป้าหมายที่จะศึกษาการใช้อนุพันธ์ที่มีประจุของไคโทซาน งานวิจัยแบ่งออกเป็นสอง ส่วน ส่วนแรกเป็นการศึกษาการเกิดเป็นฟิล์มมัลติเลเยอร์ของอนุพันธ์ที่มีประจุของไคโทซานด้วยการ ประกอบแบบชั้นต่อชั้น อนุพันธ์มีประจุของไคโทซานที่สนใจศึกษาในงานวิจัยนี้ ได้แก่ เอ็น-ซัลโฟเฟอร์ฟู ริลไคโทซาน, เอ็น-ซักซินิลไคโทซาน, และ เอ็น-[(2-ไฮดรอกซิล-3-ไทรเมทิล แอมโมเนียม)โพรพิล]ไคโท ซานคลอไรด์ ติดตามกระบวนการประกอบเป็นฟิล์มและสมบัติวิสโคอิลาสติซิตีด้วยควอร์ตซ์คริสทัลไม โครบาลานซ์ วิเคราะห์การสลับชั้นด้วยการวัดมุมสัมผัสของน้ำ ตรวจสอบการปกคลุมของฟิล์มที่ ประกอบขึ้นด้วยอะตอมมิกฟอร์ซไมโครสโกปีและเอทีอาร์เอฟทีไออาร์สเปกโทรสโกปี ศึกษาการ ตอบสนองทางชีวภาพของฟิล์มที่ประกอบขึ้นบางระบบในแง่ของการยึดเกาะและการเพิ่มจำนวนของ เซลล์ไฟโบรบลาสต์ในหลอดทดลอง ฤทธิ์ยับยั้งแบคทีเรีย และการเกาะของเกล็ดเลือด

2.1.1 Surface-quaternized Chitosan Particles as Alternative and Effective Organic Antibacterial Fillers

Taking advantage of the large surface area that is covered with permanent positive charges of quaternary ammonium entities, this research aimed to develop environmentally friendly, organic antibacterial fillers from quaternized chitosan particles that may be applicable for biomedical devices, health and textile industries. The particles were formulated by ionic crosslinking of chitosan with tripolyphosphate followed by quaternization that was conducted under heterogeneous condition via either direct methylation or reductive *Nalkylation* with a selected aldehyde followed by methylation. Sub-micron, spherical, and positively charged quaternized chitosan particles were formed, as determined by 1H-NMR, FT-IR, PCS, and TEM analysis. Antibacterial activity tests performed by viable cell counts suggested that all quaternized chitosan particles exhibited superior antibacterial activity against the model Grampositive bacteria, *S.aureus*, as compared to the native chitosan particles at neutral pH. Only some quaternized chitosan particles, especially those having a high charge density and bearing large alkyl substituent groups, were capable of suppressing the growth of the model Gram-

negative bacteria, *E. coli*. The inhibitory efficiency of the quaternized chitosan particles was quantified in terms of the minimum inhibitory concentration (MIC).

Keywords: chitosan; particle; heterogeneous quaternization; minimum inhibitory concentration

อนุภาคไคโทซานควอเตอร์ในซ์ที่ผิวเป็นฟิลเลอร์อินทรีย์ทางเลือกที่มีประสิทธ์ภาพด้านการต้าน เชื้อแบคทีเรีย

ใช้ประโยชน์จากการมีพื้นที่ผิวสูงและการถูกปกคลุมด้วยประจุถาวรของหมู่ควอเทอร์นารี แอมโมเนียมของอนุภาคควอเทอร์ในซ์ใคโทซาน งานวิจัยในส่วนที่สองสนใจศึกษาการใช้อนุภาคดังกล่าว เพื่อวัตถุประ- สงค์ สองประการ คือ เป็นสารยับยั้งแบคทีเรีย และเป็นตัวแลกเปลี่ยนแอนไอออนสำหรับ การประยุกต์ทางใบโอเซ็นเซอร์ ทั้งนี้เตรียมอนุภาคด้วยการเชื่อมขวางแบบไอออนิกของไคโทซานด้วย ไทรพอลิฟอสเฟส ตามด้วยควอเทอร์ในเซชันซึ่งส่วนใหญ่เป็นการทำปฏิกิริยาแบบวิวิธพันธ์ผ่านเมทิลเล ชันหรือเอ็น-รีดักที่ฟแอลคิเลชัน/เมทิลเลชัน จากการยืนยันการเกิดอนุภาคโดยการวิเคราะห์ด้วยเทคนิคฟู เรียทรานส์ฟอร์มอินฟราเรดสเปกโทรสโกปี, โฟตอนคอร์รีเลชันสเปกโทรสโกปี และกล้องจุลทรรศน์ อิเล็กตรอนแบบส่งกราด ผ่านพบว่า อนุภาคที่ได้มีขนาดเล็กกว่า 1 ไมครอเมตร มีลักษณะเป็นทรงกลม และมีประจุเป็นบวก จากการทดสอบฤทธิ์ในการยับยั้งแบคทีเรียด้วยการนับจำนวนแบคทีเรียที่รอดชีวิต พบว่าอนุภาคควอเทอร์ในซ์ไคโทซานทุกชนิดมีฤทธิ์ในการยับยั้ง S.aureus ซึ่งเป็นแบคทีเรียแกรมบวกที่ เหนือกว่าอนุภาคไคโทซานในสภาวะที่มีพีเอชเป็นกลาง ในขณะที่มีเพียงอนุภาคควอเทอร์ในซ์ไคโทซาน บางชนิดโดยเฉพาะอย่างยิ่งที่มีความหนาแน่นประจุสูงและมีหมู่แทนที่แอลคิลขนาดใหญ่ที่สามารถยับยั้ง การเติบโตของ E.coli ซึ่งเป็นแบคทีเรีย แกรมลบ นอกจากนี้ยังพบว่าประสิทธิภาพในการยับยั้งขึ้นกับ ปริมาณของอนุภาคซึ่งประเมินค่าเชิงปริมาณได้จากความเข้มข้นต่ำสุดที่ทำให้เกิดการยับยั้ง งานวิจัยอีก ส่วนหนึ่งเป็นการศึกษาการใช้อนุภาคควอเทอในซ์ใคโทซานเป็นตัวแลกเปลี่ยนแอนไอออนร่วมกับพิโรลิดิ นิลเพปไทด์นิวคลีอิกแอซิดที่มีคอนฟอร์เมชันถูกจำกัด (พีเอ็นเอ) สำหรับการตรวจลำดับเบสของดีเอ็นเอ จากการวิเคราะห์ด้วยมัลดิ-ทอฟแมสสเปกโทรเมทรีพบว่าอนุภาคควอเทอในซ์ไคโทซานสามารถใช้ ร่วมกับพีเอ็นเอที่มีลำดับเบสเป็น T9 ในการบอกความแตกต่างระหว่างดีเอ็นเอที่มีลำดับเบสเป็นคู่สมจาก ดีเอ็นเอที่มีลำดับเบสไม่เป็นคู่สม (มีลำดับเบสผิดไปหนึ่งตำแหน่งหรือทุกตำแหน่ง) ได้

คำหลัก: ไคโทซาน, อนุพันธ์มีประจุ, ฟิล์มมัลติเลเยอร์, ความเข้ากันได้กับสิ่งมีชีวิต, อนุภาค, ฤทธิ์ยับยั้ง แบคทีเรีย, ไบโอเซนเซอร์, ดีเอ็นเอ, พีเอ็นเอ, ตัวแลกเปลี่ยนไอออน

2.1.2 Multilayer Thin Films Assembled from Charged Derivatives of Chitosan: Formation and Biological Responses

Charged derivatives of chitosan, *N*-sulfofurfuryl chitosan (SFC) and *N*-[(2-hydroxyl-3-trimethylammonium)propyl] chitosan chloride (HTACC), were prepared by reductive alkylation using 5-formyl-2-furansulfonic acid, sodium salt (FFSA) as a reagent and ring opening of glycidyltrimethylammonium chloride (GTMAC) by amino groups of chitosan(CHI), respectively. Multilayer thin film of chitosan and its charged derivatives was fabricated by alternate layer-by-layer adsorption onto a surface-treated poly(ethylene terephthalate) (treated PET) substrate. Assembly process was monitored by quartz crystal microbalance (QCM). Stratification of the multilayer film was demonstrated by water contact angle data. The coverage of the assembled films was characterized by AFM and ATR-FTIR analyses. Alternate biological responses of the assembled films were assessed by protein adsorption and *in vitro* cell adhesion and proliferation.

Keywords: Chitosan, Charged derivative, Layer-by-layer adsorption, Multilayer film, Polyelectrolyte

ฟิล์มหลายชั้นประกอบจากอนุพันธ์ที่มีประจุของไคโตซาน: การเกิดและตอบสนองทางชีวภาพ

อนุพันธ์ที่มีประจุของไคโตซาน, เอ็น-ซัลโฟเฟอร์ฟูริลไคโตซาน (เอสเอฟซี) และเอ็น-[(2-ไฮดรอก ซิล-3-ไตรเมทิลแอมโมเนียม)โพรพิล]ไคโตซานคลอไรด์ (เอชทีเอซีซี) เตรียมขึ้นโดยปฏิกิริยารีดักทีฟ แอลคิลเลชันโดยใช้เกลือโซเดียมของ 5-ฟอร์มิล-2-ฟิวแรนซัลโฟนิกแอซิดเป็นรีเอเจนด์ และปฏิกิริยาการ เปิดวงของไกลซิดิลไทรเมทิลแอมโมเนียมคลอไรด์ (จีทีเอ็มเอซี) ด้วยหมู่แอมิโนของไคโตซาน ตามลำดับ เตรียมมัลติเลเยอร์ฟิล์มของไคโตซานและอนุพันธ์ที่มีประจุของไคโตซานบนผิวของพอลิเอ ทิลีนเทเรฟทาเลตที่มีการดัดแปรด้วยวิธีการดูดชับแบบประกอบชั้นต่อชั้นของพอลิอิเล็กโทรไลต์ที่มีประจุ ตรงข้ามกัน ติดตามกระบวนการประกอบเป็นฟิล์มด้วยเทคนิคควอร์ทซ์คริสตัลไมโครบาลานซ์ (คิวซี เอ็ม) สามารถยืนยันการสลับชั้นของฟิล์มหลายชั้นได้จากผลการวัดมุมสัมผัสของน้ำ วิเคราะห์ลักษณะ และโครงสร้างทางเคมีบนพื้นผิวของมัลติเลเยอร์ฟิล์มด้วยอะตอมมิกฟอร์ซไมโครสโกปี (เอเอฟเอ็ม) และ เอทีอาร์-เอฟทีไออาร์ ตรวจสอบการตอบสนองทางชีวภาพแบบสลับของฟิล์มที่ประกอบขึ้นโดยศึกษา การดูดซับของโปรตีน การยึดเกาะและการแพร่กระจายของเซลล์ในหลอดทดลอง

คำสำคัญ: ไคโทซาน, อนุพันธ์มีประจุ, การดูดซับแบบชั้นต่อชั้น, ฟิล์มหลายชั้น, พอลิอิเล็กทรอไลต์

2.2 Syntheses, Characterization and Antibacterial Activity of Chitosan Grafted Hydrogels and Associated Mica Containing Nanocomposite Hydrogels

Chitosan (CS) grafted poly[(acrylic acid)-co-(2-hydroxyethyl methacrylate)] (CS-g-poly(AA-co-HEMA)) at different molar ratios of AA and HEMA, and the associated nanocomposite hydrogels of CS-g-poly(AA-co-HEMA)/mica were synthesized by radical copolymerization. The grafting positions at the amino or hydroxyl groups in the CS were identified by Fourier transform infrared spectroscopy. CS-g-poly(AA-co-HEMA) hydrogels were intercalated in the mica and the amount of hydrogel insertion did not affect the spacing of the silicate layers in mica. The higher mica loadings produced rougher surfaces of the nanocomposite hydrogel. The water absorbency of the CS-g-poly(AA-co-HEMA)/mica nanocomposite hydrogels decreased with increasing levels of mica loading to a lower level than those of the CSg-poly(AA-co-HEMA) hydrogels. Both CS-g-poly(AA) and CS-g-poly(AA-co-HEMA)/mica nanocomposite hydrogels exhibited a higher antiproliferative activity against *Staphylococcus aureus* than did the neat CS hydrogel with CS-g-poly(AA) revealing a very pronounced minimum inhibition concentration (MIC) of 1.56 mg ml⁻¹. The extent of mica loading in the CS-g- poly(AA-co-HEMA) nanocomposite hydrogels did not affect the MIC (12.5 mg ml⁻¹).

Keywords: Chitosan, Acrylic acid, 2-hydroxyethyl methacrylate, Mica, Nanocomposite hydrogel, Antibacterial property

การสังเคราะห์ การตรวจคุณลักษณะ และการตรวจสอบฤทธิ์ต้านแบคทีเรียของไฮโดรเจลไคโท ซานและไฮโดรเจลไคโทซานนาโนคอมพอสิตที่มีไมกา

สังเคราะห์ใคโทซานกราฟต์พอลิเมอร์ร่วมอะคริลิกแอซิดและ 2-ไฮดรอกซีเอทิลเมทาคริเลต (CS-g-poly(AA-co-HEMA)) ที่อัตราส่วนโดยโมลต่าง ๆ ของ AA และ HEMA และไฮโดรเจลนาโนคอมพอสิต ของ CS-g-poly(AA-co-HEMA)/mica ด้วยปฏิกิริยาการเกิดพอลิเมอร์แบบอนุมูลอิสระ หาตำแหน่งการ กราฟต์ด้วยเทคนิค FTIR พบว่า เกิดกราฟต์ที่หมู่แอมิโนหรือไฮดรอกซิลในไคโทซาน ไฮโดรเจลนาโน คอมพอสิตของ CS-g-poly(AA-co-HEMA) เกิดลักษณะอินเทอร์คาเลต ซึ่งมีการแทรกสอดของสายโซ่ พอลิเมอร์ในชั้นซิลิเกตของไมกา และปริมาณการสอดแทรกของไฮโดรเจลไม่มีผลต่อระยะห่างของชั้นซิลิ

เกตในไมกา ปริมาณไมกาที่เพิ่มขึ้นทำให้ไฮโดรเจลนาโนคอมพอสิตมีพื้นผิวขรุขระมากขึ้น การดูดซึมน้ำ ของ CS-g-poly(AA-co-HEMA)/mica nanocomposite ลดลง จากการเพิ่มปริมาณไมกาในการ สังเคราะห์ และค่านี้ลดลงมากกว่าค่าการดูดซึมน้ำของ CS-g-poly(AA-co-HEMA) hydrogel ทั้ง CS-g-poly(AA) และ CS-g-poly(AA-co-HEMA)/mica composite แสดงฤทธิ์ยับยั้งการแบ่งตัวของเซลล์ (antiproliferative activity) ต่อเชื้อสเตปฟิโลคอกคัสออเรียส มากกว่าที่ไคโทซานไฮโดรเจลจะทำได้ ความเข้มข้นน้อยที่สุดที่ยับยั้งเชื้อนี้ได้ของ CS-g-poly(AA) มีค่า 1.56 มิลลิกรัมต่อมิลลิลิตร ปริมาณ ไมกาใน CS-g-poly(AA-co-HEMA)/mica nanocomposite hydrogel ไม่มีผลต่อค่า MIC ซึ่งให้ค่าเท่ากัน คือ 12.5 มิลลิกรัมต่อมิลลิลิตร

คำสำคัญ: ไคโทซาน, อะคริลิกแอซิด, 2-ไฮดรอกซีเอทิลเมทาคริเลต, ไมกา, ไฮโดรเจลนาโนคอมพอสิต, ต้านฤทธิ์เชื้อแบคทีเรีย

2.3 Surface Modification of Electrospun Chitosan Nanofibers for Antibacterial Activity

Chitosan with a degree of deacetylation of 95% in its blend with poly(ethylene oxide) (PEO) was fabricated into nanofibrous membranes by electrospinning. The introduction of PEO was to facilitate the fiber formation. The spinning solution was 6.7% w/v chitosan and 0.3% w/v PEO in 70:30 v/v trifluoroacetic acid/dichloromethane. The obtained fibers were smooth without the presence of beads, as confirmed by scanning electron microscopy (SEM). The diameters of the individual fibers were 272 \pm 56 nm. The surface of the obtained chitosan fibers was modified with N-(2-hydroxyl) propyl-3-trimethyl ammonium chloride (HTAC) with an aim of making the chitosan nanofibrous membranes into a quaternary ammonium salt (HTACC). The reaction was characterized by Fourier-transformed infrared spectroscopy (FTIR) and degree of swelling. The resulting chitosan fibers were tested with two types of bacteria and the antibacterial activities were compared and discussed.

Keywords: Surface modification, Electrospinning, Chitosan, Derivative of chitosan, Nanofiber, Antibacterial activity

การดัดแปรผิวของเส้นใยไคโทซานขนาดนาโนเมตรปั่นด้วยไฟฟ้าเพื่อต้านฤทธิ์แบคทีเรีย

ได้ผลิตเมมเบรนของเส้นใยไคโทซานขนาดนาโนเมตรจากไคโทซานที่มีระดับดีแอเซตทิเลชัน ร้อยละ 95 ผสมกับพอลิเอทิลีนออกไซด์ (PEO) ด้วยเทคนิคอิเล็กทรอสปินนิง การใส่ PEO ก็เพื่อช่วยใน การฉีดเส้นใย สารละลายสปินนิงประกอบด้วยไคโทซานร้อยละ 6.7 โดยน้ำหนัก และ PEO ร้อยละ 0.3 โดยน้ำหนัก ในสารละลายผสมระหว่างไทรฟูลออโรแอซิติกแอซิตกับไดคลอโรมีเทนสัดส่วน 70:30 โดย ปริมาตร เส้นใยเมมเบรนที่ได้มีความเรียบ ไม่มีปุ่มหรือปมตลอดเส้น ซึ่งตรวจสอบได้ด้วยกล้อง จุลทรรศน์อิเล็กทรอนแบบส่องกราด เส้นผ่าศูนย์กลางของเส้นใยมีค่า 272 ± 56 นาโนเมตร นำสารเอ็น-2-ไฮดรอกซีพรอพิล-3-ไทรเมทิลแอมโมเนียมคลอไรด์ (N-(2-hydroxyl) propyl-3-trimethyl ammonium chloride) (HTAC) มาดัดแปรผิวหน้าของเส้นใยไคโทซานที่ได้ เพื่อทำให้ผิวเส้นใยเหล่านี้มีเกลือของควอ เตอร์นารี (HTACC) ซึ่งยืนยันได้ด้วยเทคนิค FTIR และระดับขั้นของการดูดซึมน้ำ นำเส้นใยที่ได้ ทั้งหมดมาทดสอบฤทธิ์การต้านเชื้อแบคทีเรีย งานนี้ได้นำเสนอผลและวิพากย์ฤทธิ์การต้านแบคทีเรีย

คำสำคัญ: การดัดแปรผิว, อิเล็กทรอสปินนิง, ไคโทซาน, อนุพันธ์ของไคโทซาน, นาโนไฟเบอร์, ฤทธิ์ต้าน แบคทีเรีย

กลุ่มโครงการวิจัยที่ 3 ไฮโดรเจลสำหรับสิ่งแวดล้อม

3.1 Synthesis of Acrylamide/Acrylic Acid-Based Aluminum Flocculant for Dye Reduction and Textile Wastewater Treatment

Aluminum hydroxide-poly[acrylamide-co-(acrylic acid)], AHAMAA, was synthesized with a redox initiator by solution polymerization in which the effects of reactant contents were optimized. The effects of pH, temperature, and initial dye concentration on Congo red reduction were investigated. A mixture of Congo red and direct blue 71, and the composite textile dye wastewater were investigated. Adsorptions of both dyes were more effective in the non-buffered solution than those in the buffered solution, and Congo red were adsorbed more than direct blue 71 at all pHs. The adsorption of Congo red increased with increasing temperature and its initial concentration. Both dyes obeyed the Freundlich adsorption isotherm. The maximum adsorptions in 100 mg dm⁻³ solution were 109±0.5 mg g⁻¹ and 62±6.6 mg g⁻¹ for Congo red and direct blue 71, respectively. At 150 mg dm⁻³ of the mixed Congo red and direct blue 71, the adsorption was 142±2 mg g⁻¹ by 643±3 mg dm⁻³ AHAMAA. The 40 mg g⁻¹ dyes of the textile effluent wastewater were adsorbed by 500 mg dm⁻³ AHAMAA. AHAMAA could decrease turbidity of the composite wastewater containing a mixture of reactive and direct dyes from 405 to 23 NTU.

Keywords: Aluminum flocculant, Poly[acrylamide-co-(acrylic acid)], Dye adsorption, Turbidity reduction, Wastewater

การสังเคราะห์สารจับกลุ่มก้อนอะลูมิเนียมฐานอะคริลาไมด์/อะคริลิกแอซิดสำหรับการลดสีย้อม และการบำบัดน้ำเสียสิ่งทอ

สารก่อการจับกลุ่มพอลิเมอร์อะลูมิเนียมไฮดรอกไซด์-โคพอลิเมอร์ของอะคริลาไมด์และอะคริลิกแอ ซิด (AHAMAA) สังเคราะห์ได้โดยใช้สารริเริ่มปฏิกิริยารีดอกซ์ในปฏิกิริยาพอลิเมอไรเซชันแบบสารละลาย ปรับปริมาณสารตั้งต้นให้เหมาะสมในการสังเคราะห์ นำสารที่สังเคราะห์ได้มาศึกษาผลของค่า ความเป็นกรด-เบส อุณหภูมิ และความเข้มขันเริ่มต้นของสีย้อมต่อการลดสีย้อม Congo red และ direct blue 71 ในน้ำเสียสังเคราะห์ และคอมพอสิตของสีย้อมในน้ำเสียจากโรงงานอุตสาหกรรมสิ่งทอ จากผล

การทดลองพบว่า AHAMAA ดูดซับสีย้อม Congo red และ direct blue 71 ในน้ำเสียสังเคราะห์ที่ภาวะ ไม่มีสารควบคุมค่าความเป็นกรด-เบส ดีกว่าน้ำเสียสังเคราะห์ที่มีสารควบคุมความเป็นกรด-เบส และดูด ซับสีย้อม Congo red ดีกว่า direct blue 71 ทุกค่าความเป็นกรด-เบส การดูดซับสีย้อม Congo red เพิ่มขึ้น เมื่อเพิ่มความเข้มขันเริ่มต้นของสีย้อม และอุณหภูมิ การดูดซับสีย้อมของ AHAMAA เป็นแบบ Freundlich isotherm เมื่อความเข้มขันเริ่มต้นของสีย้อมเป็น 100 มิลลิกรัมต่อลูกบาศก์เดซิเมตร AHAMAA ดูดซับ Congo red ได้มากสุด 109 ± 0.5 มิลลิกรัมต่อกรัม และดูดซับ direct blue 71 ได้ มากสุด 62 ± 6.6 มิลลิกรัมต่อกรัม ในน้ำเสียสังเคราะห์ที่มีสีย้อมทั้งสองผสมกันที่ความเข้มขันรวมเป็น 150 มิลลิกรัมต่อลูกบาศก์เดซิเมตร เมื่อใช้ AHAMAA ความเข้มขัน 643 ± 3 มิลลิกรัมต่อลูกบาศก์เดซิเมตร สามารถดูดซับสีย้อมรวมได้ 142±2 มิลลิกรัมต่อกรัม และ AHAMAA ความเข้มขัน 500 มิลลิกรัมต่อลูกบาศก์เดซิเมตร สามารถดูดซับสีย้อมในน้ำเสียจากโรงงานอุตสาหกรรมสิ่งทอที่มีสี ย้อม reactive dye ผสมกับ direct dye จากความขุ่น 405 เป็น 23 NTU

คำสำคัญ: สารก่อการจับกลุ่มชนิดอะลูมิเนียม, โคพอลิเมอร์ของอะคริลาไมด์และอะคริลิกแอซิด, การดูด ซับสีย้อม, การลดความขุ่น, น้ำเสีย

3.2 Photocatalytic Efficiency of TiO₂/Poly[Acrylamide-Co-(Acrylic Acid)] Composite for Textile Dye Degradation

Poly[acrylamide-co-(acrylic acid)], (poly[AAm-co-(AAc)]), and TiO₂/Poly[AAm-co-(AAc)] composite were synthesized by an aqueous solution polymerization method. Poly[AAm-co-(AAc)] and TiO₂/Poly[AAm-co-(AAc)] composite had equilibrium water absorbency of 823±2 and 455±8 times their dry weights, respectively. The efficiency of the composite to absorb methylene blue was determined using UV-visible spectrophotometry. The results showed that 88% of 5 mg L⁻¹ of methylene blue solution was absorbed with an absorption rate of 0.1344 min⁻¹. Influential factors on the photocatalytic degradation, namely type of TiO₂, wavelength and intensity of UV radiation, were investigated. In the presence of UV radiation at 365 nm, TiO₂/Poly[AAm-co-(AAc)] composite can degrade as high as 91% of the dye in 40 min. In contrast, poly[AAm-co-(AAc)] could degrade only 3% of the dye. Degradation of the dye was not observed neither in TiO₂/Poly[AAm-co-(AAc)] composite nor poly[AAm-co-(AAc)] without

exposure to UV radiation when the dye was incorporated into the system. The reused efficiency of TiO₂/Poly[AAm-co-(AAc)] composite understudy was found that the TiO₂/Poly[AAm-co-(AAc)] composite could be reused for only 2 times before it became slurry. This result indicated that TiO₂/Poly[AAm-co-(AAc)] composite not only degraded the methylene blue but also decomposed itself under UV irradiation. This leads to a conclusion that the system does not cause any environmental problems.

Keywords: Composite, Photocatalysts, Photodegradation, Titanium dioxide

ประสิทธิภาพด้านโฟโตแคตทาลิสของคอมพอสิตไทเทเนียมไดออกไซด์/พอลิ(อะคริลาไมด์-*โค*-อะคริลิกแอซิด) สำหรับการแตกสลายของสีย้อม

ได้สังเคราะห์พอลิ(อะคริลาไมด์-โค-กรดอะคริลิก) และคอมพอสิตของพอลิ(อะคริลาไมด์-โค-กรด อะคริลิก) ที่มีไทเทเนียมไดออกไซด์โดยปฏิกิริยาพอลิเมอไรเซชันแบบสารละลาย พบว่า พอลิเมอร์ร่วม และคอมพอสิตของพอลิเมอร์ร่วมที่เตรียมได้มีค่าการดูดซึมน้ำ 823±2 และ 455±8 เท่าของน้ำหนักพอลิ เมอร์แห้ง ตามลำดับ ได้ศึกษาประสิทธิภาพการดูดซึมสีเมทิสีนบลูในสารละลายด้วยเทคนิคยูวีวิสซิ เบิลสเปกโทรโฟโตเมตรีพบว่า คอมพอสิตที่เตรียมได้สามารถดูดซึมสีเมทิสีนบลูที่ความเข้มขัน 5 มิลลิกรัมต่อลิตรได้ร้อยละ 88 โดยมีค่าคงตัวอัตราการดูดซึมสี 0.1344 ต่อนาที ศึกษาการแตกสลายของ โมเลกุลสีเมทิสีนบลูที่ถูกดูดซึมบนคอมพอสิตด้วยการศึกษาอิทธิพลของตัวแปร ได้แก่ ชนิดของอนุภาค ไทเทเนียมไดออกไซด์ ความยาวคลื่นและความเข้มของรังสียูวี พบว่า ไทเทเนียมไดออกไซด์พอลิเมอร์คอมพอสิตมีประสิทธิภาพในการแตกสลายสีเมทิสีนบลูได้มากถึงร้อยละ 91 ใช้เวลา 40 นาที ฉายด้วยรังสียูวีความยาวคลื่น 365 นาโนเมตร ในทางตรงกันข้าม พบการแตกสลายของสีย้อมด้วยพอลิเมอร์ร่วมที่ไม่ มีไทเทเนียมไดออกไซด์เพียงร้อยละ 3 และไม่เกิดการแตกสลายสีย้อมในที่มีดของพอลิเมอร์ร่วมและคอม พอสิต ศึกษาประสิทธิภาพการใช้ซ้ำของพอลิเมอร์คอมพอสิตภายใต้ภาวะที่ฉายด้วยรังสียูวี พบว่า สามารถนำกลับมาใช้ไหม่ได้ 2 ครั้งก่อนที่พอลิเมอร์คอมพอสิตจะกลายเป็นของหนิด ผลการทดลองนี้ แสดงว่า พอลิเมอร์คอมพอสิตไม่เพียงแตกสลายสีเมทิสีนบลู ยังแตกสลายตัวพอลิเมอร์เองภายใต้รังสียูวี งานวิจัยนี้นำไปสู่การสรุปว่า ระบบนี้ไม่ก่อปัญหาสิ่งแวดล้อม

คำหลัก: คอมพอสิต, โฟโตแคตทาลิสต์, การแตกสลายด้วยแสง, ไทเทเนียมไดออกไซด์

3.3 Acrylamide-Based Composite Hydrogels Initiated by Titanium Dioxide Photocatalyst for Dye and Composite Hydrogel Degradations

To synthesize the composite hydrogels, nano-sized titanium hydroxide particles were dispersed in distilled water and exposed to ultraviolet radiation (UV) for a set time while the dispersion was being stirred. When the titanium hydroxide had reacted with water to generate hydroxyl radicals, monomers and crosslinking agent were added and exposed to UV again while stirring the reaction mixture. A composite hydrogel was resulted in at the specified time, acrylamide with its co monomers namely acrylic acid and/or itaconic acid and crosslinking monomer of *N*, *N'*-methylenebisacrylamide were used for the synthesis. The resulting composite hydrogels were tested for water absorption in distilled water and dye solution such as Congo red or other dye solutions. The composite hydrogel and adsorbed dye degradations are to be experimented under UV radiation. This project is still ongoing since it has just started in January 2011.

Keywords: Acrylamide-based composite hydrogel, TiO₂ photocatalyst, Hydrogel degradations, Dye degradation

ไฮโดรเจลคอมพอสิตฐานอะคริลาไมด์ริเริ่มโดยโฟโตแคตทาลิสต์ไทเทเนียมไดออกไซด์สำหรับ การแตกสลายของสีย้อมและไฮโดรเจล

สังเคราะห์ไฮโดรเจลคอมพอสิตเริ่มด้วยการนำอนุภาคไทเทเนียมไดออกไซด์ระดับนาโนเมตรมา
กวนในน้ำ แล้วกวนพร้อมกับฉายรังสีอัลตราไวโอเลตเป็นระยะเวลาหนึ่ง เพื่อให้ไทเทเนียมไดออกไซด์
ทำปฏิกิริยากับน้ำแล้วเกิดอนุมูลไฮดรอกซิลขึ้น เติมมอนอเมอร์และสารเชื่อมขวาง แล้วกวนต่อไปพร้อม
กับฉายรังสีอัลตราไวโอเลต จนกระทั่งเกิดเป็นไฮโดรเจลคอมพอสิตขึ้น มอนอเมอร์ที่ใช้ในการสังเคราะห์
คือ อะคริลาไมด์ ซึ่งมีมอนอเมอร์ร่วมคือ กรดอะคริลิก หรือกรดอิทาโคนิก และสารเชื่อมขวางที่ใช้คือ
เอ็น, เอ็น-เมทิลีนบิสอะคริลาไมด์ นำไฮโดรเจลที่สังเคราะห์ไปวิเคราะห์หาความสามารถในการดูดซึมน้ำ
และสีย้อม Congo red พร้อมกับตรวจสอบเอกลักษณ์ต่าง ๆ ของรูปแบบการดูดซับสี ตรวจสอบการแตก
สลายของไฮโดรเจลคอมพอสิตและแตกสลายของสีย้อมที่ถูกดูดซับบนไฮโดรเจลคอมพอสิตด้วยปฏิกิริยา
เคมีทางแสง โครงการนี้เพิ่งเริ่มวิจัยเมื่อเดือนมกราคม 2554

คำสำคัญ: ไฮโดรเจลคอมพอสิตฐานอะคริลาไมด์, ไทเทเนียมไดออกไซด์โฟโตแคตาลิสต์, การแตกสลาย ของไฮโดรเจล, การแตกสลายของสีย้อม

กลุ่มโครงการวิจัยที่ 4 ไฮโดรเจลกับการใช้งานเฉพาะทาง

4.1 Gel Strength and Swelling of Acrylamide-Protic Acid Superabsorbent Copolymers

The viscoelastic and swelling properties of polyacrylamide-based superabsorbent copolymers were investigated as a function of the ionic comonomer structure. Superabsorbent copolymers were synthesized by free-radical crosslinking copolymerization of acrylamide and one of the monoprotic acids (acrylic acid and crotonic acid) or the diprotic acids (maleic acid and itaconic acid) as the investigated ionic comonomer. The reaction composition of all components, i.e. monomer, comonomer, initiator, co-initiator and crosslinker, was fixed to be the same for the synthesis of all four superabsorbent copolymer systems. Viscoelastic measurements were performed in all systems where the particles were closely packed. The network structures of all systems were evaluated via viscoelastic and swelling measurements. The results indicated that superabsorbent polymers with high water absorbency were accompanied by low gel strength and the calculated high value of molecular weight between crosslinks (\overline{M}_c) and low value of effective crosslinking density (V_e). Diprotic acid-containing superabsorbent polymers showed higher water absorbency over monoprotic acid-containing and nonionic ones. The differences in \overline{M}_c and V_e values of each system were explained with respect to the differences in the monomer reactivity ratio and hydrophilicity of the comonomers.

Keywords: Superabsorbent polymers, Swelling, Viscoelastic, Molecular weight between crosslinks, Crosslinking density

ความแข็งแรงของเจลและการบวมตัวของโคพอลิเมอร์ซูเปอร์แอบซอร์เบนต์ฐานอะครลาไมด์-กรดโปรติก

การวิจัยนี้เพื่อศึกษาโครงสร้างของไอออนิกโคพอลิเมอร์ที่มีต่อสมบัติความหยุ่นหนืดและสมบัติการ บวมตัวของโคพอลิเมอร์ซูเปอร์แอบซอร์เบนต์อะครลาไมด์-กรดโปรติก ได้สังเคราะห์โคพอลิเมอร์ซูเปอร์ แอบซอร์เบนต์โดยวิธีการเกิดปฏิกิริยาโคพอลิเมอไรเซชันแบบอนุมูลอิสระของมอนอเมอร์อะคริลาไมด์ กับกรดมอนอเมอร์โปรตอนเดียว (อะคริลิกแอซิดและโครโทนิกแอซิด) หรือกรดมอนอเมอร์สองโปรตอน (มาเลอิกแอซิดและอิทาโคนิกแอซิด) ซึ่งทำหน้าที่เป็นมอนอเมอร์ร่วมแบบมีประจุ กำหนดองค์ประกอบ ของสารต่าง ๆ ในปฏิกิริยา เช่น มอนอเมอร์ มอนอเมอร์ร่วม อินิชิเอเตอร์ อินิชิเอเตอร์ร่วม และสารเชื่อม

ขวาง ให้เป็นต่าคงตัวและมีค่าเท่ากันสำหรับการสังเคราะห์โคพอลิเมอร์ซูเปอร์แอบซอร์เบนต์ 4 ชนิดนี้ วัดสมบัติความหยุ่นหนืดของโคพอลิเมอร์ซูเปอร์แอบซอร์เบนต์ทั้ง 4 ชนิด เมื่อกำหนดให้อนุภาคของโค พอลิเมอร์เหล่านี้มีลักษณะเกาะกันแน่นเป็นก้อนปิด (closely packed) ประเมินโครงสร้างของเครือข่าย ของโคพอลิเมอร์ทั้ง 4 ชนิดจากสมบัติความหยุ่นหนืดและการบวมตัว ผลที่ได้แสดงว่า โคพอลิเมอร์ ซูเปอร์แอบซอร์เบนต์มีค่าการดูดซึมน้ำมากเมื่อพอลิเมอร์เจลมีความแข็งแรงต่ำ มีค่าน้ำหนักโมเลกุล เฉลี่ยระหว่างโซ่เชื่อมขวางสูง และมีค่าความหนาแน่นของการเชื่อมขวางต่ำ โคพอลิเมอร์ซูเปอร์แอบซอร์ เบนต์ชนิดสองโปรตอนมีค่าการดูดซึมน้ำมากกว่าโคพอลิเมอร์ซูเปอร์แอบซอร์เบนต์ชนิดหนึ่งโปรตอน และพอลิเมอร์ซูเปอร์แอบซอร์เบนต์ชนิดไม่มีประจุ ความแตกต่างระหว่างค่าน้ำหนักโมเลกุลเฉลี่ย ระหว่างโซ่เชื่อมขวางและค่าความหนาแน่นของการเชื่อมขวางของโคพอลิเมอร์ซูเปอร์แอบซอร์เบนต์มี ความสัมพันธ์กับค่าความไวของมอนอเมอร์และความชอบน้ำของมอนอเมอร์ร่วม

คำสำคัญ พอลิเมอร์ซูเปอร์แอบซอร์เบนต์, การบวมตัว, สมบัติความหยุ่นหนืด, น้ำหนักโมเลกุลระหว่าง โซ่เชื่อมขวาง, ค่าความหนาแน่นของการเชื่อมขวาง

4.2 Acrylamide-Itaconic Acid Superabsorbent Polymers and Superabsorbent Polymer/ Mica Nanocomposites

Superabsorbent polymer and its nanocomposite of acrylamide (AM)/itaconic acid (IA) were synthesized by solution polymerization in an aqueous solution of AM with IA comonomer and mica used as an inorganic additive. This reaction was initiated by a redox initiator couple of ammonium persulfate and N, N, N', N'-tetramethylethylenediamine in the presence of N, N'-methylenebisacrylamide crosslinker. The influences of the concentrations of IA, the crosslinker and mica at several reaction temperatures on water absorption of the superabsorbent polymer systems were examined. The superabsorbent copolymers and their nanocomposites were tested with a load of 0.28 or 0.70 psi in both distilled water and artificial urine. Transmission electron micrographs and X-ray diffraction confirmed that the polymer chains were successfully intercalated into the silicate layers in the mica. The water absorbency and the artificial urine absorbency of the composite with an AM-to-IA mole ratio of 95:5, 0.2% mol N-MBA, and 5% w/w mica were 748 \pm 5 and 76 \pm 2 g g $^{-1}$, respectively, whilst the neat copolymer achieved only 640 \pm 7 and 72 \pm 2g g $^{-1}$ in water and artificial urine, respectively. The viscoelastic behavior

suggested that the swollen gel of the nanocomposites exhibited mechanical stability and elasticity.

Keywords: Superabsorbent nanocomposites, Mica, Water absorbency, Intercalation

ชูเปอร์แอบซอร์แบนต์พอลิเมอร์ของอะคริลาไมด์/อิทาโคนิกแอซิดและไมกานาโนคอมพอสิต ชูเปอร์แอบซอร์แบนต์พอลิเมอร์

ได้สังเคราะห์ชูเปอร์แอบซอร์แบนต์พอลิเมอร์และคอมพอสิตของชูเปอร์แอบซอร์แบนต์พอลิเมอร์ของอะครลาไมด์และอิทาโคนิกแอซิด โดยการเกิดพอลิเมอไรเซชันในสารละลายของอะคริลาไมด์และอิทาโคนิกแอซิดโคมอนอเมอร์กับผงไมกาซึ่งเป็นสารเติมแต่งอนินทรีย์ ปฏิกิริยาได้เกิดขึ้นโดยคู่รีดอกซ์อินิ ซิเอเตอร์ของแอมโมเนียมเพอร์ซัลเฟตและเอ็น,เอ็น,เอ็น',เอ็น',เคทระเมทิลเอทิลีนใดแอมีนและมีเอ็น,เอ็น'-เมทิลีนบิสอะคริลาไมด์เป็นสารเชื่อมขวาง อิทธิพลของความเข้มข้นของอิทาโคนิกแอซิด สารเชื่อมขวาง และไมกาที่อุณหภูมิต่าง ๆ ของการเกิดปฏิกิริยามีผลต่อการดูดซึมน้ำของซูเปอร์แอบซอร์แบนต์พอลิเมอร์ทั้งสอง ภายใต้แรงกดทับ 0.28 or 0.70 ปอนด์ต่อตารางนิ้ว ในน้ำกลั่นและในปัสสาวะเทียม ภาพจากกล้อง จุลทรรศน์แบบส่องผ่านและเส้นกราฟของการเลี้ยวเบนด้วยรังสีเอกซ์บ่งบอกว่า โช่พอลิเมอร์ได้ สอดแทรกเข้าไปในชั้นซิลิเกตของไมกา การดูดซึมน้ำและน้ำปัสสาวะเทียมของพอลิเมอร์คอมพอสิตที่มี สัดส่วนโมลของอะคริลาไมด์ต่ออิทาโคนิกแอซิด 95:5, 0.2% โดยโมลของสารเชื่อมขวาง และปริมาณ ใมการ้อยละ 5 โดยน้ำหนัก มีค่า 748±5 และ 76±2 กรัมต่อกรัมของสารแห้ง ตามลำดับ พฤติกรรมด้าน ความหยุ่นหนืดบ่งว่า เจลที่บวมตัวเต็มที่ของคอมพอสิตซูเปอร์แอบซอร์แบนต์พอลิเมอร์มีความเสถียร เชิงกลและมีความอืดหยุ่น

คำสำคัญ: นาโนคอมพอสิตซูเปอร์แอบซอร์เบนต์, ไมกา, การดูดซึมน้ำ, การสอดแทรก

4.3 Synthesis of Acrylamide-*co*-(Itaconic Acid) Superabsorbent Polymers and Associated Silica Superabsorbent Polymer Composites

Superabsorbent polymers (SAPs) were synthesized from acrylamide (AM) and itaconic acid (IA) *via* a crosslinking polymerization. SAP composites (SAPCs) were formed by the incorporation of silica with three particle sizes into the polymerization to increase the gel strength of SAPs. Effects of AM: IA molar ratios, silica types and concentrations on water

absorbency, absorbency rate and absorbency under loadings (AUL) of the composites were investigated. The highest water absorbency of the SAP is $233 \pm 8 \text{ g g}^{-1}$ at an AM: IA molar ratio of 97:3 with absorbency rate of $149 \pm 2 \text{ g g}^{-1}$ within 15 min. The highest AUL of the SAPC with 0.5-2.0% w w⁻¹ silica is 13 g g⁻¹ by 1.93 x 10^3 Pa load. A pseudo-second-order kinetics for water absorbency was found in both SAPs and *in situ* SAPCs. *In situ* SAPCs and the mechanically mixed SAPCs in vertical and horizontal direction yielded similar water absorbency values. This research suggested that SAPCs can be economically prepared by mixing SAP with silica powders in a mixing machine to obtain a high water absorption capacity from SAPC.

Keywords: Acrylamide-co-(Itaconic Acid) Superabsorbent Polymers, silica, composite, mechanical mixing, vertical mixing, horizontal mixing

การสังเคราะห์พอลิเมอร์ซูเปอร์แอบซอร์เบนต์ของอะคราไมด์-*โค*-อิทาโคนิกแอซิดกับซิลิกาคอม พอสิตของพอลิเมอร์ซูเปอร์แอบซอร์เบนต์อะคราไมด์-โค-อิทาโคนิกแอซิด

ได้สังเคราะห์พอลิเมอร์ซูเปอร์แอบซอร์เบนต์ (SAP) ของอะคราไมด์-โค-อิทาโคนิกแอซิด จากอะคริ ลาไมด์ (AM) และอิทาโคนิกแอซิด (IA) โดยการเกิดปฏิกิริยาแบบเชื่อมขวาง คอมพอสิตของ SAP (SAPC) เกิดจากการผสมชิลิกาที่มีขนาดอนุภาคระดับนาโนเมตร 3 ขนาด เข้าไปขณะที่เกิดปฏิกิริยาพอ ลิเมอไรเซชันเพื่อเพิ่มความแข็งแรงต่อเจลพอลิเมอร์ ผลของสัดส่วนโดยโมลของ AM: IA, ชนิดและปริ มารของซิลิกาต่อค่าการดูดซึมน้ำ อัตราการดูดซึมน้ำ และการดูดซึมน้ำภายใต้แรงกดทับ (AUL) ของ SAPC ค่าการดูดซึมน้ำมากสุดของ SAP คือ 233 ± 8 กรัมต่อกรัมของสารแห้ง ที่สัดส่วนโดยโมลของ AM:IA 97:3 และมีอัตรการดูดซึมที่ 149 ± 2 กรัมต่อกรัมของสารแห้ง ภายใน 15 นาที AUL ของ SAPC ที่มีปริมาณซิลิการ้อยละ 0.5-2 มีค่า 13 กรัมต่อกรัมของสารแห้ง โดยแรงกดทับ 1.93 x 10³ พัสคาล จลนศาสตร์ของการดูดซึมน้ำของ SAP และ SAPC ที่เกิดพร้อมกันกับพอลิเมอร์มีลักษณะเป็น pseudo-second-order เหมือนกัน การดูดซึมน้ำของ SAPCs ที่เกิดพร้อมกันกับพอลิเมอร์มีลักษณะเป็น pseudo-second-order เหมือนกัน การดูดซึมน้ำของ SAPCs ที่เกิดพร้อมกันกับพอลิเมอร์มีลักษณะเป็น pseudo-second-order เหมือนกัน การดูดซึมน้ำของ SAPCs ที่เกิดข้ามารถดอติมน้ำของ SAPCs ที่ประหยัด โดยการผสม SAPS กับผงซิลิกาในเครื่องผสม สามารถผลิต SAPCs ที่มีค่าการดูดซึมน้ำมากได้

คำสำคัญ: พอลิเมอร์ซูเปอร์แอบซอร์เบนต์อะคริลาไมดี-โค-อิทาโคนิกแอซิด, ซิลิกา, คอมพอสิต, การผสม เชิงกล, การผสมในแนวตั้ง, การผสมในแนวนอน

4.4 Acrylamide/2-acrylamido-2-methylpropane Sulfonic Acid and Associated Sodium Salt Superabsorbent Copolymers with Mica Nanocomposites as Fire Retardants

Superabsorbent polymers (SAPs) of poly[acrylamide-co-(2-acrylamido-2-methylpropane sulfonic acid)], poly(AM-co-AMPS-H⁺), and its sodium salt, poly(AM-co-AMPS-Na⁺), were synthesized by free-radical crosslinking polymerization. A maximum water absorbency in deionized water of 1212 g g⁻¹ was achieved for poly(AM-co-AMPS-Na⁺) at an 85% mol of AMPS-Na $^{+}$. The inclusion of mica at 5 – 30% (w w $^{-1}$) into the preparation of poly(AM-co-AMPS-Na⁺) SAP leads to an intercalated structure, as detected by XRD and TEM analyses. Poly(AM-co-AMPS-Na⁺)/30% (w w⁻¹) mica SAP nanocomposite showed a tap-water absorbency of 593 g g⁻¹ with a better thermal stability, compared to the pure SAP. Cone calorimetric analyses revealed that the wood specimens coated with the prepared poly(AM-co-AMPS-Na⁺) SAP or its 30% (w w⁻¹) mica nanocomposite provided excellent protection in delaying the ignition time after exposure to an open flame when compared to that observed with the uncoated specimen (186, 136 and 13 s, respectively). The maximum reduction in the peak heat release rate, the greatest extension of time at peak heat release rate and the minimum in total heat release rate were observed with the mica SAP nanocomposite-coated surface. Intercalating structure of mica in the SAP nanocomposites provided a better shielding effect against external heat sources, and the capability of poly(AM-co-AMPS-Na⁺) SAP in holding a large amount of water.

Keywords: Superabsorbent; Acrylamide; 2-acrylamido-2-methylpropane sulfonic acid sodium salt; Mica; Nanocomposites; Cone calorimetry.

สารหน่วงไฟของอะคริลาไมด์/2-อะคริลามิโด-2-เมทิลโพรเพนซัลโฟนิกแอซิดและเกลือโซเดียม ของโคพอลิเมอร์ซูเปอร์แอบซอร์เบนต์กับไมกานาโนคอมพอสิต

ได้สังเคราะห์ซูเปอร์แอบซอร์เบนต์พอลิเมอร์ (SAP) ของพอลิ(อะคริลาไมด์-โค-2-อะคริลามิโด-2-เมทิลโพรเพนซัลโฟนิกแอซิด) หรือ poly(AM-co-AMPS-H[†]) และเกลือโซเดียมของพอลิเมอร์ poly(AM-co-AMPS-Na[†]) โดยวิธีการเกิดพอลิเมอร์แบบเชื่อมขวางด้วยอนุมูลอิสระ ค่าการดูดซึมน้ำมากที่สุดในน้ำ กลั่น คือ 1212 กรัมต่อกรัม ของสารแห้ง ที่สังเคราะห์ได้จาก poly(AM-co-AMPS-Na[†]) ที่ร้อยละ 85 โดย โมลของ 2-อะคริลามิโด-2-เมทิลโพรเพนโซเดียมซัลโฟเนต (AMPS-Na[†]) การใส่ผงไมการ้อยละ 5 -30 โดยน้ำหนักเข้าไปใน poly(AM-co-AMPS-Na[†]) SAP ทำให้เกิดโคงสร้างแบบสอดแทรกของโซ่พอลิเมอร์ เข้าไปในไมกา ดังที่ตรวจสอบได้ด้วยภาพจากกล้องจุลทรรศน์แบบสองผ่านและภาพจากการเลี้ยวเบน ของรังสีเอกซ์ นาโนคอมพอสิตของ poly(AM-co-AMPS-Na[†]) ที่มีผงไมการ้อยละ 30 สามารถดูดซึม น้ำประปาใด้ 593 กรัมต่อกรัมของสารแห้ง พร้อมมีสภาพต้านความร้อนที่อุณหภูมิสูงได้เมื่อเปรียบเทียบ กับ poly(AM-co-AMPS-Na[†]) SAP การวิเคราะห์เชิงความร้อนด้วยโคนแคลอริเมทรีเปิดเผยว่า ชิ้นไม้ที่ เคลือบด้วย poly(AM-co-AMPS-Na[†])/30 ไมกานาโนคอมพอสิต สามารถป้องกันชิ้นไม้โดยหน่วงการติด ไฟภายหลังได้รับการสัมผัสโดยตรงกับเปลวไฟเมื่อเปรียบเทียบกับไม้ที่เคลือบเฉพาะ poly(AM-co-AMPS-Na[†]) และไม้ที่ไม่ได้เคลือบเป็นเวลา 186, 136 และ 13 วินาที ตามลำดับ พบความสามารถใน การลดอัตราการปล่อยความร้อน ณ จุดยอดของพีกมากที่สุดใน poly(AM-co-AMPS-Na[‡])/30 ไมกานาโนคอมพอสิต การหน่วงเวลาไหม้ไฟมากที่สุด ณ จุดยอดของพีกที่ปลดปล่อยความร้อน และปริมาณ ความร้อนน้อยที่สุดที่ปล่อยออกมาที่ผิวของไม้ที่กำลังไหม้ไฟที่มีการเคลือบด้วยนาโนคอมพอสิต โครงสร้างการสอดแทรกของโซ่พอลิเมอร์ของ poly(AM-co-AMPS-Na[‡]) เข้าไปในไมกา เป็นฉนวน ป้องกันความร้อนจากภายนอกเข้าไปใหม้เนื้อไม้ที่เคลือบสารนี้ พร้อมกับน้ำปริมาณมากที่สารนี้กักเก็บ ไว้จะถูกปล่อยออกมาเพื่อลดอุณหภูมิของชินไม้ที่ใหม่ไฟ

คำสำคัญ: ซูเปอร์แอบซอร์เบนต์, อะคริลาไมด์, 2-อะคริลามิโด-2-เมทิลโพรเพนโชเดียมซัลโฟเนต, ไมกา, นาโนคอมพอสิต. โคนแคลอริเมทรี

4.5 Effect of fire retardant on flammability of acrylamide and 2-acrylamido-2-methylpropane sodium sulfonate copolymer nanocomposites

Poly[acrylamide-co-(2-acrylamido-2-methylpropane sodium sulfonate)] superabsor- bents and superabsorbent composites (SAPCs) with zinc borate and/or melamine as fire retardants were synthesized. Water absorbencies decreased inversely to added amount of fire retardant. Thermal stability of SAPC/zinc borate increases with increasing zinc borate. Incorporating melamine improved thermal stability of the SAPC until 300°C. Flammability analysis demonstrated that wood surface coated with SAP or SAPC emulsions extended time to ignition of the wood. Peak heat release rate and total heat release are smallest in specimens coated with SAPC/30%melamine. Wood coated with SAPC incorporating 20% zinc borate/10% melamine mixture gave the longest time to ignition at 4½ min.

Keywords: Superabsorbent, Zinc borate, Melamine, Fire retardant, Cone calorimetry.

ผลของสารหน่วงการติดไฟต่อการไหม้ไฟของนาโนคอมพอสิตโคพอลิเมอร์ของอะคริลาไมด์ และ2-อะคริลามิโด-2-เมทิลโพนเพนโซเดียมซัลโฟเนต

ได้สังเคราะห์สารหน่วงไฟที่ประกอบด้วยซูเปอร์แอบซอร์เบนต์พอลิเมอร์ของพอลิ(อะคริลาไมด์-โค-2-อะคริลามิโด-2-เมทิลโพรเพนโซเดียมซัลโฟเนต) และคอมพอสิตของซูเปอร์แอบซอร์เบนต์พอลิเมอร์ หน่วงไฟของพอลิ(อะคริลาไมด์-โค-2-อะคริลามิโด-2-เมทิลโพรเพนโซเดียมซัลโฟเนต) ซึ่งผสมกับชิงก์ บอร์เรต และ/หรือเมลามีน ค่าการดูดซึมน้ำลดลงเป็นสัดส่วนผกผันกลับกับปริมาณของสารหน่วงไฟอนิ นทรีย์ ความเสถียรเชิงความร้อนของ SAPC/ซิงก์บอร์เรตเพิ่มขึ้นตามปริมาณของชิงก์บอเรตที่เพิ่มขึ้น การเติมเมลามีนเข้าไปในนาโนคอมพอสิตของซูเปอร์แอบซอร์เบนต์พอลิเมอร์ปรับปรุงความเสภียรเชิง ความร้อนได้ถึงอุณหภูมิสูงสุดที่ 300 องศาเซลเซียส การวิเคราะห์การใหม้ไฟของชิ้นไม้ พบว่า ชิ้นไม้ที่ เคลือบด้วยอิมัลชันของ SAP หรือ SAPC สามารถยืดเวลาติดไฟของไม้ได้ อัตราการปล่อยความร้อน ณ จุดพีก และปริมาณความร้อนที่ปล่อยมากที่สุด มีค่าน้อยที่สุดในชิ้นไม้ที่เคลือบด้วย SAPC/30% เมลามีน ชิ้นไม้ที่เคลือบด้วย SAPC/20% ซิงก์บอเรต/10%เมลามีน สามารถหน่วงการติดไฟได้นานที่สุดถึง 4 นาที่ 30 วินาที

คำสำคัญ ซูเปอร์แอบซอร์เบนต์, ซิงก์บอเรต, เมลามีน, สารหน่วงไฟ, โคนแคลอริเมทรี

4.6 Swelling Properties and Strength of Poly[Acrylamide-co-(Itaconic Acid)] Gel and Clay-Modified Poly[Acrylamide-co-(Itaconic Acid)] Gel

Three types of clay (montmorillonite, bentonite and mica) and chemically modified clays were investigated for creating better superabsorbent polymer nanocomposites (SAPCs) with stronger gel strength and higher water swelling at under loading conditions. The selected types of clay were treated by two methods, one with inorganic acids (HCl, H₂SO₄) and another with organic compound, such as cetyltrimethylammonium bromide (C₁₉H₄₂BrN) and anionic surfactant (hexadecanoic acid) were used. Ionic exchange capacity and its interaction through acid-base were consideration. The SAPCs were synthesized through free radical crosslinking polymerization of acrylamide and itaconic acid in the presence of clays and modified clays.

Reaction conditions were controlled to give the optimized water absorption and high gel strength. This project has just started in January 2011.

Keyword: Superabsorbent, Clays, Modified Clays, Gel strength, AUL, Water absorption

สมบัติการบวมตัวและความแข็งแรงของเจลพอลิ(อะคริลาไมด์-โค-อิทาโคนิกแอซิด) และเจล ของพอลิ(อะคริลาไมด์-โค-อิทาโคนิกแอซิด) ที่ผสมแร่ดินและแร่ดินดัดแปร

ศึกษาชนิดของแร่ดิน (มอนต์มอริลลอในต์ เบนโทในต์ และไมกา) และการดัดแปรแร่ดินด้วยวิธีทาง เคมี เพื่อทำให้ได้วัสดุเชิงประกอบพอลิเมอร์ดูดซึมน้ำมาก (superabsorbent polymer composites, SAPCs) ที่มีความแข็งแรงภายใต้ภาวะกดทับและยังคงมีความสามารถในการบวมตัวมาก ใช้การดัดแปรแร่ ดินด้วยวิธีทางเคมี 2 วิธี คือ ทำปฏิกิริยาการกระตุ้นด้วยกรด (กรดเกลือ และกรดซัลฟิวริก) และทำปฏิกิริยากับสารอินทรีย์ เช่น ซีทิลไทรเมทิลแอมโมเนียมโบรไมด์ (C19H2BrN) และแอนไอออนิกเซอร์แฟก เตนต์ (เฮกซะเดกคาโนอิกแอซิด) การแลกเปลี่ยนประสิทธิภาพของและปฏิสัมพันธ์ระหว่างกรดและเบสจะ นำมาพิจารณา ได้สังเคราะห์ SAPCs ผ่านกระบวนการเกิดพอลิเมอร์แบบอนุมูลอิสระในสารละลายของพอ ลิเมอร์ร่วมระหว่างอะคริลาไมด์กับอิทาโคนิกแอซิดซึ่งมีแร่ดินกระจายตัวอยู่ ควบคุมภาวะการเกิดปฏิกิริยา เพื่อหาค่าการดูดซึมน้ำมากที่สุดและมีความแข็งแรงของเจลที่ดี โครงการนี้เพิ่งเริ่มวิจัยในเดือนมกราคม 2554

คำสำคัญ ซูเปอร์แอบซอร์เบนต์, แร่ดิน, แร่ดินดัดแปร, ความแข็งแรงของเจล, ค่าการดูดซึมน้ำภายใต้แรง กดทับ, ค่าการดูดซึมน้ำ

กลุ่มโครงการวิจัยที่ 5 ไมโครเอนแคปซูเลชันและการควบคุมการปล่อยของวัสดุอนินทรีย์/อินทรีย์

5.1 Microencapsulation of menthol via glass membrane emulsification and controlled release

This research studied the preparation of microcapsules of menthol with the Shirasu porous glass (SPG) membrane emulsification technique combined with a high-speed disperser. The oilin water emulsion from the SPG membrane was prepared by controlling operation pressures, the amounts of surfactant and stabilizer, and the amount of menthol loading. The average droplet size (\overline{d}) and coefficient variation (CV) of the emulsion droplets were systemically investigated. The emulsions of menthol so prepared were mixed with the chitosan solution prepared by the high-speed disperser. Tripolyphosphate (TPP) crosslinker solution was gradually dropped in the emulsion mixture. The effects of crosslinking time and pH of microcapsules on the properties of the microcapsules were investigated. The mechanism of menthol release of microcapsules was studied. The flow behavior of microcapsules formulated in a leave-on hair conditioner was also investigated. It was found that the emulsions of menthol were successfully prepared via the SPG membrane pore sizes of 5.2 µm. The droplets having the \overline{d} , of 19.6 \pm 2.3 µm and the coefficient variation (CV) of 11.5% were achieved. When the menthol loading in the dispersed phase increased from 5 to 10%wt, the size of emulsion droplets decreased but the size distribution was broader. The optimal condition of emulsion prepared with the high-speed disperser was 14000 rpm at 90 s mixing in 1.5 %w v $^{-1}$ of chitosan solution. Chitosan layer of microcapsule shell was crosslinked via ionic bonding between the positive charge of chitosan and the negative charge of TPP. The average size of microcapsules was 27.6±7.2 µm with the CV of 26.3 %. The pH of emulsion of the microcapsules was in the range of 5-7 which is good for uses in hair applications. The mechanism of menthol release was a diffusion control which depended on the amount of chitosan-to-tripolyphosphate ratio (by mole) and crosslinking time. The microcapsules formulated in a leave-on hair conditioner were found to exhibit the pseudoplastic/thixotropic flow behavior. The conditioner was stability and applicable at temperatures not higher than 40 °C. Its coating on human hair rendered soft hair and easy hair combing.

Keywords: Microencapsulation, Menthol, Glass membrane emulsification, SPG, Controlled release

ไมโครแอนแคปซูเลชันของเมนทอลผ่านกลาสเมมเบรนอิมัลซิฟิเคชันและการปล่อยแบบควบคุม

งานวิจัยนี้เป็นการศึกษาการเตรียมไมโครแคปซูลของเมนทอลด้วยเทคนิคชิราสุพอรัสกลาสเมม เบรน (เอสพีจี) อิมัลซิฟิเคชันร่วมกับเครื่องกวนสารละลายความเร็วรอบสูง เตรียมอิมัลชันของน้ำมันใน น้ำจากเอสพีจีเมมเบรน ปรับความดันที่ใช้ เปลี่ยนปริมาณของสารลดแรงตึงผิว สารเพิ่มเสถียรภาพ และ ปริมาณเมนทอล วัดขนาดและการกระจายของหยดน้ำมันในน้ำที่เตรียมได้ นำอิมัลชั้นของเมนทอลที่ เตรียมได้จากเอสพีจีเมมเบรนผสมกับอิมัลซันที่มีใคโทซานซึ่งเตรียมด้วยการกวนด้วยเครื่องกวน สารละลาย ค่อย ๆ หยดสารละลายเชื่อมขวางไทรพอลิฟอสเฟต ศึกษาผลของเวลาเชื่อมขวาง และค่า ความเป็นกรด-เบสต่อสมบัติของอิมัลชันที่เตรียมได้ ศึกษากลไกการปล่อยเมนทอลจากไมโครแคปซูล และสมบัติการใหลของครีมบำรุงเส้นผมชนิดที่ไม่ต้องล้างออกที่เตรียมด้วยไมโครแคปซูล พบว่า สามารถเตรียมหยดของน้ำมันในน้ำด้วยเอสพีจีเมมเบรนที่มีขนาดรูพรุน 5.2 ไมโครเมตร หยดน้ำมันที่ ได้มีขนาดเฉลี่ย 19.6±2.3 ไมโครเมตร และมีค่าสัมประสิทธิ์การแปรปรวนประมาณร้อยละ 11.5 เมื่อ ปริมาณเมนทอลเพิ่มขึ้นจากร้อยละ 5 เป็น 10 โดยน้ำหนัก หยดน้ำมันมีขนาดเล็กลง แต่มีการกระจายตัว ของขนาดกว้างขึ้น ภาวะที่เหมาะสมสำหรับการเตรียมหยดน้ำมันในน้ำด้วยเครื่องกวนสารละลายความ เร็วรอบสูง คือ ความเร็วการกวน 14000 รอบต่อนาที เวลา 90 วินาที และความเข้มข้นของสารละลายไค โทซานร้อยละ 1.5 โดยน้ำหนักต่อปริมาตร เปลือกของแคปซูลไคโทซานเกิดการเชื่อมขวางด้วยพันธะไอ ออนิกระหว่างประจุบวกของไคโทซานกับประจุลบของไทรพอลิฟอสเฟต เกิดเป็นไมโครแคปซูลที่มีขนาด เฉลี่ย 27.6±7.2 ไมโครเมตร และมีค่าสัมประสิทธิ์การแปรปรวนร้อยละ 26.3 ความเป็นกรด-เบสของ ระบบอิมัลชั้นที่จะนำไมโครแคปซูลไปใช้งานด้านเส้นผมควรอยู่ในช่วง 5 ถึง 7 กลไกการปล่อยเมนทอล จากไมโครแคปซูลเป็นการควบคุมแบบการแพร่ ซึ่งขึ้นอยู่กับปริมาณไทรพอลิฟอสเฟต สัดส่วนโดยโม ลของไคโทซานต่อไทรพอลิฟอสเฟต และเวลาการเชื่อมขวาง เมื่อใช้ไมโครแคปซูลเตรียมเป็นครีมบำรุง เส้นผมชนิดที่ไม่ต้องล้างออก ครีมที่ได้มีพฤติกรรมการไหลแบบซูโดพลาสติก/ทิกโซทรอปี และครีมบำรุง ผมมีเสถียรภาพที่ดี ใช้งานได้ดีที่อุณหภูมิไม่สูงกว่า 40 องศาเซลเซียส และเคลือบติดบนเส้นผมมนุษย์ ได้ ทำให้เส้นผมนุ่มลื่นและหวีง่ายขึ้น

คำสำคัญ: ไมโครเอ็นแคปซูเลชัน, เมนทอล, กลาสเมมเบรนอิมัลชิฟิเคชัน, เอสพีจี, การปล่อยแบบ ควบคุม

5.2 Synthesis of Microcapsules Containing Eucalyptus Oil via Shirasu Porous Glass Membrane Emulsification

The emulsion of eucalyptus oil was encapsulated by sodium alginate via Shirasu Porous Glass Membrane which possesses uniform pore size. The eucalyptus oil, liquid paraffin and petroleum ether were used to compose the dispersed phase while sodium dodecylsulfate surfactant and poly(vinyl alcohol) stabilizer were used as ingredients in the continuous phase to realize an oil-in-water emulsion. Calcium carbonate was used a crosslinking agent. The reaction parameters of importance namely the concentrations of encapsulating sodium alginate, and the crosslinking agent and the crosslinking time on physical and morphological properties, microcapsule size and size distribution were investigated. The extent of encapsulation and controlled release of eucalyptus oil were experimented. This project has just started in early January 2011.

Keywords: Eucalyptus oil, Sodium alginate, Shirasu Porous Glass Membrane, Microcapsules, Encapsulation, Controlled release

การสังเคราะห์ไมโครแคปซูลบรรจุน้ำมันยูคาลิปตัสโดยอิมัลซิฟิเคชันผ่านชิราซุพอรัสกลาสเมม เบรน

เดรียมอิมัลชันของน้ำมันยูคาลิปตัสที่ถูกห่อหุ้มด้วยโซเดียมแอลจิเนต ผ่านชิราสุพอรัสกลาสเมม เบรน (Shirasu Porous Glass Membrane) ที่มีขนาดรูพรุนสม่ำเสมอ ใช้น้ำมันยูคาลิปตัส พาราฟิน เหลวและปิโตรเลียมอีเทอร์เป็นวัฏภาคกระจาย ใช้โซเดียมแอลจิเนต สารลดแรงตึงผิวโซเดียมโดเดก ซิลซัลเฟต และสารเพิ่มความเสถียรแก่อิมัลชันพอลิไวนิลแอลกอฮอล์เป็นวัฏภาคต่อเนื่อง ใช้ระบบ อิมัลชันแบบน้ำมันในน้ำ สารเชื่อมขวางเป็นแคลเซียมคาร์บอเนต ศึกษาผลของตัวแปรต่าง ๆ ได้แก่ ความเข้มขันของสารห่อหุ้มโซเดียมแอลจิเนต ความเข้มขันของสารเชื่อมขวาง เวลาที่ใช้ในการทำ ปฏิกิริยาเชื่อมขวาง ต่อสมบัติทางกายภาพ วัดขนาดและการกระจายตัวของไมโครแคปซูล ตรวจสอบ สัณฐานวิทยาของไมโครแคปซูล ศึกษาปริมาณที่กักเก็บได้และการปล่อยน้ำมันยูคาลิปตัสจากไมโคร แคปซูล ได้ไมโครแคปซูลของน้ำมันยูคาลิปตัสที่มีขนาดอนุภาคสม่ำเสมอ มีการกระจายตัวของขนาด อนุภาคที่แคบ และสามารถควบคุมการปล่อยน้ำมันยูคาลิปตัสในภาวะการใช้งานได้ โครงการนี้ได้เริ่ม วิจัยเมื่อตันเดือนมกราคม 2554

คำสำคัญ: น้ำมันยูคาลิปตัส, โซเดียมแอลจิเนต, ชิราสุพอรัสกลาสเมมเบรน, ไมโครแคปซูล, การห่อหุ้ม, การปล่อยแบบควบคุม

5.3 Synthesis and Characterization of Controlled Release NPK Compound Fertilizer Hydrogel

This research studied the synthesis of controlled-release NPK compound fertilizer hydrogels. The controlled-release fertilizer hydrogels were prepared by dipping the fertilizer granules in poly(vinyl alcohol) (PVA) solution and then in chitosan (CS) solution. The PVA- and CS-coated fertilizer granules were crosslinked via vapor deposition of glutaraldehyde (GA) solution in a 2.9-L closed chamber. Water dissolution times of the un-coated fertilizer granules and the coated fertilizer granules were investigated. The fertilizer hydrogel were synthesized by grafting the crosslinked-CS layer of coated fertilizer with acrylamide (AM) and acrylic acid (AA) via inverse suspension polymerization. The existences of functional groups of the crosslinked-CS and the grafted fertilizer hydrogel were confirmed by FTIR spectroscopy. The morphologies of the un-coated and coated granules were viewed by optical microscopy. The surface morphology of hydrogel layer after swelling was also investigated by scanning electron microscopy. The effect of reactants on water absorbency of compound fertilizer hydrogel was observed. Release behaviors of the compound fertilizer hydrogel granules were investigated. It was found that water dissolution times of the grafted fertilizer increased with increasing the frequency of coating. To synthesize the compound fertilizer hydrogel, the optimal ratio of AM-to-AA was 3:97% mol and the optimal contents of N,N,N',N'-tetramethylethylenediamine (N,N,N',N'-TEMED), ammonium persulfate (APS) and N,N'-methylenebisacrylamide (N-MBA) was 0.13, 0.13 and 0.01% by mol of monomers, respectively. Water absorbency of the compound fertilizer hydrogel was 233±5 g/g in distilled water at room temperature within 24 h of immersion. The release nutrient order in 30-days of compound fertilizer hydrogel granules was 84±18, 63±12 and 36±15%, of N, P and K nutrients, respectively. The release data of the N and P nutrients of the fertilizer granules hydrogel obeyed the Korsmeyer-Peppas model while the K nutrient release followed the exponential behavior.

Keywords: NPK Compound Fertilizer, Poly(vinyl alcohol), Chitosan, Glutaraldehyde crosslinker, Fertilizer hydrogel

การสังเคราะห์และการตรวจสอบลักษณะของปุ๋ยไฮโดรเจลคอมพาวนด์เอ็นพีเคที่มีการปล่อย แบบควบคุม

งานวิจัยนี้มุ่งศึกษาการเตรียมปุ๋ยไฮโดรเจลคอมพาวนด์ชนิดควบคุมการปล่อยธาตุ NPK ได้เตรียม ปุ๋ยไฮโดรเจลด้วยการจุ่มเม็ดปุ๋ยลงในสารละลายพอลิไวนิลแอลกอฮอล์ ตามด้วยการจุ่มในสารละลายไค โทซานและเชื่อมขวางด้วยไอของสารละลายกลูทารัลดีไฮด์ หาเวลาที่ปุยไม่เคลือบและปุ๋ยเคลือบละลาย น้ำหมด นำปุ๋ยเคลือบพอลิไวนิลแอลกอฮอล์และไคโทซานที่เชื่อมขวางแล้วมาสังเคราะห์เป็นปุ๋ยไฮโดร เจล ด้วยการทำปฏิกิริยาการเกิดพอลิเมอร์แบบแขวนลอยของมอนอเมอร์อะคริลาไมด์และอะคริลิกแอซิด ตรวจสอบหมู่ฟังก์ชันของของปุ๋ยไฮโดรเจลด้วยเทคนิคฟูเรียร์ทรานฟอร์มอินฟราเรดส-เปกโทรสโกปี ศึกษาสัณฐานวิทยาของเม็ดปุ๋ยที่ไม่เคลือบและเคลือบด้วยเทคนิคกล้องจุลทรรศน์แบบแสง และตรวจสอบ สัณฐานวิทยาของชั้นไฮโดรเจลที่เคลือบเม็ดปุ๋ยหลังจากบวมน้ำด้วยกล้องจุลทรรศน์อิเล็กตรอนแบบส่อง กราด ศึกษาผลของสารตั้งต้นต่อค่าการดูดซึมน้ำของปุ๋ยไฮโดรเจลคอมพาวนด์ และศึกษาการปล่อยธาตุ อาหารเอ็นพีเคในปุ๋ยไฮโดรเจลคอมพาวนด์ พบว่า เวลาในการละลายน้ำของปุ๋ยเพิ่มขึ้นด้วยการเพิ่ม จำนวนครั้งในการเคลือบ ปริมาณสารตั้งต้นที่เหมาะสมในการสังเคราะห์ปุ๋ยไฮโดรเจลคอมพาวนด์ คือ ้อัตราส่วนของมอนอเมอร์อะคริลาไมด์ต่ออะคริลิกแอซิดมีค่าร้อยละ 3:97 โดยโมล ใช้เอ็น,เอ็น,เอ็น′, *เอ็น*'-เททระเมทิลเอทิลีนไดแอมีน แอมโมเนียมเพอร์ซัลเฟต และ*เอ็น, เอ็น'*-เมทิลีนบิสอะคริลาไมด์มี ค่า 0.13, 0.13 และ 0.01% โมลของมอนอเมอร์ทั้งหมด ให้ค่าการดูดซึมน้ำ 233±5 กรัมต่อน้ำหนักแห้ง ในน้ำกลั่น ที่อุณหภูมิห้อง ภายในเวลา 24 ชั่วโมง เม็ดปุ๋ยไฮโดรเจลคอมพาวนด์ปล่อยธาตุอาหารเอ็น พีเคได้ร้อยละ 84±18, 63±12 และ 36±15 ตามลำดับ ภายในเวลา 30 วัน ในน้ำกลั่น ค่าการปล่อยธาตุ อาหารในโตรเจนและฟอสฟอรัสสอดคล้องกับแบบจำลองจลนศาสตร์การปล่อยของ Korsmeyer-Peppas ส่วนการปล่อยธาตุอาหารโพแทสเซียมเป็นแบบเอกซ์โพเนนเชียล

คำสำคัญ: ปุ๋ยคอมพาวนด์เอ็นพีเค, พอลิไวนิลแอลกอฮอล์, ไคโทซาน, สารเชื่อมขวางกลูทารัลดีไฮด์, ปุ๋ย ไฮโดรเจล

5.4 Synthesis and characterization of hydrogel for insulin released from hydrolyzed collagen grafted poly[(acrylic acid)-co-(methacrylic acid)]

Hydrolyzed collagen grafted poly[(acrylic acid)-co-(methacrylic acid)] hydrogels were synthesized by solution polymerization. Acrylic acid (AA) and methacrylic acid (MAA), ammonium persulfate (APS), N, N, N', N'-tetramethylethylenediamine (TEMED), and N, N'-

methylenebisacrylamide (N-MBA) were used as a pair of monomer, an initiator, a co-initiator, and a crosslinking agent, respectively. The effects of reagents on the performance and water absorbency of synthesized hydrogels were investigated. The grafted hydrolyzed collagen hydrogel was confirmed by FTIR technique. The effects of pH in buffered and non-buffered solutions, sodium chloride solution, and temperature on the swelling behavior of the grafted hydrolyzed collagen hydrogel were examined. The released behavior of insulin or methylene blue (as a smaller-sized model drug) was also investigated in simulated gastric and intestinal fluids. It was found that when the APS contents were too high or low, the synthesized products were not in the hydrogel form and the water absorbency cannot be determined. The high water absorbency of grafted hydrogel was reached 476±9 gg⁻¹, when the ratio of AA-to-MAA was 92:8 and the contents of TEMED, APS and N-MBA were 0.015, 0.2 and 0.12 % by mol of monomers, respectively. The grafted hydrolyzed collagen hydrogel in the acidic and neutral pH solution was suitable for drug delivery application at a target site. It showed that the abilities to release of insulin and methylene blue were slightly less in the simulated gastric fluid and relatively high in the simulated intestinal fluid. The results obtained were in good agreement with the pH responses of the synthesized hydrogel. Thus, the hydrolyzed collagen grafted poly[(acrylic acid)-co-(methacrylic acid)] hydrogel exhibits itself as the insulin controlled release medium.

Keywords: Hydrogel, Hydrolyzed collagen, Grafted collagen, Acrylic acid, Methacrylic acid

การสังเคราะห์และการตรวจสอบคุณลักษณะเฉพาะของไฮโรเจลสำหรับการปล่อยอินซูลินจาก คอลลาเจนไฮโดรไลซ์กราฟต์พอลิ(อะคริลิกแอซิด-*โค*-เมทาคริลิกแอซิด)

สังเคราะห์ไฮโดรเจลจากคอลลาเจนไฮโดรไลซ์กราฟต์พอลิเมอร์ร่วมอะคริลิกแอซิด-เมทาคริลิกแอซิด โดยปฏิกิริยาการเกิดพอลิเมอร์ในสารละลาย ใช้อะคริลิกแอซิดเป็นมอนอเมอร์ เมทาคริลิกแอซิดเป็นมอนอ เมอร์ร่วม แอมโมเนียมเพอร์ซัลเฟตเป็นสารริเริ่มปฏิกิริยา และ เอ็น, เอ็น, เอ็น, เอ็น', เอ็น'-เททระเมทิลเอทิลีน ใดแอมีนเป็นสารริเริ่มปฏิกิริยาร่วม และ เอ็น, เอ็น'-เมทิลีนบิสอะคริลาไมด์เป็นสารเชื่อมขวาง ศึกษาผล ของสารตั้งตันต่อค่าการดูดซึมน้ำของไฮโดรเจลที่สังเคราะห์ได้ ยืนยันการเกิดการกราฟต์ของไฮโดรเจลจากคอลลาเจนไฮโดรไลซ์ด้วยเทคนิค FTIR ศึกษาผลของค่าความเป็นกรด-เบสในสารละลายไม่มี บัฟเฟอร์และสารละลายบัฟเฟอร์ ความเข้มข้นของสารละลายเกลือโซเดียมคลอไรด์ และอุณหภูมิต่อ

การตอบสนองของการดูดซึมน้ำของไฮโดรเจลจากกราฟต์คอลลาเจนไฮโดรไลซ์ ศึกษาการนำส่งยาของ อินซูลินและเมทิลีนบลูที่ใช้เป็นแบบจำลองการปล่อยยา โดยเลียนแบบสารละลายในกระเพาะอาหาร และ สารละลายภายในลำไส้ พบว่า เมื่อปริมาณสารเริ่มปฏิกิริยามีมากหรือน้อยเกินไป สารที่สังเคราะห์ได้ไม่ อยู่ในรูปของไฮโดรเจล และไม่สามารถหาค่าการดูดซึมน้ำ กราฟต์ไฮโดรเจลที่สังเคราะห์ได้มีค่าการดูด ซึมน้ำมากเท่ากับ 476±9 เท่าของน้ำหนักสารแห้ง เมื่อใช้สัดส่วนของอะคริลิกแอซิดต่อเมทาคริลิกแอซิด 92:8 โดยโมล ปริมาณแอมโมเนียมเพอร์ซัลเฟต เอ็น, เอ็น, เอ็น, เอ็น' เก็น'-เททระเมทิลเอทิลีนไดแอมีน และ เอ็น, เอ็น'-เมทิสีนบิสอะคริลาไมด์ เท่ากับ 0.015, 0.2 และ 0.12 โดยโมลของมอนอเมอร์ ตามลำดับ ไฮโดรเจลจากกราฟต์คอลลาเจนไฮโดรไลซ์มีการตอบสนองในภาวะกรดและภาวะเป็นกลาง ที่เหมาะสมกับการนำไปประยุกต์ในการนำส่งยาไปยังอวัยวะเป้าหมาย ไฮโดรเจลปล่อยอินซูลินและเมทิลีนบลูออกมาน้อยในสารละลายเลียนแบบกระเพาะอาหารที่มีสภาพเป็นกรด เมื่อไฮโดรเจลอยู่ใน สารละลายเลียนแบบลำไส้ที่มีภาวะเป็นกลาง สามารถปล่อยอินซูลินและเมทิลีนบลูออกมาในปริมาณมาก ซึ่งสอดคล้องกับผลการทดลองในส่วนของการตอบสนองต่อค่าความเป็นกรด-เบสของไฮโดรเจลที่ สังเคราะห์ได้ ดังนั้น ไฮโดรเจลจากคอลลาเจนไฮโดรไลซ์กราฟต์พอลิเมอร์ร่วมอะคริลิกแอซิด-เมทาคริลิกแอซิด สามารถแสดงผลเป็นด้วกลางควบคุมการปล่อยอินซูลินได้ดี

คำสำคัญ: ไฮโดรเจล, คอลลาเจนไฮโดรไลซ์, กราฟเทดคอลลาเจน, อะคริลิกแอซิด, เมทาคริลิกแอซิด

กลุ่มโครงการวิจัยที่ 6 การผลิตเส้นใยและกระดาษจากนุ่น

6.1 Kapok I: Properties investigation of kapok fiber as a potential pulp source for papermaking

The potential use of kapok fiber as a new source for pulping and papermaking has been investigated. The experiment was started by cooking kapok fibers with different dosages of sodium hydroxide. Then, the pulp was refined twice using a disc refiner with a disc gap of 1/100 inch. Handsheets were made and their strength properties were evaluated to determine the optimal dosage of sodium hydroxide. The optimized pulping condition was then used to prepare kapok pulp. Then, this kapok pulp was mixed with commercial hardwood pulp and/or softwood pulp at different blend ratios to make papers. Addition of the kapok pulp to the mixed pulps improved the tensile and burst strengths of the sheets but decreased the tear resistance. Water repellency of the sheets prepared from the kapok pulp mixed with the commercial pulps was also improved. These results indicate that kapok fiber can be a quality pulp source for papermaking, especially for packaging paper.

Keywords: Kapok fiber; Paper properties, Raw material, Papermaking

นุ่น 1: การประเมินสมบัติของเส้นใยนุ่นเป็นแหล่งเยื่อที่มีศักยภาพเพื่อการผลิตกระดาษ

โครงการนี้ได้ประเมินศักยภาพและความเหมาะสมของเส้นใยนุ่นเพื่อเป็นแหล่งเยื่อและการผลิต กระดาษชนิดใหม่ เริ่มต้นด้วยการตัมเยื่อนุ่นในสารละลายโซเดียมไฮดรอกไซด์ปริมาณต่าง ๆ นำเยื่อที่ ต้มแล้วมาบด 2 ครั้งในเครื่องบดเยื่อแบบจาน ใช้ระยะห่างระหว่างจานบด 1/1000 นิ้ว ผลิตกระดาษ แฮนด์ชิตจากเยื่อที่บดได้ ประเมินสมบัติด้านความแข็งแรงของแฮนด์ชิตเพื่อหาปริมาณโซเดียมไฮดรอก ไซด์ที่เหมาะสม เมื่อได้ภาวะการต้มเยื่อที่เหมาะสมแล้ว นำภาวะนี้ไปผลิตเยื่ออีกครั้งหนึ่ง นำเยื่อที่ผลิต ได้ใหม่ด้วยภาวะนี้ไปผลมกับเยื่อจากไม้เนื้อแข็ง เยื่อจากไม้เนื้ออ่อน และเยื่อผสมระหว่าเยื่อทั้งสองชนิด เยื่อนุ่นที่เดิมลงไปในเยื่อผสมปรับปรุงสมบัติเทนไซล์และความแข็งแรงทนแรงระเบิดของกระดาษแฮนด์ชิต แต่ลดความต้านทานต่อแรงฉีกขาด จากการวัดมุมสัมผัสของน้ำบนกระดาษแฮนด์ชิตที่เตรียมได้ กระดาษแฮนด์ชิตขับน้ำกลั่นที่หยดบนกระดาษนุ่นผสมเยื่อผสมทั้งสองชนิดมากขึ้น ผลที่ได้เหล่านี้บ่งชี้ ว่า เยื่อนุ่นสามารถเป็นแหล่งเยื่อที่มีคุณภาพสำหรับการผลิตกระดาษ โดยเฉพาะอย่างสำหรับกระดาษ บรรจุภัณฑ์

คำสำคัญ: เส้นใยนุ่น, สมบัติของกระดาษ, วัตถุดิบ, การผลิตกระดาษ

6.2 Kapok II: Pretreatment of Kapok Fibers for Pulping and Papermaking

Kapok fiber is naturally coated with wax and cutin which render it hydrophobic. To obtain the fiber suitable for pulping, it must be immersed in water for as long as three to four weeks. This research investigated the effects of fiber pretreatments by chemical method or biological method for varied immersion times before it could be subjected to soda pulping. These pretreatments were compared with those obtained from the controlled fiber where the kapok fibers were immersed in tap water for 3 weeks (as controlled kapok). For the chemical pretreatment, the doses of sodium hydroxide (5 and 10% based on O.D. fiber weight) were used with various immersion times (1, 2 and 3 weeks). For the biological pretreatment, the enzyme lipase doses (0.25 and 0.5% based on O.D. fiber weight) was used under the immersion times (1, 3 and 5 hours). All the pretreatment results were compared with those obtained from the control. After the kapok fibers had passed the soda pulping process and further processes, the pulp and their handsheets having 60 g/m² from each pretreatment were characterized for the pulping efficiency, physical properties and optical properties. This research elucidated the results and causes of each effect and suggested their benefits for the pulp and paper making.

Keywords: Kapok fiber, Chemical pretreatment, Biological pretreatment, Soda pulping, Lipase, Immersion times, Paper making

นุ่น II: การปรับสภาพผิวของเส้นใยนุ่นสำหรับการผลิตเยื่อและการผลิตกระดาษ

เส้นใยนุ่นมีขี้ผึ้งและเคอร์ทินเคลือบอยู่ตามธรรมชาติ จึงทำให้นุ่นไม่ชอบน้ำ ในการผลิตเยื่อจากนุ่น จำเป็นต้องแช่นุ่นในน้ำเป็นเวลานานถึง 3-4 สัปดาห์ งานวิจัยจึงได้ศึกษาผลของการปรับสภาพเส้นใยแบบ เคมี หรือแบบชีวภาพของเส้นใยนุ่น ก่อนนำเส้นใยนุ่นไปเข้ากระบวนการโซดา และเทียบผลกับเส้นใยนุ่นที่ แช่ในน้ำประปาอย่างเดียว เป็นเวลา 3 สัปดาห์ (นุ่นควบคุม) ได้ศึกษาผลจากปริมาณโซเดียมไฮดรอกไซด์ ของการปรับสภาพแบบเคมี (ร้อยละ 5 และ 10 เมื่อเทียบกับน้ำหนักของนุ่นที่อบแห้ง) และเวลาแช่นุ่น (1, 2 และ 3 สัปดาห์) ส่วนการปรับสภาพด้วยวิธีทางชีวภาพใช้เอนไซม์ไลเปส (ร้อยละ 0.25 และ 0.50 เมื่อเทียบ

กับน้ำหนักของนุ่นที่อบแห้ง) และเวลาแช่นุ่น (1, 3 และ 5 ชั่วโมง) ภายหลังที่เส้นใยนุ่นผ่านกระบวนการ โซคา และขึ้นแผ่นกระคาษแล้ว ได้ศึกษาประสิทธิภาพในการผลิต สมบัติเชิงกลและสมบัติทางแสงของเยื่อ และกระคาษที่ได้จากแต่ละกระบวนการปรับสภาพ อธิบายผลและเหตุที่ได้จากตัวแปรพร้อมทั้งเสนอแนะ การใช้ประโยชน์ของเยื่อและกระคาษ

คำสำคัญ: เส้นใยนุ่น, การปรับสภาพเชิงเคมี, การปรับสภาพเชิงชีวภาพ, การตัมเยื่อด้วยโชดา, เอ็นไซม์ ไลเปส, เวลาการแช่, การผลิตกระดาษ

Kapok III: Use of Kapok Pulp to Improve Properties of Recycled Paper

Using recycled paper is one way to reduce environment problems. However, higher cycle numbers of recycling leads to reduction of paper strength; thus, improvement of recycled paper properties is very important. One way to improve strength of recycled paper is to use kapok pulp because kapok is the long fiber with good enough pulp and paper properties. In this study, paper was made using kapok and recycled pulp to compare with those using softwood-to-recycled pulp ratios at 100:0, 10:90, 20:80, 30:70 and 0:100. As a result, it was found that recycling up to three cycles had a small effect on paper properties. Higher amount of kapok pulp in the mixed pulp between kapok pulp and recycled pulp increased porosity, opacity, density and tensile index but decreased brightness and whiteness of handsheets. On the other hand, higher amount of softwood pulp led to higher tear index only. So, the combination of the mixed pulps and amount of pulps used are really dependent on the final paper property required.

Keywords: Recycled paper, Kapok fiber, Softwood, Paper properties

นุ่น III: การใช้เส้นใยนุ่นในการปรับปรุงสมบัติของกระดาษที่ผลิตจากเยื่อเวียนทำใหม่

งานวิจัยในส่วนนี้ศึกษาผลของการใช้เยื่อนุ่นในการปรับปรุงสมบัติของกระดาษที่ผลิตจากเยื่อเวียน ทำใหม่ แต่อย่างไรก็ตาม จำนวนรอบของการเวียนทำใหม่มากเกินไปจะลดความแข็งแรงของกระดาษ เวียนทำใหม่ ดังนั้น การปรับปรุงสมบัติของกระดาษเวียนทำใหม่มีความสำคัญมาก วิธีหนึ่งที่จะเพิ่มความ แข็งแรงแก่กระดาษเวียนทำใหม่คือ การใส่เยื่อนุ่น เพราะเยื่อนุ่นเป็นเยื่อใยยาวซึ่งมีสมบัติของเยื่อและ กระดาษที่ดีพอ การทดลองเริ่มต้นจากการนำเยื่อนุ่นมาผสมกับเยื่อเวียนทำใหม่ ในสัดส่วน เยื่อนุ่น: เยื่อ เวียนทำใหม่ 100:0, 10:90, 20:80, 30:70 และ 0:100 ในแต่ละรอบของการเวียนทำใหม่ ตั้งแต่ 1- 3 รอบ นอกจากนี้ ยังนำเยื่อใยยาว (เยื่อจากไม้เนื้ออ่อน) มาผสมเยื่อเวียนทำใหม่แทนเยื่อนุ่น เพื่อใช้ เปรียบเทียบประสิทธิภาพการปรับปรุงสมบัติของเยื่อเวียนทำใหม่ผสมระหว่างเยื่อนุ่นกับเยื่อยาว จาก การทดลองพบว่า เมื่อเปรียบเทียบกับเยื่อใยยาวแล้ว การใช้ปริมาณสัดส่วนเยื่อนุ่นที่มากขึ้นในการผลิต กระดาษจากเยื่อเวียนทำใหม่ ส่งผลให้ค่าความแข็งแรงต่อแรงดึง ความหนาแน่น ความพรุน ความเรียบ และความทึบแสงของกระดาษเพิ่มมากขึ้น ในขณะที่เมื่อเปรียบเทียบกับเยื่อนุ่นในสัดส่วนที่เท่ากันแล้ว การใช้เยื่อใยยาวในสัดส่วนที่เพิ่มขึ้นส่งผลให้ค่าความต้านทานแรงฉีกมีค่าสูงขึ้นมากกว่าการใช้เยื่อนุ่น ดังนั้น การผสมผสานการใช้เส้นใยผสมและปริมาณที่พอเหมาะขึ้นกับสมบัติสุดท้ายของกระดาษที่ ต้องการ

คำสำคัญ: กระดาษเวียนทำใหม่, เส้นใยนุ่น, ไม้เนื้ออ่อน, สมบัติของกระดาษ

กลุ่มโครงการวิจัย ที่ 7 ผ้าไหมและการพิมพ์ผ้าไหมด้วยหมึกพิมพ์อิงก์เจ็ต

7.1 Modified chitosan pretreatment of polyester fabric for printing by ink jet ink

The present research deals with the use of pretreatment solutions of chitosan (CH), N-[(4dimethyl aminobenzyl)imino] chitosan (DBIC), N-[(2-hydroxy-3-trimethylammonium) propyl] chitosan chloride (HTACC), glycine (Gly), and a mixture of CH and Gly, for padding polyester fabrics prior to printing with a set of seven-color pigmented water-based ink jet inks. After padding the fabrics with the above cationic pretreatments, they were printed with a piezoelectric drop-on-demand jet printer. CH, DBIC and HTACC were characterized by IR and NMR spectroscopy. The zeta potentials of the pretreatment solutions, the inks and the fabrics were measured. The K/S values, color gamut, tone reproduction, outline sharpness, and the surface appearance of the fabrics were characterized. Statistical evaluation of the significance of the results was performed. Among the pretreatments, the HTACC at 0.1% (w/v) yielded fabrics with the highest K/S values, widest color gamut and gamut volume, more color saturation with good tonal reproduction, and the sharpest and smoothest outline of printed character, and a smooth fabric surface with less stiffness. The proposed ionic interactions between the protonated amino groups of CH and the anionic portion of the encapsulated ink pigments, and van der Waals and hydrophobic interactions between the polyester and the pigments are likely reasons for these enhanced properties of the printed fabrics.

Keywords: Chitosan; glycine, N-[(4-dimethyl aminobenzyl)imino] chitosan, N-[(2-hydroxy-3-trimethylammonium)propyl] chitosan chloride, Color properties, Outline sharpness, Stiffness

การปรับสภาพผิวผ้าพอลิเอสเทอร์ด้วยไคโทซานดัดแปรสำหรับการพิมพ์โดยหมึกอิงก์เจ็ต

งานวิจัยนี้เป็นการศึกษาผลของสารละลายปรับสภาพผิวผ้าพอลิเอสเทอร์ 5 ชนิด คือ ไคโทซาน ไค โทซานดัดแปร เอ็น-4-ไดเมทิลแอมิโนเบนซิลอิมิโน (N-[(4-dimethyl aminobenzyl)imino] chitosan, DBIC) เอ็น-2-ไฮดรอกซี-3-ไทรเมทิลแอมโมเนียมพรอพิลไคโทซานคลอไรด์ (N-[(2-hydroxyl-3-trimethylammonium)propyl] chitosan chloride, HTACC) ไกลซีน และของผสมระหว่างไคโทซานกับ ไกลซีน สำหรับการแพดดิงผ้าก่อนการพิมพ์ด้วยหมึกพิมพ์อิงก์เจ็ตฐานน้ำชนิดสารสี 7 สี ด้วย เครื่องพิมพ์อิงก์เจ็ตแบบ piezo-electric drop-on-demand ตรวจสอบลักษณะเฉพาะของไคโทซาน ไคโท

ชานดัดแปร DBIC และ HTACC ด้วยเทคเนิค IR and NMR วัดค่า zeta potentials ของสารละลายปรับ สภาพผิว และผ้าพอลิเอส- เทอร์ วัดความเข้มสี ขอบเขตสี การผลิตน้ำหนักสี ความคมชัดของตัวอักษร และตรวจสอบลักษณะพื้นผิวผ้าที่ปรับสภาพ พบว่า HTACC ความเข้มข้นร้อยละ 0.1 โดยน้ำหนัก ให้ ความเข้มสีมากสุด ขอบเขตสีและปริมาตรสีกว้างสุด ความอิ่มตัวสีและการผลิตน้ำหนักสีดี ความคมชัด ของตัวอักษรมากสุด และพื้นผิวผ้ามีความกระด้างน้อยสุด ด้วยปฏิกิริยาระหว่างประจุบวกของสารปรับ สภาพผิวผ้ากับประจุลบของสารสีในหมึกพิมพ์ และแรง van der Waals และความไม่ชอบน้ำของผ้าพอลิ เอสเทอร์และสารสีที่มีผลเพิ่มคุณภาพผ้าพิมพ์พอลิเอสเทอร์ด้วยระบบการพิมพ์อิงก์เจ็ต

คำสำคัญ: ไคโทซาน, ไกลซีน, ไคโทซานดัดแปร เอ็น-4-ไดเมทิลแอมิโนเบนซิลอิมิโน, เอ็น-2-ไฮดรอกซิ-3-พรอพิลไทรเมทิลแอมโมเนียมไคโทซานคลอไรด์, สมบัติทางสี, ความคมชัดของเส้น, ความกระด้าง

7.2 Anionically surface-modified pigment/binder ink jet inks for silk fabric printing

The purpose of this research was to prepare anionically surface-modified organic pigment/binder ink jet inks for printing on chitosan-pre-treated silk fabrics. Anionically surfacemodified organic pigment/binder ink jet inks were prepared in four colours (cyan, magenta, yellow and black). The pigment-to-binder ratio was controlled at 1:6.4 for the cyan, magenta and yellow inks, and 1:3.4 for the black ink. Ink formulations (by weight) were assembled and mixed as follows: 8% pigment dispersion, 10% diethylene glycol, 12% glycerol, 5% urea, 10% polyacrylate emulsion binder and 55% deionised water. The inks were mixed and filtered with a special type of membrane to remove the oversized particles. They were characterised in terms of their particle size, zeta potential, particle morphology, viscosity, surface tension and pH. The inks were printed onto silk or the chitosan pre-treated silk fabrics using a piezo-type ink jet printer. The fabrics were then heat cured and analysed for the effect of chitosan pre-treatment on colour gamut, wash fastness and crock fastness. The formulated ink jet inks yielded an acceptably good ink jetting reliability, one-year stability and printability. The chitosan pre-treated silk fabrics gave a wider colour gamut and colour saturation than the non-treated one. Crock fastness and wash fastness of the chitosan pre-treated fabrics where relatively better than those of non-treated fabrics. The surface modified pigments are transparent and thus their inks printed on the chitosan pre-treated fabrics produced slightly low K/S values of CMYK colours because the limited chitosan concentration in the pre-treatment is controlled by its solubility in acidic solution. The higher loading of chitosan pre-treatment gave higher K/S values and a stiffer touch of the fabrics which is uncomfortable for users. Water-based pigmented inks having the sulphonate group on the pigment surface can be printed on the fabric surface pre-treated with chitosan molecules which have the protonated amino groups to give good color appearance. It is anticipated that this type of ink can be applied to any textile surface which has been pre-treated with the protonated chitosan. Ionic interactions between the sulphonate group of the pigment and protonated amino groups of chitosan in conjunction with polyacrylate binder enhance colour strength, widen colour gamut and chroma, and produce good adhesion for fabric operational properties such as wash fastness and crock fastness.

Keywords: Anionic functional group, Surface-modified pigments, Ink jet, Fabric pre-treatment, Chitosan, Silk fabric, Polyacrylate emulsion binder

การพิมพ์ผ้าไหมด้วยหมึกพิมพ์อิงก์เจ็ตชนิดผิวสารสีมีประจุลบ/สารยึด

วัตถุประสงค์ของงานวิจัยนี้เพื่อเตรียมหมึกพิมพ์อิงก์เจ็ตชนิดผิวสารสีมีประจุลบผสมกับสารยึดเพื่อ พิมพ์ผ้าใหมปรับผิวผ้าด้วยสารละลายใคโทซานประจุลบ นำสารสีผิวมีประจุลบ 4 สี ได้แก่ สีฟ้าเขียว สี ม่วงแดง สีเหลือง และสีดำ ใช้สัดส่วนของสารสีต่อสารยึด เป็น 1: 6.4 สำหรับสีหมึกพิมพ์สีฟ้าเขียว สี ม่วงแดงและสีเหลือง ส่วนสีหมึกพิมพ์สีดำมีสัดส่วนเป็น 1:3.4 ผสมองค์ประกอบในหมึกพิมพ์ตามลำดับ ดังนี้ สารละลายของสารสีซึ่งการกระจายมาแล้วในพอลิเมอร์ ร้อยละ 8 ไดเอทิลีนไกลคอลร้อยละ 10 ไกล คอลร้อยละ 5 ยูเรียร้อยละ 10 อิมัลชันพอลิอะคริเลตไบน์เดอร์ร้อยละ 10 และน้ำกลั่นร้อยละ 55 ผสมและ เขย่าให้เข้ากัน กรองด้วยเมมเบรนพิเศษเพื่อกรองอนุภาคขนาดใหญ่ออกไป นำหมึกพิมพ์ที่เตรียมได้ ทั้งหมดไปวัดขนาดอนุภาค ความต่างศักย์ซีตา สัณฐานวิทยาของอนุภาค ความหนืด แรงตึงผิว และค่า ความเป็นกรด-เบสของหมึกพิมพ์ นำหมึกพิมพ์ทั้งสี่สีบรรจุในตลับพิมพ์และนำไปพิมพ์ผ้าไหมที่ไม่ผ่าน การจุ่มรีดและผ้าที่ผ่านการจุ่มรีดด้วยสารละลายไคโทซานด้วยเครื่องพิมพ์อิงก์เจ็ตที่ขับเคลื่อนการพิมพ์ ้ด้วยแรงดันเปียร์โซ นำผ้าพิมพ์เหล่านี้ไปอบและวิเคราะห์คุณภาพของสีพิมพ์ด้านแกมุตสี ความทนการ ซัก และความทนการขีดข่วนและขัดถู หมึกพิมพ์สูตรชุดนี้ที่กำหนดสามารถพ่นหมึกได้เส้นหมึกพิมพ์ สมบูรณ์ ลักษณะการพ่นหมึกเชื่อถือได้ และมีความเสถียรของสารสีในหมึกพิมพ์เก็บได้นาน 1 ปี ผ้า พิมพ์ที่ปรับผิวด้วยใคโทซานมีค่าแกมุตสึกว้างกว่าและมีความอิ่มตัวของสีมากกว่าผ้าที่ไม่ได้ปรับผิว ความทนการขีดข่วนและขัดถู และความทนการซักของผ้าพิมพ์ที่ปรับผิวมีค่ามากกว่าผ้าพิมพ์ที่ไม่ปรับ ผิว สารสีที่ดัดแปรด้วยสารเคมีที่ผิวมีความโปร่งใสมาก สีพิมพ์ที่ได้บนผ้าไหมที่จุ่มรีดด้วยสารละลายไค

โทซานจึงมีค่า K/S ไม่สูง เพราะปริมาณที่จำกัดของไคโทซานที่ละลายได้เฉพาะในกรดที่มีค่าความเป็น

กรด-เบสต่ำกว่า 4 และปริมาณไคโทซามที่มากขึ้นบนผ้าไหมก็จะทำให้สีพิมพ์มีค่า K/S มากขึ้นแต่ผ้า

พิมพ์มีความกระด้างมากขึ้น ผู้ใช้จับต้องไม่สบายมือและไม่สบายเมื่อสวมใส่ หมึกพิมพ์อิงก์เจ็ตฐานน้ำที่

มีกลุ่มซัลโฟเนตประจุบบนผิวของสารสีพิมพ์ได้สีเข้มดีขึ้นบนผ้าที่ปรับผิวด้วยไคโทซานที่มีประจุบวก

จากการเติมโปรตอนที่กลุ่มแอมิโน เป็นที่คาดว่า หมึกพิมพ์กลุ่มนี้สามารถใช้ได้กับผ้าได้ทุกชนิดที่ได้รับ

การปรับผิวก่อนพิมพ์ด้วยไคโทซานประจุบวก พันธะไอออนระหว่างกลุ่มซัลโฟเนตประจุลบกับสารไคโท

ซานประจุบวกเมื่อเสริมกับสารยึดพอลิอะคริเลต จะช่วยส่งให้สีพิมพ์มีความอิ่มตัวมากขึ้น สีในแกมุต

กว้างขึ้น และเกิดแรงยึดติดมากขึ้น ทำให้ทนการซักและการขีดข่วนและการขัดถูมากขึ้น

คำสำคัญ: หมู่ฟังก์ชันประจุลบ, สารสีดัดแปรผิว, หมึกพิมพ์อิงก์เจ็ต, สารปรับผิวผ้า, ใคโทซาน, ผ้าใหม,

สารยึดอิมัลชันพอลิอะคริเลต

7.3 Simulation of Printed Images on Silk Fabric by Ink Jet Printer

Silk fabric is a fabric in which its gloss is perceived differently in comparison with other

fabrics due to its specific reflectance. This research measured a Bidirectional Reflectance

Distribution Function (BRDF) of three types of silk fabric having different weaving styles in

conjunction with reflectance characteristics. We measured BRDF of the silk fabrics and its

reflection model was then proposed. The proposed reflection model incorporates a specular

reflection lobe and diffuse reflection lobe. The proposed model and the measured BRDF of the

three silk fabrics were fitted by the least-square error method. The measured BRDF of the silk

fabric were also fitted with Phong reflection model, Oren-Nayar reflection model and Torrance-

Sparrow reflection. It was found that the proposed model fitted better with the measured BRDF

than did the general models of Phong-reflection, Oren-Nayar reflection, and Torrance-reflection.

The proposed model can thus be used to approximate, analyze and elucidate the

characteristics of light reflection of the three silk fabrics.

Key words: BRDF, silk fabrics, reflection model.

การวัด Bidirectional Reflectance Distribution Function และการจำลองแบบการสะท้อนแสง

ของผ้าไหม

ผ้าใหมเป็นสิ่งทอที่มีความมันวาวมากกว่าสิ่งทอประเภทอื่น เนื่องจากผ้าใหมมีลักษณะการสะท้อน

แสงที่มีความเฉพาะตัว ดังนั้น งานวิจัยนี้จึงศึกษาลักษณะการสะท้อนแสงของผ้าไหม โดยวัดค่า BRDF

(Bidirectional Reflectance Distribution Function) และนำเสนอแบบจำลองการสะท้อนแสงของพื้นผิว

ผ้าใหมที่คำนึงถึงการสะท้อนของแสงฟุ้งและแสงกล้า โดยใช้วิธีการหาค่าความผิดพลาดกำลังสองน้อย

ที่สุด (least-square error) หาความสัมพันธ์ระหว่างค่าที่วัดกับแบบจำลอง เมื่อทดสอบแบบจำลองที่ได้

พบว่า แบบจำลองที่นำเสนอนี้มีความสัมพันธ์กับ BRDF ที่วัดได้ของผ้าไหมมากกว่าแบบจำลองการ

สะท้อนแสงที่มีอยู่ทั่วไป ได้แก่ แบบจำลองการสะท้อนแสงของ Phong reflection model, แบบจำลอง

การสะท้อนแสงของ Oren-Nayar reflection model และแบบจำลองการสะท้อนแสงของ Torrance-

Sparrow reflection model ผู้วิจัยสามารถพยากรณ์ค่าการสะท้อนแสง วิเคราะห์ และอธิบายลักษณะการ

สะท้อนแสงของผ้าใหม่ได้จากแบบจำลองที่นำเสนอนี้

คำสำคัญ : บีอาร์ดีเอฟ, ผ้าไหม, แบบจำลองการสะท้อนแสง

7.4 Effects of Chitosan and Glycine Pretreatment on Polyester Fabric Printed by Ink Jet Ink

The effects of pretreatment solutions of chitosan (CS) and glycine (Gly) on polyester fabric

and their printing results were investigated. The polyester fabrics were padded with CS (4%

w/v) or Gly (5% w/v) solution prior to printing with a set of seven-color pigmented water-based

jet inks from a piezo-electric jet printer. Hydrophobicity/hydrophilicity of the untreated and

treated polyester fabrics was measured by wicking test. K/S values and color difference of the

polyester printed fabrics were investigated. The printed fabric with Gly pretreatment had the

higher K/S values and color difference than those with CS pretreatment due to its interaction

with color inks. Gly increased hydrophilicity of the treated polyester fabric, while CS markedly

decreased the hydrophilicity. Interaction between the pretreatment agent and the active groups

on pigment color development was elucidated.

Keywords: Chitosan, Glycine, Polyester fabric, Ink jet printing

ผลของการปรับผิวด้วยไคโทซานและไกลซีนบนผ้าพอลิเอสเทอร์พิมพ์ด้วยหมึกพิมพ์อิงก์เจ็ต

ได้ศึกษาและวิเคราะห์ผลของการปรับผิวด้วยสารละลายไคโทซาน (CS) และไกลซีน (GIy) บนผ้า พอลิเอสเทอร์และผลการพิมพ์ด้วยหมึกพิมพ์อิงก์เจ็ต นำผ้าพอลิเอสเทอร์ไปจุ๋มรีดด้วยสารละลายไคโท ซานความเข้มขันร้อยละ 4 โดยน้ำหนักต่อปริมาตรตัวทำละลาย หรือ GIy ร้อยละ 5 ก่อนพิมพ์ด้วยชุด หมึกพิมพ์อิงก์เจ็ตสารสีฐานน้ำ 7 สี จากเครื่องพิมพ์แบบเปียร์โซ หาความไม่ซอบน้ำและความซอบน้ำ บนผิวผ้าที่ไม่ปรับผิวและปรับผิวด้วยวิธีวัดการซึมน้ำ (wicking test) วัดค่า K/S และ Δ E (ความ แตกต่าง) ของสีบนผ้าพิมพ์ ผ้าพิมพ์ที่ปรับผิวด้วย GIy ให้ค่า K/S และ Δ E ของสีพิมพ์มากกว่าผ้าพิมพ์ ที่ปรับผิวด้วย CS ส่วน GIy เพิ่มความซอบน้ำของผ้าพอลิเอสเทอร์ ในขณะที่ CS ลดความซอบน้ำอย่าง มีนัยสำคัญ เนื่องจากซนิดของสารปรับผิวมีปฏิสัมพันธ์กับสารสีของหมึกพิมพ์แตกต่างกัน งานวิจัยนี้จึง ได้อธิบายความสัมพันธ์ระหว่างสารปรับผิวกับหมู่ฟังก์ชันที่ไวต่อการพัฒนาสีของสารสี

คำสำคัญ: ใคโทซาน, ไกลซีน, พอลิเอสเทอร์, การพิมพ์อิงก์เจ็ต

7.5 Effects of Ink Formulation Containing Surface-Modified Pigmented Jet Inks on Jettability

Six surface-modified pigmented inkjet inks comprising black, cyan, magenta, yellow, light cyan, and light magenta colors were prepared with a pigment-to-binder ratio of 1:2. Styrene-acrylic acid emulsion was used as a binder. Fluid system composed of diethylene glycol and glycerol was examined by varying their ratios to adjust the ink viscosity. Overall particle size of pigment and polymer emulsion was controlled within the range of 100 to 300 nm. Surface tensions were varied by surfactant concentration. The range of viscosity and surface tension affecting the jettability were investigated. Good jettability range was found in a viscosity-surface tension operation window in each series of ink formulation 5 which could produce the complete test patterns.

Key words: Ink formulation, Surface modified pigment, Viscosity, Surface tension, Ink jet ink, Jetting

ผลขององค์ประกอบของหมึกพิมพ์ในหมึกพิมพ์อิงก์เจ็ตที่มีสารสีดัดแปรผิวต่อการพ่นหมึก

ได้เตรียมหมึกพิมพ์อิงก์เจ็ตประเภทสารสีจากสารสีดัดแปรผิว 6 ชนิด ซึ่งมีสารสีสีดำ สีฟ้าเขียว สี เหลือง สีม่วงแดง สีฟ้าเขียวอ่อน และสีม่วงแดงอ่อน ในสัดส่วนของสารสีต่อสารยึด 1 ต่อ 2 โดยมี อิมัลชั้นของสไตรีนและอะคริลิกแอชิดเป็นสารยึด แปรสัดส่วนของไดเอทีลีนไกลคอลและกลีเซอรอลซึ่ง เป็นระบบของไหลของหมึกพิมพ์ เพื่อปรับความหนืดของหมึกพิมพ์ให้ทำงานได้ ปรับขนาดอนุภาคของ สารสีและขนาดของอนุภาคอิมัลชั้นพอลิเมอร์โดยเฉลี่ยให้อยู่ในช่วง 100 ถึง 300 นาโนเมตร ปรับแรงตึง ผิวของหมึกพิมพ์ด้วยความเข้มขันของสารลดแรงตึงผิวที่คัดเลือก ช่วงของความหนืดและแรงตึงผิวของ หมึกพิมพ์แต่ละสีมีผลต่อความสามารถในการพ่นหมึกพิมพ์ ได้ศึกษาช่วงหน้าต่างที่ให้ขอบเขตของความ หนืดและแรงตึงผิวที่พ่นหมึกพิมพ์ได้ของหมึกพิมพ์แต่ละสีในแต่ละสูตรหมึก พบว่า หมึกพิมพ์อิงก์เจ็ต สูตร 5 ซึ่งสามารถพิมพ์เส้นหมึกทุกสีได้รูปแบบของเส้นสมบรูณ์ที่สุด

คำสำคัญ: สูตรหมึกพิมพ์, สารสีดัดแปรผิว, ความหนืด, แรงตึงผิว, หมึกพิพม์อิงก์เจ็ต, การพ่นหยดหมึก

4. ผลงานที่ได้จากโครงการ

4.1 ผลงานตีพิมพ์ในวารสารวิชาการนานาชาติ/หนังสือ/สิทธิบัตร

ก. ในวารสารวิชาการระดับนานาชาติ

- 1. Nakason, C., Wohmang, T.; Kaesaman, A., Kiatkamjornwong, S. 2010. Preparation of Cassava Starch-Graft-Polyacrylamide Superabsorbents and Associated Composites by Reactive Blending, Carbohydrate Polymers, 81, 348–357.
- 2. Vallapa, N., Wiarachai, O., Thongchul, N., Pan, J., Tangpasuthadol, V., Kiatkamjornwong, S., Hoven, P. V. 2011. Enhancing antibacterial activity of chitosan surface by heterogeneous quaternization, Carbohydrate Polymers, 83, 868—875.
- 3. Noppakundilograt, S., Nanakorn, P., Jinsart, W., Kiatkamjornwong, S. 2010. Synthesis of Acrylamide/acrylic acid-Based Aluminum Flocculant for Dye Reduction and Textile Wastewater Treatment, Polymer Engineering and Science, 50(8), 1535—1546.
- 4. Kangwansupamonkon, W, Jitbunpot, W., Kiatkamjornwong, S. 2010. Photocatalytic efficiency of TiO₂/poly[acrylamide-*co*-(acrylicacid)] composite for textile dye degradation, Polymer Degradation and Stability, 95, 1894 1902.
- 5. Seetapan, N., Wongsawaeng, J., Kiatkamjornwong, S., 2011, Gel strength and swelling of acrylamide-protic acid superabsorbent copolymers, Polymer for Advanced Technologies, DOI: 10.1002/pat.1658, online.
- 6. Foungfung, D., Seetapan, N., Phattanarudee, S., Kiatkamjornwong, S. 2011. Synthesis of acrylamide /itaconic acid superabsorbent polymers and superabsorbent polymer/mica nanocomposites. Polymer for Advanced Technologies, 22, 635 647.
- 7. Limparyoon, N., Seetapan, N., Kiatkamjornwong, S. 2011. Acrylamide/2-acrylamido-2-methylpropane Sulfonic Acid and Associated Sodium Salt Superabsorbent Copolymers with Mica Nanocomposites as Fire Retardants, Polymer Degradation and Stability, 96, 1054 —1063
- 8. Seetapan, N., Nattawut Limparyoon, N., Kiatkamjornwong, S. 2011. Effect of fire retardant on flammability of acrylamide and 2-acrylamido-2-methylpropane sodium sulfonate copolymer nanocomposites, Polymer Degradation and Stability, doi:10.1016/j.polymdegrad stab.2011.06.014

- 9. Seetapan, N., Srisithipantakul, N., and Kiatkamjornwong, S. 2011. Synthesis of acrylamide-co-(itaconic acid) superabsorbent polymers and associated silica superabsorbent polymer composites, Polymer Engineering and Science, 51(4), 764—775.
- 10. Noppakundilograt, S., Buranagul, P. Graisuwan, W., Chawan Koopipat, C., Kiatkamjornwong, S. 2010. Modified Chitosan Pretreatment of Polyester Fabric for Printing by Ink Jet Ink, Carbohydrate Polymers, 82, 1124—1135.
- 11. Chakvattanatham, K., Phattanarudee, S., Kiatkamjornwong, S. 2010. Anionically surface-modified pigment/binder in jet inks for silk fabric printing. Pigment & Resin Technology, 39(6), 327—341.

ข. วารสารในประเทศ

12. Suda Kiatkamjornwong, Boonyakiat Chaitepprasith, Chawan Koopipat, 2010. Measurement of BRDF and Modeling Reflectance of Silk Fabrics, Journal of the Royal Institute of Thailand, 35(1), 109—117.

ค. บทความที่อยู่ระหว่างการแก้ไขและการพิจารณาของวารสาร

- 13. Somporn Chaiarrekij, Apiporn Apirakchaiskul, Kuntinee Suvarnakich, and Suda Kiatkamjornwong, 2011. Kapok I: Properties investigation of kapok fiber as a potential pulp source for papermaking, Bioresources, under revision.
- 14. Noppakundilograt, S., Sonjaipanich, K., Thongchul, N., Kiatkamjornwong, S. 2011. Syntheses, Characterization and Antibacterial Activity of Chitosan Grafted Hydrogels and associated mica containing nanocomposite hydrogels, Journal of Applied Polymer Science, under revision.
- 15. Oraphan Wiarachai, Nuttha Thongchul, Suda Kiatkamjornwong, Voravee P. Hoven, Surface-quaternized chitosan particles as an alternative and effective organic antibacterial filler, Colloids and Surfaces B: Biointerfaces, under review.
- 16. Navagan Rachanark, Varawut Tangpasuthadol, Suda Kiatkamjornwong, Improvement of tensile modulus and tear strength of natural rubber dipped films by vinylated silica generated in situ, Polymer International, under review.
- 17. Stéphane Dubascoux, Chalao Thepchalerm, Eric Dubreucq, Suwaluk Wisunthorn, Laurent Vaysse, Suda Kiatkamjornwong, Charoen Nakason, Frédéric Bonfils. Comparative

study of the mesostructure of natural and synthetic polyisoprene by SEC-MALS and AF4-MALS, Journal of Chromatography A., under review.

- 18. Graisuwan, W.; Ananthanawat, C.; Wiarachai, O.; Puthong, S.; Su, X. D.; Thongchul, N.; Kiatkamjornwong, S.; Hoven, V. P. Multilayer Thin Films Assembled from Charged Derivatives of Chitosan: Formation and Biological Responses, Langmuir, in language check.
- 19. Somporn Chaiarrekij, Thippawan Hommaivai, Kuntinee Suvarnakich, and Suda Kiatkamjornwong, Kapok II: Pretreatment of kapok fibers for pulping and papermaking Bioresources, in revision before submitting to Bioresources.
- 20. Roongkarn Nuisin, Jaruwan Krongsil, Suda Kiatkamjornwong Microencapsulation of menthol via glass membrane emulsification and controlled release, to be submitted to Colloids and Surfaces A: Physicochemicals and Engineering Aspects, in language check.
- 21. Charoen Nakason, Yeampon Nakaramontee, Azizon Kaesaman, Wiyong Kangwansukpamonkon, and Suda Kiatkamjornwong' Synthesis and Characterization of Water Swellable Natural Rubber Composites, in final check of figures and tables.

ง. บทความที่จะร่างจากงานวิจัยที่เพิ่งปิดโครงการวิจัยเมื่อเดือนพฤษภาคม 2554

- 22. Supaporn Noppakundilograt, Thayarat Petcharat, Suda Kiatkamjornwong. Synthesis and characterization of controlled released NPK fertilizer hydrogel.
- 23. Wiyong Kangwansupamonkon, Wailawan Tiertrakulwattana, Pitt Suphapol, Suda Kiatkamjornwong. Surface modification of electrospun chitosan nanofiber for antibacterial activity.
- 24. Wasinee Sakathok, Suda Kiatkamjornwong, Varawut Tangpasuthadol. Physical properties of MMA grafted natural rubber film reinforced with *in situ* generated silica.
- 25. Sopinya Choopromkaw, Supaporn Noppakundilograt, Suda Kiatkamjornwong, 2010, Synthesis, characterization and controlled release of hydrogel from collagen grafted poly[(acrylic acid)-co-(methacrylic acid)]

จ. สิทธิบัตร

1. สุดา เกียรติกำจรวงศ์, วลาสินี จิตบรรพต, วิยงค์ กังวานศุภมงคล, กนิษฐา บุญภาวาณิชกุล
คอมพอสิตพอลิเมอร์ดูดซึมน้ำมากที่สามารถแตกสลายตัวเองได้โดยอาศัยการกระตุ้นด้วยรังสี
อัลตราไวโอ เลต เลขที่คำขอ 1001001273 วันที่ 26 กันยายน 2553

- สุดา เกียรติกำจรวงศ์, ณัฐวุฒิ ลิมประยูร, นิสภา ศีตปันย์ 2553 เจลอิมัลชันวัสดุเชิงประกอบ พอลิเมอร์ดูดซึมน้ำมากและเจลอิมัลชันพอลิเมอร์ดูดซึมน้ำมากที่มีสมบัติหน่วงการติดไฟ เลขที่คำขอ 1101000208 วันที่ 15 กุมภาพันธ์ 2554
- 3. สุดา เกียรติกำจรวงศ์ สุภาภรณ์ นพคุณดิลกรัตน์ ณัฏฐ์ธยาน์ เพชรรัตน์ ปุ๋ยละลายช้าและ กรรมวิธีการผลิตปุ๋ยละลายช้าดังกล่าว ยื่นผ่านสถาบันทรัพย์สินทางปัญญาเมื่อ 1 มิถุนายน 2554 ขณะนี้รอทางสถาบันพิจารณาแก้ไขเนื้อหาในแง่กฎหมาย คาดว่าจะสามารถส่งไปยังกรมทรัพย์สินทาง ปัญญาในเดือนกันยายน 2554
- 4. สุดา เกียรติกำจรวงศ์ สุภาภรณ์ นพคุณดิลกรัตน์ สวเนตร์ วงศ์แป้น ลิตสา วงศ์ศิริทรัพย์ สารปรับสภาพผิวผ้าจากไคโทซานดัดแปรละลายน้ำได้สำหรับการพิมพ์ระบบอิงก์เจ็ต ยื่นผ่านสถาบัน ทรัพย์สินทางปัญญาเมื่อ 10 พฤษภาคม 2554 ขณะนี้รอทางสถาบันพิจารณาแก้ไขเนื้อหาในแง่ กฎหมาย คาดว่าจะสามารถส่งไปยังกรมทรัพย์สินทางปัญญาในเดือนกันยายน 2554
- 5. สุดา เกียรติกำจรวงศ์ สุภาภรณ์ นพคุณดิลกรัตน์ ปัญฑ์ธร บูรณะกูล สารปรับสภาพผิวผ้า จากไคโท ซานดัดแปรสำหรับผ้าพิมพ์ด้วยหมึกพิมพ์อิงก์เจ็ต ยื่นผ่านสถาบันทรัพย์สินทางปัญญาเมื่อ 2 มิถุนายน 2554 ขณะนี้รอทางสถาบันพิจารณาแก้ไขเนื้อหาในแง่กฎหมาย คาดว่าจะสามารถส่งไปยัง กรมทรัพย์สินทางปัญญาในเดือนกันยายน 2554

4.2 ความก้าวหน้าในการสร้างทีมวิจัย

4.2.1 การสำเร็จการศึกษาของนักศึกษาปริญญาเอกและปริญญาโท

- 1. นางสาวจิราพร วงแสวง นิสิตปริญญามหาบัณฑิต สาขาวิชาปิโตรเคมีและวิทยาศาสตร์พอลิ เมอร์ คณะวิทยาศาสตร์ จุฬาลงกรณ์มหาวิทยาลัย สำเร็จการศึกษาเดือนพฤษภาคม พ.ศ. 2551
- 2. นางสาววิไลพร ไกรสุวรรณ ปริญญาโท หลักสูตรปิโตรเคมีและวิทยาศาสตร์พอลิเมอร์ คณะ วิทยาศาสตร์ จุฬาลงกรณ์มหาวิทยาลัย สำเร็จการศึกษาในเดือน พฤษภาคม พ.ศ. 2551
- 3. นางสาวรันยา บุญเวช สาขาเทคโนโลยียางและวิทยาการพอลิเมอร์ มหาวิทยาลัยสงขลา นครินทร์ วิทยาเขตปัตตานี สำเร็จการศึกษาเดือนพฤษภาคม พ.ศ. 2551
- 4. นางสาววลาสินี จิตรบรรพต นิสิตปริญญามหาบัณฑิต สาขาวิชาปิโตรเคมีและวิทยาศาสตร์ พอลิเมอร์ คณะวิทยาศาสตร์ จุฬาลงกรณ์มหาวิทยาลัย สำเร็จการศึกษาเดือนพฤษภาคม พ.ศ. 2551
- 5. นายอภิพร อภิรักษ์ชัยสกุล ปริญญาโท หลักสูตรเทคโนโลยีเยื่อและกระดาษ คณะ วิทยาศาสตร์จุฬาลงกรณ์มหาวิทยาลัย สำเร็จการศึกษาในเดือนพฤษภาคม พ.ศ. 2551
- 6. นายกิตติชัย สนใจพาณิชย์ ปริญญาโท หลักสูตรปิโตรเคมีและวิทยาศาสตร์พอลิเมอร์ คณะ วิทยาศาสตร์ จุฬาลงกรณ์มหาวิทยาลัย สำเร็จการศึกษาในเดือนพฤษภาคม พ.ศ. 2552

- 7. นางสาวซารีนา ซะยานัย สาขาเทคโนโลยียางและวิทยาการพอลิเมอร์มหาวิทยาลัยสงขลา นครินทร์ วิทยาเขตปัตตานี สำเร็จการศึกษาเดือนพฤษภาคม พ.ศ. 2552
- 8. นางสาวอรพรรณ เวียระชัย ปริญญาโท หลักสูตรปิโตรเคมีและวิทยาศาสตร์พอลิเมอร์ คณะ วิทยาศาสตร์ จุฬาลงกรณ์มหาวิทยาลัย สำเร็จการศึกษาในเดือนพฤษภาคม พ.ศ. 2553
- 9. นายนายตออา เวอะเม็ง สาขาเทคโนโลยียางและวิทยาการพอลิเมอร์มหาวิทยาลัยสงขลา นครินทร์ วิทยาเขตปัตตานี สำเร็จการศึกษาเดือนพฤษภาคม พ.ศ. 2553
- 10. นายเยี่ยมพล นัครามนตรี สาขาเทคโนโลยียางและวิทยาการพอลิเมอร์มหาวิทยาลัยสงขลา นครินทร์ วิทยาเขตปัตตานี สำเร็จการศึกษาเดือนพฤษภาคม พ.ศ. 2553
- 11. นายณัฐวุฒ ลิ้มประยูร ปริญญาโท หลักสูตรปิโตรเคมีและวิทยาศาสตร์พอลิเมอร์ คณะ วิทยาศาสตร์ จุฬาลงกรณ์มหาวิทยาลัย สำเร็จการศึกษาในเดือนพฤษภาคม พ.ศ. 2553
- 12. นางสาวจิตติมา มีบึงพร้าว ปริญญาโท หลักสูตรปิโตรเคมีและวิทยาศาสตร์พอลิเมอร์ คณะ วิทยาศาสตร์ จุฬาลงกรณ์มหาวิทยาลัย สำเร็จการศึกษาในเดือนพฤษภาคม พ.ศ. 2553
- 13. นายนวกานต์ ราชนาค ปริญญาโท หลักสูตรปิโตรเคมีและวิทยาศาสตร์พอลิเมอร์ คณะ วิทยาศาสตร์ จุฬาลงกรณ์มหาวิทยาลัย สำเร็จการศึกษาในเดือนพฤษภาคม พ.ศ. 2553
- 14. นายบุญยเกียรติ ฉายเทพประสิทธิ์ ปริญญาโท หลักสูตรเทคโนโลยีทางภาพ คณะ วิทยาศาสตร์ จุฬาลงกรณ์มหาวิทยาลัย สำเร็จการศึกษาในเดือนพฤษภาคม พ.ศ. 2553
- 15. นางสาวทิพย์วรรณ หอมไม่วาย ปริญญาโท หลักสูตรเทคโนโลยีเยื่อและกระดาษ คณะ วิทยาศาสตร์ จุฬาลงกรณ์มหาวิทยาลัย สำเร็จการศึกษาในเดือนพฤษภาคม พ.ศ. 2554
- 16. นางสาวณัฏฐ์ธยาน์ เพชรรัตน์ นิสิตปริญญาโท หลักสูตรปิโตรเคมีและวิทยาศาสตร์พอลิ เมอร์ คณะวิทยาศาสตร์ จุฬาลงกรณ์มหาวิทยาลัย สำเร็จการศึกษาในเดือนพฤษภาคม พ.ศ. 2554
- 17. นางสาวจารุวรรณ ครองศิลป์ นิสิตปริญญาโท หลักสูตรปิโตรเคมีและวิทยาศาสตร์พอลิเมอร์ คณะวิทยาศาสตร์ จุฬาลงกรณ์มหาวิทยาลัย สำเร็จการศึกษาในเดือนพฤษภาคม พ.ศ. 2554
- 18. นางสาวโสภิญญา ชูพรมแก้ว นิสิตปริญญาโท หลักสูตรปิโตรเคมีและวิทยาศาสตร์พอลิเมอร์ คณะวิทยาศาสตร์ จุฬาลงกรณ์มหาวิทยาลัย สำเร็จการศึกษาในเดือนพฤษภาคม พ.ศ. 2554
- 19. นางสาวสันนิภา พัฒนปิยะทรัพย์ นิสิตปริญญาตรี หลักสูตรเทคโนโลยีทางภาพและการ พิมพ์ คณะวิทยาศาสตร์ จุฬาลงกรณ์มหาวิทยาลัย สำเร็จการศึกษาในเดือนพฤษภาคม พ.ศ. 2554
- 20. นางสาวสุทธาทิพย์ เลขาลาวัณย์นิสิตปริญญาตรี หลักสูตรเทคโนโลยีทางภาพและการพิมพ์ คณะวิทยาศาสตร์ จุฬาลงกรณ์มหาวิทยาลัย สำเร็จการศึกษาในเดือนพฤษภาคม พ.ศ. 2554
- 21. นางสาวสุภาณี พิพัฒน์วิทยา นิสิตปริญญาตรี หลักสูตรเทคโนโลยีทางภาพและการพิมพ์ คณะวิทยาศาสตร์ จุฬาลงกรณ์มหาวิทยาลัย สำเร็จการศึกษาในเดือนพฤษภาคม พ.ศ. 2554

4.2.2 จำนวนหัวหน้าโครงการและนักวิจัยประจำโครงการ ณ วันที่ 1 สิงหาคม 2554

รายนามกลุ่มวิจัย ปี 2550-2554

1. อาจารย์นักวิจัย

		เริ่มร่วมเข้าโครงการ			สถานภาพปัจจุบัน
ชื่อ-นามสกุล	ตำแหน่งวิชาการ	สังกิด	ตำแหน่งใน	ตำแหน่งวิชาการ	ตำแหน่งอื่น
			โครงการ		
1. ୭ኜ. ଜ୍ଡା	ศาสตราจารย์ 11	รถเนากาพการการและ	หัวหน้าโครงการ	ศาสตราจารย์ 11 หรือ	
เกียรติกำจรวงศ์		เทคโนโลยีทางการพิมพ์ คณะ		ศาสตราจารย์ A 1	
		วิทยาศาสตร์ จุฬาลงกรณ์			
		มหาวิทยาลัย			
2. ดร. พิชช์ ศุภผล	รองศาสตราจารย์ 9	วิทยาลัยปิโครเลียมและปิโตร	นักวิจัยและ	ศาสตราจารย์ A2	
		เคมี จุฬาลงกรร์มหาวิทยาลัย	อาจารย์ที่ปรึกษา	(ศาสตราจารย์ ระดับ	
			ร่าม	10)	
3. ดร. เจริญ	รองศาสตราจารย์ 9	eพระทะเส _ร ียามาผนเชริคกก	หัวหน้าโครงการ	รองศาสตราจารย์ 9	คณบดี คณะวิทยาศาสตร์และเทคโนโลยี
นาคะสรรค์		ลิเมอร์ คณะวิทยาศาสตร์ และ	ย ១ខា		มหาวิทยาลัยสงขลานครินทร์
		เทคโนโลยี มหาวิทยาลัยสงขลา			วิทยาเขตปัตตานี
		นคริน วิทยาเขตป์ตตานี			
4. ตร. วรวีร์	ผู้ช่วยศาสตราจารย็	ภาควิชาเคมี คณะวิทยาศาสตร์	หัวหน้าโครงการ	รองศาสตราจารย์ 9	
โฮ่เวน	8	จุฬาลงกรณ์มหาวิทยาลัย	ย่อย		
5. ดร. ธีรยุทธ วิใล	รองศาสตราจารย์ 9	ภาควิชาเคมี คณะวิทยาศาสตร์	นักวิจัยและ	รองศาสตราจารย์ 9	อยู่ในขั้นตอนการพิจารณาตำแหน่ง
วัลย์		จุฬาลงกรณ์มหาวิทยาลัย	อาจารย์ที่ปรึกษา		ศาสตราจารย์ ระดับ 10

			ร่าม		
6. ตร. วราวุฒิ	ผู้ช่วยศาสตราจารย์	ภาควิชาเคมี คณะวิทยาศาสตร์	หัวหน้าโครงการ	ผู้ช่วยศาสตราจารย์ 8	
ะ ตงพสุธาดล	7	จุฬาลงกรณ์มหาวิทยาลัย	ย่ อย		
7. อาซีซัน	รองศาสตราจารย์ 8	ลาเทคโนโลยียางและพอ เ	นักวิจัย	รองศาสตราจารย์ 9	รองคณบดี
แกสมาน		ลิเมอร์ คณะวิทยาศาสตร์ และ			คณะวิทยาศาสตร์และเทคโนโลยี
		เทคโนโลยี มหาวิทยาลัยสงขลา			มหาวิทยาลัยสงขลานครินทร์
		นคริน วิทยาเขตปัตตานี			
8. ตร. สุภาภรณ์	นั้ช่วยศาสตราจารย็	ภาควิชา วท. ภาพถ่ายและ	หัวหน้าโครงการ	ผู้ช่วยศาสตราจารย์ 8	รองหัวหน้าภาควิชา ภาควิชา วท.
นพคุณดิลกรัตน์	7	เทคโนโลยีทางการพิมพ์ คณะ	₂ ខំខំខ		ภาพถ่ายและเทคโนโลยีทางการพิมพ์
		วิทยาศาสตร์ จุฬาลงกรณ์			คณะวิทยาศาสตร์ จุฬาลงกรณ์
		มหาวิทยาลัย			มหาวิทยาลัย
9. ตร. ชวาล	ผู้ช่วยศาสตราจารย์	ภาควิชา วท. ภาพถ่ายและ	หัวหน้าโครงการ	นักวิจัย	
คูร์พิพัฒน์	ระดับ 7	เทคโนโลยีทางการพิมพ์ คณะ	₂ ខំខ		
		วิทยาศาสตร์ จุฬาลงกรณ์			
		มหาวิทยาลัย			
10. ดร. นิสภา คีต	นักวิจัย P 3	ศูนย์เทคโนโลยีโลหะและวัสดุ	หัวหน้าโครงการ	นักวิจัย P 3	
ประย์		แห่งชาติ สำนักพัฒนา	ย่อย		
		วิทยาศาสตร์และเทคโนโลยี			
		แห่งชาติ กระทรวงวิทยาศาสตร์			
		และเทคโนโลยี			
11. ตร. รุ่งกานต์	อาจารย์พนักงาน	ภาควิชาวิทยาศาสตร์ทั่วไป	หัวหน้าโครงการ	นี้ช่วยศาสตราจารย์	

น้ยสินฏ์	มหาวิทยาลัย A 5	คณะวิทยาศาสตร์ จุพาลงกรณ์	ย่อย	พนักงานมหาวิทยาลัย	
		มหาวิทยาลัย		A 4	
12. ดร. วิยงค์	นักวิจัย P 3	ศูนย์นาโนเทคโนโลยีแห่งชาติ	หัวหน้าโครงการ	นักวิจัย P 3	หัวหน้าโครงการศูนย์วิจัย ศูนย์นาโน
กังวานศุภมงคล		สำนักพัฒนาวิทยาศาสตร์และ	ย่อย		เทคโนโลยีแห่งชาติ
		เทคโนโลยีแห่งชาติ			
		กระทรวงวิทยาศาสตร์ และ			
		เทคโนโลยี			
13. สมพร ชัยอารีย์	อาจารย์พนักงาน	ภาควิชา วท. ภาพถ่ายและ	หัวหน้าโครงการ	อาจารย์พนักงาน	
กิจ	มหาวิทยาลัย A 5	เทคโนโลยีทางการพิมพ์ คณะ	₂ ខេខ	มหาวิทยาลัย A 5	
		วิทยาศาสตร์ จุฬาลงกรณ์			
		มหาวิทยาลัย			
14 ตร. กุนทินี	อาจารย์พนักงาน	ภาควิชา วท. ภาพถ่ายและ	นักวิจัย	อาจารย์พนักงาน	
สุวรรณกิจ	มหาวิทยาลัย A 5	เทคโนโลยีทางการพิมพ์ คณะ		มหาวิทยาลัย A 5	
		วิทยาศาสตร์ จุฬาลงกรณ์			
		มหาวิทยาลัย			

2. รายหามหิสิตผู้ช่วยวิจัยที่กำลังศึกษา

		เริ่มร่วมเข้าโครงการ	
ชื่อ-นามสกุล	สาขา/ระดับการศึกษา	สังกิด	ประมาณการการสำเร็จการศึกษา
นางสาววลัยวัลย์ เตียวตระกูลวัฒน	ปิโตรเคมี ฯ /โท	คณะวิทยาศาสตร์ จุฬาลงกรณ์มหาวิทยาลัย	ภาคตัน ปีการศึกษา 2554
นางสาววาสินี สากะโทก	ปิโตรเคมี ฯ /โท	คณะวิทยาศาสตร์ จุฬาลงกรณ์มหาวิทยาลัย	ภาคตัน ปีการศึกษา 2555
นางสาวเพียงหทัย พิบูลย์	ปิโตรเคมี ฯ /โท	คณะวิทยาศาสตร์ จุฬาลงกรณ์มหาวิทยาลัย	ภาคตัน ปีการศึกษา 2555
นางสาวนิสารัตน์ อณสุววรณ์	ปิโตรเคมี ฯ /โท	คณะวิทยาศาสตร์ จุฬาลงกรณ์มหาวิทยาลัย	ภาคตัน ปีการศึกษา 2555
นายนที คล้ายแก้ว	ปิโตรเคมี ฯ /โท	คณะวิทยาศาสตร์ จุฬาลงกรณ์มหาวิทยาลัย	ภาคตัน ปีการศึกษา 2555
นางสาวปียะพร อรรคฮาต	ปิโตรเคมี/เอก	คณะวิทยาศาสตร์ จุฬาลงกรณ์มหาวิทยาลัย	ภาคปลาย ปีการศึกษา 2554
นางสาววิไลพร ไกรสุวรรณ	ปิโตรเคมี/เอก	คณะวิทยาศาสตร์ จุฬาลงกรณ์มหาวิทยาลัย	ภาคต้น ปีการศึกษา 2555
นางสาวเฉลา เทพเฉลิม	เทคโนโลฮ็พอลิเมอร์/	คณะบัณฑิตวิทยาลัย มหาวิทยาลัยสงขลานครินทร์ (วิทยา	ภาคตัน ปิการศึกษา 2556
	เอก	เขตปัตตานี)	

4.3 การนำผลจากโครงการไปใช้ประโยชน์

ได้ประชาสัมพันธ์ผลงานบางประเภทสู่นักข่าวและหนังสือพิมพ์ ดังตัวอย่างข่าวที่ได้ประชาสัมพันธ์ ไปยังสื่อต่าง ๆ ดังตัวอย่างการประชาสัมพันธ์ 1 เรื่อง



ข่าวประชาสัมพันธ์

นักวิจัยจุฬาฯ ผลิตกรีนพอลิเมอร์ย่อยสลายเร็วด้วยรังสีอัลตราไวโอเลต

ปัจจุบันพอลิเมอร์ดูดซึมน้ำมาก หรือไฮโดรเจล เป็นที่สนใจและถูกนำไปใช้ประโยชน์ใน อุตสาหกรรมหลายด้าน เนื่องจากมีความสามารถในการดูดซึมน้ำได้สูง มีสมบัติในการบวมน้ำและ สามารถเก็บกักน้ำไว้ในโครงสร้างได้มากกว่า 20 เท่าของน้ำหนักพอลิเมอร์แห้งและไม่ละลายน้ำ

ในด้านเกษตรกรรม มีการนำพอลิเมอร์ดูดซึมน้ำมากไปใช้ในการทำสวนประดับ ซึ่งจะช่วยใน การปรับปรุงคุณภาพดิน โดยเพิ่มความสามารถในการกักเก็บน้ำ และปล่อยน้ำสู่ดินและรากพืช เป็น การรักษาความสมดุลของความชื้นในดิน และช่วยกักเก็บสารอาหารของพืชที่ละลายในเจลพอลิเมอร์

ขณะที่ด้านอุตสาหกรรม มีการนำพอลิเมอร์ดูดซึมน้ำมากมาใช้ทำผลิตภัณฑ์เพื่อสุขอนามัย ผ้าอ้อมเด็ก ผ้าอ้อมผู้สูงวัย และผ้าอ้อมผู้ป่วย กระดาษชำระ เป็นต้น ด้านการแพทย์ได้นำไปทำ ผ้าพันแผล ใช้เป็นสารควบคุมอัตราการปล่อยยาสำหรับผู้ป่วย ด้านอาหารนำมาใช้เป็นสารป้องกันการ รั่วซึมของของเหลวในภาชนะบรรจุอาหาร นอกจากนี้ยังนำมาใช้ในงานด้านอื่น ๆเช่น สารดับเพลิง หิมะเทียม หมึกพิมพ์ เป็นต้น

อย่างไรก็ตามพอลิเมอร์ดังกล่าวส่วนใหญ่เป็นผลิตภัณฑ์จากปิโตรเคมี ซึ่งต้องใช้ระยะเวลา ยาวนานหลายร้อยปีในการแตกสลาย หรือไม่สามารถแตกสลายได้เองตามธรรมชาติ ประกอบกับ ปัจจุบันมีแนวโน้มการใช้พอลิเมอร์ดูดซึมน้ำมากเพิ่มขึ้นอย่างชัดเจน จึงก่อให้ขยะและปัญหาด้าน สิ่งแวดล้อมตามมา ขณะนี้หลายประเทศเริ่มตื่นตัวและพยายามหาทางแก้ไขพัฒนาวัสดุต่างๆ ที่จะ สามารถแตกสลายได้เองตามธรรมชาติ

ศ.ดร.สุดา เกียรติกำจรวงศ์ เมธีวิจัยอาวุโส สกว. ภาควิชาวิทยาศาสตร์ทางการพิมพ์และ เทคโนโลยีทางการพิมพ์ คณะวิทยาศาสตร์ จุฬาลงกรณ์มหาวิทยาลัย ได้รับการสนับสนุนทุนวิจัยจาก ฝ่ายวิชาการ สำนักงานกองทุนสนับสนุนการวิจัย (สกว.) เพื่อทำวิจัยและพัฒนาวัสดุพอลิเมอร์สีเขียว และประโยชน์ใช้งาน

ศ.ดร.สุดา เปิดเผยว่า คณะวิจัยได้ผลิตพอลิเมอร์คอมพอสิตดูดซึมน้ำมากที่มีลักษณะเป็นก้อน วุ้นหรือเจลใส หรือเป็นของเหลวที่มีความหนืดสูงและตกตะกอนก้อนเจลที่ได้เป็นก้อนแข็งและบดให้มี ขนาดเล็กต่อไป พอลิเมอร์ที่ผลิตได้นี้สามารถดูดซับสีย้อมสิ่งทอและสามารถแตกสลายทั้งสีย้อมและ ตนเองได้ โดยอาศัยการกระตุ้นด้วยรังสีอัลตราไวโอเลตจากแหล่งกำเนิดรังสีหรือจากดวงอาทิตย์ที่มาก พอ ทำให้เกิดการเปลี่ยนแปลงสมบัติและโครงสร้างทางเคมีจนแตกสลายภายในเวลาอันรวดเร็วเพียง พอที่จะไม่ทำให้เกิดการสะสมของเสียต่อภาวะแวดล้อม นอกจากนี้พอลิเมอร์คอมพอสิตดูดซึมน้ำมาก ยังสามารถดูดซับและแตกสลายสีย้อมสิ่งทดที่ก่อให้เกิดน้ำเสียหลังกระบวนการย้อมเสร็จสิ้นได้อีกด้วย

จากการทดสอบการแตกสลายสีย้อมของสิ่งทอ พบว่าสีย้อมที่ถูกดูดซับด้วยพอลิเมอร์คอมพอ สิตดูดซึมน้ำมาก จะแตกสลายได้หมดภายใต้รังสีอัลตราไวโอเลตเป็นเวลา 20-40 นาที และเมื่อฉายใน ระยะเวลา 24 ชั่วโมง พอลิเมอร์คอมพอสิตดูดซึมน้ำมากจะแตกสลายกลายเป็นของเหลวใสจนเหลือ เพียงอนุภาคไททาเนียมไดออกไซด์ปริมาณน้อยมาก

"พอลิเมอร์ดังกล่าวจัดได้เป็นวัสดุสีเขียวที่สามารถช่วยลดปัญหาสิ่งแวดล้อม และเป็นวัสดุที่ สามารถนำมาใช้กับอุตสาหกรรมได้หลากหลายประเภท เนื่องจากมีความสามารถในการแตกสลายตัว เองได้ภายใต้รังสีอัลตราไวโอเลตในระยะเวลาอันสั้น จึงมีประโยชน์ทั้งในด้านธุรกิจ สังคม และ สิ่งแวดล้อม อีกทั้งสามารถตอบสนองความต้องการของผู้บริโภคอีกด้วย ซึ่งงานวิจัยนี้ได้ยื่นจดสิทธิบัตร เป็นที่เรียบร้อยแล้ว" ศ.ดร.สุดากล่าวสรุป

นิธิปรียา จันทวงษ์ เจ้าหน้าที่บริหารโครงการ ฝ่ายวิชาการ สกว. 0-2278-8249

5 กิจกรรมอื่น ๆ ที่ เกี่ยวข้อง

- 5.1 ผลงานอื่น ๆ เช่น การไปเสนอผลงาน การได้รับเชิญไปเป็นวิทยากร การได้รับรางวัล
 - **ก. การนำเสนอผลงานของผู้ช่วยวิจัยระดับปริญญาโทในการประชุม**ต่าง ๆ ดังนี้
- 1. อภิพร อภิรักษ์ชัยสกุล, กุนทินี สุวรรณกิจ, สมพร ชัยอารีย์กิจ และ สุดา เกียรติกำจรวงศ์, "การใช้ เส้นใยนุ่นในการปรับปรุงสมบัติกระดาษ", การประชุมวิชาการ "นเรศวรวิจัย" ครั้งที่ 4: การบริหาร นวัตกรรม, คณะวิทยาศาสตร์ มหาวิทยาลัยนเรศวร, พิษณุโลก, 28-29 กรกฎาคม 2551.
- 2. <u>Graisuwan, W.;</u> Kiatkamjornwong, S. Hoven, V. P. Formation and Biocompatibility of Multilayer Film Assembled From Charged Derivatives of Chitosan 33rd Congress on Science and Technology of Thailand at Walailak University, October 18-20, 2007, บทความผู้จัดทำหายไป จากเอกสารการประชุม จึงไม่มีข้อมูลของเอกสาร
- 3. <u>Graisuwan, W.;</u> Kiatkamjornwong, S. Hoven, V. P. Formation and Biocompatibility of Multilayer Film Assembled From Charged Derivatives of Chitosan, Proceedings of the 3rd Mathematics & Physical Science International Graduate Congress, December 12-14, 2007, A038 with a poster, pp. 322-326.
- 4. <u>Walasinee Jitbunpot</u>, Wiyong Kangwansupamonkon, Suda Kiatkamjornwong, "Removal Efficiency of Methylene Blue Dye Using TiO₂/Poly[acrylamide-co-(acrylic acid)] Composites", Proceedings of the 34th Congress on Science and Technology of Thailand 2008, The Queen Sirikit National Convention Center, Bangkok, Thailand, Oct 31- Nov 2, 2008, STT 34 F_F0003.
- 5. <u>Walasinee Jitbunpot</u>, Suda Kiatkamjornwong, Wiyong Kangwansupamonkon, "Preparation and Dye Removal Efficiency Study Using Nano TiO₂/Poly[acrylamide-co-(acrylic acid)] Composite", Proceedings of the 1st Biannual NanoThailand Symposium, 2008, The Queen Sirikit National Convention Center, Bangkok, Thailand, Nov 6-8, 2008, T64, pp. 290-294.
- 6. <u>Hoven, V. P.</u>; Vallapa, N.; Thongchul, N.; Tangpasuthadol, V.; Kiatkamjornwong, S. "Antibacterial Activity of Surface-quaternized Chitosan" *The 42*nd *IUPAC World Polymer Congress (MACRO 2008), Polymer at Frontiers of Science and Technology*, June 29 July 4, 2008, Taipei, Taiwan, Poster.
- 7. <u>Punthorn Buranagul</u>, Supaporn Noppakundilograt, Suda Kiatkamjornwong. Pretreatment of Polyester Fabric Surface with Chitosan Solution for Ink Jet Printing, Proceedings of 34th Congress on Science and Technology of Thailand at Queen Sirikit National Convention Center, October 31-November 2, 2008, STT34_E_E0118.

- 8. <u>Kittichai Sonjaipanich</u>, Supaporn Noppakundilograt, Nuttha Thongchul, Suda Kiatkam-jornwong, Synthesis of Grafted Chitosan Poly[(acrylic acid)-co-(2-hydroxyethyl methacrylate)] Hydrogels for Antibacterial Activity, Proceedings of 34th Congress on Science and Technology of Thailand at Queen Sirikit National Convention Center, October 31 November 2, 2008, STT34 E E0051.
- 9. <u>Wiarachai, O.</u>; Thongchul, N.; Kiatkamjornwong, S.; Hoven, V. P. "Development of Antibacterial Fillers from Quaternized Chitosan Particles" *The* 5th *National Chitin-Chitosan Conference* July 24-25, **2008**, Bangkok, Thailand, Oral
- 10. <u>Graisuwan, W.</u>; Puthong, S.; Kiatkamjornwong, S.; Hoven, V. P. "Formation and Biocompatibility of Multilayer Films Assembled from Charged Derivatives of Chitosan" *The* 5th *National Chitin-Chitosan Conference* July 24-25, **2008**, Bangkok, Thailand, Oral
- 11. <u>Meebungpraw, J.</u>; Vilaivan, T.; Kiatkamjornwong, S.; Hoven, V. P. "Determination of DNA Sequences Using Quaternized Chitosan Particles in Combination with MALDI-TOF Mass Spectrometry" *The 2nd Polymer Graduate Conference in Thailand*, May 21-22, **2009**, Chulalongkorn University, Bangkok, Thailand, Poster
- 12. <u>Wiarachai, O.</u>; Thongchul, N.; Kiatkamjornwong, S.; Hoven, V. P. "Quaternary Ammonium-containing Chitosan Particles: Preparation and Antibacterial Activity" *Pure and Applied Chemistry International Conference 2009*, January 14-16, **2009**, Naresuan University, Phitsanulok, Thailand, Poster
- 13. <u>Meebungpraw, J.</u>; Vilaivan, T.; Kiatkamjornwong, S.; Hoven, V. P. "Detection of DNA-PNA Hybridization using Quaternized Chitosan Particles in Combination with MALDI-TOF Mass Spectrometry" *Pure and Applied Chemistry International Conference 2009*, January 14-16, **2009**, Naresuan University, Phitsanulok, Thailand, Poster.
- 14. Meebungpraw, J.; Vilaivan, T.; Kiatkamjornwong, S.; <u>Hoven, V. P</u>. "Determination of DNA Sequences using Peptide Nucleic Acid in Combination with Chitosan Particles by MALDI-TOF Mass Spectrometry" *The 11th Pacific Polymer Conference*, December 6-10, **2009**, Cairns, Australia, Poster.
- 15. <u>Limprayoon, N.</u>, Seetapan, N., and Kiatkamjornwong, S., "Water absorbency of superabsorbent copolymer of acrylamide/2-acrylamido-2-methylpropane sulfonic acid and its sodium salt" *presented in The 2nd Polymer Graduate Conference of Thailand, 21-22 May 2009*, Bangkok, Thailand, pp. 57-61.

- 16. <u>Jaruwan Krongsin</u>, Supaporn Noppakundilograt, Roongkan Nuisin, Suda Kiatkamjornwong, 2010. Microencapsulation of menthol by crosslinked chitosan via porous glass membrane emulsification technique, Proceedings of the First Polymer Conference of Thailand, October 7-8, 2010 at the Convention Center, Chulabhorn Research Institute, Bangkok, pp. 264-269.
- 17. <u>Natthaya Pheatcharat</u>, Supaporn Noppakundilograt, Suda Kiatkamjornwong, 2010, Synthesis and characterization of prolonged-dissolution NPK fertilizer hydrogel, Proceedings of the First Polymer Conference of Thailand, October 7-8, 2010 at the Convention Center, Chulabhorn Research Institute, Bangkok, pp. 124-129.
- 18. <u>Sopinya Choopromkaw</u>, Supaporn Noppakundilograt, Suda Kiatkamjornwong, 2010, Synthesis and characterization of hydrogel from collagen grafted poly[(acrylic acid)-co-(methacrylic acid)], Proceedings of the First Polymer Conference of Thailand, October 7-8, 2010 at the Convention Center, Chulabhorn Research Institute, Bangkok, pp. 165-170.
- 19. <u>Wilaiwan.Tiawtrakoonwat</u> Pitt Supapho, Wiyong Kangwansupamonkon, Suda Kiatkamjornwong, Surface modification of electrospun chitosan nanofiber, Pure and Applied Chemistry International Conference (PACCON2011), Jan 5-7 2011 at the Miracle Grand Hotel, Bangkok, pp. 465-468.
- 20. <u>Chawan Koopipat,</u> Boonyakiat Chaitepprasith and Suda Kiatkamjornwong, Modeling BRDF of Silk Fabric by modifying Phong Reflection Model, oral presentation in The 31st International Congress on Imaging Science (ICIS2010) Beijing May 12 16, 2010, in Proceedings, pp. 98-101.
- 21. <u>Hommaivai, T.</u>, Suvarnakich, K., Chaiarrekij, S., and Kiatkamjornwong, S., "Alkali Pretreatment of Kapok Fibers for Pulping and Papermaking", the 1st Polymer Conference of Thailand, the Convention Center of Chulabhorn Research Institute, Bangkok, Thailand, October 7-8, 2010 pages 118-123. (หมายเหตุ: ได้รับรางวัล the best oral presentation award in Polymers for Food and Agriculture).
- 22. สันนิภา พัฒนปิยะทรัพย์, สุทธาทิพย์ เลขาลาวัณย์, สุภาณี พิพัฒน์วิทยา, สมพร ชัยอารีย์กิจ และ สุดา เกียรติกำจรวงศ์, "การใช้เยื่อนุ่นในการปรับปรุงสมบัติของกระดาษรีไซเคิล", การประชุมวิชาการ ครั้งที่ 19 ประจำปี 2554 (The Science Forum 2011), คณะวิทยาศาสตร์ จุฬาลงกรณ์มหาวิทยาลัย, กรุงเทพมหานคร, 10-11 มีนาคม 2554 (หมายเหตุ: ได้รับรางวัลชนะเลิศอันดับที่ 1 The Hitachi Trophy 2011 สาขาวิทยาศาสตร์ประยุกต์และเทคโนโลยี) บทคัดย่อ

- 23. Sae-ung, P.; Meebungpraw, J.; Tumcharern, G.; Vilaivan, V.; Kiatkamjornwong, S.; <u>Hoven, V. P.</u> "Featuring Biosensing Applications of Chitosan" *Pure and Applied Chemistry International Conference 2011*, January 5 7, 2011, Miracle Grand Hotel, Bangkok, Thailand, Invited presentation.
- 24. <u>Chalao Thepchalerm</u>, Stephane Dubascoux1, Eric Dubreucq, Suwaluk Wisunthorn, Laurent Vaysse, Suda Kiatkamjornwong, Charoen Nakason, Frederic Bonfils. Characterization of Natural Rubber Mesostructure by Size-Exclusion Chromatography (SEC) and Asymmetric Flow Field-Flow Fractionation (AF4) Coupled with an Online Multi-Angle Light Scattering Detector (MALS), Together for Hevea and Natural Rubber Research, The Third Annual Seminar of HRPP: Prince of Songkla University, Surat Thani Campus, May 10th, 2011. Abstract.

ข. อาจารย์นักวิจัยและนิสิตในโครงการวิจัยที่ใด้รับรางวัล อาจารย์

- 1. รองศาสตราจารย์ ดร. เจริญ นาคะสรร ได้รับรางวัลดังต่อไปนี้
- 1.1 รางวัลนักวิจัยดีเด่นแห่งชาติ สภาวิจัยแห่งชาติ ประจำปี พ.ศ. 2553 สาขาวิทยาศาสตร์ กายภาพและคณิตศาสตร์ **และ**
- 1.2 รางวัลวิทยาศาสตร์และเทคโนโลยีดีเด่นสาขาพอลิเมอร์ มูลนิธิโทเร ประเทศไทย ประจำปี พ.ศ. 2553
- 2. รองศาสตราจารย์ ดร. ธีรยุทธ วิไลวัลย์ รางวัลนักวิจัยดีเด่นแห่งชาติ สภาวิจัยแห่งชาติ ประจำปี พ.ศ. 2553 สาขาวิทยาศาสตร์เคมีและเภสัช

นิสิต

- 1. **นางสาวอรพรรณ เวียรชัย** ได้รับรางวัลชนะเลิศ การแข่งขันเสนอผลงานประเภท โปสเตอร์ ในสาขา Nanomaterials จากงานวิจัยในหัวข้อเรื่อง "Development of Antibacterial Fillers from Quaternized Chitosan Particles"จากการประชุม The 16th Science Forum ซึ่งจัดขึ้นที่คณะ วิทยาศาสตร์ จุฬาลงกรณ์มหาวิทยาลัย ในระหว่างวันที่ 13-14 มีนาคม 2551
- 2. **นางสาวจิตติมา มีบึงพร้าว** ได้รับรางวัล The Outstanding Poster Presentation Award สาขา Material Science and Nanotechnology จากงานวิจัยในหัวข้อเรื่อง "Determination of DNA Sequences using Peptide Nucleic Acid in Combination with Chitosan Particles by MALDI-TOF Mass Spectrometry" จากการประชุม Pure and Applied Chemistry International Conference (PACCON 2009) ซึ่งจัดขึ้นที่มหาวิทยาลัยนเรศวร ในระหว่างวันที่ 14-16 มกราคม 2552
- 3. **นางสาวทิพวรรณ หอมไม่วาย** ได้รับรางวัล the best oral presentation award in Polymers for Food and Agriculture โดยการนำเสนอผลงาน Alkali Pretreatment of Kapok Fibers

for Pulping and Papermaking" Hommaivai, T., Suvarnakich, K., Chaiarrekij, S., and Kiatkamjornwong, S., in the 1st Polymer Conference of Thailand, the Convention Center of Chulabhorn Research Institute, Bangkok, Thailand, October 7-8, 2010 pages 118-123.

4. นางสาวสันนิภา พัฒนปิยะทรัพย์, นางสาวสุทธาทิพย์ เลขาลาวัณย์, นางสาวสุภาณี พิพัฒน์วิทยา นำเสนองานวิจัยเรื่อง การใช้เยื่อนุ่นในการปรับปรุงสมบัติของกระดาษรีไซเคิล ได้รับรางวัล บรรยายชนะเลิศอันดับที่ 1 The Hitachi Trophy 2011 สาขาวิทยาศาสตร์ประยุกต์และเทคโนโลยี) การ ประชุมวิชาการครั้งที่ 19 ประจำปี 2554 (The Science Forum 2011), คณะวิทยาศาสตร์ จุฬาลงกรณ์ มหาวิทยาลัย, กรุงเทพมหานคร, 10-11 มีนาคม 2554

ค. ข้อมูลนิสิตที่ได้รับทุนเครือข่าย

1. ชื่อนิสิต: นางสาวปิยะพร อรรคฮาต

หลักสูตร: ปิโตรเคมี

หัวข้อวิทยานิพนธ์: Synthesis and sensor application of carboxyl-containing polymer brushes

อาจารย์ที่ปรึกษาหลัก: รองศาสตราจารย์ ดร. วรวีร์ โฮเว่น ภาควิชาเคมี คณะวิทยาศาสตร์ จุฬาลงกรณ์มหาวิทยาลัย

อาจารย์ที่ปรึกษาร่วม: ศาสตราจารย์ ดร. สุดา เกียรติกำจรวงศ์ ภาควิชาวิทยาศาสตร์ทาง ภาพถ่ายและเทคโนโลยีทางการพิมพ์ คณะวิทยาศาสตร์ จุฬาลงกรณ์มหาวิทยาลัย

อาจารย์ที่ปรึกษาร่วม: Professor Dr. Yasuhiko Iwasaki, Department of Chemistry and Materials Engineering, Faculty of Chemistry, Materials and Bioengineeringม Kansai University, Japan

ปีที่เข้าศึกษา: 2549

สถานภาพปัจจุบัน: สอบป้องกันวิทยานิพนธ์แล้วในเดือนเมษายน 2554 ขณะนี้อยู่ระหว่าง การแก้ไขบทความเพื่อส่งตีพิมพ์ในวารสารวิชาการระดับนานาชาติ นิสิตจะจบการศึกษาเมื่อบทความ ได้รับการตีพิมพ์ในวารสารวิชาการระดับนานาชาติแล้ว

หน่วยงานที่จะเข้าทำงานหลังจากจบการศึกษา: ภาควิชาเคมี คณะวิทยาศาสตร์ มหา-วิทยาลัยบูรพา

2. ชื่อนิสิต: นางสาววิไลพร ไกรสุวรรณ

หลักสูตร: ปิโตรเคมี

หัวข้อวิทยานิพนธ์: Synthesis and characterization of active functional copolymers of N-isopropylacrylamide

อาจารย์ที่ปรึกษาหลัก: รองศาสตราจารย์ ดร. วรวีร์ โฮเว่น ภาควิชาเคมี คณะวิทยาศาสตร์ จุฬาลงกรณ์มหาวิทยาลัย

อาจารย์ที่ปรึกษาร่วม: ศาสตราจารย์ ดร. สุดา เกียรติกำจรวงศ์ ภาควิชาวิทยาศาสตร์ทาง ภาพถ่ายและเทคโนโลยีทางการพิมพ์ คณะวิทยาศาสตร์ จุฬาลงกรณ์มหาวิทยาลัย

ปีที่เข้าศึกษา: 2551

สถานภาพปัจจุบัน: สอบโครงร่างวิทยานิพนธ์แล้วในเดือนธันวาคม 2553 ขณะนี้อยู่ระหว่างการทำวิจัย

หน่วยงานที่จะเข้าทำงานหลังจากจบการศึกษา: ยังไม่มี

3. ชื่อนักศึกษา: นางสาวเฉลา เทพเฉลิม

หลักสูตร ปรัชญาดุษฎีบัณฑิต (เทคโนโลยีพอลิเมอร์) คณะ บัณฑิตวิทยาลัย มหาวิทยาลัย สงขลานครินทร์ (วิทยาเขตปัตตานี)

หัวข้อวิทยานิพนธ์ทั้งไทยและอังกฤษ

ภาษาไทย ปรากฏการณ์แข็งขึ้นของยางธรรมชาติ: กลไกเชิงโมเลกุลและความเกี่ยวข้องของ ส่วนที่ไม่ใช่ยางที่มีผลกระทบต่อโครงสร้างและสมบัติการไหล

ภาษาอังกฤษ Storage hardening of natural rubber: Molecular mechanisms and non-isoprene compounds involved: influence of the phenomenon on structure and rheological properties.

ชื่ออาจารย์ที่ปรึกษาทั้งคนไทยและต่างประเทศ พร้อมสถานที่ทำงานของอาจารย์ที่ปรึกษาทั้ง

- 1) Dr. Frederic Bonfils (UMR IATE 1208, CIRAD, INRA, Montpellier SupAgro, UMII, 2 Place Viala, 34060 Montpellier Cedex 1, France)
- 2) Dr. Laurent Vaysse (¹UMR IATE 1208, CIRAD, INRA, Montpellier SupAgro, UMII, ²KU-CIRAD laboratory Agroindustry building 3, 7th Floor, Kasetsart University, Bangkok 10900, Thailand)
- 3) Dr. Suwaluk Wisunthorn (Faculty of Science and Industrial Technology, Prince of Songkla University, Surat Thani Campus, Muang District, Surat Thani, Thailand)

- 4) Assoc. Prof. Dr. Charoen Nakason (Center of Excellence in Natural Rubber Technology, Faculty of Science & Technology, Prince of Songkla University, Pattani campus, Thailand)
- **5) Prof. Dr. Suda Kiatkamjornwong** (Department of Imaging and Printing Technology, Faculty of Science, Chulalongkorn University, Bangkok, Thailand)

4. ความร่วมมือกับเครือข่ายต่างประเทศ

- 1) CIRAD (Agricultural Research for Development), Montpellier, France
- 2) Mixed Research Unit (Unité Mixte de Recherche, UMR), Montpellier, France
- 3) Montpellier SupAgro (International Center for Higher Education in Agricultural Sciences), France
- 5. **ความก้าวหน้าของการทำวิจัย** ผลการนำเสนอผลงานวิจัย เช่น การประชุมวิชาการในประเทศ นอก ประเทศ การส่งบทความไปยังวารสารนานาชาติ
- 1) การประชุมวิชาการ The 3rd "Hevea Research Platform in Partnership" (HRPP) Annual Seminar, Workshop and Field trip ณ มหาวิทยาลัยสงขลานครินทร์ วิทยาเขตสุราษฎร์ธานี, วันที่ 10 12 พฤษภาคม 2554
- 2) ชื่อที่สอง ในการตีพิมพ์วารสาร Journal of Chromatography A (Submitted paper on June 7, 2011) ดังนี้ Stephane Dubascoux, Chalao Thepchalerm, Eric Dubreucq, Suwaluk Wisunthorn, Laurent Vaysse, Suda Kiatkamjornwong, Charoen Nakason, Frederic Bonfils Comparative study of the mesostructure of natural and synthetic polyisoprene by SEC-MALS and AF4-MALS. Journal of Chromatography A, submitted.
 - 6. รางวัลที่ได้ของนักศึกษา ยังไม่มี
- 7. การคาดคะเนเวลาที่จะจบการศึกษา ประมาณเดือนชั้นวาคม พ.ศ.2555 ถึงเดือนมิถุนายน พ.ศ. 2556
 - 8. การคาดคะเนวิชาชีพในอนาคต อาจารย์ในสังกัดมหาวิทยาลัยของรัฐบาล

เอกสารแนบ

บทความพิมพ์เผยแพร่ในวารสาร



Contents lists available at ScienceDirect

Carbohydrate Polymers

journal homepage: www.elsevier.com/locate/carbpol



Preparation of cassava starch-graft-polyacrylamide superabsorbents and associated composites by reactive blending

Charoen Nakason^a, Toha Wohmang^a, Azizon Kaesaman^a, Suda Kiatkamjornwong^{b,*}

- ^a Center of Excellence in Natural Rubber Technology, Department of Rubber Technology and Polymer Science, Faculty of Science and Technology, Prince of Songkla University, Pattani, 94000, Thailand
- ^b Multidisciplinary Program of Petrochemistry and Polymer Science, Department of Imaging and Printing Technology, Faculty of Science, Chulalongkorn University, Bangkok, 10330, Thailand

ARTICLE INFO

Article history: Received 11 January 2010 Received in revised form 11 February 2010 Accepted 15 February 2010 Available online 4 March 2010

Keywords: Batch reactor High water absorbing polymer Cassava starch Acrylamide

ABSTRACT

Cassava starch-g-polyacrylamide (PAM) was successfully prepared by a reactive batch processing using a specially designed batch reactor resulting in a superabsorbent polymer (SAP) with water absorption of 605 g/g being obtained under the optimized reaction conditions. The occurrence of a graft copolymer was confirmed by FT-IR spectra, where it was found to exhibit all characteristic bands of both starch and acrylamide (AM) units. SEM micrographs of the starch granules showed an irregular shape and varied particle sizes with a smooth surface, while the graft copolymers had a coarse porous structure and broad network. Various types of inorganic filler were added to the graft copolymer to prepare the SAP composites (SAPC). It was found that the SAPC with bentonite clay exhibited the highest water absorption of approximately 730 g/g. Conversely, the incorporation of silica to the graft copolymer gave a significantly lower water absorption capability than the copolymer alone.

© 2010 Elsevier Ltd. All rights reserved.

1. Introduction

Biodegradable polymers have drawn considerable attention in both academia and industry due to the problem of environmental pollution caused by the disposal of synthetic polymer waste. Therefore, the development of biodegradable polymers has been one of the main areas of current interest. One of the simple practical approaches to prepare biodegradable polymers is to blend polymers with various types of starch. Since Thailand is one of the world's largest exporters of cassava products it, therefore, has a great opportunity to search for a reliable process to use cassava starch by modifying its molecular structure to produce biodegradable products, such as superabsorbent polymers (SAPs) (Lanthong, Nuisin, & Kiatkamjornwong, 2006). SAPs are a lightly crosslinked network of hydrophilic polymer chains that can absorb and retain a large quantity of aqueous fluids, and where the absorbed fluids are hardly removed even under pressure (Zhang, Li, & Wang, 2006). Most of the current SAPs are synthetic polymers that have a poor biodegradability leading to environmental problems with their disposal. The development of starch-based SAPs could potentially be used to solve this problem. Potential applications of starch-based SAPs are fairly diverse and include personal care products, firefighting gels, agricultural uses, and so forth (Willett & Finkenstadt, 2006). Starch-based SAPs are developed by grafting starch with unsaturated hydrophilic monomers, such as acrylic, acrylamide (AM) (Athawale & Lele, 1998; Karadağ, Üzüm, & Saraydin, 2005; Lanthong et al., 2006; Mostafa, 1995; Willett & Finkenstadt, 2006; Zhang et al., 2006) and ϵ -caprolactone (Chen et al., 2005), and can be formed by radical chain copolymerization via chemical initiation (Athawale & Lele, 2000; Chen, Park, & Park, 1999) or by the use of γ -ray irradiation (Caykara, Bozkaya, & Kantoğlu, 2003; Kiatkamjornwong, Mongkolsawat, & Sonsuk, 2002).

Although reactive extrusion has been used as a continuous process (Carr, Kim, Yoon, & Stanley, 1992; Willett & Finkenstadt, 2006; Yoon, Carr, & Bagley, 1992), processing of most starch-based graft copolymers is typically done in a batch process, but this consumes a large amount of water (Fanta, 1996; Weaver et al., 1977). Starch-gpolyacrylamide (PAM) has been successfully prepared before using a co-rotating twin screw extruder (Finkenstadt & Willett, 2005; Willett & Finkenstadt, 2003), but the maximum water absorption capacity of the SAPs obtained using this process was relatively low at only approximately 300 times their dry weight in water (Carr et al., 1992).

In this work, a specially designed batch reactor was built and used to prepare starch-g-PAM based SAPs via reactive processing with low quantities of water. This was aimed to enhance the water retention capability of the saponified starch-g-PAM SAP obtained and also to improve some other important properties (see below). The influence of the reaction time, temperature, concentration of

^{*} Corresponding author. Tel.: +66 2 218 5587; fax: +66 2 255 3021.

E-mail addresses: ncharoen@bunga.pn.psu.ac.th (C. Nakason), ksuda@chula.ac.th

Kiatkamiornwong)

the initiator and the molar ratio of starch:AM on the conversion, graft efficiency, graft content and water absorbency were investigated. SAP composites (SAPC) of the starch-g-PAM with silica, bentonite clay and China clay were also prepared and their water absorption was tested.

2. Experimental

2.1. Materials

The cassava starch used as the polymer substrate was obtained from Siam Starch (1966) Co., Ltd., Rayong, Thailand. AM, used as a grafting monomer, was manufactured by Fluka (Buchs, Switzerland). Potassium persulfate (KPS), used as a free radical initiator, was manufactured by Asia Pacific Specialty Chemicals

Ltd. (Seven Hills, Australia). Hydroquinone, used as a free radical scavenger, was manufactured by Merck (Darmstadt, Germany). N,N'-Methylenebisacrylamide (N,N'-MBA), used as a crosslinker, was manufactured by Fluka (Buchs, Switzerland). For the preparation of SAPCs, Ultrasil VN 3 GR silica obtained from Evonik Degussa GmbH (Essen, Germany), bentonite clay, grade SAC-1, manufactured by Thai Nippon Chemical Industry, Co., Ltd. (Samut Sakhon, Thailand) and China clay manufactured by Renuka Minchem Pvt. Ltd. (Udaipur, India) were each mixed in the reactive batch processing.

2.2. Reactive polymerization

Reactive batch processing was performed using an in-house specially designed and built batch reactor with a capacity of approx-

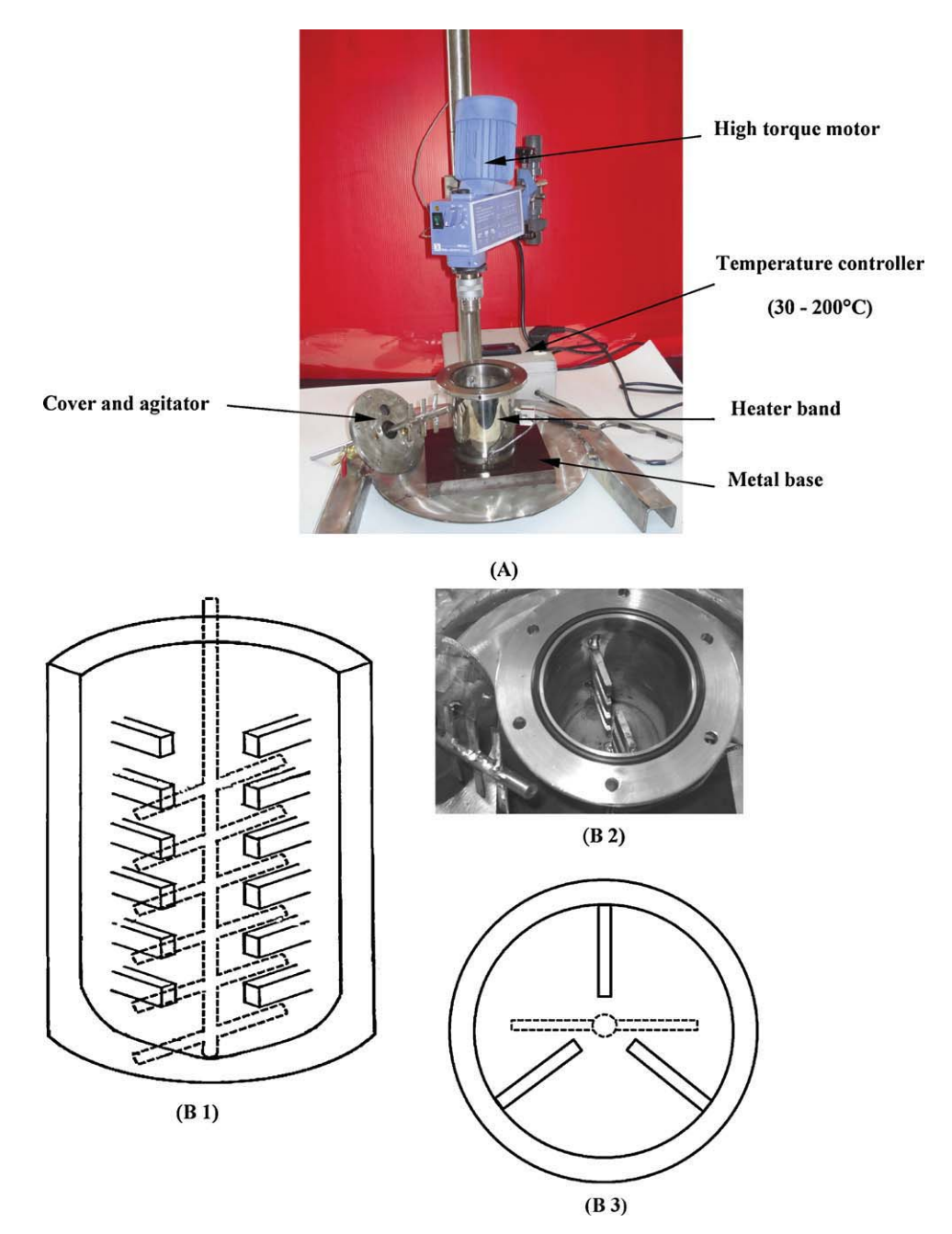


Fig. 1. Components of a specially designed batch reactor. A: Batch reactor, and B: specially designed mixing elements showing (B1) side view of total stirring blades, (B2) top view of the reactor stirring blades, and (B3) top view of total stirring blades.

Table 1Relationship of the Reynolds number and mixing speed.

Reynolds number	Mixing speed
<10 10 < N _{rev} < 10 ⁴	Low speed for laminar flow Medium speed for transition
>10 ⁴	High speed for turbulent flow

imately 1 L, as shown in Fig. 1. It is a stainless steel reactor with a specially designed internal geometry containing an agitator. A programmable heating element surrounded the outside cylinder of the reactor, and a stainless steel cover for the inlet and outlet of nitrogen gas was also built. A high torque motor with a maximum torque of 3000 N cm (RW 47D High-Viscosity Mechanical Overhead Stirrer powered by a $3\times230\,\text{V}$, $60\,\text{Hz}$, $570\,\text{W}$, IKA, Staufen Germany) was fitted to an in-house made specially designed agitator to cause a thorough mixing of the highly viscous material during the graft copolymerization.

Graft copolymerization was begun by drying cassava starch in a hot air oven for at least 4 h at $60\,^{\circ}\text{C}$ before incorporating it into the batch reactor. Nitrogen gas was purged thoroughly into the reactor and stirred for at least 1 min to eliminate oxygen gas. Distilled water and cassava starch was added at a 1:1 (w/w) ratio and stirred at $60\,^{\circ}\text{C}$ for 20 min to form the gelatinized starch. The temperature of the mix was then increased to $80\,^{\circ}\text{C}$ and stirred for 2 min before incorporating 3.70 mM KPS initiator and then stirring continuously for another 30 min. An aqueous solution of 23.81% (w/w) AM was then added drop wise to the reactor with a continual stirring for the indicated time intervals (a range of $110-260\,\text{min}$). The actual concentration of the starch was also $23.81\%\,(\text{w/w})$ of the total mass, i.e., starch:AM = 1:1 by weight. The reactor is capable of handling gelatinized starch at this mixture ratio with the small amount of water because the high torque motor is used. In this part of experiment, no

crosslinker was incorporated for characterization purposes. Then, the ungrafted homopolymer (PAM) was soluble in ethanol/water whereas the starch grafted PAM was insoluble.

The reaction and newly synthesized product was then quenched by adding 0.5% (w/w) of hydroquinone in ethanol and left overnight to remove the un-reacted monomer. The solid products were finally collected by filtration and dried.

2.3. Saponification

To enhance the water absorbing capability of the resultant SAP, 40 g of the graft copolymer was transferred to a flask containing 100 mL of 1 mol/L of sodium hydroxide solution and 100 mL of distilled water and the content was saponified at 90 °C for 2 h. The final concentration of the graft copolymer in NaOH solution was 16.67% (w/w) of the total mass, i.e., 40 g of the graft copolymer in 240 g of the mixture. The pH of the saponified products was then adjusted to 7 by the addition of a 1 M HCl solution and the graft copolymer was coagulated and precipitated by the rapid addition of an excess amount of methanol. The solid saponified copolymer was then filtered and washed thoroughly to remove the ungrafted starch as well as the un-reacted monomer. The thoroughly washed products were then dried in a vacuum oven at 60 °C until the weight of the polymer was constant. They were then ground and filtered through an 80-mesh screen to leave the powdery SAP.

2.3.1. Influence of the inorganic filler

Three types of inorganic filler, namely silica, China clay and bentonite clay, were incorporated in the starch-g-PAM copolymer SAP to form SAPCs. The graft copolymer was first prepared using a 1:1 (w/w) ratio of starch:AM at a reaction time and temperature of 140 min and 80 °C with KPS at 1.5 wt% of starch and 0.3 wt% of N,N'-

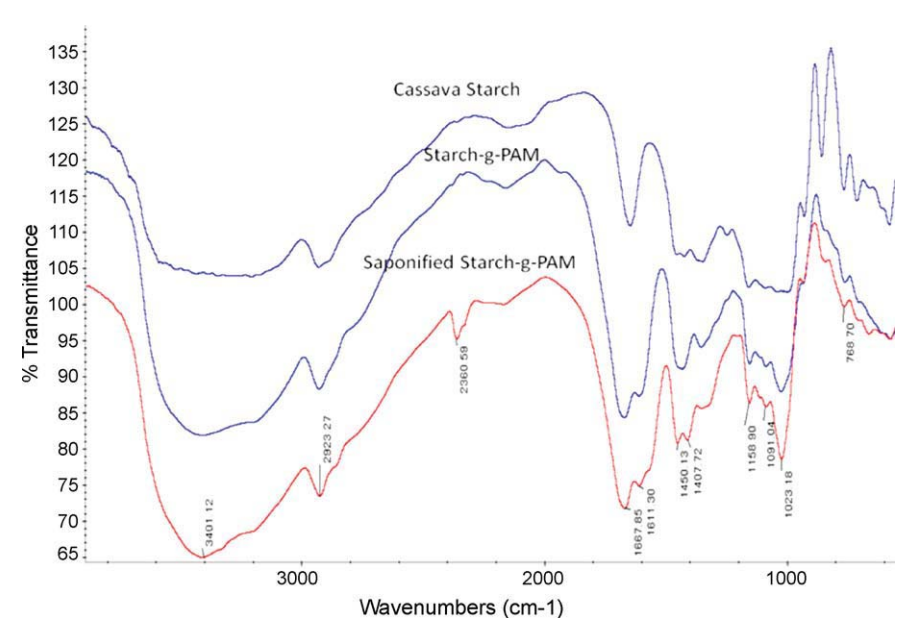


Fig. 2. Representative FT-IR spectra of cassava starch, the starch-g-PAM copolymer and its saponified product.

$$R - C - NH_2 \xrightarrow{\triangle} R - C = N - H \xrightarrow{OH} R - C = N + H_2O$$

Scheme 1. Proposed mechanism for the formation of nitrile group from dehydration of amide group by alkaline hydrolysis at 90 °C.

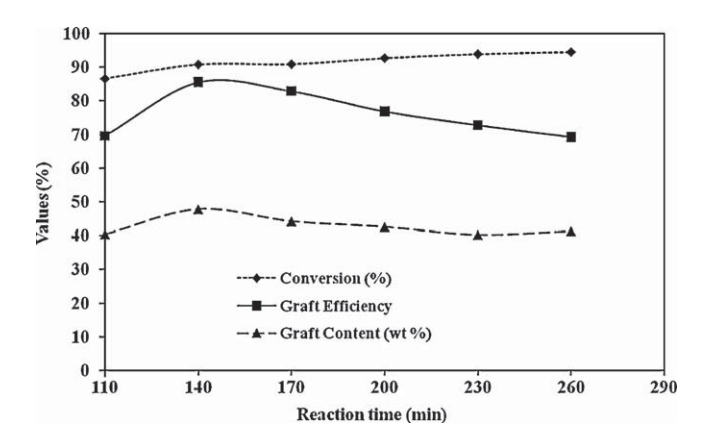


Fig. 3. Relationship between the level of conversion, graft efficiency and graft content of the saponified starch-*g*-PAM copolymer SAP against the reaction time employed for the copolymer formation.

MBA under a stirring speed of 300 rpm. The fillers were filtered through a 325-mesh stainless steel screen before incorporating in the reaction mixture at a loading level of 10 wt% of graft copolymer.

2.4. Water absorbency

The powdery SAP (0.1 g) was immersed in distilled water (250 mL) for 24 h at ambient temperature (25–30 °C) to reach an equilibrium swelling. The residual water was removed by filtration through an 80-mesh stainless steel screen with the water absorbed polymer left on the screen for at least 1 h to drain off the additional unabsorbed water. During this period, the screen was gently shaken with an alternate lined angle of 15–20° to ensure that most of the un-absorbed water was separated. The un-absorbed water which was held in the free spaces among the SAP particles, due to variation in particle sizes, by capillary force must be excluded. The water absorption was determined by weighing the swollen graft copolymer and its dried polymer in Eq. (1) as follows:

water absorbency
$$(g/g) = \frac{W_1 - W_0}{W_0}$$
, (1)

where W_0 is the weight of the dried SAP and W_1 is the weight of the swollen sample.

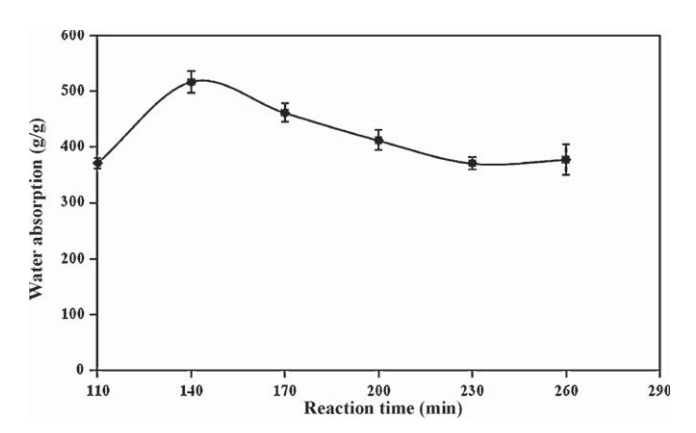


Fig. 4. Relationship between the reaction time used for the starch-g-PAM copolymer SAP formation and the resultant water absorption obtained by the SAP. Data are shown as the mean \pm 1 S.D. and are derived from 3 replicate samples.

2.4.1. Characterization

The nitrogen contents were measured using a Kjeldahl digestion unit consisting of Kjeldatherm block digestion units (702001 KBL 20S), a programmable distillation unit with a titration unit (Vapodest 45s) and a scrubber unit, all manufactured by Gerhardt (Königswinter, Germany). Details for the determination of nitrogen content were as described elsewhere (McGill & Figueiredo, 1993). The conversion, graft content and graft efficiency were each calculated using the following equations (2)–(4) (Willett & Finkenstadt, 2003):

$$conversion = \frac{100N_{crud}}{N_f},$$
 (2)

$$graft content = \frac{100N_i}{19.72},$$
 (3)

graft efficiency =
$$\frac{100(1-f)N_i}{(1-f)N_i + fN_s},$$
 (4)

where N_{crud} is the nitrogen content (wt%) of the newly synthesized (crude) product. N_f is the theoretical nitrogen content based on the feeding amount of the monomer. N_i is the nitrogen content of the EtOH/H₂O-insoluble fraction and f is the weight of the soluble fraction in the EtOH/H₂O. The nitrogen content of the PAM was 19.72 wt% by the above method. Graft efficiency is based on the amount of monomer polymerized, and is equal to the ratio

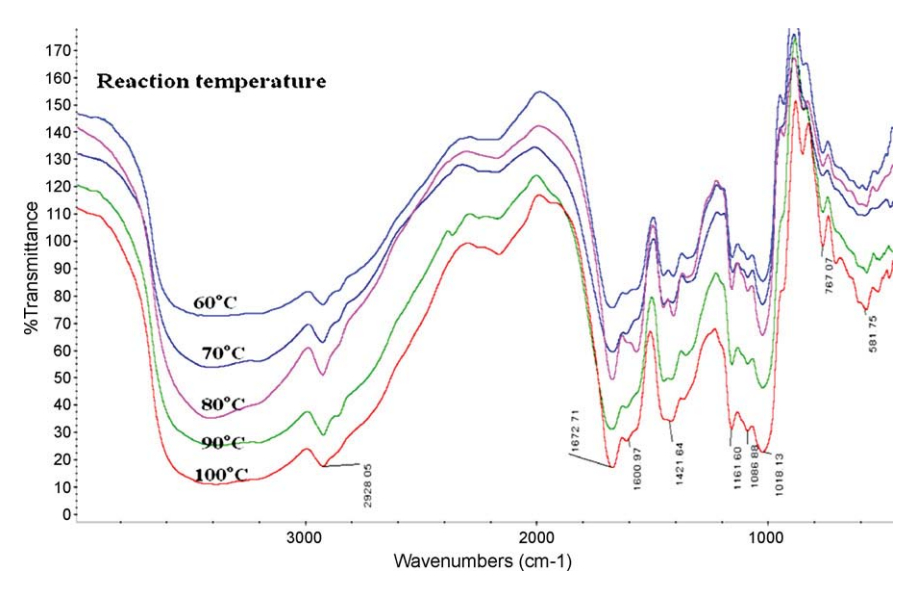


Fig. 5. Representative FT-IR spectra of the purified starch-g-PAM copolymer prepared at the indicated five different reaction temperatures.

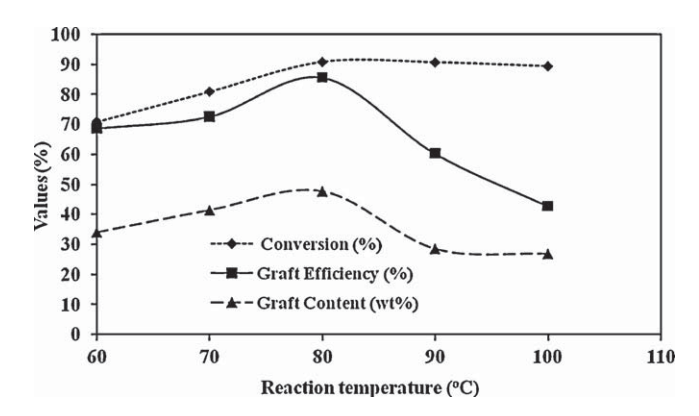


Fig. 6. Relationship between the reaction temperature used to form the starch-g-PAM copolymer SAP and the level of conversion, graft efficiency and graft content of the obtained SAP.

of the insoluble amount of PAM to the total amount of PAM (the insoluble and soluble parts). It should be mentioned that GE was calculated only in the reaction system without incorporation of the crosslinking agent.

2.4.1.1. Morphology of SAP and SAPC. The SAP and SAPC samples were dried at 105 °C for 2 h to eliminate moisture. They were cooled in a desiccator, and coated with gold and characterized using a scanning electron microscopy (JOEL SEM, JSM-5200, Tokyo, Japan) at 15 kV.

3. Results and discussion

Based on the specially designed reactor (Fig. 1), the mixing speeds for the polymerization reaction can be controlled based on the relationship between the Reynolds number of the reactor and the mixing speed of the reaction mixture (Table 1). The Reynolds number (N_{Re}) equation is shown in Eq. (5):

$$N_{Re} = \frac{\rho n D^2}{\mu},\tag{5}$$

where D is the diameter of the propeller (0.31 in), n is the speed of the propeller (300 rpm), ρ is the initial density of the starch (1.50 g/cm³) and μ is the initial viscosity of the starch (0.018 Pa s). Based on Eq. (5), the specially designed reactor has a Reynolds number of 224.7 and it is possible to state that the reactor is capable of handling viscous dispersion and thus it can mix the reaction mixture by the transition mode at a medium speed (see Table 1).

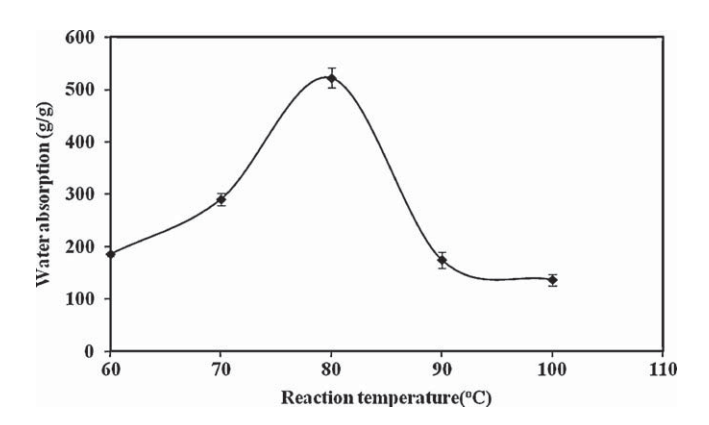


Fig. 7. Relationship between the reaction temperature used to form the starch-g-PAM copolymer SAP and the level of water absorption of the obtained SAP. Data are shown as the mean \pm 1 S.D. and are derived from 3 replicate sample.

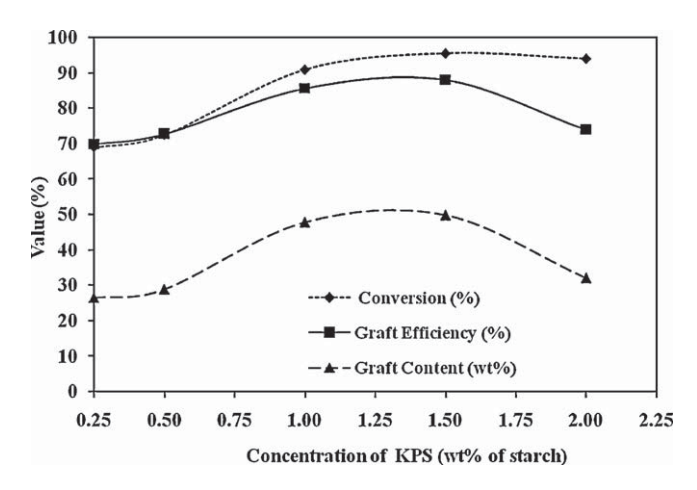


Fig. 8. Relationship between the KPS concentration used to form the starch-g-PAM copolymer SAP and the level of conversion, graft efficiency and graft content of the obtained SAP.

3.1. Influence of reaction time

The total time from the start of stirring, to mix the starch with water, until the end of the stirring is termed the reaction time. In this work, the reaction time was varied at 110, 140, 170, 200, 230 and 260 min, with a fixed 1:1 (w/w) ratio of starch:AM, KPS at 1 wt% of starch, a reaction temperature of 80 °C with a stirring speed of 300 rpm.

Fig. 2 shows the representative FT-IR spectra of the cassava starch, the purified starch-g-PAM and its saponified product. The broad absorption bands in the region of wave number 3550-3200 cm⁻¹, which represent the O-H stretching vibration, are clearly seen, and the medium absorption peak at 2923 cm⁻¹ represents the C-H stretching vibration. Furthermore, the triplet peaks with a strong absorption at 1156, 1051 and 1023 cm⁻¹ indicate the presence of the C-O-C stretching vibration. The IR spectrum of the starch-g-PAM copolymer gives all the absorption bands of cassava starch plus, additionally, the absorption peaks at 3401, 1667 and 1611 cm⁻¹, which indicate the N-H stretching, C=O stretching and N-H bending of the amide groups, respectively. Therefore, these are the characteristics of the -CONH₂ groups in the grafted PAM. Furthermore, the peak at 1407 cm⁻¹ that represents -C-N stretching, and that at $766-710\,\mathrm{cm}^{-1}$ that represents the weak band of N-H out of plane bending, all are also characteristic bands of the amide grafted onto the cassava starch backbone. After the saponification, the following absorption peaks were observed

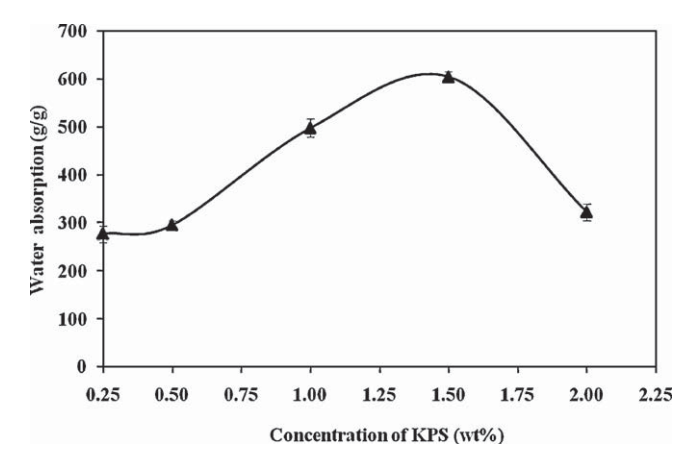


Fig. 9. Relationship between the KPS concentration used to form the starch-g-PAM copolymer SAP and the level of water absorption of the obtained SAP. Data are shown as the mean \pm 1 S.D. and are derived from 3 replicate samples.

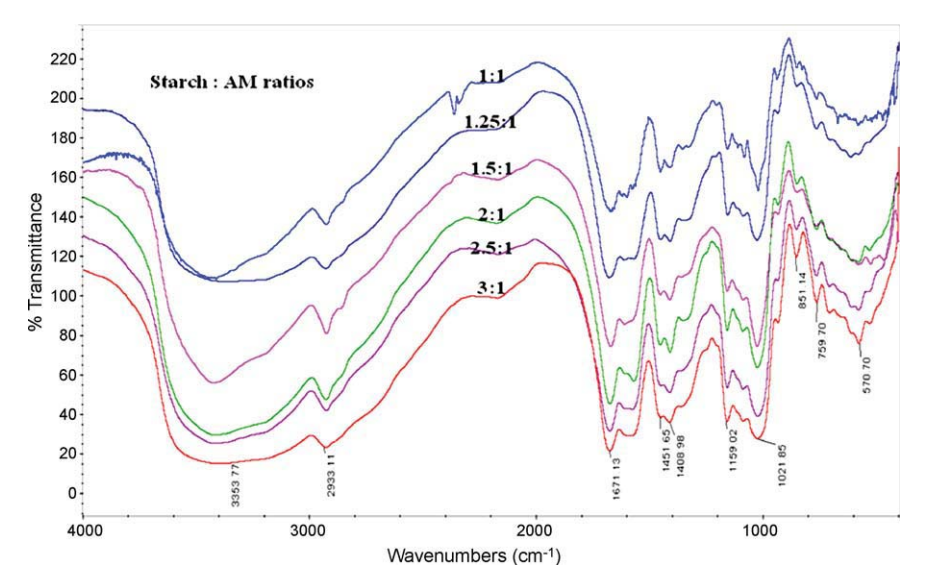


Fig. 10. Representative FT-IR spectra of the purified starch-g-PAM copolymer prepared from six different (w/w) ratios of starch:AM.

that confirm the occurrence of PAM; the N-H stretching of O=C-NH (amide band), the C=O stretching, the N-H bending at 1450 cm⁻¹ for the -C-N stretching and a relatively intense and sharp peak at 2360 cm⁻¹ which is the -C≡N (nitrile or cyanyl) peak, an intermediate peak from the saponification in alkaline solution of the amide group converted to the nitrile or cyanyl group. Although an amide is considered a neutral functional group, it is both weak acid and weak basic, and amide is hydrolyzed by strong acid or strong base. Even though POCl₃ is widely used as a dehydrating agent to convert O=C-NH (amide) to R-C≡N (nitrile or cyanyl) (Wade, 1991) it is possible that heat generated at the saponification condition can act as a dehydrating agent to dehydrate acrylamide moiety to nitrile moiety for the SAP prepared from high content of acrylamide (starch:AM = 1:1). This is because the two hydrogen atoms of the amino group can be abstracted by the hydroxide anion under heat. The carbonyl oxygen of acrylamide moiety is simultaneously protonated to become the hydroxyl group as a leaving group which can promote the formation of the nitrile or cyanyl group as shown

It is further observed (see the effect of starch:AM ratio) that at the higher starch:AM ratios, this peak (2360 cm⁻¹ peak) disappeared because more starch active sites were available for AM grafting.

Fig. 3 shows the influence of the reaction time on the conversion from monomer to polymer, graft efficiency and graft content (based on Eqs. (2)–(4)). The conversion level slightly increased with increasing reaction time from \sim 88% at 100 min to a maximum value of approximately 95% at a reaction time of 260 min (the longest reaction time). On the other hand, the graft efficiency and graft content initially increased more significantly as the reaction time was increased from 110 to 140 min (70–85% and 40–50%, respectively), and then decreased with longer reaction times. The decrease

in graft efficiency with longer reaction times was slightly more marked for graft content but nevertheless the maximum graft efficiency and content were both attained at a reaction time of 140 min. This might be attributed to a higher level of PAM homopolymer formation with reaction times of longer than 140 min. Furthermore, there is a possibility that the crosslinked PAM can be simply degraded by mechanical shear into lower molecular weight fragments during a prolonged reaction time. Regardless, the graft copolymer prepared with a reaction time of 140 min incorporated the highest grafted PAM, content and this corresponded to the highest water absorption capability of the saponified graft copolymer (Fig. 4) which was also obtained from a reaction time of 140 min at ca. 520 g/g). Increasing the reaction time above 140 min caused a decreased water absorption capability, and this is also likely to be due to a lower amount of the grafted PAM which becomes saponified and so more hydrophilic in nature.

Given that reaction times over 140 min only slightly increased the level of conversion but markedly reduced that of the graft efficiency, graft content and water absorbance, a reaction time of 140 min was selected for further investigation.

3.2. Influence of the reaction temperature

Fig. 5 shows the representative FT-IR spectra of the purified starch-g-PAM copolymer prepared from five different reaction temperatures (60, 70, 80, 90 and 100 °C) with a fixed reaction time of 140 min, a starch:AM (w/w) ratio of 1, KPS at 1% (w/w) and a stirring speed of 300 rpm. The characteristic bands of cassava starch and amide groups are present, similar to those observed for the purified starch-g-PAM copolymer in Fig. 2, which confirms the formation of a cassava starch-g-PAM copolymer. The influence of the reaction temperature upon the graft efficiency, graft con-

 Table 2

 Properties of the cassava starch-g-PAM copolymer SAP derived from various (w/w) ratios of starch:AM.

*		` ' '		
Starch:AM (w/w) ratio	Conversion (%)	Graft efficiency (%)	Graft content (wt%)	Absorbency in DI water (g/g)
1:1	90.9 ± 1.5	85.6 ± 2.1	47.8 ± 1.7	606 ± 10.2
1.25:1	86.7 ± 1.8	80.6 ± 3.5	44.0 ± 3.7	479 ± 9.8
1.5:1	76.4 ± 2.1	76.7 ± 3.9	31.3 ± 3.1	407 ± 11.1
2:1	73.2 ± 3.2	71.1 ± 2.7	28.3 ± 4.7	349 ± 9.7
2.5:1	61.7 ± 3.8	55.6 ± 3.9	23.1 ± 3.1	222 ± 8.9
3:1	48.2 ± 2.7	39.4 ± 4.1	16.8 ± 2.9	132 ± 10.4

The experiment was carried out in triplicate and the data was presented within ± 1 S.D.

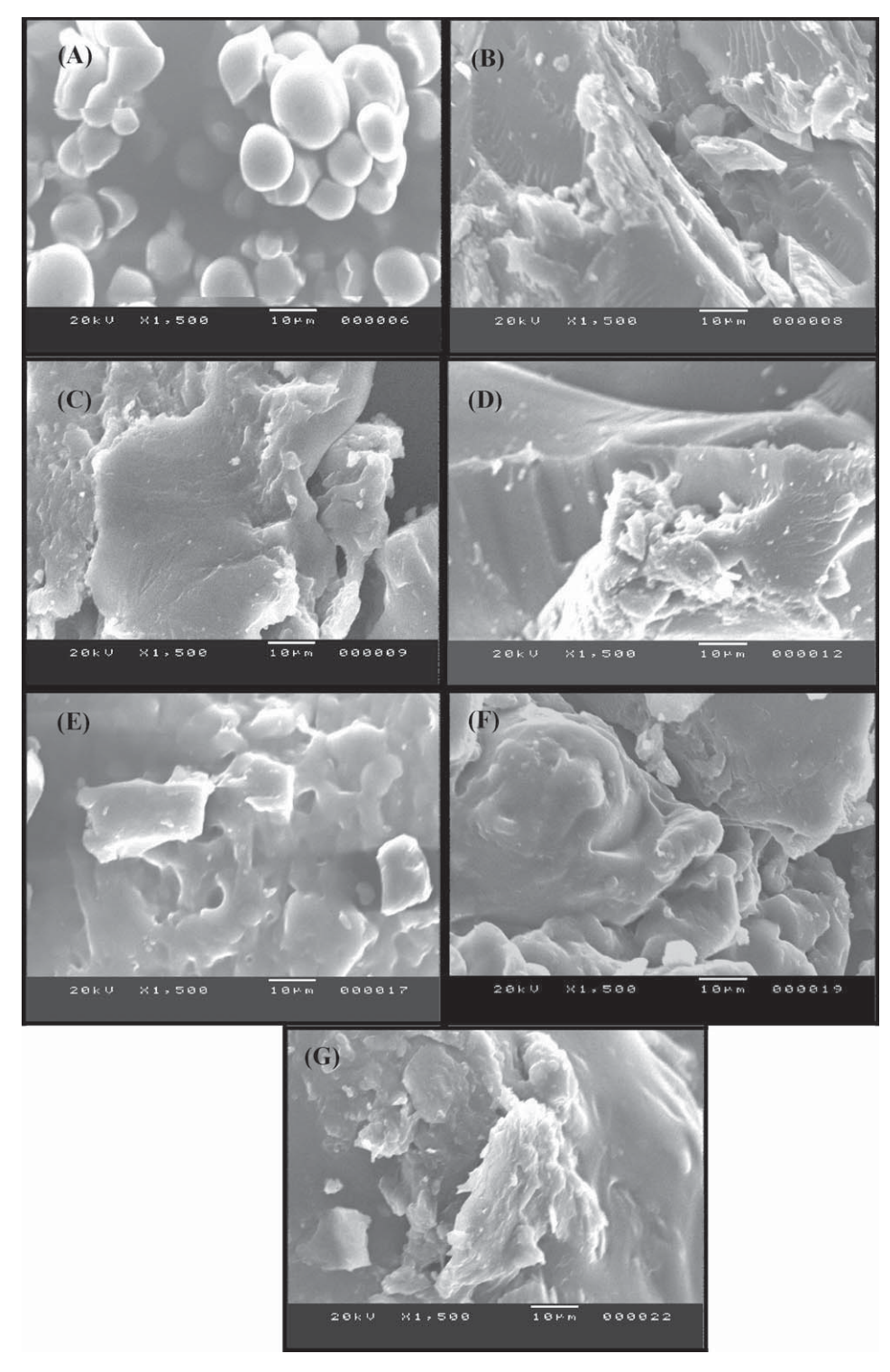


Fig. 11. Representative SEM micrographs of (A) cassava starch, and the purified starch-g-PAM copolymer SAP prepared from starch:AM (w/w) ratios of (B) 1:1, (C) 1.25:1, (D) 1.5:1, (E) 2:1, (F) 2.50:1 and (G) 3:1.

tent and level of conversion of monomer to polymers is shown in Fig. 6, where the conversion linearly and significantly increases with increasing temperature within the range of $60-80\,^{\circ}\text{C}$ and then reaches a smooth plateau (or mild decrease) region at reaction temperatures higher than $80\,^{\circ}\text{C}$. This might be related to the optimum decomposition temperature of KPS at $80\,^{\circ}\text{C}$, where at temperatures lower than $80\,^{\circ}\text{C}$ the initiator molecules decompose less to give fewer free radicals. On the other hand, at temperatures higher than $80\,^{\circ}\text{C}$ too high a rate of free radical generation

is attained which then recombine and so reduce the efficiency of the initiator. The graft efficiency and graft content also increased with increasing reaction temperatures up to $80\,^{\circ}$ C, and thereafter at higher temperatures an abrupt decrease in the graft efficiency and graft content was observed (Fig. 6). This is attributed to the increasing rate of graft copolymerization in reaction temperatures in the range of $60\text{--}80\,^{\circ}\text{C}$, but at higher temperatures a greater rate of PAM homopolymer formation occurred at the expense of the graft copolymerization. In addition, chain transfer at higher

temperatures is likely to significantly reduce the extent of graft copolymerization. These results correlated well with the water absorption ability of the saponified starch-g-PAM copolymer based SAP at various reaction temperatures, where the maximum water absorption was obtained in the saponified starch-g-PAM copolymer prepared at 80 °C (Fig. 7). This is because the graft copolymer contains the highest grafted PAM that thereafter was hydrolyzed by the saponification process to result in the presence of the more hydrophilic carboxamide and carboxylic acid groups and therefore a greater level of water absorption.

3.3. Influence of the concentration of potassium persulfate initiator

The conversion level, graft efficiency and graft content of the starch-g-PAM copolymer prepared using KPS at five different concentrations (0.25, 0.50, 1.00, 1.50 and 2.00 wt% of the cassava starch), with a fixed starch:monomer (w/w) ratio of 1, a 140 min reaction time at 80°C and a stirring speed of 300 rpm is summarized in Fig. 8. The conversion level obtained increased with increasing KPS concentrations up to a maximum conversion value at 1.50-2.00 wt% KPS. This may be attributed to the increasing availability of reactive free radicals to initiate the polymerization of PAM to form the grafted PAM and PAM homopolymer. Increasing the concentration of KPS from 1.50-2 wt% did not cause any further significant effect upon the conversion level, although a slight numerical decrease was seen. Although an abundant level of free radicals were formed in the system, the amount of monomer available for the reaction was limiting and, therefore, any further excess production of free radicals might recombine.

The graft efficiency and graft content of the starch-g-PAM copolymer also increased with increasing KPS concentrations within the range of 0.25–1.00 by 1.50 wt% KPS, with the maximum values observed between 1 and 1.5 wt%. Likewise, the graft efficiency and content both decreased with further increases in the KPS concentration above 1.50 wt% (Fig. 8). The higher concentrations of initiator (KPS) produced a higher grafted PAM level in cassava starch molecules but at 2 wt% the KPS concentration is too high and chain transfer to monomer or homopolymer formation was more pronounced causing lower graft content and graft efficiency (Fig. 8) as well as the lower water absorption capability (Fig. 9). Indeed, as expected, the water absorption of the saponified cassava starch-g-PAM copolymer prepared using KPS at 1.50 wt% exhibited the highest water absorption capability (ca. 605 g/g), which is approximately 2-3 times higher than those of the graft copolymers prepared by reactive extrusion reported elsewhere (Willett & Finkenstadt, 2006).

3.4. Influence of the starch:acrylamide ratios

The influence of the starch:AM ratios, at six different (w/w) ratios of 1:1, 1.25:1, 1.5:1, 2:1, 2.5:1 and 3:1, was analyzed using a 140-min reaction time at $80\,^{\circ}\text{C}$, a stirring speed of 300 rpm and a KPS concentration of 1.5 wt% of the starch.

The FT-IR spectra of the purified starch-g-PAM derived from the six different starch:AM (w/w) ratios revealed all the characteristic bands of both cassava starch and PAM (Fig. 10), as shown respectively in Figs. 2 and 5, supporting the formation of a starch-g-PAM copolymer in all six different starch:AM (w/w) ratios. The characteristics and properties of these six different starch-g-PAM copolymers based SAPs are shown in Table 2, where it is clear that increasing the starch content decreased the level of conversion, graft efficiency, graft content and water absorption of the SAP. This is attributed to the lowering level of the newly formed graft PAM, which plays the main role in water absorp-

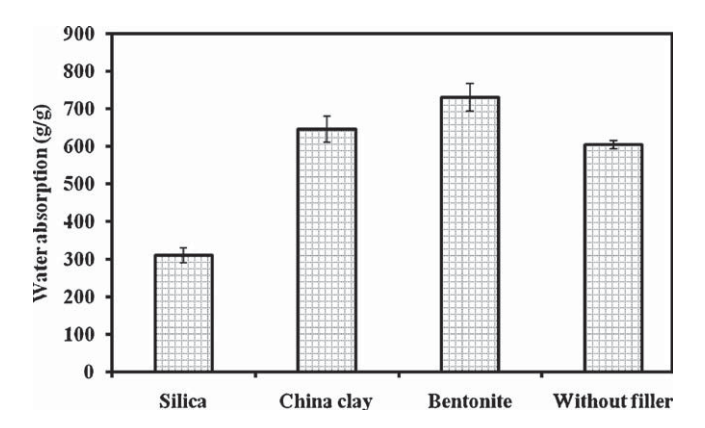


Fig. 12. Water absorption of the saponified starch-g-PAM copolymer SAP (without filler) and the derived composite based SAPCs with the indicated inorganic fillers. Data are shown as the mean \pm 1 S.D. and are derived from 3 replicate samples.

tion of the polymer. Therefore, a starch:AM (w/w) ratio of 1:1 was selected to prepare the graft copolymer for further studies.

Representative SEM micrographs of starch and of the starch-g-PAM copolymers with different starch:AM (w/w) ratios are illustrated in Fig. 11. Starch granules (Fig. 11(A)) had an irregularly oval shape and a fairly diverse array of particle sizes (in the range of 0.3– $1.2\,\mu m$ in diameter) with a smooth surface. On the other hand, the graft copolymers had a clearly different surface morphology in that the oval particle shape was absent but rather they had a coarse and broad network structure with a rather rough surface. This yields a higher water absorption capability for the copolymer, especially in the case of the SAP derived from a starch:AM (w/w) ratio of 1:1 (Fig. 11(B).

3.5. Influence of inorganic fillers

The water absorption of the saponified starch-g-PAM copolymer based SAP and the three SAPCs derived from the SAP is shown in Fig. 12, where the water absorption of the bentonite (730 g/g) and China clay (650 g/g) based SAPCs are significantly higher than those of the base SAP, i.e., without filler (606 g/g) or the silica based SAPC (310 g/g). This is because the hydration of bentonite powder is higher than that of China clay and especially silica and also that the bentonite powder dispersed more readily and produced more particulates in water than did either the China clay or the silica. Unfortunately, the incorporation of the silica resulted in a significantly lower water absorption of the resulting SAPC than that of the original starch-g-PAM copolymer based SAP. Perhaps this type of silica caused a smooth surface with a low content of coarse pores, a notion that is supported to some extent by the SEM micrographs (Fig. 13(A)). In contrast, the SAPCs formed with bentonite clay (Fig. 13(C)) and China clay (Fig. 13(B)) both showed a more porous surface which allowed a higher water intension capability of the composite.

Bentonite is an aluminium phyllosilicate absorbent and consists mostly of montmorillonite. Both bentonite and China clay are hydrous aluminium phyllosilicates, while silica is a porous silica dioxide. The former two phyllosilicates can both graft and intercalate the polymer chains but the latter cannot. The work (Foungfung, Seetapan, Phattanarudee, & Kiatkamjornwong, 2010) showed that the inclusion of phyllosilicate clay at an appropriate amount in the *in situ* polymerization of the monomer both enhances the superabsorbent polymer strength and gives a higher level of water absorption. The bentonite, after alkaline saponification, becomes

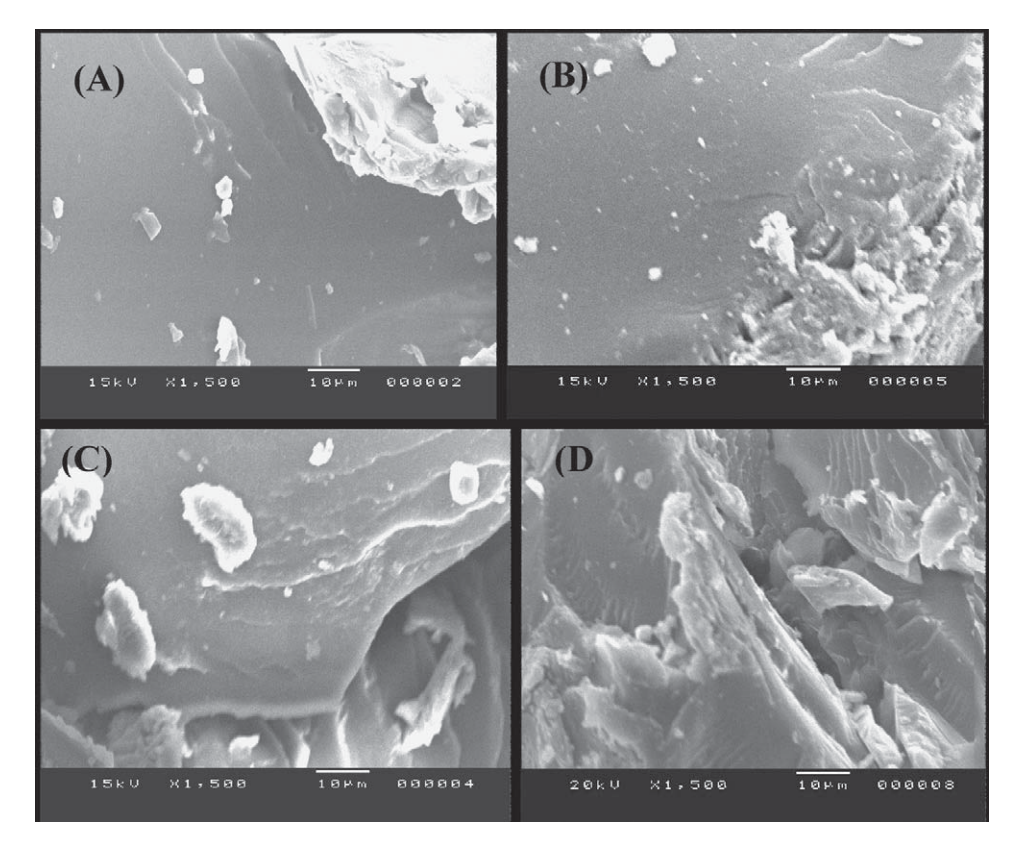


Fig. 13. Representative SEM micrographs of the purified starch-g-polyacrylamide composites with (A) silica, (B) China clay, (C) bentonite clay, and (D) without filler.

sodium bentonite which can increase the water absorption more than the kaolinite in the China clay. The *N*,*N*′-MBA crosslinker at 0.3 wt% was used for connecting the acrylamide units to starch or the acrylamide itself. Then the crosslinker could be used to crosslink the ungrafted PAM to be the crosslinked homopolymeric SAPC which can influence water absorption of the whole system. Besides, the clay powder can act as a crosslinking point and plays an important role in the formation of network structure of the SAPC (Wu, Wei, Lin, & Wu, 2003). Likewise, the *N*-MBA crosslinker might also crosslink the active site of the clay with acrylamide monomer or the starch graft PAM SAP (Foungfung et al., 2010; Wu et al., 2003).

4. Conclusions

A high water absorbing copolymer, based on the graft copolymerization of cassava starch and AM, was successfully prepared by reactive batch processing using a specially designed batch reactor. The reactor has a Reynold number of 224.7 and can mix the mixture effectively even at low water content. The highest obtained water absorption capability of the saponified starch-g-PAM copolymer was 605 g/g when prepared with a reaction time and temperature of 140 min and 80 °C, a KPS concentration of 1.5 wt% of starch and a starch: AM (w/w) ratio of 1:1. The FT-IR spectra confirmed the formation of saponified starch-g-PAM copolymer by exhibiting all the characteristic bands of both starch and AM units. The starch granules, as viewed by SEM, had irregularly oval shaped particles of variable sizes with a smooth surface. However, the graft copolymers exhibited coarse porous structures and a broad network, which may contribute to the higher water absorption capability of the copolymer and the SAPCs over the SAP. The bentonite clay SAPC exhibited the highest water absorption capability (ca. 730 g/g), significantly higher than that of the unfilled graft copolymer SAP (606 g/g). This is due to larger hydration of bentonite powder than those of the China clay and silica.

Acknowledgements

The authors thank the Thailand Research Fund for funding the research project under the Senior Scholarly Consolidation (Grant no. RTA5080004). Many thanks go to the Prince of Songkla University (Pattani Campus) and Chulalongkorn University for research facilities and other support from Publication Consultation Unit of the Research Division, Faculty of Science, Chulalongkorn University.

References

Athawale, V. D., & Lele, V. (1998). Graft copolymerization onto starch. II. Grafting of acrylic acid and preparation of it's hydrogels. *Carbohydrate Polymers*, 35(1–2), 21–27.

Athawale, V. D., & Lele, V. (2000). Thermal studies on granular maize starch and its graft copolymers with vinyl monomers. *Starch/Stärke*, 52(6–7), 205–213.

Carr, M. E., Kim, S., Yoon, K. J., & Stanley, K. D. (1992). Graft polymerization of cationic methacrylate, acrylamide, and acrylonitrile monomers onto starch by reactive extrusion. *Cereal Chemistry*, 69, 70–75.

Caykara, T., Bozkaya, U., & Kantoğlu, Ö. (2003). Network structure and swelling behavior of poly(acrylamide/crotonic acid) hydrogels in aqueous salt solutions. *Journal of Polymer Science Part B: Polymer Physics*, 41(14), 1589–1778.

Chen, J., Park, H., & Park, K. (1999). Synthesis of superporous hydrogels: Hydrogels with fast swelling and superabsorbent properties. *Journal of Biomedical Materials Research Part A*, 44, 53–62.

Chen, L., Ni, Y., Bian, X., Qiu, X., Zhang, X., Chen, X., et al. (2005). A novel approach to grafting polymerization of ε -caprolactone onto starch granules. *Carbohydrate Polymers*, 60(1), 103-109.

Fanta, G. F. (1996). Starch graft copolymers. In J. C. Salamone (Ed.), Polymeric materials encyclopedia (pp. 7901–7910). Florida: CRC Press.

Finkenstadt, V. L., & Willett, J. L. (2005). Reactive extrusion of starch-polyacrylamide graft copolymers: Effects of monomer/starch ratio and moisture content. *Macromolecular Chemistry and Physics*, 206(16), 1648–1652.

Foungfung, D., Seetapan, N., Phattanarudee, S., & Kiatkamjornwong, S. (2010). Acrylamide-itaconic acid superabsorbent polymers and superabsorbent polymer/mica nanocomposites. *Polymers for Advanced Technologies*, 10.1002/pat.1559.

Karadağ, E., Üzüm, O. B., & Saraydin, D. (2005). Water uptake in chemically crosslinked poly(acrylamide-co-crotonic acid) hydrogels. *Materials & Design*, 26(4), 265–270.

- Kiatkamjornwong, S., Mongkolsawat, K., & Sonsuk, M. (2002). Synthesis and property characterization of cassava starch-g-poly[acrylamide-co-(maleic acid)] via gamma-irradiation. *Polymer*, 43(14), 3915–3924.
- Lanthong, P., Nuisin, R., & Kiatkamjornwong, S. (2006). Graft copolymerization, characterization and degradation of cassava starch-g-acrylamide/itaconic acid superabsorbents. *Carbohydrate Polymers*, 66, 229–245.
- McGill, W. B., & Figueiredo, C. T. (1993). Chapter 22, Total nitrogen. In M. R. Carter (Ed.), Soil sampling and methods of analysis (pp. 201–211). Boca Raton: Lewis.
- Mostafa, Kh. M. (1995). Graft polymerization of acrylic acid onto starch using potassium permanganate acid (redox system). *Journal of Applied Polymer Science*, 56(2), 263–269.
- 56(2), 263–269.
 Wade, L. G., Jr. (1991). Organic chemistry (p. 967). Englewood Cliffs: Prentice Hall.
 Weaver, M. O., Montgomery, R. R., Miller, L. D., Sohns, V. E., Fanta, G. F., & Doane, W. M.
 (1977). A practical process for the preparation of Super Slurper, a starch-based
 polymer with a large capacity to absorb water. Starch/Stärke, 29(12), 413–422.
- Willett, J. L., & Finkenstadt, V. L. (2003). Preparation of starch-graft-polyacrylamide copolymers by reactive extrusion. *Polymer Engineering and Science*, 43(10), 1666–1674.
- Willett, J. L., & Finkenstadt, V. L. (2006). Reactive extrusion of starch–polyacrylamide graft copolymers using various starches. *Journal of Polymers and the Environment*, 14(2), 125–129.
- Wu, J, Wei, Y., Lin, J., & Wu, S. L. (2003). Study of starch-graft-acrylamide/mineral powder superabsorbent composite. *Polymer*, 44(21), 6513–6520.
- Yoon, D. J., Carr, M. E., & Bagley, E. B. (1992). Reactive extrusion vs. batch preparation of starch-g-polyacrylonitrile. *Journal of Applied Polymer Science*, 45(6), 1093–1100.
- Zhang, J., Li, A., & Wang, A. (2006). Study on superabsorbent composite. VI. Preparation, characterization and swelling behaviors of starch phosphate-graft-acrylamide/attapulgite superabsorbent composite. Carbohydrate Polymers, 65(2), 150–158.



Contents lists available at ScienceDirect

Carbohydrate Polymers

journal homepage: www.elsevier.com/locate/carbpol



Enhancing antibacterial activity of chitosan surface by heterogeneous quaternization

Napanporn Vallapa ^{a,b}, Oraphan Wiarachai ^{a,b}, Nuttha Thongchul ^c, Jisheng Pan ^d, Varawut Tangpasuthadol ^e, Suda Kiatkamjornwong ^f, Voravee P. Hoven ^{e,*}

- a Program in Petrochemistry and Polymer Science, Faculty of Science, Chulalongkorn University, Phayathai Road, Pathumwan, Bangkok 10330, Thailand
- b Center for Petroleum, Petrochemicals, and Advanced Materials, Chulalongkorn University, Phayathai Road, Pathumwan, Bangkok 10330, Thailand
- c Institute of Biotechnology and Genetic Engineering, Chulalongkorn University, Phayathai Road, Pathumwan, Bangkok 10330, Thailand
- d Institute of Materials Research and Engineering, A*STAR (Agency for Science, Technology and Research), Research Link, Singapore 117602, Singapore
- e Organic Synthesis Research Unit, Department of Chemistry, Faculty of Science, Chulalongkorn University, Phayathai Road, Pathumwan, Bangkok 10330, Thailand
- Department of Imaging and Printing Technology, Faculty of Science, Chulalongkorn University, Phayathai Road, Pathumwan, Bangkok 10330, Thailand

ARTICLE INFO

Article history: Received 24 July 2010 Received in revised form 26 August 2010 Accepted 29 August 2010 Available online 6 September 2010

Keywords:
Chitosan
Antibacterial activity
Quaternary ammonium group
Hydrophobicity
Surface modification

ABSTRACT

This research aimed to increase the antibacterial activity of the chitosan surface by introducing quaternary ammonium groups via a heterogeneous two-step process: reductive alkylation using a series of different aldehydes followed by methylation with methyl iodide. ATR-FTIR and XPS analyses, together with water contact angle and zeta potential measurements, confirmed the success of the surface quaternization. The antibacterial activity of the surface-quaternized chitosan film against *Staphylococcus aureus* and *Escherichia coli*, as model Gram-positive and Gram-negative bacteria, respectively, were superior to that of the virgin chitosan film. The apparent damaged bacterial morphology upon contact with the surface-quaternized chitosan film was verified by SEM. Thus, the introduction of additional positive charges to the chitosan surface via the versatile and yet simple process of heterogeneous quaternization can significantly improve the antibacterial activity of the chitosan surface, especially in a neutral environment.

© 2010 Elsevier Ltd. All rights reserved.

1. Introduction

Chitosan has progressively attracted attention due to its multiple bioactivities, such as antimicrobial (Lim & Hudson, 2004; Ong, Wu, Moochhala, Tan, & Lu, 2008) and antitumor (Gorbach et al., 1994). The antibacterial activity, in particular, has been followed with great interest. Chitosan inhibits the growth of a fairly diverse range of bacteria (Choi et al., 2001; Fujimoto, Tsuchiya, Terao, Nakamura, & Yamamoto, 2006) and thus offer great benefit to a wide variety of applications, ranging from medical (Alves & Mano, 2008) to agriculture (Campaniello, Bevilacqua, Sinigaglia, & Corbo, 2008) The exact mechanism of the antimicrobial action of chitosan is still ambiguous, although six main mechanisms, none of which are mutually exclusive, have been proposed (Raafat, von Bargen, Haas, & Sahl, 2008; Rabea, Badawy, Stevens, Smagghe, & Steurbaut, 2003) as follows: (1) Interactions between the positively charged moieties on the chitosan molecules and those negatively charged ones on the microbial cell outer membranes leads to changes in the cell membrane structure and permeability inducing the leakage of proteinaceous and other intracellular constituents and so challenging the biochemical and physiological competency of the bacteria leading to loss of replicative ability and eventual death. (2) Chitosan acts as a chelating agent that selectively binds trace metals and subsequently inhibits the production of toxins and microbial growth. (3) Chitosan activates several defense processes in the host tissue, acts as a water binding agent and inhibits various enzymes. (4) Low molecular weight chitosan penetrates the cytosol of the microorganisms and, through the binding of chitosan with DNA, results in the interference with the synthesis of mRNA and proteins. (5) Chitosan on the surface of the cell can form an impermeable polymeric layer which alters the cell permeability and prevents nutrients from entering the cell. (6) Finally, since chitosan can adsorb the electronegative substances in the cell and flocculate them, it disturbs the physiological activities of the microorganism leading to their death

Nonetheless, chitosan, shows its antibacterial activity only in acidic medium, which is ascribed to the poor solubility of chitosan above its pK_a (pH 6.5). For this reason, a number of chitosan derivatives have been developed not only to expand the use of chitosan into a broader pH range and so media but also to improve the bactericidal actions of chitosan. Amongst all the derivatives that exhibit superior antibacterial activity to native

^{*} Corresponding author. Tel.: +66 2218 7626–7; fax: +66 2218 7598. E-mail address: vipavee.p@chula.ac.th (V.P. Hoven).

chitosan, quaternary ammonium-containing ones have gained the most attention. They are typically synthesized either by direct quaternization of the amino groups of chitosan using alkyl halides under alkaline conditions (Domard, Rinaudo, & Terrassin, 1986; Polnok, Borchard, Verhoef, Sarisuta, & Junginger, 2004), by reductive N-alkylation reaction of chitosan with aldehydes via Schiff's base intermediates followed by quaternization with methyl iodide (Muzzarelli & Tanfani, 1985; Sajomsang, Gonil, & Saesoo, 2009) or by reductive N-alkylation reaction of chitosan with quaternary ammonium-type aldehydes (Suzuki, Oda, Shinobu, Saimoto, & Shigemasa, 2000). Reaction of the amino groups of chitosan with glycidyltrimethylammonium chloride (GTMAC) has been introduced as an alternative for N-selective reaction under acidic and neutral conditions (Seong, Whang, & Ko, 2000; Sun, Du, Fan, Chen, & Yang, 2006). A recent review on the synthesis and applications of quaternized derivatives of chitosan have been available in published literatures (Mourya & Inamdar, 2009; Sajomsang, 2010).

Chitosan in its solid form (film, fiber or particles) holds promising values in many applications for which interfacial contact inhibition is sufficient, although its bactericidal action is only favorable in acidic media (pH < 6.5) when most of its amino groups hold their cationic character. As a means to permanently introduce a positive charge to solid chitosan, without having to incorporate additional cationic species or altering the processability of chitosan, heterogeneous quaternization seems to be an attractive approach. The reactions can be accomplished in the absence of tedious purification process that are certainly required if the quaternization is done homogeneously in solution. Chitosan can be fabricated into the desired solid form (film, fiber or particle) prior to the surface modification. Previously, we have demonstrated that it is conceivable to tune the surface properties of chitosan, namely hydrophilicity/hydrophobicity, and protein adsorption, by chemical modification of the chitosan surface by choosing the suitable reagents under a heterogeneous condition (Amornchai, Hoven, & Tangpasuthadol, 2004; Hoven, Tangpasuthadol, Angkitpaiboon, Vallapa, & Kiatkamjornwong, 2007; Tangpasuthadol, Pongchaisirikul, & Hoven, 2003).

This research aimed to conduct the quaternization of chitosan by a well-developed chemistry based on a two-step approach using firstly a reductive *N*-alkylation reaction of chitosan with aldehydes via the formation of Schiff's base intermediates, followed by quaternization with methyl iodide. Besides the positive charge of quaternary ammonium groups, it is envisaged that the hydrophobicity introduced from the hydrocarbon chains of the different aldehydes should help elevate the antibacterial activities, as has been formerly described by others (Badawy, 2010; Kim & Choi, 2002; Ye et al., 2007).

2. Materials and methods

2.1. Materials

Chitosan flakes (DAC of 92%, M_V = 550,000 Da) were purchased from Seafresh Chitosan (Lab) Co., Ltd. (Thailand). Chitosan films and particles were prepared according to the published procedure by Hoven et al. (2007) and Qi, Xu, Jiang, Hu, and Zou (2004), respectively. Methanol, as commercial grade, was distilled over 4A molecular sieves prior to use. Methyl iodide (CH₃I), acetaldehyde, glutaraldehyde, sodium borohydride (NaBH₄), sodium iodide (NaI) and were all purchased from Fluka (Switzerland), and used as received. Benzaldehyde and butyraldehyde were purchased from Merck (Germany) and Sigma Chemical Co. (USA), respectively, and used as received. *Staphylococcus aureus* (*S. aureus*) and *Escherichia coli* (*E. coli*) were purchased from the National Center for Genetic Engineering and Biotechnology (Thailand). Trypicase soy agar (TSA)

and Trypicase soy broth (TSB) were purchased from PPL System Co., Ltd. (Thailand). Phosphate buffer saline (PBS) was supplied by Aldrich (USA). Ultrapure distilled water was obtained after purification using a Millipore Milli-Q system (USA).

2.2. Preparation of N-alkyl chitosan films or particles

An anhydrous methanol solution of each selected aldehyde (10 mL) at the desired concentration (0.4–1 M) was added into a flask containing chitosan films (2 cm \times 2 cm) or particles (0.03 g). After stirring for a given time at ambient temperature (\sim 28–30 $^{\circ}$ C), NaBH₄ (0.3 g, 0.8 mol) was added into the reaction mixture and the solution was stirred for 24 h. The films were removed from the solution, rinsed thoroughly with methanol, and dried *in vacuo*. In the case of particles, they were isolated by centrifugation at 6000 rpm. The supernatant was discarded and the particles were resuspended in and centrifugally washed with methanol three times prior to being dried *in vacuo*.

2.3. Preparation of quaternized N-alkyl chitosan films or particles

An anhydrous methanol solution of NaI (0.2 M) was added via syringe into a flask containing N-alkyl chitosan films (2 cm \times 2 cm) or particles (0.03 g) and NaOH (0.13 g, 0.3 mol). The total volume of the reaction mixture was 10 mL and the concentration of CH₃I was varied within a range of 0.4–2.4 M. The reaction mixture was stirred at 50 °C for the indicated time and then the films were removed from the solution, rinsed thoroughly with methanol, and dried in vacuo. In the case of particles, they were isolated by centrifugation, washed with methanol and dried in vacuo as detailed above.

2.4. Characterization of surface-quaternized chitosan films/particles

A contact angle goniometer, model 100-00, equipped with a Gilmont syringe and a 24-gauge flat-tipped needle (Ramé-Hart, Inc., USA), was used for the determination of water contact angles. The reported angle expressed as the mean ± 1 standard deviation is the average of five measurements on different areas of each sample. All attenuated total reflectance-Fourier transform infrared (ATR-FTIR) spectra were collected at a resolution of 4 cm⁻¹ and for 128 scans using a Nicolet Magna 750 FT-IR spectrometer (USA) equipped with a liquid-nitrogen-cooled mercury-cadmium-telluride (MCT) detector using a variable angle reflection accessory (SeagullTM, Harrick Scientific, USA) with a hemispherical Ge IRE. X-ray photoelectron spectroscopy (XPS) analysis was performed using a VG ESCALAB 220i-XL instrument (UK) equipped with a monochromatic Al Kα (1486.7 eV photons) and an unmonochromated Mg Kα X-ray source (1253.6 eV photons). The zeta potential of chitosan particles was determined using a Zetasizer Nano-ZS (Malvern Instruments, UK) at 25 °C using a scattering angle of 173°. All data are displayed as the mean \pm 1 standard deviation and are derived from at least three independent experiments.

2.5. Evaluation of antibacterial activity

All glasswares used for the tests were sterilized in an autoclave at 121 °C for 15 min prior to use. The quaternized N-alkyl chitosan films or particles were sterilized by exposing to UV radiation for 30 min prior to the tests. The quaternized N-alkyl chitosan films (1 cm \times 1 cm) were placed one per well of a 24-well plate containing 2 mL TSB. Then 12 μ L of bacterial suspension in distilled water (OD₆₀₀ = 0.5) was pipetted into each well and the plate incubated in a shaking incubator (Model G-25, New Brunswick Scientific Co., Inc., USA) at 37 °C, 110 rpm, for 24 h. The bacterial suspension (100 μ L) was then transferred from each well into a well of a 96-well plate

R = ethyl (QECS), butyl (QBuCS), benzyl (QBzCS)

Scheme 1. Surface quaternization of chitosan.

to determine the OD $_{600}$ by UV–vis spectroscopy (Multi-Detection Microplate Reader Model All, Bio-Tek TM Instruments Inc., USA). Another 100 μ L of each of the bacterial suspensions was diluted 10^{10} times and 100 μ L of this diluted bacterial suspension was then spread onto TSA. After incubating at 37 °C for 24 h, the number of colonies, and thus replication competent bacteria were then counted as a measure of assumed viability. The results, after correction for the dilution factor, were expressed as the mean number of colony forming units per volume (CFU/mL). All tests of antibacterial activity were performed in triplicate per sample and upon at least three independent samples. The antibacterial ratio was calculated using the following relationship:

antibacterial ratio (%) =
$$\frac{A-B}{A} \times 100$$
 (1)

where A is a number of original viable bacterial cell after incubation in media alone (control) and B is a number of viable bacterial cell after incubation with the designated chitosan film.

Statistical analysis was performed using the Statistical Package for the Social Science (SPSS) version 17.0 software. Statistical comparisons were made by One-Way Analysis of Variance (ANOVA) with the Least Square Difference (LSD) tests post hoc evaluations of differences between groups. The threshold level for accepting statistical significance was set at p < 0.05.

2.6. Determination of bacterial morphology

Bacterial morphology on the quaternized N-alkyl chitosan films was examined under a scanning electron microscope (SEM, JEOL Model JSM-5800L, Japan). After incubation with the bacterial suspension (OD $_{600}$ = 0.5) for 24 h, the quaternized N-alkyl chitosan films were removed from the bacterial suspension by sterile forceps and immersed in 3% (w/v) glutaraldehyde solution at 4 °C in order to fix the adherent bacteria on the films. After 24 h, the glutaraldehyde solution was removed and the films were washed with PBS, followed by a stepwise dehydration with 30%, 50%, 70%, 90% and 100% (v/v) ethanol in water for 10 min each. The films were then dried and sputter-coated with a thin film of gold before being characterized by SEM.

3. Results and discussion

3.1. Surface quaternization

The methods used for modifying the chitosan surface are outlined in Scheme 1. The reaction introduces quaternary ammonium groups via a heterogeneous two-step process, the reductive N-alkylation using selected aldehydes followed by methylation with methyl iodide to form quaternized N-alkyl chitosan surface. Contact angle analysis was used to monitor the extent of both reductive N-alkylation and quaternization as a function of reaction time and reagent concentrations. As shown in Fig. S1 (Supplementary data), the reaction with butyraldehyde and benzaldehyde, but not acetaldehyde, intrinsically introduced additional hydrophobicity to the chitosan films. Water contact angle of the virgin chitosan film is $79.8 \pm 3.1^{\circ}$. The trend was reversed, however, in the case

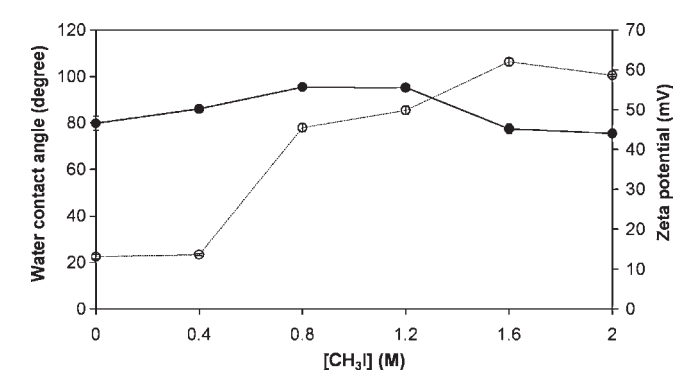


Fig. 1. Water contact angle (\bullet) and zeta potential (\bigcirc) of the quaternized *N*-benzyl chitosan film/particle prepared by methylation of the *N*-benzyl chitosan film/particle using varied [CH₃I].

of acetaldehyde. Upon using the optimized condition that yield the maximum extent of surface reductive N-alkylation (summarized in Table S1, Supplementary data), the water contact angle of N-ethyl chitosan film, N-butyl chitosan film, and N-benzyl chitosan film was $82.1 \pm 0.7^{\circ}$, $93.8 \pm 0.8^{\circ}$, and $93.0 \pm 2.3^{\circ}$, respectively. A series of quaternized N-alkyl chitosan films were subsequently obtained by methylation of these three different N-alkyl chitosan films. According to Fig. S2 shown in the Supplementary data, the surface of all N-alkyl chitosan films essentially became more hydrophilic after quaternization. Upon using a reaction time of $12 \, h$, the optimized methyl iodide [CH $_3$ I] for the step of methylation of all N-alkyl chitosan substrates together with their lowest water contact angles obtained are displayed in Table S2 (Supplementary data).

In order to verify that the reductive N-alkylation followed by methylation can increase the magnitude of positive charges on the chitosan surface, a series of surface-quaternized chitosan particles prepared by conditions equivalent to those used for the films were subjected to zeta potential measurements. The results, also summarized in Table S2, reveal that, as anticipated, all surfacequaternized chitosan particles possessed higher zeta potential values than the virgin unmodified chitosan particles (zeta potential = +13.11 \pm 0.6 mV). The highest zeta potential (+58.60 \pm 0.3 mV) was achieved in the case of the quaternized N-benzyl chitosan (QBzCS) particles implying that its charge magnitude can be broadly tailored. To test this hypothesis, a series of QBzCS films/particles were prepared from N-benzyl chitosan films/particles using varied concentrations of CH₃I (Fig. 1), where the degree of quaternization, expressed in terms of zeta potential value, clearly increased as a function of the CH₃I concentration used. The water contact angle, on the other hand, was initially raised as the CH3I concentration was increased up to 0.8-1.2 M, reaching a maximal value of $\sim 95^{\circ}$, but the surface then became more hydrophilic as the CH₃I concentration was increased further to 1.6-2.0 M. This trend can be explained as a result of the balance between two competing effects. The methyl groups introduced from CH₃I during quaternization enhance the hydrophobicity of the N-benzyl chitosan film. However, the higher level of methylation leads to the greater magnitude of surface positive charge density due to the formation of quaternary ammonium groups. The surface of the modified chitosan film thus became more hydrophilic at high levels of quaternization. The lowest water contact angle obtained in the series was $\sim 75^{\circ}$.

ATR-FTIR spectroscopy was also used to confirm the success of quaternization of *N*-alkyl chitosan (Fig. 2). Absorption peaks at 1650 cm⁻¹ and 1590 cm⁻¹ were assigned to the C=O stretching (Amide I) and N-H bending (Amide II) of the glucosamine unit, respectively. After the reaction, the peak intensity of the N-H bending of chitosan at 1590 cm⁻¹ correspondingly decreased, whereas the intensity of C-H deformation peaks at 1470 cm⁻¹ increased, indicating that the substitution of the alkyl groups occurred at the

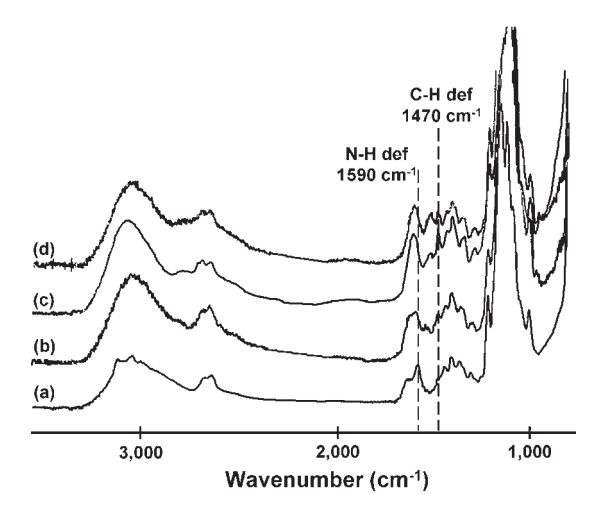


Fig. 2. ATR-FTIR spectra of the (a) chitosan, (b) QECS, (c) QBuCS, and (d) QBzCS films.

amino group of the chitosan film. The results from the ATR-FTIR analysis apparently indicated that the reaction should proceed to a depth of at least $1-2~\mu m$ (estimated depth of ATR-FTIR sensitivity).

XPS analysis further supports the success of surface quaternization on QBuCS and QBzCS films (Fig. 3), which were selected as representative samples from the series to be characterized by XPS. Besides C, O, and N, the basic elements already present in the chitosan film, there were no additional elements introduced to the chitosan surface after reductive N-alkylation and methylation. The only way to detect the quaternary ammonium groups after surface modification is by considering the N 1s spectrum of the surfacequaternized chitosan film in comparison with the virgin chitosan film. As seen from Fig. 3(a), the N 1s peak of the virgin chitosan film can be fitted with one peak at 400 eV. The N 1s signals of both QBuCS and QBzCS films (Fig. 3(b) and (c)), on the other hand, can be split into two peaks. One appears at the same binding energy as the chitosan film (Peak A). The other having higher binding energy emerges at 403 eV (Peak B). This latter peak can be regarded as a signal from the positively charged nitrogen atom of the quaternary

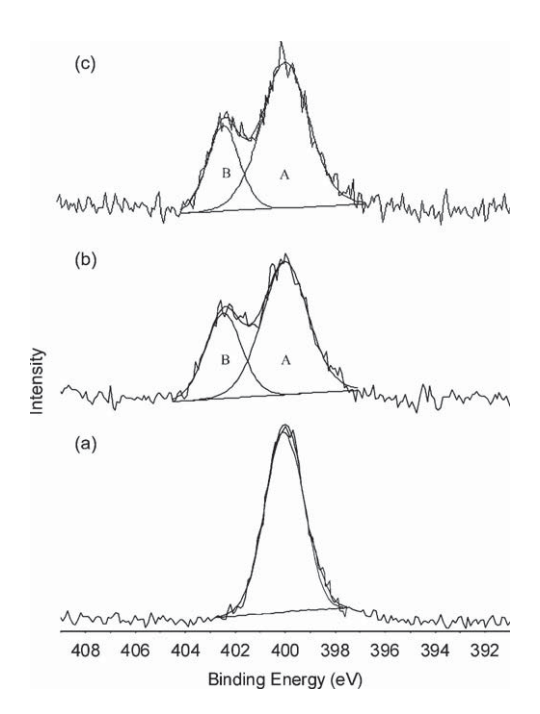
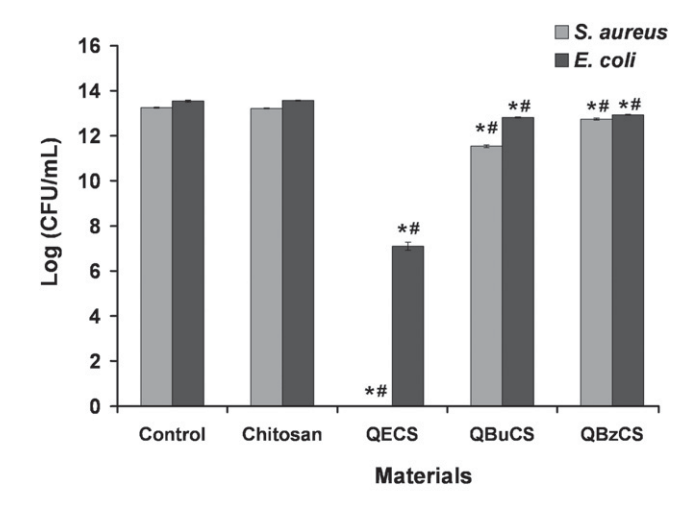


Fig. 3. XPS N 1s spectra of (a) chitosan, (b) QBuCS, and (c) QBzCS films.



	11	% Antibacter	ial ratio		
S.aureus	0.00	7.80	100.00	98.04	69.27
E.coli	0.00	0.00	99.99	81.00	75.00

Fig. 4. Total replication competent (viable) cell counts of bacteria grown for 24h in media alone (control) or in the presence of chitosan and different quaternized N-alkyl chitosan films, and below in the table, the corresponding antibacterial ratio. Statistical significance with p < 0.05 of the viable count is compared with the control (*) and the chitosan film (#).

ammonium moiety. The %DQ in the surface region could be estimated from the relative ratio of atomic composition of Peak A to Peak B. For the QBzCS series, it was found that the %DQ of the *N*-benzyl chitosan film after quaternization with 0.4 M and 1.6 M CH₃I was equal to 19.2% and 39.6%, respectively. To some extent, these values corresponded with the zeta potential values measured on the quaternized chitosan particles (see Fig. 1 for comparison).

3.2. Evaluation of antibacterial activity

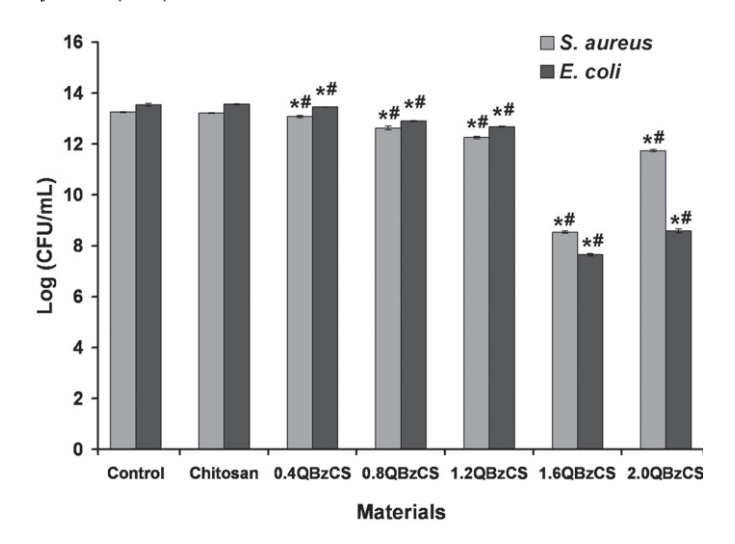
The antibacterial activity of the quaternized *N*-alkyl chitosan films was tested against the Gram-positive and Gram-negative representative bacteria, S. aureus and E. coli, respectively, in terms of the total number of replication competent (viable) cells as mean colony forming units per volume (CFU/mL). In order to determine the effect of the alkyl substituent on the antibacterial activity of the three quaternized N-alkyl chitosan films, QECS, QBuCS and QBzCS, having a similar zeta potential of ~30 mV were selected for the investigation. It is interesting to see from Fig. 4 that the chitosan film, at pH 7.4, showed almost no antibacterial action in comparison with the control of which the bacteria were grown in the absence of chitosan film. This is not quite unexpected, considering that the amino groups on the surface of chitosan films are in the neutral form, not positively charged, at that pH. This also implied that the chelation of the amino groups of chitosan, which has been proposed by others (Cuero, Osuji, & Washington, 1991; Kong et al., 2008) as one of the antibacterial mechanism, does not play a major role in this particular case. This outcome, in fact, suggests a potential significance for the surface quaternization in promoting antibacterial activity under a neutral environment.

Apparently, the QECS and QBuCS films exhibited a greater antibacterial activity than the QBzCS film against both bacterial species. Among all surface-quaternized chitosan films, it seems that the greater the hydrophobicity of the film was, the lower the antibacterial activity was obtained considering that all samples having the similar zeta potential. With the highest water contact angle value $(93.0 \pm 1.4^{\circ})$, the QBzCS film was not the best

substrate to interact with the bacteria, as previously anticipated based on the assumption that the hydrophobic character should favor the interaction with the lipid bilayers, another major component of the bacterial membrane and subsequently enhances the antibacterial activity. The QECS, on the other hand, exhibited the highest antibacterial activity despite its lowest water contact angle $(71.7 \pm 0.9^{\circ})$ in the series. This somewhat suggested that the bactericidal action of the surface-quaternized chitosan film may take place through not only the contact-inhibitory mechanism as previously expected, but also through a release-inhibitory mechanism similar to what has been observed for soluble chitosan and its quaternized derivatives. A similar speculation that the surface leaching of a soluble protonated glucosamine fraction from the chitosan film as being responsible for the antibacterial activity has also been made recently by Fernandez-Saiz, Lagaron, and Ocio (2009). The extent of weight loss which is presumably caused by surface erosion of all surface-quaternized chitosan films determined by gravimetric analysis was varied roughly in a similar range of 0.1–0.2%. Although there was no specific correlation between the magnitude of weight loss and the type of quaternized derivative, it should be more likely for the QECS to possess the greatest ability to erode out considering its lowest hydrophobicity in the series. It should be noted that there was no detectable weight loss in the case of the virgin, unmodified chitosan film.

The QECS film was detrimental to both S. aureus and E. coli, although perhaps at a greater magnitude to S. aureus, where it yielded a 100% and almost a 100% antibacterial ratio against S. aureus and E. coli, respectively. The QBuCS film delivered a better inhibitory effect on the Gram-positive bacteria, S. aureus than the Gram-negative bacteria, E. coli, but neither was as strong as that seen for the QECS film. It is conceivable that the absence of an outer membrane and the presence of negatively charged teichoic acid within a thick peptidoglycan layer (20–80 nm) on the surface of S. aureus (Talaro, 2005) should make them more attractive to the positively charged, quaternized chitosan films and easier to be damaged through the contact-inhibitory mechanism than E. coli (Fernandez-Saiz et al., 2009). Although E. coli, with its thinner double protective layer (the outer lipopolysaccharide layer embedded with a number of small channels of porins and the inner peptidoglycan layer (7–8 nm)) (Talaro, 2005) should be more structurally vulnerable to damage than S. aureus, which has a peptidoglycan layer that is several magnitudes thicker than that of *E. coli*, it has been recently been reported, based on AFM analysis, that the stiffness of S. aureus is indeed lower than that of E. coli (Fernandez-Saiz et al., 2009). However, that did not seem to be the case for the QBzCS films. The antibacterial activity against E. coli was relatively comparable to that against S. aureus. In fact, the higher susceptibility of E. coli than S. aureus towards chitosan has also been reported before by others (Chung et al., 2004; Devlieghere, Vermeulen, & Debevere, 2004) For comparison, the investigation was also conducted on the chitosan film that was quaternized by direct methylation with $1.2\,M\ CH_3I$ for $8\,h.$ It was found that the methylated chitosan film having a comparable zeta potential of +29.3 mV exhibited %antibacterial ratio of ~26 and 29% against *S. aureus* and *E. coli*, respectively. These significantly lower antibacterial efficiency values as opposed to those of the QECS, QBuCS, and QBzCS films helped verifying the indispensable role of the alkyl groups namely ethyl, butyl, and benzyl, respectively, introduced in the step of reductive alkylation, in enhancing the antibacterial activity of the chitosan surface via heterogeneous quaternization.

To further demonstrate the influence of the chitosan surface positive charge density on the antibacterial activity, the latter was examined against *E. coli* and *S. aureus* on a series of QBzCS films in which the charge magnitude was varied as a function of the CH₃I concentration used in the quaternization step. It should be noted that the number written in front of QBzCS displayed in the hor-



% Antibacterial ratio							
S.aureus	0.00	7.80	27.00	75.90	89.94	99.99	96.92
E.coli	0.00	0.00	17.00	77.00	86.28	99.99	99.99

Fig. 5. Total replication competent (viable) cell counts of bacteria grown for 24h in media alone (control) or in the presence of chitosan and QBzCS films having different degree of quaternization (varied as a function of the CH₃I concentration) and below in the table, the corresponding antibacterial ratio. Statistical significance with p < 0.05 of the viable count is compared with the control (*) and the chitosan film (#)

izontal axis of Fig. 5 represents the CH_3I concentration used for preparing each QBzCS film. The viable count data shown in Fig. 5 suggested that the antibacterial activity of the surface-quaternized chitosan carrying the same hydrocarbon moiety from the step of N-reductive alkylation, benzyl group in this case, can be proportionally tailored as a function of the CH_3I concentration. Besides the increase in charge density, the elevated hydrophilicity introduced by quaternization may also help promote antibacterial activity of the QBzCS films, perhaps through the same mechanism previously described based on surface erosion. This may be the reason why the highly quaternized QBzCS films that were prepared from 1.6 M and 2.0 M of CH_3I and possessed relatively low water contact angles (see Fig. 1 for data) are so potent that they can almost entirely suppress the bacterial growth ($\sim 100\%$ antibacterial ratio).

In order to determine the morphological changes of bacteria upon prolonged contact with the surface-quaternized chitosan, and to be able to simultaneously correlate the extent of damage with charge magnitude of the chitosan surface, SEM analysis was conducted on the surface of the series of QBzCS films having varied charge magnitude which can be manipulated as a function of CH₃I concentration. It was our intention not to rinse the surfacequaternized film after incubation with the bacterial suspension in order to keep as many bacterial cells adhered onto the film surface as possible, so that both normal and damaged cells can be observed in case they, as is likely, vary in their adherent strength. As revealed in Fig. 6(a) and (b), the typical spherical shape and clustered formation of S. aureus cells (Eaton, Fernandes, Pereira, Pintado, & Malcata, 2008) was evident on the surface of chitosan and 0.4QBzCS films with no detectable signs of damage. This corresponds quite well with the fact that the CS and 0.4QBzCS film exhibited no and low antibacterial action against S. aureus, respectively. Although most of bacteria on the surface of the 0.8QBzCS and 1.2QBzCS films appear normal in morphology, the cells became less clustered and apparent morphological damage can be easily visualized, especially by those pointed out by arrows and magnified images shown in the inset in Fig. 6(c) and (d). Some cells were ruptured with broken

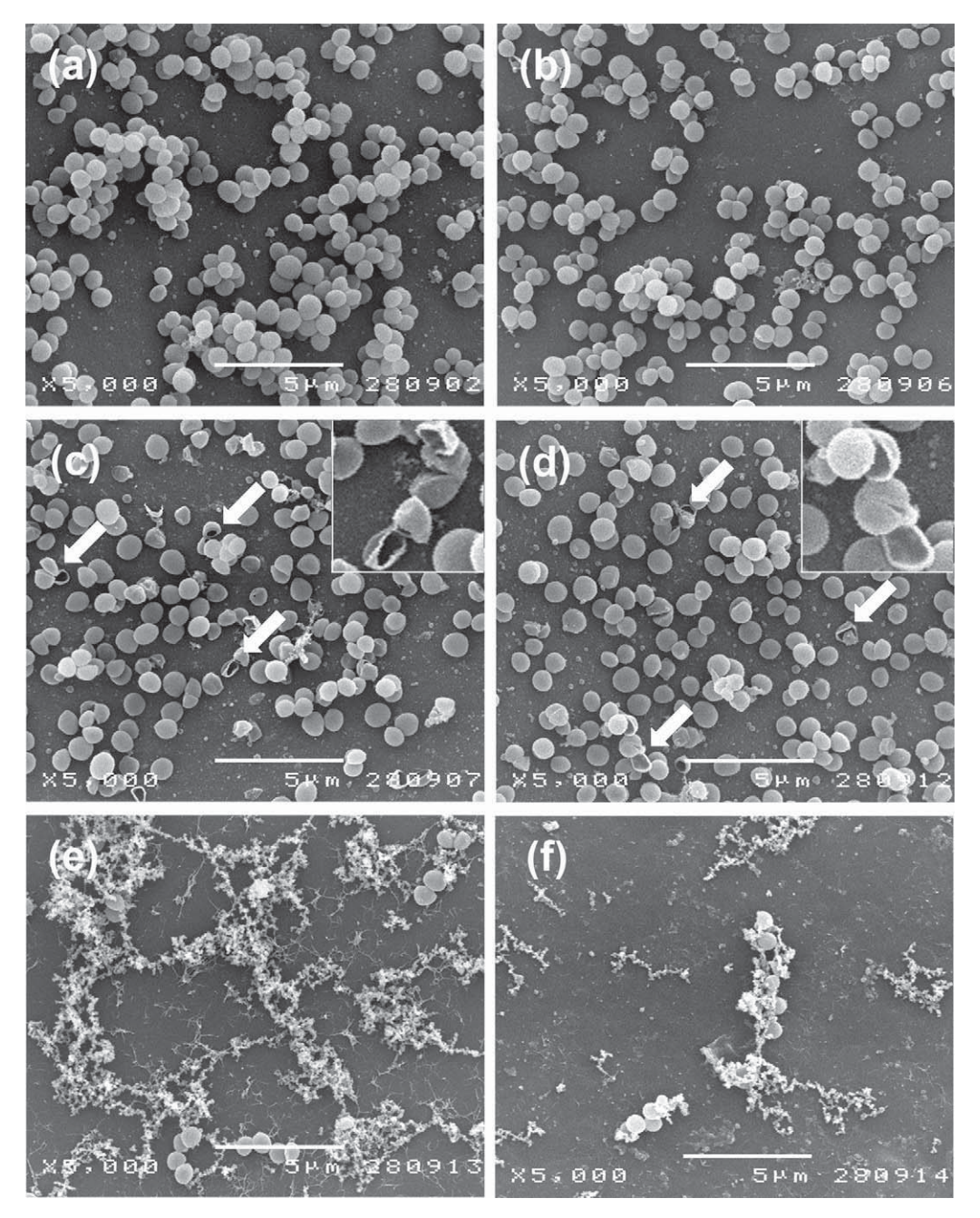


Fig. 6. SEM micrographs of (a) chitosan, (b) 0.4QBzCS, (c) 0.8QBzCS, (d) 1.2QBzCS, (e) 1.6QBzCS, and (f) 2.0QBzCS films after being incubated with the suspension of *S. aureus* (OD₆₀₀ = 0.5) for 24 h. Micrographs shown are representative of at least 5 such fields of view per sample and 3 independent samples.

cell membranes, others were deformed, collapsed and shrunken in size. A further increase in the surface charge density caused extensive lysis of the cells and only few intact bacteria remained on the surface of the 1.6QBzCS and 2.0QBzCS films (Fig. 6(e) and (f)). It is feasible that what appear on those surfaces are fragments of disrupted cytoplasmic membrane and/or intracellular components of the bacteria.

Similar destructive features were also observed in the case of *E. coli* (Fig. 7), even though there was a higher density of *E. coli* cells in the suspension containing chitosan and 0.4QBzCS films than those containing other QBzCS films (see Fig. 5), very few of them adhered onto the surface of chitosan and 0.4QBzCS films, even despite the absence of agitation and washing prior to fixation of the samples, as can be seen from Fig. 7(a) and (b). This may imply that there

are no particular attractive forces between the virgin and slightly surface-modified chitosan films under a neutral pH environment. This is entirely the opposite behavior to that observed for S. aureus under the same conditions. Nevertheless, the damage to E. coli cells became apparent with the QBzCS films having a greater extent of quaternization. As indicated by the arrows, and shown in the insets, in Fig. 7(c)–(f), E. coli were severely damaged and appeared in the form of deformed and collapsed rods. Fewer E. coli cells in the suspension, together with remnants of destroyed cell membranes and/or intracellular materials of the bacteria that were left on the surface of the E0.00 grad film (Fig. E1), indicate that most of them were lysed and did not survive. This outcome is in excellent agreement with the antibacterial activity based on the total viable cell count data.

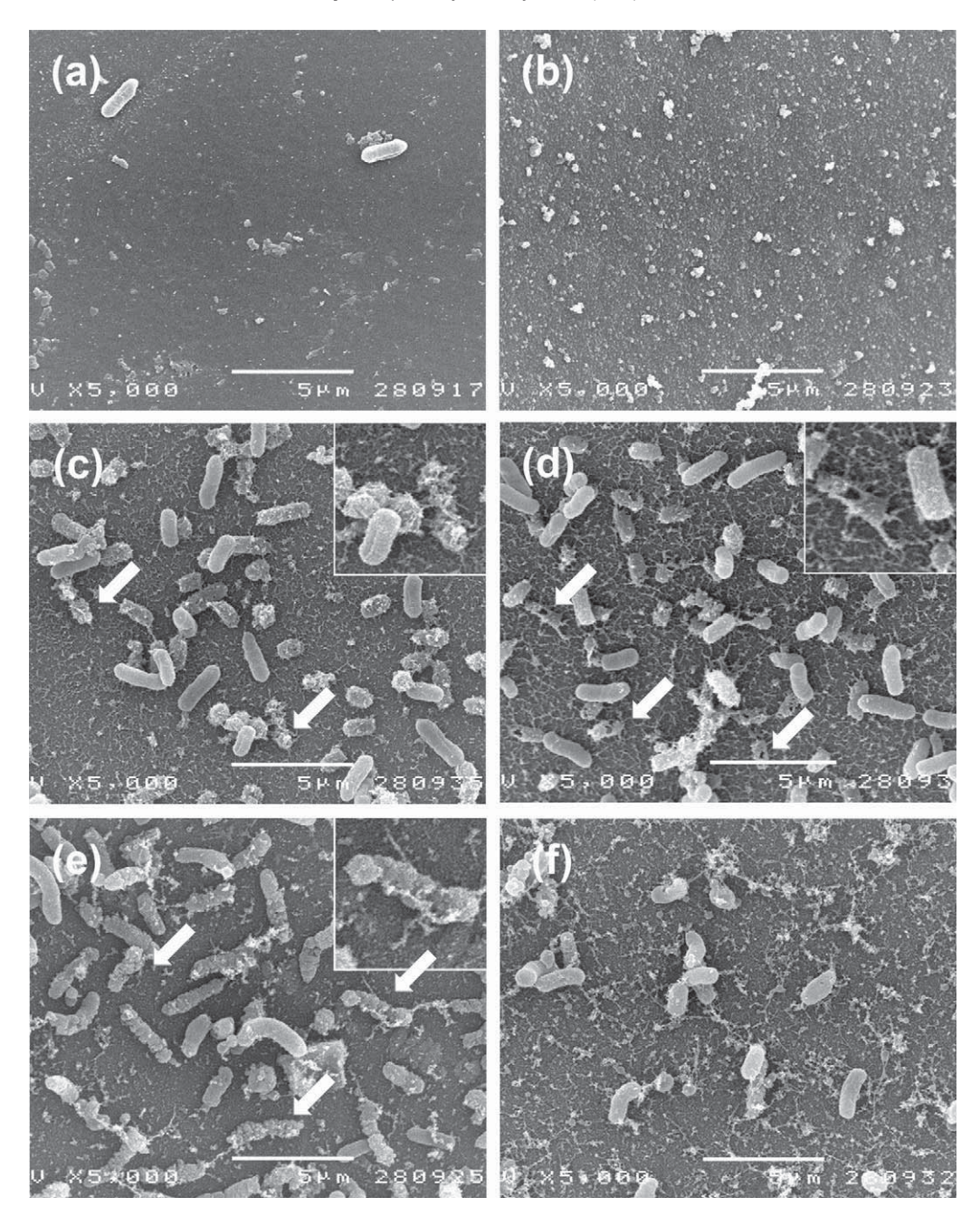


Fig. 7. SEM micrographs of the (a) chitosan, (b) 0.4QBzCS, (c) 0.8QBzCS, (d) 1.2QBzCS, (e) 1.6QBzCS, and (f) 2.0QBzCS chitosan films after being incubated with the suspension of *E. coli* $(OD_{600} = 0.5)$ for $24 \, h$. Micrographs shown are representative of at least 5 such fields of view per sample and 3 independent samples.

4. Conclusions

Quaternized *N*-alkyl chitosan films/particles having different alkyl substituents were successfully prepared. Conventional antibacterial test based on total viable plate counts, as well as microscopic evidences obtained from SEM analysis, support that all surface-modified chitosan samples exhibited greater antibacterial activity against *S. aureus* (Gram-positive bacteria) and *E. coli* (Gramnegative bacteria) than the virgin chitosan surface at neutral pH. The additional positive charges introduced by surface quaternization apparently made the chitosan films more antibacterial. The ability to fine tune the antibacterial activity of the chitosan surface by controlling the degree of quaternization which can readily be varied as a function of CH₃I concentration, renders the heterogeneous quaternization a powerful route for enhancing the

antibacterial efficacy of chitosan. This is particularly desirable considering that the process can be done simply on the pre-fabricated solid form of chitosan without the need for a tedious purification process. These surface-quaternized chitosan films/particles should potentially be useful for many technologically important applications requiring antibacterial activity.

Acknowledgements

This research is supported financially by Research Team Promotion Grant from the Thailand Research Fund (RTA47800004). The authors are indebted to Associate Professor Sanong Ekgasit of Chulalongkorn University for the access to the ATR-FTIR facility. Contact angle goniometer provided by the National Metal and Materials Technology Center (MTEC) is gratefully acknowledged.

The authors appreciated a language editing service provided by Dr. Robert Butcher, the Publication Counselling Unit (PCU), Faculty of Science, Chulalongkorn University.

Appendix A. Supplementary data

Supplementary data associated with this article can be found, in the online version, at doi:10.1016/j.carbpol.2010.08.075.

References

- Alves, N. M., & Mano, J. F. (2008). Chitosan derivatives obtained by chemical modifications for biomedical and environmental applications. *International Journal of Biological Macromolecules*, 43(5), 401–414.
- Amornchai, W., Hoven, V. P., & Tangpasuthadol, V. (2004). Surface modification of chitosan films-grafting ethylene glycol oligomer and its effect on protein adsorption. *Macromolecular Symposia*, 216, 99–107.
- Badawy, M. E. I. (2010). Structure and antimicrobial activity relationship of quaternary N-alkyl chitosan derivatives against some plant pathogens. *Journal of Applied Polymer Science*, 117(2), 960–969.
- Campaniello, D., Bevilacqua, A., Sinigaglia, M., & Corbo, M. R. (2008). Chitosan: Antimicrobial activity and potential applications for preserving minimally processed strawberries. *Food Microbiology*, 25(8), 992–1000.
- Choi, B. K., Kim, K. Y., Yoo, Y. J., Oh, S. J., Choi, J. H., & Kim, C. Y. (2001). In vitro antimicrobial activity of a chitooligosaccharide mixture against Actinobacillus actinomycetemcomitans and Streptococcus mutans. International Journal of Antimicrobial Agents, 18(6), 553–557.
- Chung, Y. C., Su, Y. P., Chen, C. C., Jia, G., Wang, H. I., Wu, J. C. G., et al. (2004). Relationship between antibacterial activity of chitosan and surface characteristics of cell wall. Acta Pharmacologica Sinica, 25(7), 932–936.
- Cuero, R. G., Osuji, G., & Washington, A. (1991). N-Carboxymethylchitosan inhibition of aflatoxin production: Role of zinc. *Biotechnology Letters*, 13(6), 441–444.
- Devlieghere, F., Vermeulen, A., & Debevere, J. (2004). Chitosan: Antimicrobial activity, interactions with food components and applicability as a coating on fruit and vegetables. Food Microbiology, 21(6), 703–714.
- Domard, A., Rinaudo, M., & Terrassin, C. (1986). New method for the quaternization of chitosan. *International Journal of Biological Macromolecules*, 8(2), 105–107. Eaton, P., Fernandes, J. C., Pereira, E., Pintado, M. E., & Malcata, F. X. (2008). Atomic
- Eaton, P., Fernandes, J. C., Pereira, E., Pintado, M. E., & Malcata, F. X. (2008). Atomic force microscopy study of the antibacterial effects of chitosans on *Escherichia* coli and *Staphylococcus aureus*. *Ultramicroscopy*, 108(10), 1128–1134.
- Fernandez-Saiz, P., Lagaron, J. M., & Ocio, M. J. (2009). Optimization of the biocide properties of chitosan for its application in the design of active films of interest in the food area. *Food Hydrocolloids*, 23(3), 913–921.
- Fujimoto, T., Tsuchiya, Y., Terao, M., Nakamura, K., & Yamamoto, M. (2006). Antibacterial effects of chitosan solutions[®] against Legionella pneumophila, Escherichia coli, and Staphylococcus aureus. International Journal of Food Microbiology, 112(2), 96–101.
- Gorbach, V. I., Krasikova, I. N., Lukyanov, P. A., Loenko, Y. N., Soloveva, T. F., Ovodov, Y. S., et al. (1994). New glycolipids (chitooligosaccharide derivatives) possessing immunostimulating and antitumor activities. *Carbohydrate Research*, 260(1), 73–82.

- Hoven, V. P., Tangpasuthadol, V., Angkitpaiboon, Y., Vallapa, N., & Kiatkamjornwong, S. (2007). Surface-charged chitosan: Preparation and protein adsorption. *Carbohydrate Polymers*, 68(1), 44–53.
- Kim, C. H., & Choi, K. S. (2002). Synthesis and antibacterial activity of quaternized chitosan derivatives having different methylene spacers. *Journal of Industrial and Engineering Chemistry*, 8(1), 71–76.
- Kong, M., Chen, X. G., Liu, C. S., Liu, C. G., Meng, X. H., & Yu, L. J. (2008). Antibacterial mechanism of chitosan microspheres in a solid dispersing system against E. coli. Colloids and Surfaces B: Biointerfaces, 65(2), 197–202.
- Lim, S. H., & Hudson, S. M. (2004). Synthesis and antimicrobial activity of a water-soluble chitosan derivative with a fiber-reactive group. *Carbohydrate Research*, 339(2), 313–319.
- Mourya, V. K., & Inamdar, N. N. (2009). Trimethyl chitosan and its applications in drug delivery. *Journal of Materials Science: Materials in Medicine*, 20(5), 1057–1079.
- Muzzarelli, R. A. A., & Tanfani, F. (1985). The N-permethylation of chitosan and the preparation of N-trimethyl chitosan iodide. Carbohydrate Polymers, 5(4), 297–307.
- Ong, S. Y., Wu, J., Moochhala, S. M., Tan, M. H., & Lu, J. (2008). Development of a chitosan-based wound dressing with improved hemostatic and antimicrobial properties. *Biomaterials*, 29(32), 4323–4332.
- Polnok, A., Borchard, G., Verhoef, J. C., Sarisuta, N., & Junginger, H. E. (2004). Influence of methylation process on the degree of quaternization of N-trimethyl chitosan chloride. European Journal of Pharmaceutics and Biopharmaceutics, 57(1), 77–83.
- Qi, L. F., Xu, Z. R., Jiang, X., Hu, C. H., & Zou, X. F. (2004). Preparation and antibacterial activity of chitosan nanoparticles. Carbohydrate Research, 339(16), 2693–2700.
- Raafat, D., von Bargen, K., Haas, A., & Sahl, H.-G. (2008). Insights into the mode of action of chitosan as an antibacterial compound. Applied and Environmental Microbiology, 74(12), 3764–3773.
- Rabea, E. I., Badawy, M. E. T., Stevens, C. V., Smagghe, G., & Steurbaut, W. (2003). Chitosan as antimicrobial agent: Applications and mode of action. *Biomacro-molecules*, 4(6), 1457–1465.
- Sajomsang, W. (2010). Synthetic methods and applications of chitosan containing pyridylmethyl moiety and its quaternized derivatives: A review. Carbohydrate Polymers, 80(3), 631–647.
- Sajomsang, W., Gonil, P., & Saesoo, S. (2009). Synthesis and antibacterial activity of methylated N-(4-N,N-dimethylaminocinnamyl) chitosan chloride. European Polymer Journal, 45(8), 2319–2328.
- Seong, H. S., Whang, H. S., & Ko, S. W. (2000). Synthesis of a quaternary ammonium derivative of chito-oligosaccharide as antimicrobial agent for cellulosic fibers. *Journal of Applied Polymer Science*, 76(14), 2009–2015.
- Sun, L. P., Du, Y. M., Fan, L. H., Chen, X., & Yang, J. H. (2006). Preparation, characterization and antimicrobial activity of quaternized carboxymethyl chitosan and application as pulp-cap. *Polymer*, 47(6), 1796–1804.
- Suzuki, K., Oda, D., Shinobu, T., Saimoto, H., & Shigemasa, Y. (2000). New selectively N-substituted quaternary ammonium chitosan derivatives. *Polymer Journal*, 32(4), 334–338.
- Talaro, K. P. (2005). Foundations in microbiology. New York: McGraw-Hill.
- Tangpasuthadol, V., Pongchaisirikul, N., & Hoven, V. P. (2003). Surface modification of chitosan films: Effects of hydrophobicity on protein adsorption. *Carbohydrate Research*, 338(9), 937–942.
- Ye, X. L., Li, X. G., Yuan, L. J., Ge, L. H., Zhang, B. S., & Zhou, S. B. (2007). Interaction of houttuyfonate homologues with the cell membrane of gram-positive and gram-negative bacteria. Colloids and Surfaces A: Physicochemical and Engineering Aspects, 301(1–3), 412–418.

Synthesis of Acrylamide/Acrylic Acid-Based **Aluminum Flocculant for Dye Reduction** and Textile Wastewater Treatment

Supaporn Noppakundilograt, Praon Nanakorn, Wanida Jinsart, Suda Kiatkamjornwong ¹ Department of Imaging and Printing Technology, Faculty of Science, Chulalongkorn University, Bangkok 10330, Thailand

Aluminum hydroxide-poly[acrylamide-co-(acrylic acid)], AHAMAA, was synthesized with a redox initiator by solution polymerization in which the effects of reactant contents were optimized. The effects of pH, temperature, and initial dye concentration on Congo red reduction were investigated. A mixture of Congo red and direct blue 71, and the composite textile dye wastewater were investigated. Adsorptions of both dyes were more effective in the nonbuffered solution than those in the buffered solution, and Congo red adsorbed more than direct blue 71 at all pHs. The adsorption of Congo red increased with increasing temperature and its initial concentration. Both dyes obeyed the Freundlich adsorption isotherm. The maximum adsorptions in 100 mg dm $^{-3}$ solution were 109 \pm 0.5 mg g $^{-1}$ and 62 \pm 6.6 mg g $^{-1}$ for Congo red and direct blue 71, respectively. At 150 mg dm $^{-3}$ of the mixed Congo red and direct blue 71, the adsorption was 142 \pm 2 mg g⁻¹ by 643 \pm 3 mg dm⁻³ AHAMAA. The 40 mg g⁻¹ dyes of the textile effluent wastewater were adsorbed by 500 mg dm⁻³ AHAMAA. AHAMAA could decrease turbidity of the composite wastewater containing a mixture of reactive and direct dyes from 405 to 23 NTU. POLYM. ENG. SCI., 50:1535-1546, 2010. © 2010 Society of Plastics Engineers

INTRODUCTION

Wastewater from the textile dyeing and finishing industries is often polluted by azo dyes which can

Correspondence to: Suda Kiatkamjornwong; e-mail: ksuda@chula.ac.th Grants (Thailand Research Fund); contract grant numbers: RTA4780004, RTA5080004.

DOI 10.1002/pen.21694

Published online in Wiley InterScience (www.interscience.wiley.com). © 2010 Society of Plastics Engineers

Contract grant sponsor: Senior Scholar Research Team Consolidation

decompose to hazardous aromatic amines that are highly carcinogenic. These potent pollutants are highly toxic to organisms and cause skin irritation, cancer, and mutation of aquatic organisms and humans [1, 2]. Therefore, it is mandated to remove those hazardous chemicals before discharging the wastewater into natural water sources [3–6].

Congo red, C.I. 22120, is a hazardous azo dye [7], and its use in many countries is prohibited but in those where it is allowed it has gained favor for textile dyeing especially in silk due to its vivid, bright, and striking color. However, it is difficult to degrade, making its disposal from wastewater which is a severe problem. Attempts to remove Congo red from wastewater by several kinds of absorbents, such as activated carbon [8], fly ash [9], chitosan [10], acid activated red mud [11], and electrocoagulated metal hydroxide sludge [12] have been reported. Some low-cost absorbents have typically attained a low adsorption capacity. Direct blue 71, C.I. 34140, having a slightly larger structure than Congo red, it is also widely used in the textile industry but in contrast to Congo red, there have been a few research work reporting its adsorption isotherm [13, 14].

Anionic polymeric flocculant hydrogels have been reported to be able to remove cationic dyes [15] but not for anionic dyes such as Congo red [16]. In general, the usage of polymeric flocculants could decrease the consumption of alum or aluminum complex and may be an alternative method for solving the problematic Alzheimer's disease in human, which is induced from the leaking aluminum ions from aluminum complex in the drinking water. Moreover, an increase in the concentration of residual Al ions in sewage sludge became a potential problem as a toxic source in water treatment processes [17-19].

² Program of Petrochemistry and Polymer Science, Faculty of Science, Chulalongkorn University, Bangkok 10330, Thailand

Department of General Science, Faculty of Science, Chulalongkorn University, Bangkok 10330, Thailand

FIG. 1. The molecular structures of (a) Congo red (C.I. 21120) and (b) direct blue 71 (C.I. 34140).

However, there are still needs to have some new adsorbents for treating a wide variety of textile wastewater. The synthetic polymer of aluminum hydroxide poly[acrylamide-co-(acrylic acid)], AHAMAA, used for turbidity reduction in synthetic wastewater as a complex polymeric flocculant (CPF) [20] has been reported. In the research, decreases in Congo red and direct blue 71 by AHAMAA considered as a model of anionic dye in wastewater are evaluated since AHAMAA can be an alternative remedy material for the textile industry. Here we report on the synthesis and characterization of AHA-MAA, the active ingredients needed for synthesizing the AHAMAA and its capacities to adsorb and decrease the dye concentrations under different pHs and initial dye concentrations. The adsorption isotherms of the two dyes by AHAMAA are studied. Decreases in color and turbidity, by AHAMAA, of the textile effluents containing mixtures of reactive, acid, and direct dyes from the two textile finishing plants are also investigated.

EXPERIMENTAL

Materials

Acrylamide (AM) was provided by Siam Chemical Industry Co. (Bangkok, Thailand). Acrylic acid (AA), N,N'-methylenebisacrylamide (N-MBA) and N,N,N',N'-tetramethylethylenediamine (TEMED) were purchased from Fluka (Buchs, Switzerland) and used as a co-monomer, crosslinking agent, and polymeric modifier, respectively. Ammonium persulfate initiator (APS) was purchased from Merck (Hohenbrunn, Germany). Sodium carbonate and aluminum sulfate (both were AR grade) were supplied by BDH (Poole, U.K.). Congo red (molecular weight = 696.68) in Fig. 1a [11], and direct blue 71 (molecular weight = 965.94) in Fig. 1b [13], were purchased from Fluka (Buchs, Switzerland) and Sigma-Aldrich (St. Louis, USA), respectively. Deionized water was processed by Elga Deionizer (Model LA611, Buckinghamshire, U.K.). Composite mixtures of reactive dyes, direct dyes, and acid dyes from the textile dyeing and finishing effluents were supplied from two volunteer factories.

Synthesis of Aluminum Hydroxide Suspension

A suspension of $Al(OH)_3$ was prepared by slowly dropping 22.5 cm³ of 0.2 M sodium carbonate into 20 cm³ of 0.1 M aluminum sulfate at a constant rate with stirring at room temperature. The $Al(OH)_3$ suspension was then used as it was.

Synthesis of Polymeric Flocculants of Aluminum hydroxide-poly[acrylamide-(acrylic acid)] (AHAMAA)

AHAMAA was synthesized by the polymerization of AM and AA in the presence of the Al(OH)₃ suspension. AM and AA were added to a 500-cm3 four-necked roundbottomed reaction flask containing the newly prepared Al(OH)₃ suspension. This reaction flask was equipped with a mechanical stirrer, a condenser, and an inlet tube for nitrogen gas feed, and it was then immersed in a water bath at a controlled temperature of $45^{\circ}C \pm 2^{\circ}C$. The mixture was stirred with a small bladed propeller at 250 rpm under a constant nitrogen gas atmosphere fed through the gas inlet tube for 30 min. The crosslinking agent (N-MBA), initiator (APS), and TEMED were subsequently added (see Table 1) and stirred for another 30 min. The copolymer was filtered, dehydrated with acetone, cut into small pieces of ~ 1 cm \times 1 cm, and dried in a vacuum oven at 50°C for 24 h to a constant weight. The dried samples were then milled and sieved through a 100-mesh sieve. Existence of the synthesized polymers was identified by Fourier Transform Infrared Spectroscopy (FTIR, model Nicolet Impact 410, Madison, WI), and ²⁷Al nuclear magnetic resonance (²⁷Al-NMR, model Unity Inova-500, Palo Alto, CA). The ²⁷Al-NMR measurement was performed in a solid state method and the frequency of ²⁷Al was at 130 MHz. The sample powder was put in a cylindrical sample cell (0.64 cm diameter and 2.0 cm height) and it was then measured at 26°C. The measurement conditions were set as follows: relaxation delay was 1.000 s (first pulse at 58.5° and the second pulse at 9.0°), acquisition time was 0.006 s, and a total time was 16 min 15 s.

TABLE 1. The synthesis parameters of AHAMAA.

Reactants	Quantity
Acrylamide: acrylic acid ($\times 10^{-3}$ mol)	98:2, 96:4, 94:6, 92:8, 90:10
N-MBA ($\times 10^{-4}$ mol)	1.2, 2.3, 4.6, 9.2
APS ($\times 10^{-4}$ mol)	0.8, 1.6, 3.1, 6.2
TEMED ($\times 10^{-4}$ mol)	1.5, 3.0, 6.0, 12.0
Synthesized Al(OH) ₃ suspension (cm ³)	42.5

Stability of AHAMAA in Water

Stability of the AHAMAA in water was performed by determining the leaching aluminum ion concentration from its complex. Portions of the dry AHAMAA polymer composite material weighing 0.04 g were added into 200 cm³ of deionized water and kept covered at room temperature for 15, 30, 45, and 60 days. The swollen material was filtered through a 100-mesh aluminum screen sieve. The filtrate was then collected and the aluminum ion concentration in the filtrate was determined by the ICP-AES (PerkinElmer model PLASMA-1000, Waltham, MA).

Effect of the Reactant Contents on Dye Reduction of AHAMAA

The effects of the AM:AA, N-MBA, APS, and TEMED contents on the efficiency of the resultant AHAMAA polymer to decrease Congo red were investigated at room temperature and pH 5. A 50 cm³ solution containing 24 mg dm⁻³ of Congo red was added to 0.03 g of the dry AHAMAA powder and they were allowed to swell for 24 h. The swollen material was then filtered through a 100-mesh aluminum screen sieve at ambient temperature. The filtrate absorption was measured by a UV–visible spectrophotometer (UV-2550, Shimadzu, Tokyo, Japan) at a wavelength of 497 nm and the amount of the decreased dye expressed as dye removal can be calculated from *Eq. 1*:

%Dye removal =
$$\frac{C_i - C_e}{C_i} \times 100$$
 (1)

where C_i is the initial dye concentration and C_e is the equilibrium dye concentration.

Evaluation of the equilibrium water absorbency of each AHAMAA polymer was carried out using the deionized water at room temperature in a closed system. The deionized water (200 cm³) was added to 0.1 g of dry AHAMAA, which was then allowed to reach equilibrium swelling for 24 h. The swollen material was then filtered through a 100-mesh aluminum sieve screen for 2 h. The water absorbency was then obtained from the increased weight in the cross-linked AHAMAA and was recorded as water absorbency (Q) expressed as a weight ratio of the absorbed water in the polymer over the dry polymer, calculated from Eq. 2:

Water absorbency
$$(Q) = (W_s - W_d)/W_d$$
 (2)

where W_d is the weight of dry AHAMAA (g), and W_s is the weight of the equilibrium swollen material (g). The resultant water absorption is the average of three replications with one standard deviation.

Effect of pH upon Dye Adsorption by AHAMAA

The AHAMAA polymer was prepared from AM, AA, N-MBA, APS and TEMED contents at 96×10^{-3} , 4×10^{-3}

 10^{-3} , 2.3×10^{-4} , 1.6×10^{-4} , and 12×10^{-4} mol, respectively. The dye adsorption was tested at room temperature using 50 cm³ solution containing 50 mg dm⁻³ of Congo red or direct blue 71 in 0.3 g dry weight of the polymer material in the two systems. The first system is the nonbuffered solution where pH of the dye solution was adjusted to within the range of 5-11 by using 0.1 M HCl or 0.1 M NaOH. The buffered solution as the second system in which pH of the dye solution was adjusted with a buffer solution consisting of a mixture of 0.2 M boric acid, 0.05 M citric acid, and 0.1 M tri-sodium phosphate, and the pH was maintained in the same range as those in the nonbuffered system [21]. The absorption was measured by the same UV-visible spectrophotometer (UV-2550, Shimadzu, Tokyo, Japan) at their maximum absorptions at 497 nm and 587 nm for Congo red and direct blue 71, respectively.

Effect of Temperature upon Dye Adsorption by AHAMAA

The effect of solution temperature on the decrease of Congo red by AHAMAA was studied at 35, 40, and 50°C using 50 cm³ of the dye solution containing 100 mg dm⁻³ of Congo red at pH 7 in the nonbuffered system.

Effect of the Initial Dye Concentration

The effect of the initial dye concentration on Congo red reduction was evaluated using the dye solution concentrations of 24, 50, 75, and 100 mg dm⁻³ in the non-buffered system.

Adsorption Isotherm

The dye solutions of Congo red and direct blue 71 were prepared. Each solution was measured by the same UV–visible spectrophotometer at their maximum absorption wavelength. The amount of the dye adsorbed was calculated from Eq. 3:

$$q_{\rm e} = (C_0 - C_{\rm e}) \frac{v}{m} \tag{3}$$

where q_e is the equilibrium amount of the dye adsorbed per unit weight of AHAMAA (mg g⁻¹), C_0 is the initial concentration of Congo red or direct blue 71 (mg dm⁻³), C_e is the concentration of dye at equilibrium (mg dm⁻³), v is the solution volume (dm⁻³), and m is the mass of AHAMAA (g) [4].

A linear form of the Langmuir isotherm represents a model of monolayer adsorption on a surface containing a finite number of identical sites. This isotherm is given in Eq. 4:

$$\frac{C_{\rm e}}{q_{\rm e}} = \frac{1}{Q_{\rm max}K_{\rm L}} + \frac{C_{\rm e}}{Q_{\rm max}} \tag{4}$$

where C_e is the concentration of the dye solution (mg dm⁻³) at equilibrium, q_e is the amount of dye adsorbed per unit weight of AHAMAA (mg g⁻¹), Q_{max} is the monolayer capacity of the adsorbent (mg g⁻¹) and K_L is the Langmuir adsorption constant (dm³ mg⁻¹). A plot of C_e/q_e against C_e gives a linear line where the Q_{max} and K_L values are obtained from the slope and intercept, respectively.

The Freundlich isotherm reveals a multilayer adsorption model on a heterogeneous surface. This model is formulated in a linear form as shown in Eq. 5 [22]:

$$\ln q_{\rm e} = \ln K_{\rm F} + \frac{1}{n} \ln C_{\rm e} \tag{5}$$

where $C_{\rm e}$ is the concentration of dye solution (mg dm⁻³) at equilibrium, $K_{\rm F}$ is the adsorption capacity representing a quantity of dye adsorbed onto adsorbent (mg g⁻¹) and n is an empirical parameter representing a heterogeneity factor for measuring the deviation from linearity of the adsorption between solution concentration and adsorption. A plot of $\ln q_{\rm e}$ versus $\ln C_{\rm e}$ gives n and $K_{\rm F}$ values from the slope and intercept, respectively.

Wastewater Treatment

The decreases in color and turbidity were investigated by AHAMAA from textile wastewater provided by the two textile factories. The sample from the Factory A, named as sample A, contained a mixture of reactive and direct dyes, whereas the sample from the Factory B was mainly acid dye, named as sample B1, and a mixture of disperse and acid dyes, named as sample B2. A synthetic wastewater was also prepared from a mixture of 75 mg dm⁻³ Congo red and 75 mg dm⁻³ direct blue 71 as a model dye wastewater for the quantitative analysis of the color.

The amount of 500 mg dm⁻³ AHAMAA was added into 500 cm³ of each wastewater sample from which the solution pH was adjusted to 7. It was stirred at 120 rpm for 3 min and at 30 rpm for 30 min. It was then filtered and the color and turbidity of the filtrate were measured. Turbidity of the textile wastewater was measured by a portable turbidity meter (model 2100P, Hach, Loveland, CO). The decrease in turbidity by AHAMAA was calculated from the turbidity before and after the AHAMAA addition.

The decrease in color by AHAMAA for the wastewater treatment was measured using a simple spectrophotometric technique. The filtrate was measured at its maximum absorbance wavelength. The dye concentrations were measured before and after the AHAMAA addition.

The absorption spectral data of the wastewater samples were recorded from 200 to 700 nm. For a quantitative analysis, a calibration curve of the mixture of model dye concentration (mg dm⁻³) against the absorbance at the $\lambda_{\rm max}$ of 519 nm was plotted. The dye concentrations were

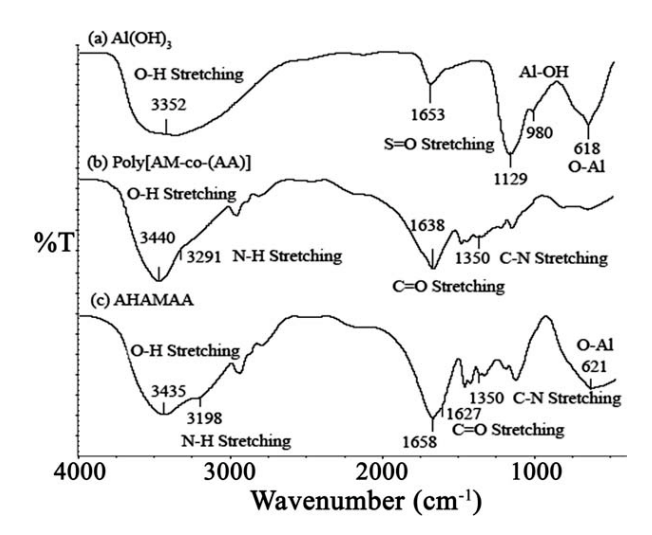


FIG. 2. FTIR spectra of (a) Al(OH)₃, (b) poly[AM-co-(AA)], and (c) AHAMAA

quantified according to the calibration curve of the mixed model dye. Then the decrease in relative dye concentration of the textile wastewater was calculated.

RESULTS AND DISCUSSION

Characterization of Functional Groups by FTIR Spectroscopy

The FTIR spectra of the synthesized Al(OH)3 and AHAMAA are shown in Fig. 2 in which Al(OH)₃ in spectrum (a) shows a peak of —OH stretching at 3352 cm⁻¹ indicating the presence of the hydroxide group. In addition, it also shows the peaks of Al-OH and O-Al at 980 and 618 cm⁻¹, respectively. The strong and broad absorption band centered at 618 cm⁻¹ is probably resulted from the combined absorptions of sulfate, the Al-O stretching vibrations and the Al-OH wagging vibration mode of molecular water [23]. This result strongly supports that the hydrolysis product of the aluminum sulfate was aluminum hydroxide, and the absorption peaks at 1129 and 1653 cm⁻¹ are the sulfate group of residual aluminum sulfate within the Al(OH)₃ suspension [24]. The IR spectrum (b) of poly[AM-co-AA] shows the peaks of O-H stretching and C=O stretching of carboxylic acid group at 3440 and 1638 cm⁻¹, respectively. Moreover, it shows the peaks of N—H stretching and C—N stretching of carboxamide group at 3291 and 1350 cm⁻¹, respectively. The spectrum (c) (see Fig. 2) of AHAMAA shows evidence of the coordination between the carboxylate anion and aluminum ion at the strong absorption peak of 1658 cm⁻¹, indicating a complex formation of the poly[AM-co-AA] and Al(OH)₃ [23]. This result also supports the presence of the carboxylic acid group (3435 and 1627 cm^{-1}) and carboxamide group (3198 and 1350 cm⁻¹) in the three-dimensional crosslinked structure of the copolymer.

Characterization of Al(OH)₃ and AHAMAA by ²⁷Al-NMR

Figure 3 indicates the form of Al(OH)₃, and the coordination of the aluminum ions from the ²⁷Al-NMR signals. There is one signal at 9.132 ppm designated for Al(OH)₃ in spectrum (a) which indicates that Al(OH)₃ was the monomeric species because its signal appears near 0 ppm [25]. On the other hand, the AHAMAA gave the signal at 8.008 ppm of peak (b). It confirms that the aluminum atoms in AHAMAA were mostly in an octahedral coordination [26]. A possible structure of AHAMAA is postulated in Fig. 4.

Stability of the AHAMAA in Water

The amount of aluminum ions leached from AHA-MAA in deionized water was found to be in the range of $0.09-0.2 \text{ mg dm}^{-3} \text{ regardless of the soaking time } (15-60)$ days), which suggests that the stability of the aluminum ions in the AHAMAA is high. Under these conditions, the free aluminum ion concentration remained in the treated water is not likely to be harmful to fish, plant, or human health. For example, the aluminum ions in natural groundwater are found from 0.4 mg dm⁻³ to 5 mg dm⁻³ in acidic soils, and the maximum contaminant level of aluminum ions in the human body is not higher than 0.2 mg dm^{-3} [27]. Indeed, the highest stringent amount that is limited by WHO for aluminum ions in human drinking water is as high as 0.2 mg dm⁻³. Thus, the AHAMAA seems to be quite stable and is safe to be used as a sorbent in aqueous solution to decrease Congo red or direct blue 71 before discharging the treated water to natural water resources.

Dye Decreasing Efficiency

Congo red was used a model to investigate the dye decreasing efficiency of AHAMAA. Considering the molecular structure of Congo red (Fig. 1a) and AHAMAA (see Fig. 3), there are several active points, namely the amino and azo groups, which can interact with the carboxylic acid groups of AHAMAA. To achieve the opti-

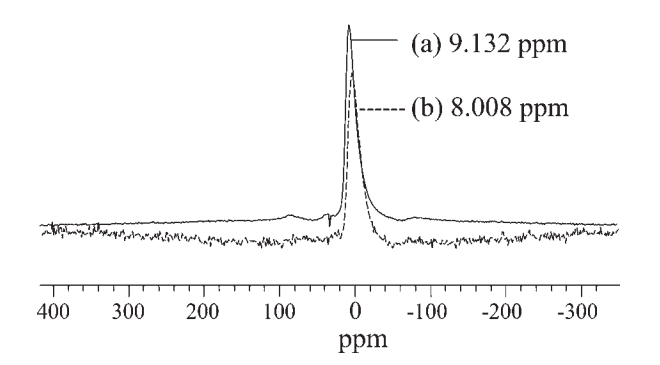


FIG. 3. The 27 Al-NMR spectra of (a) Al(OH)₃ and (b) AHAMAA synthesized with 4 \times 10⁻³ mol AA, 2.3 \times 10⁻⁴ mol N-MBA, 1.6 \times 10⁻⁴ mol APS, and 12 \times 10⁻⁴ mol TEMED.

FIG. 4. The structure of AHAMAA.

mized performance of AHAMAA in decreasing the dye content, the comonomer is a key factor. Other important factors for the dye adsorption are dye permeability, the extent of contact surface and interaction between the dye and the adsorbent via carboxylic acid and aluminum ion. Water absorption can be one of the indicators for the dye molecules to access and permeate into the adsorbent.

Effects of Reactant Contents in AHAMAA Polymerization on Decreasing Congo Red Content

Monomer Contents. Basically, Congo red is a dipolar molecule which exists in a cationic form with positively charged azo (-N=N⁺-H) and amino (-N⁺H₂) groups at pH 5 [8]. Thus, subjecting to the solution pH relative to the dye and the AHAMAA respective pKa values, AHAMAA can remove Congo red through the ionic interactions between the negatively charged carboxylate anion of AHAMAA and the positively charged azo or amino groups of Congo red [4]. The efficiency of Congo red reduction (q_e) by the crosslinked AHAMAA synthesized with different contents of AA and N-MBA are illustrated in Fig. 5. The Congo red reduction efficiency increased with increasing the AA content, which is likely to be due to the increasing amount of the resultant carboxylate anions, leading to more ion-ion interactions between AHAMAA and Congo red. In addition, a twofold increase in the AA content also caused water absorbency to increase by 1.3-folds due to increases in hydrophilicity of the polymer chains with increasing levels of the carboxylate anions [28]. The higher the repulsion between carboxylate groups in crosslinked polymer chains, the greater the water absorbency [29]. The highest water absorbency was achieved when the AA content was 4×10^{-3} mol and declined slightly afterward but not significantly with further increases in AA contents (Fig. 5a). This could be caused by a complex formation between the carboxylate anions and the aluminum cations, similarly to another type of crosslinking reaction, to yield a more rigid chain structure. Moreover, this complex structure can certainly decrease the anionic repulsion, which lowers the water absorption [30, 31]. Likewise, the formation of complex along with the decreased amount of free carboxylate anions in AHAMAA may account for the lower Congo

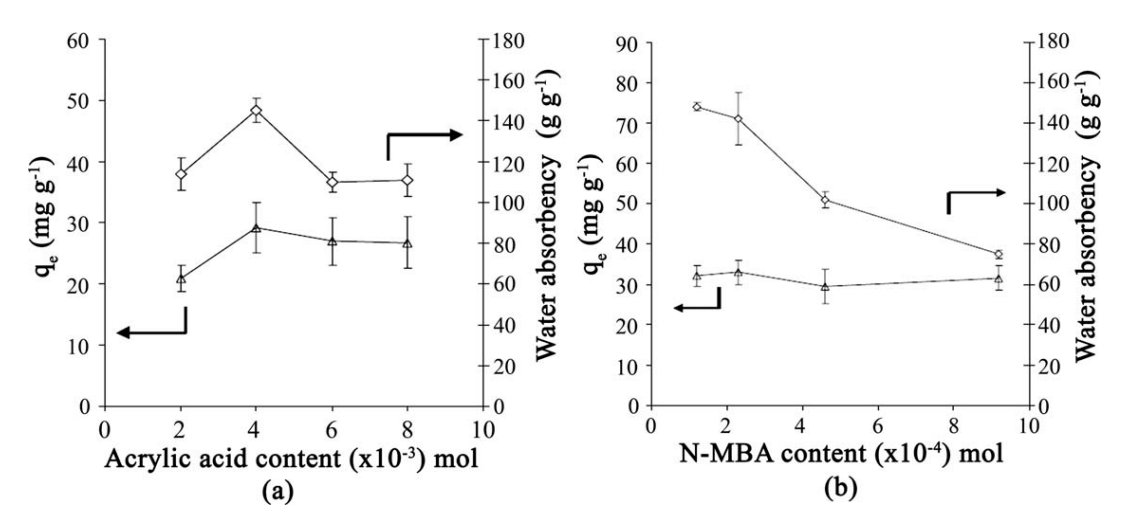


FIG. 5. Effect of the acrylic acid and N-MBA contents on Congo red adsorption efficiency and water absorbency of AHAMAA synthesized by 3.2×10^{-4} mol APS, 12×10^{-4} mol TEMED, 250 rpm, at 45° C and 1 h polymerization time with: (a) 4.6×10^{-4} mol N-MBA with varied contents of AA and (b) 4×10^{-3} mol AA with varied contents of N-MBA.

red reduction efficiency by AHAMAA polymers synthesized with the higher amounts of AA. Thus, when all other conditions remain constant, the Congo red reduction efficiency by AHAMAA was optimal when the AA amount was 4×10^{-3} mol.

Since the crosslinked AHAMAA may principally remove Congo red via the contributions of the negatively charged carboxylate group, any positive effect on decreasing Congo red content could not be expected when increasing the amount of N-MBA. Changing the N-MBA contents did not impose any significant effect on the dye reduction efficiency of AHAMAA (Fig. 5b) because N-MBA is a crosslinking agent, which affects only the double bonds in the network structure but not the number of cations or anions on the polymeric backbone. However, the increasing N-MBA levels did decrease the water absorbency of the resultant AHAMAA polymer (Fig. 5b). This is because increasing rigidity of the crosslinked chains [32] is in a sense analogous to that with AA contents higher than 4×10^{-3} mol as discussed above. From these findings, 4×10^{-3} mol of AA and 2.3×10^{-4} mol of N-MBA were selected to synthesize AHAMAA to investigate the effect of APS content on decreasing Congo red content.

Effect of Initiator and TEMED Contents. In the redox initiated polymerization by APS and TEMED, TEMED is normally the coinitiator or starter to induce the decomposition of the APS initiator. The role of APS is to generate free radicals to control the length of polymer chains, which affects the water absorbency. The water absorbency was low when using low contents of APS in the polymerization (Fig. 6a) because a few radicals were generated and led to short polymer chains having a few carboxylate anions to induce low anionic repulsions. However, increasing the APS level by twofold to 1.6×10^{-4} mol

yielded a 10% increase in water absorbency. Further increase in AA contents decreased the water absorption gradually and markedly by 30% at further increases in APS content. Basically, an abundance of radicals was generated at the higher APS contents resulting in the formation of too many short polymer chains in the AHA-MAA. The chains can swell less due to the lower chain flexibility and the less repulsion caused by the smaller number of carboxylate groups [32]. Surprisingly, increasing APS contents did not increase Congo red reduction efficiency at all (Fig. 6a), which may be caused by the limited amount of ions in the polymer chains. However, 4×10^{-3} mol of AA, 2.3×10^{-4} mol of N-MBA, and 1.6×10^{-4} mol of APS were selected to synthesize AHAMAA to investigate the effect of TEMED content on dye decreasing efficiency of AHAMAA.

The water absorbency increased markedly with increasing TEMED concentrations in the polymerization reaction (Fig. 6b). In the APS/TEMED initiation, the free radicals $[(CH_3)_2NCH_2CH_2(CH_3)N^*CH_2)]$ and (OSO_3H) are both responsible for the initiation of vinyl polymerization [33]; thus, TEMED accelerates free radical production rates resulting in longer and more flexible polymer chains. The lower the TEMED content, the lower the water absorption (Fig. 6b). The highest Congo red reduction efficiency by AHAMAA polymers was observed at 91% (36 mg g⁻¹) when TEMED content used was 12×10^{-4} mol. The low TEMED content at 1.5×10^{-4} mol can produce AHA-MAA polymer that removes 25 mg g⁻¹ of Congo red, despite its low water absorption (27 \pm 2 g g⁻¹). The decrease in dye content depends more or less upon water absorption because water is a medium, where dye is dissolved, diffused, and transported to the AHAMAA gel.

It is necessary to mention that TEMED is a strong base having a pH value of 11. This implies that TEMED can hydrolyze the carboxamide in acrylamide moiety to give

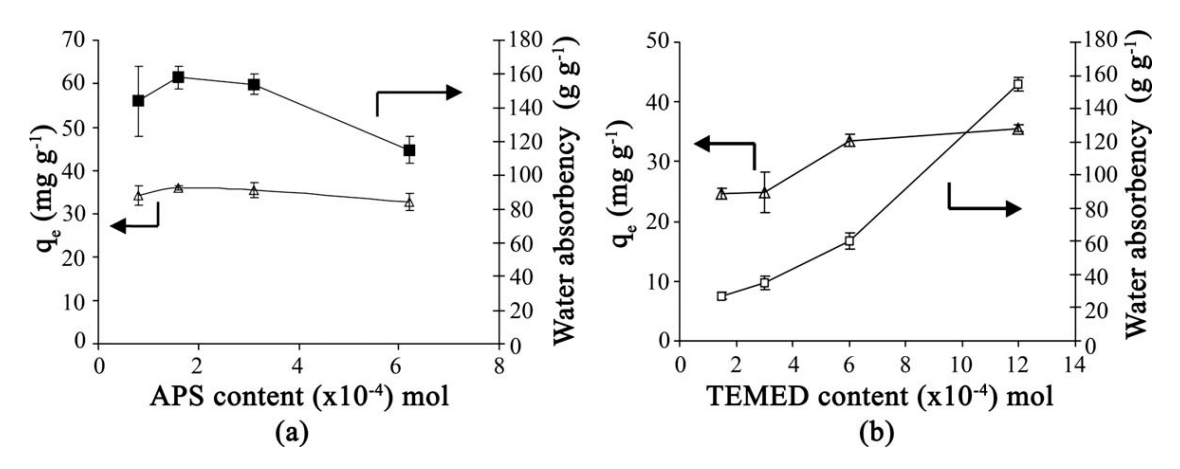


FIG. 6. Effect of the initiator and TEMED contents on Congo red adsorption efficiency and water absorbency of AHAMAA synthesized by 4×10^{-3} mol AA, 2.3×10^{-4} mol N-MBA, 250 rpm, at 45°C and 1 h polymerization time with: (a) 12×10^{-4} mol TEMED with varied contents of APS and (b) 1.6×10^{-4} mol APS with varied contents of TEMED.

the carboxylate group which is the functionality in acrylic acid. Such a hydrolysis at the solution temperature of 45°C which is similar to the NaOH saponification of polyacrylamide could be another attribute to the higher water absorption when higher concentrations of TEMED are used.

Effect of pH on Dye Reduction by AHAMAA Polymer

In a Low Ion Content, the Nonbuffered System. Congo red has a propensity to form ribbon-like micellar mesophases in water solution [34], and is pH dependence (pKa of the azo, sulfonate, and amine functional groups). The molecular form of Congo red in a solution medium changed markedly in the pH range of 3–5, and at a high alkaline pH of 12, e.g., the color of Congo red changes from dark blue at pH 3–5 to red at pH 12 from the original red in a solid form [11]. Therefore, pH of the 50 mg dm⁻³ Congo red solution was adjusted to pH 5, 7, 9, or 11 with 0.1 M HCl or 0.1 M NaOH.

At pH 5, the dipolar Congo red exists in a cationic which is positively charged at the $(-N=N^+-H)$ and the amino $(=N^+H_2)$ groups [8]. Thus, AHAMAA can remove Congo red from the solution by strong ionic interactions between the positive charge of the dye and the negative charge of the carboxylate groups in AHAMAA outcompeting the hydrogen bonding of water with the dye, leading to a rather highly dye decreasing level (89% ± 1%) at pH 5, as summarized in Table 2. On the other hand, at pH 7, Congo red in an anionic form is negatively charged at the sulfonate group [8], again allowing Congo red reduction by AHAMAA via ionic interactions, but this time between the aluminum ion in the complex of AHAMAA and the sulfonate anion of the dye, at an apparently higher dye removal efficiency $(95\% \pm 1\%)$. Further increases in pH to 9 and to 11 resulted in a predominance of deprotonated carboxylate

groups of AHAMAA, leading to the repulsion between the sulfonate and carboxylate anions of the dye and AHAMAA, respectively, and a lower decreasing efficiency from 95% \pm 1% at pH 7 to 43% \pm 2% at pH 9 and none at all at pH 11. In addition, the aluminum ion (the cationic part) in AHAMAA might react with the hydroxide ion at the higher pH values instead of the anionic group of the dye [35], leading to a smaller deplete in the dye content.

Direct blue 71 is a triazo dye (Fig. 1b), where the azo form appears to be the predominant species in solution, and it has a tendency to form a nonaggregated state due to the four negatively charged sulfonate groups [36]. Here, AHAMAA was able to moderately deplete direct blue 71 from the solution at pH 5 (59% \pm 3%) when the sulfonate groups are partially protonated and thus are weakly anionic. However, as direct blue 71 has a more sulfonate group per molecule than does Congo red, and thus the higher net charge density and repulsion from the AHAMAA carboxylate anions, the efficiency of AHAMAA in removing direct blue 71 was, of course, lower than that observed for Congo red at all pH values tested

TABLE 2. Effect of pH in the buffered and nonbuffered systems on the dye removal efficiency of the synthesized AHAMAA.^a

		% Dye removal						
	Con	igo red	Direct blue 71					
рН	Buffer	Nonbuffer	Buffer	Nonbuffer				
5 7 9	62 ± 2 13 ± 2 ND^{b} ND^{b}	89 ± 1 95 ± 1 43 ± 2 ND^{b}	ND ^b ND ^b ND ^b	59 ± 3 43 ± 1 35 ± 3 ND^{b}				

 $[^]a$ Polymerization reactions were carried out with 4 \times 10^{-3} mol AA, 2.3 \times 10^{-4} mol N-MBA, 1.6 \times 10^{-4} mol APS, 12 \times 10^{-4} mol TEMED, 42.5 cm³ Al(OH)3, 250 rpm, at 45°C and 1 h polymerization.

^b Cannot be detected.

FIG. 7. A possible structure of Al-citrate complex in the buffered system.

(5, 7, 9, and 11), and especially at the higher pH values. Thus, as the pH increases to 7, 9, and 11, the direct blue 71 reduction efficiency by AHAMAA (Table 2) decreases with no detectable decrease in color at pH 11 as discussed above in the case of Congo red.

In a Relatively High Ion Content, the Buffered System. Very interestingly, the dye reduction efficiency in the nonbuffered (a low ion content) system of AHA-MAA was significantly greater than that of the buffered system (relatively high ion content) at pHs 5, 7, and 9 (Table 2). This is because the low molecular weight citrate and borate anions of the buffer system created a complex formation with the aluminum ion complexes in AHAMAA [26, 37] as shown in Fig. 7, leading to a decreased ionic attraction between the aluminum cations in the AHAMAA polymer and the sulfonate anions in the dye, and thus resulted in a lower dye reduction. Moreover, the repulsion between the citrate and sulfonate anions would further decrease the dye reduction efficiency.

Effect of Temperature on Congo red Reduction by AHAMAA

The adsorption capacity of dye reduction generally depends on the temperature of the dye solution [38, 39], whilst Congo red has been reported to have a high water solubility of 50–100 g dm⁻³ at 80°C [3]. Thus, the effect of temperature on Congo red adsorption by AHAMAA was studied at 35, 40, and 50°C at pH 7 with a 100 mg dm⁻³ Congo red solution. Its adsorption capacity on AHAMAA in the nonbuffered system increased with increasing solution temperatures (Table 3) because thermal energy enhances the adsorbent to swell more and facilitates higher diffusion of Congo red molecules onto the adsorbent surface and causes more dye penetration into the internal structure of AHAMAA [40].

TABLE 3. Effect of the temperature on the Congo red removal efficiency of the synthesized AHAMAA.^a

Temperature (°C)	Adsorption capacity (mg g ⁻¹)
35 40 50	109 ± 1 110 ± 0.3 118 ± 0.6

 $[^]a$ Polymerization reactions were carried out with 4×10^{-3} mol AA, 2.3×10^{-4} mol N-MBA, 1.6×10^{-4} mol APS, 12×10^{-4} mol TEMED, $42.5~cm^3$ Al(OH)3, 250 rpm, at $45^\circ C$ and 1 h polymerization time.

Effect of the Initial Dye Concentration on Congo Red Reduction

The effect of the initial Congo red concentration on dye reduction by AHAMAA at 30°C at pH 7 was investigated with four Congo red concentrations at 24, 50, 75, and 100 mg dm⁻³. The results in Fig. 8 indicate that when the initial Congo red concentration increased from 24 to 100 mg dm⁻³, the adsorption capacity for Congo red increased from 38 to 109 mg g⁻¹, i.e., the dye content was gradually decreased. The dose-dependent response at the low dye concentrations (0–50 mg dm⁻³) is linear but the response declines as a linear asymptote at the higher dye concentrations (75–100 mg dm⁻³). The higher Congo red concentrations adsorbed on the AHAMAA gel could be caused by the absorbed water as a medium to dissolve and transport the dye to the gel.

Adsorption Isotherm Analysis

The adsorption isotherms of Congo red and direct blue 71 by AHAMAA did not obey the Langmuir isotherm at all. The data (not shown here) did not fit well to the Langmuir isotherm model with nonlinearity when a plot of $C_{\rm e}/q_{\rm e}$ versus $C_{\rm e}$ was constructed, and the correlation coefficient R^2 values of the lines were 0.6273 and 0.0037 for Congo red and direct blue 71, respectively. The Lang-

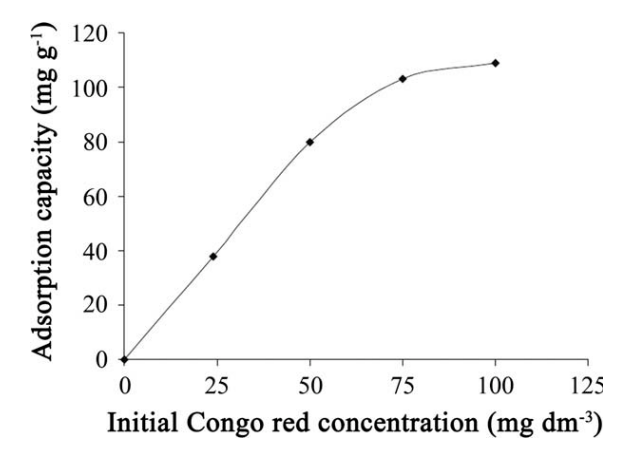


FIG. 8. Effect of the initial dye concentration on the Congo red removal by AHAMAA.

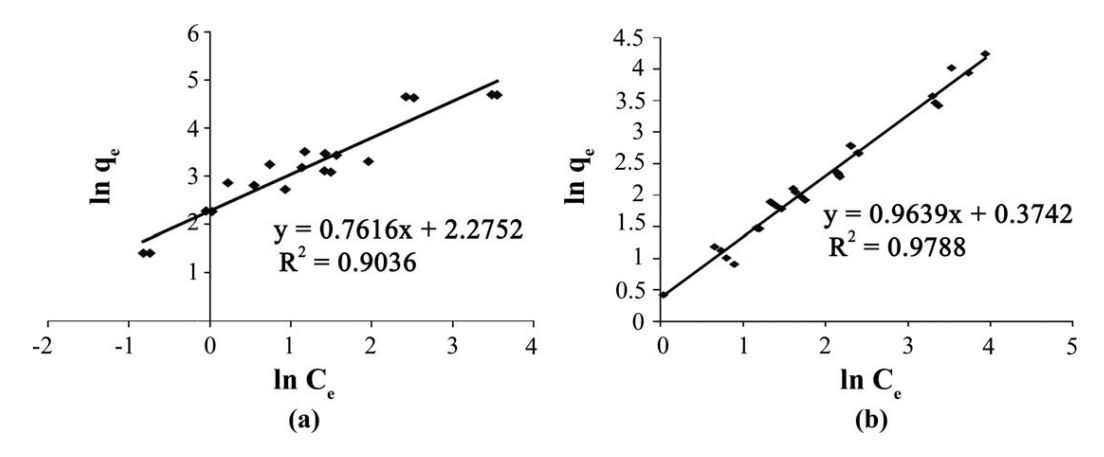


FIG. 9. Freundlich isotherm of: (a) Congo red by AHAMAA and (b) direct blue 71 by AHAMAA.

muir adsorption isotherm is only valid for adsorption of a solute from a solution as a monolayer on an adsorbent surface containing a finite number of identical sites with uniform energy of adsorption.

In contrast, the plots of $\ln q_{\rm e}$ versus $\ln C_{\rm e}$ (Fig. 9a and b) give a linear relationship with R^2 of 0.9036 and 0.9788 for Congo red and direct blue 71, respectively. That is, the result fits well with the Freundlich isotherm, which characterizes a multilayer adsorption model and describes the adsorption behavior on a heterogeneous surface [22]. In fact, the polyacrylamide-based hydrogel synthesized by a redox initiation is a heterogeneous gel. For Congo red and direct blue 71, the $K_{\rm F}$ values were 9.73 and 1.45,

respectively, whereas the n values were 1.31 and 1.04, respectively. The n value of Congo red (1.31) is higher than unity and also higher than that of direct blue (1.04), indicates that the adsorption of Congo red favors a physical process rather than a chemical process. However, one can also state that both dye adsorptions took place by a physical process such as Van der Waal force and electrostatic force. The difference in K_F between the two dyes reflects the higher q_e value of Congo red, and that AHAMAA can adsorb more Congo red than direct blue 71. These results are in good agreement with those presented the above section in the dye reduction. The maximum dye adsorption capacities were 109 ± 0.5 mg g^{-1}

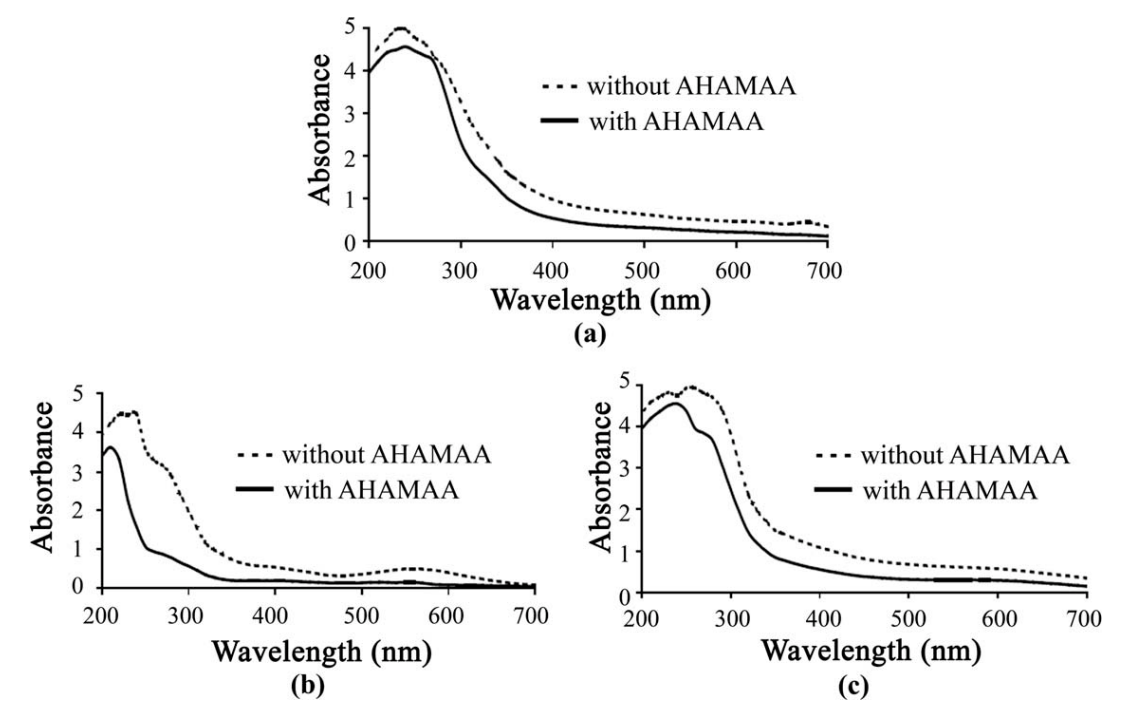


FIG. 10. Absorption spectra of wastewater from factories without and with AHAMAA: (a) A (mixture of reactive and direct dyes), (b) B1 (acid dyes), and (c) B2 (mixture of disperse and acid dyes).

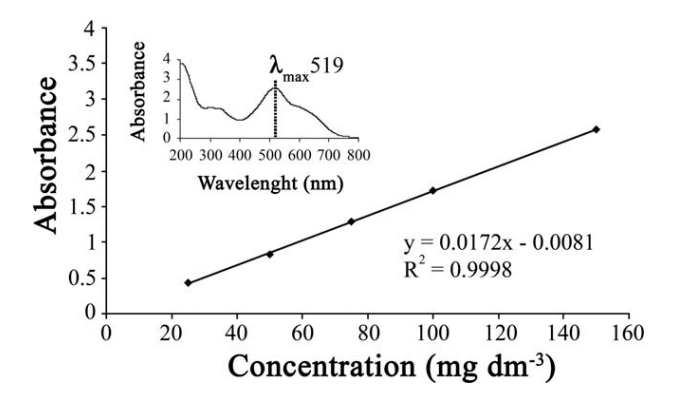


FIG. 11. Calibration line of the mixed dye solutions of Congo red and direct blue 71 (inset figure of absorption spectrum of a mixed aqueous solution of Congo red and direct blue 71).

 $(65\% \pm 1\%)$ and 62 ± 6.6 mg g⁻¹ $(42\% \pm 6\%)$ for Congo red and direct blue 71, respectively, from a 100 mg dm⁻³ solution of each dye.

Wastewater Treatment

The spectral absorptions of the industrial wastewater of sample A (a mixture of reactive dyes and direct dyes), sample B1 (only acid dyes) and sample B2 (a mixture of disperse dyes and acid dyes) before and after AHAMAA addition are shown in Fig. 10. All of the absorbances were dramatically decreased with wavelengths after the AHAMAA treatment. That means that the AHAMAA is an effective polymer flocculant in decreasing dye contents of the three samples.

The estimated dye concentrations were quantified from the synthetic dye wastewater. A calibration curve of the mixture of Congo red and direct blue 71 was constructed as shown in Fig. 11 in which an inset for the maximum absorption of the mixed dyes at $\lambda_{\rm max}$ at 519 nm is illustrated. The decrease in dye content in the mixed dye system was 92 \pm 3 mg dm⁻³ (61% \pm 2%) using 643 \pm 3 mg dm⁻³ of AHAMAA. The adsorption capacity in the mixed dye system was 142 \pm 2 mg g⁻¹. Table 4 presents

the dye contents by measuring the dye absorbance and converting their absorbance to dye concentrations without and with 500 mg dm⁻³ of AHAMAA. The result shows that AHAMAA is able to decrease color of the textile wastewater containing reactive, direct, and acid dyes. The highest dye decrease was 68% (19.9 mg dm⁻³) for 40 mg g⁻¹ of the B1 nondiluted sample containing only acid dyes. The dye reduction decreased with increasing dilution of the wastewater. It is also found that the presence of impurity and unknown additives in the textile effluent wastewater might decrease the dye reduction efficiency of AHAMAA, which could be caused by the charge neutralization or destabilization of the polymer bridge.

Generally, textile wastewater is comprised not only dye molecules but also various negatively charged compounds, such as, anionic detergents, dispersing agents and inorganic compounds such as salts. The flocculation mechanism of anionic textile dyes of reactive, acid, and direct dyes involved the electrostatic interaction between negative charges of the dye with positive charges of AHAMAA. The hydrophobic disperse dyes interacted with negatively charged compounds in textile wastewater to form a dye anionic compound, which behaved as an anionic dye. It interacted then with AHAMAA via the electrostatic attraction [41], resulting in a color reduction of the dyes in textile wastewater.

Based on the ICP analysis, the amount of aluminum ion of AHAMAA is 12 ± 2 mg dm⁻³ and it is responsible for the turbidity experiment. Table 5 shows that the turbidity of the textile wastewater is decreased in the presence of AHAMAA. The initial turbidity of wastewater from factories A and B was decreased with dilution. This may be caused by increasing amounts of the soluble dye and contaminated anionic compounds with water addition. The highest turbidity reduction was found in sample A at 94.4%. Interaction between the colloidal reactive and direct dyes and contaminated anionic compounds with AHAMAA flocculant can take place via the charge neutralization and bridge formation with the AHAMAA [25]. However, AHAMAA did not affect the turbidity of wastewater in sample A/100 having 1.84 NTU because the very low initial turbidity might not be sensitively detected by

TABLE 4. Dye removal of industrial wastewater by AHAMAA.

Wastewater		Without AHAMAA		With		
(factory/dilution)	λ_{max} (nm)	Absorbance	Conc. (mg dm ⁻³)	Absorbance	Conc. (mg dm ⁻³)	Dye removal (%)
A/0	509	0.60	35.1	0.30	17.8	50
A/10		0.14	8.3	0.07	4.5	45
A/100		0.04	2.6	0.02	1.5	42
B1/0	557	0.50	29.4	0.16	9.5	68
B1/5		0.12	7.3	0.05	2.9	60
B1/10		0.07	4.4	0.04	2.6	40
B2/0	549	0.61	35.8	0.29	17.3	52
B2/5		0.15	8.7	0.08	5.0	42
B2/10		0.09	5.4	0.08	4.7	13

TABLE 5. Turbidity reduction of industrial wastewater by AHAMAA.

			Indust	rial wastewa	ter (factory/di	lution)		
Properties	A	A/10	A/100	B1	B1/5	B1/10	B2	B2/10
Initial turbidity (NTU)	405	22.7	1.84	52.9	12.7	9.49	86.7	8.8
Turbidity after AHAMAA treatment (NTU)	23.0	8.5	1.97	24.3	5.23	3.94	74.5	8.8
% Reduction	94.4	62.6	NA	54.1	58.9	58.5	14.1	NA

the meter. The turbidity reduction for the sample B1, B1/5, and B1/10 were in the range of 54.1–58.9% at a similar initial turbidity. In sample B2, the turbidity reduction was only 14.1% even if its initial turbidity was rather high (86.7 NTU). This is because sample B2 contained the disperse dyes which cannot react directly with AHAMAA leading to the low turbidity reduction. Thus, when sample B2 was diluted by 10 times to become sample B2/10, AHAMAA cannot decrease its turbidity because of its low initial turbidity (8 NTU).

The investigation indicated that AHAMAA functions as an adsorbent and a flocculant. Because it can be applied in wastewater treatment as a flocculant to make flocs in the turbidity reduction of the kaolin suspension as described [20], and it can also be applied for the removal of dyes in the wastewater by the adsorption mechanism. Thus, it functions as an adsorbent as well.

CONCLUSIONS

AHAMAA was prepared by radical chain copolymerization in solution in which the residual aluminum ion concentration of AHAMAA in water was found in the range of 0.09-0.2 mg dm⁻³ regardless of the soaking time which indicates that AHAMAA is highly stable. AHAMAA can adsorb Congo red and direct blue 71, as validated by the Freundlich isotherm, through ionic interactions between the positively charged aluminum ion of AHAMAA and the sulfonate anion of the dyes. Both dyes are better removed by AHAMAA at pH 5-9 in the nonbuffered system. The dye reduction efficiency in the buffered system is lower than that of the nonbuffered. The adsorption capacity of AHAMAA for Congo red increases with increasing temperature and initial concentration of the dye solution. By adding AHAMAA, the color of the synthetic wastewater was decreased by 61% \pm 2% with the addition of 643 \pm 3 mg dm⁻³ of AHA-MAA, and 68% reduction for the industrial wastewater by 500 mg dm⁻³ of AHAMAA. The turbidity reduction of the wastewater from Factory A by AHAMAA was 94.4% when the initial turbidity was 405 NTU to become 23 NTU after the treatment. This new compound was designed to apply in wastewater treatment to reduce or replace alum consumption in a convention method. Although the cost of AHAMAAA is somewhat higher than the conventional alum they are ecological friendly and safe.

ACKNOWLEDGMENTS

Research facilities provided by the Imaging Polymer Laboratory of Chulalongkorn University's Imaging and Printing Technology Department are gratefully acknowledged. The authors thank the Publication Counseling Unit of the Research Division, Faculty of Science, Chulalongkorn University, for language corrections. Many thanks to Ms. Arunnee Sodsree for the dye and wastewater measurement.

REFERENCES

- C. Novotny, N. Dias, A. Kapanen, K. Malachova, M. Vandrovcova, M. Itavaara, and N. Lima, *Chemosphere*, 63, 1436 (2006).
- L.E. Gray and J.S. Ostby, Fundam. Appl. Toxicol., 20, 177 (1993).
- 3. B. Acemioglu, J. Colloid Interface Sci., 274, 371 (2004).
- 4. P. Baskaralingam, M. Pulikesi, V. Ramamurthi, and S. Sivanesan, *J. Hazard. Mater. B*, **136**, 989 (2006).
- M. Alkan, S. Celikcapa, O. Demirbas, and M. Dogan, *Dyes Pigm.*, 65, 251 (2005).
- T. Robinson, B. Chandran, and P. Nigam, Water Res., 36, 2824 (2002).
- L.E. Gray, J.S. Ostby, R.J. Kavlock, and R. Marshall, Fundam. Appl. Toxicol., 19, 411 (1992).
- M.K. Purkait, A. Maiti, S. DasGupta, and S. De, *J. Hazard. Mater.*, **145**, 287 (2007).
- V.V. Basava Rao and S. Ram Mohan Rao, Chem. Eng. J., 16, 77 (2006).
- S. Chatterjee, S. Chatterjee, B.P. Chatterjee, and A.K. Guha, Colloids Surf. A, 299, 146 (2007).
- A. Tor and Y. Cengeloglu, J. Hazard. Mater. B, 138, 409 (2006).
- A.K. Golder, A.N. Samanta, and S. Ray, *Chem. Eng. J.*, 122, 107 (2006).
- A.A. Ahmad, B.H. Hameed, and N. Aziz, *J. Hazard. Mater.*, 141, 70 (2007).
- Y. Bulut, N. Gozubenli, and H. Aydin, J. Hazard. Mater., 144, 300 (2007).
- E. Karadag, D. Saraydin, and O. Guven, Water Air Soil Pollut., 106, 369 (1998).
- S. Duran, D. Solpan, and O. Guven, *Nucl. Instrum. Methods* B, 151, 196 (1999).
- O.S. Fatoki and A.O. Ogunfowokan, Water SA., 28, 293 (2002).
- N. Kaneko, T. Sugioka, and H. Sakurai, *J. Inorg. Biochem.*, 101, 967 (2007).

- 19. M. Kabsch-Korbutowicz, Desalination, 185, 327 (2005).
- S. Noppakundilograt, P. Nanakorn, K. Sonjaipanich, N. Seetapan, and S. Kiatkamjornwong, *J. Appl. Polym. Sci.*, 114, 2564 (2009).
- 21. G.L. Shugar and J.A. Dean, *The Chemist's Ready Hand-book*, McGraw-Hill, New York (1990).
- E.Y. Ozmen and M. Yilmaz, J. Hazard. Mater., 148, 303 (2007).
- 23. C.A. Contreras, S. Sugita, and E. Ramos, *AZojomo*, **2**, 3 (2006).
- G.A. Mazzocchin, F. Agnoli, and S. Mazzocchin, Anal. Chim. Acta., 475, 181 (2003).
- B.Y. Gao, Y.B. Chu, Q.Y. Yue, B.J. Wang, and S.G. Wang, J. Environ. Manage., 76, 143 (2005).
- W.H. Kuan, M.K. Wang, P.M. Huang, C.W. Wu, C.M. Chang, and S.L. Wang, *Water Res.*, 39, 3457 (2005).
- S.M.Z. Al-Kindy, S.S. Al-Ghamari, and F.E. Suliman, Spectrochim. Acta A, 68, 1174 (2007).
- J. Gregory, "Polymer Adsorption and Flocculation," in *Industrial Water Soluble Polymers*, C.A. Finch, Ed., The Royal Society of Chemistry, London, 62 (1996).
- 29. T. Caykara, I. Akcakaya, Eur. Polym. J., 42, 1437 (2006).
- N.A. Peppas and A.R. Khare, Adv. Drug. Deliv. Rev., 11, 1 (1993).
- 31. Z. Chen, M. Liu, and S. Ma, React. Funct. Polym., 62, 85 (2005).

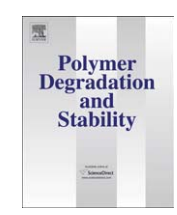
- 32. P. Lanthong, R. Nuisin, and S. Kiatkamjornwong, *Carbohydr. Polym.*, **66**, 229 (2006).
- 33. S. Kiatkamjornwong and R. Wongwathansatien, "Superabsorbent Polymer of Poly[acrylamide-co-(acrylic acid)] by Foamed Polymerization. I. Synthesis and Water Swelling Properties." in *Fundamentals and Applications of Polymer Gels*, Macromolucule Symposia Series 207, R.A. Siegel, Ed., Wiley-VCH, Weinheim, New York, 229 (2004).
- M. Skowronek, I. Roterman, L. Konieczny, B. Stopa, J. Rybarska, B. Piekarska, A. Gorecki, and M. Krol, *Comput. Chem.*, 24, 429 (2000).
- B.C. Faust, W.B. Labiosa, K.H. Dai, J.S. MacFall, B.A. Browne, A.A. Ribeiro, and D.D. Richter, *Geochim. Cosmo-chim. Acta*, 61, 3261 (1997).
- 36. T. Ren, Z. Yuan and B. Su, *Colloids Surf. A*, **300**, 79 (2007).
- 37. B. Tagirov, J. Schott, J.-C. Harrichoury, and J. Escalier, *Geochim. Cosmochim. Acta*, **68**, 1333 (2004).
- 38. L. Wang and A. Wang, J. Hazard. Mater., 147, 979 (2007).
- 39. F.A. Pavan, S.L.P. Dias, E.C. Lima, and E.V. Benvenutti, *Dyes Pigm.*, **76**, 64 (2008).
- 40. L. Wang and A. Wang, *Bioresour. Technol.*, 99, 1403 (2008).
- 41. R.J. Zemaitaitiene, E. Zliobaite, R. Klimaviciute, and A. Zemaitaitis, *Colloids Surf. A*, **214**, 37 (2003).



Contents lists available at ScienceDirect

Polymer Degradation and Stability

journal homepage: www.elsevier.com/locate/polydegstab



Photocatalytic efficiency of TiO₂/poly[acrylamide-co-(acrylic acid)] composite for textile dye degradation

Wiyong Kangwansupamonkon^a, Walasinee Jitbunpot^b, Suda Kiatkamjornwong^{c,*}

- ^a National Nanotechnology Center, National Science and Technology Development Agency; 111 Thailand Science Park, Paholyothin Road, Klong 1, Klong Luang, Pathumthani 12120, Thailand
- ^b Program of Petrochemistry and Polymer Science, Faculty of Science, Chulalongkorn University, Phyathai Road, Bangkok 10330, Thailand
- ^c Department of Imaging and Printing Technology, Faculty of Science, Chulalongkorn University, Phyathai Road, Bangkok 10330, Thailand

ARTICLE INFO

Article history: Received 13 February 2010 Accepted 23 April 2010 Available online 12 May 2010

Keywords: TiO₂ Hydrogel Photocatalytic degradation Dye removal

ABSTRACT

A novel photocatalytically degradable TiO₂/poly[acrylamide-co-(acrylic acid)] composite hydrogel (TiO₂/poly[AAm-co-AAc]) was synthesized by polymerization in an aqueous solution with N,N'-methylenebisacrylamide as the crosslinker and ammonium persulphate and TEMED as the initiator pair. The combined and separate effects of photodegradation and adsorption processes for dye removal were evaluated using methylene blue (MB) as the model dye for a photodegradation target, and compared with those of the neat poly[AAm-co-AAc], and a commercially available TiO₂ photocatalyst (Degussa P-25). Without photodegradation (i.e. in the dark), the TiO₂/poly[AAm-co-AAc] composite adsorbed up to 85% of the MB from a 5 mg L⁻¹ MB solution in 15 min compared to only 10% for the pristine TiO₂. The reproducibility in photodegradation of the reused poly[AAm-co-AAc] composite was also investigated, where poly[AAm-co-AAc] was found to be photocatalytically degraded under UV irradiation. Therefore, the TiO₂/poly[AAm-co-AAc] composite hydrogel is a good dye adsorber with self-photodegradability and it also can easily be separated from the reaction by simple filtration. With these properties, the TiO₂/poly[AAm-co-AAc] hydrogel can be called a green polymer for use in the photodegradation—adsorption process for the abatement of various pollutants.

 $\ensuremath{\texttt{©}}$ 2010 Elsevier Ltd. All rights reserved.

1. Introduction

In recent years, pollution from dye wastewater has become a serious environmental problem due to the vast and increasing uses of a variety of dyes [1–4]. The dyes usually have a synthetic origin and typically have complex aromatic molecular structures that are more stable and difficult to degrade. The textile, paper, plastics and cosmetic industries use a wide variety of dyes to color their products and discharge large amounts of effluents, including dyes, which are toxic and could cause serious ecological problems. Therefore, dye pollution in water, such as discharge effluent into streams and ground water, is a major environmental problem.

Methylene blue (MB) has wide applications, which includes coloring paper, temporary hair colorant, dyeing cottons and wools. Although it is not strongly hazardous, it can cause some harmful effects, such as heartbeat increase, vomiting, shock, cyanosis, jaundice, quadriplegia, and tissue necrosis in humans. Color

removal from effluents polluted with dyes of textile industries has been considered a challenge due to the difficulty of treating such wastewaters by conventional methods. The effluents of the manufacturing and textile industries are discarded into rivers and lakes, changing their biological life [5,6].

The current methods of dye removal from industrial wastewaters can require many processes and steps, such as biological treatment, coagulation, flotation, electrochemical techniques, adsorption and oxidation. Among these methods, adsorption is generally preferred due to its high efficiency, ease of handling and the availability of different adsorbents [7]. However, new environmental laws may consider the used adsorbents or sludge as hazardous waste materials themselves that will require further treatment prior to disposal. Consequently, novel technologies with a higher efficiency and lower energy consumption are required and have stimulated intensive research. An alternative to conventional methods includes the advanced oxidation processes (AOPs), which are based on the generation of very reactive species, such as hydroxyl radicals (*OH), that oxidize a broad range of organic pollutants quickly and non-selectively.

Photocatalytic oxidation using a semiconductor, such as TiO_2 as a photocatalyst, is one of the AOPs being developed. When TiO_2 is

^{*} Corresponding author. Tel.: +662 2185587; fax: +662 2553021.

E-mail addresses: wiyong@nanotec.or.th (W. Kangwansupamonkon), yoghurt55@hotmail.com (W. Jitbunpot), ksuda@chula.ac.th (S. Kiatkamjornwong).

illuminated by radiation with a wavelength below 380 nm, the photons excite the valence band electrons across the band gap into the conduction band, leaving holes behind in the valence band that will then react with water molecules or hydroxide ions (OH⁻) to produce hydroxyl radicals (*OH) [8]. Oxygen is usually supplied as an electron acceptor to prolong the recombination of electron-hole pairs during the photocatalytic oxidation. TiO₂ photocatalysts have been successfully used to purify water and air, to degrade some organic pollutants and to kill microbes including bacteria [9–12]. Several investigations have reported that TiO₂ based photocatalysis is an effective method for discoloring and oxidizing organic dyes in wastewater, [13–15] including optimization of the method with the model dye, methylene blue (MB) [16–19].

However, as a photocatalyst TiO_2 is usually used in a powdery form in aqueous suspension, which requires separation of the TiO_2 particles from the purified water after the discoloring reaction. In addition, the process is generally equipped with an artificial UV radiation source, leading to a considerable increase in the operation and environmental costs. These drawbacks may be an obstacle to the use of TiO_2 photocatalysis for practical applications.

The development of new adsorbents having superior properties, such as a high adsorption capacity, fast adsorption rate and mechanical strength, has generated a great deal of interest in their application for wastewater treatment. Using several polymers with different functional groups is of increasing importance due to their high adsorption capacities and, especially, their regeneration abilities allowing repeated use or application in a continuous treatment processes [20,21]. Hydrogels possessing different functional groups have also been investigated for this purpose [22-24]. Hydrogels can be defined as water-swollen, three-dimensional networks. They can absorb a large amount of water compared to other water absorbing materials, and can also show stimuli-responsive properties to various external stimuli, such as temperature, pH, solvent composition and ionic strength in salt composition, depending on the type of functional groups in the materials [25,26]. In recent years, the preparation of hydrogel composites has spurred research efforts to produce new materials and novel applications in different areas, such as drug delivery, medical materials, agriculture industry and various fractionation/separation processes. However, investigation of the potential applicability of hydrogel composites in the dye removal process is less well studied. Hafez et al. [27] reported the photocatalytic efficiency of TiO2 immobilized on a PVP/AAc hydrogel for the removal of Remazol Red RB-133 textile dye and under the same experimental conditions (an equal amount of TiO₂ and pH), the PVP/AAc hydrogel supported catalysts rendered 58% and 35% efficiency relative to the non-supported ones of the commercially available Degussa P-25, and freshly prepared colloidal photocatalysts, respectively. Tang et al. [28] studied the use of a TiO₂/polyacrylamide hydrogel composite for the removal and photodegradability of the methyl orange dye, and the TiO₂/ PAAm composite had a good photocatalytic degradability, the composite also possessed a good reproducibility of photocatalytic degradability, which is possible to be applied for a practical process.

In the work reported here, a novel hydrogel composite (TiO₂/poly[AAm-co-AAc]) was prepared with acrylamide (AAm), acrylic acid (AAc) and TiO₂, and was then evaluated for the ability to remove MB dye from aqueous solutions. The combined effect of photodegradation—adsorption mediated by the TiO₂/poly[AAm-co-AAc] composite was investigated. The photocatalytic degradation process utilizing TiO₂ has been shown to be very effective for the degradation of various organic pollutants, but it is ineffective for the abatement of heavy metal ions which are generally non-degradable [29] and only reactive under UV irradiation. In contrast, poly[AAm-co-AAc] is known to have a very promising capability in this regard. Therefore, it was expected, and here is evaluated and

reported, that TiO_2 and poly[AAm-co-AAc] could complement each other with their own advantages and so provide a comprehensive method in the abatement of various wastewater pollutants. Composite gels also have many other advantages, such as a low cost and easy separation from the reaction solution.

2. Experimental

2.1. Materials

AAm and AAc (both commercial grade) were obtained from Siam Chemical Industry, Thailand. N,N'-methylenebisacrylamide (N-MBA, Fluka, analytical grade) was used as a crosslinking agent. The photocatalyst employed was titanium dioxide (TiO₂, commercial grade, P-25, Degussa Corporation). According to the manufacturer's specification, P-25 has an elementary particle size of 30 nm and a BET surface area of ca. $54 \text{ m}^2 \text{ g}^{-1}$. Ammonium persulfate (APS, analytical grade, Merck, Germany) and N,N,N'N'-tetramethylenediamine (TEMED, analytical grade, Aldrich, Germany) were used as a redox initiator pair for the free radical polymerization reaction. Methanol (MeOH, commercial grade, BDH U.K.) was used for dehydrating water from the gel. Basic blue 9 (MB having a C.I. of 52015, a light blue dye powder) was from Dystar Thai Co. Ltd. (Bangkok, Thailand) and was used as received. All other chemicals were used without further purification.

2.2. Preparation of TiO₂/poly[acrylamide-co-(acrylic acid)] composite hydrogel

The TiO₂/poly[acrylamide-co-(acrylic acid)] composite hydrogel was synthesized by polymerization from an aqueous solution containing acrylic acid (2.5×10^{-1} M) and acrylamide (2.5×10^{-1} M) in a four-necked round bottomed flask, equipped with a mechanical stirrer set at 200 rpm and an inlet tube for feeding nitrogen gas. The reaction temperature was controlled at 60 °C. Then 2.5×10^{-2} M of N-MBA, 2.5×10^{-3} M of APS, 5–20 %wt of TiO₂ and 0.5 mL of TEMED were sequentially added to the reaction mixture. The mixture was stirred for 30 min and the resulting polymer was dehydrated with methanol, cut into small pieces of about 4–5 mm in diameter, and then dried at 50 °C for 24 h.

2.3. Characterization

2.3.1. Morphological study by SEM

The surface morphologies of TiO_2 , poly[AAm-co-AAc] and the $TiO_2/poly[AAm-co-AAc]$ composite were investigated using scanning electron microscopy (SEM, model JSM-T 220A, JEOL, Japan) without cross-section. The thickness of gold coating on the copolymer and its composites was 25 nm, and the SEM was operated with an accelerating voltage of 15 kV. The elemental analyses from SEM micrographs were used to calculate the percentage (in weight) of titanium by energy dispersive X-ray spectrometry (EDXS).

2.3.2. X-ray diffraction analysis

X-ray diffraction measurements of TiO₂, poly[AAm-co-AAc] and the TiO₂/poly[AAm-co-AAc] composite were carried out using a JOEL JDX-3530 diffractometer (CuK \propto radiation, $\lambda=0.15405$ nm, 2 kW). The X-ray diffraction (XRD) patterns were recorded from 10° to 60° in 2 θ at a scanning rate of 0.02° min⁻¹. The dried copolymer powder was mounted on a sample holder with smooth double-sided adhesive tape.

2.3.3. The decolorization of the dye solution in the dark

Dye removal behavior from aqueous suspension of the TiO_2 /poly [AAm-co-AAc] composite in comparison with the pristine TiO_2 was

investigated in continuous adsorption equilibrium experiments using the MB dye solution in the dark (to exclude photodegredation) as follows. A sample of the $TiO_2/poly[AAm-co-AAc]$ composite weighing 0.2 g, or 0.0153 g of the pristine TiO_2 (the weight was selected from the TGA results), was transferred directly into a 200 mL aqueous solution of 5 mg L $^{-1}$ MB. The MB solution in each sample was agitated magnetically at a moderate speed and then allowed to sediment. At various time intervals, t, an aliquot of the solution was taken and the remaining dye concentration in the solution was subsequently monitored by a UV—visible spectrophotometer (Perkin—Elmer, model Lambda 650, Shelton, Connecticut, U.S.A) at an incident wavelength, λ_{max} , of 664 nm. The initial and equilibrium dye concentrations are determined using a calibration curve based on the absorbance at λ_{max} versus dye concentration in standard dye solutions.

To construct a calibration curve, the MB concentrations of 0.5, 1.0, 2.5, 5.0, 7.5 and 10 mg L $^{-1}$ were prepared in volumetric flasks and the absorbance of each of the standard MB solutions was measured at the maximum absorption wavelength of 664 nm. Therefore, the concentration of MB could be calculated from the regression equation: $y = 0.1777 \times$, $R^2 = 0.9892$ as shown in Fig. 1. The amount of dye adsorbed per unit mass of the sample at equilibrium, $q_{\rm max}$ (mg g $^{-1}$), is calculated by using Equation (1):

$$\begin{array}{c} + H^{+} + 2e \\ + H^{-} - 2e \\ + H_{3}C)_{2}N \end{array}$$
methylene blue
$$\begin{array}{c} + H^{+} + 2e \\ + H_{3}C)_{2}N \end{array}$$
leucomethylene blue

$$q_{\text{max}} = (C_0 - C_{\text{eq}}) \times V/M \tag{1}$$

where C_0 and C_{eq} (mg L⁻¹) are the liquid phase concentrations of dye initially and at equilibrium, respectively, and the dye removal of MB from solution was calculated by Equation (2):

% Dye Removal =
$$\frac{C_0 - C_1}{C_0} \times 100$$
 (2)

where C_1 (mg L⁻¹) is the liquid phase concentrations at time, t.

2.3.4. Photocatalytic degradation of methylene blue

Photocatalytic degradation of the MB dye was studied using $0.2 \, \mathrm{g}$ of the $\mathrm{TiO_2/poly[AAm-}\mathit{co-}\mathrm{AAc]}$ composite or the poly[AAm- $\mathit{co-}\mathrm{AAc}$] without $\mathrm{TiO_2}$ (as a control). Each sample was poured into

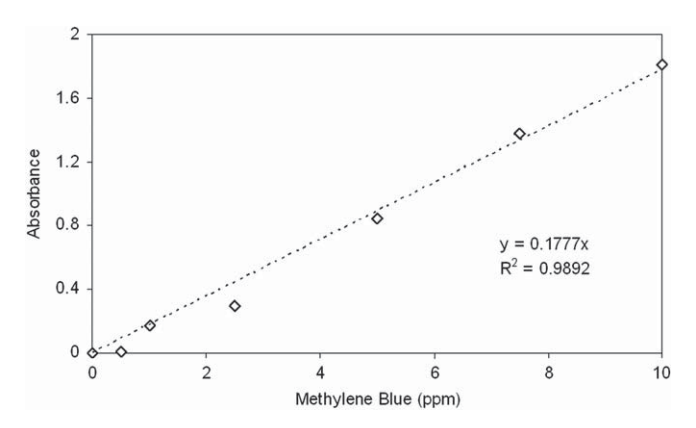


Fig. 1. Calibration curve for MB dye detection by absorbance at 664 nm.

a 200 mL MB solution (5 mg L $^{-1}$) and kept at room temperature for 24 h. After the equilibrium absorption, the unabsorbed dye solution was removed by filtration over a 100-mesh sieve aluminum screen and left for 30 min to drain off the unabsorbed solution. The swollen hydrogels were placed in a quartz cuvette having a path length of 1 cm, capped and exposed on its side to 365 nm UV radiation by a UV lamp at an intensity of 1 mW cm $^{-2}$. The decolorization of MB at the equilibrium absorption of the neat poly [AAm-co-AAc] and TiO2/poly[AAm-co-AAc] composite were measured at the indicated time intervals between 0 and 40 min exposure to UV radiation by a UV—visible spectrophotometer at a wavelength of 608 nm.

The absorbance measurements of the dye concentration in solution were performed with the UV—visible absorption spectroscopy at $\lambda_{\rm max}=664$ nm and the absorbance measurements of the dye concentration in poly[AAm–co–AAc] hydrogel and TiO2/poly [AAm–co–AAc] composite were performed at $\lambda_{\rm max}=608$ nm. The experimental conditions show that the maximum absorption occurred at 664 and 608 nm at pHs 1—7 as depicted in Fig. 2. The latter absorption band was selected to monitor the temporal concentration changes of methylene blue in poly[AAm–co–AAc] and TiO2/poly[AAm–co–AAc] composite. The blue shifts of the absorption bands of methylene blue in poly[AAm–co–AAc] and TiO2/poly [AAm–co–AAc] composite are pH dependent as that shown in Equation (3): [18]

The dye removal of MB from within the hydrogel under different conditions, such as in darkness (without UV irradiation) or under UV irradiation, was calculated by Equation (2) where C_0 and C_1 are the concentrations of MB dye measured at 608 nm in equilibrium absorption of the hydrogel before and after the irradiation, respectively.

As per the preliminary kinetics study, it showed that the degradation of MB by the TiO₂/poly[AAm-co-AAc] composite was best fitted by pseudo-first-order kinetics. The related kinetic model is shown in Equation (4):

$$-\ln\left(\frac{C}{C_0}\right) = kt \tag{4}$$

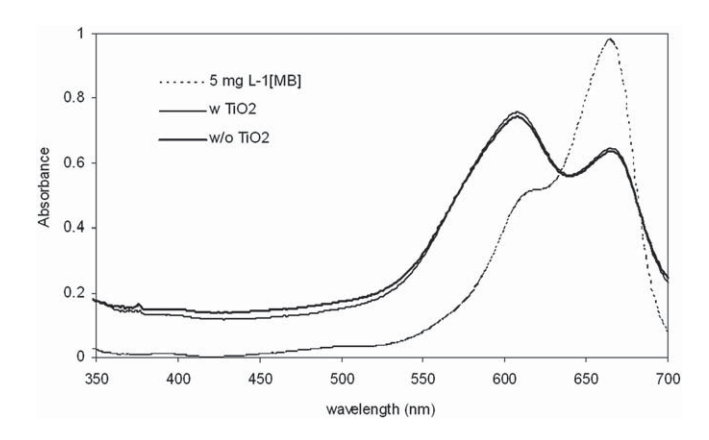


Fig. 2. Temporal spectral changes of MB in TiO₂/poly[AAm-co-AAc] composite and poly[AAm-co-AAc].

where C_0 and C are the initial dye concentration and that at time t (min), respectively, t is the irradiation time (min) and k is the rate constant (min⁻¹) [30].

2.3.5. Rheological measurement of the TiO₂/poly[AAm-co-AAc] composite for degradation evaluation

The degradation of the $TiO_2/poly[AAm-co-AAc]$ composite hydrogel was evaluated by rheological measurements using a strain controlled rheometer (Bohlin Gemini HR nano, Malvern, UK) with parallel plates of 25 mm diameter. Oscillatory experiments and mechanical spectra were recorded in the frequency range of 0.01-35 Hz at 37 °C. The linear viscoelastic region was assessed at 0.1 Hz by assaying the strain sweep with a constant deformation strain of 0.5%. The samples were analyzed 24 h after sample preparation to attain the maximum swelling. The storage or elastic (G') and loss or viscous (G'') moduli were determined as a function of the frequency.

2.3.6. Photodegradation of the TiO₂/uncrosslinked poly[AAm-co-AAc] by GPC

The TiO₂/uncrosslinked poly[AAm-co-AAc] was synthesized by polymerization from an aqueous solution as detailed above except that the *N*-MBA crosslinker was omitted in the synthesis step. The TiO₂/uncrosslinked poly[AAm-co-AAc] was then irradiated with 365 nm UV radiation at an intensity of 1.6 mW cm⁻² for 4 h and 24 h and compared to the neat uncrosslinked poly[AAm-co-AAc] synthesized under the same conditions. The number average molecular weight ($\overline{M}_{\rm m}$), weight average molecular weight ($\overline{M}_{\rm w}$) and polydispersity index (PDI) were analyzed by gel permeation chromatography (GPC). It is important to state that the TiO₂/uncrosslinked poly[AAm-co-AAc] must be totally soluble in water. Samples of the polymer composite weighing 10 mg was dissolved in 5 mL of sodium bicarbonate buffer at pH 11, filtered through

a 0.45 µm filter, and then the solution was transferred to the auto-sampler vial for molecular weight determination by GPC.

3. Results and discussion

3.1. Morphological study by SEM

The morphologies of TiO_2 (Degussa P-25) particles, poly[AAm-co-AAc] and TiO_2 /poly[AAm-co-AAc] composite, as observed by SEM, are shown in Fig. 3. TiO_2 (P-25) particles, utilized as a nanocatalyst, were largely small spherical particles of 35–67 nm diameter (mean 50 ± 7 nm) but tended to agglomerate together (Fig. 3 (a)). The pulverized poly[AAm-co-AAc], obtained from the radical chain polymerization in aqueous solution, was essentially a smooth sheet free of any significant particulate nature (Fig. 3 (b)). The TiO_2 loadings at 15 and 20%wt were immobilized in the TiO_2 /poly[AAm-co-AAc] composite showed the TiO_2 particles to be well dispersed and so were found to reside on both the surface and the inner depths (Fig. 3 (c,d)). The TiO_2 particle distribution increased with increasing TiO_2 content. However, the fine nanoscaled TiO_2 particles are susceptible to agglomerate when their content was raised to 20%wt of TiO_2 /poly[AAm-co-AAc] composite (Fig. 3 (d)).

3.2. X-ray diffraction analysis

To get some information on the TiO₂ content and structure in the hydrogel composites, XRD analysis was performed and typical diffractogram patterns are shown in Fig. 4.

No diffraction peaks in the spectrum for the synthesized poly [AAm-co-AAc] hydrogel were obtained. In contrast, a number of sharp peaks were clearly visible in the TiO₂/poly[AAm-co-AAc] composite, indicating the presence of crystalline moieties in the composite samples. The (101) and (110) basal plane spacing of TiO₂

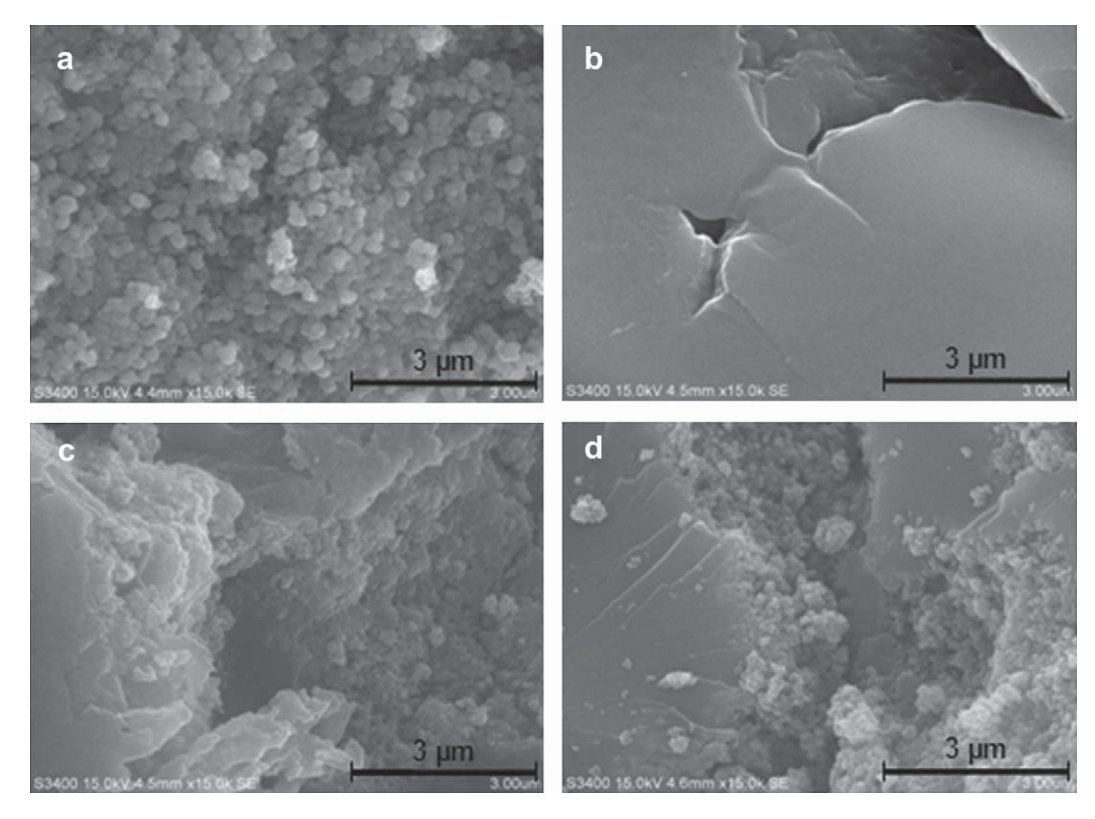


Fig. 3. Representative SEM micrographs of the (a) pristine TiO₂ (P-25), (b) neat poly[AAm-co-AAc] hydrogel, (c) 15%wt TiO₂/Poly[AAm-co-AAc] composite, and the (d) 20%wt TiO₂/Poly[AAm-co-AAc] composite. (Images are taken at 15,000× magnification representing at least 3 of such fields of view per sample and 3 independent samples).

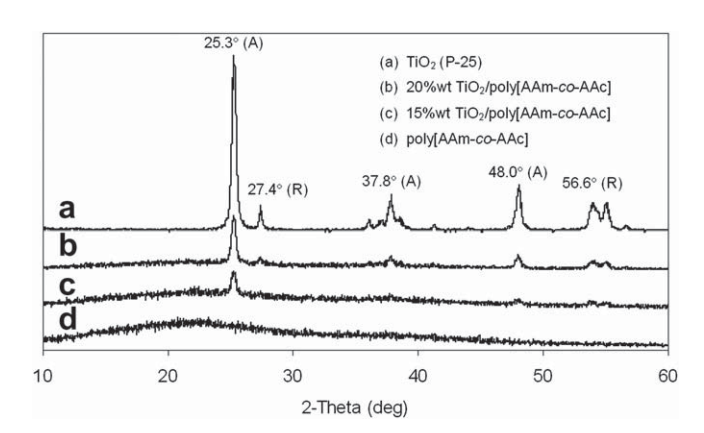


Fig. 4. Representative XRD patterns of (a) TiO₂ (P-25), (b) 20%wt TiO₂ (P-25)/poly [AAm-co-AAc], (c) 15%wt TiO₂(P-25)/poly[AAm-co-AAc] and (d) poly[AAm-co-AAc] (Diffractograms shown are representative of 3 independent samples).

are reported to be the anatase and rutile crystalline phases at $2\theta=25.3^{\circ}$ and 27.4° , respectively [31]. The result here shows that the TiO₂ (P-25)/poly[AAm-co-AAc] composites have observed peaks at $2\theta=25.3^{\circ}$, 37.8° and 48.0° for the anatase crystalline phase and at $2\theta=27.4^{\circ}$ and 56.6° for the rutile crystalline phase (Fig. 4 (b,c)).

The intensity of the characteristic TiO_2 peaks increased with increasing amounts of TiO_2 loading in the TiO_2 /poly[AAm-co-AAc] composite, in comparison with the poly[AAm-co-AAc] without TiO_2 (Fig. 4 (b,c)). This confirms that TiO_2 is incorporated in the poly [AAm-co-AAc] matrix, and therefore that the poly[AAm-co-AAc] and the TiO_2 /poly[AAm-co-AAc] composite were successfully synthesized.

3.3. Effect of TiO₂ content on photocatalytic degradation

The photocatalytic degradation of the MB dye within the adsorbent, after exposure to a 200 mL 5 mg $\rm L^{-1}$ MB solution and subsequent removal of the solution by filtration, was carried out in a quartz cuvette as described previously. The effects of $\rm TiO_2$ loading from 5 to 20%wt in the hydrogel on dye degradation, measured with a UV—visible spectrophotometer at a wavelength of 608 nm, were evaluated following exposure to a 365 nm

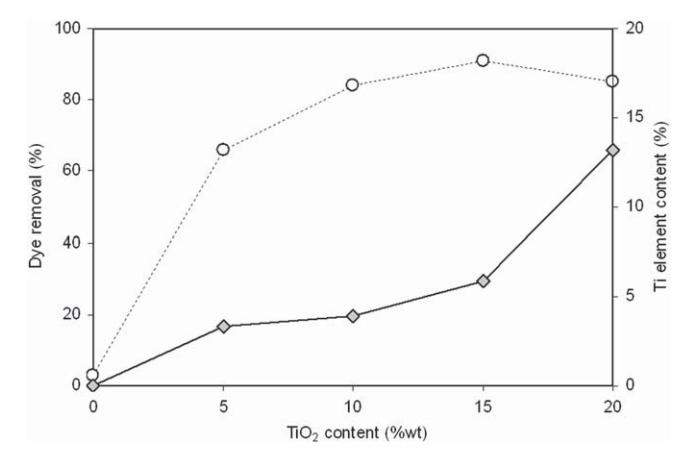


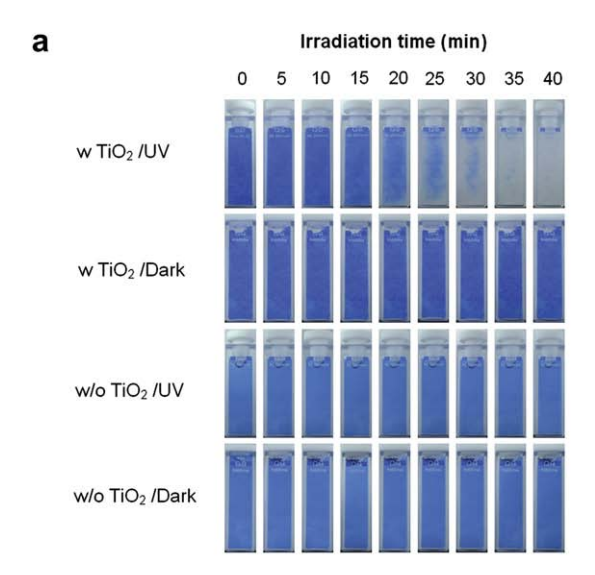
Fig. 5. MB dye removal from the hydrogel as a function of the TiO_2 (P-25) loading (%wt TiO_2 and the % elemental Ti) in the poly[AAm-co-AAc] hydrogel, when exposing to 365 nm wavelength UV irradiation at 1 mW cm⁻² for 40 min (Data are shown as the mean \pm 1 S.D. and are derived from 3 replications). Means with a different letter are significantly different (p < 0.05; Mann–Whitney U test).

wavelength UV radiation source at an intensity of 1 mW cm^{-2} for 0 or 40 min (Fig. 5).

The dependence of the MB dye removal from the adsorbent hydrogel on the ${\rm TiO_2}$ loading in the hydrogel (Fig. 5), evaluated as either %wt ${\rm TiO_2}$ or the % Ti element content, indicates that the dye removal efficiency increases with increasing ${\rm TiO_2}$ concentration until 15%wt of ${\rm TiO_2}$ (5.9% Ti elemental composition). Although ${\rm TiO_2}$ is a good photocatalytic degradation agent, and so as the ${\rm TiO_2}$ amount in the polymer increased, the photocatalytic degradation is enhanced by the increased number of available catalyst active sites, the ${\rm TiO_2}$ nanoparticles are, however, prone to conglomerate at concentrations above 15%wt ${\rm TiO_2}$ loading, which results in a decreased photocatalytic degradability due to the decrease in the number of available catalyst active sites.

3.4. Photocatalytic degradation of methylene blue in the hydrogel composite

The photodegradation of MB dye within the adsorbent hydrogel was found to be enhanced in the presence of TiO₂/poly[AAm-co-AAc] composite (Fig. 6). Thus, in the presence of 15%wt TiO₂/poly [AAm-co-AAc] composite, approximately 91% of the dye was degraded after 40 min UV irradiation at room temperature, in contrast to the 3% seen following UV irradiation without TiO₂.



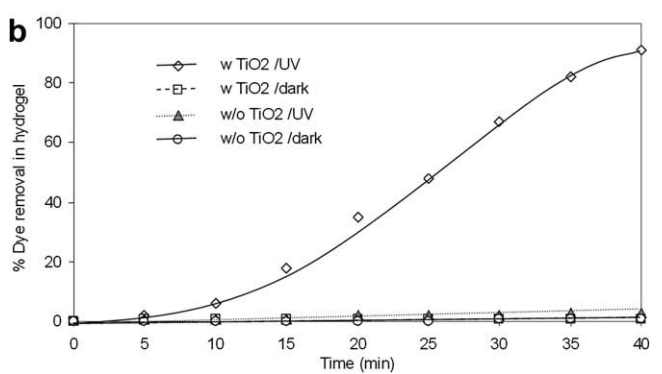


Fig. 6. MB dye removal from the hydrogel with time with (UV) or without (dark) exposure to 365 nm UV radiation at 1 mW cm $^{-2}$ in the presence (w TiO₂) or absence (w/o TiO₂) of 15%wt TiO₂ in the poly[AAm-co-AAc] hydrogel. The dye concentration was 5 mg L $^{-1}$ MB (200 mL). (a) Color appearance of MB degradation, where each cuvette is representative of 3 independent repeats. (b) MB dye removal vs. irradiation time, where data are shown as the mean \pm 1 S.D., derived from 3 replications.

Likewise, there were no changes in the dye concentration, when poly[AAm-co-AAc] or TiO₂/poly[AAm-co-AAc] composites were used in the dark (i.e., without UV irradiation). Thus, both UV radiation and the TiO₂ photocatalyst are needed for the effective destruction of MB. Following UV radiation, the irradiated MB molecule is excited and acts as a photosensitizer capable of injecting electrons into the conduction band of the TiO₂ semiconductor particles to form oxidized radicals, whilst the oxidized species of the MB molecules then undergo further degradation, such as via peroxylated or hydroxylated intermediates to further degradation products such as mineralized products [16,32].

3.5. Dye removal from solution in the dark and photocatalytic degradation of methylene blue

Fig. 7 shows the comparison of MB dye removal via adsorption by TiO_2 (P-25), poly[AAm-co-AAc] and the TiO_2 /poly[AAm-co-AAc] composite in contact with the MB solution in the dark (to exclude photodegradation). The poly[AAm-co-AAc] hydrogel and TiO_2 /poly [AAm-co-AAc] composite both adsorbed MB dye to a significant extent with similar kinetics, with essentially equilibrium adsorption, $q_{\text{max}} = 5.3 \text{ mg g}^{-1}$, (% dye removal = $\sim 87\%$) being attained within 15 min. In contrast, the TiO_2 (P-25) alone was a poor adsorbent, reaching a much lower equilibrium (saturation) level of only 0.7 mg g $^{-1}$ (% dye removal = 12%) absorbance after 30–45 min. Thus, the role of poly[AAm-co-AAc] as an adsorbent, with the formation of an ionic complex between the MB molecules and the poly[AAm-co-AAc] hydrogel [33], and potentially aiding TiO_2 photooxidation should not be ignored.

The adsorption rate constants are summarized in Table 1, where the close $k_{removal}$ values for the poly[AAm-co-AAc] and the TiO₂/poly[AAm-co-AAc] composite before UV irradiation, compared to the large difference between them after the UV irradiation, are due to interaction of the charged groups of the polymer networks and the dye imines groups to support the adsorption [34]. In contrast, a very small amount of MB molecules could be adsorbed onto the surface of TiO2 (P-25), although the BET surface area of TiO_2 (P-25) is 54 m² g⁻¹. Thus, the ionic functional groups on the poly[AAm-co-AAc] backbone can adsorb and trap the cationic dye through ionic interactions. With the TiO₂ alone, the k_{degrad} is very low but it is better than that of poly[AAmco-AAc] alone. To ascertain more details on the photocatalytic degradation of MB, the amount of MB dye removed by the TiO₂/ poly[AAm-co-AAc] composite, poly[AAm-co-AAc] and TiO₂ (P-25) were plotted (Fig. 8). The TiO₂/poly[AAm-co-AAc] composite starts with a weak dye removal process within 5 min, accelerates to an

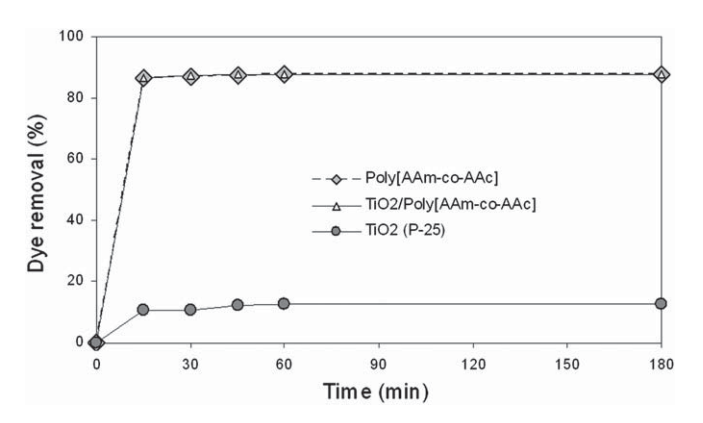


Fig. 7. Adsorption of a 5 mg L^{-1} MB solution (200 mL) by TiO_2 immobilized in poly [AAm-co-AAc], neat poly[AAm-co-AAc] or the pristine TiO_2 (Degussa P-25) in the dark. Data are shown as the mean \pm 1 S.D., derived from 3 replications.

Table 1Equilibrium dye adsorption, dye removal rate and photodegradation rate constants of MB dye by the pristine TiO₂, TiO₂/poly[AAm-co-AAc] and the neat poly[AAm-co-AAc].

Sample	$q_{ m max}~({ m mg~g^{-1}})$	Rate constant (k), min ⁻¹				
		$k_{\text{removal}}^{\text{a}}$	R^2	$k_{ m degrad}^{ m b}$	R^2	
Poly[AAm-co-AAc]	5.3	0.1346	1	0.0008	0.9865	
TiO ₂ /Poly[AAm-co-AAc]*	5.3	0.1344	1	0.1161	0.9936	
TiO ₂ (P-25)	0.7	0.0006	0.9103	0.0185	0.9916	

*loaded with 15%wt TiO $_2$. UV irradiation at a wavelength of 365 nm and 1 mW cm $^{-2}$.

almost linear rate between 15 and 30 min and reaches equilibrium at approximately 40 min with a maximum dye removal of 91%. In contrast, the dye removal by TiO2 (P-25) particles is only 53% at 40 min, but is not yet at equilibrium. Note that the MB dye removal by poly[AAm-co-AAc] showed only a very slight increase, attaining only some 3% removal by a 40-min adsorption. According to the rate of photodegradation after the irradiation (Table 1), the extent of dye degradation strongly depended on the presence of TiO2 particles while poly[AAm-co-AAc] did not change the dye degradation at all. However, the k_{degrad} values for the dye removal by the TiO₂/poly[AAm-co-AAc] composite and TiO₂ particles alone were significantly greater (145- and 23.1-fold higher, respectively) than that for the poly[AAm-co-AAc] alone which had a very low k_{degrad} value (Table 1). Besides its effectiveness in dye removal and the practical advantages of the ease of separation, the photocatalyst can be reused to some extent and then degraded which is described below.

3.6. Reproducibility of the reused TiO₂/poly[AAm-co-AAc] composite

The reproducibility of the photocatalytic degradation activity of a 0.2 g sample TiO_2 (P-25)/poly[AAm-co-AAc] composite performed on a 5 mg L⁻¹ MB dye solution (200 mL) is expressed as the number of cycles (Fig. 9), where the photocatalytic degradation of TiO_2 /poly[AAm-co-AAc] composite was reduced from 91% on the first usage to 82, 22 and 17% after the second, third and fourth cycles of reuse, respectively. This reduced dye photodegradation activity is in accord with the appearance of the recycled TiO_2 /poly[AAm-co-AAc] composite, which was clearly changed in the morphology as a hydrogel due to the photodegradation (Fig. 10).

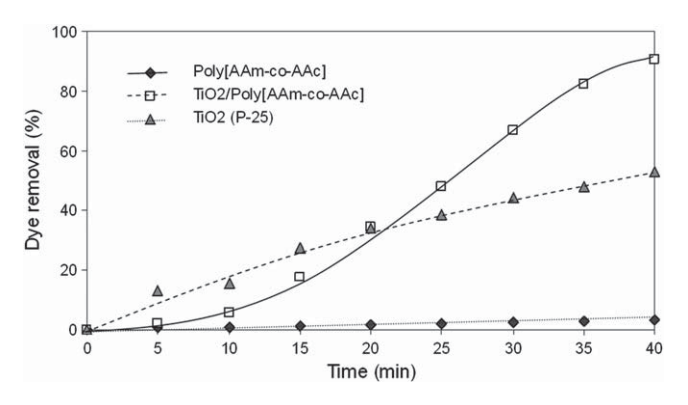


Fig. 8. Photocatalytic degradation of a 5 mg L^{-1} MB solution (200 mL) by TiO_2 immobilized in poly[AAm-co-AAc], the neat poly[AAm-co-AAc] and the pristine TiO_2 (Degussa P-25) following 365 nm wavelength UV irradiation at 1 mW cm⁻² for the indicated time. Data are shown as the mean \pm 1 S.D., derived from 3 replications.

^a k_{removal} were calculated from the curve of Fig. 7 (in the dark).

b k_{degerad} was calculated from the curve of Fig. 8 (under UV irradiation).

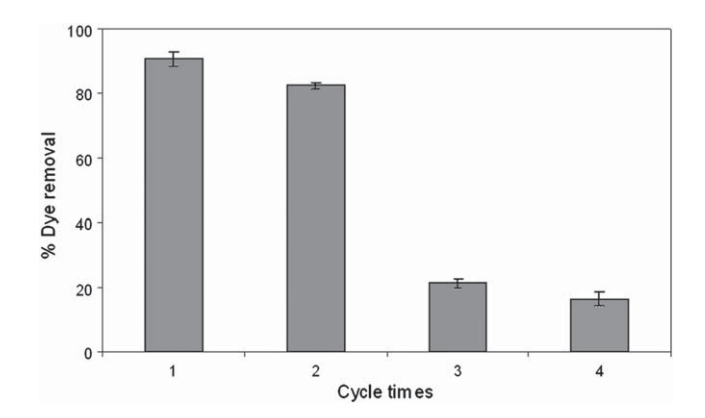


Fig. 9. Photocatalytic degradation of MB with 15%wt $TiO_2/poly[AAm-co-AAc]$ composite after the indicated number of recycling times. Data are shown as the mean \pm 1 S.D., derived from 3 replications.

3.7. Degradation of TiO₂/poly[AAm-co-AAc] hydrogel composite by rheological measurement

The storage modulus or elasticity modulus (G'), is a measure of the gel elastic behavior associated with the storage of energy, and the loss modulus or viscous modulus (G''), is a measure of the gel viscous behavior associated with the dissipation of energy. The frequency dependence of the storage moduli and loss moduli of poly[AAm-co-AAc] and the TiO2/poly[AAm-co-AAc] composite before and after UV irradiation for 8 and 24 h is shown in Fig. 11. It can be seen that G' for both the poly[AAm-co-AAc] and the TiO2/poly[AAm-co-AAc] composite before UV irradiation was higher than their corresponding G'' values, which indicates that the elastic response of the material is stronger than the viscous response. After 8 h of UV irradiation, the G' value for the poly[AAm-co-AAc] still remained higher than the corresponding G'' but the G'' value for the

TiO₂/poly[AAm-co-AAc] composite was largely higher than the corresponding G' value. It is well known that the storage modulus can be considered as a measure of the extent of the gel network formation and that the higher the *G'* value of the gel, the stronger is the gel elasticity. This indicates that the swollen TiO₂/poly[AAm-co-AAc] hydrogel composite can be photodegraded faster than the swollen poly[AAm-co-AAc] hydrogel without TiO2 after 8-h UV irradiation, presumably by both photocleavage and photocatalytic reactions. Furthermore, after 24-h of UV irradiation time, the G" values of both the poly[AAm-co-AAc] and the TiO2/poly[AAm-co-AAc] composite were mostly higher than the *G*′, indicating that the viscous response of the material is more predominant than the elastic response and these hydrogel systems displayed a liquid-like behavior. Thus, as well as degrading the MB dye molecules adsorbed into the network, the existence of TiO₂ nanoparticles in the hydrogel composite can also assist the self-degradation of the hydrogel matrix. From the bond energies available (Table 2), the crosslinking molecules in the hydrogel networks can be easily photodegraded because of the lower bond energy (305 kJ mol⁻¹) of the C-N linkage via the N-MBA crosslinker.

3.8. Photodegradation of TiO₂/uncrosslinked poly[AAm-co-AAc] by GPC

The initiation step in the photocatalytic degradation process of poly[AAm-co-AAc] can be quite different. According to the literature [32–34], TiO₂ molecules are stimulated by absorbing UV radiation of a wavelength lower than 390 nm to generate various active oxygen species. The photocatalytic degradation of the poly [AAm-co-AAc] matrix [35–37] may be initiated at the same time as MB photodegradation [16–18] by active oxygen species, such as O₂•-, HOO• and HO•, forming on the surface of the TiO₂. These active oxygen species then attack the neighboring polymer chains to extract a hydrogen atom and form carbon-centered radicals, such as $-CH_2 \cdot CONH_2^-$ and $-CH_2 \cdot COCOOH-$. Their successive reactions

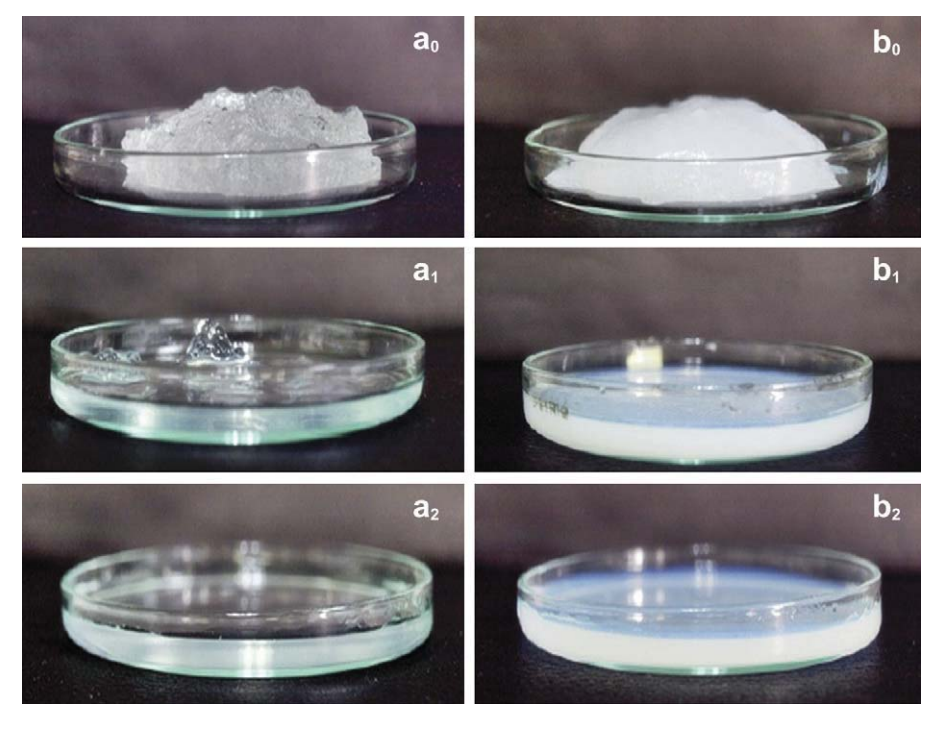
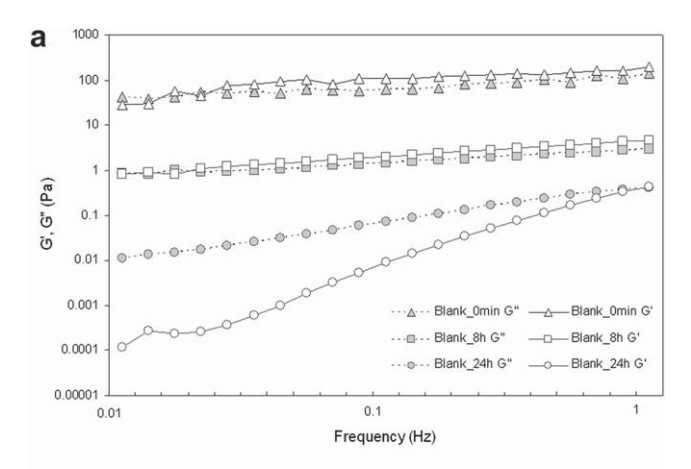


Fig. 10. Appearance of the (a) poly[AAm-co-AAc] hydrogel and (b) 15%wt TiO₂/Poly[AAm-co-AAc] composite after UV irradiation at 365 nm and 1 mW cm⁻¹ for (0) 0 h, (1) 8 h and (2) 24 h. Images shown are representative of 3 independent replications.



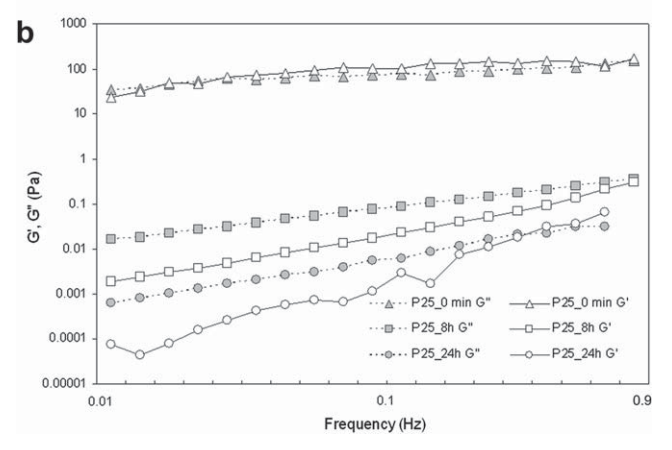


Fig. 11. Frequency dependence of the dynamic storage modulus (G') and the dynamic loss modulus (G'') of the (a) poly[AAm-co-AAc] hydrogel and (b) 15%wt TiO₂/Poly [AAm-co-AAc] composite after exposure to 365 nm wavelength UV irradiation at 1 mW cm⁻¹ for the indicated periods of time. Data are shown as the mean \pm 1 S.D., derived from 3 replications.

with $O_2^{\bullet-}$, HOO^{\bullet} and HO^{\bullet} produce hydroxyl derivatives and carbonyl intermediates, leading to the cleavage of the carbon chains and finally the release of carbon dioxide.

The photocatalytic degradation of the uncrosslinked poly [AAm-co-AAc] was accompanied by a decrease in the molecular weight of the uncrosslinked poly[AAm-co-AAc], as measured by GPC (Table 3). The $\overline{M}_{\rm W}$ of poly[AAm-co-AAc] homopolymer incorporated with TiO₂ decreased some 40% from 991 \times 10³ to 596 \times 10³ g mol⁻¹ after 24 h of UV irradiation, a decrease in the $\overline{M}_{\rm W}$ of ~400 kg mol⁻¹. A similar analysis for the neat poly[AAm-co-AAc] shows that the $\overline{M}_{\rm W}$ was only decreased ~200 kg mol⁻¹ and so may imply that the bond scission in the polymer backbone of the TiO₂/poly[AAm-co-AAc] composite is caused by both the direct photolytic and the TiO₂ photocatalytic reactions.

Table 2 Average energy for selected bond types.

Type of bond	Energy (kJ mol ⁻¹)
C-N	305
C-C	347
C-0	358
N-H	391
C—H	413
O-H	467
C=C	614
C=0	745

Table 3The variation of molecular weights of poly[AAm-co-AAc] with irradiation time.

Sample	\overline{M}_n^a	\overline{M}_{W}^{b}	PDI
	$(10^{-3} \text{ g mol}^{-1})$	$(10^{-3} \text{ g mol}^{-1})$	_
Poly[AAm-co-AAc]. before irradiation	234	1000	4.3
Poly[AAm-co-AAc]. 365 nm, 4 h	222	972	4.4
Poly[AAm-co-AAc]. 365 nm, 24 h	174	790	4.6
TiO ₂ /Poly[AAm-co-AAc];	242	991	4.1
before irradiation			
TiO ₂ /Poly[AAm-co-AAc]; 365 nm, 4 h	220	950	4.3
TiO ₂ /Poly[AAm-co-AAc]; 365 nm, 24 h	196	596	3.1

 $^{^{\}mathrm{a}}$ $\overline{\mathit{M}}_{\mathrm{n}}$: number average molecular weight.

4. Conclusions

A photocatalytically degradable TiO₂/poly[AAm-co-AAc] hydrogel composite was prepared by polymerization from an aqueous solution. XRD and SEM characterizations of the composite indicated that the TiO₂ particles were dispersed throughout the poly[AAmco-AAc] hydrogel composite. TiO₂/poly[AAm-co-AAc] composite adsorbed at least 85% of a 5 mg L^{-1} MB solution in 15 min, compared to only 10% by pristine TiO2 without photodegradation (in the dark). Approximately, 91% of the total MB present was photocatalytically degraded. The obtained results indicate that the newly prepared TiO₂/poly[AAm-co-AAc] is capable of removing the MB dve via the combined effect of adsorption-photodegradation. The ease of separation and removal of TiO₂/poly[AAm-co-AAc] hydrogel composite from the reactors by filtration and self-photcatalytic degradation, render it a potentially somewhat more green material by coupling with the photodegradation-adsorption process in the abatement of various wastewater pollutants.

Acknowledgments

This research is financially supported by a Research Team Consolidation Grant for Senior Research Scholars from the Thailand Research Fund — Higher Education Commission (contract number RTA5080004). The authors are also grateful for the partial research funding from the National Nanotechnology Center, NSTDA, Thailand (Grant number P-00-60064). Research facilities provided by the Polymer Imaging Laboratory of Chulalongkorn University's Imaging and Printing Technology Department and the National Nanotechnology Center, National Science and Technology Development Agency, are highly appreciated. Research materials donated by the mentioned manufacturers are also acknowledged.

References

- Sanghi R, Bhattacharya B, Singh V. Cassia angustifolia seed gum as an effective natural coagulant for decolourisation of dye solutions. Green Chem 2002:4:252–4.
- [2] Namasivayam C, Arasi DJSE. Removal of Congo red from wastewater by adsorption onto waste red mud. Chemosphere 1997;34:401–17.
- [3] Moozyckine AU, Davies DM. Green S as a prototype for an environmentallydegradable dye: the concept of a 'green dye' in future. Green Chem 2002:4:452–8.
- [4] Akhtar S, Khan AA, Husain Q. Potential of immobilized bitter gourd (Momordica charantia) peroxidases in the decolorization and removal of textile dyes from polluted wastewater and dyeing effluent. Chemosphere 2005;60:291–301.
- [5] Ho YS, Mckay G. The kinetics of adsorption of basic dyes from aqueous solutions by sphagnum moss peat. Can J Chem Eng 1998;76:822-7.
- [6] Walker GM, Hansen L, Hanna JA, Allen SJ. Kinetics of a reactive dye adsorption onto dolomitic sorbents. Water Res 2003;37:2081–9.
- [7] Crini G. Recent developments in polysaccharide-based materials used as adsorbents in wastewater treatment. Progress Polym Sci 2005;30:38–70.

 $^{^{\}mathrm{b}}$ $\overline{M}_{\mathrm{W}}$: weight average molecular weight.

- [8] Crittenden JC, Zhang Y, Hand DW, Perram DL, Marchand EG. Solar detoxification of fuel-contaminated groundwater using fixed-bed photocatalysts. Water Environ Res 1996;68:270–8.
- [9] Hou H, Zhu D, Cheng J. Application of nanometer TiO₂ photocatalysis material in air purification. Proceedings of the Int Conf Integrat Commercial Micro & Nanosystems; 2007:89.
- [10] Li BJ, Yang DH, Wu SQ, Li BS, Meng H, Jiang SP, et al. Application of nano-sized TiO₂ photocatalysis to air purification and sterilization. Zhonghua yu fang yi xue za zhi [Chinese Journal of Preventive Medicine] 2008;42(11):831–5.
- [11] Rajeshwar K, Osugi ME, Chanmanee W, Chenthamarakshan CR, Zanoni MVB, Kajitvichyanukul P, et al. Heterogeneous photocatalytic treatment of organic dyes in air and aqueous media. J Photochem Photobio C: Photochem Rev 2008;9(4):171–92.
- [12] Kangwansupamonkon W, Lauruengtana V, Surassmo S, Ruktanonchai U. Antibacterial effect of apatite-coated titanium dioxide for textiles applications. Nanomedicine: Nanotech Bio Med 2009;5(2):240–9.
- [13] Matthews LR, Avnir D, Modestov AD, Sampath S, Lev O. The incorporation of Titania into modified silicates for solar photodegradation of aqueous species. I Sol-Gel Sci Technol 1997:8:619–23.
- [14] Zhan H, Chen K, Tian H. Photocatalytic degradation of acid azo dyes in aqueous TiO₂ suspension II. The effect of pH values. Dyes Pigm 1998;37:241–7.
- [15] Li XZ, Zhao YG. Advanced treatment of dyeing wastewater for reuse. Water Sci Technol 1999;39:24955.
- [16] Kuo WS, Ho PH. Solar photocatalytic decolorization of methylene blue in water. Chemosphere 2001;45:77–83.
- [17] Houas A, Lachheb H, Ksibi M, Elaloui E, Guillard C, Herrmann JM. Photocatalytic degradation pathway of methylene blue in water. Appl Cat B: Environ 2001;31:145–57.
- [18] Zhang T, Oyama T, Aoshima A, Hidaka H, Zhao J, Serpone N. Photooxidative N-demethylation of methylene blue in aqueous TiO₂ dispersions under UV irradiation. J Photochem Photobio A: Chem 2001;140:163—9.
- [19] Yu Z, Chuang SSC. The effect of Pt on the photocatalytic degradation pathway of methylene blue over TiO₂ under ambient conditions. Appl Cat B: Environ 2008:83:277–85.
- [20] Senkal BF, Yavuz E. Preparation of poly(vinyl pyrrolidone) grafted sulfonamide based polystyrene resin and its use for the removal of dye from water. Polym Adv Technol 2006;17:928–31.
- [21] Hashem A, Abdel-Halim ES, Sokker HH. Bi-functional starch composites prepared by γ-irradiation for removal of anionic and cationic dyes from aqueous solutions. Polymer Plast Technol Eng 2007;46:71–7.

- [22] Kasgoz H. Aminofunctionalized acrylamide-maleic acid hydrogels: adsorption of indigo carmine. Colloids Surf A: Physicochem Eng Aspects 2005; 266:44–50.
- [23] Kasgoz H. New sorbent hydrogels for removal of acidic dyes and metal ions from aqueous solutions. Polym Bull 2006;56:517–28.
- [24] Dadhaniya PV, Patel MP, Patel RG. Removal of anionic dyes from aqueous solution using poly[N-vinyl pyrrolidone/2-(methacryloyloxyethyl) trimethyl ammonium chloride] super-swelling hydrogels. Polym Bull 2007;58: 359–69.
- [25] Ohmine I, Tanaka T. Salt effects on the phase transition of ionic gels. J Chem Phys 1982:77:5725–9.
- [26] Katayama S, Hirokawa Y, Tanaka T. Reentrant phase transition in acrylamidederivative copolymer gels. Macromolecules 1984;17(12):2641–3.
- [27] Hafez HS, El-Hag Ali A, Abdel-Mottaleb MSA. Photocatalytic efficiency of titanium dioxide immobilized on PVP/AAc hydrogel membranes: a comparative study for safe disposal of wastewater of Remazol Red RB-133 textile dye. Int J Photoenergy 2005;7:181–5.
- [28] Tang Q, Lin J, Wu Z, Wu J. Preparation and photocatalytic degradability of TiO₂/polyacrylamide composite. Euro Polym J 2007;43(6):2214–20.
- [29] Chen D, Ray AK. Removal of toxic metal ions from wastewater by semiconductor photocatalysis. Chem Eng Sci 2001;56:1561-70.
- [30] Abbasi M, Asl NR. Sonochemical degradation of Basic Blue 41 dye assisted by $nanoTiO_2$ and H_2O_2 . J Hazard Mater 2008;153(3):942–7.
- [31] Mozia S, Morawski AW, Toyada M, Inagaki M. Application of anatase-phase TiO₂ for decomposition of azo dye in a photocatalytic membrane reactor. Desalination 2009;241(1–3):97–105.
- [32] Zainal Z, Hui LK, Hussein MZ, Abdullah AH, Hamadneh IMKR. Characterization of TiO₂-Chitosan/Glass photocatalyst for the removal of a monoazo dye via photodegradation—adsorption process. J Hazard Mater 2009;164:138—45.
- [33] Paulino AT, Guilherme MR, Resi AV, Campese GM. Removal of methylene blue from an aqueous media using superabsorbent hydrogel supported on modified polysaccharide. J Colloid Interface Sci 2006;301(1):55–62.
- [34] Solpan D, Duran S, Torun M. Removal of cationic dyes by poly(acrylamide-co-acrylic acid) hydrogels in aqueous solutions. Rad Phys Chem 2008; 77:447–55.
- [35] Shukla NB, Daraboina N, Madras G. Oxidative and photooxidative degradation of poly(acrylic acid). Polym Degrad Stab 2009;94(8):1238–44.
- [36] Vijayalakshmi SP, Madras G. Photocatalytic degradation of poly(ethylene oxide) and polyacrylamide. J Appl Polym Sci 2006;100:3997–4003.
- [37] Vinu R, Madras G. Photocatalytic degradation of poly(acrylamide-co-acrylic acid). J Phys Chem B 2008;112:8928–35.

Received: 28 October 2008,

Revised: 1 June 2009.

Accepted: 28 August 2009,

Published online in Wiley Online Library: 23 September 2009

(wileyonlinelibrary.com) DOI: 10.1002/pat.1559

Acrylamide-itaconic acid superabsorbent polymers and superabsorbent polymer/mica nanocomposites

Daungtawan Foungfung^a, Siriwan Phattanarudee^b, Nispa Seetapan^c and Suda Kiatkamjornwong^{b*}

Superabsorbent polymer acrylamide (AM)/itaconic acid (IA) and its nanocomposite were synthesized by redox polymerization in an aqueous solution of both monomers with mica used as an inorganic additive. The influences of IA concentration, mica content, and crosslinker concentration on the water absorption and physical properties of the superabsorbent polymer and its nanocomposite were examined. Water absorbency in artificial urine by the synthesized copolymers, and the gel strength of the superabsorbent copolymers and their nanocomposites, were tested with loads of 0.28 or 0.70 psi. Transmission electron micrographs and X-ray diffraction confirmed that the polymer chains were successfully intercalated into the silicate layers in the mica. The water absorbency and the artificial urine absorbency of the composite with an AM-to-IA mole ratio of 95:5, 0.2% mol N-MBA, and 5% w/w mica were 748 ± 5 and 76 ± 2 g g⁻¹, respectively, whilst the neat copolymer achieved only 640 ± 7 and 72 ± 2 g g⁻¹ in water and artificial urine, respectively. The viscoelastic behavior suggested that the swollen gel of the nanocomposites exhibited mechanical stability and elasticity. Copyright © 2009 John Wiley & Sons, Ltd.

Keywords: superabsorbent polymer; superabsorbent polymer nanocomposite; mica; water absorbency

INTRODUCTION

Superabsorbent polymers are lightly crosslinked hydrophilic polymers that can absorb, swell, and retain aqueous solutions or fluids up to hundreds of times their own dry weight giving them many advantages over traditional water absorbing materials such as cotton, pulp, or sponges. They are widely used in agriculture, horticulture, disposable diapers, cosmetics, controlled drug delivery systems, and wound dressings.^[1-9] The first superabsorbent polymer was reported by the US Department of Agriculture in 1961, whilst later research has focused upon attempting to modify these absorbent polymers to enhance their absorbency, gel strength, and absorption rate. 11-15]

In recent years, increasing attention has been paid to the incorporation of inorganic materials in the preparation of superabsorbent polymers including kaolin,^[16] montmorillonite,^[17,18] attapulgite,^[19–22] laponite,^[23] vermiculite,^[24] bentonite,^[25] and mica.^[8,26–28] The incorporation of these mineral powders can reduce production costs as well as improve water absorption, gel strength, and the mechanical and thermal stabilities of superabsorbent polymers. Among these clays is mica, a plate-like crystalline aluminosilicate with a 2:1 phyllosilicate type structure with an octahedral Al sheet and two tetrahedral Si sheets. Mica has been widely used as a reinforcing filler in polymeric matrices due to its excellent mechanical, electrical, and thermal properties.^[29] Lin et al. synthesized a poly(acrylic acid)/mica superabsorbent composite by a graft polymerization reaction between partially neutralized acrylic acid and ultrafine mica powder. The water absorbency of the composite was higher than 1100 g g⁻¹ at a 10% w/w mica addition.^[26] However, further increase in the mica content

decreased the water absorbency. The influence of the degree of neutralization of the acrylic acid was found to be optimal at 65%. A series of superabsorbent polymers based on sodium acrylate, mica, and *N*, *N'*-methylenebisacrylamide (N-MBA) were prepared by inverse suspension polymerization.^[27] The results showed that the water absorbency and the initial absorption rate gradually decreased with increasing amounts of pure K⁺-mica and intercalated mica. In addition, the water absorbency of the composite gels obtained from K⁺-mica was higher than that of gels from intercalated-mica. The water absorbency of these gels decreased with increase in the ionic strength of the external salt solution. Zhang and Wang^[28] researched a series of clay-based superabsorbent composites prepared from acrylamide (AM) and

- * Correspondence to: S. Kiatkamjornwong, Department of Imaging and Printing Technology, Faculty of Science, Chulalongkorn University, Phayathai Road, Bangkok 10330, Thailand. E-mail: ksuda@chula.ac.th
- a D. Foungfung

Petrochemistry and Polymer Science, Faculty of Science, Chulalongkorn University, Phayathai Road, Bangkok 10330, Thailand

- b S. Phattanarudee, S. Kiatkamjornwong

 Department of Imaging and Printing Technology, Faculty of Science,
 Chulalongkorn University, Phayathai Road, Bangkok 10330, Thailand
- c N. Seetapan

National Metal and Materials Technology Center, National Science and Technology Development Agency, 114 Thailand Science Park, Paholyothin Rd, Klong 1, Klong Luang, Pathumthani 12120, Thailand

Contract/grant sponsor: Thailand Research Fund, Senior Research Grant. Grantcontract/grant number: RTA4780004.



various clays, and reported that mica incorporation improved the thermal stability of superabsorbent composites to a higher degree than the other tested clays. The effect of intercalant content of mica on the properties of the charged nanocomposite poly(*N*-isopropyl acrylamide) hydrogels was investigated. The mica was first intercalated with different levels of intercalant, trimethyl (acrylamido propyl) ammonium chloride (TMAACI), based on the cationic exchange capacity (CEC) of mica.^[8] The results showed that mica could intercalate with TMAACI under a low CEC value with the significantly enhanced swelling behavior and mechanical properties being related to the intercalated mica content and CEC values.

AM can be used to copolymerize with a number of vinyl monomers to synthesize superabsorbent polymers. Graft copolymer of starch with acrylic acid/AM, [30,31] AM/maleic acid, [32] acrylic acid/itaconic acid (IA),[33] as superabsorbent polymers could be used for agricultural and environmental applications. Copolymerization of partially hydrolyzed AM with *n*-vinyl pyrrolidone produced superabsorbent polymers for oil recovery applications.^[34–36] AM can be also used with acrylic acid,^[37] methacrylic acid, [38] and crotonic [39] to produce various properties of superabsorbent polymers for enzyme immobilization or dye removal. However, none of them has involved the inclusion of filler into superabsorbent polymers. For the present investigation, swelling synthetic mica was chosen for in situ polymerization of AM-IA superabsorbent polymer nanocomposites. The main aim for adding the mica particles was to form composites with increased swollen gel strength and without loss of water absorbency for personal care products such as baby disposal diapers.

EXPERIMENTAL

Materials

AM (Siam Resin and Chemicals, Thailand) and ionic comonomer, IA (Merck, Hohenbrunn, Germany), were used as monomers. N-MBA (Fluka, Buchs, Switzerland) was utilized as a crosslinker. Ammonium persulphate (APS, Merck, Hohenbrunn, Germany) and N, N, N', N'-tetramethylethylenediamine (TEMED, Fluka, Buchs, Switzerland) were added as a redox initiator pair. The swelling mica with exchangeable sodium ions and a CEC of about 120 meq/100 g was purchased from Wako Pure Chemical Industries, Osaka, Japan. The average particle size, as measured by SEM, was approximately 3 μm . The deionized water used in the experiment was obtained from ELGA Labwater (model reservoir 25L, purelab option, UK). All the materials were used as received.

Preparation of the superabsorbent nanocomposite

A mixture of $60\,\mathrm{cm}^3$ aqueous solution containing AM, IA monomers, and mica was placed in a 500-cm^3 four-necked round-bottomed flask. The mixture was mechanically stirred by a small-bladed propeller at 250 rpm, within a temperature range of $50\pm2\,^\circ\mathrm{C}$ for 2 hr for monomer intercalation. Then, $20\,\mathrm{cm}^3$ (0.2% mole) of N-MBA aqueous solution was added within 5 min. The mixture was purged with N_2 gas to remove oxygen from the solution during the reaction. Next, 0.3 mole ($20\,\mathrm{cm}^3$) of the APS aqueous solution was added and stirred for 5 min. Lastly, 1.2% mole ($0.2\,\mathrm{cm}^3$) of the co-initiator (TEMED) was added and the polymerization was continued for 30 min. The resulting polymer

Table 1. Composition variables investigated in crosslinked polymerization of poly(AM-co-IA)/mica nanocomposites

Ingredients	Amount
Monomer (AM/IA) ratios (% mol)	99/1, 98/2, 97/3, 96/4, 95/5
Mica (% w/w)	0, 2, 5, 10, 15
N, N'-methylenebisacrylamide (% mole) ^a	0.2, 0.5, 0.7, 0.9
Ammonium persulfate (% mole) ^a	0.3
N, N, N', N'-tetramethyl-	1.2
ethylenediamine (% mole) ^a	
Reaction temperature (°C)	50
Agitation speed (rpm)	250
Reaction time (min)	30
^a % mole based on the monomer conce	ntration.

was then dewatered with methanol, cut into small pieces, with diameters of about 0.5 cm, and dried at 50°C for 24 hr in a vacuum oven to constant weight. The dried polymer was then milled and separated through a 100-mesh aluminum screening sieve to form the superabsorbent composite particles (powder). Superabsorbent nanocomposites at other AM/IA ratios, different mica contents, and various crosslinker concentrations, listed in Table 1, were prepared in the same manner.

Determination of the unreacted amount of AM monomer in the superabsorbent polymer by gas chromatography

The superabsorbent polymer derived from the polymerization reaction was stirred in 300 cm³ of deionized water at room temperature for 30 min. Then 50 cm³ of the solution was used to determine the trace amounts of AM monomer in the polymerization reaction by Method 8032A, which consists of three steps: bromination, extraction, and calibration. Bromination of the AM double bond gave 2, 3-dibromopropionamide which was extracted from the reaction mixture with ethyl acetate. After salting out with sodium sulfate, the extract was analyzed by gas chromatography.

Determination of density of the superabsorbent nanocomposite

The standard method (ASTM D 792) for determining the polymer density was used to evaluate the densities of mica, poly(AM-co-IA), and poly(AM-co-IA)/mica nanocomposites in n-heptane in a pycnometer.

Measurement of water absorbency

In deinoized water and its absorption with time

Deionized water (200 g) was added to 0.1 g of the superabsorbent polymers or its nanocomposites in a $250\,\mathrm{cm}^3$ glass beaker at room temperature. The nanocomposite was allowed to swell for 24 hr. The residual water was removed by filtration with a 100-mesh screen sieve for 2 hr in a closed system at room temperature and the swollen gel was weighed. The water absorbency, as grams of water per gram of sample (g g $^{-1}$) was



calculated as shown in eqn (1), from a minimum number of at least three repeats.

Water absorbency
$$(Q) = \frac{B - A}{A}$$
 (1)

where A and B are the weights of the dry polymer and the swollen gel, respectively.

Deionized water (200 g) was added to 0.1 g of the dried nanocomposites in a 250 ml glass beaker covered with a glass lid. The polymer was allowed to swell first for 1 min. The swollen gel was then separated from the water by filtering it through a 100-mesh sieve aluminum screen for 2 hr at room temperature to drain out the unbound water, and the swollen copolymer was then weighed. Similar experiments were carried out for each gel at the swelling times of 1, 5, 10, 30, 60, 180, 300, and 480 min.

In artificial urine

The same experimental procedures as described above were carried out using artificial reference urine (ARU) instead of deionized water. The ARU was prepared by mixing equal amounts of 0.1055 M sodium chloride, 0.0323 M sodium dihydrogen phosphate, 0.00321 M sodium citrate, 0.00385 M magnesium sulphate, 0.01695 M sodium sulfate, and 0.0637 M potassium chloride. The pH was adjusted to 6.5. The ARU had an ionic strength of 0.0747 mol-ion dm⁻³, based on the method of Skoog et al.^[41,42]

Absorbency under load

Deionized water (25 cm³) was placed in a Petri dish as shown in Fig. 1. Dried copolymer weighing about 0.16 g was carefully sprinkled onto the filter screen of the testing device, which was comprised of an aluminum cylinder with a stainless steel cloth 100-mesh screen sieve placed at the bottom of the cylinder. The device has a diameter of 26 mm and a height of 35 mm. A piston assembly, including appropriate weights to achieve a load of either 0.28 or 0.70 psi, was placed on top of the dry copolymer. After assembly with added dry copolymer with appropriate weight (for a load of 0.28 or 0.70 psi), the entire device was weighed and then placed in the water filled Petri dish for 1 hr to allow the absorption to reach equilibrium, whereupon the entire device was reweighed. The absorbency under load (AUL), as gram of water absorbed per gram of the dry copolymer (g g⁻¹) was calculated as eqn (2).^[43]

Absorbency under load (AUL) =
$$\frac{B - A}{A}$$
 (2)

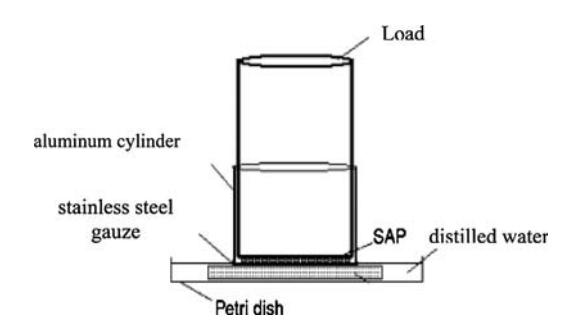


Figure 1. Scheme of the absorbency under load (AUL) setup.

where A and B are the weights of the dry polymer and the swollen gel, respectively. The water absorbency was calculated as gram of water per gram of sample. The number of repeats was not less than three.

Characterization of the superabsorbent nanocomposites

Identification of the functional groups

The functional groups of the copolymers and nanocomposites were identified using Fourier-Transform Infrared Spectrometry (FT-IR) (Nicolet Infrared Spectrometer, model Impact 410). The dried sample was ground with the dried KBr powder. The KBr disk was dried again, pressed, and subjected to the FT-IR spectrometry.

Morphology by scanning and transmission electron microscopic analyses

The surface morphology of the superabsorbent composites was investigated using scanning electron microscopy (SEM, model JSM-6400, JEOL, Japan), without cross-section. The thickness of the gold coating on the sample was 25 nm, and SEM was operated with an accelerating voltage of 15–20 kV to give good image contrast.

For TEM analysis, the superabsorbent nanocomposite particles were dispersed in ethyl alcohol and the suspension was then sonicated for 5 min. The diluted suspension was then dropped onto a 300-mesh copper grid, and left to dry in a control room atmosphere before performing the TEM analysis. TEM micrographs of the samples were obtained at an acceleration voltage of 120 kV (JEOL JEM-2100, Japan).

X-ray diffraction analysis

X-ray diffraction measurements were performed using an X-ray diffractometer, Bruker AXS Model D8 Discover (Cu $K\alpha$ radiation, 40 kV, 40 mA, with $\lambda = 0.15406$ nm and n = 1) at a scanning range from 2 to 25° and a scanning rate of 0.025° min⁻¹. The interlayer spacing (d) of mica and mica-superabsorbent nanocomposites was calculated using Bragg's equation (eqn 3):

$$n\lambda = 2d\sin\theta$$
 (3)

where d is the interplanar distance of the (001) reflection plane, θ is the diffraction angle, and λ is the wavelength.

Viscoelastic properties

The rheological experiments of the swollen gel particles having an irregular shape were carried out in a strain-controlled rheometer (ARES, TA Inc., New Castle, USA) equipped with a solvent trap to prevent water evaporation during measurements. The experiments were operated at 25° C using parallel plate geometry (50 mm diameter, 1 mm gap) made of stainless steel. The strain sweeps, at a fixed frequency of 1 rad sec⁻¹, were conducted in a range of 0.1–100% for determining a linear viscoelastic (LVE) range, where G' (storage modulus) and G'' (loss modulus) are independent of the strain amplitude. After a strain sweep test, the dynamic frequency sweeps were performed within the determined LVE range. The samples were prepared as follows. A dry superabsorbent (0.1 g) was dispersed in $200 \, \text{cm}^3$ distilled water and allowed to swell for 24 hr to reach equilibrium swelling. The swollen superabsorbent was filtered through a



100-mesh aluminum screen for 2 hr. Pieces of tissue papers were used to rub off the unabsorbed water at the bottom of the screen until the swollen gel did not flow when the screen was held vertically. Afterwards, the swollen gel particles were removed from the screen to investigate their rheological behavior.

Thermal stability analysis

The superabsorbent composites were investigated using a PerkinElmer TGA-7 thermogravimetric analyzer for their thermal property. The measurements were carried out over a temperature range of 25–800°C at a heating rate of $10^{\circ}\text{C min}^{-1}$ with a nitrogen flow rate of $60~\text{cm}^3~\text{min}^{-1}$. In order to compare the residue of the superabsorbent composite, the polymer was burned in an oven. The dry nanocomposite copolymer samples, weighing $1.00\pm0.01~\text{g}$, were each individually placed in a $25~\text{cm}^3~\text{porcelain}$ crucible, weighed, and transferred into a furnace at 800°C for 10~hr or until combustion of the remaining white mica powder had been completed. The crucible was removed from the furnace, cooled to room temperature, weighed, and the remaining mica weight was evaluated.

RESULTS AND DISCUSSION

FT-IR spectra of mica, synthesized copolymer, and superabsorbent nanocomposites

The FT-IR spectra of mica, poly[acrylamide-co-(itaconic acid)], and poly[acrylamide-co-(itaconic acid)]/mica nanocomposites are shown in Fig. 2. The absorption bands at 3452 cm⁻¹ (broad) and 1638 cm⁻¹ (Fig. 2a) correspond to the O–H stretching and interlayer water vibration present in the mica, whilst those at 1003 cm⁻¹ (broad peak), 702, and 476 cm⁻¹ are the Si–O stretching, Al–O stretching, and Si–O bending, respectively. The copolymer exhibits a broad absorption band at 3400 cm⁻¹, and strong peaks were observed at 1659 and 1448 cm⁻¹, which correspond to O–H stretching, C=O stretching of -COO⁻, and C–N stretching of O=C–N–H, present in the IA and AM monomers

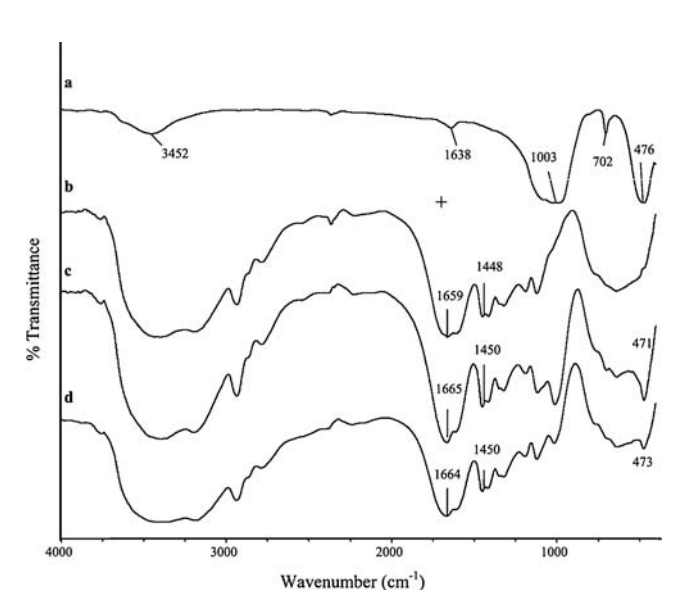


Figure 2. FT-IR spectra of (a) mica, (b) poly(AM-co-IA) copolymer, (c, d) poly(AM-co-IA)/mica nanocomposite at a 97:3 mole ratio crosslinked by 0.2% mole N-MBA with either (c) 15% w/w of mica or (d) 5% w/w of mica.

(Fig.2b). In comparing the spectra of pure mica and the copolymer, the spectra of nanocomposites synthesized using 5 and 15% (w/w) mica showed a similar broad band in the 3400- $3370\,\mathrm{cm}^{-1}$ range and strong peaks at $1665-1664\,\mathrm{cm}^{-1}$ and 1450 cm⁻¹ for the -COO⁻ indicating the characteristics of the copolymer. However, the -COO⁻ group on the IA might have experienced a conformation change during the reaction. [16] With mica addition, the absorption band of the -C-N stretching (-CONH₂) was shifted from 1448 to 1450 cm⁻¹. Furthermore, the weak absorption bands at 1016–1011 cm⁻¹, and the strong bands at 473–471 cm⁻¹ intimate the existence of a Si–OH group in the nanocomposites (Fig. 2c,d), which have possibly acquired a conformation change during the reaction. Taken together, these observed peaks strongly support that the reaction product is the desired composite. Since the characteristic absorption peaks for the -COO⁻ group on the IA and the mica Si-OH group are changed after the copolymerization, it is suggested that they have reacted together during the copolymerization.^[16] One possible reaction is a grafting reaction (via the esterification reaction) of the OH groups on mica with the -COO group on the IA,[44,45] where the OH groups in mica esterifies with the -COOgroup on the IA and then radical chain polymerization takes place. Another possible mechanism is that the hydroxyl groups may react with the radicals and liberate free radicals on the mica structure and the graft polymerization can take place on these free radicals, giving IA-AM branches on the mica backbone. [45] We favor the latter suggestion that the grafting reaction takes place on the mica surface since it is observed that the amount of mica present influences the interaction between AM/IA and mica, as well as the swelling properties of the corresponding superabsorbent nanocomposites.

Micro-morphology and TEM analyses

The representative SEM micrograph of mica particles is shown in Fig. 3a which reveals their platelet and flake-like appearance with an average particle size of 3 μm . In contrast, surface of the copolymer without mica is rather smooth (Fig. 3b). Upon mica incorporation, the mica particles were evenly and well dispersed in the matrix of the superabsorbent nanocomposite, but as clusters (loose agglomerates or tight aggregates) of about 30–50 μm , rather than individual particles, imbedded in the polymer matrix (Fig. 3c,d). Strong particle adhesive forces might have caused this agglomeration. Mica has a plate-like structure (platelet) with a high aspect ratio of reinforcing particles and it has good adhesion to the matrix polymer. Both are of great importance because they control the final properties of the composites.

Internal structures of the nanocomposites, on a nanometer scale, were investigated using TEM since this allows a qualitative understanding of the internal structure through direct observation. It was postulated that some of the polymer chains, polymerized by the incorporation of the monomers, are distributed between the silicate layers resulting from the initial intercalation of both acrylate monomers with mica in solution. In some support for this notion was that poly(AM-co-IA)/2% w/w mica nanocomposites had a partially intercalated structure, displayed as the dark cross lines, indicating the parts of the polymeric intercalation into the interlayer spacing of mica (Fig. 4). The thickness of the cross lines were approximately 1 nm, which corresponds to the typical thickness of the clay layers, whereas the distance between the cross lines are the interlayer spaces,



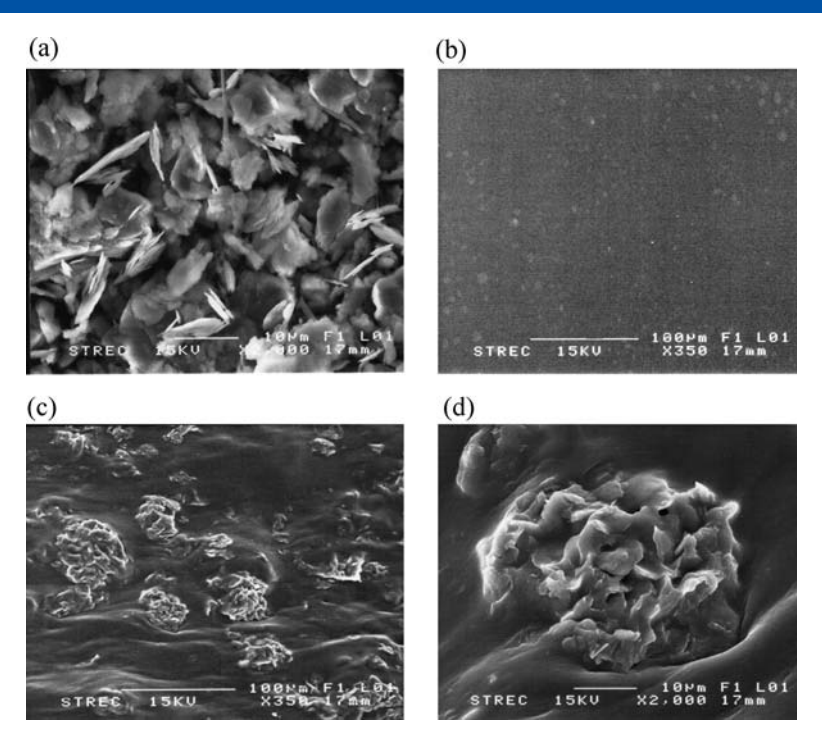


Figure 3. Representative SEM micrographs of (a) mica, (b) mica-free superabsorbent polymer, and (c, d) superabsorbent polymer/mica nanocomposites at a magnification of either (c) $350 \times \text{ or (d)}$ at $12,000 \times \text{ or (d)}$

and the gray bases are the polymer matrix. These micrographs demonstrate that the inorganic phase (the mica particles) is dispersed at the nanometer level in the organic phase (copolymer). Consequently, the nanocomposites exhibit unique properties not being shared by their micro-scale counterparts or conventionally filled polymer. The interlayer distance of mica in the nanocomposites obtained from TEM micrograph is about 13 Å, correlating well with the interlayer spacing characterized by XRD analysis.

X-ray diffraction analysis

XRD patterns supply very useful information on the gallery size of the final intercalated nanocomposites by measuring the increase in the basal (001) d-spacing, as depicted in the representative X-ray diffractograms in Fig. 5. The measured d_{001} of mica is 12.4 Å ($2\theta=7.1^{\circ}$), and that of the mica composites (AM/IA mole ratio of 97:3) with 15 and 5% w/w mica have peaks at about d=14 and 13.8 Å, corresponding to $2\theta=6.3$ and 6.4° , respectively. According to the above TEM results, the increase in the basal interlayer spacing of mica implies that there is polymer intercalation within the stacked silicate galleries of mica. A substantial increase in the intensity of the XRD peak is observed for the mica loading from 5 to 15% w/w which corresponds to the increased content in intercalated mica.

Table 2 summarizes the XRD analysis results which show that the peak position of the (001) basal plane remained approximately the same at different AM/IA ratios and mica contents, and thus the basal spacing is apparently independent of the content of IA and mica (within these tested ranges) in the prepared composites. However, the differing amounts of IA and mica at 0.2% mole N-MBA are responsible for the different water absorptions of the composites, which might imply that the limited amount of AM and IA monomers

penetrated between the layers of clay during the dispersion of the clay into the monomer mixture. Hence, after the polymerization, the interlayer spacing of mica is widened due to the presence of the intercalated copolymer chains. The rest of the added IA content, which cannot penetrate within the clay interlayer, distributes within the mixture and copolymerizes with AM resulting in the enhancement of the water absorbency as the content of IA increases. Additionally, the increase in the hydrogen-bonding formation from the interaction of the carboxylic groups of IA with clay outside the gallery leads to the improved water absorbency. A 2-dimensional schematic representation of the composites containing low and high IA content is shown in Scheme 1. The data summarized in Table 2 also reveals that the different mica contents influence the water absorption capacity of the composite, which will be discussed later in "Effect of IA concentration and mica content on water absorbency" section.

Density of the synthesized poly(AM-co-IA)/mica nanocomposites

The main application of synthesized superabsorbent nanocomposites is to produce personal care products such as adult and baby diapers. Importantly then, the desired superabsorbent polymer or composite should not add extra weight to the diapers and this would provide discomfort to users. The densities relative to the poly(AM-co-IA) nanocomposite at 95:5 mole ratio of AM/IA, the poly(AM-co-IA)/mica nanocomposite densities were increased to 8.76 and 20.44% for 5 and 15% w/w of mica inclusion, respectively (Table 3). Given that optimal water absorption was attained at 5% w/w mica (Table 2) which inflicts only an 8.8% increase in the density of the polymer nanocomposites (Table 3), this should not prevent the development of an optimum product design that is comfortable for users.



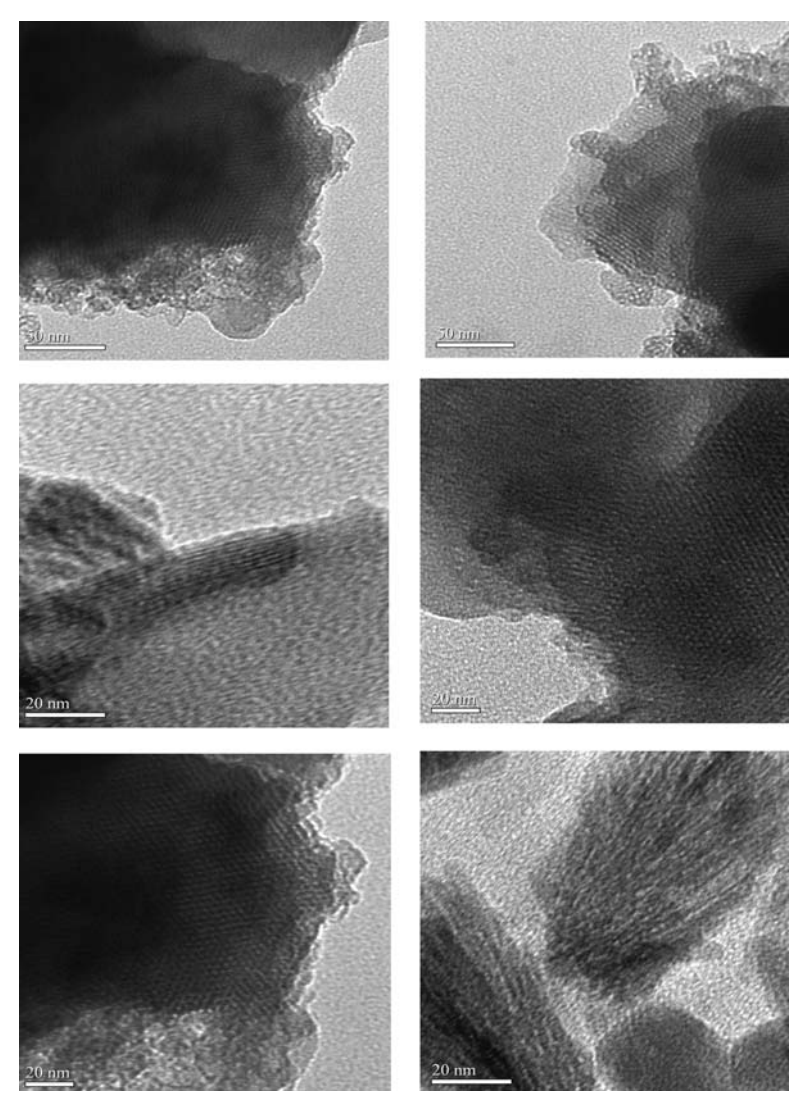


Figure 4. Representative TEM micrographs of poly(AM-co-IA)/mica nanocomposites at a 97:3 mole ratio with 2% w/w mica and crosslinked by 0.2% mole N-MBA.

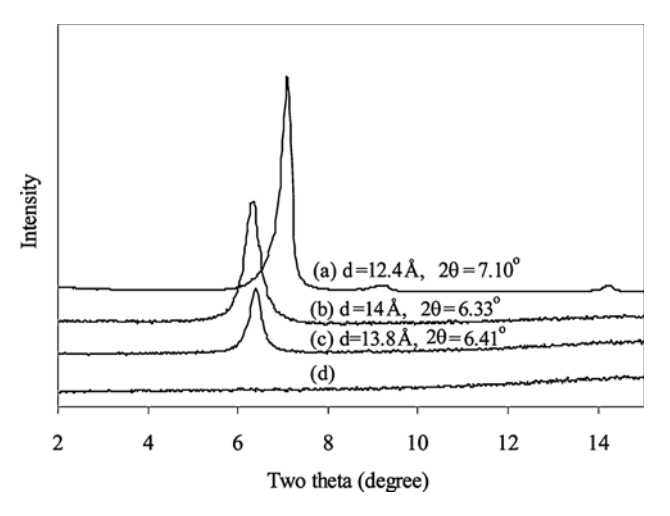


Figure 5. Representative X-ray diffraction patterns of (a) mica powder, (b, c) poly(AM-co-IA)/mica nanocomposites with either (b) 15 w/w mica or (c) 5% w/w mica, and (d) poly(AM-co-IA) copolymer. All copolymers had an AM/IA mole ratio of 97:3 and were crosslinked with 0.2% mole N-MBA.

The effect of N-MBA and IA concentrations on water absorbency

The relationship between water absorbency and N-MBA crosslinker concentration at three levels of IA concentration and two levels of mica incorporation is summarized in Fig. 6. The results show that the effect of mica addition at 5% w/w enhances the water absorbency and this is more marked at the high levels (5% mole) of IA and low N-MBA concentrations (0.2% mole). For the composite with 1% mole IA, the effect of the crosslinker is less effective when its contents were higher than 0.5% mole, implying that the crosslinker has crosslinked most of the IA molecules due to the higher reactivity ratios of N-MBA and IA. Thus, the crosslinking effect dominates the other minor effects to give nearly constant water absorption at higher N-MBA and mica contents. The effect of N-MBA crosslinker on decreasing the water absorption of the copolymers and their nanocomposites was obviously discernable at low levels of the crosslinker. However, at a higher concentration of crosslinker, the water absorption decreased gradually and was seen to level off. This behavior results from the cyclization and the multiple crosslinking reactions at pendant vinyl groups of the N-MBA.[47]



Table 2. The effect of AM/IA ratios and mica content on the XRD patterns and water absorption of crosslinked poly(AM-co-IA) and nanocomposites with 5 and 15% w/w mica

AM/IA ratio of composite	Mica content (% w/w)	Typical diffraction peak (°)	Basal spacing (Å)	Water absorption $(g g^{-1})$
_	100	7.1	12.4	_
99:1	5	6.3	14	330
	15	6.4	13.9	250
97:3	5	6.4	13.8	420
	15	6.3	14	390
95:5	5	6.3	14	750
	15	6.4	13.9	590

Residual amount of AM monomer in the superabsorbents polymer

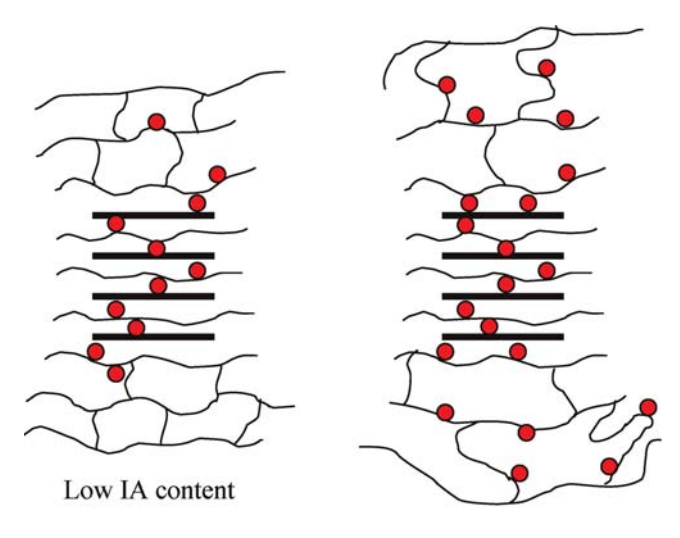
The residual amount of AM monomer in the superabsorbents polymer is another important issue of concern because the AM monomer is classified as a probable carcinogen and a known cumulative neurotoxin in humans. On the other hand, polyacrylamide is not known to display either bioactivity or harmful and is not considered hazardous for users. The unreacted AM level in (nano) composites is summarized in Table 4. Note that although residual N-MBA will also be detected as well as free monomer by this method, this will serve to increase and not hide the free monomer estimates and thus they can be seen as conservative estimates of safe levels. In any case, and to err on the side of caution, we consider that such errors are likely to be small because the reactivity ratio, r_1 and r_2 , values for AM/N-MBA are

0.64 and 1.77, respectively, [49] and N-MBA was only added at a final concentration of 2% mole, and thus would have rapidly reacted with the other monomers. Thus the analyzed value of the residual monomer will principally reflect the level of the AM monomer. Regardless, the residual amount of the AM monomer retained in the polymer was very low (about 0.1%) and its content will not be harmful to users because users are not in direct

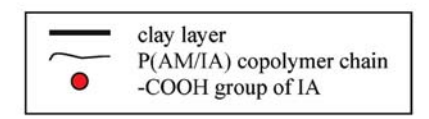
Table 3. The densities of mica, crosslinked poly(AM-co-IA), and poly(AM-co-IA)/mica nanocomposites

Crosslinked poly(AM- <i>co</i> -IA), % w/w	Mica Content Added, % w/w	Density (g cm ⁻³) ^a of AM/IA at 95:5 mole ratio
— 100 100	100 0 5	1.94 ± 0.03 1.37 ± 0.04 1.49 ± 0.01
100	15	$\textbf{1.65} \pm \textbf{0.03}$

 $^{\rm a}\,\text{Data}$ are displayed as the average $\pm\,1$ SD and are derived from four independent repeats.



High IA content



Scheme 1. A two-dimensional schematic representation of poly(AM-*co*-IA) intercalated within the mica galleries and grafted on the mica surface at low (1% mole) and high (5% mole) IA contents.

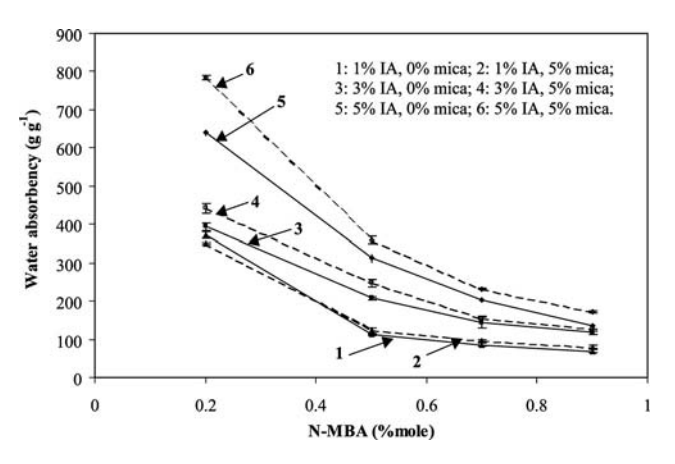


Figure 6. The effect of varying the N-MBA crosslinker concentration on the water absorbency (*Q*) of the crosslinked poly(AM-co-IA) copolymers and their nanocomposites with 5% w/w of mica addition at various IA concentrations.



Table 4. The residual amounts of acrylamide monomer in the crosslinked polymer and polymer nanocomposites

	Initial acrylamide monomer	monome crossl	Residual acrylamide monomer in the crosslinked polymer ^a	
AM/IA ratio	concentration (ppm)	ppm	%	
100:0 99:1 95:5	71,080 70,369 67,526	94.2 54.7 56.5	0.13 0.08 0.08	

 $^{^{\}rm a}$ Data are displayed as the mean $\pm\,1$ SD and are derived from two independent repeats.

contact with the superabsorbent polymer enveloped in a napkin pad.

Effect of IA concentration and mica content on water absorbency

In deinoized water

Polyacrylamide superabsorbent prepared with 0.2% mole of crosslinker can absorb water at $35\pm 1\,\mathrm{g\,g^{-1}}$ dry weight, whereas the water absorbency of the synthesized poly(AM-co-IA) superabsorbents using the same amount of crosslinker vary from 372 ± 9 to $640\pm 7\,\mathrm{g\,g^{-1}}$ dry weight corresponding to the addition of 1–5% mole IA (as seen in Fig. 7 without the addition of mica). The increase in water absorbency of the copolymers is caused by the addition of IA into the polymer network. An increase in the IA concentrations increases the amount of free carboxyl groups (–COOH), and thus increases the electrostatic repulsive forces between the charge sites on the carboxylate ions upon their complete dissociation, [50] leading to expansion of the structure. The expanded structure with high IA contents causes a high degree of swelling and higher water absorption of the superabsorbent polymers and their composites.

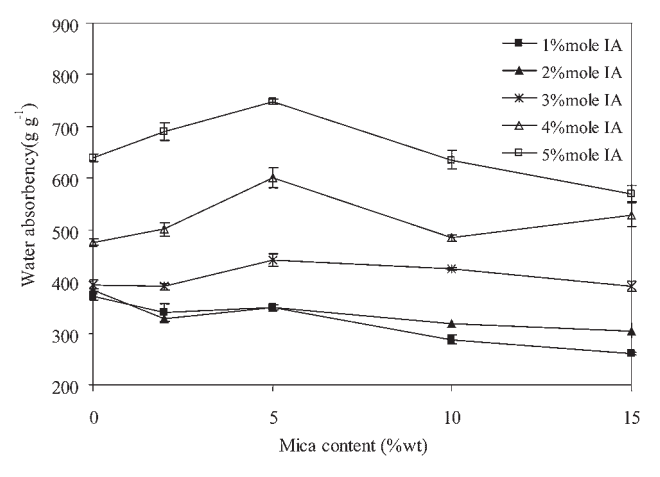


Figure 7. The effect of mica content on water absorbency (*Q*) of the 0.2% mole of N-MBA crosslinked poly(AM-*co*-IA)/mica nanocomposites.

In our superabsorbent preparation, we observed the formation of slurry if an IA content of higher than 5% mole was employed in the reaction mixture. This prohibits its use in personal care applications. The product cannot be dewatered with methanol and the dry gel could not be obtained. This result is in good agreement with the findings by Pulat and Eksi, [50] who reported that increase in the IA levels in copolymeric structures decreased the effective crosslinking densities of the polymer networks. As IA could not form superabsorbent polymers by itself, an excessive amount of IA in the monomer mixture made it more difficult to form a copolymer gel. The degree of swelling of the synthesized copolymers of AM and IA mainly depended on the repulsive forces between the hydrophilic pendants (amide and carboxylic groups) in their structures. The reactivity ratios of AM, IA, and N-MBA are 0.77, 1.36, and 1.77, respectively,^[51] i.e. IA molecules are used up via a crosslinking reaction with N-MBA before AM monomer, even if the monomer feed concentrations are equal or higher. In the present case, the structure of the copolymer contained more units of uncrosslinked PAM moiety than crosslinked IA units owing to a higher AM concentration.

The water absorbency of superabsorbent polymer nanocomposites shows a similar trend to that of poly(AM-co-IA) copolymer in which the water absorbency increases with an increase in IA concentration (Fig. 7). The same rationale described previously is applicable here, where the highest swelling and the largest basal spacing of the superabsorbent polymer nanocomposites were achieved at 5% mole of IA. The result shows that the water absorbency tends to increase as the mica content increases from 0–5% w/w for the nanocomposite systems containing 3–5% mole IA, whereas the highest water absorption was found at 5% w/w mica. However, above a 5% w/w mica content, the water absorbency decreased, suggesting a rigidity effect from the added mica on the copolymer. As described in the previous section, it is likely that the intercalated structure was increased in the composite and the grafting reaction took place on the surface of mica. Increase in the mica levels will increase the crosslinking density of superabsorbent nanocomposites with decrease in the entropy of the chains as they become stiffer, giving a stronger gel with fewer available spaces for water to enter, and a decreased water swelling capacity.[27]

In contrast, mica inclusion does not significantly improve the water absorbency of the superabsorbent nanocomposites with 1 and 2% mole IA. As discussed above, the water absorbency of all the nanocomposites is decreased as the mica content increases beyond 5% w/w.

The mechanisms of the intercalation are complex and are not known in much detail. Gao^[52] conjectured that there are three states in the composite structure. Here, we present such interactions occurring in our system using the speculation of Gao as indicated in Scheme 1. The first stage involves the polymer molecules intercalating into the interlayer spaces of the clay facilitated by Van der Waals interactions and hydrogen bonding between the polymer molecules (containing ionic groups from IA) and the hydrated interlayer cations and the silicate layer. The second stage is the binding of polymer chains to the outer surface of the clay particles via hydrogen bonds. Lastly, polymer chains located far from clay particles form networks by reacting with the N-MBA crosslinking agent. The latter has no interaction with the clay particles. Therefore, the overall structure of the composite would be quite complex. Understanding this complex structure will assist in predicting or searching the composite properties.



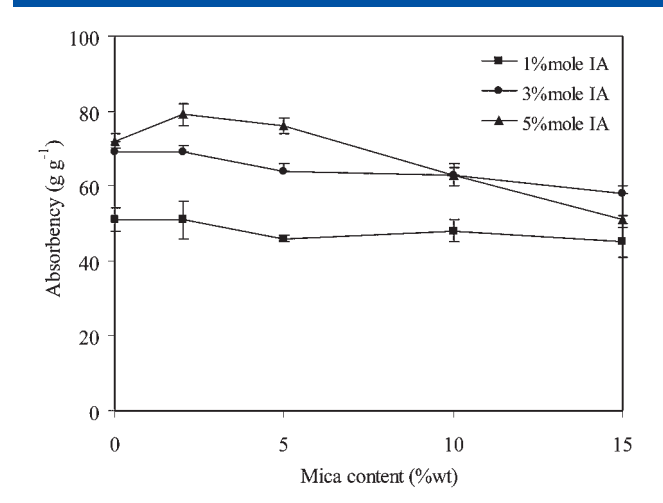


Figure 8. Water absorbency in artificial urine of the superabsorbent nanocomposites at AM/IA ratios of 99:1, 97:3, and 95:5, 0.2% mole of N-MBA, with various levels of mica content.

In ARU

A critical property in selecting a superabsorbent product for commercial use in personal care applications is the extent of swelling in ionic and osmoactive body-waste liquids such as urine and blood.^[53] An acceptable swelling capacity is approximately 20-40 g of urine per gram of polymer. The amount of urine absorbed by various poly(AM-co-IA)/mica nanocomposites prepared with AM/IA ratios of 99:1, 97:3, and 95:5, at different mica contents were investigated and the results are summarized in Fig. 8. In general, the swelling of the superabsorbent nanocomposite in ARU is much lower than the swelling obtained in deinoized water due to the presence of salts in the urine solution, leading to a decrease in expansion of the gel networks caused by the repulsive forces of counter ions on the polymeric chain shielded by the bound ionic charges. Therefore, the osmotic pressure differences between the gel network and the external solution decrease with increase in ionic strength of the artificial

urine. [54] The forces for the absorption of ionic solutions are attributed to the osmotic pressure based on the movable counter ions, the polymer-solvent affinity, and the rubber elasticity. The ionic strength of the artificial urine used in these studies was calculated $^{[42]}$ to be 0.0747 mol-ion $\rm dm^{-3}$ or 74.7 mM. Normal urine usually has an ionic strength of 10–800 mM or up to 1500 mM ionic strength in the mild dehydration, a superabsorbent polymer with higher urine absorption is needed to compensate the reduction of urine absorption caused by the salt effect. The ionic strength of the swelling liquid (e.g. urine) has an inversely proportional effect on the equilibrium-swelling ratio. The results show that the urine absorbency of the nanocomposites containing 1 and 3% mole of IA decreased slightly with increase in the content of mica. However, the nanocomposite with 5% mole IA yielded the highest urine absorption of all the samples, and this was maximal with the addition of 2% w/w mica, with higher mica levels significantly decreasing the urine absorbency of the nanocomposite. Likely, the decrease in the concentration difference of counterions inside and outside the superabsorbent particles is responsible for the decrease in urine absorption. Nanocomposites with high IA content (5% mole) showed a slight increase in urine absorbency with small mica additions (2 and 5% w/w), which is probably due to the increase in the osmotic pressure difference in the low chemically-crosslinking density system. However, why nanocomposites with 5% mole IA should show such a marked decrease in water absorption, with increasing mica levels above 5% w/w compared to those with lower IA levels, cannot currently be explained.

Water AUL

The poly(AM-co-IA) and poly(AM-co-IA)/mica nanocomposites with 5 and 15% w/w mica can absorb water up without load to 251 ± 4 , 239 ± 10 , and 201 ± 9 g g⁻¹ of the dry copolymer within 1 min, respectively. The results shown in Table 5 indicate that the more the mica content in the nanocomposites, the lower the absorption rate for poly(AM-co-IA)/mica nanocomposites due to

Table 5.	Effect	of swelling	time on	water	absorbency	of the	e superabsorb	ent polymer*

poly(AM- <i>co</i> -IA) copolymer			Poly(AM-co-IA)/mica nanocompsoite				
		5	5%wt mica		15%wt mica		
Time (min)	Water absorbency (Q) g g $^{-1}$	Time (min)	Water absorbency (Q) g g $^{-1}$	Time (min)	Water absorbency (Q) g g^{-1}		
1	251 ± 4	1	239 ± 10	1	201 ± 9		
5	310 ± 7	5	290 ± 9	5	212 ± 8		
10	313 ± 6	10	305 ± 7	10	230 ± 8		
30	337 ± 9	30	327 ± 5	30	238 ± 7		
60	340 ± 6	60	$\textbf{330} \pm \textbf{4}$	60	235 ± 6		
180	347 ± 8	180	341 ± 7	180	248 ± 10		
300	357 ± 4	300	348 ± 8	300	255 ± 5		
480	371 ± 10	480	350 ± 8	480	350 ± 9		

*Polymerizations were carried out at the AM/IA ratio of 99:1, 0.2% mole of N-MBA, 0.3% mole of APS, 1.2% mole of TEMED, mica contents at 5 and 15% wt, 50°C, and 30 min. Each result was an average of three repeats with one standard deviation.



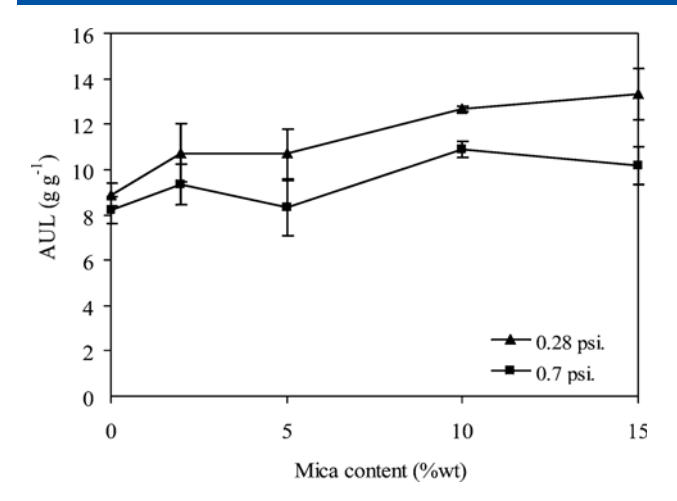


Figure 9. The effect of mica content on the absorbency under load (AUL) of the 0.2% mole of N-MBA crosslinked poly(AM-co-IA)/mica nanocomposites at a AM/IA mole ratio of 99:1.

the rigidity of the polymer chains resulting from a larger number of the crosslink density of the nanocomposites. The absorption rate sharply increased in the beginning, and the equilibrium absorbency could be achieved in 60 min for all of the polymers. Therefore, it is logical to carry out water AUL for 1 hr based on the extent of water absorbency and a few hours used as personal care products.

AUL measures the ability of a polymer to absorb fluid under a static load, and can be considered as a measurement of gel stability or gel strength. A high value of AUL correlates to a high gel strength. The water AUL (0.28 and 0.7 psi) of the poly(AM-co-IA)/mica nanocomposites in Fig. 9 was drastically reduced compared to those without a load, as depicted in Fig. 8. The heavier load at 0.7 psi yields a significantly lower absorbency at all levels of mica inclusion tested (0–15% w/w), presumably a larger compressive load restricts the flexibility and mobility of the polymer chains resulting in the lower water absorbency. Interestingly, the water AUL increased with the increase in the mica content, which is attributed to the fact that the mica particles act as crosslink points in combination with the polymer intercalation. When the mica levels are increased, the polymer

crosslink density and rigid structure are simultaneously enhanced, thereby increasing the gel strength at the expense of water absorption underweight loading. Consistent with this notion, the results presented in Table 6 indicate that the gel strength attained in the nanocomposites of other AM/IA ratios also tend to increase with the mica content as well.

Viscoelastic properties of poly(AM-co-IA)/mica nanocomposites

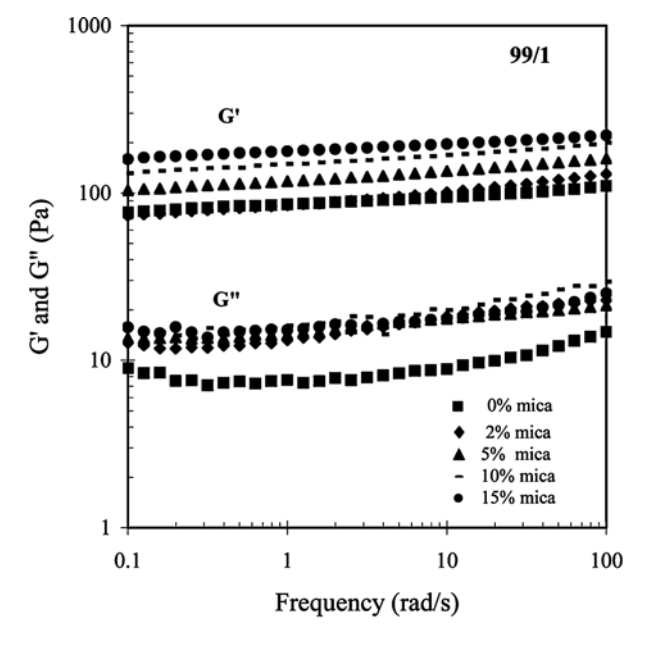
The storage (G') and loss (G'') moduli, as a function of frequency, for the superabsorbents (AM/IA mole ratios of 99:1 and 97:3) at various mica contents are summarized in Fig. 10. The experiments were performed within the LVE region, as predetermined from stress sweep experiments (data not shown here). All the superabsorbents behaved as elastic networks where G' was approximately tenfolds larger than G'' at all studied frequencies. An elastic network is endowed with the formation of chemical crosslinking between the copolymers and N-MBA, and the physical interaction of the copolymer chains and mica particles.^[55] The more distinct frequency-independent G' was observed in the system of 99:1 mole ratio of AM/IA, which means that this gel system has a more stable network structure when exposed to high frequencies. In contrast, the nanocomposites with a 97:3 mole ratio of AM/IA showed obvious frequencydependent G' and G'' due to the ability of the superabsorbent to absorb high levels of water molecules. The frequency-dependent G' is characteristic of soft gels, which is sensitive to the applied frequency, especially at high frequency. Since the G' of all the nanocomposites were weak if they were frequency-dependent at the low frequency range, the equilibrium modulus (G_e) , corresponding to the effective crosslink density, was determined from the value of G' at 0.1 rad sec⁻¹. Unfortunately, the experiments for nanocomposites with AM/IA ratios of 96:4 and 95:5 could not be performed due to the soft gel formation, which could not be used for the test.

Figure 11 shows the plots of equilibrium modulus and δ of the superabsorbents, extracted from the information in Fig. 10, as a function of mica contents. Tan δ is taken from the ratio of G''/G' and a value of tan $\delta < 1$ means that the system is elastic. In contrast, if tan $\delta > 1$, the system shows fluid-like behavior. The increase in $G_{\rm e}$ (the equilibrium modulus) with an increase in mica

Table 6. Water absorption under load of the crosslinked poly(AM-co-IA) and its nanocomposites at various mica contents						
		Water absorbency under load (g g^{-1}) at AM/IA mole ratio				
Load (psi)	Mica (% w/w)	99:1	98:2	97:3	96:4	95:5
0.28	0	8.9 ± 0.5	$\textbf{9.6} \pm \textbf{1.05}$	$\textbf{10.5} \pm \textbf{0.4}$	10.6 ± 0.1	$\textbf{10.4} \pm \textbf{0.2}$
	5	$\textbf{10.7} \pm \textbf{1.1}$	$\textbf{9.7} \pm \textbf{0.6}$	12.1 ± 0.5	10.6 ± 1.5	$\textbf{10.6} \pm \textbf{0.1}$
	10	$\textbf{12.7} \pm \textbf{0.1}$	11.7 ± 0.4	12.4 ± 0.6	11.7 ± 1.7	9.5 ± 0.8
0.7	0	8.2 ± 0.6	$\textbf{7.2} \pm \textbf{1.4}$	8.9 ± 1.3	$\textbf{9.2} \pm \textbf{0.9}$	7.6 ± 1.3
	5	8.3 ± 1.2	$\textbf{9.2} \pm \textbf{0.1}$	10 ± 0.7	7.7 ± 0.4	8.1 ± 0.5
	10	10.9 ± 0.4	8.7 ± 0.3	10.5 ± 0.4	9.3 ± 1.0	7.7 ± 0.5

Data are displayed as the mean \pm 1 SD and are derived from three independent repeats at the N-MBA content of 0.2% mole based on the monomer concentration.





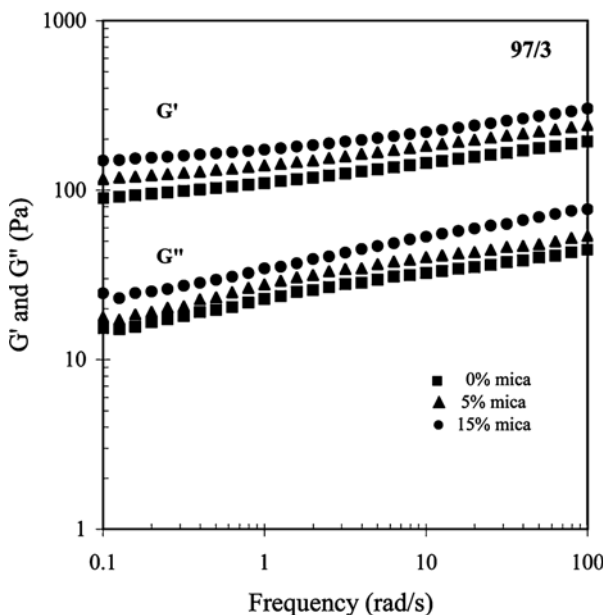


Figure 10. Angular frequency dependence of G' and G'' at the constant strain (1% strain) for the synthesized poly(AM-co-IA)/mica nanocomposites at the AM/IA ratio of 99:1 and 97:3, 0.2% mole of N-MBA, and at various mica contents.

content of both superabsorbent systems indicates an increase in the additional crosslinking density acquired from the formation of network structures between the copolymer chains and the mica particles. Typically, the increase in $G_{\rm e}$ due to an increase in network density results in a decrease in water absorbency (Q), as seen in composites with a 99:1 mole ratio of AM/IA (Fig. 11 inset). However, for composites containing 3% mole IA, although the network density increases (corresponding to an increase in $G_{\rm e}$), Q increases as well up to 5% w/w mica addition. This strange behavior might be due to the alteration in the osmotic pressure exerted in the superabsorbent particles from the presence of counterions of the added mica; the more the counterion

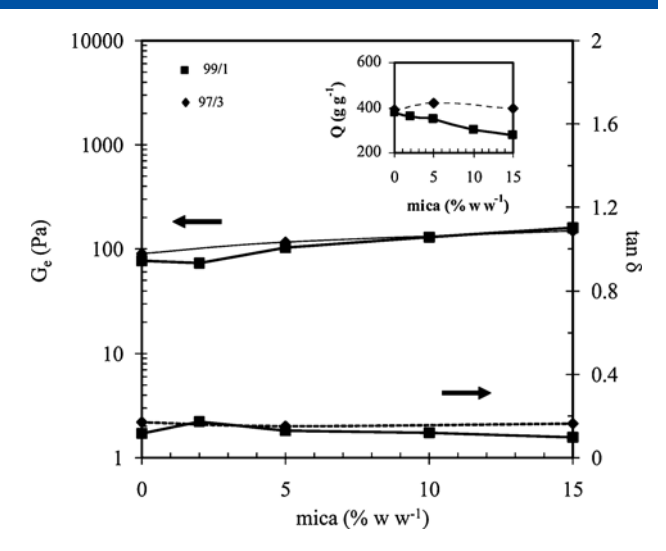


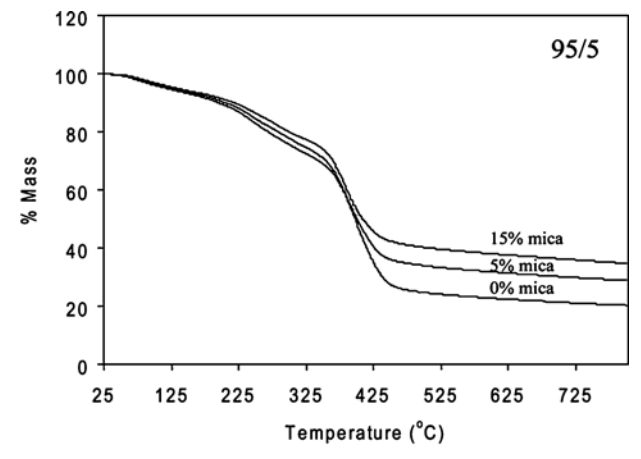
Figure 11. Equilibrium modulus (G_e) and $\tan \delta$ (at 0.1 rad \sec^{-1} where the G_e was taken) of the superabsorbent copolymers and the nanocomposite copolymer hydrogels prepared from AM/IA ratio of 99:1, 97:3 and at various mica contents. An inset is a plot of water absorption (Q) vs. mica content redrawn for a discussion.

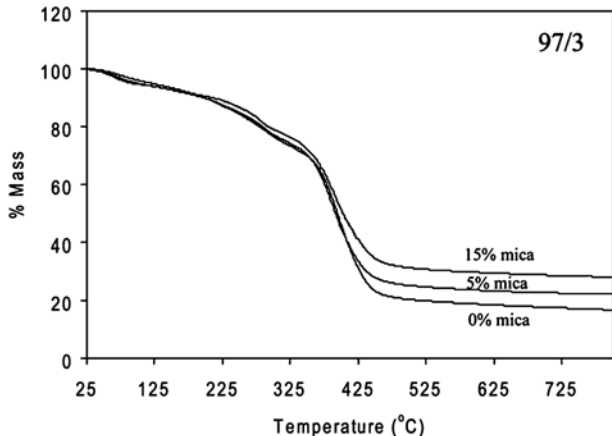
concentration within the superabsorbent increases then so does the osmotic pressure. Therefore, the ionic nature of mica predominates its crosslinker effect and so the increase in superabsorbent swelling is induced by increase in the mica content. Nevertheless, for both 1 and 3% mole composites, as the mica content is further increased, the crosslinking effect dominated.

Thermal properties of poly(AM-co-IA)/mica nanocomposites

For poly(AM-co-IA)/mica nanocomposites, the thermal stability of mica and composite residues at 800°C are both increased with increase in the mica content in comparison with the poly(AM-co-IA) without mica. The TGA results are shown in Fig. 12a-c. The increase in the thermal stability can be attributed to the high thermal stability of mica and to the interaction between the mica particles and the polymer matrix.^[46] Moreover, the thermal stability of the composites is enhanced with increase in the mica contents from 5 to 15% w/w, which provides additional evidence of mica dispersion within the polymer matrix. Under mild stirring for a certain mixing time, the mica powder could be well dispersed and stabilized in the monomer solution. Mica acts as a heat barrier, thus delaying the diffusion of volatile thermooxidation products into gas, which results in the enhanced thermal stability of the system. [54] The amount of mica retained in the composites are in the range of 79-80%, regardless of the mica content added, as determined by the furnace test, which suggests that most of the mica was intercalated into the polymer network or was grafted, and a smaller amount (approximately 20% w/w) was dispersed in the suspension during the preparation of the superabsorbent polymer and was not used in the reactions and was removed during the process. Based on the above characterized properties of absorbency, viscoelastic, and thermal stability properties, we conclude that the gas permeability properties of the composites should not be affected in comparison with the neat polymer.







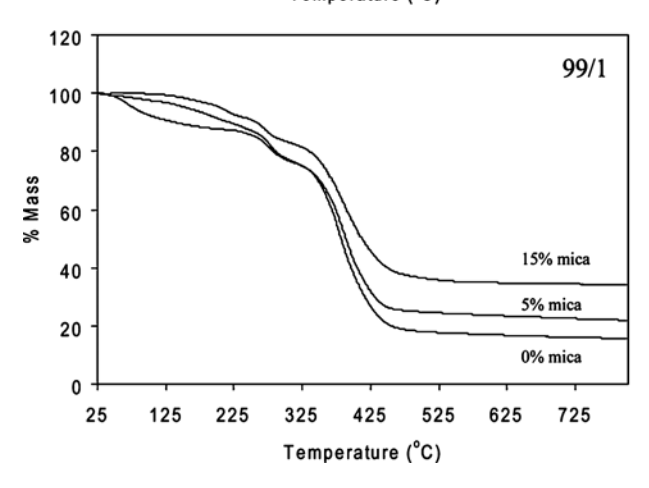


Figure 12. Representative TGA thermograms of the 0.2% mole of N-MBA crosslinked poly(AM-co-IA)/mica nanocomposites at AM/IA mole ratios of: (a) 99:1, (b) 97:3, and (c) 95:5, with various mica contents.

CONCLUSIONS

Crosslinked poly(AM-co-IA) copolymers and poly(AM-co-IA)/mica nanocomposites were successfully prepared in solution by redox polymerization. The FTIR characterization of the poly(AM-co-IA)/mica nanocomposites also gave the characteristic absorption peaks of -COO⁻ from the carboxylic acid group in the IA moiety at 1665–1664 cm⁻¹ and the absorption peaks of Si-OH group in mica at 1016–1011 cm⁻¹ and 473–471 cm⁻¹. Increasing the IA concentration in the copolymer resulted in enhanced water absorbency of the superabsorbent polymers or polymer

composites. By dispersing mica prior to polymerization, the swollen gel strength was increased as verified by the AUL and viscoelastic behavior. The TEM and XRD analyses of the composites indicated that the interlayer spacings of mica were enlarged, suggesting that the intercalation was successfully achieved. The addition of small (up to 5% w/w) mica content increased water absorption of the nanocomposites containing IA molecules at 3% mole and higher, but water absorption decreased with further increase in the mica content. The artificial urine absorption was found to decrease slightly with increase in the content of mica in the nanocomposites. However, at the AM/IA mole ratio of 95:5 with 2% w/w of mica, the water absorbency in the ARU of the superabsorbent nanocomposite reached its maximum at approximately 80 g g^{-1} . Thermal gravimetric analysis showed enhanced physical properties evidenced from the increased thermal stability with increasing mica content. Increase in the crosslinker concentration decreased the water absorbency of the nanocomposites. The residual amounts of AM monomer in the polymer and a high mica amount incorporated indicates that the solution polymerization is an acceptable synthesis route to prepare the superabsorbent polymer and superabsorbent polymer nanocomposite.

Acknowledgements

The authors are thankful for research facilities provided by the Polymer Imaging Laboratory of Chulalongkorn University's Imaging and Printing Technology Department, Faculty of Science. The authors would also like to thank the Publication Counseling Unit, especially Dr Robert Butcher, of the Research Division, Faculty of Science, Chulalongkorn University, for language correction and valuable suggestions.

REFERENCES

- F. L. Buchholz, A. T. Graham, Chapter 1. Modern Superabsorbent Polymer Technology. Wiley-VCH, New York, 1998,
- [2] G. Xu, G. Y. Wu, L. Li, Special Petrochem. 2002, 1, 42-44.
- [3] T. Sakiyama, C. H. Chu, T. Fujii, T. Yano, J. Appl. Poly. Sci. 1993, 50, 2021– 2025
- [4] T. Shiga, Y. Hirose, A. Okada, T. Kurauchi, J. Appl. Polym. Sci. 1992, 44, 249–253.
- [5] T. Shiga, Y. Hirose, A. Okada, T. Kurauchi, J. Appl. Polym. Sci. 1993, 47, 113–119.
- [6] P. Riccardo, J. Macromol, Sci., Rev. Macromol. Chem. Phys. 1994, 34, 607–662.
- [7] A. Kikuchi, T. Okano, Adv. Drug. Deliver. Rev. 2002, 54, 53-77.
- [8] W. F. Lee, K. T. Tsao, J. Appl. Polym. Sci. 2007, 104, 2277–2287.
- [9] M. Kokabi, M. Sirousazar, Z. M. Hassan, Eur. Polym. J. 2007, 43, 773–781.
- [10] United States Department of Agriculture. US Patent 3,981,100, 1961.
- [11] M. Yoshinobu, M. Morita, I. Sakata, J. Appl. Polym. Sci. 1992, 45, 805–812.
- [12] M. J. Molina, M. R. Gómez-Antón, I. F. Piérola, *Macromol. Chem. Phys.* 2002, 203, 2075–2082.
- [13] W. F. Lee, Y. C. Chen, J. Appl. Polym. Sci. 2005, 97, 855–861.
- [14] X. Li, W. Wu, J. Wang, Y. Duan, Carbohydr. Polym. 2006, 66, 473–479.
- [15] J. Z. Yi, L. M. Zhang, Eur. Polym. J. 2007, 43, 3215-3221.
- [16] J. Wu, Y. Wei, J. Lin, S. Lin, Polymer 2003, 44, 6513-6520.
- [17] W. F. Lee, L. G. Yang, J. Appl. Polym. Sci. 2004, 92, 3422–3429.
- [18] Z. Weian, L. Wei, F. Yue'e, Mater. Lett. 2005, 59, 2876–2880.
- [19] A. Li, A. Wang, Eur. Polym. J. 2005, 41, 1630–1637.
- [20] J. Zhang, H. Chen, A. Wang, *Eur. Polym. J.* **2005**, *41*, 2434–2442.
- [21] J. Zhang, H. Chen, A. Wang., Eur. Polym. J. 2006, 42, 101–108.
- [22] Y. Xiang, Z. Peng, D. Chen, Eur. Polym. J. 2006, 42, 2125–2132.
- [23] J. Z. Yi, L. M. Zhang, Eur. Polym. J. **2007**, 43, 3215–3221.



- [24] Y. Zheng, P. Li, J. Zhang, A. Wang., Eur. Polym. J. 2007, 43, 1691–1698.
- [25] F. Santiago, A. E. Mucientes, M. Osorio, C. Rivera, Eur. Polym. J. 2007, 43, 1–9.
- [26] J. Lin, J. Wu, Z. Yang, M. Pu, Macromol. Rapid. Commun. 2001, 22, 422–424.
- [27] W. F. Lee, Y. C. Chen, Eur. Polym. J. 2005, 41, 1605–1612.
- [28] J. Zhang, A. Wang, React. Funct. Polym. 2007, 67, 737-745.
- [29] I. S. Miles, S. Rostami, Multicomponent Polymer Systems. Wiley, New York, 1992.
- [30] S. Kiatkamjornwong, W. Chomsaksakul, M. Sonsuk, *Radiat. Phys. Chem.* **2000**, *59*, 413–427.
- [31] W. Jiraprasertkul, R. Nuisin, W. Jinsart, S. Kiatkamjornwong, J. Appl. Polym. Sci. 2006, 102, 2915–2928.
- [32] S. Kiatkamjornwong, K. Mongkolsawat, M. Sonsuk, Polymer 2006, 43, 3915–3924.
- [33] P. Lanthong, R. Nuisin, S. Kiatkamjornwong, *Carbohydr. Polym.* **2006**, *66*, 229–245.
- [34] S. Kiatkamjornwong, P. Suwanmala, *Radiat. Phys. Chem.* **1997**, *50*, 617–624.
- [35] S. Kiatkamjornwong, P. Suwanmala, *Radiat. Phys. Chem.* **1998**, *52*, 217–221.
- [36] S. Kiatkamjornwong, P. Suwanmala, J. Appl. Polym. Sci. **1998**, 68, 191– 203
- [37] S. Kiatkamjornwong, R. Wongwatthanasatien, *Macromol. Symp.* **2004**, *207*, 229–240.
- [38] S. Kiatkamjornwong, N. Siwarungson, A. Nganbunsri, *J. Appl. Polym. Sci.* **1999**, *73*, 2273–2291.
- [39] D. Yiamsawas, W. Kangwansupamonkon, O. Chailapakul, S. Kiatkamjornwong, React. Funct. Polym. 2007, 67, 865–882.

- [40] U.S. EPA Method8032A. SW-846 Rev 1. U.S. Environmental Protection Agency. Office of Solid Waste; 1996: http://www.ultrasci.com/analytical method.aspx?analyticalmethod (accessed April14, 2007).
- [41] V. S. Joshi, M. J. Parekh, M. J. Joshi, A. D. B. Vaidya, *Urol. Res.* 2005, 33, 80–86.
- [42] D. A. Skoog, D. M. West, F. J. Holler, Fundamentals of Analytical Chemistry (7th edn), Harcourt Brace & Company, Florida, 1991.
- [43] M. J. Ramazani-Harandi, M. J. Zohuriaan-Mehr, A. A. Yousefi, A. Ershad-Langroudi, K. Kabiri, *Polym. Test* 2006, 25, 470–474.
- [44] P. S. Liu, L. Li, N. L. Zhou, J. Zhang, S. H. Wei, J. Shen, J. Appl. Polym. Sci. 2006, 102, 5725–5730.
- [45] F. Zhang, Z. Guo, H. Gao, Y. Li, L. Ren, L. Shi, L. Wang, *Polym. Bull.* 2005, 55, 419–428.
- [46] J. H. Chang, Y. U. An, D. Cho, E. P. Giannelis, *Polymer* **2003**, *44*, 3715–3720.
- [47] J. N. Hamid, O. Oguz, J. Appl. Polym. Sci. 1996, 60, 971–979.
- [48] A. Y. Gamel, H. A. Al-Maskati, A. Y. Ali, M. G. Dairi, Mutat. Res. 1993, 300, 91–97.
- [49] J. Baselga, M. A. Llorente, J. L. Nieto, I. F. P. Hernández-Fuentes, Eur. Polym. J. 1988, 24, 161–165.
- [50] M. Pulat, H. Eksi, J. Appl. Polym. Sci. 2006, 102, 5994-5999.
- [51] N. Uyanik, C. Erbil, Eur. Polym. J. 2000, 36, 2651-2654.
- [52] D. Gao, Superabsorbent polymer composite (SAPC) materials and their industrial and high-tech applications. *Ph.D. Thesis*, **2003**, Bergakademie, Freiberg University, Freiberg.
- [53] H. A. Abd El-Rehim, Radiat. Phys. Chem. 2005, 74, 111–117.
- [54] P. S. Keshava, Y. Mohan, J. Sreeramulu, K. Mohana, *React. Funct. Polym.* 2006, 66, 1482–1493.
- [55] O. Okay, W. Oppermann, Macromolecules 2007, 40, 3378–3387.

polymers advanced technologies

Received: 17 July 2009,

Revised: 19 November 2009.

Accepted: 18 December 2009.

Published online in Wiley InterScience: 2010

(www.interscience.wiley.com) DOI: 10.1002/pat.1658

Gel strength and swelling of acrylamide-protic acid superabsorbent copolymers

Nispa Seetapan^a, Jiraporn Wongsawaeng^b and Suda Kiatkamjornwong^{b*}

The viscoelastic and swelling properties of polyacrylamide-based superabsorbent copolymers were investigated as a function of the ionic comonomer structure. Superabsorbent copolymers were synthesized by free-radical crosslinking copolymerization of acrylamide and one of the monoprotic acids (acrylic acid and crotonic acid) or the diprotic acids (maleic acid and itaconic acid) as the investigated ionic comonomer. The reaction composition of all components, i.e. monomer, comonomer, initiator, co-initiator, and crosslinker, was fixed to be the same for the synthesis of all four superabsorbent copolymer systems. Viscoelastic measurements were performed in all systems where the particles were closely packed. The network structures of all systems were evaluated via viscoelastic and swelling measurements. The results indicated that superabsorbent polymers (SAPs) with high water absorbency were accompanied by low gel strength and the calculated high value of molecular weight between crosslinks (\overline{M}_c) and low value of effective crosslinking density (ν_e). Diprotic acid-containing SAPs showed higher water absorbency over monoprotic acid-containing and non-ionic ones. The differences in \overline{M}_c and ν_e values of each system were explained with respect to the differences in the monomer reactivity ratio and hydrophilicity of the comonomers. Copyright © 2010 John Wiley & Sons, Ltd.

Keywords: superabsorbent polymers; swelling; viscoelastic; molecular weight between crosslinks; crosslinking density

INTRODUCTION

Superabsorbent polymers (SAPs) are polymers that can absorb and retain water, saline solutions, or physiological fluids up to thousands times their dry weight. These properties correspond to the three-dimensional hydrophilic network structure of the polymers. They have received considerable attention not only in the fields of personal care products, biosorbent, biomaterials, [1] but also for agricultural soil, [2] wastewater treatment, [3-7] and other applications where water absorbency or water retention is important. Besides their hydrophilic nature, SAPs containing an ionic moiety have enhanced water absorbency compared to non-ionic ones.^[8] Several ionic vinyl monomers, i.e. acrylic acid, itaconic acid, and so forth, have been selected to copolymerize with a non-ionic hydrophilic monomer like acrylamide to prepare SAPs with high degree of swelling. [6,7,9,10] Besides, one of the desired characteristics of SAPs is the optimum gel strength suitable for many applications. Both the desired properties (high swelling capacity and optimum gel strength) are in correlation with the network structure within the SAPs, which can be expressed as the average molecular weight between crosslinks (\overline{M}_c) and the effective crosslinking density (v_e) . The degree of crosslinking, the type and degree of ionic comonomer incorporated can be used to control the network structure, and thus the degree of swelling of SAPs.

Unlike the extensive determination of swelling behavior, few studies on the characterization of swollen gel strength of SAPs have been reported; for instance, Ramazani-Harandi *et al.*^[11] recently determined the swollen gel strength of the commercial acrylic-based SAP polymer via rheological characterization based on non-destructive oscillatory measurements. Oscillatory measurement is typically used to measure viscoelastic properties of

material. [12,13] Basically, the material is exposed to a small amplitude oscillatory stress (or strain), which is smaller than the critical value; the resulting strain (or stress) and phase lag between the input stress and the output strain are measured. This type of deformation can provide information on elastic energy storage and viscous energy dissipation, quantitatively represented as storage modulus (G') and loss modulus (G''), respectively. G' is proportional to the extent of the elastic component and G'' is rational to the extent of the viscous component of the system. The strength of materials is measured by the magnitude of $tan \delta$ (the ratio G''/G'), where δ is a phase angle.

In this study, the gel strength and equilibrium water absorption capacity of acrylamide-based SAPs were examined through viscoelastic and swelling measurements, respectively. Four representative mono- and di-protic acids comonomers, namely,

- * Correspondence to: S. Kiatkamjornwong, Multidisciplinary Program of Petrochemistry and Polymer Science, Department of Imaging and Printing Technology, Faculty of Science, Chulalongkorn University, Phayathai Road, Bangkok 10330, Thailand. E-mail: ksuda@chula.ac.th
- a N. Seetapan

National Metal and Materials Technology Center, National Science and Technology Development Agency, 114 Thailand Science Park, Paholyothin Road, Pathumthani 12120, Thailand

b J. Wongsawaeng, S. Kiatkamjornwong Multidisciplinary Program of Petrochemistry and Polymer Science, Department of Imaging and Printing Technology, Faculty of Science, Chulalongkorn University, Phayathai Road, Bangkok 10330, Thailand

Contract/grant sponsor: Thailand Research Fund; contract/grant number: RTA5080004.



acrylic, crotonic, maleic, and itaconic acids, having different hydrophilicity and monomer reactivity ratios toward the growing radicals, were selected to copolymerize with acrylamide. For comparison, acrylamide-based SAPs having four ionic comonomers were synthesized. All SAPs were synthesized via free-radical crosslinking polymerization. The reaction components, i.e. monomer, comonomer, initiator, co-initiator, and crosslinker, were fixed to be the same for all copolymeric systems. The network structure of each system was calculated via the equilibrium elastic modulus, obtained from the viscoelastic measurement using the polymer network theory. Likewise, the determination of the network structure in the prepared SAPs was performed using swelling data. Based on the monomer reactivity ratio and the hydrophilicity of comonomers, the obtained \overline{M}_c and v_e were correlated to the network structure, swelling behavior, and the measured gel strength of the SAPs.

EXPERIMENTAL

Materials

Acrylamide monomer (AM, 99% (w w⁻¹) purity) received from Siam Chemical Industry, Samutprakarn, Thailand, was used as a monomer. Acrylic acid (AA, Fluka, Buchs, Switzerland), crotonic acid (CA, Fluka, Buchs, Switzerland), maleic acid (MA, Merck, Darmstadts, Germany), and itaconic acid (IA, Merck, Darmstadts, Germany), were used as received. The chemical structures of the acrylamide monomer and comonomers are shown in Fig. 1. Ammonium persulfate (APS, Merck, Darmstadts, Germany), N,N,N',N'-tetramethylethylenediamine (TEMED, Fluka, Buchs, Switzerland), and methylenebisacrylamide (MBA, Fluka, Buchs, Switzerland) were used as the initiator, coinitiator, and crosslinker, respectively. Glacial acetic acid (CH₃COOH, BDH, Poole, England), phosphoric acid (H₃PO₄, 85% (w w⁻¹), Ajax, Sevenhills, Australia), boric acid (H₃BO₃, Merck, Darmstadts, Germany), and standardized sodium hydroxide (NaOH, Ajax, Sevenhills, Australia) were used to prepare 0.1 M Britton-Robinson buffers with pH values of the buffer adjusted to between 2 and 9 as desired by the addition of the appropriate amount of 0.2 M NaOH.[14] Deionized water (Elga Deionizer, Model LA611, Buckinghamshire, UK) was used for all solutions.

Preparation of polyacrylamide and acrylamide superabsorbent copolymers

SAPs were prepared by free-radical crosslinking polymerization. The concentrations of APS (initiator), TEMED (co-initiator), and MBA (crosslinker) were selected at 1.0, 2.0, and 1.0% by weight of

Figure 1. Chemical structures of acrylamide monomer and comonomers employed in the polymerization.

the monomers, respectively. For the synthesis of copolymers, the molar ratio of acrylamide: anionic comonomer was fixed at 96:4. The reaction compositions for all (co)polymer synthesis are summarized in Table 1. Briefly, a mixture containing AM, comonomer, MBA, APS, and 100 cm³ of deionized water was placed in a 500-cm³ four-necked round-bottomed flask equipped with a mechanical stirrer (IKA Euro-ST B, Germany), a condenser, and an inlet tube of nitrogen gas. The reaction flask was immersed in a controlled thermostat water bath (Mammert, Swabach, Germany) and heated to 45°C with stirring at 250 rpm for 5 min. Then, TEMED was added to the mixture and polymerization was allowed to proceed for 30 min to ensure a complete polymerization.^[7] The obtained product was dried at 60°C for 24 hr, milled, and then sieved through a 100-mesh sieve aluminum screen to obtain a dry irregular-shape powder with particle sizes <150 \(\mu m \). To extract the uncrosslinked polymer and/or residual monomers from the gel particles, 1 g of the dry SAPs was then stirred in 300 cm³ of distilled water at room temperature for 24 hr. The mixture was then separated to obtain the washed SAP and an aqueous extract. The washed SAP was dehydrated in methanol, dried at 60°C for 24 hr, ground, and then sieved via a 100-mesh sieve aluminum screen. To detect the unreacted comonomers, the aqueous extract was titrated with 0.05 M NaOH to a phenolphthalein end point. The existence of the synthesized superabsorbent copolymers was confirmed by Raman spectroscopy (Perkin Elmer, Spectrum GX, Massachusetts, USA).

Swelling measurements

The swelling measurements of the superabsorbent copolymer particles were performed at room temperature. Deionized water and Britton–Robinson buffers at a pH ranging from 2 to 9, all with an ionic strength of 0.1 M, were employed as swelling media. The obtained 0.1 g of dry particles were allowed to swell in the $200\,\mathrm{cm}^3$ deionized water for 24 hr to ensure the equilibrium (or maximum) swelling of the superabsorbent copolymers (based on our kinetic study of swelling). Subsequently, the fully swollen particles were separated from the unabsorbed medium by filtering through a 100-mesh sieve aluminum screen for 2 hr. Pieces of soft paper towel were used to absorb the unabsorbed water at the bottom of the screen until the swollen gel did not flow when the screen was held vertically. The swollen gel particle was then weighed and the water absorbency at equilibrium (Q_{er} g g⁻¹) was calculated by

$$Q_e = rac{ ext{mass of fully swollen particle} - ext{mass of dry particle}}{ ext{mass of dry particle}}$$
 $= q_w - 1$ (1)

where q_w is the equilibrium weight swelling ratio of the superabsorbent copolymer particles.

The equilibrium volume swelling ratio (q_v) was then determined by eqn (2):

$$q_{\rm v} = 1 + Q_{\rm e} \left(\frac{\rho_{\rm polymer}}{\rho_{\rm water}} \right)$$
 (2)

where $\rho_{\rm polymer}$ and $\rho_{\rm water}$ are densities of the dry SAP particles and water, respectively.



Table 1. Feeding composition of monomers, crosslinker, initiator, coinitiator, and water^a for the synthesized superabsorbent polymers

		Monomers			
Superabsorbent polymers	AM (g)	Comonomer (g)	Crosslinker MBA (g)	Initiator APS (g)	Co-initiato TEMED (g)
PAM	7.1080	_	0.0711	0.0711	0.1085
P(AM/AA)	6.8238	0.2838	0.0713	0.0714	0.1395
P(AM/CA)	6.8237	0.3446	0.0718	0.0717	0.1395
P(AM/MA)	6.8238	0.4644	0.0730	0.0729	0.1473
P(AM/IA)	6.8238	0.5204	0.0730	0.0735	0.1473

Swelling measurements were done in triplicate to obtain the average value of the water absorbency at equilibrium swelling.

Density measurements

The density of polyacrylamide superabsorbent and their copolymers was determined by the Ultrapycnometer 1000 (Quantachrome, Boynton Beach, Florida, USA), involving Archimedes' principle of fluid displacement and Boyle's law to determine the sample volume. The displacing material is helium gas, which can penetrate pores within samples. The experiment was performed by purging helium gas into the SAP samples at 23°C. The density was reported as an average value from five measurements, with the standard deviation (not shown here) being less than 0.002 g cm⁻³ for all samples.

Viscoelastic measurements

The viscoelastic experiments of the fully swollen SAP particles were carried out in a stress-controlled Gemini HR^{nano} rheometer (Malvern Instruments Ltd., Worcestershire, UK), and equipped with a solvent-trap and moisture controlling systems to prevent water evaporation during measurements. The operating temperature was 25° C, which was controlled by a peltier plate. The experiments were performed using acrylic parallel plate geometry (40 mm diameter, 1 mm gap). Firstly, a linear viscoelastic (LVE) region, where G' and G'' are independent of the stress amplitude, was determined by performing a dynamic stress sweep from $0.1-100\,\mathrm{Pa}$ at a fixed frequency of 1 Hz. Subsequent dynamic frequency sweep experiments were carried out within the evaluated LVE range.

The swollen SAP particles, after removing the unabsorbed water by filtering through the 100-mesh screen for 2 hr, were removed from the screen and placed on the measuring acrylic parallel plate of the rheometer. After loading the samples, they were allowed to relax for 10 min before carrying out each measurement in order to eliminate shear history from the sample loading. After the stress sweep experiment, a new swollen sample was loaded to perform the frequency sweep experiment at a fixed stress in the pre-determined LVE range. Three repetitions of viscoelastic measurements were performed for each sample and the obtained values of moduli were checked for reproducibility.

RESULTS AND DISCUSSION

Synthesis of acrylamide-based superabsorbent copolymers

The synthesized superabsorbent copolymers along with their functional groups were confirmed via Raman spectrometry (whose spectra are not shown here). The strong peak of the carboxylate group at 1648–1651 cm⁻¹ for all SAPs, attributed to the C=O stretching, corresponds to a conformational change during the crosslinking reaction. The peaks at 3330, 3200, 2920, and 1320 cm⁻¹ represent N–H, O–H, C–H, and C–N stretching, respectively. The results indicate that all SAP samples are acrylamide-based copolymers. Based on the titration experiment of the extracted solution, the end point detection was very low. Thus, one may conclude that acrylamide and anionic comonomer were essentially completely consumed in the crosslinking copolymerization.

Swelling experiments

Swelling in deionized water

As summarized in Table 2, the equilibrium water absorbency (Q_e) of each of the crosslinked ionic copolymers in deionized water was larger than that of crosslinked PAM, most likely as a result of the ionic (carboxylic acid) pendants in the copolymer structure to increase osmotic pressure inside the gel. The superabsorbent copolymers containing diprotic acid moieties, P(AM/MA) and

Table 2. Equilibrium water absorbency (Q_e) , equilibrium volume swelling ratio (q_v) , and equilibrium elastic modulus (G_e) of the superabsorbent polymers swollen in deionized water

Superabsorbent polymers	$Q_e (g g^{-1})$	q_{v}	G_e (Pa)		
PAM P(AM/AA)	$33\pm1\\131\pm7$	46 ± 2 174 \pm 10	$1,\!020 \pm 20 \\ 480 \pm 15$		
P(AM/CA) P(AM/MA)	44 ± 2 160 ± 4	59 ± 4 210 + 6	870 ± 20 330 ± 15		
P(AM/IA)	294 ± 6	393 ± 9	200 ± 15		
The data were obtained from three replicates.					



P(AM/IA), absorbed more water than the monoprotic acid-containing superabsorbent copolymers, P(AM/AA) and P(AM/CA). The possible reason is that more resultant density of ionic groups present in the copolymer network derived from the diprotic acid comonomers leads to an increase in electrostatic repulsive forces between charged sites on the carboxylate anions upon their complete dissociation and thus leads to a more extended configuration. The result also showed that although the P(AM/CA)-SAPs contain monoprotic acid in the network structure, the water absorbency was insignificantly different from that of the non-ionic PAM-SAPs. We postulate that the reason might be attributed to the huge difference in the reactivity ratio between AM and CA, and the relatively low hydrophilicity of CA (to be discussed below).

Swelling in Britton-Robinson buffer at various pHs

Figure 2 summarizes the data showing the pH dependence of the equilibrium water absorbency of PAM and the four copolymeric SAPs in Britton–Robinson buffers with pH values from 2 to 9 and a fixed ionic strength of 0.1 M. The water absorbency of pure PAM was not influenced by the pH of the swelling medium, as expected due to its non-ionic hydrophilic nature. In contrast, the

swelling behavior of three of the four anionic SAPs, P(AM/AA), P(AM/MA), and P(AM/IA), increased with increase in the pH of the swelling medium, due to their polyelectrolyte nature. However, the swelling behavior of the P(AM/CA)-SAPs merely responded to the variation in the pH of medium. This result is consistent with those of Çaykara et al., [15] who reported that there was very little effect of pH on the swelling behavior of crosslinked P(AM/CA) synthesized at a 95.3:4.7 molar ratio of AM:CA, which is very similar to the 96:4 ratio used here. However, as the content of CA in the copolymer was increased, so the pH-dependent swelling behavior of the copolymer was apparently increased, and they concluded that the equilibrium volume swelling depended greatly on the mole fraction of ionizable carboxylic acid groups in the network.^[15] We postulate that other reasons for the fairly pH-sensitive swelling of P(AM/CA) (96:4 molar ratio) might be attributed to the significant difference of the reactivity ratio between AM and CA, and the hydrophobicity of CA (to be discussed below).

Swelling of an ionic network is expected to significantly increase with a higher content of the ionic moiety within its structure. Anionic copolymeric SAPs are ionizable because of the presence of charged carboxylic acid groups. Each of the two monoprotic acids tested has a single dissociation constant with a

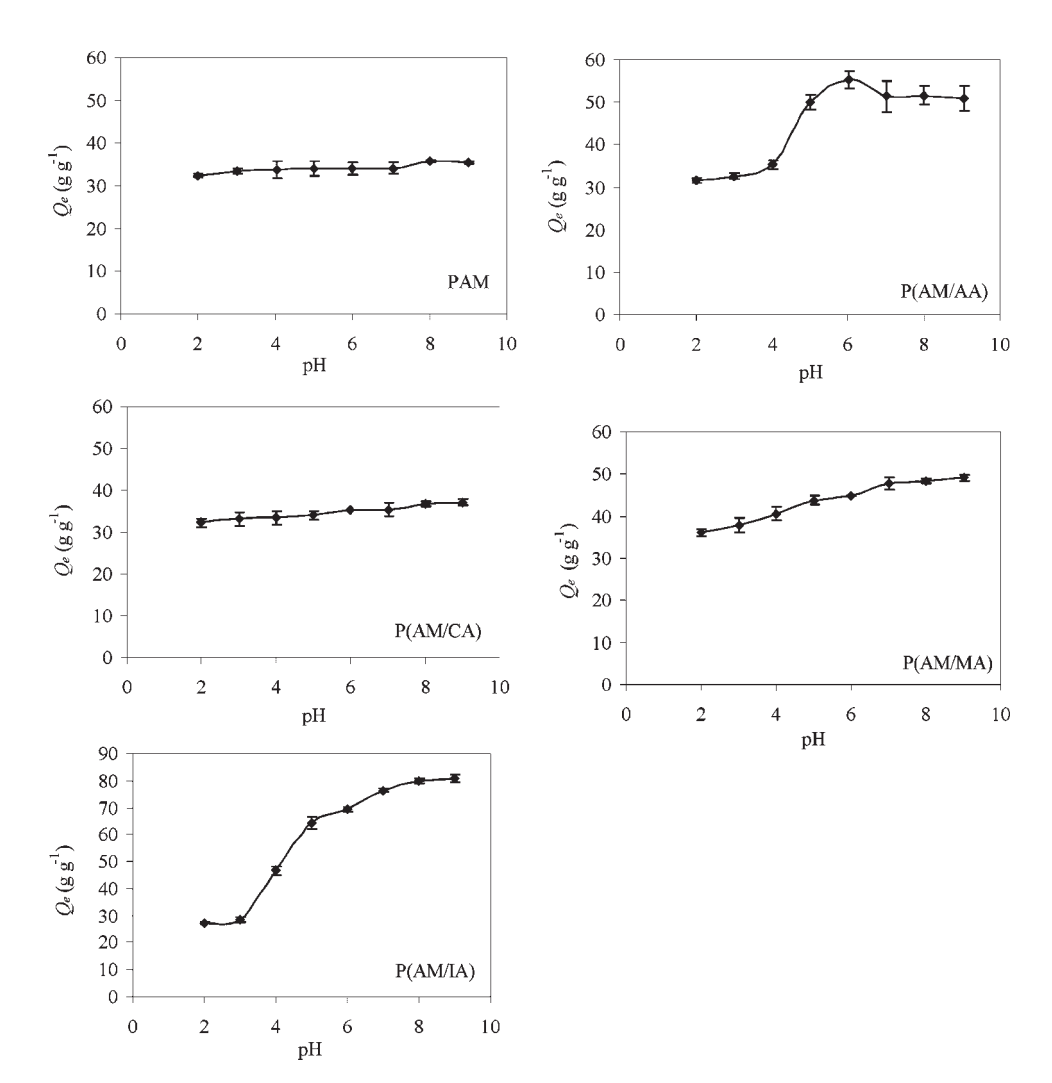


Figure 2. The effect of pH on the equilibrium water absorbency (Q_e) of SAPs: PAM, P(AM/AA), P(AM/CA), P(AM/MA), and P(AM/IA).

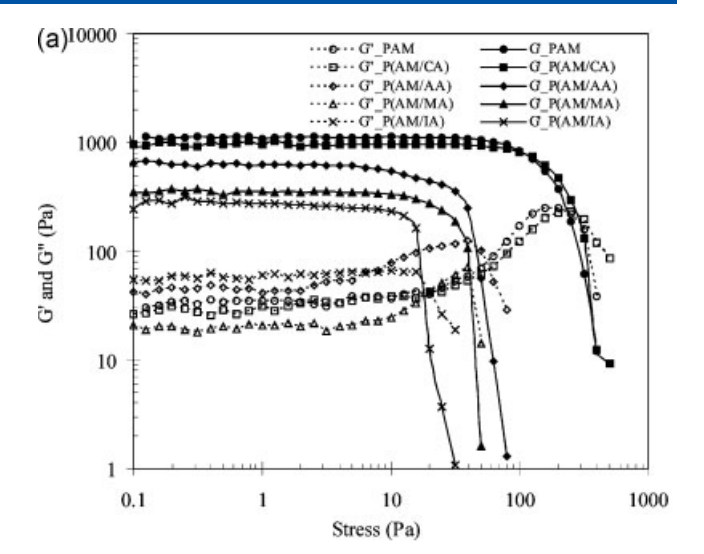


 pK_a of 4.25 and 4.69 for AA and CA, respectively, whilst the two diprotic acids have two dissociation constants, i.e. a pK_{a1} of 1.83 and 3.85, and a pK_{a2} of 6.07 and 5.45 for MA and IA, respectively. Theoretically, as the pH is increased there should be a sudden increase in the gel swelling as the pH nears the pK_a of the monoprotic acid containing SAPs, with a two-step swelling pattern for diprotic acid containing SAPs corresponding to their respective pK_{a1} and pK_{a2} . Of course, experimentally, these may be less sharp due to local environments changing some of the effective pK_a values within the copolymer and, if the two dissociation constants are relatively close, their overlapping (merging) would lead to a single broad swelling of the network at around these pH values, as was reported for crosslinked poly[(N-vinyl-2-pyrrolidone)-co-(itaconic acid)]. p-163

In this study (Fig. 2), an increase in the buffer pH resulted in an increase in the equilibrium water absorbency. At a low pH, ionization of the ionic groups in the SAPs is suppressed by H⁺ ions in the swelling medium and so flexibility of the chain is rather low. As the pH is increased, the ionic units dissociate and attract cations into the SAPs to replace H⁺ ions. The concentration of mobile ions inside the SAPs is, therefore, enhanced, which causes an increase in the ion swelling pressure. As a consequence, the equilibrium water absorbency increases. Such a trend is clearly seen for P(AM/AA)- and P(AM/IA)-SAPs, the latter showing the expected partial mergence of the p K_{a1} and p K_{a2} responses, whilst allowing for the fact that the p K_{a1} of IA is below the pH range tested, the expected trend for gel swelling around the p K_{a2} range was also noted for P(AM-IA). However, no such a trend was easily discernable for P(AM-CA)-SAPs (Fig. 2)

Viscoelastic experiments

Viscoelastic studies of our swollen SAP particles in deionized water were determined by means of the rheological method. Our investigated swollen particles consist completely of a system of closely packed gel particles. Their viscoelastic behaviors could be explained by interparticle interactions. The strength of such interactions, therefore, determined viscoelastic properties of the systems. Firstly, stress sweep experiments were performed to determine the LVE regime, where G' and G'' are independent of the stress amplitude, as shown in Fig. 3(a). The storage modulus was always larger than the loss modulus at the LVE regime. The extent of LVE range extended differently in each sample as observed from the deviation of the value of both moduli from linearity as the applied stress increased. The maximum stress up to which G' remains constant is called the critical stress (σ_c) which indicates a transition between linear and nonlinear regimes. The critical stress can be taken as the dynamic yield stress value. This means that below the critical stress the system behaves like an elastic solid. At the external applied stress beyond σ_{cr} the internal network structure started to break down and subsequently material flowed like a liquid. The result showed that the LVE range and the critical stress increased in sequence of P(AM/IA) < P(AM/MA) < P(AM/AA) < P(AM/CA) <PAM. The wide LVE region and large σ_c indicated that the system had good ability to resist external stresses to a greater extent. Furthermore, the values of tan δ are plotted in Fig. 3(b). Tan δ is the ratio of G''/G', where δ is a phase angle. If the value of tan δ is larger than 1 (G'' > G'), the system behaves like a liquid; whereas, if the value of tan δ is smaller than 1 (G'' < G'), the system shows solid-like (gel or network) behavior. Therefore, the strength of the interaction or internal structure is basically measured by the



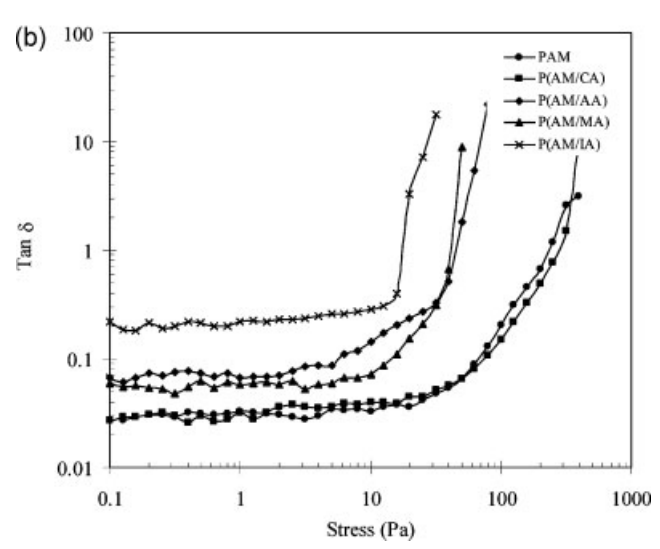


Figure 3. Viscoelastic properties of the SAPs swollen in deionized water, (a). storage (G') and loss (G'') moduli, and (b). $\tan \delta$ as a function of stress.

magnitude of $\tan\delta$. The smaller the $\tan\delta$ is, the stronger the interaction becomes. The results indicated that the strength of SAP particles inversely correlated to the water absorption capability. As a comparison to other systems, PAM and P(AM/CA) SAPs had indifferent ability to hold water and could absorb a small amount of water; thus, the larger G' and the smaller $\tan\delta$ were found in both the systems. On the contrary, P(AM/IA) SAP had ability to absorb the largest amount of water, and thus, it possessed the lowest gel strength.

It is interesting to note that for all the systems, except P(AM/IA), above the critical stress where a destruction of the gel particles occurred, a maximum in G'' was observed at a stress level close to where the viscoelastic response became primarily dissipative (tan $\delta \sim$ 1) and subsequently dropped at the larger applied stress. This behavior was very similar to a characteristic of nonlinearity, observed in the behavior of close-packed colloidal dispersions. [17–19] A slightly gradual drop in G' whereas G'' began to increase and reflected the onset of nonlinear, yielding when the stress approached a critical value where the particles were forced



to exchange positions with their neighbors, and hence the material could more effectively dissipate energy. At a larger stress where a progressive drop in G' was observed in association with a decrease in G'' after passing through a maximum, indicating the onset of plastic flow region.

Unlike the others, the SAP of P(AM/IA) did not show a maximum in G'' when the applied stress was increased. However, it behaved somewhat like a linear polymer solution. This was likely from the ability to absorb a large amount of water in P(AM/IA). As a result, when the applied stress approached the critical stress, the swollen particles, which were comparatively very soft, did not have enough strength to hop over the neighboring particles; therefore, the system flowed instead, which was consistent to the decreases in both moduli beyond the LVE region.

Figure 4 summarizes the observed storage (G') and loss (G'')moduli as a function of frequency for all the swollen SAP particles. The experiments were performed within the LVE region, as determined from stress sweep experiments. The viscoelastic behavior was dominated by an elastic character where G' was 10-fold larger than G'' at all frequencies studied (0.01–10 Hz). Additionally, no significant frequency-dependent changes in G' were observed for SAPs of PAM, P(AM/CA), P(AM/AA), and P(AM/ MA), whereas a slightly frequency-sensitive G' was observed for the P(AM/IA)-SAPs over the whole range of tested frequencies. Systems containing a higher level of small molecules (water molecules in this case) can dissipate more energy and thus, at a high frequency (corresponding to a short time scale), an increase in G'' is expected for a system absorbing a large amount of water such as P(AM/IA) SAPs. The flatness of G' over an appreciable decade of frequencies indicates a characteristic of a gel system. $^{[12]}$ Since G^{\prime} of all the systems at a low frequency range was not distinctly frequency-dependent, the equilibrium modulus (G_e) , shown in Table 2, was determined from G' at 0.01 Hz. Table 2 indicates that Q_e was found to be inversely correlated with G_e . A higher amount of water molecules inside the SAPs causes a higher mobility of the network chains and so leads to a lower strength of the system as observed from a lower G_e and larger tan δ .

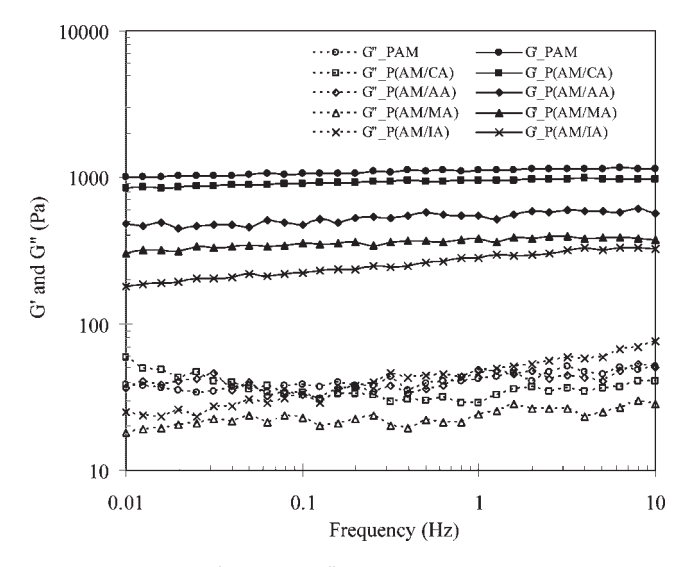


Figure 4. Storage (G') and loss (G'') moduli as a function of frequency for SAP particles swollen in deionized water.

Determination of \overline{M}_c from viscoelastic and swelling experiments

Viscoelastic behavior of particle dispersions is influenced by particle size, particle dispersity, volume fraction occupied by particles, and the gel strength of particles. Our investigated dried SAP particles with classified particle size were allowed to swell into an equilibrium stage. Each system had different ability to absorb water depending on the type of ionic comonomer, degree of crosslinking density within the particles, and the balanced osmotic pressure of the system. Therefore, the swollen particle size of each system was unequal. However, all systems were characterized in the close-packed region, where all of the spaces were occupied by the swollen particles. The swollen particles contacted one another; as a result, the elastic response dominated over the dissipative energy. Within this region, the magnitude of storage modulus and the strength of the system were strongly influenced by the degree of crosslinking within the particles. Crosslinking density is related to the average molecular weight between crosslinks (M_c), which can be determined via viscoelastic measurements. The theory of polymer networks predicts the equilibrium elastic modulus (Ge) for polymer gels obtained by the crosslinking polymerization as given in

$$G_{e} = \left(1 - \frac{2}{\phi}\right) \left(\frac{\rho_{2}}{\overline{M}_{c}}\right) RT v_{2r}^{2/3} v_{2m}^{1/3}$$
 (3)

where ϕ is the number for branches originating from a crosslinking site ($\phi=4$ for tetrafunctional networks), ρ_2 is the polymer network density, R is the gas constant, and T is the temperature. The factor $(1-2/\phi)$ is introduced for systems in a highly swollen state such as hydrogel (Phantom networks). The value of G_e is reported in Table 2. The v_{2m} is the volume fraction of polymer network, which can be calculated by

$$v_{2m} = \frac{1}{q_v} \tag{4}$$

The v_{2r} is the volume fraction of the network after the polymerization, which can be identified as shown in eqn (5):

$$v_{2r} = c_o V_r \tag{5}$$

where c_o is the initial concentration of monomers (mol cm⁻³).^[21] V_r is the average molar volume of polymer repeating units, and can be calculated as shown in eqn (6):

$$V_r = M_r/\rho_2 \tag{6}$$

where M_r is the molecular weight of the repeating unit in the copolymers, [21] and is determined from eqn (7):

$$M_r = [M_n(1 - f_i) + M_i(f_i)]$$
 (7)

where M_n is molecular weight of a neutral unit (acrylamide monomer), and M_i is the molecular weight of an ionic unit (comonomer) in the system, f_i is a mol fraction of the ionic unit in the system ($f_i = 0.04$). Table 3 contains parameters essential for calculating \overline{M}_c , according to eqn (3). The determined values of \overline{M}_c (from eqn (3)) obtained from viscoelastic measurement are listed in Table 4. The result indicated that SAPs with higher swelling capability exhibited lower gel strength as a result of the larger \overline{M}_c .



Table 3. Density and essential parameters used to determine network parameters					
Superabsorbent polymers	$ ho_2 (\mathrm{g cm^{-3}})$	M_r (g mol ⁻¹)	V_r (cm ³ mol ⁻¹)	c_o (mol cm ⁻³)	v _{2r}
PAM	1.3669	71.08	52.00	0.001	0.0519
P(AM/AA)	1.3174	71.12	53.98	0.001	0.0537
P(AM/CA)	1.3369	71.68	54.41	0.001	0.0543
P(AM/MA)	1.3116	72.88	55.57	0.001	0.0555
P(AM/IA)	1.3321	73.44	55.13	0.001	0.0550

We attempted to determine \overline{M}_c of all prepared SAPs from the equilibrium degrees of swelling. The average molecular weight between crosslinks for non-ionic phantom networks is expressed as shown in

$$\overline{M}_c = -\frac{\left(1 - \frac{2}{\phi}\right) V_1 \rho_2 \nu_{2r}^{2/3} \nu_{2m}^{1/3}}{\left[\ln(1 - \nu_{2m}) + \nu_{2m} + \chi \nu_{2m}^2\right]} \tag{8}$$

where V_1 is the molar volume of the swelling agent, and χ is the Flory polymer–solvent interaction parameter. Therefore, as also shown in Table 4, the $\overline{M}_{c \, \text{swelling}}$ values of PAM superabsorbents were calculated according to eqn (8) using the literature reported χ values. The has to be noted that a small difference in the reported χ values gives a very large difference in the calculated \overline{M}_c . Mahmudi $et \, al.$ Suggested that the values of \overline{M}_c and crosslink density can be correctly determined from swelling experiments if the χ parameter is reliably accepted or experimentally evaluated.

The swelling behavior of non-ionic network is thermodynamically dominated by contributions from the chemical potentials of mixing and elasticity. Upon swelling in an aqueous solvent, the diffusion of water into the network is driven by forces generated from the difference between the chemical potential of water inside and outside of the network until the equilibrium swelling is reached. This elastic contribution prevents the network from becoming completely dissolved. If networks contain ionizable groups within polymer chains, an additional force from the ionic contribution influences the swelling, where an increase in swelling is expected due to charge localization within the ionic network. [27,28] Therefore, the equation to determine \overline{M}_{c} of monoprotic acid-containing networks synthesized by the

simultaneous polymerization and crosslinking reaction of the monomers was derived, as shown in eqn (9):

$$\left[\frac{K_a}{10^{-pH} + K_a}\right]^2 \frac{V_1 f_i^2}{4I\overline{V}_r^2} - \nu_{2m}^{-2} \ln(1 - \nu_{2m}) - \nu_{2m}^{-1}$$

$$= \chi + \frac{\left(1 - \frac{2}{\phi}\right) V_1 \rho_2 \nu_{2r}^{2/3} \nu_{2m}^{-5/3}}{\overline{M}_c} \tag{9}$$

where K_a is the dissociation constant of monoprotic acid, l is the ionic strength of the swelling medium, and f_i is the weight fraction of ionizable polymer in the gel system.¹⁵

In case of diprotic-acid containing networks, the equation was proposed by Çaykara *et al.*^[29] as given in

$$\left[\frac{2K_{a1}K_{a2} + 10^{-pH}K_{a1}}{2\left[(10^{-pH})^2 + 10^{-pH}K_{a1} + K_{a1}K_{a2}\right]}\right]^2 \frac{V_1 f_i^2}{4I\overline{V}_r^2} - \nu_{2m}^{-2} \ln(1 - \nu_{2m}) - \nu_{2m}^{-1} \\
= \chi + \frac{\left(1 - \frac{2}{\phi}\right)V_1 \rho_2 \nu_{2r}^{2/3} \nu_{2m}^{-5/3}}{\overline{M}} \tag{10}$$

where K_{a1} and K_{a2} are the first and second dissociation constants of diprotic acid, respectively.

Therefore, data obtained from swelling experiments as a function of the pH (Fig. 2) were used to evaluate \overline{M}_c using eqns (9) and (10) for mono- and di- protic acid-containing copolymeric SAPs, respectively. The equations also provided the χ parameter of each system. If one defines the left-hand side, and the coefficient of $1/\overline{M}_c$ on the right-hand side of eqns (9) and (10) to be constant values of A and B, respectively, as described in

Table 4. Network parameters of the superabsorbent particles					
Superabsorbent polymers	$\overline{M}_{c \text{ viscoelastic}} (g \text{mol}^{-1})$	$\overline{M}_{c \text{ swelling}} (\text{g mol}^{-1})$	Χswelling	$\overline{M}_{c \text{ stoi}} (\text{g mol}^{-1})$	
PAM	$65,\!000\pm1,\!800$	37,000*, 76,000**	0.480*, 0.494**	7,726	
P(AM/AA)	$87,000 \pm 3,800$	$51,200 \pm 2,800$	0.491 ± 0.001	7,730	
P(AM/CA)	70,000 \pm 2,300	$\textbf{8,750} \pm \textbf{150}$	0.401 ± 0.004	7,625	
P(AM/MA)	$120,\!000\pm7,\!700$	$\textbf{3,6450} \pm \textbf{50}$	0.477 ± 0.003	7,753	
P(AM/IA)	$163,000 \pm 17,000$	$184,000 \pm 3,400$	0.503 ± 0.001	7,650	
* Literature reported χ values ** Literature reported χ value					



eqn (11), the plot of A against B correspondingly gives χ and \overline{M}_c as the intercept and inverse slope via a linear regression analysis.

$$A = \chi + B/\overline{M}_c \tag{11}$$

In this study, the related experimental parameters used with eqns (9) and (10) are the ionic strength of the swelling medium ($I=1\times10^{-4}\,\mathrm{mol\,cm^{-3}}$), the molar volume of the swelling medium (water) ($V_1=18\,\mathrm{cm^3\,mol^{-1}}$), and the others as shown in Table 3.

The plots of eqn (11) for each copolymeric SAPs are shown in Fig. 5. The determined \overline{M}_c and χ values of the SAPs from their swelling behavior are listed in Table 4.

On the other hand, if one assumes that all MBA crosslinkers were involved in the formation of effective crosslinks in the network, the stoichiometric molecular weight between crosslinks, $M_{\rm c}$ (stoi.), can be then calculated by

$$M_c(\mathsf{stoi}) = M_r/2X \tag{12}$$

where X is crosslinking ratio (the mol ratio of crosslinker to monomers). ¹⁰

Table 4 shows that the experimentally calculated \overline{M}_c values from both measurements of all SAP particles are higher than their respective stoichiometrically calculated values. This difference is attributed to the fact that a significant portion of the divinyl crosslinker (MBA) may not be employed in the crosslinking copolymerization. It is well known that gelation during free-radical crosslinking copolymerization occurs non-randomly, probably due to the cyclization and the multiple crosslinking reactions at pendant vinyl groups of MBA. [30,31] In addition, several researchers have reported that a high degree of monomer dilution during SAPs preparation and a higher crosslinker

reactivity are predominantly accountable for these cyclizations and multiple crosslinking reactions, which lead to a heterogeneous crosslinking distribution in the system. [32,33] The inhomogeneously crosslinking density distribution, known as the spatial gel inhomogeneity, is disadvantageous because it drastically reduces the optical clarity and strength of gels. [34] Since the spatial gel inhomogeneity results in local concentration fluctuations in gels, scattering methods, such as small angle X-ray scattering, [35,36] small angle neutron scattering, and light scattering, have been employed to investigate such inhomogeneity. Scattering theories of inhomogeneous gel have been proposed. [40–42] A more comprehensive theory has been recently constructed by Panyukov and Rabin [43,44] for a randomly crosslinked neutral polymer gels. Subsequently, the scattering theory was extended by Rabin and Panyukov [45] to describe weakly charged polymer gels.

The experimentally determined values of \overline{M}_c were used to calculate the effective crosslinking densities (ν_e) from the ratio of ρ_2/\overline{M}_c , which are shown in Fig. 6 along with the values of Q_e for all copolymeric SAPs. Although the absolute values of ν_e from both techniques were not in good agreement with each other, the same tendency was observed; that is, the effective crosslinking density decreased as the equilibrium water absorbency increased. It is interesting to note that large difference in both of the determined ν_e values was observed in SAPs containing crotonic acid as a comonomer.

Interpretation of the calculated network parameters from the reactivity ratio and structure of the ionic comonomers

The prepared copolymeric SAPs exhibited different degrees of crosslinking density, responding to the discrepancy in water absorbency and gel strength, although the content of MBA

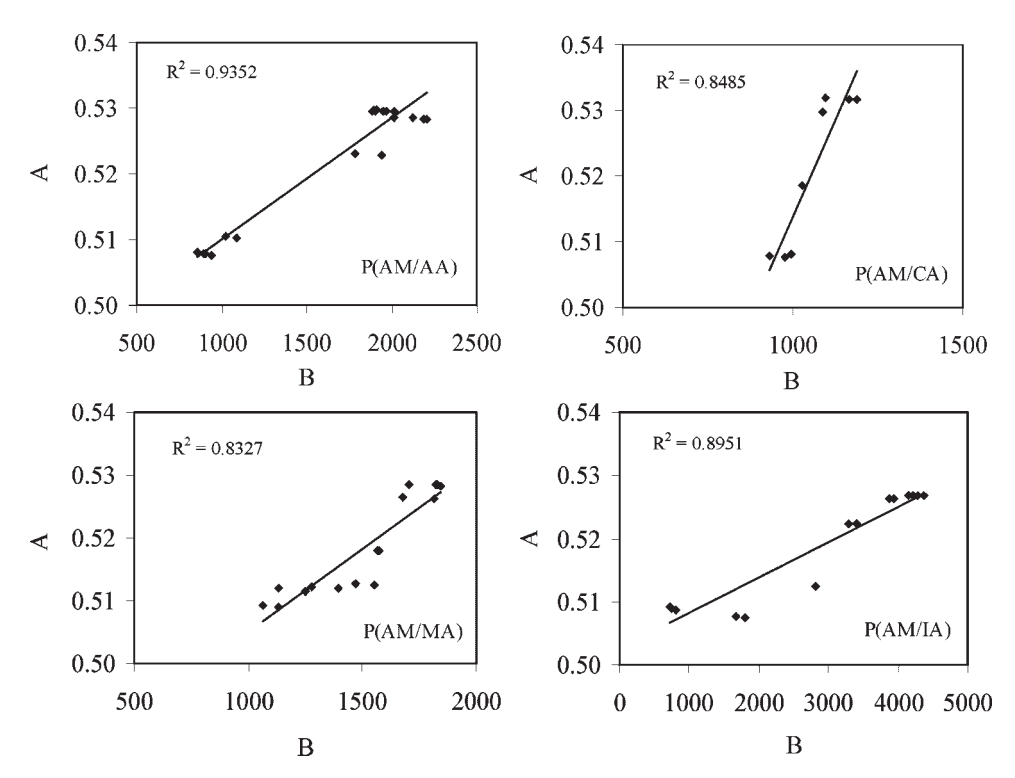


Figure 5. Determination of χ and \overline{M}_c values from the equilibrium swelling behaviors of copolymeric SAPs: P(AM/AA), P(AM/CA), P(AM/MA), and P(AM/IA). See the text for an explanation of A and B.



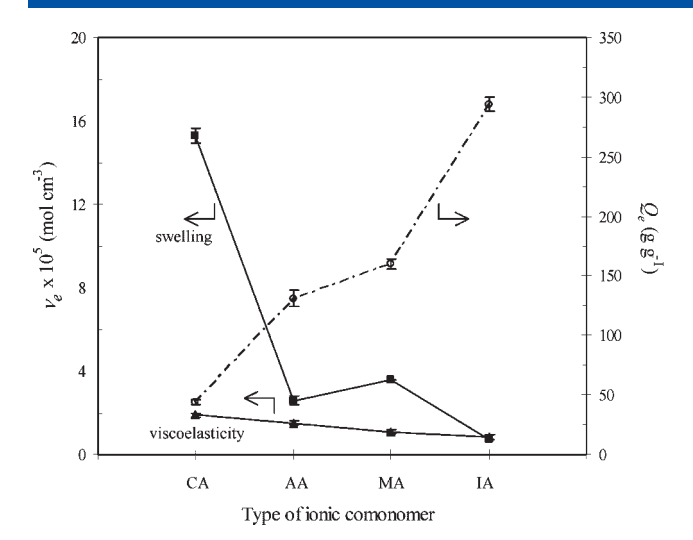


Figure 6. Effective crosslinking density (ν_e) and equilibrium water absorbency (Q_e) of polyacrylamide-SAPs containing various types of ionic comonomer.

crosslinker was equal in all preparations. Therefore, the type of ionic comonomer present in the SAP particles strongly influenced their network structure, which was discussed via the reactivity ratio and the structure of the employed ionic comonomers.

Acrylamide-based copolymer containing monoprotic acid monomer

Poly[acrylamide-co-(crotonic acid)]. In radical copolymerization, the monomer reactivity ratios (r) of a pair of monomers generally determine the distribution of each composition along the copolymer chain. It involves the reactivity of a monomer toward a radical. [46] For P(AM/CA), r_{AM} is 4.72–5.32 and r_{CA} is 0.11–0.12. [47] Due to its very low reactivity ratio, CA does not homopolymerize efficiently under these conditions. In a crosslinking copolymerization, the reactivity of the crosslinking agent MBA must also be considered, i.e. $r_{\rm AM}$ and $r_{\rm MBA}$ are 0.64 and 1.77, respectively. [33] The MBA has a high tendency to homopolymerize unless steric effects prevent its self-polymerization. Therefore, AM preferentially reacts with MBA to form a PAM crosslinked polymer. However, as mentioned previously, a high amount of MBA in the crosslinking reaction was used for cyclization and multiple crosslinking reactions.[30] In view of the extent of monomer reactivity and the relative concentration of all the components in the reaction, one may state that AM was crosslinked by MBA when the polymerization reaction was initially started but that as the AM and MBA were locally depleted, then CA was increasingly subsequently reacted to the growing radicals to yield an SAP with the CA moieties at the chain ends. [7] Thus, the obtained SAP might be in the form of the crosslinked AM/MBA at the center with peripherally-distributed CA chains. This is consistent with the observed poor swelling of the P(AM/CA)-SAPs and the large magnitude of G_e similar to that of PAM superabsorbents.

The low reactivity ratio of CA is due to the steric hindrance of the methyl group adjacent to vinyl group and the induction or resonance effects. The methyl group is an electron donating group which increases the electron density on the vinyl group and may facilitate its bonding to a cationic species. At the same time, the carboxylate anion in the carboxylic acid at the α carbon tends to ionize and delocalize between the carbon and oxygen atoms, facilitating the attack of an anionic species by decreasing the electron density on the carbon–carbon double bond. Due to the balance between the electron donating and withdrawing effects, CA could be effectively neutral and, without stringent requirements for the attacking of the π -bond, stabilization of the propagating radical species can take place. Thus, in this scenario the effect of steric hindrance is the dominant effect for radical chain polymerization, which limits the amount of CA distributed within the copolymer network, and the water absorption is restricted. Moreover, the hydrophobic nature of CA could limit the level of water absorption of the copolymer.

Poly[acrylamide-co-(acrylic acid)]. In comparison to P(AM/CA), a higher amount of AA incorporated within the copolymer network of P(AM/AA) is expected due to the higher reactivity ratio of AA than that of CA ($r_{\rm AM}$ is 1.08–1.34 and $r_{\rm AA}$ is 0.29–0.34). The higher amount of incorporated hydrophilic moieties will then create greater water absorption to P(AM/AA). Due to the high reactivity ratio of MBA, MBA will tend to incorporate into the polymer chain and can crosslink both AM and AA. This leads to a higher density of ionic components within the copolymer, and then the growing chains presume a more extended conformation resulting in the larger \overline{M}_{c} and, thus, the smaller ν_{e} .

Acrylamide-based copolymer containing diprotic acid monomer

Poly[acrylamide-co-(maleic acid)]. The reactivity ratios of the AM and MA pair have not been reported in the literature. However, as a result of its 1, 2-disubstituted vinyl structure, MA has low tendency to copolymerize. Yet, it is still much greater than its reactivity toward homopolymerization to such an extent that MA does not homopolymerize, [48] and the 1, 2-disubstituted vinyl monomer structure decreases its reactivity toward growing radicals due to steric hindrance. [46] However, in the presence of a monomer with a high polymerization tendency, such as AM, MA is randomly incorporated along the copolymer backbone, [49] which may account for the lower observed Q_e and the larger ν_e when compared to those seen with the P(AM/IA)-SAPs.

Poly[acrylamide-co-(itaconic acid)]. The IA contains a methylene group, connected to one carboxylic group, at the β carbon, whereas MA has no methylene group (Fig. 1). The presence of the methylene group renders a high reactivity ratio of IA, i.e. the r_{AM} is 0.48–0.88 and r_{IA} is 1.24–1.65. [47] Due to its significantly higher reactivity ratio over AM, IA has a larger tendency to incorporate into the growing polymer chains. As a result, IA might be incorporated as a block in the copolymer backbone. The presence of a higher density of negative charges from the carboxylic groups along the backbone can cause the growing chains to extend more than the system of P(AM/MA) due to the higher electrostatic repulsion. The more extended conformation normally lowers the tendency of growing radicals to cyclize, and to form crosslinked and multiple crosslinked branches during free-radical crosslinking copolymerization. Thus, a relatively low value of v_e was obtained.

Besides, Table 4 also shows the values of χ parameter determined via swelling experiments. The result shows that the obtained χ values of P(AM/AA)-, P(AM/MA)-, and P(AM/IA)-SAPs were close to that of crosslinked PAM (reported to be $0.48^{[23,24]}$



and 0.494^[25]); whereas the χ value of P(AM/CA)- SAPs was lower (0.401 $\pm\,0.004$). Note that χ is also used to analyze the polymer-solvent miscibility, where lower χ values represent a greater miscibility between the polymer and solvent. Flory stated that if χ < 0.5, then the polymer and solvent are completely miscible. The χ values of P(AM/AA)-, P(AM/MA)-, and P(AM/ IA)-SAPs were close to 0.5, which may suggest that those copolymers are likely to be miscible with their swelling medium, but cannot dissolve due to the presence of the crosslinked junctions. However, the still lower χ value of the P(AM/CA)-SAPs, which is less than 0.5, was neither matched by a complete dissolution of the SAPs in the swelling medium, nor a better miscibility with the medium over the other SAPs. Rather, it might result from the indifferent ability to absorb water at the various pHs of the SAPs. As shown in Fig. 2, the observed water absorbency of the P(AM/CA)-SAPs was somewhat pH-independent (over the pH range from 2 to 9), despite the presence of ionic groups from CA (p $K_a = 4.69$). The increase in water absorption of the P(AM/CA)-SAPs over that of PAM-SAPs is rather more likely to be due to the increase in hydrogen bonding between the carboxylic groups and water molecules at pH < p K_{a} . Since most CA may be located at the end of the crosslinked copolymer chains, or may be present as dangling chains, due to its very low reactivity (as discussed previously), the dissociation of its ionic groups (carboxylic groups) at pHs above its pK_a will not radically influence the swelling of the network. That is, the inclusion of CA at a 4% molar ratio did not effectively change the osmotic pressure exerted by the counterions in the network. In contrast, the addition of the other three ionic comonomers at the same molar ratio rapidly increased the water absorption of the systems (at pH > p K_a) as a consequence of the increased osmotic pressure due to the concentration difference between the counterions inside and outside of the SAPs. Therefore, the application of eqn (9), which includes the ionic contribution on swelling into the chemical potential of the system and the inclusion of ionic moieties into the system, to calculate χ and \overline{M}_c is not suitable for our P(AM/CA)-SAPs, which may result in the low value of χ and the large magnitude of v_e determined from the swelling experiments.

As a result, this study suggested that to enhance the water swelling capacity of the SAPs, an ionic comonomer is typically included in the polymerization system. However, a loss of the SAPs mechanical properties might be observed as a trade-off consequence. Experimental data from our findings reveal that if one needs to synthesize SAPs with good swelling and mechanical properties, it is essential to carefully consider the structure and hydrophilicity of the selected ionic comonomer since these parameters determine the distribution of the ionic comonomer in the SAPs system which controls the final desired properties, such as high swelling capacity, fast swelling rate, and sufficient gel strength for a particular application.

CONCLUSION

Four types of acrylamide-based SAPs, derived from two monoprotic acid monomers and two diprotic acid monomers, were synthesized at a fixed molar ratio of acrylamide to anionic comonomer of 96:4 under the same reaction conditions with APS, MBA, and TEMED at 1, 1, and 2% (w w⁻¹) of monomers, respectively. The SAPs were allowed to freely swell into an equilibrium state and the water absorbency was measured.

Viscoelastic behavior was determined in a system of closely packed swollen superabsorbent particles. SAPs containing diprotic acid predominantly influenced on the increased water absorbency. An increase in swelling capability led to a decrease in gel strength. Viscoelastic and swelling approaches in determining the network structure parameters provided the similar tendency in which the values of \overline{M}_c and ν_e of the prepared SAPs decreased with increase in the swelling capability. The postulations on these observations were elucidated from the reactivity ratios and hydrophilicity of the ionic comonomers.

Acknowledgements

The authors gratefully acknowledge the kind support from the Thailand Research Fund under the Research Scholar Team Consolidation Program Contract no. RTA5080004. Research facilities provided by the Imaging Polymer Laboratory of Chulalongkorn University's Department of Imaging and Printing Technology, Faculty of Science are gratefully acknowledged. The authors would like to thank the Publication Counseling Unit of the Research Division, Faculty of Science, Chulalongkorn University, for language suggestions.

REFERENCES

- D. Saraydin, S. Unver-Saraydin, E. Karadağ, E. Koptagel, O. Güven, Nucl. Instr. Meth. B 2004, 217, 281.
- [2] E. Karadağ, D. Saraydin, Y. Caldiran, O. Güven, Polym. Adv. Technol. 2000, 11, 59.
- [3] S. Duran, D. Solpan, O. Güven, Nucl. Instr. Meth. B 1999, 151, 196.
- [4] E. Karadağ, O. B. Uzüm, D. Saraydin, Eur. Polym. J. 2002, 38, 2133.
- [5] H. K. Can, B. Kirci, S. Kavalak, A. Güner, Radiat. Phys. Chem. 2003, 68, 811.
- [6] W. Jiraprasertkul, R. Nuisin, W. Jinsart, S. Kiatkamjornwong, J. Appl. Polym. Sci. 2006, 102, 2915.
- [7] D. Yiamsawas, W. Kangwansupamonkon, O. Chailapakul, S. Kiatkamjornwong, React. Funct. Polym. 2007, 67, 865.
- [8] S. Kiatkamjornwong, W. Chomsaksakul, M. Sonsuk, Radiat. Phys. Chem. 2000, 59, 413.
- [9] B. Taşdelen, N. Kayaman-Apohan, O. Güven, B. M. Baysal, Int. J. Pharm. 2004, 278, 343.
- [10] O. Okay, S. B. Sarıışık, Eur. Polym. J. 2000, 36, 393.
- [11] M. Ramazani-Harandi, M. Zohuriaan-Mehr, A. Yousefi, A. Ersha-d-Langroudi, K. Kabiri, Polym. Test. 2006, 25, 470.
- [12] G. M. Kavanagh, S. B. Ross-Murphy, Prog. Polym. Sci. 1998, 23, 533.
- [13] S. Gunasekaran, M. Mehmet Ak, Trends Food Sci. Tech. 2000, 11, 115.
- [14] J. A. Dean, Lange's Handbook of Chemistry (15th edn), McGraw-Hill, Inc., New York, 1999.
- [15] T. Çaykara, U. Bozkaya, O. Kantoğlu, J. Polym. Sci. Part B: Polym. Phys. 2003, 41, 1656.
- [16] M. Şen, A. Yakar, O. Güven, Polymer 1999, 40, 2969.
- [17] R. J. Keltz, R. K. Prud'homme, W. W. Graessely, Rheo. Acta 1988, 27, 531.
- [18] C. Raquois, J. F. Tassin, S. Rezaiguia, A. V. Gindre, Prog. Org. Coat. 1995, 26, 239.
- [19] I. Kaneda, A. Sogobe, Colloids Surf. A Physicochem. Eng. Asp. 2005, 270–271, 163.
- [20] G. Hild, Prog. Polym. Sci. 1998, 23, 1019.
- [21] T. Çaykara, İ. Akçakaya, Eur. Polym. J. 2006, 42, 1437.
- [22] J. E. Mark, B. Erman, Rubberlike Elasticity a Molecular Primer. Wiley, New York, 1988.
- [23] J. P. Baker, L. H. Hong, H. W. Blanch, J. M. Prausnitz, *Macromolecules* 1994, 27, 1446.
- [24] M. Y. Kizilay, O. Okay, Macromolecules 2003, 36, 6856.
- [25] J. Rosiak, K. Burczak, T. Zolozynzka, W. Pekala, *Radiat. Phys. Chem.* 1983, 22, 917.



- [26] N. Mahmudi, M. Şen, S. Rendevski, O. Güven, Nucl. Instr. Meth. B 2007,
- [27] P. J. Flory, Principles of Polymer Chemistry. Cornell University, Ithaca, NY, 1953.
- [28] H. H. Hooper, J. P. Baker, H. W. Blanch, J. M. Prausnitz, Macromolecules 1990, 23, 1096.
- [29] T. Çaykara, M. Doğmuş, Ö. Kantoğlu, J. Polym. Sci. Part B: Polym. Phys. **2004**, 42, 2586.
- [30] H. J. Naghash, O. Okay, J. Appl. Polym. Sci. **1996**, 60, 971.
- [31] E. A. Kuru, N. Orakdogen, O. Okay, *Eur. Polym. J.* **2007**, *43*, 2913.
 [32] H. Tobita, A. E. Hamielec, *Polymer* **1990**, *31*, 1546.
- [33] J. Baselga, M. A. Llorente, J. L. Nieto, I. Hernández-Fuentes, I. F. Piérola, Eur. Polym. J. 1988, 24, 161.
- [34] I. Yazici, O. Okay, Polymer 2005, 46, 2595.
- [35] S. Mallam, F. Horkay, A. M. Hecht, E. Geissler, Macromolecules 1989, 22, 3356.
- [36] Y. Cohen, O. Ramon, I. J. Kopelman, S. Mizraki, J. Polym. Sci. Polym. Phys. Ed. 1992, 30, 1055.

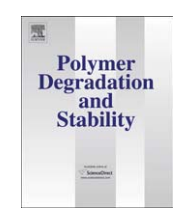
- [37] T. Norisuye, N. Masui, Y. Kida, D. Ikuta, E. Kokufuta, S. Ito, S. Panyukov, M. Shibayama, Polymer 2002, 43, 5289.
- [38] M. Y. Kizilay, O. Okay, Polymer 2003, 44, 5239.
- [39] M. Y. Kizilay, O. Okay, Polymer 2004, 45, 2567.
- [40] S. J. Candau, C. Y. Toung, T. Tanaka, P. Lemarechal, J. Bastide, J. Chem. Phys. 1979, 70, 4694.
- [41] P. N. Pusey, W. van Megen, Physica A 1989, 157, 705.
- [42] A. Onuki, J. Phys. II France 1992, 2, 45.
- [43] S. Panyukov, Y. Rabin, Phys. Rep. 1996, 269, 1.
- [44] S. Panyukov, Y. Rabin, Macromolecules 1996, 29, 7960.
- [45] Y. Rabin, S. Panyukov, *Macromolecules* **1997**, *30*, 301.
- [46] G. Odian, Principles of Polymerization (3rd edn), Wiley-Interscience, New Jersey, 2004.
- [47] R. J. Andrews, E. A. Grulke, Polymer Handbook, (Eds. A. Brundorf S. Immergut), John Wiley & Sons, New York, 1999.
- [48] P. Akkas, O. Güven, J. Appl. Polym. Sci. 2000, 78, 284.
- [49] D. Saraydin, E. Karadağ, O. Güven, Polym. Adv. Technol. 1995, 6,



Contents lists available at ScienceDirect

Polymer Degradation and Stability

journal homepage: www.elsevier.com/locate/polydegstab



Acrylamide/2-acrylamido-2-methylpropane sulfonic acid and associated sodium salt superabsorbent copolymer nanocomposites with mica as fire retardants

Nattawut Limparyoon a,1, Nispa Seetapan b,2, Suda Kiatkamjornwong c,*

- ^a Program of Petrochemistry and Polymer Science, Faculty of Science, Chulalongkorn University, Bangkok 10330, Thailand
- b National Metal and Materials Technology Center, 114 Thailand Science Park, Paholyothin Rd., Klong 1, Klong Luang, Pathumthani 12120, Thailand
- ^cDepartment of Printing and Imaging Technology, Faculty of Science, Chulalongkorn University, Bangkok 10330, Thailand

ARTICLE INFO

Article history: Received 28 November 2010 Received in revised form 15 March 2011 Accepted 27 March 2011 Available online 2 April 2011

Keywords:
Superabsorbent
Acrylamide
2-Acrylamido-2-methylpropane sulfonic
acid sodium salt
Mica
Nanocomposites
Cone calorimetry

ABSTRACT

Acrylamide (AM) and 2-acrylamido-2-methylpropane sulfonic acid (AMPS-H $^+$) or its sodium salt (AMPS-Na $^+$) were copolymerised by free-radical crosslinking polymerization to obtain poly(AM-co-AMPS-H $^+$) and poly(AM-co-AMPS-Na $^+$) superabsorbent polymers (SAPs). A maximum water absorbency in deionised water of 1200 g g $^-$ 1 was achieved for poly(AM-co-AMPS-Na $^+$) at a 85% mol of AMPS-Na $^+$. The inclusion of mica at 5–30% (w w $^-$ 1) into the preparation of poly(AM-co-AMPS-Na $^+$) SAP leads to an intercalated structure, as detected by XRD and TEM analyses. Poly(AM-co-AMPS-Na $^+$)/30% (w w $^-$ 1) mica SAP nanocomposite showed a tap water absorbency of 593 g g $^-$ 1 with a better thermal stability, compared to the pure SAP. Cone calorimetric analyses revealed that the wood specimens coated with the prepared poly(AM-co-AMPS-Na $^+$) SAP or its 30% (w w $^-$ 1) mica nanocomposite provided excellent protection in delaying the ignition time after exposure to an open flame when compared to that observed with the uncoated specimen. The maximum reduction in the peak heat release rate and the greatest extension of time at peak heat release rate were observed with the nanocomposite-coated surface, but the total heat release rate was increased. The delayed burning mechanism is brought by the intercalating structure of mica in the SAP nanocomposites, which provided a better shielding effect against external heat sources, and the capability of the SAP nanocomposite in holding a large amount of water.

© 2011 Elsevier Ltd. All rights reserved.

1. Introduction

Superabsorbent polymers (SAPs) are polymers that can absorb and retain water, saline solutions or physiological fluids up to several thousand times their dry weight. These properties correspond to the three-dimensional hydrophilic network structure of the polymers. Besides their hydrophilic nature, SAPs containing an ionic moiety have an enhanced water absorbency compared to non-ionic ones. This is due to the fact that the ionic groups in the copolymer network lead to an increase in electrostatic repulsive forces between charged sites along the copolymer chains and so a more extended copolymer network [1,2]. Several ionic vinyl monomers; i.e. acrylic acid, itaconic acid, and so forth, have been selected to copolymerise with a non-ionic hydrophilic monomer,

like acrylamide (AM), to prepare SAPs with a high degree of swelling [3–7]. The sodium salt form of the ionic monomer 2-acrylamido-2-methylpropane sulfonic acid (AMPS-H⁺), that is AMPS-Na⁺ has been of great interest in the past few years since the strongly ionisable sulfonate groups can totally dissociate in the overall pH range [1,8–15], resulting in copolymeric hydrogels with a pH-independent swelling behaviour. Based on their superior water swellable characteristics, SAPs have been widely used not only in the fields of personal care products, biosorbents and biomaterials [16], but also for agricultural soil [17], wastewater treatment [5,6,18-20] and other applications where water absorbency or water retention is important, including fire-fighting applications [21–24]. In this last scenario water is typically used to extinguish fires or to prevent combustible objects from burning by reducing the temperature of the combustible material below the burning temperature. However, when a fire is extinguished by spraying water onto it, less than about 10% of the water is generally effective in extinguishing the fire, due to the loss of the rest of the water, such as by run-off or pre-evaporation of the water away from the material surface. Therefore, SAPs have been proposed as a method to greatly improve the resistance to combustion of

^{*} Corresponding author. Tel.: +66 2218 5587; fax: +66 2255 3021. *E-mail addresses:* winny047@hotmail.com (N. Limparyoon), nispam@mtec.or.th
(N. Seetanan), ksuda@chula.ac.th, ksuda@sc.chula.ac.th (S. Kiatkamiornwong).

¹ Tel.: +66 2 594 1344.

² Tel.: +66 2 564 6500.

objects, or to prevent the penetration of extreme heat or fire to combustible materials. To prevent the spreading of fire, a sufficient amount of swollen SAP has to be sprayed onto the burnable objects to continuously coat their surface when nearby the burning fire. The mechanism of preventing the fire spreading is to cool the surface of the object and to reduce the quantity of oxygen from the surface of the burnable object to such a degree that the flame is extinguished [22]. However, SAPs are organic materials which lose their thermal stability when exposed to high temperatures. Typically, their structures are degraded to more than 50% of their original weight at 400 °C. Therefore, for fire-fighting applications, SAP nanocomposites with the inorganic fillers can be a promising system due to the ability to absorb a high amount of water together with the thermal stability provided by the added inorganic materials. Unlike the extensive studies on improving the fire-retardant properties of thermoplastics, thermosets and elastomers [25–29], the investigation of SAPs with enhanced thermal stability for firefighting applications is now drawing much more interest than before due to global warming and the need to preserve the environment [30].

Therefore, in this study, SAPs of AM and an ionic comonomer (AMPS-H⁺ or AMPS-Na⁺) with a high water swelling capacity were synthesized using free-radical crosslinking polymerization. AMPS-Na⁺ was selected as the ionic comonomer because of its strongly ionisable sulfonate groups. For comparison, the free acid form (AMPS-H⁺) was also employed to synthesize the network copolymer in order to investigate if the form of the ionic comonomer (either the salt or the acid) yielded SAPs with a higher swelling capability in water. The quantities of ionic comonomer, initiator, co-initiator and crosslinker, and the amount of reaction medium (water) on the water absorbency of the obtained poly(AM-co-AMPS-Na⁺) and poly(AM-co-AMPS-H⁺) SAPs were investigated. Furthermore, poly(AM-co-AMPS-Na⁺)/ mica nanocomposites were prepared in order to attempt to form SAP nanocomposites with an enhanced thermal stability, since polymer nanocomposites with various types of clay, such as attapulgite, kaolinite, mica, vermiculite and montmorillonite, have been reported to contribute remarkably improved thermal properties to the polymer matrix [31-34]. The range of mica content introduced into the poly(AM-co-AMPS-Na⁺) SAP matrix was varied from 0 to 30% w w^{-1} . The water absorbency capacity in both deionised and tap waters, and the morphology and thermal properties of the poly(AM-co-AMPS-Na⁺)/mica SAP nanocomposites were evaluated. Furthermore, the flammability of the prepared poly(AM-co-AMPS-Na⁺) SAP and its poly(AM-co-AMPS-Na⁺)/mica nanocomposite was examined using a cone calorimeter by coating these different types of SAPs on the wood specimen. All the data were then correlated to determine the poly(AM-co-AMPS-Na⁺)/mica SAP nanocomposite with the most suitable properties for inhibiting the spreading of fire.

2. Experimental

2.1. Materials

Acrylamide (AM) was gifted from Siam Chemical Industry Co., Ltd. (Bangkok, Thailand). 2-acrylamido-2-methylpropane sulfonic acid sodium salt (AMPS-Na⁺) and 2-acrylamido-2-methylpropane sulfonic acid (AMPS-H⁺) were purchased from Aldrich (Steinheim, Germany). The chemical structures of the monomers are shown in Fig. 1. *N,N'*-methylenebisacrylamide (N-MBA) and *N,N,N',N'*-tetramethylethylenediamine (TEMED) were received from Fluka (Buchs, Switzerland). Ammonium persulfate (APS) was from Ajax (Seven Hills, Australia). Swelling mica (industrial grade) was from Wako Pure Chemical Industries, Osaka, Japan. Deionised water (Elga

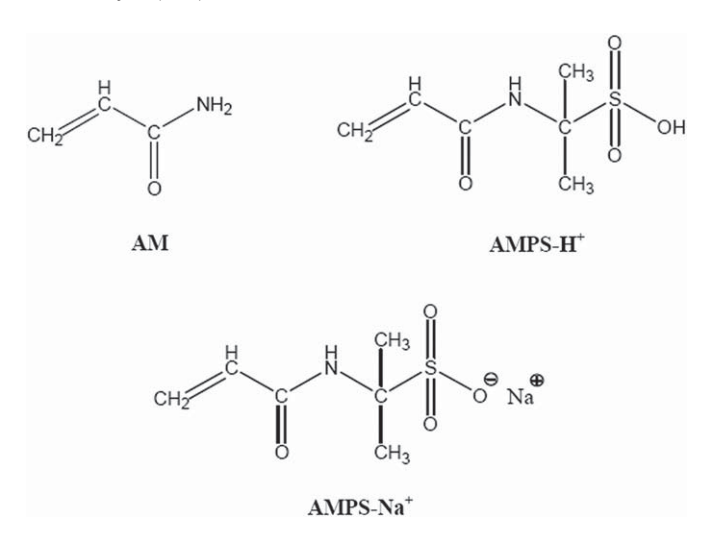


Fig. 1. Chemical structures of the monomers employed in polymerization: acrylamide (AM), 2-acrylamido-2-methylpropane sulfonic acid (AMPS-H⁺) and 2-acrylamido-2-methylpropane sulfonic acid sodium salt (AMPS-Na⁺).

Deionizer, Model LA611, U.K.) was used for the synthesis and the swelling experiment.

2.2. Preparation of poly(AM-co-AMPS- H^+) and poly(AM-co-AMPS- Na^+) SAPs and their mica-containing nanocomposites

Poly(AM-co-AMPS-Na⁺) and poly(AM-co-AMPS-H⁺) SAPs were prepared by free-radical crosslinking polymerization. The concentrations of APS (initiator), TEMED (co-initiator) and N-MBA (crosslinker) were selected at 1.2, 1.2 and 0.2% mol of the monomers, respectively. For the synthesis of copolymers, the molar ratio of AM:ionic comonomer was varied from 98:2 to 15:85. AM was dissolved in 20 cm³ of deionised water in a 1000-cm³ four-necked round-bottomed reactor equipped with a mechanical stirrer, a condenser and an inlet tube of nitrogen gas. The ionic comonomer (AMPS-Na⁺ or AMPS-H⁺) was added, and the mixture was stirred at room temperature for 5 min before being heated to 60 °C under a nitrogen atmosphere. N-MBA and APS were sequentially dissolved in 5 ml of deionised water, added to the mixture and stirred for 5 min. Finally, TEMED was added to the mixture and the reaction proceeded for 30 min to ensure complete polymerization. The product obtained was dewatered with acetone, dried, milled and then sieved through a 100-mesh sieve aluminium screen.

The amount of water, crosslinker, co-initiator and initiator present in the polymerization reaction was investigated in order to obtain the SAP with maximum water absorbency. Poly(AM-co-AMPS-Na⁺)/mica SAP nanocomposites were prepared using the same procedure as above but with the addition of the mica (ranging from 5 to 30% w w⁻¹) into the aqueous solution of monomers prior to the polymerization reaction.

2.3. Fourier Transform Infrared Spectroscopy (FT-IR)

The existence of the functional groups of the synthesized copolymers and the mica nanocomposites was confirmed by Fourier Transform Infrared Spectroscopy (FT-IR; System 2000, Perkin Elmer, U.S.A.). The dried sample and KBr powder were mixed, ground, pressed, and then subjected to the FT-IR spectrometry.

2.4. Water absorbency

The water absorbencies of the poly(AM-co-AMPS-Na⁺) and poly(AM-co-AMPS-H⁺) SAPs and the poly(AM-co-AMPS-Na⁺)/mica SAP nanocomposites were evaluated out in deionised and tap water at room temperature. Each 0.1 g portion of dry SAP was allowed to swell in 200 cm³ of deionised or tap water for 24 h. Subsequently, the fully swollen SAPs were separated from the unabsorbed medium by filtering through a 100-mesh sieve aluminium screen for 2 h and then weighed. The water absorbency at equilibrium (g g⁻¹) was calculated by Equation (1):

$$Water\ absorbency\ = \frac{weight\ of\ swollen\ gel-weight\ of\ dry\ gel}{weight\ of\ dry\ gel}$$

Swelling measurements were done in triplicate for each system to obtain the average and standard deviation of the water absorbency at equilibrium swelling.

2.5. Transmission electron microscopy (TEM)

Morphologies of the poly(AM-co-AMPS-Na⁺) SAP and its respective mica-containing SAP nanocomposite were characterized by transmission electron microscopy (TEM). The particles were dispersed in ethyl alcohol and the mixture was then sonicated for 5 min. The diluted suspension was then dropped onto a 300-mesh copper grid and left to dry in a controlled atmosphere. TEM micrographs of the samples were then obtained from the transmission electron microscopy (JOEL JEM-2100, Japan) at an acceleration voltage of 120 kV.

2.6. X-ray diffraction (XRD) analysis

X-ray diffraction (XRD) measurements were performed using an X-ray diffractometry (Bruker AXS Model D8 Discover, CuK α radiation, 40 kV, 40 mA, with $\lambda=0.15406$ nm and n=1) at a scanning range from 1 to 15° and a scanning rate of 0.5° min⁻¹. The interlayer spacings (d) of mica and poly(AM-co-AMPS-Na⁺)/mica SAP nanocomposites were calculated using Bragg's equation (Equation (2)):

$$n\lambda = 2d\sin\theta \tag{2}$$

where *d* is the interplanar distance of the (001) reflection plane, θ is the diffraction angle and λ is the wavelength.

2.7. Thermal stability analysis

The thermal properties of the poly(AM-co-AMPS-Na⁺) SAP and the poly(AM-co-AMPS-Na⁺)/mica SAP nanocomposites were investigated using a thermogravimetric analyzer (TGA/SDTA 851^e, Mettler Toledo Corporation, Switzerland). The measurements were carried out over a temperature range of 25–800 °C at a heating rate of 10 °C min⁻¹ and with a nitrogen flow rate of 60 cm³ min⁻¹. In addition, TGA under a zero air atmosphere at a flow rate of 60 cm³ min⁻¹ was examined as well.

2.8. Flammability test

Flammability analysis was evaluated using a cone calorimeter (Fire Testing Technology Ltd., UK), according to ISO 5660, at an incident heat flux (50 kW m^{-2}) in an air atmosphere, and under the free convective air flow condition. The SAPs were prepared in the form of an oil-in-water emulsion by adopting the procedure of Sortwell [35] as follows.

The dry poly(AM-co-AMPS-Na+)SAPs and their respective mica-containing SAP nanocomposites were dispersed at 40% w w⁻¹ in a mixture of 50% w w⁻¹ of palm oil and 10% w w⁻¹ of a non-ionic surfactant blend (54% w w⁻¹ of Tween 80 or polyoxyethylenesorbitan monooleate/46% w w⁻¹ of Span 80 or sorbitan (Z)-mono-9-octadecenoate), having a net hydrophilic/ lipophilic balance (HLB) value of 10. Then, a 5% v v⁻¹ of the poly(AM-co-AMPS-Na⁺) SAP or poly(AM-co-AMPS-Na⁺)/mica SAP nanocomposite suspension in the oil was dispersed in tap water, which resulted in the formation of a viscous slurry gel. This poly(AM-co-AMPS-Na⁺) SAP or poly(AM-co-AMPS-Na⁺)/mica SAP nanocomposite dispersion was then coated to give a 3-mm thickness layer on a $100 \times 100 \times 3 \text{ mm}^3 \text{ wood (Apocynaceae,})$ Wrightia religiosa Benth.) board surface. The surfaces of the SAPand mica-containing SAP nanocomposite-coated wood specimens were exposed directly to an open flame generated by a propane gas jet. The distance between the bottom surface of the cone heater and the specimen surface is adjusted to 25 mm. An uncoated wood board (from the same batch of wood as those coated) was used as the reference control. The time to ignition, time to burn through the coatings, and the heat release rate were recorded. The charred samples left from the experiments were captured by a digital camera after the specimen self-extinguished.

3. Results and discussion

3.1. Preparation and characterization of poly(AM-co-AMPS-H⁺) and poly(AM-co-AMPS-Na⁺) SAPs

3.1.1. Effect of acid and salt forms of the AMPS ionic monomer on the swelling behaviour in deionised water

Poly(AM-*co*-AMPS-H⁺) and poly(AM-*co*-AMPS-Na⁺) SAPs were synthesized by varying the molar ratios of AM:ionic comonomer (AMPS-H⁺ or AMPS-Na⁺) from 98:2 to 15:85 with the concentration of APS, TEMED and N-MBA fixed at 1.2, 1.2 and 0.2% mol, respectively. The presence of the functional groups of the SAPs was evaluated via FT-IR spectra (Fig. 2). Both spectra show a broad coupling peak of N–H and O–H stretching at around $3000-3500~\rm cm^{-1}$, peaks of C–H stretching of CH and CH₂ at around $2900-3000~\rm cm^{-1}$, a sharp peak of C=O stretching of the amide I at around $1663~\rm cm^{-1}$ (Fig. 2(a)) and $1664~\rm cm^{-1}$ (Fig. 2(b)) and a strong peak of the N–H bending of amide II at $1552~\rm cm^{-1}$ (Fig. 2(a)) and $1542~\rm cm^{-1}$ (Fig. 2(b)). The relative weak peaks at $1450~\rm cm^{-1}$

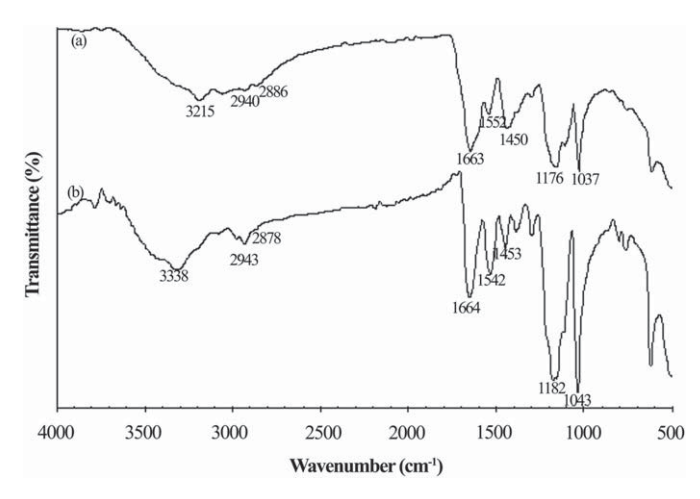


Fig. 2. Representative FT-IR spectra of the (a) poly(AM-co-AMPS-Na $^+$) and (b) poly(AM-co-AMPS-Na $^+$) SAPs prepared from a 20:80% mol AM: ionic comonomer with 1.2% mol of APS, 1.2% mol of TEMED and 0.2% mol of MBA.

(Fig. 2(a)) and 1453 cm⁻¹ (Fig. 2(b)) along with those at 1663 cm⁻¹ and 1664 cm⁻¹ are the symmetrical and asymmetrical $C(=O)_2$ stretching. Importantly, the sharp and strong peaks of the S=O stretching of AMPS-H⁺ and AMPS-Na⁺ at 1037 cm⁻¹ (Fig. 2(a)) [36] and 1043 cm⁻¹ (Fig. 2(b)) [1] were observed, respectively. Another two strong and sharp peaks at 1176 cm⁻¹ (Fig. 2(a)) and 1182 cm⁻¹ (Fig. 2(b)) arose from the C-C(=O)-O stretching. A relatively board and strong peak at 3338 cm⁻¹ in Fig. 2(b) is for the NH or the OH stretching of poly(AM-co-AMPS-Na⁺) where that for poly(AM-co-AMPS-H⁺) (Fig. 2(a)) becomes very board at 3215 cm⁻¹ because the OH group in the free acid superimposed the NH stretching of acrylamide moiety. Therefore, the SAP samples synthesized are poly(AM-co-AMPS-H⁺) and poly(AM-co-AMPS-Na⁺).

The water absorbency of the poly(AM-co-AMPS-Na⁺) SAP was found to increase sharply just over four-fold (from 60 to 244 g g⁻¹) when the content of AMPS-Na⁺ in the SAP was increased from 2 to 10% mol (Fig. 3(a)). Beyond this content, the water absorbency increased continuously but gradually until it reached 516 g g⁻¹ at 60% mol of AMPS-Na⁺. Further increases in the AMPS-Na⁺ content abruptly enhanced the water absorbency to a maximum of 986 \pm 31 g g⁻¹ at 85% mol of AMPS-Na⁺. The increase in water absorbency corresponded to the increase in the ionic group content (sulfonate groups) in the prepared SAPs. At 90% mol AMPS-Na⁺ gel formation could not be obtained but rather weak gel slurry was achieved instead.

By adopting the proposed model from Buchholz and Burgert [37], the mechanism of the swelling and water absorbency of the poly(AM-co-AMPS-Na⁺) SAPs can be postulated as follows. The SAP consists of many hydrophilic polymer chains with sulfonate groups and crosslinking points between the chains to prevent an infinite swelling. The dissociated sodium sulfonate groups increase the osmotic pressure inside the polymer, and the negative charges of sulfonate groups repel each other to expand the polymer coils, but are compensated for by the positive charges of the sodium salt to prevent an infinite expansion. When the polymer is in contact with water, water diffuses into the polymer network and solvates the sodium ions and the negatively charged sulfonates. The driving force for swelling is the difference between the osmotic pressure inside and outside the polymer membrane.

The water absorbency of poly(AM-*co*-AMPS-H⁺) SAP (Fig. 3(b)) also increased constantly with the content of AMPS-H⁺ up to 60% mol, but to a much less marked degree (1.81- to two-fold lower over the 10–60% mol range) than that of the poly(AM-*co*-AMPS-Na⁺) SAP (Fig. 3(a)) at the same mol % content of ionic comonomer.

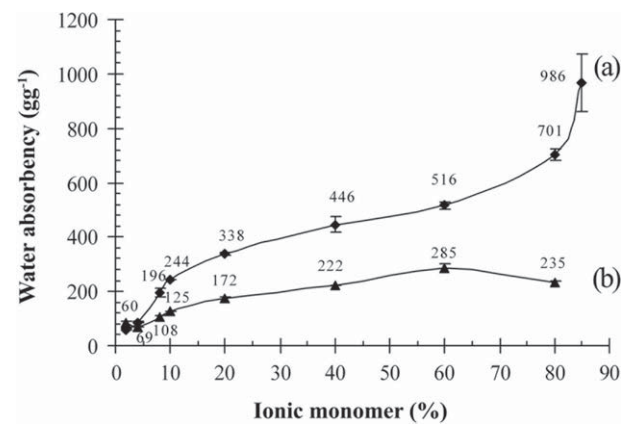


Fig. 3. Water absorbency of the (a) poly(AM-co-AMPS-Na⁺) and (b) poly(AM-co-AMPS-H⁺) SAPs as a function of the ionic comonomer contents (% mol). All SAPs were prepared using 1.2% mol of APS, 1.2% mol of TEMED and 0.2% mol of MBA.

The higher water absorbency of poly(AM-co-AMPS-Na⁺) can be explained by three attributes: 1) the presence of the salt form (AMPS-Na⁺) yielded a higher difference in the ionic osmotic pressures between the hydrogel and the swelling medium (water); 2) the larger Na⁺ ions trapped in the SAP can induce the copolymer chain between crosslinking points to presume a more extended conformation; and 3) the strong acidity of AMPS-H⁺ might induce a chain scission reaction [38] in the copolymer, as observed from the developed yellowish colour in the product attributed by the increased in AMPS-H⁺ content.

3.1.2. Effect of the initial degree of monomer dilution and the crosslinker content on the swelling behaviour in deionised water of poly(AM-co-AMPS-Na⁺) SAP

In solution polymerization, the initial degree of dilution of the monomers has been shown to strongly influence the obtained hydrogel structure and properties [39–42]. As the water present in the polymerization increases, the network structure becomes increasingly loose. Since this is especially the case when using ionic monomers, then SAPs were prepared with 85% mol of the AMPS-Na⁺ ionic monomer rather than the AMPS-H⁺ form, using both 10 and 40 ml of water reaction volume, and a crosslinker (N-MBA) content of 0.05, 0.10 or 0.20% mol. The water absorbencies of the poly(AM-co-AMPS-Na⁺) SAPs obtained from these preparations are reported in Table 1, where it was clear that increasing the N-MBA content in the SAPs formed in a 10-ml reaction volume system led to a significant decrease in the water absorbency (1.35- and 2.77fold as the N-MBA was increased from 0.05 to 0.1 and 0.2% mol, respectively). This is likely to be due to the increase in the crosslinking density that will then restrict the movement of the copolymer chains and limit the swelling capability of the SAPs. When the polymerization reaction was performed in 40 ml water, gel formation could not be achieved at the two lower N-MBA concentrations (0.05 and 0.10% mol) indicating that the continuous network could not be formed with this amount of water in the polymerization reaction [43].

3.1.3. Effect of the co-initiator and the initiator concentrations on the swelling behaviour of poly(AM-co-AMPS-Na $^+$) SAPs in deionised water

In a redox polymerization, an oxidant and a reductant pair is generally used to generate one radical and a cation and anion pair as the reaction by-product. The use of APS and TEMED is an example of an oxidation—reduction reaction to produce radicals that can initiate polymerization. The APS oxidant needs to receive an electron from a reductant to start the radical initiation reaction.

The effect of varying the TEMED content (0.6—1.8% mol) on the water absorbency of the formed poly(AM-co-AMPS-Na⁺) SAPs is shown in Table 2. The water absorbency of the poly(AM-co-AMPS-Na⁺) SAPs increased as the co-initiator concentration was increased up to 1.2% mol, with then no significant further increase in the

Table 1Water absorbency of the poly(AM-co-AMPS-Na⁺) SAP^a as a function of the amount of water present in the polymerization reaction and the amount of N-MBA crosslinker.

	Amount of water (ml)	Amount of N-MBA (% mol)	Water absorbency (g g^{-1})
_	10	0.05	1006 ± 95
		0.10	746 ± 26
		0.20	399 ± 31
	40	0.05	No gel formation
		0.10	No gel formation
		0.20	986 ± 31

 $^{^{\}rm a}$ AM: AMPS-Na $^{\rm +}$ of 15:85% mol, 1.2% mol of APS and 1.2% mol of TEMED.

Table 2Water absorbency of the poly(AM-co-AMPS-Na⁺) SAPs^a as a function of the amount of reactants.

Amount of re	eactants (% mol)	Water absorbency (g g ⁻¹)		
N-MBA	TEMED	APS		
0.10	0.6 0.9 1.2 1.8	1.2	580 ± 13 573 ± 12 746 ± 26 738 ± 23	
0.05	0.6 0.9 1.2 1.8	1.2	981 ± 8 983 ± 21 1006 ± 95 No gel formation	
0.05	0.6	0.6 1.2 1.8	$\begin{array}{c} 1212 \pm 54 \\ 981 \pm 8 \\ 797 \pm 85 \end{array}$	

^a AM: AMPS-Na⁺ of 15:85% mol in 10 ml of water as the reaction medium.

water absorbency as the TEMED concentration increased further to 1.8% mol. Since TEMED is the co-initiator or starter to induce the decomposition of the APS initiator, then at low TEMED concentrations the concentration of activated TEMED molecules is not enough to produce hydroxyl radicals. Thus, long polymer chains are not produced, resulting in the low water absorbency. In contrast, at high TEMED concentrations, short polymer chains were produced which could recombine to create many long-chains polymers, thus providing the high water absorbency. In addition, TEMED is a strong base so it may hydrolyze or neutralize the sulfonate groups to enhance water absorbency.

The effect of the APS initiator concentration on the water absorbency of the resultant poly(AM-co-AMPS-Na⁺) SAPs is shown in Table 2, where increasing the APS concentration from 0.6% to 1.2 and 1.8% mol led to a significant decrease (1.23- and 1.52-fold) in the equilibrium water absorbency. At a low APS concentration, a few radicals were generated allowing the polymer chain to propagate into long chains and so a large amount of water was absorbed into the SAP. In contrast, at high APS concentrations too many radicals were generated resulting in short polymer chains being produced and so the poly(AM-co-AMPS-Na⁺) SAP formed cannot swell to such a large extent.

3.2. Preparation and characterization of poly(AM-co-AMPS-Na⁺)/mica SAP nanocomposite

3.2.1. Water absorbency measurement in deionised water and tap water

The results from the previous section revealed the maximum water absorbency in deionised water of 1212 g g⁻¹ was attained from SAPs synthesized from a 15:85% mol ratio of AM:AMPS-Na⁺ in the presence of 10 ml of reaction medium (water), and with 0.6% mol of APS, 0.6% mol of TEMED and 0.05% mol of N-MBA. Thus, poly(AM-co-AMPS-Na⁺)/mica SAP nanocomposites were prepared as above except with mica loadings from 0 to 30% w w⁻¹ in order to evaluate any enhanced thermal stability that was afforded by the inclusion of mica into the prepared SAPs for the fire-retardant applications whilst maintaining their high water absorbency. The functional groups of the prepared nanocomposites investigated via FT-IR spectra are shown in Fig. 4. A strong peak of Si-O stretching at 972 cm⁻¹ and a sharp peak of Al–O stretching at 694 cm⁻¹ were evident in the pristine mica [44]. The spectra of the poly(AM-co-AMPS-Na⁺)/mica SAP nanocomposites show the overlapped broad peak of N-H stretching and O-H stretching at 3418 cm⁻¹ and 3307 cm⁻¹, the strong peak of C=O stretching of amide I at 1641 cm⁻¹ [45], the strong peak of the N–H bending of amide II at

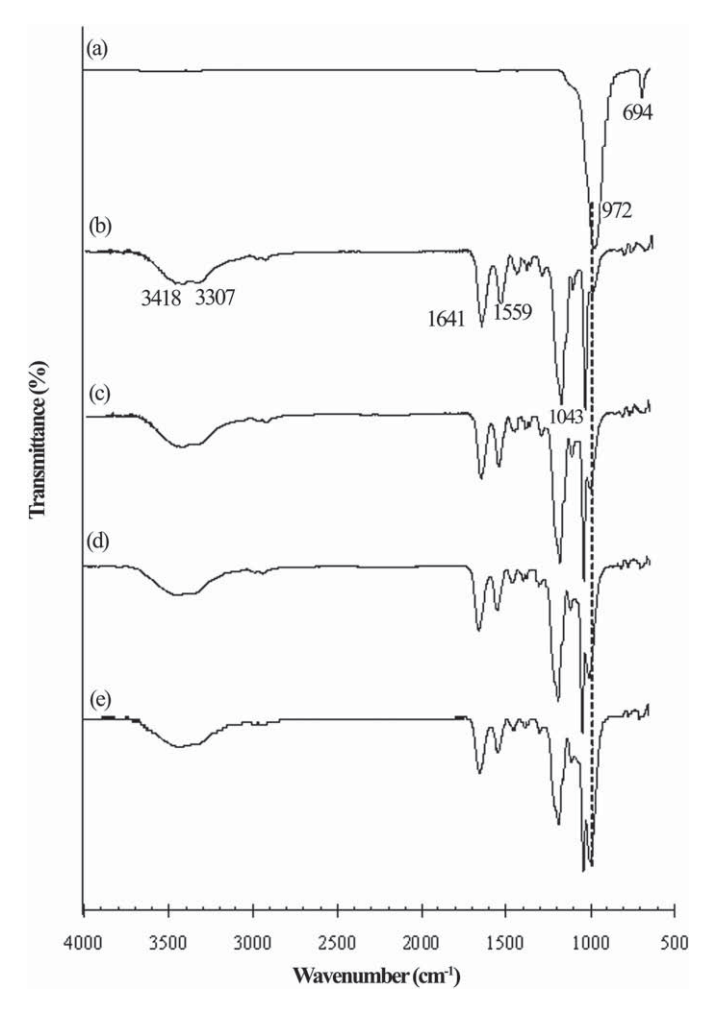


Fig. 4. Representative FT-IR spectra of (a) pristine mica, and poly(AM-co-AMPS-Na $^+$)/mica nanocomposites with mica contents of (b) 5%, (c) 10%, (d) 20% and (e) 30% w w $^{-1}$. All SAPs were prepared from a AM: ionic comonomer of 15:85% mol, 0.6% mol of APS, 0.6% mol of TEMED and 0.05% mol of MBA.

1559 cm⁻¹, the sharp peak of the S=O group of AMPS-Na⁺ at 1043 cm⁻¹ [1], and a characteristic peak of the Si–O stretching at 972 cm⁻¹ that increases in peak area in relationship to the amount of mica loaded in the synthesized nanocomposites. The results indicated that the resulting products were the desired poly(AM-co-AMPS-Na⁺)/mica SAP nanocomposites.

The water absorbency capacities in deionised and tap waters of the poly(AM-co-AMPS-Na+)/mica SAP nanocomposites with different mica loadings are shown in Fig. 5. In all cases the water absorbency level in tap water was lower than that in the deionised water, due to the presence of several major cations, such as Fe³⁺ (7.2 ppm), Ca²⁺ (27.2 ppm) and Mg²⁺ (0.05 ppm), provided by the Metropolitan Waterworks Authority. These cations cause a decrease in the gel expansion because the repulsive forces of the anionic groups along the polymer chains were shielded by the bound ionic charges. Therefore, the difference in osmotic pressure between the gel network and the external solution decreases as the quantity of the cations in the swelling medium increases. Note, however, that this difference between the swelling level in deionised and tap water becomes less marked with the inclusion of increasing mica levels in the poly(AM-co-AMPS-Na⁺)/mica nanocomposite. In addition, the water absorbency decreased with increasing mica content, showing a pronounced reduction in water absorbency (1.46- and 1.12-fold in deionised and tap waters,

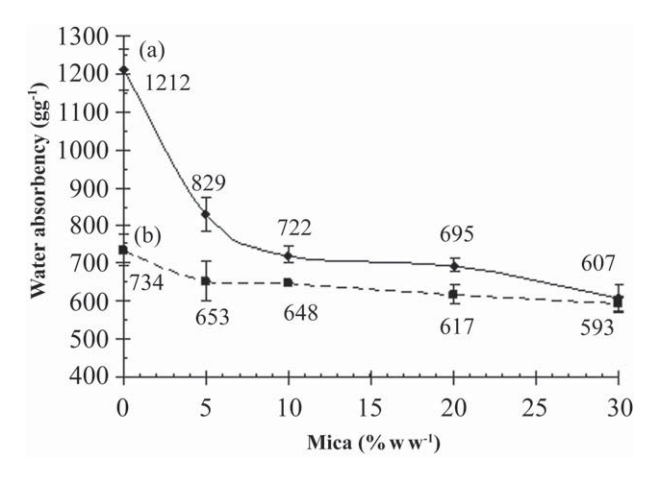


Fig. 5. Water absorbency of the poly(AM-co-AMPS-Na⁺) SAP and poly(AM-co-AMPS-Na⁺)/mica SAP nanocomposites in (a) deionised water and (b) tap water as a function of the mica loading levels. SAPs were prepared using 15:85% mol AM:AMPS-Na⁺ with 0.6% mol of APS, 0.6% mol of TEMED and 0.05% mol of MBA in 10 ml of water.

respectively) when 5% (w w $^{-1}$) of mica was added into the neat SAP. Beyond this value, a steady but slight reduction in the water swelling was observed with increasing mica levels. The presence of mica in the poly(AM-co-AMPS-Na $^+$)/mica SAP nanocomposites acts as a physical crosslink junction within the composite in which the polymer chain intercalated within the layers of mica. Thus, the water absorbency reduces proportionally to the content of mica [34].

3.2.2. XRD and TEM analyses

The intercalated structures of the prepared poly(AM-co-AMPS-Na $^+$)/mica SAP nanocomposites were investigated via XRD and TEM analyses. XRD patterns provide useful information related to the variation in the basal (001) d-spacing of the final nanocomposites and representative diffractograms are shown in Fig. 6. The measured d_{001} of mica is 12.4 Å (2 θ = 7.2°) and the mica composites at 5, 10, 20 and 30% w w $^{-1}$ of mica have a d_{001} spacing at 13.9, 13.9, 13.7 and 13.1 Å, corresponding to the peaks of 2 θ at 6.4, 6.4, 6.5 and 6.6°, respectively. Thus, the in-situ intercalated nature of the mica within the polymerised poly(AM-co-AMPS-Na $^+$)/mica

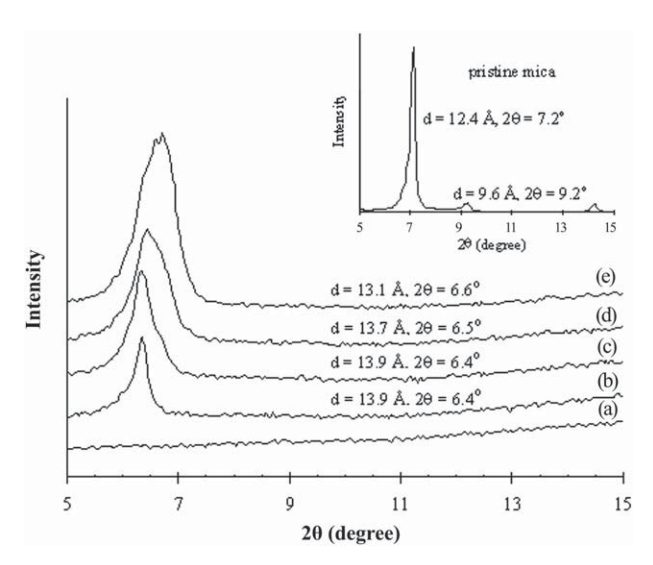


Fig. 6. Representative XRD patterns of poly(AM-co-AMPS-Na $^+$)/mica SAP nanocomposites as a function of the mica loadings for (a): 0%, (b): 5%, (c): 10%, (d): 20% and (e): 30%. The inset shows the XRD pattern of pristine mica.

SAP nanocomposite is revealed. In addition, a slight increase in the value of 2θ was observed with increasing mica contents representing a decrease in the distance between the interlayers of mica.

TEM micrographs (Fig. 7) support the intercalated poly(AM-co-AMPS-Na⁺)/mica SAP nanocomposite structure obtained from the XRD data. The dark cross lines indicate the parts of the polymer intercalated into the interlayer spacing of mica. The thickness of the cross lines is approximately 1 nm, corresponding to the typical thickness of the clay layers, whereas the distance between the cross lines are interlayer spaces and the grey bases are the polymer matrix. These micrographs demonstrate that mica particles are dispersed at the nanometer level in the SAP matrix. The interlayer distance of mica in the nanocomposites obtained from the TEM micrographs is approximately 13 Å, correlating well with the interlayer spacing characterized by XRD analysis.

3.2.3. Thermal gravimetric analysis (TGA)

The thermal stability of the poly(AM-co-AMPS-Na⁺)/mica SAP nanocomposites and the pristine mica was evaluated using TGA under a nitrogen atmosphere, with representative thermograms shown in Fig. 8(a). Pure mica had a single degradation stage at 68-87 °C with a weight loss of 7.3%, which was the loss of the moisture retained in the mica. Thermograms of poly(AM-co-AMPS-Na⁺)/mica SAP nanocomposites at mica loadings of 10, 20 and 30% w w⁻¹ are similar to the thermal decomposition of poly(AMco-AMPS-Na⁺) SAPs without mica in that the four similar stages of decomposition are seen. The first stage of degradation takes place in the range of 40-125 °C and corresponds to the absorbed and bound water. The second sharp degradation stage, in the range of 307–329 °C, is ascribed to the amide side group of the AMPS-Na⁺. The third stage, in the range of 329-413 °C, is interpreted as the amide side group of AM and the crosslinker. The final stage in the range of 450-800 °C is assigned to the thermal degradation of the backbone chain [32].

From these TGA thermograms, the temperature at which a 50% weight loss occurs was found to increase from 380 to 415 °C as the mica loading increased from 0 to 30% w w⁻¹. The thermal stability of the nanocomposites and the amount of residue at 800 °C increased as the amount of mica present in the systems increased. This improvement in the thermal stability of the nanocomposites could be attributed to the pronounced thermal stability of mica and to the interaction between the mica particles and the polymer matrix [46]. By calculating the amount of residues left at 800 °C from the thermograms, 70% by weight of the mica was retained in the SAP nanocomposites regardless of the mica content loaded. Thus, the remaining amount of mica (~30%) was not incorporated into the SAPs and was removed during the precipitation process.

Prior to the flammability analysis, the thermal stability under air of poly(AM-co-AMPS-Na⁺) SAP and its 30% w w⁻¹ mica-containing nanocomposite was examined as a model system to represent the thermal degradation of the materials exposed to a normal air atmosphere. TGA analysis under an air atmosphere shows a significantly increased temperature at which a 50% weight loss was attained $(340-480 \, ^{\circ}\text{C} \text{ as the mica level increases from 0 to } 30\% \, \text{w} \, \text{w}^{-1})$ (Fig. 8(b)) and residual weight content of the char residue (36% in comparison to the 20% weight of residue from poly(AM-co-AMPS-Na⁺)) at 800 °C. DTG thermograms (Fig. 8(c)) revealed similar thermal decomposition stages for the poly(AM-co-AMPS-Na⁺) SAP and its mica-containing nanocomposite. The first stage of degradation is from the loss of absorbed and bound water at 90-100 °C. The second stage, where the maximum weight loss rate was detected at 330 °C, corresponds to degradation of the amide side chain. The third degradation stage occurs at 580 °C and corresponds to the main chain pyrolysis. Therefore, these results confirm that mica inclusion led to an improved thermal stability for the poly(AM-co-AMPS-Na⁺)/mica

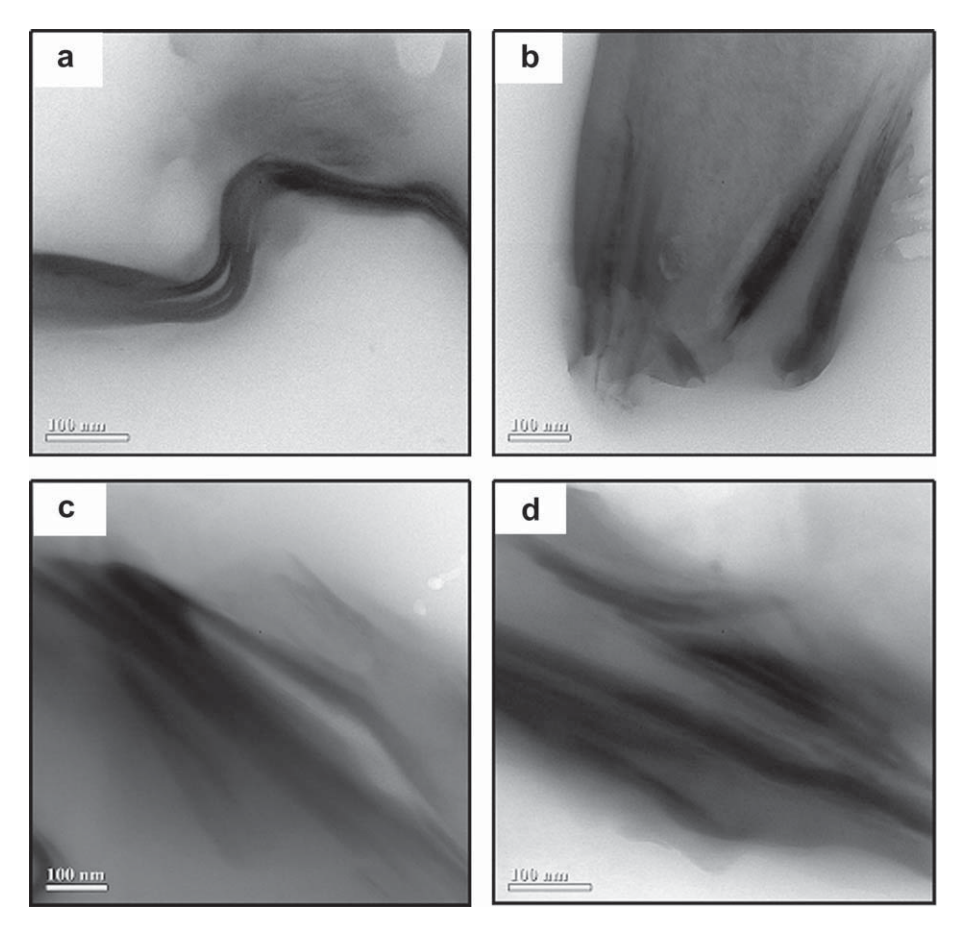


Fig. 7. Representative TEM micrographs of poly(AM-co-AMPS-Na⁺)/mica SAP nanocomposites with mica loading levels of 5, 10, 20 and 30% w w⁻¹ for a,b,c and d, respectively.

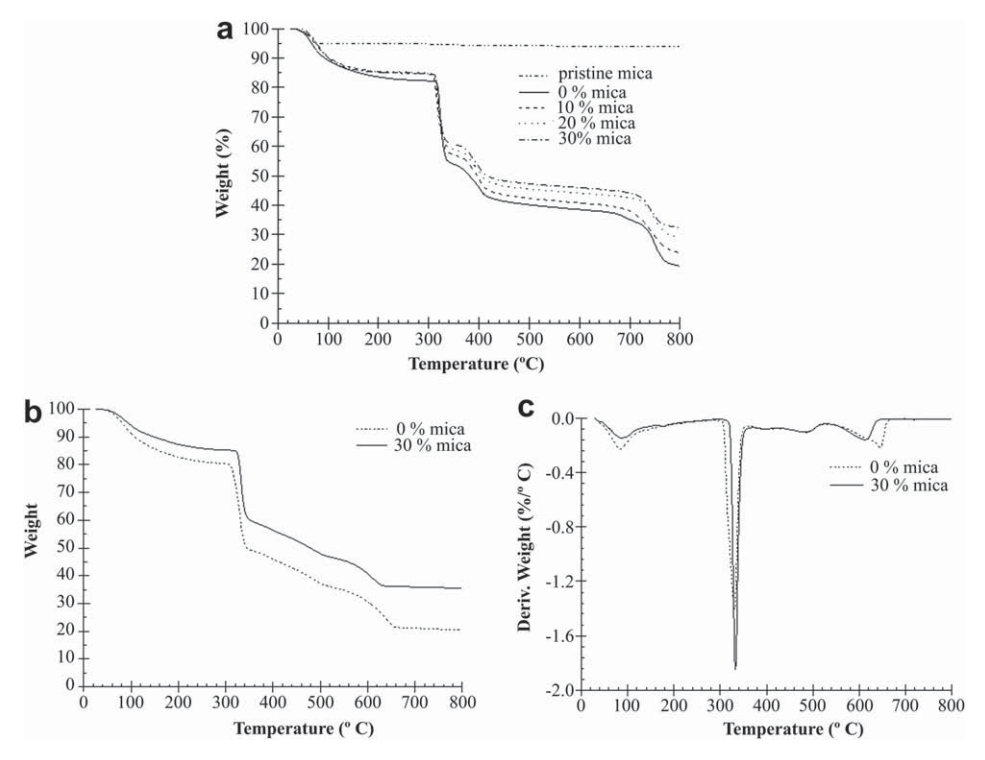


Fig. 8. Representative TGA thermograms, obtained under a N_2 atmosphere, of (a) poly(AM-co-AMPS-Na⁺)/mica SAP nanocomposites at various mica loadings (0–30% w w⁻¹), shown in comparison with that for pristine mica; (b) TGA and (c) DTG thermograms, obtained under a zero air atmosphere, of poly(AM-co-AMPS-Na⁺) SAPs and poly(AM-co-AMPS-Na⁺)/30% w w⁻¹ mica SAP nanocomposites.

Table 3Cone calorimetric data for the uncoated, mica-free and 30% w w⁻¹ mica-containing SAP-coated wood specimens.

Specimen	Time to ignition (s)	Time to burn the coated gel ^a (s)	Peak HRR (kW m^{-2})	Time at peak HRR (s)	Total HRR (MJ $\rm m^{-2}$)
Uncoated wood	13 ± 2	_	309	79	22
SAP-coated wood	125 ± 2	4 ± 2	222	224	26
SAP/30% mica-coated wood	186 ± 3	84 ± 6	213	302	25

^a Time to burn the coated gel was measured after sample ignition.

SAP nanocomposites at all temperature ranges because the mica acts as a heat barrier to delay the diffusion of volatile thermo-oxidation products to gas, and the escape of gas from the nanocomposite [34,47].

3.2.4. Flammability analysis

Cone calorimetric analyses were investigated for the poly(AM-co-AMPS-Na $^+$)/30% w w $^-$ 1 mica SAP nanocomposite-coated wood surface due to its superior thermal stability among the other poly(AM-co-AMPS-Na $^+$)/mica SAP nanocomposites studied. Poly(AM-co-AMPS-Na $^+$) SAP-coated wood and uncoated wood specimens from the same wood batch were used as controls. The flammability characterization was carried out at an incident heat flux of 50 kW m $^{-2}$, in an air atmosphere with a flame temperature of 885 °C. After being exposed to the direct flame, the time to ignition of each specimen was fast for the uncoated wood board (13 s), but was about ten-fold longer for the poly(AM-co-AMPS-Na $^+$) SAP-coated specimens, illustrating the excellent protection in delaying the ignition time after exposing to an open flame (Table 3).

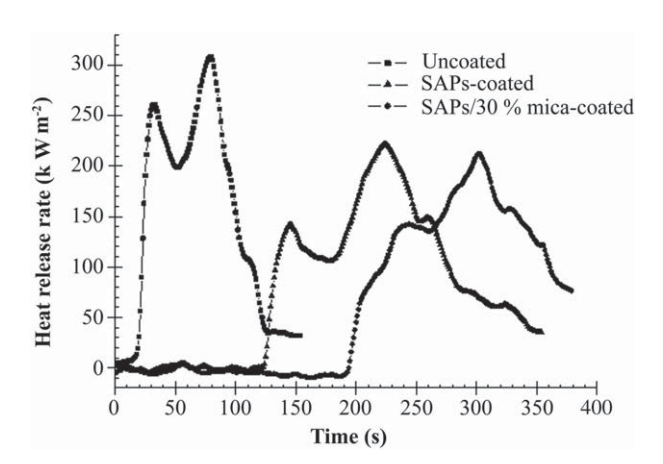


Fig. 9. Representative heat release rate per burning surface area of the uncoated, the poly(AM-co-AMPS-Na $^+$) SAP-coated, and the poly(AM-co-AMPS-Na $^+$)/30% w w $^{-1}$ mica SAP nanocomposite-coated wood boards.

Moreover, the presence of 30% w w⁻¹ mica significantly enhanced the thermal barrier, retarded the diffusion of heat and slowed down the burning, as observed from the longer time to ignition (1.49- and 14.31-fold longer than the mica-free SAP treated and untreated wood, respectively) and the 21-fold longer time to burn the coated gel (Table 3).

Heat release is defined as the heat generated due to various chemical reactions when a material is exposed to fire, and provides information on the size of the fire and hence the corresponding fire hazard [26]. Materials with a low heat release rate gives less damage to the surroundings than those with high heat release rate. Thus, the heat release rate, particularly the peak value, is the primary characteristic in determining the size, growth and suppression requirements of a fire environment [48]. A 1.39-fold reduced peak heat release rate per unit of burning surface (PHRR) and a 2.83-fold prolonged time at the PHRR (t_{PHRR}) were found in the poly(AM-co-AMPS-Na⁺) SAP-coated specimens compared to the uncoated one (Table 3 and Fig. 9), which might be attributed by the cooling effect of water trapped within the SAP particles and the formation of chars covering on the surface of the coated specimens. The inclusion of 30% w w^{-1} mica into the poly(AM-co-AMPS-Na⁺)/ mica SAP nanocomposite slightly decreased further (1.04-fold) the PHRR and markedly increased (1.35-fold) the t_{PHRR} over that seen with the mica-free poly(AM-co-AMPS-Na⁺) SAP alone. This enhanced slow burning process is brought by the formation of clay barrier, which provided a better shielding effect against external heat sources, as well as the capability of the SAP nanocomposite in holding a large amount of water.

However, when considering the total heat release rate (THRR) defined as a total heat at the end of burning. As mentioned in this study, the combustion experiment was performed until flame was self-extinguished. It was found that, for the uncoated specimen, the observed THRR of 22 MJ m⁻² was obtained from the combustion of the wood itself. Flame eventually extinguished because the entire wood specimen was completely burnt out. When comparing with the uncoated wood surface, it is interesting to mention that THRR values of the mica-free and mica-added poly(AM-co-AMPS-Na⁺) SAPs-coated specimens were found increased to 26 MJ m⁻² and 25 MJ m⁻², respectively. The explanation could be from the fact that the neat SAP and the SAP/mica nanocomposite are both fuels which







Fig. 10. Representative optical photographs of the charred specimens of (a) the uncoated wood, (b) poly(AM-co-AMPS-Na⁺) SAP-coated wood and (c) poly(AM-co-AMPS-Na⁺)/30% w w⁻¹ mica SAP nanocomposite-coated wood.

finally combusted under heat, consecutively with the burnout of wood to cause an increased THRR as compared to the uncoated wood surface. This means that both coated specimens can only delay the fire ignition, reduce PHRR and increase time at PHRR, but do not reduce THRR. This observation has been previously observed for polymer/clay nanocomposite where HRR is significantly reduced in the nanocomposite, but THRR remains unaffected [49] or increased [50].

Fig. 10 shows the char characteristics after the flame was self-extinguished. The uncoated wood gave a dark grey char, whereas the chars of the wood boards coated with the mica-free poly(AM-co-AMPS-Na $^+$)/SAPs are white and those coated with the poly(AM-co-AMPS-Na $^+$)/30% w w $^{-1}$ nanocomposite are black lump char. Furthermore, the maximum reduction in PHRR and the greatest extension of $t_{\rm PHRR}$ were observed in the poly(AM-co-AMPS-Na $^+$)/mica SAP nanocomposite-coated surface, possibly due to the intercalating structure of the mica in the nanocomposite providing a better barrier against external heat [51].

4. Conclusions

Poly(AM-co-AMPS-Na⁺) and poly(AM-co-AMPS-H⁺) SAPs were synthesized by free-radical crosslinking polymerization. The water absorbency of poly(AM-co-AMPS-H⁺) was lower than that of poly(AM-co-AMPS-Na⁺), presumably because the strong acidity of the AMPS-H⁺ monomer resulted in a chain scission reaction in the SAP. Poly(AM-co-AMPS-Na⁺)/mica SAP nanocomposite at 30% w w⁻¹ mica showed a tap water absorbency of 593 g g⁻¹ and a better thermal stability compared to the pure poly(AM-co-AMPS-Na⁺) SAP. The emulsions of the swollen poly(AM-co-AMPS-Na⁺) SAP and its 30% w w⁻¹ mica-containing nanocomposite were made by mixing with vegetable oil and surfactant, and subsequently were coated on the wood specimens. Flammability analysis revealed that both coated wood specimens showed an excellent reduction in the peak heat release rate, and prolonged the time at peak heat release rate. However, the total heat release rate was found increased. This might be from the fact that poly(AM-co-AMPS-Na⁺) SAP and its mica nanocomposite are both fuels, which finally combusted under heat.

Acknowledgements

The authors are indebted for the full financial support from the Thailand Research Fund under the Research Team Aided Program Contract no. RTA5080004. The provision of research facilities by the Imaging Polymer Laboratory of Chulalongkorn University's Department of Imaging and Printing Technology, Faculty of Science is highly acknowledged. Cone Calorimetric experiment provided by the Department of Civil Engineering, Faculty of Engineering, Chulalongkorn University, and English edition of the manuscript by the Publication Counsellor Unit of the Research Division, Faculty of Science, Chulalongkorn University, are highly appreciated. The authors thank Siam Chemical Industry Co., Ltd., for donating acrylamide monomer for the research.

References

- Durmaz S, Okay O. Acrylamide/2-acrylamido-2-methylpropane sulfonic acid sodium salt-based hydrogels: synthesis and characterization. Polymer 2000; 41:3693-704.
- [2] Kiatkamjornwong S, Chomsaksakul W, Sonsuk M. Radiation modification of water absorption of cassava starch by acrylic acid/acrylamide. Radiat Phys Chem 2000;59:413–27.
- [3] Okay O, Sarıışık SB. Swelling behaviour of poly(acrylamide-co-sodium acrylate) hydrogels in aqueous salt solutions: theory versus experiments. Eur Polym J 2000;36:393–9.

- [4] Taşdelen B, Kayaman-Apohan N, Güven O, Baysal BM. Preparation of poly(N-isopropylacrylamide/itaconic acid) copolymeric hydrogels and their drug release behaviour. Int J Pharm 2004;278:343—51.
- [5] Jiraprasertkul W, Nuisin R, Jinsart W, Kiatkamjornwong S. Synthesis and characterization of cassava starch graft poly(acrylic acid) and poly[(acrylic acid)-co-acrylamide] and polymer floculants for wastewater treatment. J Appl Polym Sci 2006;102:2915–28.
- [6] Yiamsawas D, Kangwansupamonkon W, Chailapakul O, Kiatkamjornwong S. Synthesis and swelling properties of poly[acrylamide-co-(crotonic acid)] superabsorbents. React Funct Polym 2007;67:865–82.
- [7] Seetapan N, Wongsawaeng J, Kiatkamjornwong S. Gel strength and swelling of acrylamide-protic acid superabsorbent copolymers. Polym Adv Technol; 2010. doi:10.1002/pat.1658.
 [8] Tong Z, Liu X. Swelling equilibria volume phase transition in hydrogels with
- [8] Tong Z, Liu X. Swelling equilibria volume phase transition in hydrogels with strongly dissociating electrolytes. Macromolecules 1994;27:844–8.
- [9] Liu X, Tong Z, Hu O. Swelling equilibria of hydrogels with sulfonate groups in water and in aqueous salt solutions. Macromolecules 1995;28: 3813-7.
- [10] Fisher LW, Sochor AR, Tan JS. Chain characteristics of poly(2-acrylamido-2-methylpropanesulfonate) polymers. 1. Light-scattering and intrinsic-viscosity studies. Macromolecules 1977;10:949–54.
- [11] Churochkina NA, Starodoubtsev SG, Khokhlov AR. Swelling and collapse of the gel composites based on neutral and slightly charged poly(acrylamide) gels containing Na-montmorillonite. Polym Gels Netw 1998;6:205–15.
- [12] Okay O, Sarıışık SB, Zor SD. Swelling behavior of anionic acrylamide-based hydrogels in aqueous salt solutions: comparison of experiment with theory. J Appl Polym Sci 1998;70:567–75.
- [13] Ozmen MM, Okay O. Superfast responsive ionic hydrogels with controllable pore size. Polymer 2005;46:8119–27.
- [14] Gad YH. Preparation and characterization of poly(2-acrylamido-2-methyl-propanesulfonic acid)/chitosan hydrogel using gamma irradiation and its application in wastewater treatment. Radiat Phys Chem 2008;77:1101–7.
- [15] Kaşgöz H, Durmuş A, Kaşgöz A. Enhanced swelling and adsorption properties of AAM-AMPSNa/clay hydrogel nanocomposites for heavy metal ion removal. Polym Adv Technol 2008;19:213–20.
- [16] Saraydin D, Unver-Saraydin S, Karadağ E, Koptagel E, Güven O. In vivo biocompatibility of radiation crosslinked acrylamide copolymers. Nucl Instrum Meth B 2004;217:281–92.
- [17] Karadağ E, Saraydin D, Caldiran Y, Güven O. Swelling studies of copolymeric acrylamide/crotonic acid hydrogels as carriers for agricultural uses. Polym Adv Technol 2000;11:59–68.
- [18] Duran S, Solpan D, Güven O. Synthesis and characterization of acrylamideacrylic acid hydrogels and adsorption of some textile dyes. Nucl Instrum Meth B 1999;151:196–9.
- [19] Karadağ E, Uzüm OB, Saraydin D. Swelling equilibria and dye adsorption studies of chemically crosslinked superabsorbent acrylamide/maleic acid hydrogels. Eur Polym J 2002;38:2133–41.
- [20] Can HK, Kirci B, Kavalak S, Güner A. Removal of some textile dyes from aqueous solutions by poly(N-vinyl-2-pyrrolidone) and poly(N-vinyl-2-pyrrolidone)/K₂S₂O₈ hydrogels. Radiat Phys Chem 2003;68:811–8.
- [21] Bashaw RN, Harper BG. Method for controlling the spread of fire. US patent 3229769; 1966.
- [22] Pascente JE, Pascente TJ. Method of preventing combustion by applying an aqueous superabsorbent polymer composition. US patent 5849210; 1998.
- [23] Beck M, Champ S, Tonnessen M, Ziemer A, Goebel G, Pfeiffer M. Fire extinguishing and/or fire retarding compositions. US patent 2007/0289752 A1; 2007.
- [24] Erdner S, Pakan D. Fire control composition and method. US patent 7670513 B2; 2010.
- [25] Beyer G. Organoclays as flame retardants for PVC. Polym Adv Technol 2008; 19:485–8.
- [26] Chigwada G, Wang D, Jiang DD, Wilkie CA. Styrenic nanocomposites prepared using a novel biphenyl-containing modified clay. Polym Degrad Stabil 2006; 91:755–62.
- [27] Glodek TE, Boyd SE, McAninch IM, LaScala JJ. Properties and performance of fire resistant eco-composites using polyhedral oligomeric silsesquioxane (POSS) fire retardants. Compos Sci Technol 2008;68:2994–3001.
- [28] Karlsson L, Lundgren A, Jungqvist J, Hjertberg T. Influence of melt behaviour on the flame retardant properties of ethylene copolymers modified with calcium carbonate and silicone elastomer. Polym Degrad Stabil 2009;94: 527–32.
- [29] Morgan AB. Flame retarded polymer layered silicate nanocomposites: a review of commercial and open literature systems. Polym Adv Technol 2006;17:206–17.
- [30] Bordado JCM, Gomes JFP. New technologies for effective forest fire fighting. Int J Environ Stud 2007;64:243–51.
- [31] Zeng QH, Yu AB, Lu GQ, Paul DR. Clay-based polymer nanocomposites: research and commercial development. J Nanosci Nanotechnol 2005;5: 1574–92.
- [32] Zhang J, Wang A. Study on superabsorbent composites. IX: synthesis, characterization and swelling behaviors of polyacrylamide/clay composites based on various clays. React Funct Polym 2007;67:737–45.
- [33] Lu H, Hu Y, Li M, Song L. Clay intercalation and influence on flammability and crystallization behaviors of POE-based nanocomposites. Polym Composite 2008:29:1358–63.

- [34] Foungfung D, Phattanarudee S, Seetapan N, Kiatkamjornwong S. Acrylamideitaconic acid superabsorbent polymers and superabsorbent polymer/mica nanocomposites. Polym Adv Technol; 2010. doi:10.1002/pat.1559.
- [35] Sortwell ET. Method of preventing or extinguishing fires. US patent 2009/ 0151963 A1; 2009.
- [36] Lin SB, Yuan CH, Ke AR, Quan ZL. Electrical response characterization of PVA-P(AA/AMPS) IPN hydrogels in aqueous Na₂SO₄ solution. Sens Actuators B 2008;134:281-6.
- [37] Buchholz FL, Burgert JH. Synthesis and application of superabsorbent polymers. In: Finch CA, editor. Industrial water soluble polymers. Cambridge: Royal Society of Chemistry; 1996. p. 93.
- [38] Odian G. Principles of polymerization. 4th ed. New Jersey: John Wiley & Sons, Inc; 2004.
- [39] Ilavsky M, Prins W. Rheo-optics of poly(2-hydroxyethyl methacrylate) gels. II. Effect of cross-linking density and stage of dilution during network formation. Macromolecules 1970;3:425–33.
- [40] Dusek K, Janacek J. Hydrophilic gels based on copolymers of 2-hydroxyethyl methacrylate with methacrylamide and acrylamide. J Appl Polym Sci 1975;19: 3061–75.
- [41] Baker JP, Hong L-H, Blanch HW, Prausnitz JM. Effect of initial total monomer concentration on the swelling behaviour of cationic acrylamide-based hydrogels. Macromolecules 1994;27:1446–54.
- [42] Naghash HJ, Okay O. Formation and structure of polyacrylamide gels. J Appl Polym Sci 1996;60:971–9.

- [43] Huang Y, Seitz U, Funk W. Synthesis and characterization of bisacrylamide microgels containing sulfo groups. Macromol Chem 1985;186:273–81.
- [44] Dai H, Li H, Wang F. An alternative process for the preparation of Cu-coated mica composite powder. Surf Coat Tech 2006;201:2859–66.
- [45] Tang Q, Wu J, Sun H, Fan S, Hu D, Lin J. Superabsorbent conducting hydrogel from poly(acrylamide-aniline) with thermo-sensitivity and release properties. Carbohydr Polym 2008;73:473–81.
- [46] Chang JH, An YU, Cho D, Giannelis EP. Polylactide nanocomposites: comparison of their properties with montmorillonite and synthetic mica (II). Polymer 2003;44:3715–20.
- [47] Zhang J, Wang Q, Wang A. Synthesis and characterization of chitosan-g-poly(acrylic acid)/attapulgite superabsorbent composites. Carbohydr Polym 2007;68:367-74.
- [48] Koo JH, editor. Polymer nanocomposites: processing, characterization, and applications. New York: The McGraw-Hill Companies, Inc; 2006.
- [49] Bartholmai M, Schartel B. Layered silicate polymer nanocomposites: new approach or illusion for fire retardancy? Investigations of the potentials and the tasks using a model system. Polym Adv Technol 2004;15:355–64.
 [50] Hussain M, Varley RJ, Mathys Z, Cheng YB, Simon GP. Effect of organo-phos-
- [50] Hussain M, Varley RJ, Mathys Z, Cheng YB, Simon GP. Effect of organo-phosphorus and nano-clay materials on the thermal and fire performance of epoxy resins. J Appl Polym Sci 2004;91:1233–53.
- [51] Schartel B, Bartholmai M, Knoll U. Some comments on the main fire retardancy mechanisms in polymer nanocomposites. Polym Adv Technol 2006;17: 772-7

ARTICLE IN PRESS

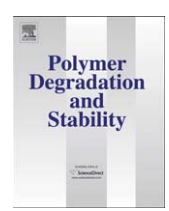
Polymer Degradation and Stability xxx (2011) 1-7



Contents lists available at ScienceDirect

Polymer Degradation and Stability

journal homepage: www.elsevier.com/locate/polydegstab



Effect of fire retardant on flammability of acrylamide and 2-acrylamido-2-methylpropane sodium sulfonate copolymer composites

Nispa Seetapan ^{a,1}, Nattawut Limparyoon ^{b,2}, Suda Kiatkamjornwong ^{c,*}

- a National Metal and Materials Technology Center, 114 Thailand Science Park, Paholyothin Rd., Klong 1, Klong Luang, Pathumthani 12120, Thailand
- ^b Program of Petrochemistry and Polymer Science, Faculty of Science, Chulalongkorn University, Bangkok 10330, Thailand
- ^c Department of Printing and Imaging Technology, Faculty of Science, Chulalongkorn University, Bangkok 10330, Thailand

ARTICLE INFO

Article history: Received 9 April 2011 Received in revised form 1 June 2011 Accepted 22 June 2011 Available online xxx

Keywords: Superabsorbent Zinc borate Melamine Fire retardant Cone calorimetry

ABSTRACT

Poly[acrylamide-co-(2-acrylamido-2-methylpropane sodium sulfonate)] superabsorbents and superabsorbent composites (SAPCs) with zinc borate and/or melamine as fire retardants were synthesized. Water absorbencies decreased inversely to added amount of fire retardant. Thermal stability of SAPC/zinc borate increases with increasing zinc borate. Incorporating melamine improved thermal stability of the SAPC until 300 °C. Flammability analysis demonstrated that wood surface coated with SAP or SAPC emulsions extended time to ignition of the wood. Peak heat release rate and total heat release are smallest in specimens coated with SAPC/30% melamine. Wood coated with SAPC incorporating 20% zinc borate/10% melamine mixture gave the longest time to ignition at 4½ min.

© 2011 Elsevier Ltd. All rights reserved.

1. Introduction

Superabsorbent polymers (SAPs) are lightly crosslinked hydrophilic polymers that can absorb and retain water, saline solutions, or physiological fluids up to thousands times their dry weight. Several ionic vinyl monomers have been copolymerized with a nonionic hydrophilic monomer to prepare SAPs with high degree of swelling [1–7]. Based on the superior water swellable characteristic, SAPs have been widely used in the fields of personal care products [8], agricultural soil [9], wastewater treatment [5,6,10-14], as well as in fire-fighting application [15–17]. In the later case, water is typically used to extinguish the fire or to prevent combustible objects from burning by reducing the temperature of the combustible material below the burning temperature. However, when a fire is extinguished by spraying water onto it, only a small amount of the total water applied is generally effective in extinguishing the fire, due to loss of most of the water, such as by run-off or evaporation of the water. Therefore, SAPs have been proposed as a method to prolong a combustible object from burning, or to prevent the penetration of

0141-3910/\$ – see front matter © 2011 Elsevier Ltd. All rights reserved. doi:10.1016/j.polymdegradstab.2011.06.014

extreme heat or fire to a combustible material. To prevent the spreading of fire, a sufficient amount of swollen SAPs have to be sprayed onto an ignitable or burnable object so as to continuously coat the surface of the object nearby the burning fire. Here, the mechanism of preventing the fire spreading is to both cool the surface of the object below the ignition temperature and to reduce the quantity of oxygen at the surface of the burnable object to a degree such that the flame is extinguished [16]. However, SAPs are organic materials which lose their thermal stability when exposed to high temperatures. Therefore, for fire-fighting applications, the incorporation of a fire retardant into SAPs can offer thermal protection from fire due to the ability to absorb high amount of water together with the thermal stability provided by the added inorganic materials. However, unlike the extensive studies on improving fire-retardant property of thermoplastics, thermosets, elastomer, and wood [18-22], the investigation of SAPs with thermal stability and fire-retardant properties for fire-fighting applications is rather limited [23,24]. Our previously published results on flammability analysis using cone calorimetry technique revealed that the wood specimens coated with SAP or SAP/mica nanocomposite showed an excellent reduction in the peak heat release rate, and extended the time at peak heat release rate, but did not reduce the total heat release [24].

Among several characterized fire retardants, zinc borate has been found to be an effective inorganic fire retardant that possesses

^{*} Corresponding author. Tel.: +66 2218 5587; fax: +66 2255 3021. *E-mail addresses*: nispam@mtec.or.th (N. Seetapan), winny047@hotmail.com (N. Limparyoon), ksuda@chula.ac.th (S. Kiatkamjornwong).

¹ Tel.: +662 564 6500.

² Tel.: +662 594 1344.

key characteristic properties of flame retardants, such as smoke suppression and promoting charring, and so on [25], that are required by new fire standards. It has been postulated that the mechanism of the zinc borate induced flame retardancy in polymeric materials involves the formation of a protective char layer at surface of the materials, which then obstructs the access of oxygen and subsequently prevents the oxidation of carbon [26]. As such, zinc borate is commonly used as a multifunctional flame retardant in combination with other halogenated or halogenated free flame retardant systems to boost flame retardancy properties [27]. Melamine is another type of nitrogen-containing flame retardants and has been used in thermoplastics [28,29]. The mechanism of melamine's fire retardancy has been reviewed and is proposed to be due to the sublimation and vapor-phase dissociation, where it is converted to non-volatile products and ammonia [30]. Therefore, in this study, we have incorporated different loadings of zinc borate and melamine into the synthesis of acrylamide (AM) and 2-acrylamido-2-methylpropane sodium sulfonate (AMPS-Na⁺) SAPs. These potential fire retardants of the obtained superabsorbent composites (SAPCs) were evaluated for their water absorbency, thermal stability and flammability. AMPS-Na⁺ was chosen because its strongly ionizable sulfonate groups can provide SAPs with a high water swelling capability. The novel fire retardant incorporating SAPCs that showed the best tap-water swelling, thermal stability and flammability might be appropriate for inhibiting the spreading of fire.

2. Experimental

2.1. Materials

Acrylamide (AM) was gifted from Siam Chemical Industry Co., Ltd. (Bangkok, Thailand). 2-acrylamido-2-methylpropane sodium sulfonate (AMPS-Na⁺) was purchased from Aldrich (Steinhiem, Germany). *N,N'*-methylenebisacrylamide (MBA) and *N,N,N'*,*N'*-tetramethylethylenediamine (TEMED) were received from Fluka (Buchs, Switzerland). Ammonium persulfate (APS) was from Ajax (Seven Hills, Australia). Zinc borate (2ZnO₂B₂O₃·3H₂O, Aldrich, Steinhiem, Germany) and melamine (C₃H₆N₆, Thai Mitsui Specialty Chemicals Co., Ltd., Chachoengsao, Thailand) were employed as fire retardants. Deionized water (Elga Deionizer, Model LA611, U.K.) was used for the synthesis and the swelling experiment.

2.2. Preparation of AM-co-AMPS-Na⁺ SAPs

SAPs were synthesized by free-radical crosslinking polymerization of AM and AMPS-Na⁺ at the molar ratio of 15:85, with 0.05% mol of MBA (crosslinker). An equal concentration of APS (initiator) and TEMED (co-initiator) was used at 1.2% by mol of the monomers. These concentrations were selected as being found previously to yield the SAP with the highest water absorbencies [24]. Firstly, AM was dissolved in deionized water in a 500-cm³ reactor equipped with a mechanical stirrer, a condenser, and an inlet tube of nitrogen gas. AMPS-Na⁺ was then added and the mixture was stirred at room temperature for 5 min, before heating to 60 °C under nitrogen atmosphere. Next, MBA and APS were sequentially added to the mixture and stirred for 5 min. Finally, TEMED was added and the polymerization was proceeded for 30 min to ensure complete polymerization. The obtained product was dehydrated with acetone, dried, milled, and then sieved through a 100-mesh sieve aluminum screen.

SAPs/fire retardant composites were synthesized by incorporating the desired amount of fire retardant into the polymerization mixture before MBA, APS, and TEMED were added. In this study, zinc borate, melamine, and their mixtures were chosen as fire retardant systems.

2.3. Fourier transform infrared spectroscopy (FT-IR)

The existence of the components of each SAP or SAPC was evaluated by analysis of their respective functional groups by Fourier Transform Infrared Spectroscopy (FTIR; System 2000, Perkin Elmer, U.S.A.). The dried sample and KBr powder were mixed, ground, pressed, and then subjected to the FT-IR spectrometry.

2.4. Water absorbency measurement

The water absorbency of the SAP and its derived SAPCs containing zinc borate, melamine or both, was carried out at room temperature. Each 0.1 g aliquot of dried SAP or SAPC product was allowed to swell in $200~{\rm cm}^3$ of deionized or tap water for 24 h. Subsequently, the fully swollen superabsorbents were separated from the unabsorbed medium by filtering through a 100-mesh sieve aluminum screen for 2 h. The swollen superabsorbents were then weighed and the water absorbency at equilibrium (g g $^{-1}$) was calculated by Eq. (1) and they were performed in triplicate for each system:

$$Water absorbency = \frac{weight of swollen gel - weight of dry gel}{weight of dry gel}$$
(1)

2.5. Thermal stability analysis

The SAP and its derived SAPCs were investigated for thermal properties using a TGA/SDTA 851e (Mettler Toledo Corporation, Switzerland). The measurements were carried out over a temperature range of 25–800 $^{\circ}\text{C}$ at a heating rate of 10 $^{\circ}\text{C}$ min $^{-1}$ with a nitrogen gas flow rate of 60 cm 3 min $^{-1}$.

2.6. Flammability test

Flammability analysis was evaluated using a cone calorimeter (Fire Testing Technology Ltd., UK), according to ISO 5660, at an incident heat flux (50 kW m^{-2}) in an air atmosphere, and under the free convective air flow condition. The SAPs were prepared in the form of an oil-in-water dispersion as follows [31].

The dry SAPs or SAPCs $(40\% \text{ w w}^{-1})$ were dispersed in a mixture of 50% w w⁻¹ of palm oil and 10% w w⁻¹ of nonionic surfactant blends containing 54% w w⁻¹ of Tween 80 or poly(oxyethylenesorbitan monooleate) having the HLB of 15 and 46% w w⁻¹ of Span 80 or sorbitan (Z)-mono-9-octadecenoate having the HLB of 4.3 to give the HLB value of the blend is 10. Each suspension (5% v v^{-1}) in the oilsurfactant mixture was then dispersed in tap water, to subsequently obtain a viscous slurry gel that was used as an emulsion to coat wood (Apocynaceae, Wrightia religiosa Benth.) board dimension $100 \times 100 \times 3$ mm to a surface depth of 3 mm. The surface of the wood, both uncoated and coated from the same batch, was subsequently exposed directly to an open flame generated by a propane gas jet. The uncoated wood board was used as the relative control to compare the effectiveness of the SAP and SAPC gels as fire retardants. The time to ignition (t_{ign}), peak of heat release rate (PHRR), time to PHRR (t_{PHRR}) and total heat release (THR) were recorded. The charred samples left after the flame extinguished were photographed by a digital camera.

3. Results and discussion

3.1. Synthesis of poly(AM-co-AMPS-Na⁺)/fire retardant SAPCs

The IR spectra shown in Fig. 1(a)–(e) of zinc borate alone and that after the nominal incorporation of 5, 10, 20, and 30% w w⁻¹ into the SAPCs revealed that the zinc borate alone shows peaks as

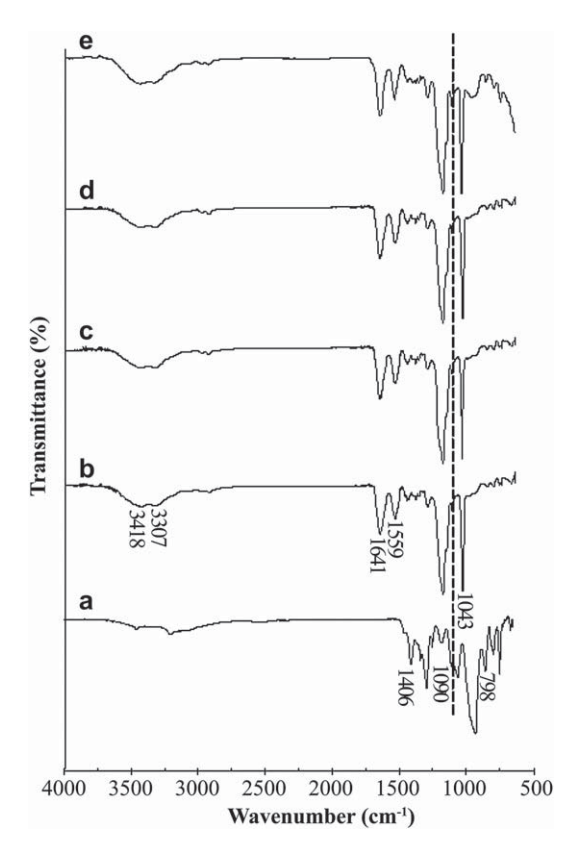


Fig. 1. Representative FT-IR spectra of (a) zinc borate, and poly(AM-co-AMPS-Na $^+$)/zinc borate SAPCs with nominal zinc borate loadings of (b) 5%, (c) 10%, (d) 20% and (e) 30% (w w $^{-1}$).

follows: 1406 cm $^{-1}$ (s), $\nu_{B(3)-O}$ as; 1090 cm $^{-1}$ (sh) and 798 cm $^{-1}$ (sh), $\nu_{B(4)-O}$ [32]. For zinc borate SAPCs, the overlapping peaks of ν_{N-H} and ν_{O-H} are found at 3418 cm $^{-1}$ (b) and 3307 cm $^{-1}$ (b), respectively; the $\nu_{C} =_{0}$ peak amide I at 1641 cm $^{-1}$ (s) [33], the δ_{N-H} peak of amide II at 1559 cm $^{-1}$ (s) and the $\nu_{S} =_{0}$ peak of AMPS-Na $^{+}$ at 1043 cm $^{-1}$ (sh) [2]. The $\nu_{B(4)-O}$ peak at 1090 cm $^{-1}$ was also present and increased in relation to the amount of zinc borate in the synthesized composites. However, when a nominal of 30% w w $^{-1}$ loading of zinc borate was prepared, some zinc borate was seen to precipitate and so separate from the obtained SAPC.

The FT-IR spectra of melamine and poly(AM-co-AMPS-Na $^+$)/ melamine SAPCs with melamine contents of 5, 10, 20, and 30% w w $^{-1}$ in Fig. 2(a)—(e) show the characteristic peaks of melamine as follows: 3468–3117 cm $^-$ 1 (s), v_{N-H}; 1647 cm $^-$ 1(s), v_C— $_N$; 1535 cm $^-$ 1 (sh), δ_{N-H} ; 1433 cm $^-$ 1 (sh), v_{C-N}; \sim 800 cm $^-$ 1, δ_{N-H} (op) [34]. Besides, the overlapping peak of v_{N-H} and v_{O-H} peaks are found at \sim 3500–3000 cm $^-$ 1 (b), the δ_{C-H} at 1186 cm $^-$ 1 (s), and the v_S— $_0$ peak of AMPS-Na $^+$ at 1043 cm $^-$ 1 (sh) [2]. The v_{N-H} and δ_{N-H} (op) peaks of melamine increased in relation to the amount of melamine loaded in the SAPCs.

Mixtures of zinc borate and melamine at 20:10, 15:15, and 10:20 by % w were incorporated in the respective SAPCs. The FT-IR spectra (Fig. 3(a)–(c)) of these prepared SAPCs showed the characteristic peaks of both zinc borate and melamine at about 1090 $\rm cm^{-1}$ and 3468–3117 $\rm cm^{-1}$, respectively.

3.2. Swelling behavior of poly(AM-co-AMPS-Na⁺)/fire retardant SAPCs

Water absorbency in tap water of the SAP and zinc borate containing SAPCs were always significantly lower than those in

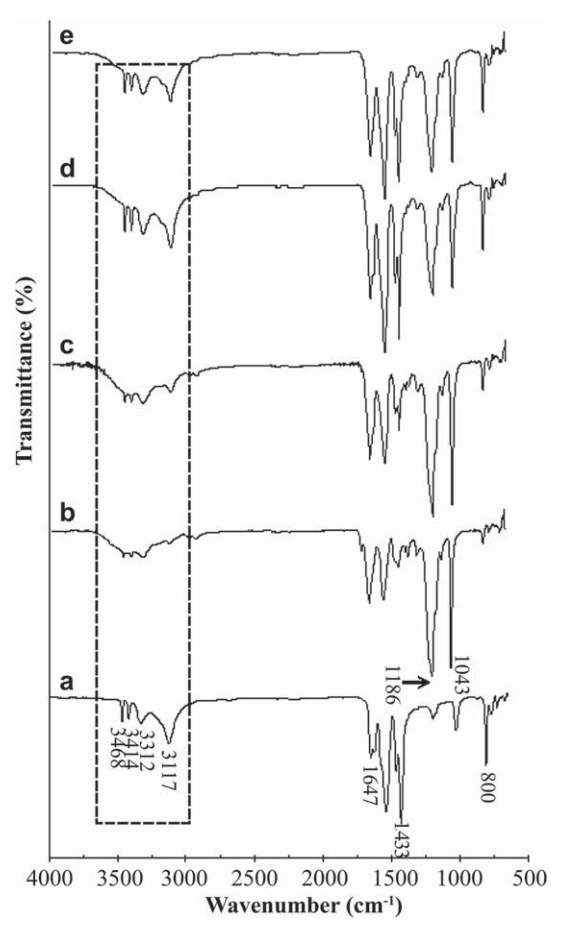


Fig. 2. Representative FT-IR spectra of (a) melamine and poly(AM-co-AMPS-Na⁺)/melamine SAPCs with nominal melamine loadings of (b) 5%, (c) 10%, (d) 20% and (e) 30% (w w⁻¹).

deionized water (Fig. 4(a)), being about 1.65-fold lower for the SAP and from 2.56- to 3.93-fold lower for the SAPCs (the difference increases as the nominal zinc level increases). The same trend was also seen for melamine containing SAPCs, but the difference between the water absorbency in tap and deionized water was less marked (Fig. 4(b)). The difference in water absorption is caused by the presence of ions in the tap water, which was used here contains Fe^{3+} (7.2 ppm), Ca^{2+} (27.2 ppm) and Mg^{2+} (0.05 ppm) as the dominant ions. The main reason is the shielding or screening effects of the cations that reduce the osmotic pressure of SAPCs. Comparing the effect of the ions on the SAPCs, one can see that the zinc borate incorporated SAPCs were affected more than melamine because the water absorption was reduced the most (Fig. 4(a) and (b)). One possible cause is the negatively synergistic effect of Zn^{2+} in the SAPC with the three main cations (Fe³⁺, Ca²⁺ and Mg²⁺). For the SAPC incorporating melamine, the effect of the cation salts in tap water on the water absorbency was not so strong due to the lower polarity of melamine (Fig. 4(b)).

The equilibrium water absorbency of the mixed zinc borate and melamine SAPCs synthesized with 30% w $\rm w^{-1}$ fire retardant in Fig. 5 for the three zinc borate-to-melamine w $\rm w^{-1}$ ratios shows that the zinc borate-to-melamine ratio at 20:10 (% w $\rm w^{-1}$) strongly decreases the equilibrium water absorbency in deionized and tap water by 1.76- and 1.50-fold respectively compared with poly(AM-co-AMPS-Na⁺) SAP (Fig. 4(b)). As the zinc borate-to-melamine ratios (% w $\rm w^{-1}$) were decreased to 15:15 and 10:20, the equilibrium water absorbency in both tap and deionized water slightly

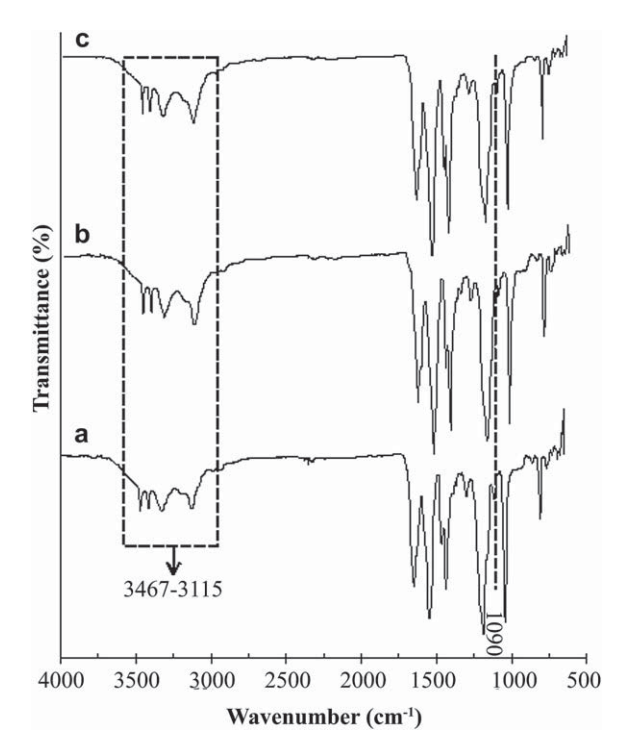


Fig. 3. Representative FT-IR spectra poly(AM-co-AMPS-Na $^+$)/zinc borate and melamine SAPCs loaded with nominal zinc borate: melamine w w $^{-1}$ ratios of (a) 20:10, (b) 15:15 and (c) 10:20.

increased (compared with zinc borate-to-melamine ratios of 20:10 (% w w^{-1})). This is because the polarity of the SAPCs increases with increasing melamine contents.

3.3. Thermal analysis of poly(AM-co-AMPS-Na⁺)/fire retardant SAPCs

The thermal behaviors of poly(AM-co-AMPS-Na⁺)/zinc borate SAPCs were similar to that seen with poly(AM-co-AMPS-Na⁺) SAP, as revealed by TGA thermograph analyses shown in Fig. 6. Zinc borate degraded via the dehydration of zinc borate crystals in the range of 341–416 °C [35]. The first degradation stage (~ 100 °C) of all SAPs and SAPCs takes place due to the loss of absorbed and bound water. The second (313–328 °C) and third (325–433 °C) stages of degradation are ascribed to the amide side group of the AMPS-Na⁺ and AM, respectively [36], and the dehydration of zinc borate crystal. The final decomposition stage (711–800 °C) is assigned to the degradation of chain backbone and rearranged zinc borate [35]. The results indicated the enhanced thermal stability at

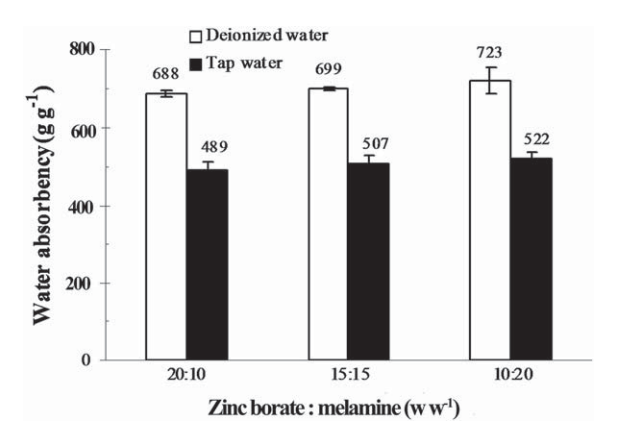


Fig. 5. Effect of the zinc borate-to-melamine ratios on the equilibrium water absorbency in deionized water and tap water of poly(AM-co-AMPS-Na $^+$)/mixed zinc borate and melamine SAPCs at zinc borate: melamine ratios of 20:10, 15:15 and 10:20% w w $^{-1}$ of total monomers.

all the tested temperatures was detected as a function of zinc borate loading because zinc borate rearranges its structure and so acts as a heat barrier to delay the diffusion of volatile thermo-oxidation products to gas, and gas to the composite [35].

Pure melamine shows two degradation stages (Fig. 7), the generation of nitrogen volatile side groups in the first stage $(315-381 \, ^{\circ}\text{C})$ and then, in the second stage $(416-748 \, ^{\circ}\text{C})$, the decomposition of main chain and nitrogen volatiles from the first stage [37]. In comparison, thermograms of the poly(AM-co-AMPS- Na^{+})/melamine SAPCs show a first degradation stage ($\sim 100 \, ^{\circ}$ C), due to the loss of absorbed and bound water, whilst the second stage (282–310 °C) is ascribed to the decomposition of the nitrogen compounds from melamine. The third (313-346 °C) and fourth (345-412 °C) stages are interpreted as the degradation of AMPS-Na⁺ and AM, respectively, whilst the final decomposition stage (742–800 °C) is assigned to the degradation of the backbone chain (Fig. 7). Overall, the incorporation of melamine improved the thermal stability of the SAPCs up to about 310 °C but thereafter melamine started to show an almost complete decomposition at higher temperature due to the loss of nitrogen compounds [38], and was completely decomposed at about 750 °C. Therefore, beyond ~330 °C, the thermal stability of the melamine-based SAPCs decreased with increasing melamine loadings.

The TGA thermograms of the SAPCs composed of poly(AM-co-AMPS-Na⁺) with either zinc borate or melamine incorporated to make SAPCs, revealed that the incorporation of zinc borate apparently promoted the thermal stability to the SAPCs over the studied temperature range (0–800 °C) (Fig. 6), whilst melamine showed a better thermal stability at temperatures only below 310 °C (Fig. 7).

576

30

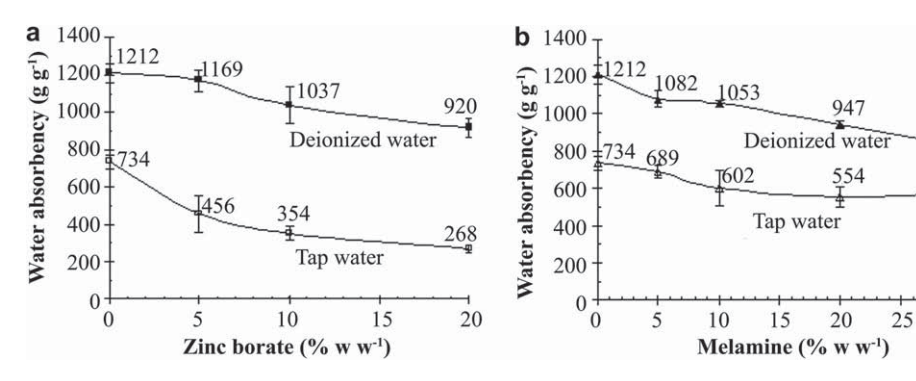


Fig. 4. Water absorbency of (a) zinc borate, and (b) melamine incorporated SAPC in deionized water and tap water.

N. Seetapan et al. / Polymer Degradation and Stability xxx (2011) 1-7

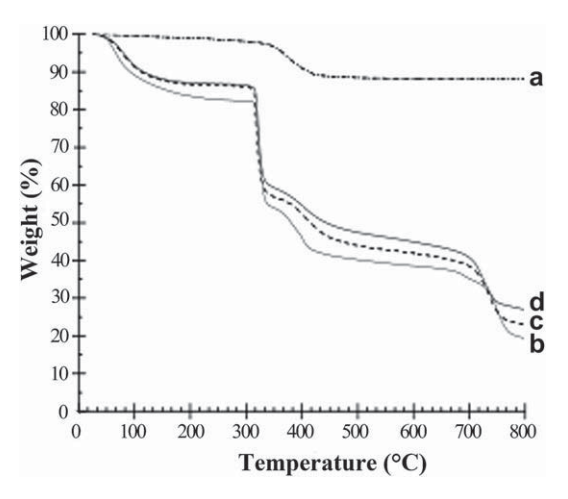


Fig. 6. Representative TGA thermograms of (a) zinc borate, (b) poly(AM-co-AMPS-Na $^+$) SAPs and the zinc borate derived SAPCs with (c) 10 and (d) 20% w w $^{-1}$ nominal loadings of zinc borate.

The latter is because at higher temperatures most of the melamine dissociated to the vapor phase [30] that can then dilute the content of oxygen gas in the area of burning objects. Therefore, the addition of both zinc borate and melamine into SAPCs could potentially offer a better thermal protection over the wide temperature from 0 to 800 °C and so was evaluated next. The TGA thermograms of the mixed zinc borate and melamine SAPCs, at a zinc borate-tomelamine addition ratios of 20:10, 15:15, and 10:20 (% w w⁻¹) of total monomers (Fig. 8) were similar to that seen for both melamine SAPC (Fig. 7) and zinc borate SAPC (Fig. 6). At temperatures below about 300 °C there was no different weight loss in thermal decomposition profiles among all the composites with varying melamine contents (Fig. 8). In addition, thermal stability was found to increase with an increasing zinc borate ratio at temperatures above 350 °C. Compared to the parental SAP, these derived SAPCs show a better thermal stability at all evaluated temperatures (0-800 °C).

3.4. Flammability analysis

Heat release is defined as the heat generated due to various chemical reactions when a material is exposed to fire, and provides information on the size of the fire and hence the corresponding fire hazard [18]. Materials with a low heat release rate (HRR) gives less damage to the surroundings than those with high HRR. Thus, the

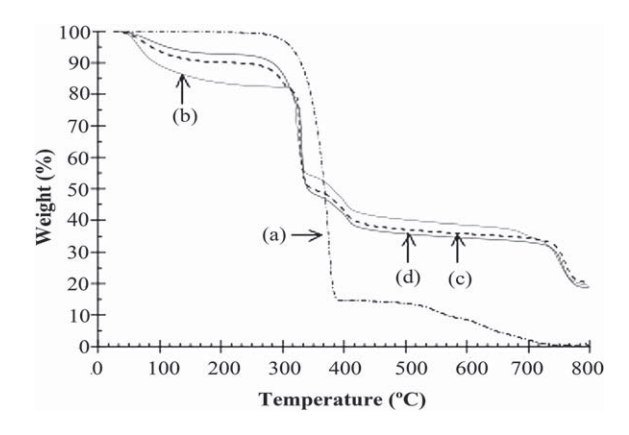


Fig. 7. Representative TGA thermograms of (a) melamine, (b) poly(AM-co-AMPS-Na⁺) SAPs and the melamine derived SAPCs with (c) 20 and (d) 30% w w⁻¹ nominal loadings of melamine.

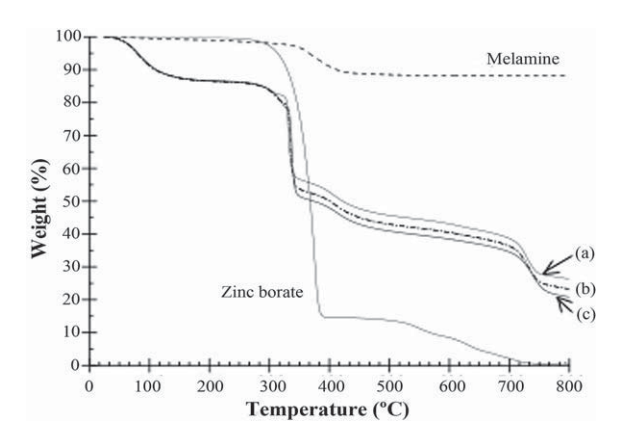


Fig. 8. Representative TGA thermograms of poly(AM-co-AMPS-Na⁺)/mixed zinc borate and melamine SAPCs at nominal zinc borate:-to-melamine ratios of (a) 20:10, (b) 15:15, and (c) 10:20% w w⁻¹ of total monomers. Redrawn for a discussion are thermograms of zinc borate and melamine.

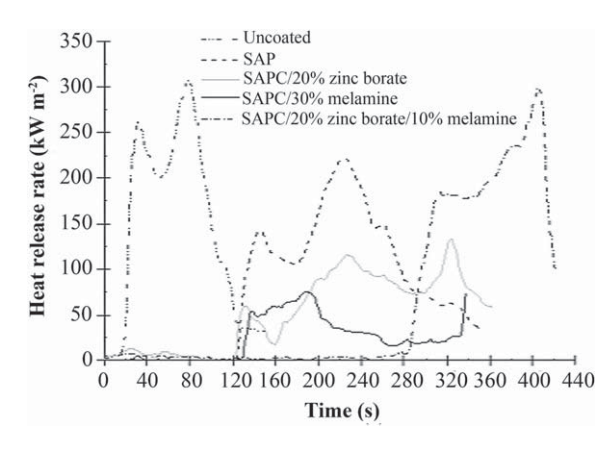


Fig. 9. Heat release rate plots for the uncoated wood and the woods coated with different emulsion systems.

HRR, and particularly the PHRR, is the primary characteristic in determining the size, growth and suppression requirements of a fire environment [39]. The THR is defined as a total heat release at the end of burning. In this study, the combustion experiment was performed until flame was self-extinguished. The HRR plots for the uncoated and the coated wood specimens revealed that the $t_{\rm ign}$ was fastest for the uncoated wood board (13 s), but was about ten-fold to twenty-fold longer for all the SAP- or SAPC-coated specimens (Fig. 9), illustrating the excellent protection obtained in delaying the flammability after exposure to an open flame (Table 1). For the uncoated specimen, the observed THR of 22 MJ m $^{-2}$ was obtained from the combustion of the wood itself, where the flame eventually extinguished because the entire wood specimen was completely

 Table 1

 Flammability parameters obtained from the cone calorimetry.

Specimen	t_{ign} (s)	PHRR (kW m ⁻²)	t_{PHRR} (s)	$^{\mathrm{THR}}$ $(\mathrm{MJ}~\mathrm{m}^{-2})$
Uncoated wood	13	309	79	22
Wood coated with SAPs	125	222	224	26
Wood coated with SAPs, 20% zinc borate	118	132	324	18
Wood coated with SAPs, 30% melamine	117	75	188	8
Wood coated with SAPs, 20% zinc borate	278	300	405	26
and 10% melamine				

 $t_{\rm ign}$, time to ignition; PHRR, peak heat release rate; $t_{\rm PHRR}$, time to PHRR; THR, total heat release.

N. Seetapan et al. / Polymer Degradation and Stability xxx (2011) 1-7

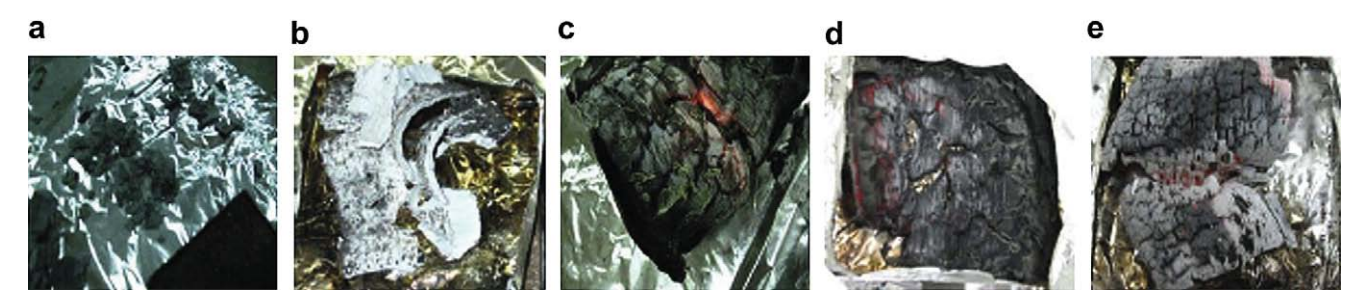


Fig. 10. Charred samples of (a) the uncoated, (b) the poly(AM-co-AMPS-Na⁺) SAP-coated, (c) the poly(AM-co-AMPS-Na⁺)/20% zinc borate SAPC-coated, (d) the poly(AM-co-AMPS-Na⁺)/30% melamine SAPC-coated, and (e) the poly(AM-co-AMPS-Na⁺)/20% zinc borate/10% melamine SAPC-coated wood boards.

burnt out. PHRR and t_{PHRR} were observed at 309 kW m⁻² and 79 s, respectively, for the uncoated wood specimen.

When compared to the uncoated wood surface, that coated with the neat SAP gel reduced the PHRR 1.39-fold, and delayed both the $t_{\rm ign}$ 9.62-fold to 125 s and the $t_{\rm PHRR}$ 2.83-fold to 224 s, whereas the THR was increased slightly (1.18-fold) to 26 MJ m $^{-2}$. This delayed-burning mechanism is explained as being due to the cooling effect of water trapped within the SAP particles. After ignition, the trapped water is slowly released causing a lower HRR for the duration of the burning process. After all water evaporated, the neat SAP, which is a fuel itself, finally combusted under heat, consecutively with the burnout of wood, and so increased the THR compared to the uncoated wood surface.

In case of the wood coated with the SAPC gels incorporating either of 20% w w⁻¹ zinc borate or 30% w w⁻¹ melamine, the t_{ign} values were broadly similar to that of the neat SAP-coated specimen, but showed a clear reduction in the PHRR, being 1.68-fold and 2.96fold lower, respectively, and is due to the fire retardant effect of zinc borate and melamine. The role of zinc borate is likely to be due to formation of a protective zinc oxide covering on the surface during combustion, which will obstruct the access of oxygen and so preventing complete combustion. The presence of melamine in the coating gel offers high potential in reducing the PHRR, due to the conversion of melamine to non-volatile products and ammonia [30], then effectively diluted the oxygen gas during combustion. Experimentally, 120 s after the specimen started to flame, it selfextinguished for about 80 s and then, at about 330 s, the flame ignited itself, as observed by the increase in the HRR (Fig. 9), due to the depletion of volatile phase and the remaining wood specimen.

The wood coated with the mixture of zinc borate and melamine containing SAPC gel provided the best delay in fire ignition ($t_{\rm ign}=258$ s), some 21.4-fold longer than the untreated wood and 2.2–2.4-fold long than the other SAP or SAPC treated samples, presumably attributed to the combined effect of zinc borate and melamine. However, after ignition, the specimen demonstrated a rapid increase in the HRR and the PHRR, the latter at 300 kW m $^{-2}$, which is a level broadly similar to that seen in the uncoated specimen. This is likely due to the burning of both wood specimen and SAP particles.

Fig. 10 shows representative images of the residues after the flame was self-extinguished. The uncoated wood gave a dark gray ash (Fig. 10(a)), whereas the residue of the wood coated with the poly(AM-co-AMPS-Na⁺) SAP after burning appeared as a white charred layer and a dark gray residue, representing the combustion of the coated SAP particles and the wood, respectively (Fig. 10(b)). The char was found to be fragile and easily cracked. Specimens coated with the SAPC containing either zinc borate (Fig. 10(c)) or melamine (Fig. 10(d)) showed a more compact black char protective layer, preventing the penetration of gases and the complete combustion. As a result, there was a reduction in the PHRR and THR in both coated samples

(Table 1). In case of a mixed zinc borate and melamine containing SAPC-coated specimen (Fig. 10(e)), the residual char was white and gray indicating a complete burning of the SAP particles and wood.

4. Conclusion

Poly(AM-co-AMPS-Na⁺) SAPs and their zinc borate and/or melamine containing SAPCs as fire retardants were synthesized by free-radical crosslinking polymerization. Water absorbencies of SAPCs decreased inversely to the amount of added fire retardant. The thermal stability of SAPCs increased as the zinc borate loadings increased, whilst melamine incorporation improved the thermal stability up to 300 °C. Both SAP and SAPC gels, coated onto the wood surface, delayed the specimen fire ignition, reduced the PHRR and extended the t_{PHRR} . The SAPC/30% w w⁻¹ melamine provided the lowest PHRR and THR. The co-incorporation of 20% w w⁻¹ zinc borate and 10% w w⁻¹ melamine in the SAPC gel provided an excellent coating system with the time to ignition of the coated specimen being delayed to about 4.5 min compared to 13 s and 2 min for the uncoated and SAP-coated wood, respectively. This may allow sufficient time for the evacuation of premises and prevention fires from spreading.

Acknowledgments

The authors would like to acknowledge the financial support from the Thailand Research Fund under the Research Scholar Team Consolidation Program Contract no. RTA5080004. Research facilities provided by the Imaging Polymer Laboratory of Chulalongkorn University's Department of Imaging and Printing Technology, Faculty of Science are highly appreciated. English edition of the manuscript by the Publication Counselor Unit of the Research Division, Faculty of Science, Chulalongkorn University, are highly appreciated.

References

- [1] Kiatkamjornwong S, Chomsaksakul W, Sonsuk M. Radiation modification of water absorption of cassava starch by acrylic acid/acrylamide. Radiat Phys Chem 2000;59:413–27.
- [2] Durmaz S, Okay O. Acrylamide/2-acrylamido-2-methylpropane sulfonic acid sodium salt-based hydrogels: synthesis and characterization. Polymer 2000; 41:3693-704.
- [3] Okay O, Sarıışık SB. Swelling behavior of poly(acrylamide-co-sodium acrylate) hydrogels in aqueous salt solutions: theory versus experiments. Eur Polym J 2000;36(2):393–9.
- [4] Taşdelen B, Kayaman-Apohan N, Güven O, Baysal BM. Preparation of poly(N-isopropylacrylamide/itaconic acid) copolymeric hydrogels and their drug release behavior. Int J Pharm 2004;278:343–51.
- [5] Jiraprasertkul W, Nuisin R, Jinsart W, Kiatkamjornwong S. Synthesis and characterization of cassava starch graft poly(acrylic acid) and poly[(acrylic acid)-co-acrylamide] and polymer flocculants for wastewater treatment. J Appl Polym Sci 2006;102:2915–28.

- [6] Yiamsawas D, Kangwansupamonkon W, Chailapakul O, Kiatkamjornwong S. Synthesis and swelling properties of poly[acrylamide-co-(crotonic acid)] superabsorbents. React Funct Polym 2007;67:865–82.
- [7] Seetapan N, Wongsawaeng J, Kiatkamjornwong S. Gel strength and swelling of acrylamide-protic acid superabsorbent copolymers. Polym Adv Technol; 2010. doi:10.1002/pat.1658.
- [8] Saraydin D, Unver-Saraydin S, Karadağ E, Koptagel E, Güven O. In vivo biocompatibility of radiation crosslinked acrylamide copolymers. Nucl Instr Meth B 2004;217:281–92.
- [9] Karadağ E, Saraydin D, Caldiran Y, Güven O. Swelling studies of copolymeric acrylamide/crotonic acid hydrogels as carriers for agricultural uses. Polym Adv Technol 2000;11(2):59–68.
- [10] Duran S, Solpan D, Güven O. Synthesis and characterization of acrylamideacrylic add hydrogels and adsorption of some textile dyes. Nucl Instr Meth B 1999;151(1-4):196-9.
- [11] Karadağ E, Uzüm OB, Saraydin D. Swelling equilibria and dye adsorption studies of chemically crosslinked superabsorbent acrylamide/maleic acid hydrogels. Eur Polym J 2002;38:2133–41.
- [12] Can HK, Kirci B, Kavalak S, Güner A. Removal of some textile dyes from aqueous solutions by poly(N-vinyl-2-pyrrolidone) and poly(N-vinyl-2pyrrolidone)/K₂S₂O₈ hydrogels. Radiat Phy Chem 2003;68:811–8.
- [13] Noppakundilograt S, Nanakorn P, Sonjaipanich K, Seetapan N, Kiatkamjornwong S. Synthesis and characterization of acrylamide-based aluminium flocculants for wastewater treatment. I Appl Polym Sci 2009:114:2564—75.
- wastewater treatment. J Appl Polym Sci 2009;114:2564–75.
 [14] Noppakundilograt S, Nanakorn P, Jinsart W, Kiatkamjornwong S. Synthesis of acrylamide/acrylic acid-based aluminum flocculant for dye reduction and textile wastewater treatment. Polym Eng Sci 2010;50(8):1535–46.
- [15] Bashaw RN, Harper BG. Method for controlling the spread of fire. US patent 3229769; 1966.
- [16] Pascente JE, Pascente TJ. Method of preventing combustion by applying an aqueous superabsorbent polymer composition. IJS patent 5849210: 1998
- aqueous superabsorbent polymer composition. US patent 5849210; 1998.
 Beck M, Champ S, Tonnessen M, Ziemer A, Goebel G, Pfeiffer M. Fire extinguishing and/or fire retarding compositions. US patent 2007/0289752 A1; 2007.
- [18] Chigwada G, Wang D, Jiang DD, Wilkie CA. Styrenic nanocomposites prepared using a novel biphenyl-containing modified clay. Polym Degrad Stab 2006;91: 755–62.
- [19] Karlsson L, Lundgren A, Jungqvist J, Hjertberg T. Influence of melt behaviour on the flame retardant properties of ethylene copolymers modified with calcium carbonate and silicone elastomer. Polym Degrad Stab 2009;94:527–32.
- [20] Morgan AB. Flame retarded polymer layered silicate nanocomposites: a review of commercial and open literature systems. Polym Adv Technol 2006;17:206–17.
- [21] Hirata T, Kawamoto T, Nishimoto T. Thermogravimetry of wood treated with water-soluble retardants and a proposal for development of fire retarded wood materials. Fire Mater 1991;15:27–36.
- [22] Hagen M, Hereid J, Delichatsios MA, Zhang J, Bakirtzis D. Flammability assessment of fire-retarded Nordic Spruce wood using thermogravimetric analyses and cone calorimetry. Fire Saf J 2009;44:1053–66.

- [23] Bordado JCM, Gomes JFP. New technologies for effective forest fire fighting. Int J Environ Stud 2007;64:243–51.
- [24] Limparyoon N, Seetapan N, Kiatkamjornwong S. Acrylamide/2-acrylamido-2-methylpropane sulfonic acid and associated sodium salt superabsorbent copolymers with mica nanocomposites as fire retardants. Polym Deg Stab 2011;96:1054–63.
- [25] Nazare S, Kandola BK, Horrocks AR. Smoke, CO, and CO₂ measurements and evaluation using different fire testing techniques for flame retardant unsaturated polyester resin formulations. J Fire Sci 2008;26:215–42.
- [26] Chen L, Wang Y-Z. A review on flame retardant technology in China. Part I: development of flame retardants. Polym Adv Technol 2010;21:1–26.
- [27] Wu W, Yang CQ. Comparison of different reactive organophosphorus flame retardant agents for cotton. Part II: Fabric flame resistant performance and physical properties. Polym Deg Stab 2007;92:363–9.
- [28] Levchik SV, Balabanovich AI, Levchik GF, Costa L. Effect of melamine and its salts on combustion and thermal decomposition of polyamide 6. Fire Mater 1997;21:75—83.
- [29] Balabanovich AI. The effect of melamine on the combustion and thermal decomposition behaviour of poly(butylenes terephatalate). Polym Deg Stab 2004;84:451–8.
- [30] Weil ED, Choudhary V. Flame-retarding plastics and elastomers with melamine. J Fire Sci 1995;13:104—26.
- [31] Sortwell ET. Method of preventing or extinguishing fires. US patent 2009/ 0151963 A1; 2009.
- [32] Yongzhong J, Shiyang G, Shuping X, Jun L. FT-IR spectroscopy of supersaturated aqueous solutions of magnesium borate. Spectrochim Acta A 1999; 56(7):1291–7.
- [33] Tang Q, Wu J, Sun H, Fan S, Hu D, Lin J. Superabsorbent conducting hydrogel from poly(acrylamide-aniline) with thermo-sensitivity and release properties. Carbohyd Polym 2008;73:473–81.
- [34] Hu Y, Ye L, Zhao X. Synthesis of the melamine—formaldehyde polycondensate and its thermal stabilization effect on polyoxymethylene. Polymer 2006;47: 2649–59.
- [35] Genovese A, Shanks RA. Structural and thermal interpretation of the synergy and interactions between the fire retardants magnesium hydroxide and zinc borate. Polym Deg Stab 2007;92:2–13.
- [36] Zhang J, Wang A. Study on superabsorbent composites. IX: synthesis, characterization and swelling behaviors of polyacrylamide/clay composites based on various clays. React Funct Polym 2007;67:737–45.
- [37] Liang H, Asif A, Shi W. Thermal degradation and flame retardancy of a novel methacrylated phenolic melamine used for UV curable flame retardant coatings. Polym Deg Stab 2005;87:495–501.
- [38] Costa L, Camino G, Luda di Cortemiglia MP. Mechanism of thermal degradation of fire-retardant melamine salts. In: Nelson G, editor. Fire and polymers: hazards identification and prevention. ACS Symposium Series 425. Washington, DC: ACS; 1990. p. 211e38.
- [39] Koo JH, editor. Polymer nanocomposites: processing, characterization, and applications. New York: The McGraw-Hill Companies, Inc.; 2006.

Synthesis of Acrylamide-Co-(Itaconic Acid) Superabsorbent Polymers and Associated Silica Superabsorbent Polymer Composites

Nispa Seetapan,¹ Natsiri Srisithipantakul,² Suda Kiatkamjornwong³

¹ National Metal and Materials Technology Center, National Science and Technology Development Agency, Pathumthani 12120, Thailand

Superabsorbent polymers (SAPs) were synthesized from acrylamide (AM) and itaconic acid (IA) via a crosslinking polymerization. SAP composites (SAPCs) were formed by the incorporation of silica with three particle sizes into the polymerization to increase the gel strength of SAPs. Effects of AM: IA molar ratios, silica types and concentrations on water absorbency, absorbency rate and absorbency under loadings (AUL) of the composites were investigated. The highest water absorbency of the SAP is 233 \pm 8 g g⁻¹ at an AM: \not IA molar ratio of 97:3 with absorbency of 149 \pm 2 g g $^{-1}$ within 15 min. The highest AUL of the SAPC with 0.5%–2.0% w w $^{-1}$ silica is 13 g g $^{-1}$ by 1.93 \times 10 3 Pa load. A pseudo-second-order kinetics for water absorbency was found in both SAPs and in situ SAPCs. In situ SAPCs and the mechanically mixed SAPCs in vertical and horizontal direction yielded similar water absorbency values. POLYM. ENG. SCI., 51:764-775, 2011. © 2011 Society of Plastics Engineers

INTRODUCTION

Superabsorbent polymers (SAPs) and their associated SAP composites (SAPCs) have drawn much interest since the early 1970s. During that period, Fanta et al. investigated graft copolymerization of vinyl acrylate or acrylonitrile onto starch and other polysaccharides, which yielded products that could absorb from several hundred to sev-

Correspondence to: Suda Kiatkamjornwong; e-mail: ksuda@chula.ac.th Contract grant sponsor: Thailand Research Fund; contract grant number: RTA5080004; contract grant sponsor: Imaging Polymer Laboratory of the Faculty of Science's Department of Imaging and Printing Technology, Chulalongkom University.

DOI 10.1002/pen.21882

Published online in Wiley Online Library (wileyonlinelibrary.com). © 2011 Society of Plastics Engineers

eral thousand times their own weight in water and also had a high water holding capacity under pressure, also known as absorbency under load (AUL) [1], and thus the name "superabsorbent polymer" was adopted. Research and development into SAPs have focused on their extraordinarily high-water absorbency and applications. Indeed, over 80% of SAPs have found extensive commercial applications as sorbents in personal care products, such as infant diapers [2], feminine hygiene products, and incontinence products [3]. Not only that, but also many new applications have already been investigated through such active research and development, leading to the successful application of SAPs in new fields, such as matrices for enzyme immobilization [4, 5], bio-sorbents in preparative chromatography [6], materials for agricultural mulches and fertilizers [7, 8], matrices for controlled release devices [9], drug delivery [10], bioactive scaffolds for bone engineering [11], bio-separation [12], moisture retention in soil [13, 14], SAPCs as a sealing material [15], debris flow control, artificial snow [16, 17], a gel actuator [18], and fire fighting [19]. The desired features of superabsorbents are a high swelling capacity, high swelling rate, and a greater strength of the swollen gel. The majority of the reported superabsorbents comprise of only the first mentioned feature, i.e., a high absorbency, but there are few studies concerning improvements of the absorbency rate and gel strength. Absorbent particles are conventionally strengthened through surface crosslinking [20]. Traditionally, an inorganic component is used as a filling material for the purpose of improving the material properties and reducing the product cost. The addition of inorganic powder (usually <5% w w⁻¹) to a SAP provides a method for increasing the gel strength [21-23]. The utility of the inorganic nanoparticles as additives to enhance the polymer performance has been increased. Such inorganic materials for the preparation of SAPCs can be laponite

² Faculty of Science, Chulalongkorn University, Bangkok 10330, Thailand

³ Program of Petrochemistry and Polymer Science, Faculty of Science, Chulalongkorn University, Bangkok 10330, Thailand

[21], kaolin [24], montmorillonite [22, 25], attapulgite [26–28], mica [23, 29], bentonite [30], sercite [31], or rectorite [32] to form the layered silicate structures.

A novel SAPC based upon starch-g-AM/mineral powder, with a water absorbency of about 4000 times its own weight, was synthesized by a graft-copolymerization reaction of AM, potato starch, and mineral ultrafine powder, followed by hydrolysis with sodium hydroxide [33]. The SAPCs doped with kaolinite powder possessed a higher water absorbency than those doped with bentonite or sercite powder, since the kaolinite powder can moderately disperse in the water and crosslink with the AM and starch. Moreover, the collaborative absorbent effect of -CONH₂, -COONa, and -COOH groups has been found to be superior to that of a single -CONH₂, -COONa, or -COOH group. The ultrafine mineral powder as a crosslinking point plays an important role in the formation of a network structure in SAPCs. Incorporation of kaolin into hydrogel SAPCs caused a reduced equilibrium swelling and swelling rate to as low as 17-31% and 19-29% (w w⁻¹), respectively, but resulted in an enhanced gel strength by as much as 21-35% above that of the corresponding SAP as a control [34]. Grafted sodium carboxymethylcellulose (CMC) - silica gel SAPC with a water absorbency capacity as high as 4000 g g⁻¹ in distilled water has been reported [35]. Super porous hydrogel composites with the inclusion of modified cellulose gum or an internally cross-linked form of CMC typically gave a significant improvement in the properties of superporous hydrogels, such as a high mechanical strength and a high swelling ratio. Indeed, the inclusion of a suitable composite material typically increases the physical crosslinking density and so provides a high strength and prevents the polymer chains from collapsing during air drying [36]. The in situ sol-gel method used to prepare bioactive hydrogels [11, 37, 38] is considered to be quite expensive for industrial use. Therefore, the use of amorphous silica powder to form the non-layered silica SAPCs is a cheaper way for industries to manufacture personal care products. On the other hand, the mechanical mixing of SAP with silicate powder can be another economical way to prepare SAPCs.

In this research, poly[acrylamide-co-(itaconic acid)]/silica composites as potential SAPCs were made by in situ solution polymerization with three different sizes of silica. The SAPCs with a high water absorbency rate and

TABLE 1. Silica types and their physical properties.

Physical properties	Aerosil 90	Aerosil 200	Aerosil 300
BET surface area, (m ² g ⁻¹) Average primary particle size, (nm) pH SiO ₂ (% w w ⁻¹) Al ₂ O ₃ (% w w ⁻¹) Fe ₂ O ₃ (% w w ⁻¹)	90 ± 15 20 3.7-4.7 >99.8 <0.05 <0.003	200 ± 25 12 3.7-4.7 >99.8 <0.05 <0.003	300 ± 30 7 3.7-4.7 >99.8 <0.05 <0.003
HCl (% w w ⁻¹)	< 0.005	< 0.025	< 0.005

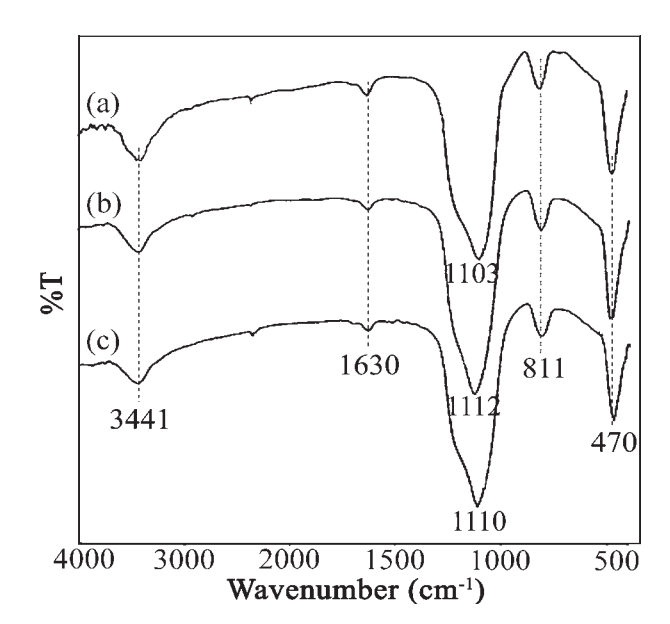


FIG. 1. IR spectra of the three types of silica used in the synthesis: (a) Aerosil 90, (b) Aerosil 200, and (c) Aerosil 300.

capacities were compared with the SAPCs prepared by mechanical mixing between the P(AM-IA) SAP and silica powder of the same composition.

EXPERIMENTAL PROCEDURES

Materials and Methods

Acrylamide (AM, Siam Chemicals, Bangkok, Thailand), itaconic acid (IA, Merck, Hohenbrunn, Germany), N,N'-methylenebisacrylamide (N-MBA, Fluka, Buchs, Switzerland), ammonium persulfate (APS, Merck, Hohenbrunn, Germany), N,N,N',N'-tetramethylethylenediamine (TEMED, Fluka, Buchs, Switzerland), and silica (SiO₂, J.J-Degussa-Huts, Thailand) were used. The three types of silica used in this research, and their properties, are shown in Table 1 and their IR spectra are given in Fig. 1.

Polymerization

A 100-cm³ mixture of AM: IA of 100:0, 99:1, 98:2, and 97:3 (by % molar ratios) was supplemented with 0.5% w w⁻¹ N-MBA crosslinker, the initiator couple of APS (1.0% w w⁻¹) and TEMED (0.20 cm³), and then poured into a 500-cm³ four-necked round-bottomed flask equipped with a mechanical stirrer (Ika-Ruhrwerke RW20, Staufen, Germany), a spiral condenser and a thermometer. The polymerization reaction was allowed to proceed at 45°C in a water bath (WBU 45 Memmert, Schwabach, West Germany) under a nitrogen gas atmosphere for 30 min with stirring at 250 rpm The resulting polymer was dehydrated with methanol, cut into small pieces of half a centimeter in diameter, dried in a vacuum

TABLE 2. Basic formulation for the preparation of P(AM-IA) SAPs and P(AM-IA)/silica SAPCs.

Ingredient	In situ polymerization method	Mechanical mixing method
AM / IA (mole/mole)	100/0, 99/1,	100/0, 99/1,
	98/2, 97/3	98/2, 97/3
Aerosil 90 silica (w w ⁻¹)	0.1, 0.2, 0.5, 2.0	0.1, 0.5, 2.0
Aerosil 200 silica (w w ⁻¹)	0.1, 0.2, 0.5, 2.0	_
Aerosil 300 silica (w w ⁻¹)	0.1, 0.2, 0.5, 2.0	0.1, 0.5, 2.0
N-MBA (w w ⁻¹)	0.5	0.5
APS (w w^{-1})	1.0	1.0
TEMED (cm ³)	0.2	0.2
Horizontal mixing (rpm)	600	600
Vertical mixing (rpm)	100	100

oven (Hotpack, USA) for 24 h to a constant weight, and then milled. The obtained copolymer powders were then investigated for their water absorbency capacity. The monomer AM: IA molar ratio from which the synthesized P(AM-IA) copolymer possessed the highest water absorbency was then selected to prepare the P(AM-IA)/silica SAPC.

To prepare the SAPCs, three types of silica, namely Aerosil 90, Aerosil 200, and Aerosil 300, each at four different concentrations of 0.1, 0.2, 0.5, and 2% w w⁻¹, were added in situ with the other ingredients in the polymerization process as shown in Table 2.

Characterization of the Copolymers

Identification of the Functional Groups of the Synthesized Copolymers. The functional groups of the copolymers were investigated by Fourier transform infrared spectroscopy (FTIR model Nicolet Impact 410) using a KBr pellet method with 32 scans and 4 cm⁻¹ resolution. The interface software (Nicolet Omnic) was connected to the Nicolet FTIR in a data acquisition system.

Surface Morphology of the Synthesized Copolymers. The surface morphology of the copolymers was investigated using scanning electron microscopy (SEM, model JSM-6400, Japan) without cross-sectioning. The thickness of gold coated on the copolymer was 25 nm, and SEM was operated with a 15 kV accelerating voltage. The elemental analyses of the SEM micrographs were investigated by energy dispersive X-ray spectrometry (EDXS).

Equilibrium Water Absorbency

In deionized Water. Deionized water (150 g) was added to 0.1 g of the dry copolymer (A) in a 250 cm³ glass beaker covered with a lid and it was allowed to swell for 30 min. The completely swollen copolymer gel was filtered through 100-mesh aluminum sieve screen for 3 h

and the remaining swollen copolymer gel was weighed (B). The water absorbency (g g⁻¹ of the dry copolymer) was calculated by Eq. I shown below:

Water absorbency of copolymer
$$(g g^{-1}) = (B - A)/A$$
 (1)

Absorbency Under Load (AUL). Deionized water (25 cm³) was placed in a Petri dish. A 0.16 g (A) aliquot of the dry copolymer was carefully scattered onto the filter screen of the test device (a flexiglass cylinder of 26 mm diameter, 35 mm height, and a 100 mesh stainless steel cloth in the bottom). A piston assembly, including an additional weight to achieve a load of 0.28 psi $(1.93 \times 10^3 \text{ Pa})$ was placed on the top of the dry copolymer. After weighing the assembly device (B), it was placed on the Petri dish, and absorbency was allowed to proceed for 1 h after which time the entire device was reweighed (C). Similar experiments were carried out for a load of 0.70 psi $(4.83 \times 10^3 \text{ Pa})$. The AUL (g g⁻¹) was calculated by Eq. 2:

$$AUL(g g^{-1}) = (C - B)/A$$
 (2)

Swelling Kinetics of the SAPs and SAPCs. Deionized water of 1000 cm^3 was placed in a 2-dm³ beaker. The dry copolymer of 0.1 g was sealed in a teabag and placed in a beaker where it was allowed to swell for 15 min. The soaked teabag was removed from the beaker and the swollen copolymer was weighed after excess water on the bag was blotted out on filter paper. Similar experiments were carried out but for gel swelling times of 15, 45, 105, 225, 1125, and 1605 min. Schott's equation [39], as shown in Eq. 3, is used to describe a well-known pseudo second-order absorbency kinetics equation and was used in these studies to test for pseudo second-order absorbency kinetics of water absorbency by the SAPs and SAPCs. Since:

$$t/Q_{\rm t} = t/Q_{\infty} + 1/kQ_{\infty}^2,\tag{3}$$

where $Q_{\rm t}$ and Q_{∞} are the absorbencies at time t and infinite time for full swelling and k is the absorbency coefficient which describes the rate constant of swelling, then by plotting $t/Q_{\rm t}$ vs. t, Q_{∞} and k can be calculated.

The Level of Retained Silica in the P(AM-IA) Gel. A 1.00 g (A) aliquot of the dry copolymer was placed in a 100 cm^3 porcelain crucible on a hot plate and heated at 100°C for 45 min before being placed in a muffle furnace (Vulcan 3-550 PD) at 600°C for 90 min until all the powder became white. The crucible was removed from the furnace and cool. The white powder was weighed (B), and the amount of retained silica in the gel was calculated by Eq. 4:

Silica retained in the gel =
$$(B - A)/A$$
 (4)

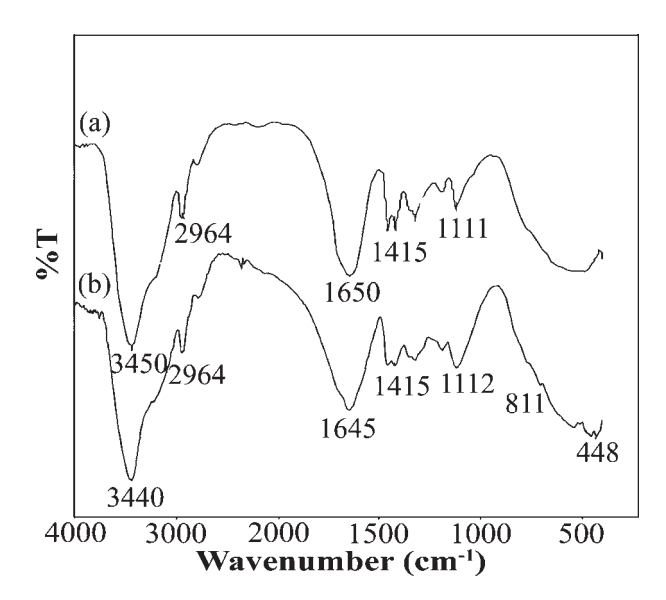


FIG. 2. IR spectra of (a) P(AM), and (b) P(AM)/Aerosil 90 silica composite.

SAPCs by Mechanical Mixing. A 0.2 g aliquot of the dried P(AM-IA) copolymer powder having a mesh size of not larger than 100 and the specified amount of silica were mixed in the bottle by a home-made mixing rotator with a controllable speed at 600 rpm for 30 min for horizontal mixing (HM). For the vertical mixing (VM), the mixture was shaken with a speed of 100 rpm in a rolling type mixer (MS1 Minishaker, IKA-Work, Inc, Wilmington). After mixing (either HM or VM), the sample was transferred for the water absorbency experiment. The types of silica and copolymer used for the mixing are shown in Table 2.

RESULTS AND DISCUSSION

The assignments of the FTIR spectra of the three silicas are shown in Fig. 1. All three types of silica (Aerosil 90, Aerosil 200, and Aerosil 300) gave the similar IR peaks with a medium OH stretching peak at 3444–3441 cm⁻¹, a weak C=O stretching peak at 1630 cm⁻¹, a strong peak at 1112–1103 cm⁻¹ for Si—O—Si bending, a medium peak at 811–810 cm⁻¹ for Si—OH and a sharp peak at 474–470 cm⁻¹ for Si—O—Si bending. Table 1 shows that their BET surface areas and average primary particle sizes are significantly different.

The peaks of P(AM) (Fig. 2a), P(AM)/Aerosil 90 silica SAPC (Fig. 2b, P(AM-IA) (Fig. 3a) and P(AM-IA)/Aerosil 90 silica SAPC (Fig. 3b) indicated that silica was attached onto both the AM and IA moieties via covalent bonding. All copolymers showed the strong peak at 3450–3440 cm⁻¹ for the N—H stretching overlapping with the OH— stretching, the medium peak at 2939–2936 cm⁻¹ for the C—H stretching, the medium peak at about 1650 cm⁻¹ of the C=O stretching for amide I, the peak at 1415–1452 cm⁻¹ for the C—H bending of amide, and the medium peak at 1112–1120 cm⁻¹ for the N—H (am-

ide II) bending. Besides the aforementioned peaks, the Si—O—Si sharp peak of Aerosil 90 silica at 470 cm⁻¹ was shifted to 448 cm⁻¹ in the P(AM)/Aerosil 90 silica (Fig. 2b) and to 447 cm⁻¹ in the P(AM-IA)/Aerosil 90 silica SAPCs (Fig. 3b). Other SAPCs with either Aerosil 200 or Aerosil 300 silica addition demonstrated the similar spectra (not shown here) as the Aerosil 90 silica-co-polymer composites.

The existence of silica particles in the SAPCs was confirmed by SEM micrographs (see Fig. 4). PAM and P(AM-IA) copolymers have a rough morphology (Fig. 4a and b), while the micrograph of P(AM-IA)/Aerosil 90 silica composite shows a similar morphology but with large agglomerates of white particles of silica trapped on the rough surface of polymer matrix (Fig. 4c). EDXS analysis of P(AM-IA) and P(AM-IA)/Aerosil 90 silica composite (Fig. 4d and e) indicates that besides common elements such as carbon and oxygen found in both copolymers, the presence of silicon element was also detected in the prepared copolymer composite at the energy peak at 1.75 keV. Therefore, data from SEM-EDXS confirmed that the silica particles were retained within the SAPCs.

Effect of Itaconic Acid Concentration

The Water Absorbency of the Synthesized Copolymer. The water absorbency of the copolymers synthesized in situ by solution polymerization with three concentrations (0, 1, 2, and 3% molar ratio) of IA is shown in Table 3. Because the reactivity ratios r_1 and r_2 values for AM/N-MBA are 0.64 and 1.77, respectively, the PAM was thus rigid due to more effective crosslinking density to cause the low water absorbency [40]. The effective

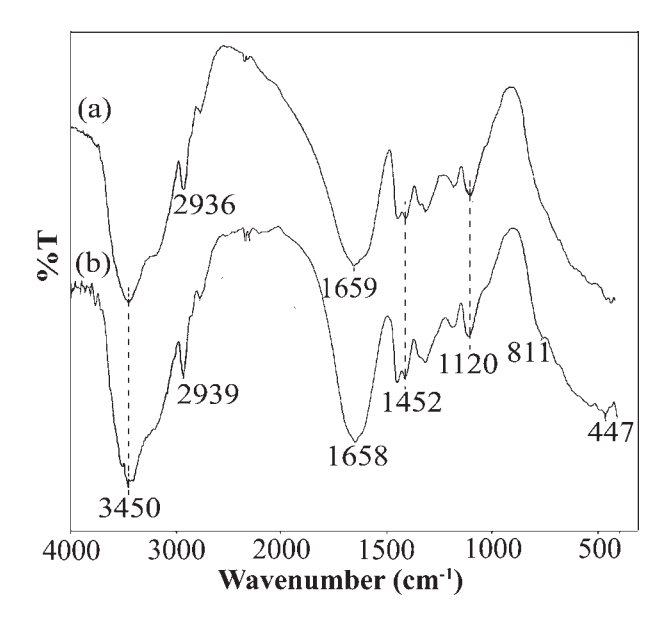


FIG. 3. IR spectra of (a) P(AM-IA), and (b) P(AM-IA)/Aerosil 90 silica composite.

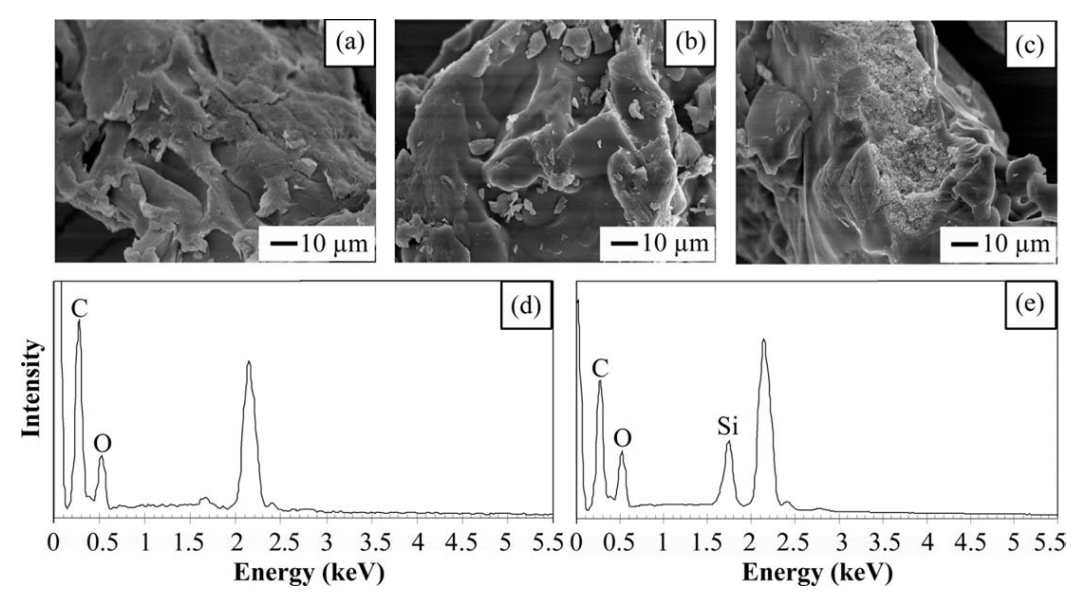


FIG. 4. SEM micrographs of (a) P(AM), (b) P(AM-IA), and (c) P(AM-IA)/Aerosil 90 silica composite; and EDXS spectra of (d) P(AM-IA) and (e) P(AM-IA)/Aerosil 90 silica composite.

crosslinking density is defined as the number of moles of elastically effective crosslinks per unit volume of polymer. Therefore, an increase of hydrophilic monomer (IA) in the SAPs enhances the swelling capability and, hence, decreases the effective crosslinking density. This statement has been investigated by several researches. Our previous investigation, for example, found that SAPs with high water absorbency were accompanied by low gel strength and the calculated low value of effective crosslinking density [41]. The water absorbency increases with increasing concentrations of the hydrophilic and ionic functional groups of IA, in good agreement with the previous findings by Uyanik and Erbil [42] and Pulat and Eksi [43], who reported that increasing IA concentrations in copolymer structures decreases the effective crosslinking densities of the polymer networks. As IA cannot form superabsorbent polymers by itself, an excessive amount of IA in the monomer mixture made it more difficult to form a copolymer gel. Thus, here we could show the results of IA concentrations up to only 3% (molar ratio). The degree of swelling of the synthesized P(AM-IA) copolymers mainly depends on the repulsive forces between the hydrophilic pendants (amide and carboxylic groups) in their structures. For AM/IA copolymer, IA was reported to be more reactive than AM ($r_{\rm IA} > r_{\rm AM}$) [42]. Therefore, IA molecules are used up via a crosslinking reaction with N-MBA before AM monomer, even if AM feed concentrations are higher. In the present case, the structure of the copolymer should contain more units of the uncrosslinked PAM moiety than crosslinked IA units owing to a higher AM concentration and higher reactivity of N-MBA. The synthesized copolymer must have an optimum ratio of AM-to-IA to balance hydrophilic or ionic functional groups and chain flexibility to produce the copoly-

mer with the highest water absorbency capacity. The copolymer synthesized by an AM: IA molar ratio of 97:3 can absorb deionized water to as high as 233 \pm 8 g g $^{-1}$ (Table 3). However, the AUL values were nearly constant at 11–12 g g $^{-1}$ and 12–14 g g $^{-1}$ for a load of 0.28 psi (1.93 \times 10 3 Pa) and 0.70 psi (4.83 \times 10 3 Pa), respectively, regardless of the IA concentration. Thus, the AUL was essentially constant regardless of the loads and the concentration of the hydrophilic or ionic functional groups and chain flexibility.

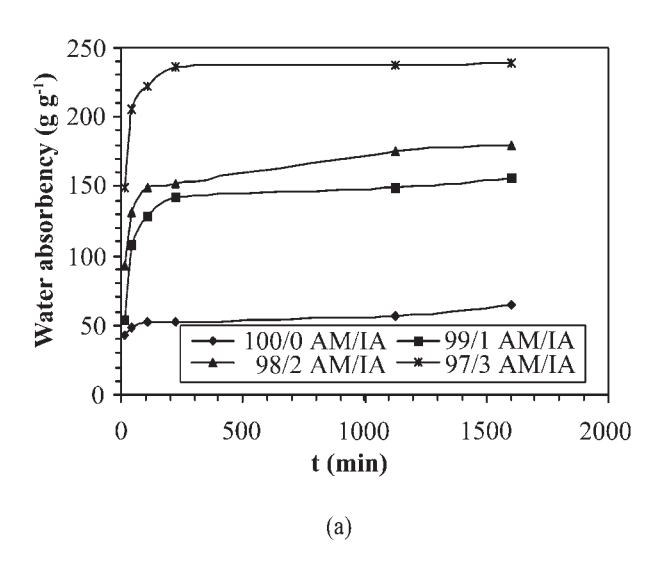
The AUL is a measure of the ability of an SAP to absorb a liquid while the SAP is under an application of load or restraining force. The value of AUL is altered proportionally to the strength of the swollen gel, thus, AUL is often reported in the technical data sheets and patent articles in order to quantify the gel strength suitable for a particular application such as diapers for baby and adult [44, 45].

In free swelling (without an application of external load), the presence of ionic charges along polymer chains significantly increases the swelling of SAPs due to an increase in electrostatic repulsive forces between charged

TABLE 3. Effect of itaconic acid concentration (molar ratio) on the water absorbency of the P(AM-IA) SAP.

Itaconic acid	Water abso	Water absorbency under load (AUL [Pa]) of						
concentration (% molar ratio)	0	1.93×10^{3}	4.83×10^{3}					
0	51 ± 2	14	12					
1	157 ± 9	14	12					
2	191 ± 6	13	11					
3	233 ± 8	12	11					

APS, $1.0\% \text{ w w}^{-1}$; N-MBA, $0.5\% \text{ w w}^{-1}$; at 45°C , 250 rpm, 30 min.



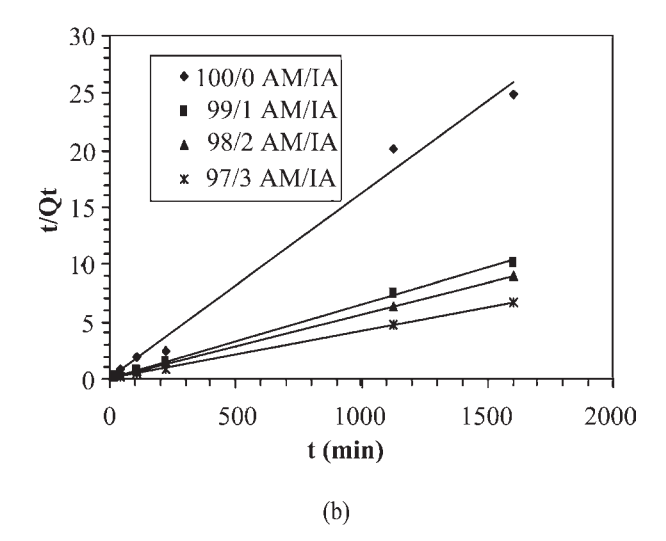


FIG. 5. Effect of the itaconic acid concentration (molar ratio) on the swelling kinetics of: (a) water absorbency vs. absorption time, (b) t/Q_t vs. absorption time (the linear regression equations and correlation coefficients were given in Table 4).

sites on the carboxylate anions (in case of IA) upon their complete dissociation and thus leads to a more extended configuration, as seen in Table 3 that the copolymer system of 3% mole of IA yielded the water absorbency of around 233 g g^{-1} , while the water absorbency of the P(AM) SAP was about 51 g g^{-1} .

However, under an application of load, the swelling ability of SAP is decreased with respect to the load-free absorbency (see Table 3) as a result of the restricted mobility of polymer chain. Therefore, the diffusion of a liquid into the SAP particle is counterbalanced by the external pressure applied on the SAP particles. As a result, our data imply that the extended conformations of the main chain, especially in SAP containing ionic charges, are prohibited under an application of load. Therefore, the observed AUL value was insignificantly altered irrespective of the applied loads and the concentration of ionic groups within the SAP.

The Swelling Kinetics of the Synthesized Copolymers. In practical applications, not only is a higher absorbency capacity required for the absorbent, but also a high swelling rate. The swelling kinetics of hydrogels have been characterized as occurring in two stages; an initial first order (Fickian diffusion model) stage followed by a later second order (Schott model) stage. In the initial stage, the swelling of hydrogel in water is governed by a

first order diffusion process which involves migration of water to fill the spaces between polymer chains. The Fick model is thus valid for the initial swell stage where the fractional swelling value (Q_t/Q_{∞}) is less than or equal to 0.6 [46]. The Schott model is used for longer swelling times when the density of the hydrogel has increased. At this second order swelling, the swelling kinetic is not controlled by diffusion, but by the relaxation of the polymer chains [39, 47]. The evaluated swelling kinetics of the P(AM-IA) copolymer, synthesized by in situ solution polymerization of various concentrations (0, 1, 2, and 3% molar ratios) of IA revealed that the higher the IA concentration, the larger the water absorbency became (Fig. 5a). In other words, the P(AM) SAP gave the lowest water absorbency and the 97:3 (molar ratio) P(AM-IA) SAP gave the highest water absorbency (233 \pm 8 g g⁻¹) due to the hydrophilic nature of the carboxylic acid of the IA monomer. The 97:3 (molar ratio) P(AM-IA) SAP could absorb deionized water up to $149 \pm 2 \text{ g g}^{-1}$ of the dry copolymer within 15 min and reached the highest absorbency within 200 min. A plot of t/Q_t vs. t reveals that all the absorbency data almost perfectly fit in a linear line with small positive intercepts and high r^2 values, in support of pseudo-second order kinetics (Fig. 5b). The fitting equation and the r^2 value are reported in Table 4. Indeed, the experimentally determined water absorbency values fit the theoretically determined values from the

TABLE 4. Equilibrium water absorbency (Q_{∞}) and rate constant of swelling of P(AM-IA) SAPs prepared from various IA contents.

IA content (% molar)	Q_{∞} (Schott model)	$K (\min^{-1})$	Q_{∞} (experimental)	Fitting second order kinetic equation	r^2
0	62	6.14e-3	51 ± 2	y = 0.0161x + 0.0422	0.9894
1	156	2.53e-4	157 ± 9	y = 0.0064x + 0.162	0.9996
2	182	2.27e-4	191 ± 6	y = 0.0055x + 0.1333	0.9997
3	238	5.44e-4	233 ± 8	y = 0.0042x + 0.0324	1

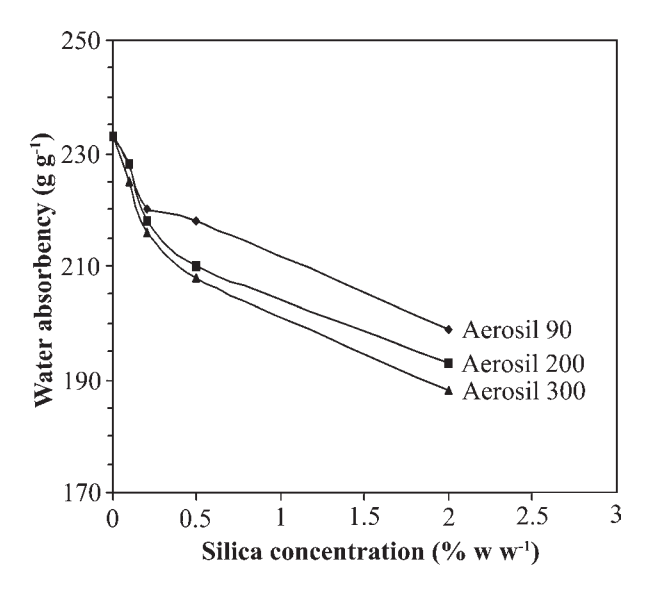


FIG. 6. Effect of silica concentration on water absorbency of SAPCs synthesized from 97:3% molar ratio of AM:IA.

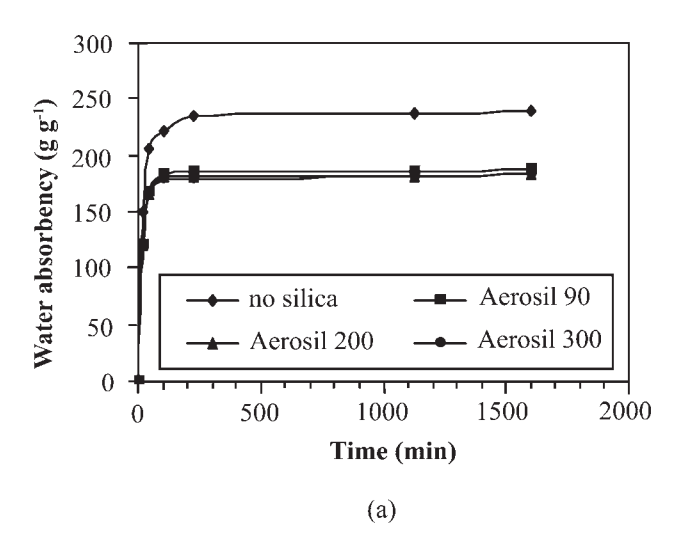
Schott model (Eq.~3) supporting pseudo-second order kinetics for the swelling behavior of the P(AM-IA) SAPs (Table 4). In comparison to the P(AM) SAP, the presence of IA in the hydrogel lowered the swelling rate constant (k), although the k value at a 3% molar ratio of IA was higher than that for 1 and 2% IA but still less than that seen in the P(AM) SAP (Table 4). Likewise, the first order kinetics model also tested (not shown here) does not give a good straight line but gives low regression values.

Effect of Silica

Type and Concentration of Silica on the Water Absorbency of SAPCs. The incorporation of each type

of silica (Aerosil 90, 200, and 300) into the 97:3 (molar ratio) P(AM-IA) copolymer to form P(AM-IA)/silica composites reduced the water absorbency of the SAPC in a dose dependent manner, reaching a level of some 15-20% lower at 2% w w⁻¹ silica than that seen without silica, 0% (see Fig. 6). In addition, there was a dependency upon the type of silica, with the larger silica particles yielding a SAPC with lower water absorbency at the same nominal silica concentration. For example, compared to that at 0% silica, the water absorbency was decreased from 233 \pm 8 g g⁻¹ to 199 \pm 4, 193 \pm 6, and 188 \pm 1 g g⁻¹, a reduction of 15, 17, and 20%, with the incorporation of Aerosil 90, Aerosil 200, and Aerosil 300 at 2% w w⁻¹, respectively. This is to be expected since water absorbency is related to the higher hydrophilic properties of the hydrophilic chain and the silica particle size, as shown in Table 1, the BET surface areas of the three silicas differ significantly. As to the dose-dependent effect, the silica particles present in SAPs act as crosslinking points [5], and so more crosslinking points are available with the increased addition of SiO₂ in addition to the N-MBA crosslinking agent. Although more hydrogen bonding takes place between the hydrophilic silanol group on the silica, water absorbency through this bonding may increase the rigidity of the chain. Since the surface physical-chemical properties are the same, and so do not differentially affect the water absorbency of the SAPCs, their surface areas and average primary particle size are, therefore, the important attributes controlling the extent of water absorbency.

Type of Silica and Silica Content on the Swelling Kinetics. The swelling kinetics of the SAPCs, synthesized from a 97:3 molar ratio of AM:IA with in situ incorporation of 2.0% w w⁻¹ of silica were essentially the same for all three types of silica (Fig. 7a) and showed pseudo second-order absorbency kinetics regardless of the



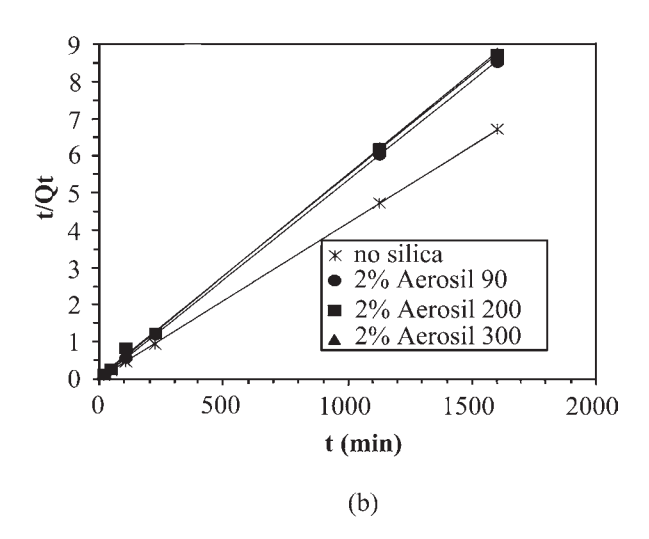


FIG. 7. Effect of the type of silica on the swelling kinetics of a P(AM-IA)/2% w w⁻¹ silica composite (97:3 molar ratio of AM: IA) showing the (a) water absorbency vs. absorption time, and (b) t/Q_t vs. absorption time (the linear regression equations and correlation coefficients were given in Table 5).

TABLE 5. Equilibrium water absorbency (Q_{∞}) and rate constant of swelling (k): of SAPCs prepared from P(AM-IA)/2% w w w¹ silica (97:3 molar ratio of AM: IA), with the indicated different types of silica particles.

System	Q_{∞} (Schott model)	k (min ⁻¹)	Q_{∞} (experimental)	Fitting second order kinetic equation	r^2
No silica	238	5.44e-4	233 ± 8	y = 0.0042x + 0.0324	1
Aerosil 90	189	9.03e-4	188 ± 6	y = 0.0053x + 0.0311	1
Aerosil 200	185	3.14e-4	184 ± 2	y = 0.0054x + 0.0928	0.9994
Aerosil 300	182	6.53e-4	183 ± 4	y = 0.0055x + 0.0463	1

presence of silica and its concentration (Fig. 7b). The high quality of linear curve fitting is represented by the value of r^2 equal to 1 (Table 5). Again the experimental water absorbency values were very close to those derived theoretically from the Schott model of pseudo secondorder kinetics (Table 5). In the presence of 2.0% w w⁻¹ silica, the resulting 97:3 molar ratio P(AM-IA)/silica SAPC could absorb water at the very similar values of 121 ± 8 , 119 ± 8 , and 118 ± 8 g g⁻¹ of the dry polymer within 15 min for Aerosil 90, Aerosil 200, and Aerosil 300, respectively. The dependence of swelling time on the equilibrium swelling rate arises because the mass of liquid absorbed during the swelling, so that the rate increases until constant at the absorbency time longer than 300 min. The water swelling rate depends on the equilibrium swelling capacity of the polymer. The swelling absorbency values of the 97:3 P(AM-IA)/silica SAPCs with Aerosil 90, Aerosil 200, and Aerosil 300 are not much different to each other but decreased with increasing concentrations of silica (Table 6). As mentioned before, the fine silica particles act as additional crosslinking junctions and so the crosslink density increased with increasing silica levels, leading to a decreased swelling.

The swelling kinetics of the P(AM-IA)/silica SAPCs, synthesized from a 97:3 molar ratio of AM: IA with four contents of Aerosil 90, are shown in Fig. 8a, and replotted as t/Q_t vs. t in Fig. 8b. As mentioned earlier, all the t/Q_t vs. t plots are linear and fit well with the calculated values using the Schott's pseudo second-order absorbency kinetics model (Table 7). The incorporation of silica causes a dose-dependent decrease in the water absorbency, but the rate constant of swelling (k) was accelerated by increasing silica contents, due to the increasing level of crosslinking density within the SAPCs.

In view of the second-order absorbency kinetics observed in a later time course (Figs. 5, 7, and 8), one

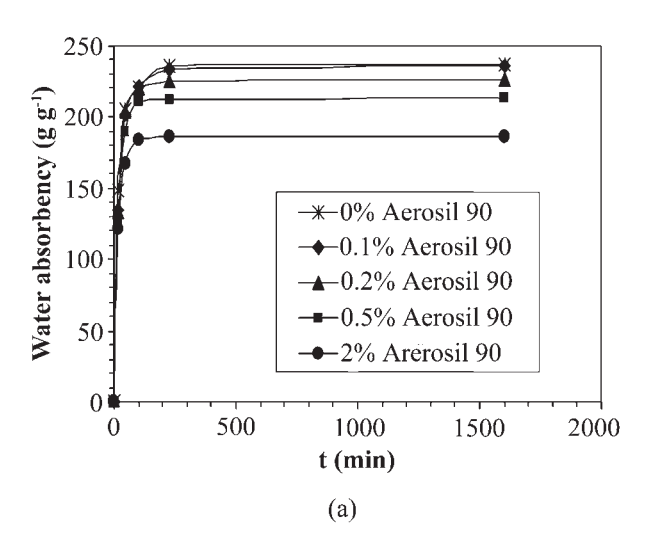
can describe the absorbency behavior as follows. When the P(AM-IA) SAP or P(AM-IA)/silica SAPC contacts with the excess amount of water, diffusion takes place which is governed by a first-order process on a short time scale (Fick model), and then subsequently the rate of swelling at long swelling times is not governed by the diffusion, but rather is mainly controlled by stress relaxation of the amorphous regions of the polymer network which follows a pseudo second-order kinetics control (Scott model).

The Effect of the Type of Silica and its Content on the Water AUL of the Synthesized Copolymers. The water AUL $(1.93 \times 10^3 \text{ Pa})$ and $4.83 \times 10^3 \text{ Pa}$ of the P(AM-IA)/silica SAPCs, synthesized from a 97:3 molar ratio of AM: IA in the presence of the three silica types (Aerosol 90, 200, and 300) and four contents $(0.1, 0.2, 0.5, \text{ and } 2\% \text{ w w}^{-1})$ of silica is shown in Table 6. The AULs at $1.93 \times 10^3 \text{ Pa}$ and $4.83 \times 10^3 \text{ Pa}$ for the 97:3 P(AM-IA) SAP were very similar at 12 g g⁻¹ and 11 g g⁻¹, respectively (Table 3), and were not significantly changed by the addition of silica, type or concentration, with all tested P(AM-IA)/silica SAPCs having an AUL of 11-13 g g⁻¹ at both evaluated loads.

In general, silica has been used to help improve the gel strength so as to provide a higher AUL to swollen gels with an otherwise reduced water absorbency. The swelling in the present work was observed to decrease slightly with increasing contents of silica in the P(AM-IA)/silica composite. The additional amounts of silica probably act as nonreactive filler dispersed in the network. It may be attributed to the fact that fine silica particles act as additional junctions. Therefore, silica imposes effects on gel strength or AUL improvement, in that the higher the silica concentration, the higher the gel strength becomes.

TABLE 6. Effect of silica types and concentrations on the water absorbency of SAPCs (97:3 molar ratio of AM:IA).

				Water absorbe	ncy (g g ⁻¹) und	der loads (Pa) o	f		
Concentration of silica (% w w ⁻¹)		0		1.93×10^{3}			4.83×10^{3}		
	Aerosil 90	Aerosil 200	Aerosil 300	Aerosil 90	Aerosil 200	Aerosil 300	Aerosil 90	Aerosil 200	Aerosil 300
0.1	228 ± 1	228 ± 7	225 ± 2	12	12	12	11	11	11
0.2	220 ± 1	218 ± 2	216 ± 3	12	12	13	11	11	12
0.5	218 ± 1	210 ± 5	208 ± 5	13	13	13	12	12	12
2.0	199 ± 4	193 ± 6	188 ± 1	13	13	13	12	12	12



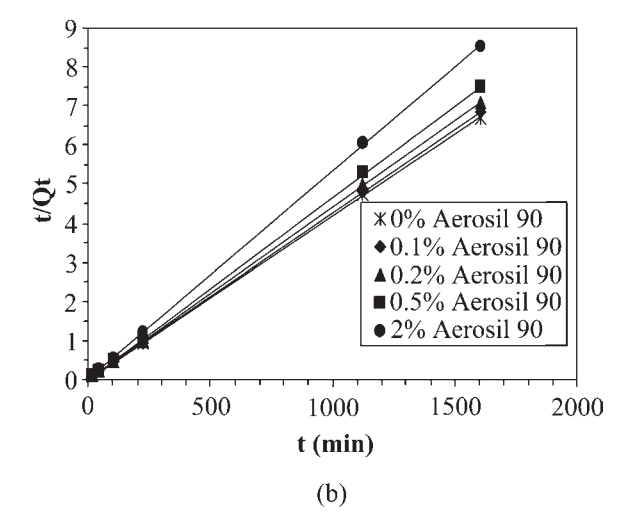


FIG. 8. Effect of silica concentration on the (a) water absorbency vs. absorption time and (b) t/Q_t vs. absorption time for a P(AM-IA)/Aerosil 90 silica composite (97:3 molar ratio of AM: IA) (the linear regression equations and correlation coefficients were given in Table 7).

Besides the crosslinking reaction, these characteristics may be attributed to the fact that the fine silica particles act as additional junctions for grafting reaction on their surface to increase the SAPC density. Increasing silica contents led to increased gel strength, although the water absorbency value of the SAPCs with different silica types (particle sizes) is not different at all. Increasing the water absorbency was achieved by a lower crosslinking reaction, AUL decreased because the swollen particles easily deformed and clumped together under load, liquid supplying voids or spaces were closed. If this is the case, then to increase the AUL, a second polymerization on the surface with a small amount of additional crosslinking density may be needed.

The Retained Silica in the Gel

The actual amount of silica that is incorporated into the 97:3 P(AM-IA)/silica SAPC was evaluated by the difference in silica contents between those in the initial prepolymerization and the final products after the polymerization (Table 8). The amounts of silica retained in the SAPCs are lower than the added amounts of silica added, i.e., the whole amount of silica is not incorporated into the polymer network, but rather only some 86–95% is retained. This is not linearly dependent upon the silica content in the polymerization reaction and, although their average primary particle sizes are significantly different, the interaction between SAPCs and the three different silica types cannot be differentiated. The retention of silica within the SAPCs is in agreement with the IR spectra (see Fig. 3) and the SEM-EDXS data (see Fig. 4).

Effect of Mechanical Mixing on Water Absorbency of SAPCs

Since it is possible to mix or blend the SAP with the silica particles as an organic and inorganic composite, it is of interest if the resulting composite will perform similarly to the in situ polymerized SAPCs. That is, the performance of the silica-filled SAPC can match that the in situ silica SAPC arises because the silica can leak out from the composite. Then, its strength might be somewhat lower compared to the in situ polymerized SAPCs.

Effect of the Mixing Method

The VM motion uses an eccentric motion in the vertical direction with a constant speed of 100 rpm while the

TABLE 7. Equilibrium water absorbency (Q_{∞}) and rate constant of swelling (k): of SAPCs prepared from P(AM-IA)/Aerosil 90 silica (97:3 molar ratio of AM: IA) with the incorporation of the indicated final Aerosil 90 concentration.

Aerosil 90 (w w ⁻¹)	Q_{∞} (Schott model)	k (min ⁻¹)	Q_{∞} (experimental)	Fitting second order kinetic equation	R^2
0	238	5.44e-4	233 ± 8	y = 0.0042x + 0.0324	1
0.1	238	5.78e-4	235 ± 6	y = 0.0042x + 0.0305	1
0.2	227	7.53e-4	227 ± 1	y = 0.0044x + 0.0257	1
0.5	213	8.09e-4	214 ± 6	y = 0.0047x + 0.0273	1
2	189	9.39e-4	188 ± 6	y = 0.0053x + 0.0299	1

TABLE 8. The silica retained in the gel at various silica concentrations.

Type of Aerosil	Silica concentration added in polymerization (% w w ⁻¹)	Silica concentration after sintering (% w w ⁻¹)	Silica concentration retained in the gel (% w w ⁻¹)
Aerosil 90	0.1	0.09	90
	0.2	0.19	95
	0.5	0.44	88
	2.0	1.79	90
Aerosil 200	2.0	1.85	93
Aerosil 300	2.0	1.71	86

HM method uses a constant rotation speed of 600 rpm in the horizontal direction. To this are added the SAP particles with silica powder, and dispersion of the components in the cylindrical bottle is accomplished by rotating the bottle and its contents about the horizontal axis of the cylindrical bottle at a rate sufficient to lift the silica particles to one side and then cause them to roll, slide and tumble or cascade to the lower side. At this speed, the rotation movement is the cascade manner. When the HM rotation of SAP and silica particles in the cylindrical bottle takes place, some parts of the particles contact with the cylindrical wall in the diameter direction of the roller movement, contact sites of the SAPs for silica particles decrease when the movement of the cylindrical bottle is continued. In the VM motion, both the SAPs and silica particles move up and down along the length of the cylindrical bottle. Therefore, the contact sites of the SAPs and silica particles in the VM direction are higher than the HM motion leading to the larger probability of silica particles in adhering to the SAP surface. The adsorption of silica is strengthened by hydrogen bonding between hydroxyl groups on silica surface and carboxylic and amine groups on P(AM-IA) SAP. Based on the mixing mechanism and speed, the Aerosil 300 having larger surface area (BET surface area of $300 \pm 30 \text{ m}^2 \text{ g}^{-1}$ and 7 nm particle size) adsorbed on SAP particles more than the Aerosil 90 silica did (BET surface area of 90 \pm 15 m^2 g^{-1} and 20 nm particle size). As a result Aerosil 300SAPC should provide the lower water absorbency since the adsorbed silica might interrupt the diffusion or the binding of water into the SAP particle. However, the results in Table 9 indicated that both the mixing direction and types of the investigated silica particles did not significantly alter the water absorbency of the SAPC comparative to the in situ SAPC polymerization.

When the mixture of SAPs and silica particles is mixed by an eccentric rotation (VM), they move up and down along the length of the cylindrical bottle. Therefore, the mixing force is controlled by a centrifugal acceleration, α , as shown in Eq. 5 [48, 49]:

$$\alpha = (r_{\rm h} + r_{\rm e})\omega^2 \tag{5}$$

where r_b is the radius of the glass bottle, r_e is the eccentric radius, and ω is the rotation angular velocity. According to the theory of the elasticity contact between spheres [48], the contact area S increases as indicated in Eq. 6:

$$S\alpha F^{2/3} \tag{6}$$

where F is the force worked on the spheres. The Aerosil 300 silica has a stronger force to hold silica particles on the surface of the SAP due to its larger surface area and smaller size. Thus, the SAPs and Aerosil 300 can physically interact, aggregate, or agglomerate together more strongly than those of Aerosil 90.

It is necessary to mention that SAPs at various AM:IA ratios without silica were also mixed horizontally or vertically as for a control purpose at the same condition for the SAPCs. The mixing force given to SAPs actually helps only disperse the particle agglomeration and imposes a slight effect on water absorbency as shown in Table 9. Regardless of the dependence of the mixing time on the SAPs-silica contact, the HM rotation rate is higher than the VM rotation and, therefore, the force between the SAP and silica particles by HM rotation increases rapidly. The mixing force between the SAP and silica particles can be divided into three regions: elastic, plastic and destructive. In the low mixing force region, the con-

TABLE 9. Mechanical mixing of the superabsorbent copolymer with silica by horizontal mixing or vertical mixing.

Silica surface	Silica		100/0			99/1			of SAPCs from AM/IA (mol %) 98/2			97/3		
area	content		100/0			77/1			70/2			7113		
$\frac{(m^2 g^{-1})}{}$	(% w)	In situ	VM	HM	In situ	VM	HM	In situ	VM	HM	In situ	VM	HM	
90	0	51 ± 2	35 ± 1	35 ± 1	157 ± 9	144 ± 8	144 ± 8	191 ± 6	201 ± 5	201 ± 5	233 ± 8	225 ± 4	225 ± 4	
	0.1	_	36 ± 2	19 ± 2	_	177 ± 7	182 ± 41	_	178 ± 9	174 ± 9	228 ± 1	239 ± 29	228 ± 17	
	0.5	_	37 ± 5	20 ± 3	_	165 ± 2	183 ± 24	_	155 ± 7	176 ± 11	218 ± 1	250 ± 13	340 ± 63	
	2.0	_	34 ± 0	21 ± 3	_	189 ± 35	136 ± 19	_	165 ± 19	164 ± 6	199 ± 4	225 ± 22	228 ± 8	
300	0	51 ± 2	35 ± 1	35 ± 1	157 ± 9	144 ± 8	144 ± 8	191 ± 6	201 ± 5	201 ± 5	233 ± 8	225 ± 4	225 ± 4	
	0.1	_	41 ± 2	37 ± 1	_	147 ± 19	151 ± 6	_	191 ± 6	213 ± 51	225 ± 2	166 ± 5	220 ± 48	
	0.5	_	40 ± 1	40 ± 1	_	143 ± 8	132 ± 12	_	198 ± 14	208 ± 5	208 ± 2	209 ± 23	195 ± 23	
	2.0		40 ± 2	42 ± 2	_	141 ± 19	135 ± 3	_	193 ± 6	205 ± 2	188 ± 1	201 ± 3	212 ± 5	

0.2 g sample, mixing time = 30 min, vertical mixing (VM) at 100 rpm and horizontal mixing (HM) at 600 rpm, "—" for do not measure.

tact between SAPs and silica particles is supposed to be elastic, in good approximation, and after the mixing, the shapes of SAPs and silica do not change. Over the elastic force range, some plastic region can be observed, and if the force becomes greater than plastic region, SAP destruction may arise.

The results in Table 9 indicate that all the SAPs having various silica types and contents mixed under VM or HM motions are linear and it can be concluded that their mixing forces are elastic because the water absorbency values are in a linear trend. The extent of water absorbency of the in situ SAPCs containing a 97:3 molar AM: IA ratio with various silica contents used in comparison with the mechanical mixing SAPCs at the same monomer ratio are similar with only a small deviation in most cases.

The Role of Silica in SAPCs

The preparation of SAPs needs to have a crosslinking agent to control the gel properties. However, when a crosslinking agent, such as N-MBA, is used, the water absorbency decreased. To control the desirable level of water absorbency through the chemical crosslinking reaction, a well-designed recipe and reaction condition must be strictly controlled. Inorganic particulate filler with a hydrophilic surface, such as silica, is normally recommended for incorporation during the polymerization of SAPs as another crosslinking site or grafting site for the in situ prepared SAPCs or mechanical mixing of SAPs and silica to give SAPCs. As shown above, the silica particles can be embedded in the polymer to give a better overall strength. Moreover, the presence of silica in the SAPCs reduces the load-free water absorbency very slightly. Data from the water AUL, however, were not significantly different between the SAP and SAPCs due to the aforementioned discussion. When the SAPCs are assembled as a baby diaper or famine napkins, the absorbed fluid is still held within the superabsorbent network and silica also helps the polymer to flow easily from the sack and can improve fluid permeability of the hydrated SAPs. In this work, we tuned the combination between the chemical crosslinking reaction by N-MBA and the minimum silica incorporation to obtain the desirable water absorbency behavior.

CONCLUSIONS

The P(AM-IA) SAPs prepared by in situ solution polymerization produced a high level of water absorbency and a much lower AUL water absorbency. Increasing the IA concentration in the SAPs significantly increased the water absorbency. In situ polymerized SAPCs containing various molar ratios of AM: IA and incorporating three types of silica particles at various contents were synthesized. The water absorbency of SAPCs was lower than those of SAPs, the extent of which depended on the amount of silica incorporated. However, the AUL of

SAPs and SAPCs at a 97:3 molar ratio of AM: IA was almost unchanged regardless of the type and amount of silica added. The amounts of silica retained in the SAPCs of the three silica types and contents were in the range of 88-95% by weight. Water absorbency kinetics of the P(AM-IA) SAPs or the P(AM-IA)/silica SAPCs obeys Langmuir absorbency isotherm with a pseudo secondorder absorbency phenomenon. Horizontal or vertical mixed SAPs with two types of silica at 0.1, 0.5, and 2% by weight did not give significant differences in water absorbency. In addition, the levels of water absorbency of the mechanically mixed SAPCs did not significantly vary from the levels obtained from the in situ SAPCs. Therefore, the obtained results indicated that in order to prepare SAP with improved mechanical properties via the addition of silica particles, one could avoid the complicated in situ polymerization reaction in the presence of the silica particles by mechanical mixing the neat SAP with silica particles to obtain the associated SAPC.

ACKNOWLEDGMENTS

The authors thank Publication Counseling Unit (PCU) for the language check and some useful suggestion.

REFERENCES

- F.L. Buchholz, "Preparation and Structure of Polyacrylate," in *Absorbent Polymer Technology*, L. Brannon-Peppas and R.S. Harland, Eds., Amsterdam, Elsevier Science, 23 (1990).
- K. Kosemund, H. Schlatter, J.L. Ochsenhirt, E.L. Krause, D.S. Marsman, and G.N. Erasala, *Regul. Toxicol. Pharma-col.*, 53(2), 81 (2008).
- 3. F. Masuda, "Trends in the Development of Superabsorbent Polymers for Diaper," in *Superabsorbent Polymers: Science and Technology*; ACS Symposium Series # 573, F.L. Buchholz and N.A. Peppas, Eds., The American Chemical Society, Washington, DC, 88 (1994).
- 4. R. Chandra and R. Rustgi, *Prog. Polym. Sci.*, **23**, 1273
- 5. M.J. Ham and Y.H. Kim, Polym. Eng. Sci., 48, 2439 (2008).
- S. Dalal, S. Raghava, and M.N. Gupta, *Biochem. Eng. J.*, 42, 301 (2008).
- R. Liang, M. Liu, and L. Wu, React. Funct. Polym., 67, 769 (2007).
- 8. R.E. Sojka, D.L. Bjorneberg, J.A. Entry, R.D. Lentz, and W.J. Orts, *Adv. Agronomy*, **92**, 75 (2007).
- A. P. Nikolaos and R.K. Atul, Adv. Drug Delivery Rev., 11, 1 (1993).
- M.H.A. Azadi and P. Rafiei, Adv. Drug Delivery Rev., 60, 1638 (2008).
- A. Costantini, G. Luciani, B. Silvestri, F. Tescione, and F. Branda, J. Biomed. Mater. Res. Part B: Appl. Biomater., 86B(1), 98 (2007).
- 12. M. Kiremitci and H. Cukurova, Polymer, 33, 3257 (1992).
- E. Karadağ, D. Saraydin, Y. Caldiran, and O. Güven, *Polym. Adv. Tech.*, 11, 59 (2000).

- 14. T. Masuda, "Absorptivity of Water (Moisture Absorptivity and Retention of Water)," in *Gels Handbook*, Y. Osada, K. Kajiwara, T. Fushimi, O. Irasa, Y. Hirokawa, T. Matsunaga, T. Shimomura, L. Wang, and H. Ishida, Eds., Academic Press, New York, 17 (2001).
- T. Toyoda, "Water-Swelling Rubbers," in *Gels Handbook*,
 Y. Osada, K. Kajiwara, T. Fushimi, O. Irasa, Y. Hirokawa,
 T. Matsunaga, T. Shimomura, L. Wang, and H. Ishida, Eds.,
 Academic Press, New York, 295 (2001).
- Y. Osada, K. Kajiwara, T. Fushimi, O. Irasa, Y. Hirokawa, T. Matsunaga, T. Shimomura, L. Wang, and H. Ishida, "Artificial Snow," in *Gels Handbook*, Y. Osada, K. Kajiwara, T. Fushimi, O. Irasa, Y. Hirokawa, T. Matsunaga, T. Shimomura, L. Wang, and H. Ishida, Eds., Academic Press, New York, 491 (2001).
- 17. H.-W. Jacobi, T. Annor, and E. Quansah, J. Photochem. Photobiol. A, 179, 330 (2006).
- T. Shimura and T. Namba, "Preparation and Application of High-Performance Superabsobent Polymers," in *Superab*sorbent Polymers: Science and Technology; ACS Symposium Series # 573, F.L. Buchholz and N.A. Peppas, Eds., The American Chemical Society, Washington, DC112 (1994).
- 19. J.C.M. Bordado and J.F.P. Gomes, *Int. J. Environ. Stud.*, **64**(2), 243 (2007).
- T.L. Staples, D.E. Henton, and F.L. Buchholz, "Chemistry of Superabsorbent Polyacrylates," in *Modern Superabsorb*ent Polymer Technology, F.L. Buchholz and A.T. Graham, Eds., Wiley-VCH, New York, 55 (1998).
- P. Li, N.H. Kim, D. Hui, K.Y. Rhee, and J.H. Lee, *Appl. Clay Sci.*, 46, 414 (2009).
- 22. K. Haraguchi, Curr. Opin. Solid State Mater. Sci., 11, 47 (2007).
- D. Foungfung, S. Phattanarudee, N. Seetapan, and S. Kiatkamjornwong, *Polym. Adv. Tech.* (2009), DOI: 10.1002/ pat.1559.
- M. Taniguchi, K. Kato, A. Shimauchi, X. Ping, K. Fujita, T. Tanaka, Y. Tarui, and E. Hirasawa, *J. Biosci. Bioeng.*, 99(2), 130 (2005).
- 25. D. Depan, A.P. Kumar, and R.P. Singh, *Acta Biomater.*, **5**, 93 (2009).
- 26. A. Li and A. Wang, Eur. Polym. J., 41, 1630 (2005).
- J. Zhang, H. Chen, and A. Wang, Eur. Polym. J., 42, 101 (2006).
- J. Zhang, Q. Wang, and A. Wang, Carbohydr. Polym., 68, 367 (2007).

- S. Sharma and S. Komarneni, Appl. Clay Sci., 42, 553 (2009).
- X. Huang, S. Xu, M. Zhong, J. Wang, S. Feng, and R. Shi, *Appl. Clay Sci.*, 42, 455 (2009).
- 31. J. Wu, J. Lin, M. Zhou, and C. Wei, *Macromol. Rapid Commun.*, **21**, 1032 (2000).
- 32. W. Wang and A. Wang., *Carbohydr. Polym.*, **77(4)**, 891 (2009).
- 33. U.Y. Kim, "Recent Developments in High Water Absorbing Polymers and Applications", in *The Proceedings of the International Conference on Recent Developments in Petro-chemical and Polymer Technologies*, 6–1, December 12–16, 1989, Chulalongkorn University Press, Bangkok, Thailand.
- H.F. Mark, N.M. Bikales, C.G. Overberger, and G. Mengel, *Encyclopedia of Polymer Science and Engineering*, 2nd ed., Wiley, New York, Vol. 7, 783 (1989).
- A. Pourjavadi, F. Seidi, and R. Soleyman, J. Appl. Polym. Sci., 108(5), 3281 (2008).
- 36. F.L. Buchholz, J. Chem. Ed., 73, 512 (1996).
- B. Silvestri, G. Luciani, A. Costantini, F. Tescione, F. Branda, and A. Pezzella, J. Biomed. Mater. Res. Part B: Appl. Biomater., 89, 369 (2009).
- 38. X. Shi, S. Xu, J. Lin, S. Feng, and J. Wang, *Mater. Lett.*, **63**(2), 527 (2009).
- 39. H. Schott, J. Macromol. Sci. Phys., 31(1), 1 (1992).
- 40. J. Baselga, M.A. Llorente, J.L. Nieto, and I.F.P. Hernández-Fuentes, *Eur. Polym. J.* 24, 161 (1988).
- 41. N. Seetapan, J. Wongsawaeng, and S. Kiatkamjornwong, *Polym. Adv. Tech.* (2010), DOI: 10.1002/pat.1658.
- 42. N. Uyanik and C. Erbil, Eur. Polym. J., 36, 2651 (2000).
- M. Pulat and H. Eksi, J. Appl. Polym. Sci., 102, 5994 (2006).
- M.J. Ramazani-Harandi, M.J. Zohuriaan-Mehr, A.A. Yousefi, A. Ershad-Langroudi, and K. Kabiri, *Polym. Test.*, 25, 470 (2006).
- 45. J. Qin, U.S. Pat. 6,998,367 B2 (2006).
- 46. D. Saraydin and Y. Caldiran, Polym. Bull., 46(1), 91 (2001).
- 47. N. Martinez-Vázquez, R. del, C. Antonio-Cruz, A. Álvarez-Castillo, A.M. Mendoza-Martinez, and A.B. Morales-Cepeda, *Rev. Mex. Ingenieria Quim.*, **6(3)**, 337 (2007).
- 48. W. Saelow, S. Kiatkamjornwong, T. Watanabe, and Y. Hoshino, *J. Imaging Soc. Jpn.*, **38**(4), 310 (1999).
- 49. C. Poomtien, S. Kiatkamjornwong, and Y. Hoshino, *Part. Sci. Technol.*, **16**(4), 295 (1999).



Contents lists available at ScienceDirect

Carbohydrate Polymers

journal homepage: www.elsevier.com/locate/carbpol



Modified chitosan pretreatment of polyester fabric for printing by ink jet ink

Supaporn Noppakundilograt^a, Punthorn Buranagul^a, Wilaiporn Graisuwan^b, Chawan Koopipat^a, Suda Kiatkamjornwong^{a,*}

- ^a Department of Imaging and Printing Technology, Faculty of Science, Chulalongkorn University, Phyathai Road, Bangkok, 10330, Thailand
- ^b Program of Petrochemistry, Faculty of Science, Chulalongkorn University, Phyathai Road, Bangkok, 10330, Thailand

ARTICLE INFO

Article history: Received 24 April 2010 Received in revised form 14 June 2010 Accepted 22 June 2010 Available online 26 June 2010

Keywords:
Chitosan
Glycine
N-[(4-dimethyl aminobenzyl)imino]
chitosan
N-[(2-hydroxy-3trimethylammonium)propyl] chitosan
chloride
Color properties
Outline sharpness
Stiffness

ABSTRACT

The present research deals with the use of pretreatment solutions of chitosan (CH), N-[(4-dimethyl aminobenzyl)imino] chitosan (DBIC), N-[(2-hydroxy-3-trimethylammonium)propyl] chitosan chloride (HTACC), glycine (Gly), and a mixture of CH and Gly, for padding polyester fabrics prior to printing with a set of seven-color pigmented water-based ink jet inks. After padding the fabrics with the above cationic pretreatments, they were printed with a piezo-electric drop-on-demand jet printer. CH, DBIC and HTACC were characterized by IR and NMR spectroscopy. The zeta potentials of the pretreatment solutions, the inks and the fabrics were measured. The K/S values, color gamut, tone reproduction, outline sharpness, and the surface appearance of the fabrics were characterized. Statistical evaluation of the significance of the results was performed. Among the pretreatments, the HTACC at 0.1% (w/v) yielded fabrics with the highest K/S values, widest color gamut and gamut volume, more color saturation with good tonal reproduction, and the sharpest and smoothest outline of printed character, and a smooth fabric surface with less stiffness. The proposed ionic interactions between the protonated amino groups of CH and the anionic portion of the encapsulated ink pigments, and van der Waals and hydrophobic interactions between the polyester and the pigments are likely reasons for these enhanced properties of the printed fabrics.

© 2010 Elsevier Ltd. All rights reserved.

1. Introduction

The pretreatment of fabrics with a suitable agent is a requirement in textile-ink jet printing because the deposited pretreatment chemical on the fabric surface limits excessive ink spreading and controls ink migration and penetration into the fabric fibers, and yet allows the ink to dry after the ink has been jetted (applied) onto the fabric surface. This interaction of the pretreatment agent and the jet ink results in an increase in color gamut, sharpness and other properties of the printed fabric (Hakeim, El-Gabry, & Abou-Okeil, 2008; Leelajariyakul, Noguchi, & Kiatkamjornwong, 2008; Phattanarudee, Chakvattanatham, & Kiatkamjornwong, 2009; Wang et al., 2007; Yuen, Ku, Kan, & Choi, 2007).

Polyester, one of the more popular textile fabrics, needs dyeing and printing to provide the color and pattern ranges required by customers and hence the higher add-on value. Although polyester fabric is hydrophobic, it has a negative zeta potential value (Espinosa-Jiménez, Padilla-Weigand, Ontiveros-Ortega,

Ramos-Tejada, & Perea-Carpio, 2003). Thus, a prospective pretreatment agent with positive charges should be adsorbed onto the polyester fabric due to the requirement of an ionic interaction in enhancing the color and other properties (Samu, Moulee, & Kumar, 1999). Some types of cationic pretreatment agents have been reported to be able to increase the printed polyester color strength (K/S) by as much as 36% with ink jet printing when compared with the untreated polyester fabric (Wang et al., 2007).

Chitosan (CH) is widely used as a pretreatment reagent for synthetic polymers due to its green environmental advantages, easy to use and relatively low cost yet abundant supply. Indeed, CH has been extensively used for the dyeing and finishing of various textile fabrics, where the pretreatment of fabrics with CH produced a high color yield, good shrink resistance and provided some degree of antimicrobial activity (Abou-Okeil & Hakeim, 2005; Hakeim, Abou-Okeil, Abdou, & Waly, 2005; Julia, Pascual, & Erra, 2000). In textile-ink jet printing, CH has generally been used as a pretreatment agent for silk fabrics to expand the color gamut and to improve the crock fastness of the printed fabric (Chakvattanatham, Phattanarudee, & Kiatkamjornwong, 2010; Phattanarudee et al., 2009; Yuen, Ku, & Kan, 2008), whilst CH modified with dimethyl aminobenzaldehyde (DBIC) affected the color gamut of the printed polyester (Hakeim et al., 2008). CH is dissolved in acetic acid where upon its amino groups are protonated to form quaternary ammo-

^{*} Corresponding author. Tel.: +66 2 218 5587; fax: +66 2 255 3021.

E-mail addresses: supaporn.n@chula.ac.th (S. Noppakundilograt),
puntune@hotmail.com (P. Buranagul), porn_grai@yahoo.com (W. Graisuwan),
chawan.k@chula.ac.th (C. Koopipat), ksuda@chula.ac.th (S. Kiatkamjornwong).

nium ions, which interact with anionic dyes through electrostatic attraction (Jocic et al., 2005). CH-padded fabrics result in a higher level of pigment adsorption onto the pretreated fabric surface compared to that of uncoated fabrics, and also gave a high color quality on the surface (Chakvattanatham et al., 2010; Phattanarudee et al., 2009).

Unfortunately, the retained acetic acid (from the CH) of the pretreated cotton fabric yields reduced color gamut, compared with the untreated one, and the acrid odor is retained in the printed fabrics after the post-treatment (Yuen et al., 2007), whilst CH also increases the stiffness of the fabrics (Phattanarudee et al., 2009). To solve these problems, the water-soluble CH derivatives with highly positive charges, O-acrylamidomethyl-N-[(2-hydroxy-3-trimethylammonium)propyl] chitosan chloride (NMA-HTACC) and N-[(2-hydroxy-3-trimethylammonium)propyl] chitosan chloride (HTACC), were synthesized (Kim, Lee, Lee, & Park, 2003; Lim & Hudson, 2004a, 2004b). Previously, the use of NMA-HTACC was reported to increase the color yield in the dyeing of cotton fabrics, whilst HTACC generated antimicrobial activity in the textile (Seong, Whang, & Ko, 2000).

The aim of this research was to modify CH to a cationic form with better solubility. To this end, CH with two different molecular weights and deacetylation degrees were modified to HTACC and DBIC, respectively, so as to improve the pretreatment properties of CH. Due to the solubility of CH in acid, the low average molecular weight CH was used for direct pretreatment and the synthesis of DBIC. The synthesized HTACC and DBIC were then used as pretreatment agents for polyester fabrics, color printed with an ink jet ink. The effects of fabric pretreatment with HTACC, DBIC, CH, Glycine (Gly) and a mixture of CH and Gly were investigated in depth for the color appearance yield in terms of color gamut and gamut volume, color strength and tone reproduction of the subsequently ink jet printed fabrics. In addition, the outline sharpness and evenness of density of the positive and negative characters of the printed polyester fabrics were also investigated along with the stiffness of the printed fabrics.

2. Experimental

2.1. Materials

A plain weave polyester fabric, constructed of 182 ends/in. (warp) \times 87 picks/in. (weft) with a basic weight of 127 g m⁻², was used. Triton X-100, a non-ionic surfactant, was supplied by Merck (Frankfurt, Germany). CH flakes of 57,000 g/mol of average molecular weight and 85% deacetylation degrees (DD) was used for the synthesis of N-[(4-dimethyl aminobenzyl)imino] chitosan (DBIC) due to its lower water solubility while CH flakes of 100,000 g/mol of average molecular weight and 95% DD was used to synthesize N-[(2-hydroxy-3-trimethylammonium)propyl] chi-

tosan chloride (HTACC) due to its higher water solubility. Both types of CH were purchased from Seafresh Industry Public Co., Ltd. (Bangkok, Thailand). Gly (98.5% pure) was purchased from Ajax Finechem (Seven Hills, NSW, Australia). N,N'-dimethyl aminobenzaldehyde was purchased from Asia Pacific Specialty Chemical Ltd. (Seven Hills, NSW, Australia). Glycidyl trimethylammonium chloride (GTMAC) was purchased from Sigma–Aldrich (St. Louis, MO). A commercial set of seven-color, pigmented water-based jet inks (Epson UltrachromeTM Ink), supplied from Seiko Epson Corporation (Suwa, Nagano, Japan), was used for printing the fabrics. Based on the manufacturer's claims, the pigment dispersions were treated by polymeric dispersant and polymer encapsulation to give an average particle size of the encapsulated pigment of approximately 100 nm.

2.2. Synthesis of the modified chitosans

2.2.1. N-[(4-dimethyl aminobenzyl)imino] chitosan (DBIC)

DBIC was prepared based on the method of Hakeim et al. (2008). CH (5 g, average molecular weight = $57,000 \, \text{g/mol}$ and 85% DD) and dimethyl aminobenzaldehyde (9.3 g) were mixed in 150 mL methanol for 10 h. The product was filtered through a 100-mesh aluminum screen sieve, washed with 300 ml of a 1:1 (v/v) ratio of mixed methanol–acetone solution and then dried overnight at room temperature. The intense yellowish dried product obtained was then characterized by IR spectroscopy (Spectrum One, PerkinElmer Life and Analytical Sciences Inc, MA). The synthetic route is shown in Scheme 1.

2.2.2. N-[(2-hydroxy-3-trimethylammonium)propyl] chitosan chloride (HTACC)

The synthesis of HTACC was modified from that of Seong et al. (2000). In brief, 0.50 g of CH (average molecular weight = 100,000 g/mol with DD = 95%) was dissolved in 25 cm³ of 1% (v/v) aqueous acetic acid. Then 0.9 g of GTMAC was slowly added into the CH solution whilst maintaining the reaction temperature at 70 °C during the mixing and over the subsequent 24 h. The solution was then poured in a dialysis tubing cellulose membrane (average flat width of 76 mm, Sigma, St. Louis, MO) for dialysis for 5 days against 1000 cm³ of deionized water, changed every day. The white colored product obtained was freeze dried in a freeze drier (Labconco, MO), and aliquots were then characterized by IR spectroscopy (Spectrum GX, PerkinElmer Life and Analytical Sciences Inc, MA.) and NMR spectrometry (Advance 300 MHZ NMR Spectrometer, Bruker, Switzerland). The reaction is shown in Scheme 2.

2.2.3. Preparation of pretreatment solutions

The pretreatment agents of the unmodified CH, having 0.1, 1, 2, 3 and 4% (w/v), were prepared by stirring in 2% (v/v) of acetic acid until the CH (57,000 g/mol) was dissolved. Gly concentrations, from

Scheme 1. Synthesis route of N-[(4-dimethyl aminobenzyl)imino] chitosan from chitosan.

Scheme 2. Synthesis route of N-[(2-hydroxy-3-trimethylammonium)propyl] chitosan chloride (HTACC) from chitosan.

5 to 15% (w/v) in deionized water (Elga Deionizer, LA1, Elga Labwater, UK), were prepared. Likewise, 15% (w/v) of Gly was mixed with 1% (w/v) of CH to give a mixed pretreatment solution. The solutions of the two modified CH (HTACC and DBIC) at a concentration of 0.1% (w/v) were prepared by dissolving 0.25 g HTACC in deionized water in a $250\,\mathrm{cm}^3$ volumetric flask, whereas 0.25 g of DBIC was dissolved in $250\,\mathrm{cm}^3$ of 2% (v/v) acetic acid.

2.2.4. Purity of the polyester fabric

Purity of the polyester fabric was evaluated by testing the presence of starch and poly(vinyl alcohol) by iodine in potassium iodide solution by observing the development of purple color. Carboxyl methyl cellulose (CMC) was examined by mixed solution of ferric chloride and potassium thiosulfate which was followed by dropping solution of potassium ferrocyanide. The presence of CMC can develop a purple color on the fabric surface (Livengood, 1983). The optical brightener may interfere the color data therefore the fabric was viewed in an MEDA light color viewing booth under ultraviolet irradiation where the presence of visible fluorescent light shall be detected.

2.2.5. Zeta potential measurement

The ink jet inks, pretreatment solutions, polyester fabric and the pretreated polyester fabrics were all measured for zeta potential using a Nano-ZS, Zeta potential Analyzer (Malvern Instruments Ltd., UK) in a disposable U-shaped cell with each wall accommodating one small piece of a Cu electrode. The zeta potential of the untreated polyester fabric and the pretreated polyester fabrics were measured by first preparing a fabric suspension by pulling out the fibers from the piece of fabric and then cutting the fibers into small pieces of approximately 0.05 cm long. They were then soaked in deionized water for 24 h. The suspension obtained was used for measuring the zeta potential of the pretreated fabrics.

2.2.6. Fabric pretreatment

The polyester fabrics were cleaned with Triton X-100, rinsed in distilled water and dried at room temperature. The cleaned polyester fabrics (23 cm \times 32 cm) were then padded with the above mentioned pretreatment solutions using a padding machine (PB-1, Copower Technology Co., Ltd., Taiwan) with a 70% wet pick up. The pretreated fabrics were then dried in an oven (M-3, Copower Technology Co., Ltd., Taiwan) at 80 $^{\circ}$ C for 5 min and cured at 110 $^{\circ}$ C for 2 min.

2.2.7. Ink jet printing and post-treatment

The untreated and pretreated polyester fabrics were printed with a set of seven-color, pigmented ink jet inks (cyan, light cyan, magenta, light magenta, yellow, black and light black colors), using commercially available water-based inks on a piezo-electric dropon-demand type ink jet printer (Epson Stylus Photo 2100, Seiko Epson Corporation, Nagano, Japan). A color test chart, composed of 294 color patches, several lines and characters, was used for investigating the quality of the printed polyester fabrics. Post-treatment of the printed fabric was performed by steaming at 100 °C for 5 min in a steamer (HTS-3, Copower Technology Co., Ltd., Taiwan).

2.2.8. Color gamut evaluation

The color test chart of each printed fabric was measured in tristimulus values using an X-Rite spectrophotometer (SP62, X-Rite Inc., MI) with an illuminant D50, the CIE 1931 2° observer in a specular light excluded mode. The tristimulus values (X, Y, Z) were transformed to chromaticity coordinates (x, y, z) for creating a color gamut in a two-dimensional color space. The L^* , a^* and b^* color values were used to calculate a gamut volume in a three-dimensional space by SHIPP program (Fair, 1997; Putthimai, 2003). In the same manner, the L^* vs. C^* space was also created by measuring the sample lightness and chroma in the CIE $L^*C^*H^*$ spaces.

2.2.9. Color strength (K/S) measurement

The color strength of inks was determined based on the Kubelka–Munk equation, and expressed as a *K*/*S* value, fluctuating from the maximum absorption wavelength of each color within the visible spectrum. The percentage of reflectance was measured by the same spectrophotometer with a specular light excluded condition. The *K*/*S* value was calculated according to Eq. (1) (James, 1997):

$$\frac{K}{S} = \frac{(1 - R_{\infty})^2}{2R_{\infty}} \tag{1}$$

where K is the absorption coefficient of the printed color on the surface, S is the scattering coefficient caused by the colored substrate, and R_{∞} is reflectance of the colored sample at an infinite opacity. Evaluation of the significance level of K/S values of the pretreated fabrics compared with the untreated fabric was performed by oneway analysis of variance (ANOVA) with the least square difference (LSD) tests used for post hoc evaluations of differences between groups in Statistical Package for the Social Science (SPSS) version 14.0 software, at a confidence level of 95.0% (α = 0.05).

2.2.10. Tone reproduction measurement

The tone reproduction was evaluated by plotting the optical density versus the percentage of the dot area. The optical density was measured by a densitometer (R730, IHARA Electronic Ind. Co., Ltd., Nagoya, Japan).

2.2.11. Outline sharpness and contrast assessment

The printed outline sharpness on the fabrics was measured by optical microscopy (PM10-AD, Olympus Corporation, Tokyo, Japan) with a $4\times$ magnification of 10-point printed positive and negative "E" characters. The black and white line strips printed on the fabrics at the applied spatial frequencies of 0.5, 1 and 2 lines mm $^{-1}$ in the two directions (weft and warp) of the polyester fabric of the bar target were measured by a microdensitometer (Konica, PDM-7, Tokyo, Japan). The scanning aperture was set at a width of 20 μm and a reflection mode of 500 μm , and data were then acquired at 20 data points per second to give a total scanning of 400 data points. The densities in each sample were measured and normalized to the untreated fabrics. The contrast at each frequency was calculated from Eq. (2):

$$Contrast(\omega) = D_{max}(\omega) - D_{min}(\omega)$$
 (2)

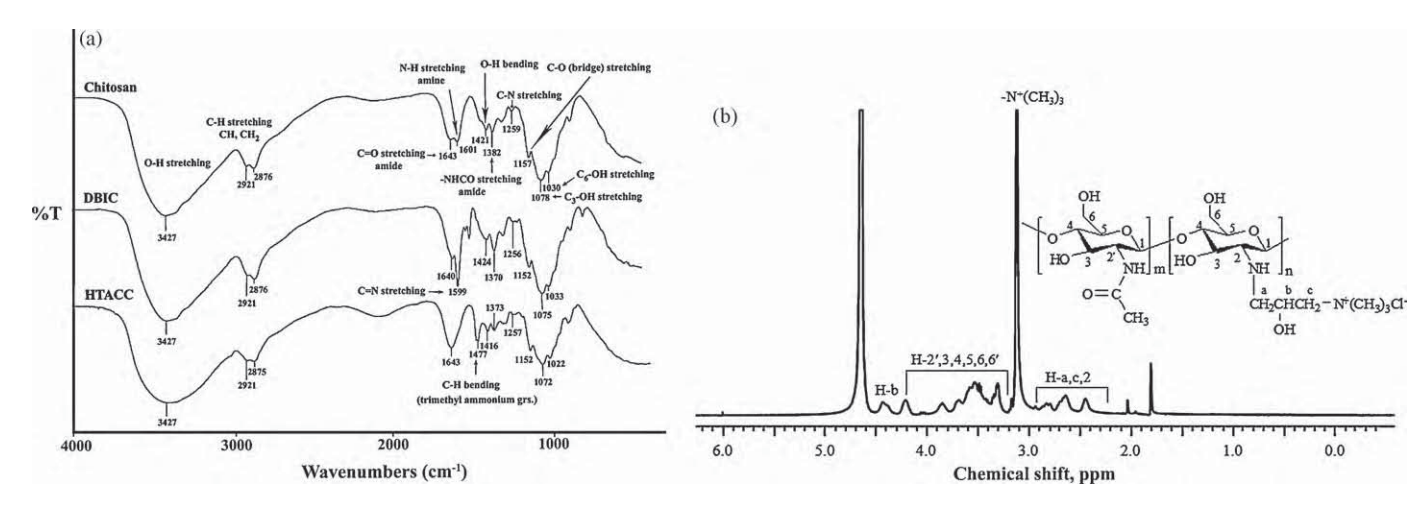


Fig. 1. Confirmation of modified chitosans: (a) IR spectra of chitosan, DBIC and HTACC; (b) 1H NMR spectra of HTACC (solvent: D2O, 25°C).

where $D_{\rm max}$ and $D_{\rm min}$ are average maximum and minimum densities, respectively, and ω is the spatial frequency. Plots of the densities against the measured frequencies in both the weft and warp fabric directions were constructed. However, calculation of the contrast in the warp direction could not be measured because of the problems in measuring both the densities.

2.2.12. Surface appearance of the pretreated polyester fabrics

The surface of the pretreated polyester fabrics was examined by scanning electron microscopy on a Spectrum One (PerkinElmer Life and Analytical Sciences, Inc., MA) at a magnification of 2000×.

2.2.13. Stiffness of the treated fabrics

The stiffness of the fibers was measured in terms of the bending length by following the JISI 1096:1999 stiffness 145° cantilever method (Stiffness Method A, 1999). Pieces of each fabric, sized $2\,\mathrm{cm} \times 15\,\mathrm{cm}$, were measured and the average bending length in the warp and weft directions, obtained from five measurements, were expressed as the average stiffness. The bending length of the fabrics treated with the selected loadings of the pretreatments were then compared with that for the untreated fabrics, within the same pretreatment agent at various levels, and at the same selected loadings of the five pretreatment agents. The significance of the test was performed by one-way analysis of variance (ANOVA) with the least square difference (LSD) tests being used for post hoc evaluations of differences between groups in Statistical Package for the Social Science (SPSS) version 14.0 software, at a confidence level of 95.0% (α = 0.05).

2.2.14. Color fastness to washing and rubbing

The effects of the pretreatment agents on color fastness to washing and to rubbing of the fabrics were investigated based on ISO 105-C10:2006 (E), and AATCC TM 8, respectively.

3. Results and discussion

3.1. Characterization of the fabric and the modified chitosans

Under the test conditions mentioned above, it showed that the polyester fabrics were free from starch, poly(vinyl alcohol), and CMC, because the mixed solution of iodine and potassium iodide for starch and poly(vinyl alcohol) did not give the purple color, and a mixed solution of ferric chloride and potassium thiosulfate for CMC did not produce the purple color on the fabric surface either. It was also found that the polyester fabric was free from optical brightener, because the visible fluorescent light

was not observed on the exposed surface under ultraviolet irradiation.

The IR spectra of the unmodified CH and the two modified CHs (DBIC and HTACC) are given in Fig. 1(a). That for CH shows the overlapped peaks of N–H stretching and O–H stretching at 3427 cm⁻¹ and O–H bending at 1421 cm⁻¹ which indicates the presence of hydroxyl groups (Sun, Zhou, Xie, & Mao, 2007). The weak absorption peaks at 2921 and 2876 cm⁻¹ are assigned to the C–H stretching (Huacai, Wan, & Dengke, 2006). The strong characteristic peaks of CH at 1643, 1601, 1382 and 1259 cm⁻¹ are assigned to the C=O stretching, N–H bending and –NHCO stretching of the amide (Zhang, Wang, & Wang, 2007), and C–N stretching (Singh, Sharmaa, Tripathi, & Sanghib, 2009), respectively. In addition, the weak characteristic peaks at 1157, 1078 and 1030 cm⁻¹ are ascribed to the stretching of the C–O bridge (Huacai et al., 2006; Mun et al., 2008) and the C₃–OH and C₆–OH groups (Zhang et al., 2007), respectively.

The CH amine N–H bending at 1601 cm⁻¹ in the IR spectrum of DBIC is absent, but rather the spectrum displays a strong absorption peak at 1599 cm⁻¹ corresponding to the C=N stretching of DBIC (Hakeim et al., 2008). This confirms that DBIC was synthesized by the reaction between the amino groups of CH and the aldehyde groups of dimethyl aminobenzaldehyde to become the imino groups (C=N) in DBIC.

The IR spectrum of HTACC reveals that the characteristic amine N–H bending peak at $1601\,\mathrm{cm^{-1}}$ is absent, but rather reveals the presence of the peak at $1477\,\mathrm{cm^{-1}}$ assigned for the C–H bending of the trimethylammonium groups (Lim & Hudson, 2004a). In addition, the N–H bending of primary amine groups is absent due to changes to the secondary amine. The peak at $3400\,\mathrm{cm^{-1}}$ was somewhat broadened, caused by the overlapping of the O–H group with the N–H stretching. A weak and broad band at $2200-2000\,\mathrm{cm^{-1}}$ was observed, potentially assigned to a combination of the asymmetrical N(CH₃)₃+ bending vibration and to the torsional oscillation of the N(CH₃)₃+ group.

The ¹H NMR spectrum of HTACC in Fig. 1(b) shows the integrations of the trimethyl ammonium group equals to 1, and the integration of the Hs at the positions 2′, 3, 4, 5, 6 and 6′ equal to 0.8. The degree of substitution (DS) of GTMAC in HTACC was calculated from Eq. (3):

$$\% DS = \left\{ \frac{integral \, of \, the \, N^+(CH_3)_3/9}{(integral \, of \, the \, H-2', \, 3, \, 4, \, 5, \, 6, \, 6'/6) \times (95/100)} \right\} \times 100 \tag{3}$$

where %DD is the degree of deacetylation (95/100). From the results, it confirms that HTACC contained 87.7% DS. The calculated

Table 1Zeta potentials of the materials used.

Type of material	Zeta potential, ζ (mV)
Ink jet inks	
Cyan	-43.1
Magenta	-56.5
Yellow	-34.7
Black	-36.7
Pre-treating solutions	
1% (w/v) CH	+83.4
15% (w/v) Gly	+24.7
1% (w/v) CH + 15% (w/v) Gly	+65.1
0.1% (w/v) DIBC	+73.2
0.1% (w/v) HTACC	+36.6
Fabrics	
Untreated fabric	-22.6
Treated fabric with 1% (w/v) CH	-21.6
Treated fabric with 15% (w/v) Gly	-26.4
Treated fabric with 1% (w/v) CH + 15% (w/v) Gly	-28.8
Treated fabric with 0.1% (w/v) DIBC	-24.6
Treated fabric with 0.1% (w/v) HTACC	-23.1

average molecular weight of HTACC based on the above mentioned data is 165,000 g/mol with an aqueous solution pH of 6.8.

3.2. Zeta potential measurement

The zeta potentials of all four base ink colors were found to be negatively charged, with the magenta color having the highest negative value and the yellow color the lowest, but still relatively high (Table 1). To the best of our knowledge, the pigments of Epson inks are encapsulated by a type of crosslinked polymer to prevent coagulation. It implies that the encapsulated pigmented inks had anionic functional groups (generated negative charges), consistent with their good dispersion stability. Similarly, the polyester fabric also had a negative zeta potential, although of a lower magnitude but still sufficient to likely prevent agglomeration of the particles. For the pretreatment solutions, all of them had positive zeta potentials with CH having the highest value, some 2.3-fold higher than HTACC, whilst Gly had the lowest zeta potential. However, all can be considered to highly likely be stable in an aqueous state. Nevertheless, when the fabrics had been padded with the pretreatment solutions, all the zeta potentials of the treated fabrics became negative at around 22–29 mV, which can be considered to be less stable in terms of agglomeration and aggregation. It is clear that the fabric has a dominant effect because the analyzer measured the entire bulk solution of the substrate with thus only a relatively small (by mass) influence from the deposited thin film from the pretreatment agent. One may assume that at least a minute amount of the pretreatment solution and thus agent could be absorbed on the surface and a larger amount penetrated into the polyester fabric, leaving a very thin layer on the fabric surface.

3.3. Effects of the pretreatment agents

3.3.1. Color strength

The ink jet inks are transparent due to the inherent nature of the pigments used. The CH solutions in acetic acid (CH having average molecular weight of 57,000 g/mol) were slightly yellow to yellowish brown and so made the background yellowish. The CH having average molecular weight of 100,000 g/mol can dissolve slightly in acetic acid, therefore, CH with average molecular weight of 57,000 g/mol was used as a representative for the fabric treatment. The background color of the fabric interfered with the printed ink color, resulting in inappropriate color assessments. The color value so measured is basically the combined data of both the background color and the ink color. The background color of the fabric was, therefore, used as a reference for all the measured color values so as to obtain the real color yield of the ink and the resultant effect of the pretreatment agent and the ink.

The color strength (K/S) of the fabrics subjected to the various pretreatment solutions is summarized in Table 2. Theoretically, all of the pretreated fabrics gave generally the higher *K*/*S* values than the untreated fabrics. For the CH-treated fabrics, lower *K*/*S* values were obtained for cyan, magenta and yellow inks at all CH loadings compared to the untreated fabric. Only the black ink showed a numerically, but not statistically significantly, increased K/S level at three out of the five CH loadings, that is not for those at 2 and 4% (w/v) CH which had lower K/S values. In contrast to CH, compared to the untreated fabric, the K/S values were higher for cyan, yellow and black inks for all Gly loadings tested, whereas for magenta the K/S values were higher than the untreated fabric at 5% (w/v) Gly, but decreased with increasing Gly loadings to equal to and lower than the untreated fabric at 10 and 15% (w/v) Gly, respectively. However, when the mixed pretreatment of 1% (w/v) of CH with 15%(w/v) of Gly was used, the K/S values were all lower than that for the untreated fabric and were not as high as those of the pure Gly or CH at the same respective loading levels, except for the yellow ink which was higher than that for 1% (w/v) CH alone. However, none of these numerical differences in the K/S values relative to the untreated fabric were statistically significant except for those at 1% (w/v) CH for cyan color, 15% (w/v) Gly and the 15% (w/v) Gly mixed with 1% (w/v) CH for cyan, black and magenta colors.

Pretreatment of the fabric with DBIC also gave lower K/S values than the untreated fabric for all four inks. In contrast, pretreatment of the fabric with HTACC gave a remarkable and the highest improvement in the K/S values with the concentration of HTACC

The color strength (K/S) and gamut volume of untreated and pretreated polyester fabrics.

Polyester fabrics		K/S at λ_{\max}							
Pretreatment	Concentration (%, w/v)	Cyan 620 nm	Magenta 540 nm	Yellow 400 nm	Black 400 nm	Gamut volume			
Untreated	-	2.53	4.79	5.38	3.61	6859			
CH-	0.1	2.61	3.54	5.11	4.25	6967			
treated	1	1.77	3.25	2.78	4.40	7535			
	2	1.54	2.56	3.05	2.93	6820			
	3	2.12	3.21	3.37	5.74	6961			
	4	1.57	2.47	5.20	2.40	7205			
Gly	5	3.57	5.07	6.77	3.77	7557			
treated	10	3.04	4.80	7.00	8.50	7703			
	15	2.90	4.19	6.26	7.57	7846			
CH + Gly treated	1+15	1.67	3.10	4.56	2.61	6277			
DBIC treated	0.1	2.28	4.48	4.2	3.02	7219			
HTACC treated	0.1	8.74	14.15	29.14	30.40	12950			

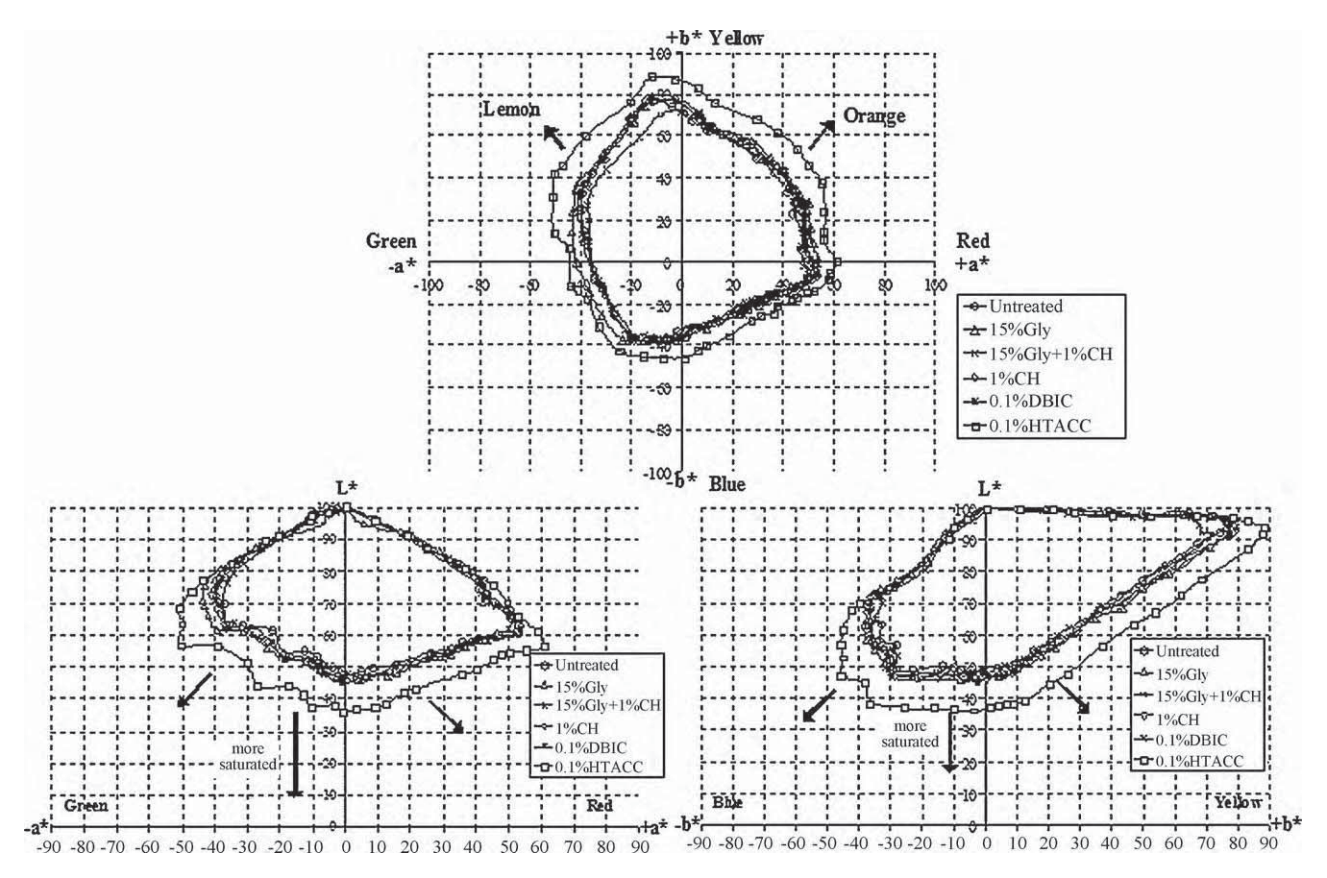


Fig. 2. Color gamuts of the printed fabrics after various pretreatments expressed as a^*b^* for the red-green color vs. yellow-blue color; L^*a^* for lightness vs. red-green color; L^*b^* for lightness vs. yellow-blue color. Data are the mean values, derived from 3 independent repeats.

as low as 0.1% (w/v). Indeed, HTACC pretreatment increased the K/S values of the cyan, magenta, yellow and black inks by some 5-, 4-, 9- and 11-fold, respectively, above that of the untreated fabric. These numerical increases in K/S values were statistically significant (p < 0.05).

3.3.2. Color gamut and gamut volume

A more meaningful presentation of color is the color gamut in the CIE $L^*a^*b^*$ and $L^*C^*H^*$ system because a more complete color information can be obtained. The color gamut produced by the pretreatment solutions is given in Fig. 2, in which the CIE a^*b^* , L^*a^* and L^*b^* gamuts are shown separately. In all the three gamuts, the 0.1% (w/v) HTACC pretreatment clearly gave the widest gamut followed by 15% (w/v) Gly, while the rest of the pretreatment solutions were only slightly different from each other and the untreated reference fabric. The HTACC treatment produced a far more saturated lemon and orange color, as shown in the CIE a^*b^* gamut, a saturated green and red color, as shown in the L^*a^* gamut, and saturated blue and yellow colors, as seen in the L^*b^* gamut. Moreover, the calculated gamut volumes of the untreated and treated fabrics are summarized in Table 2. One can see that increasing the pretreatment solution increased the gamut volume of the printed colors whereas only 0.1% (w/v) of HTACC padded fabric produced the highest gamut volume. Interestingly, the K/S values and the size of gamut volume were not really related in every case, as seen in the case of 0.1 and 1% (w/v) treatment by CH (Table 2). This is due to the fact that the K/S was calculated from colors of the cyan, magenta, yellow and black inks, whereas the gamut volume was calculated from all colors produced in the color sphere. Thus, the gamut volume is a better tool for comparison of the effect of pretreatment of the fabric on the color yield from subsequent printing because it represents the colors that are actually seen.

3.3.3. Tone reproduction

Tone reproduction represents the reproduced optical density with respect to the dot area in a continuous range. The higher the density, the more saturated the printed fabric becomes. Fig. 3(a) shows the tone reproduction of the pretreated fabrics, revealing that different sloped tone reproduction plots were observed for each of the different pretreated fabrics. The tonal densities of the fabrics pretreated with CH, Gly, the CH–Gly mixture and DBIC were all relatively close at the lower dot areas but they gave relatively higher tone densities at the higher dot areas. Very interestingly, the HTACC pretreated fabrics revealed a steadily increasing tonal density for the whole range of dot areas, with a much higher optical density when the dot areas were higher than 40%.

3.3.4. Chroma or color saturation

The components of color appearance are represented by L^* (lightness), C^* (chroma) and H^* (hue angle), and so an L^*C^* plot is another method to observe the extent of color saturation after printing on fabrics pretreated with the different solutions. In this representation, the higher the C^* value is, the greater the color saturation becomes. Most of the pretreated fabrics gave higher color saturations at all lightness, even at the low lightness areas (Fig. 3(b)). Pretreatment brings out a higher color saturation, as indicated by the scattering of the points in the L^*C^* plot. Basically, an ideal color production is judged by the evenly and widely scattering of the points at all lightness and chroma values, i.e., from the low to high values of both axes. With a wide scattering of the points on the L^* and C^* plot, a better tone reproduction with more details can be obtained.

When considering the CH pretreated fabrics, the color saturation was slightly increased as the CH concentrations increased. In the Gly pretreated fabrics, the color saturation increased gradu-

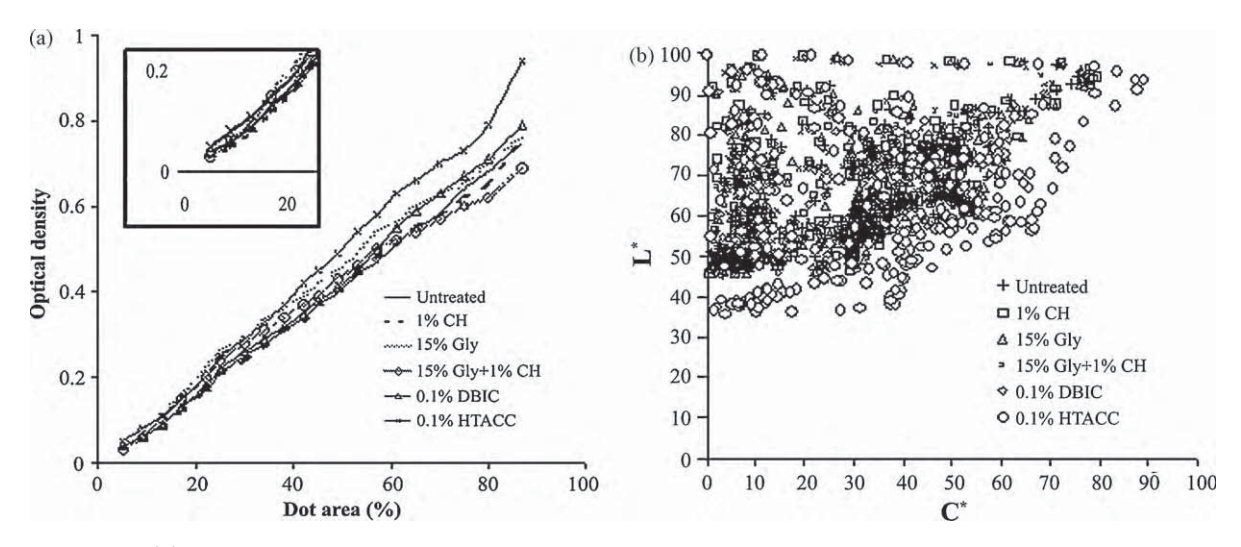


Fig. 3. Color yield: (a) The *L**C* boundary of the printed fabrics with various pretreatments; (b) tone reproduction (shown as a plot of dot area against optical density) of the printed fabrics with various pretreatments. Data are the mean values, derived from 3 independent repeats.

ally with increasing Gly concentrations up to a maximum at 15% (w/v) Gly. However, when a 1% (w/v) CH and 15% (w/v) Gly mixture was used, the color saturation obtained was lower, being at the same level as that observed with the 1% (w/v) CH pretreated fabric samples. In contrast, when the HTACC was used, higher color saturation was found in the HTACC pretreatment compared to that found with DBIC pretreatment at the same concentration. Indeed, the 0.1% (w/v) DBIC treatment resulted in similar color saturation as that of fabrics pretreated with 1% (w/v) CH.

The extent of the interaction depends on the pretreatment agent concentration, the molecular weight, degree of deacetylation, the location of remaining acetyl units and the local environment, as influenced by the pH, the molecular size of the colorant (Jocic et al., 2005; Leelajariyakul et al., 2008; Phattanarudee et al., 2009), and physical phenomena of surface properties. The major contributor towards the higher K/S values and wider color gamut can be obtained by the adsorption onto the modified CHs, or onto Gly, of the polymer treated pigment molecules under the environmental conditions. It is now realized that chemisorption, such as ion-exchange, electrostatic attractions and so forth, is the most prevalent mechanism, with the pH being the main factor affecting adsorption (Crini & Badot, 2008; Jocic et al., 2005; Pillai, Paul, & Sharma, 2009). Under acidic conditions, the amino groups of CH are protonated to positively charged amine ions (-NH₃⁺) that can electrostatically interact with the negative charge of the polymer encapsulated pigmented inks. It has been experimentally confirmed that the printed fabric color is enhanced under such acidic conditions. Furthermore, Jocic et al. (2005) elucidated the possible ionic states and interactions between wool, CH, CH-treated wool and dye, in an aqueous solution at either pH 4.2 or pH 6.5. This led to the postulation about the possible interactions between the polyester and the negative charge of the polymer encapsulated pigmented ink in the present case. Only one terminal end of the hydroxyl group per polyester molecule can be hydrogen bonded with the oxygen atom of the acetyl group of the adsorbed CH or the modified CH, or through van der Waals and hydrophobic interactions (Polyester/CH). Similar van der Waals and hydrophobic interactions between the polyester and the pigmented ink dispersion are also possible (Jocic et al., 2005).

Gly, a small amino acid molecule, has an isoelectric point (PI) at 5.97, the point or pH at which Gly will be centered between the pK_a of the two ionizable groups, the amino group and the carboxylic acid group. Therefore, electrostatic interactions between the protonated amino groups $(-NH_3^+)$ with the negative charge of polymer

encapsulated pigmented ink are also possible at a pH of less than 5.97.

When Gly was mixed with CH in an acidic condition (pH < PI), the additional protonation of H^+ to the amino group of Gly was, at first, expected because the solution pH was lower than the isoelectric point and thus Gly should be in the protonated form. Unfortunately, the opposite result was obtained in that for the mixed Gly and CH pretreatment, a lower pH yielded fabric prints with lower K/S values and a narrower color gamut. This could be caused by the fact that the acid (H^+) used for dissolving CH might protonate the carboxyl group of Gly instead.

For the DBIC pretreatment solution, there are two nitrogen atoms per glucosamine unit, and so the *K*/*S* values and color gamut were thus larger than those of the untreated fabric and the CH-treated fabrics.

Introducing a quaternary ammonium group has long been known to enhance the solubility of CH. The conjugation of glycidyltrimethylammonium chloride (GTMAC) to CH produces a CH derivative, HTACC, a water-soluble polymer at all pH values. Therefore, having two nitrogen atoms, one secondary amino group and one quaternary ammonium group, the HTACC pretreatment can synergistically produce higher *K*/*S* values of each color, a higher gamut volume and a better color saturation when compared with the low effectiveness of the primary amino group of CH alone in neutral or dilute acid solutions.

The stable positive charges may interact with the negative charge of the polymer encapsulated pigmented ink via amidation or electrostatic interaction. The much higher *K/S* values and the larger color gamut boundary and volume induced by the HTACC pretreatment can be further caused by the ease of site accessibility due to the longer side chain. It is anticipated that this long side chain can allow both chemisorption and physical surface adsorption of the pigmented inks to take place. The protonated CH and HTACC can provide a rapid surface adsorption followed by diffusion and chemisorption of the modified pigment molecules in the CH network via electrostatic interactions (Bahmani, East, & Holme, 2000). Furthermore, HTACC has been reported to generate antibacterial activity to cellulosic fibers (Seong et al., 2000), which is another advantage to use HTACC in textiles.

3.3.5. Outline sharpness and contrast assessment

The outline sharpness of the printed character "E" visualized and then as measured by the optical microscopy, is illustrated for the positive characters in Fig. 4(a)–(f) and negative characters in

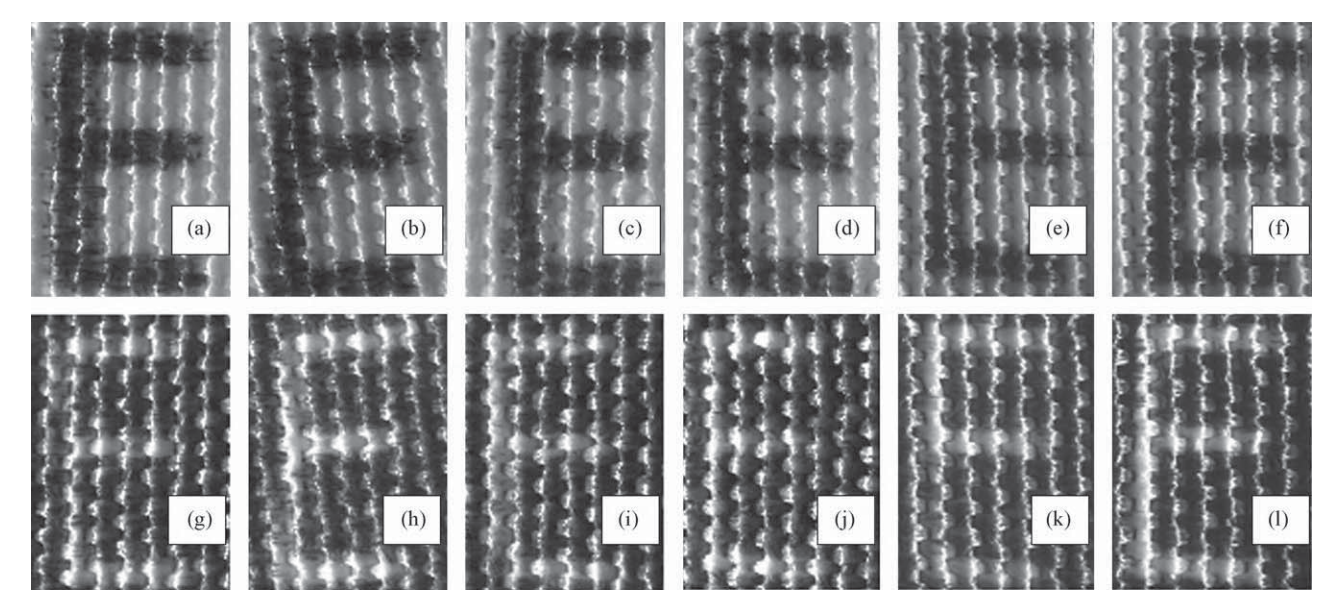


Fig. 4. Outline sharpness and printed character quality of the "E" on fabrics with various pretreatments: Positive character: (a) the untreated fabric, and the fabrics pretreated with (b) 1% (w/v) CH, (c) 15% (w/v) glycine, (d) mixture of 1% (w/v) CH and 15% (w/v) glycine, (e) 0.1% (w/v) DBIC and (f) 0.1% (w/v) HTACC; negative character: (g) the untreated fabric, and the fabrics pretreated with (h) 1% (w/v) CH, (i) 15% (w/v) glycine, (j) mixture of 1% (w/v) CH and 15% (w/v) glycine, (k) 0.1% (w/v) DBIC and (l) 0.1% (w/v) HTACC

Fig. 4(g)-(l), printed on polyester fabrics after various pretreatments. In principle, the good printed qualities of characters are sharpness, even ink deposition and legibility. The sizes of the positive characters (Fig. 4(a)–(f)) are larger and shaper than those of the negative characters (Fig. 4(g)–(1)). Ink spreading in both vertical and horizontal directions was observed in the untreated fabric (Fig. 4(a) and (g)) and all the CH-treated fabrics (Fig. 4(b) and (h)). The edges of the positive characters were not so ragged but the negative characters were more ragged and unevenly printed. The printed positive characters and negative characters on 0.1% (w/v) DBIC pretreated fabrics in Fig. 4(e) and (k) or 0.1% (w/v) HTACC pretreated fabric in Fig. 4(f) and (l) gave a much better legibility with sharper edges, more evenly printed color densities and a higher contrast between the letter and the background than those of the untreated fabric. One obvious point was also seen in the blurred "E" characters (Fig. 4(c) and (i)) on the Gly pretreated fabrics, due to the lower viscosity resulting from the small molecular size of Gly. This observation is even more obvious in the negative characters (Fig. 4(i)).

The data of the treatments disclose that the contrast transfer function (CTF) in the warp direction is higher than those in the weft direction. The trace lines of micro-density vs. distance in pixel, and their contrast calculated from the average micro-density in the weft direction are revealed in Table 3. The contrast in the warp direction cannot be calculated due to the configuration of the fiber and thus no data could be presented. One should bear in mind that the densities of the fabrics were bared. From these results, the 0.1% (w/v) HTACC pretreated fabric gave the highest contrast, followed by the 0.1% (w/v) DBIC pretreatment, whilst fabric pretreated with the mixed 15% (w/v) Gly and 1% (w/v) CH gave the lowest contrast. All the measured samples rendered a decreasing contrast with increasing spatial frequencies at each resolution. Therefore, among all the pretreatments, the fabrics treated with 0.1% (w/v) HTACC gave the highest smoother trace lines and resolution especially at the frequency of 2 lines per mm (data are not shown here). Two possible attributes to the above observations are the extent of ink absorption, spreading and fixation. The lower ink absorption produced a higher ink density and better contrast, while the better color fixation controls an adequate ink penetration and limited ink spreading to result in the fine and smooth edges of the characters.

3.3.6. Surface appearance and stiffness of the pretreated polyester fabrics

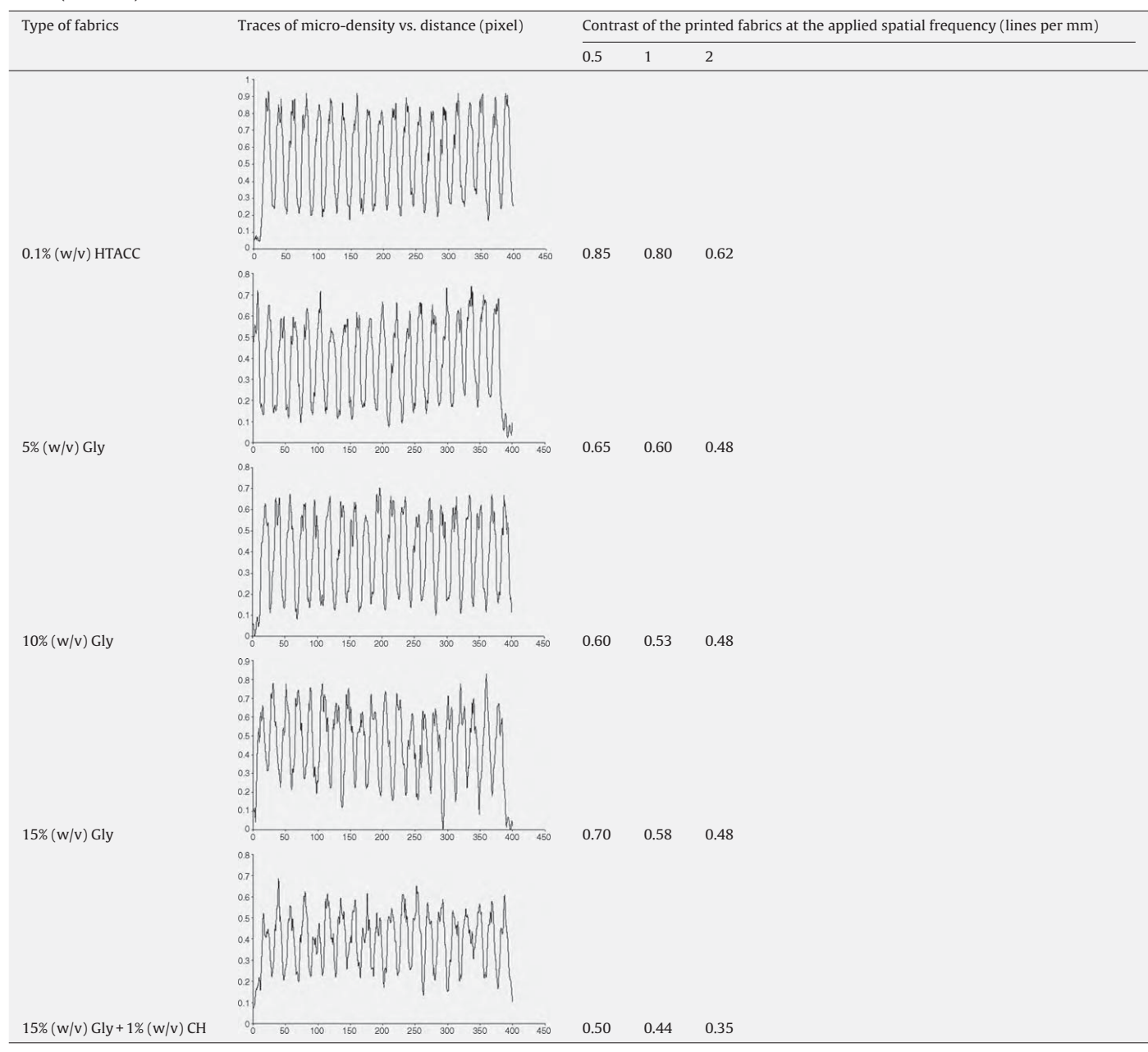
Fig. 5 shows the surface appearance of the untreated polyester fabrics and the various treated polyester fabrics. The untreated polyester fabric, as depicted in Fig. 5(a) is not smooth and has minute and shallow channels distributed widely on the fiber. When it was treated with 1% (w/v) of CH, the channels were reduced because the CH solution could fill up the channels. With higher CH concentrations, at 2, 3 and 4% (w/v), an uneven and rough layer of CH was deposited on the fiber surfaces which made the fibers become distorted (micrographs are not shown here). This behavior may induce stiffness to the fabrics. When an excessive amount of 15% (w/v) Gly was padded, small specks, agglomerates and layers of the pretreatment Gly were deposited widely on the fiber, as shown in Fig. 5(b). The fibers became smoother and less swollen when the mixed CH and Gly solution was padded (Fig. 5(c)). The stiffness of the fabric at this level of padding was hard to hand touch. The CH and Gly pretreated fabrics were not soft to hand touch because the fabric stiffness was increased appreciably. On the other hand, the fabrics padded with 0.1% (w/v) of DBIC or 0.1% (w/v) of HTACC (Fig. 5(e) and (f), respectively) had a smooth surface texture somewhat similar to that of the untreated fabric. For softness to hand touch, the 0.1% (w/v) DBIC or 0.1% (w/v) HTACC pretreatment gave a relatively similar stiffness as that for the untreated fabric regardless of the high molecular weight of HTACC. Based on Crutzen (1995) model of ditallowdimethyl ammonium chloride deposition on cotton, this model was adopted to explain the similar softening result of the high molecular weight HTACC. The long side chain of N-(2-hydroxyl-3-trimethylammonium)propyl chloride attached at the nitrogen atom of the amine occupied more spaces on the fabric. The combined effects of adsorption and the softening power of quaternaries enable the fabric to behave somewhat like the cationic softener treated fabric.

Fig. 6 shows the extent of the bending length of the printed fabrics in the warp and weft directions for the fabrics pretreated with the different solutions. The stiffness of the untreated warp direction was higher because it is naturally stronger than that of the weft direction, due to having more incorporated fibers (182 ends in. $^{-1}$ for the warp fiber vs. 87 picks in. $^{-1}$ for the weft). When 0.1% (w/v) CH, 0.1% (w/v) HTACC and 0.1% (w/v) DBIC were used to treat the

Table 3Print contrast in the weft direction of polyester fabrics printed by ink jet inks after pretreatment with the indicated solutions.

Type of fabrics	Traces of micro-density vs. distance (pixel)	Contrast of the printed fabrics at the applied spatial frequency (lines per mm)		
	0.9 1	0.5	2	
Untreated	0.8 0.7 0.6 0.5 0.4 0.1 0.2 0.1 0.5 0.1 0.1 0.2 0.1 0.3 0.3 0.3 0.3 0.3 0.3 0.3 0.3	0.69	0.58	0.53
	0.9 0.8 0.7 0.6 0.5 0.4 0.3 0.2			
.1% (w/v) CH	0 50 100 150 200 250 300 350 400 450	0.57	0.51	0.47
% (w/v) CH	0.8 0.7 0.6 0.5 0.4 0.3 0.2 0.1 0.0 0.0 0.0 0.0 0.0 0.0 0.0	0.63	0.60	0.51
% (w/v) CH	0.8 0.7 0.6 0.3 0.2 0.1 0.0 150 200 250 300 350 400 450	0.59	0.52	0.36
	0.8- 0.7- 0.6- 0.5- 0.4- 0.3- 0.2-			
% (w/v) CH	0 50 100 150 200 250 300 350 400 450	0.55	0.48	0.37
4% (w/v) CH	0.7- 0.6- 0.6- 0.4- 0.3- 0.2- 0.11- 0 50 100 150 200 250 300 350 400 450	0.57	0.52	0.44
0.1% (w/v) DBIC	0.5 0.4 0.3 0.2 0.1 0 50 100 150 200 250 300 350 400 450	0.69	0.69	0.51

Table 3 (Continued)



fabrics prior to printing, the stiffness in the warp direction in each pretreated fabric increased, which was influenced by the strength of the warp fibers and the pretreatment solution ($p \ll 0.05$). The HTACC pretreated fabric gave significantly lower fabric stiffness. The stiffness of the weft direction in the untreated and treated fabrics showed a similar trend as those seen for the warp direction. In contrast, when more concentrated pretreatment solutions were used, the stiffness in the weft direction increased rapidly. This is because the pretreatment solutions were absorbed easily by the fibers in the weak weft fibers due to the lower fiber density at 87 picks in. $^{-1}$ in this direction. Increasing the pretreatment of both chitosan solutions from 0.1 to 4% (w/v), and Gly solutions from 5 to 15% (w/v) significantly increased the stiffness in both the warp and the weft fiber directions, but with a greater increase in the weft fiber direction. When the fabrics were pretreated with the mixture of 1% (w/v) CH and 15% (w/v) Gly, the stiffness increased markedly and this was statistically significant ($p \ll 0.05$). The greater the stiffness of the fabrics, the less comfortable they became. It is also anticipated that the electrostatic interaction between the positive charges of the pretreatment agents and the negative charge of the polyester surface and the inks might be the major contribution to the increase in fabric stiffness. Therefore, there is a trade-off in the amount of pretreatment solution on the required printing property vs. the fabric performance properties. In the present case, HTACC is a good candidate as a pretreatment agent because only 0.1% (w/v) is required to obtain a satisfactory color strength, which does not yield too high a fabric stiffness and also has the advantage of potentially adding antibacterial activity, as reported elsewhere (Seong et al., 2000).

3.3.7. Effect of pretreatment agent on color fastness to washing and rubbing

Based on the ISO 105-C10:2006 (E) for evaluating color fastness to washing, and AATCC TM 8 for color fastness to rubbing, the results presented below are based on the five levels of evaluation that 5 stands for excellent, 4 for good, 3 for fair, 2 for poor, and 1

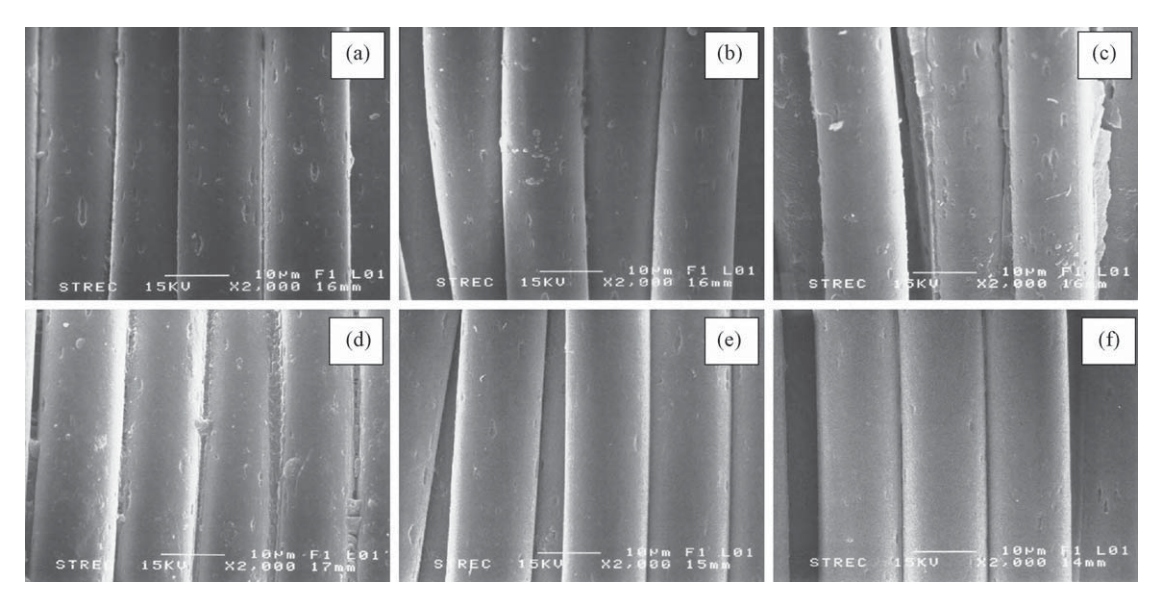


Fig. 5. Surface appearances of (a) the untreated fabric, and the fabrics pretreated with (b) 1% (w/v) CH, (c) 15% (w/v) glycine, (d) mixture of 1% (w/v) CH and 15% (w/v) glycine, (e) 0.1% (w/v) DBIC and (f) 0.1% (w/v) HTACC.

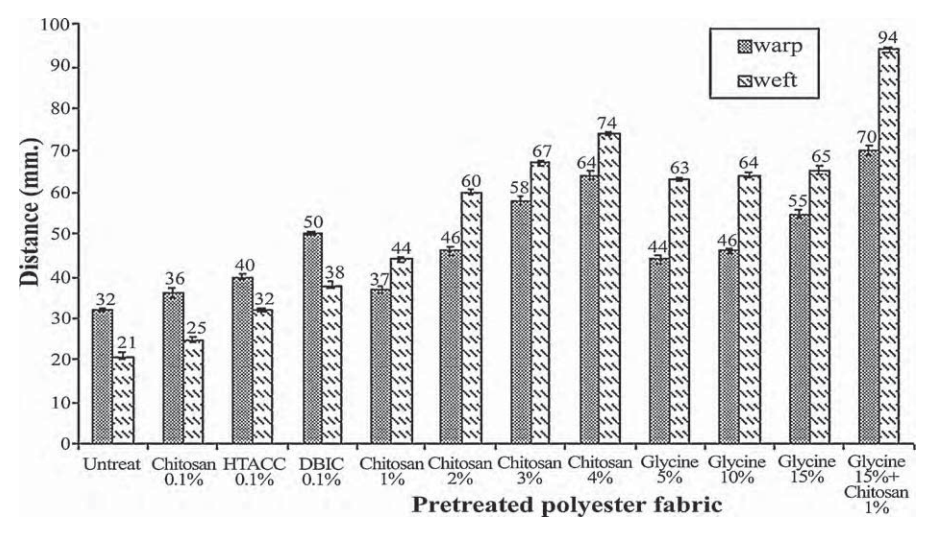


Fig. 6. Stiffness of the printed fibers of (a) untreated fabrics, weft direction, (b) untreated fabrics, warp direction, (c) treated with 0.1% (w/v) HTACC, weft direction and (d) treated with 0.1% (w/v) HTACC, warp direction. (Data are shown as the mean values ± 1 SD, derived from five independent repeats.)

for very poor:

Treatment	Color fastness level	Dry fastness level	Wet fastness level
Untreated	1	3-3.5	2.5
CH, Gly, DBIC	2	3-4	2.5-3, 2-3, 1.5-2.5
HTACC	3-4	3-4	2.5
Gly-CH mixture	3-4	3-4	2.5-3.5

The pretreated fabrics gave the higher color fastness to washing than the untreated one. The HTACC gave better color fastness to washing of the printed polyester fabric which might be contributed by HTACC as an interlayer between the ink and the fabric. Similar result was also observed for the Gly–CH mixture pretreated fabric. Color fastnesses to wet rubbing for all fabrics with all pretreatments are lower than those for dry rubbing. This could be caused by the weakness of the swollen film in the wet condition which can be easily rubbed off. One can also see that Gly–CH mixture pretreatment having the higher stiffness contributes somewhat the better color fastness to both dry and wet rubbings. It may be then said that the higher flexural modulus is also another contribution to rubbing.

Both HTACC and DBIC pretreatments gave the lower color fastness to wet rubbing because they are relatively hydrophilic in nature with low flexural modulus and the pretreated films are weak in water and under rubbing.

With a very smooth interface adhesion for the ink and substrate, the only forces holding the substrate and pretreatment agent together are the interfacial attractive forces. Internal stresses act to reduce adhesion and less external force is required to disrupt the adhesive bond. As film formation proceeds, $T_{\rm g}$ rises and free volume is reduced; the film becomes fixed in unstable conformations, and internal stress increases. Stresses also result from volume expansions, such as swelling of films by exposure to high humidity or water immersion. Thus delaminating of the printed ink film under rubbing can occur easily.

4. Conclusions

The use of CH, Gly, and the two modified CHs (DBIC and HTACC) as the pretreatment reagents of polyester fabrics prior to ink jet printing indicated that these pretreated fabrics produced a much

better color quality than the untreated fabrics, but that the extent of this improvement largely depended on the type and concentration of the pretreatment solutions. Although polyester is a hydrophobic fabric, it had a negative zeta potential implying that it has negative charges on its surface. The important properties of the K/S value, color gamut and gamut volume, color saturation, tone reproduction, outline sharpness and surface appearance were evaluated. Overall, HTACC pretreatment gave overwhelming excellent properties over the rest of the pretreatments. Only 0.1% (w/v) of HTACC was required to provide a high color gamut and color saturation, good tone reproduction and outline sharpness, smooth surface and less fabric stiffness. Nevertheless, Gly could also be used as a pretreatment agent for good color reproduction, but it is not as good for outline sharpness because it produced rather poor outline sharpness and low contrast print, due to its high spreading caused by the low solution viscosity. Based on the numerical observation and statistical evaluation, the pretreatment agents gave better qualities than the untreated fabric and their efficiency can be ranked as follows for (i) color properties: HTACC ≫ Gly > CH ≈ DBIC > Gly–CH mixture (15% and 1% (w/v), respectively); (ii) for outline sharpness: HTACC > CH \approx DBIC \approx Gly–CH mixture (15% and 1% (w/v), respectively); and (iii) less stiffness: HTACC < DBIC < Gly < CH < Gly - CH mixture (15% and 1% (w/v), respectively); (iv) color fastness to washing: HTACC \approx Gly–CH mixture > CH > gly \approx DBIC; (v) color fastness to rubbing: Gly–CH mixture > gly ≈ CH > HTACC > DBIC.

Acknowledgements

The authors would like to acknowledge the research grant support by the National Research Council of Thailand under contract number GRB_19_51_23_03 and the Research Team Aids coded RTA5080004 for their financial support. Deep gratitude also goes to the Polymer Research Laboratory of the Department of Imaging and Printing Technology, Chulalongkorn University, for providing research facilities. The authors are indebted to the Department of Textile Chemical Engineering, the Faculty of Textile Industries, Rajamangala University of Technology, KrungThep, for permission to use their padding machine and steamer. Many thanks go to Assistant Professor Voravee, P. Hoven, Ph.D. for useful comments on the manuscript, to Publication Counseling Unit of the Research Affairs, Faculty of Science, Chulalongkorn University for language editing.

References

- Abou-Okeil, A., & Hakeim, O. A. (2005). Effect of metal ion binding of chitosan on the printability of pretreated wool fabric. *Coloration Technology*, 121, 41–44.
- Bahmani, S. A., East, G. C., & Holme, I. (2000). The application of chitosan in pigment printing. *Coloration Technology*, 116, 94–99.
- Chakvattanatham, K., Phattanarudee, S., & Kiatkamjornwong, S. (2010). Anionically surface-modified pigment/binder ink jet inks for silk fabric printing. *Pigment & Resin Technology*, 39(6).
- Crini, G., & Badot, P. M. (2008). Application of chitosan, a natural aminopolysaccharide, for dye removal from aqueous solutions by adsorption processes using batch studies: A review of recent literature. Progress in Polymer Science, 33, 399–447
- Crutzen, A. M. (1995). Study of the ditallowdimethylammonium chloride interaction with cellulose. *Journal of the American Oil Chemists' Society*, 72, 137–143.

- Espinosa-Jiménez, M., Padilla-Weigand, R., Ontiveros-Ortega, A., Ramos-Tejada, M. M., & Perea-Carpio, M. R. (2003). Interpretation of colloidal dyeing of polyester fabrics pretreated with ethyl xanthogenate in terms of zeta potential and surface free energy balance. *Journal of Colloid and Interface Science*, 265, 227–233.
- Fair, M. D. (1997). Colorimetry in color appearance models. MA: Addison-Wesley-Longman., p. 61.
- Hakeim, O. A., Abou-Okeil, A., Abdou, L. A. W., & Waly, A. (2005). The influence of chitosan and some of its depolymerized grades on natural color printing. *Journal* of Applied Polymer Science, 97, 559–563.
- Hakeim, O. A., El-Gabry, L., & Abou-Okeil, A. (2008). Rendering synthetic fabrics acid printable using chitosan and binder. *Journal of Applied Polymer Science*, 108, 2122–2127.
- Huacai, G., Wan, P., & Dengke, L. (2006). Graft copolymerization of chitosan with acrylic acid under microwave irradiation and its water absorbency. *Carbohydrate Polymers*, 66, 372–378.
- James, H. N. (1997). In M. Roderick (Ed.), Color physics for industry (p. 296). West Yorkshire, England: Society of Dyers and Colourists.
- Jocic, D., Vîlchez, S., Topalovic, T., Navarro, A., Jovancic, P., Julià, M. R., et al. (2005). Chitosan/acid dye interactions in wool dyeing system. *Carbohydrate Polymers*, 60, 51–59.
- Julia, M. R., Pascual, E., & Erra, P. (2000). Influence of the molecular mass of chitosan on shrink-resistance and dyeing properties of chitosan treated wool. *Coloration Technology*, 116, 62–67.
- Kim, J. Y., Lee, J. K., Lee, T. S., & Park, W. H. (2003). Synthesis of chitooligosaccharide derivative with quaternary ammonium group and its antimicrobial activity against Streptococcus mutans. International Journal of Biological Macromolecules, 32, 23–27.
- Leelajariyakul, S., Noguchi, N., & Kiatkamjornwong, S. (2008). Surface-modified and micro-encapsulated pigmented inks for ink jet printing on textile fabrics. *Progress in Organic Coatings*, 62, 145–161.
- Lim, S. H., & Hudson, S. M. (2004a). Application of a fibre-reactive chitosan derivative to cotton fabric as a zero-salt dyeing auxiliary. Coloration Technology, 120, 108–113.
- Lim, S. H., & Hudson, S. M. (2004b). Structure of the O-polysaccharide of Citrobacter youngae O1 containing an α-D-ribofuranosyl group. Carbohydrate Research, 339, 313–325.
- Livengood, C. D. (1983). Spot tests for identification of warp sizes on fabric. Textile Industries, September, 114–116.
- Mun, G. A., Nurkeeva, Z. S., Dergunov, S. A., Nama, I. K., Maimakov, T. P., Shaikhut-dinov, E. M., et al. (2008). Studies on graft copolymerization of 2-hydroxyethyl acrylate onto chitosan. Reactive and Functional Polymer, 68, 389–395.
- Phattanarudee, S., Chakvattanatham, K., & Kiatkamjornwong, S. (2009). Pretreatment of silk fabric surface with amino compounds for ink jet printing. *Progress in Organic Coatings*, 64, 405–418.
- Pillai, C. K. S., Paul, W., & Sharma, C. P. (2009). Chitin and chitosan polymers: Chemistry, solubility and fiber formation. *Progress in Polymer Science*, 34, 641–678.
- Putthimai, P. (2003). Appendix B, in print qualities of screen and ink jet printings on cotton fabrics (p. 105, ISBN 974-17-194-9). Masters Thesis, Chulalongkorn University
- Samu, R., Moulee, A., & Kumar, V. G. (1999). Effect of charge and hydrophobicity on adsorption of modified starches on polyester. *Journal of Colloid and Interface Science*, 220, 260–268.
- Seong, H., Whang, H. S., & Ko, S. (2000). Synthesis of a quaternary ammonium derivative of chito-oligosaccharide as antimicrobial agent for cellulosic fibers. *Journal of Applied Polymer Science*, 76, 2009–2015.
- Singh, V., Sharmaa, A. K., Tripathi, D. N., & Sanghib, R. (2009).
 Poly(methylmethacrylate) grafted chitosan: An efficient adsorbent for anionic azo dyes. Journal of Hazardous Materials, 161, 955–966.
- Stiffness Method A. (1999). JIS published standard. JIS L, 1096.
- Sun, T., Zhou, D., Xie, J., & Mao, F. (2007). Preparation of chitosan oligomers and their antioxidant activity. European Food Research and Technology, 225, 451–456.
- Wang, C., Wu, G., Fang, K., Tian, A., Zhang, X., Fu, S., et al. (2007). Cationic pretreatment for improving image quality of inkjet printing on polyester fabrics. In *Proceedings* of NIP23 and digital fabrication Anchorage, United States of America, (2nd ed., pp. 500–503).
- Yuen, C. W., Ku, S. K., & Kan, C. (2008). Use of a biomaterial as a thickener for textile ink-jet printing. Journal of Applied Polymer Science, 107, 1057–1065.
- Yuen, C. W. M., Ku, S. K. A., Kan, C. W., & Choi, P. S. R. (2007). Enhancing textile ink-jet printing with chitosan. Coloration Technology, 123, 267–270.
- Zhang, J., Wang, Q., & Wang, A. (2007). Synthesis and characterization of chitosan-g-poly(acrylic acid)/attapulgite superabsorbent composites. *Carbohy-drate Polymers*, 68, 367–374.

Anionically surface-modified pigment/binder ink jet inks for silk fabric printing

K. Chakvattanatham, S. Phattanarudee and S. Kiatkamjornwong
Imaging Technology Research Unit, Department of Imaging and Printing Technology, Faculty of Science,
Chulalongkorn University, Bangkok, Thailand

Abstract

Purpose — The purpose of this paper is to prepare anionically surface-modified organic pigment/binder ink jet inks for printing on chitosan-pre-treated silk fabrics.

Design/methodology/approach — Anionically surface-modified organic pigment/binder ink jet inks were prepared in four colours (cyan, magenta, yellow and black). The pigment-to-binder ratio was controlled at 1:6.4 for the cyan, magenta and yellow inks, and 1:3.4 for the black ink. Ink formulations (by weight) were assembled and mixed as follows: 8 per cent pigment dispersion, 10 per cent diethylene glycol, 12 per cent glycerol, 5 per cent urea, 10 per cent polyacrylate emulsion binder and 55 per cent deionised water. They were characterised in terms of their particle size, zeta-potential, particle morphology, viscosity, surface tension and pH. The inks were printed onto silk or the chitosan pre-treated silk fabrics using a piezo-type ink jet printer. The fabrics were then heat cured and analysed for the effect of chitosan pre-treatment on colour gamut, wash fastness and crock fastness.

Findings — The formulated ink jet inks yielded an acceptably good ink jetting reliability, one-year stability and printability. The chitosan pre-treated silk fabrics gave a wider colour gamut and colour saturation than the non-treated one. Crock fastness and wash fastness of the chitosan pre-treated fabrics were relatively better than those of non-treated fabrics.

Research limitations/implications — The surface-modified pigments are transparent and thus their inks printed on the chitosan pre-treated fabrics produced slightly low K/S values of cyan, magenta, yellow, and black colours because the limited chitosan concentration in the pre-treatment is controlled by its solubility in acidic solution. The higher loading of chitosan pre-treatment gave higher K/S values and a stiffer touch of the fabrics. Practical implications — The water-based pigmented inks having the sulphonate group on the pigment surface can be printed on the fabric surface pre-treated with chitosan molecules which have the protonated amino groups to give good colour appearance. It is anticipated that this type of ink can be applied to any textile surface which has been pre-treated with the protonated chitosan.

Originality/value — The modified organic pigments having the sulphonate group on their surface can be used to produce novel water-based ink jet inks which can print on the chitosan pre-treated silk fabric. Ionic interactions between the sulphonate group of the pigment and protonated amino groups of chitosan in conjunction with polyacrylate binder enhance colour strength, widen colour gamut and chroma, and produce good adhesion for fabric operational properties such as wash fastness and crock fastness.

Keywords Inks, Colour fastness, Silk, Pigments, Ink jet printers

Paper type Research paper

Introduction

Organic pigments that are used in ink formulations for fabric printing need to be surface modified if they are to be suitable for printing and application. Limitations on the pigments in this context usually relate to the colour gamut, the stability of the ink, the nature of the continuous medium and the drying time. In applications, various problems, such as in the development of a concentration gradient, the blocking of jets, inconsistency in colour and the low optical density of the resultant prints, are of a major concern (Fu, 2006). The pigment dispersion needs to demonstrate colloid stability with a limited and controllable particle growth in size with time, the size remaining less than 150 nm. The formulated ink must have a low viscosity and a

The current issue and full text archive of this journal is available at www.emeraldinsight.com/0369-9420.htm



Pigment & Resin Technology 39/6 (2010) 327–341 © Emerald Group Publishing Limited [ISSN 0369-9420] [DOI 10.1108/03699421011085821] high surface tension. There is a need, therefore, to consider both the thermal and long-term shelf life stabilities of the inks coupled with the need for colour purity (Leelajariyakul *et al.*, 2008). The stability of the pigment dispersion within the ink depends on particle separation forces (type and magnitude), whereby the separated distance can be maintained by stabilising groups that are adsorbed to polymer surface via steric and/or electrostatic forces. These stabilising groups can be covalently attached to the pigment surface in ways that ensure that the functional groups, such as carboxylic or sulphonic acid groups are available on the pigment surface (Belmont, 1994; Johnson and Belmont, 1997).

Like other fabrics, silk, which is directly printed by ink jet printing, does not provide high-quality printing because the surface of the silk fabric is not smooth. A pre-treatment

This research was supported by a Senior Scholar Research Grant Number RTA4780004 from the Thailand Research Fund. The research facilities, provided by the Polymer Imaging Laboratory of Chulalongkorn University's Imaging and Printing Technology Department, are highly appreciated. The authors are grateful to Professor J.T. Guthrie for his valuable suggestions in paper improvement. Material donations from Cabot (Tokyo) and Shin Nakamura are highly acknowledged.

Volume 39 · Number 6 · 2010 · 327-341

process to limit the excessive spreading of the ink is necessary before ink jet textile printing because the fabric is porous, soft and pliable. The treating system helps to smooth out the fabric surface and ink absorption becomes more uniform (Phattanarudee *et al.*, 2009). The functional groups provided by the pre-treatment compounds are designed to absorb additional ink, resulting in a better deposition of ink on the fabric surface or a higher ink holdout (Bajai, 2002).

The majority of interest in textile and printing has been involved with cotton (Bahmani *et al.*, 2000; Oktem, 2003) or synthetic textiles as the substrate- and dye-based ink jet inks (Yuen *et al.*, 2007) have been used. The limited research into the use of the ink jet colouration of silk is a suppressing factor. The major objectives of the current research were to use the anionic, surface-modified pigments/binders to formulate four pigmented ink jet inks and to investigate those parameters that were considered to be of relevance to their printing on pre-treated silk fabrics.

Experimental

Materials

Preparation of pigmented ink jet inks

The pigmented ink jet inks that were used in the study are listed in Table I with the surface-modified pigments being supplied by Cabot Corporation, Billerica, Massachusetts, USA (Jason, 2004). The four pigments used were a cyan pigment, IJXTM 253 C, modified from C.I. Pigment Blue 15:4; a magenta pigment, IJXTM266D, modified from C.I. Pigment Red 122; a yellow pigment, IJXTM273B, modified from C.I. Pigment Yellow 74 (Johnson and Belmont, 1997; Johnson *et al.*, 2002); and a black pigment, CAB-O-Jet 200, modified from C.I. Pigment Black 7 (Belmont, 1994; Belmont *et al.*, 1996a, b). The pigments were provided as an aqueous dispersion. The relevant structures of the pigments are shown in Figure 1, whilst the properties of the surface-modified pigment dispersions are given in Table I.

Methods

Each pigmented ink formulation was assembled as follows (total composition by per cent volume): 8 per cent pigment dispersion, 10 per cent diethylene glycol, 12 per cent glycerol, 5 per cent urea, 10 per cent polyacrylate emulsion binder and 55 per cent deionised water. The pigment/binder ratios were prepared at 1:6.4 for the cyan, magenta and yellow inks, and 1:3.4 for the black ink (Leelajariyakul *et al.*, 2008; Phattanarudee *et al.*, 2009). The polymer binder for the anionically surface-modified pigment dispersions was a polyacrylate emulsion, Vanatex S-711 polyacrylate binder (Shin Nakamura, Wakayama, Japan), added at 10 per cent

w/v of dispersion in 63 per cent w/v de-ionised water. The mean diameter of the polymer particles was 116 nm. The Vanatex S-711 contained non-ionic surfactant at 48.5 per cent w/v. The viscosity was 1,000 mPa s at a shear-strain rate of 320 s⁻¹ at 25°C. The pH of the dispersion was 5. The glass transition temperature of Vanatex S-711 was 1.2°C. Urea, a good hydrotropic agent, which works as an anti-hydrogen bonding additive was used to improve the stability and to provide the required reduced viscosity and clogging problems that are inherent in on-demand piezo nozzle-jetting devices.

Each component was added individually to the total system. Diluted NaOH solution was added to the ink in order to adjust the pH to within the desired range of 7-9. After mixing, the inks were filtered through a cellulose acetate filter (pore size $0.45 \,\mu m$, Sartorius Stedim Biotech GmbH, Göettingen, Germany) to remove all coarse particles and so the risk of their clogging the orifices of the ink jet printer was reduced.

Characterisation of pigmented ink jet inks

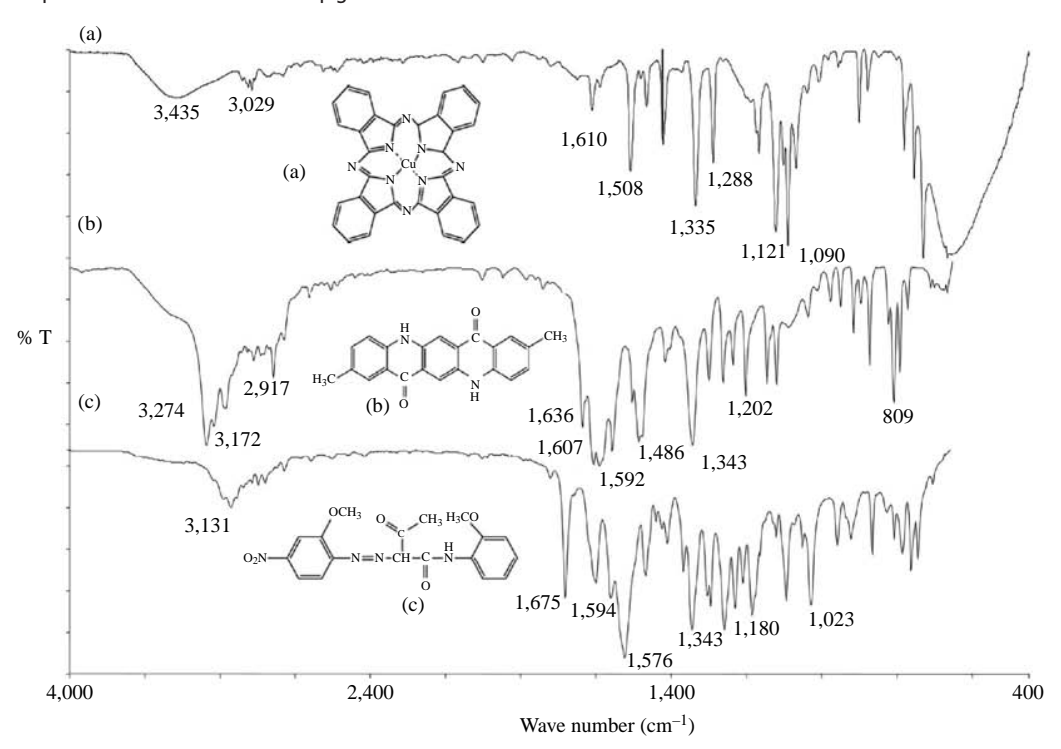
The pigment dispersion was dried on a glass support, and the resulting film was dried and ground. The dried powder was subjected to Fourier transform infrared (FTIR) measurement (Perkin Elmer System 2000, UK). The pH of the ink was adjusted to the suitable range for printing (pH meter, pH Tester 20, Oaklon, Eutech instruments, Vernon Hills, Illinois, USA) at room temperature. A Brookfield viscometer (DV III, programmable rheometer, Stoughton, Massachusetts, USA) was used to measure the viscosity of the pigment dispersion and of the formulated inks, at 25°C. A particle size distribution analyser (Malvern laser scattering analyser, model Mastersizer S, long bed Ver. 2.11, Worcestershire, UK) was used for the particle size analyses of the pigment dispersions and of the formulated inks. The particle size distributions of the ink formulations were measured after various storage periods (one day, one, ten and 12 months) to confirm the stability of the inks. The surface tension of each ink preparation was measured using a surface tensiometer (K8, Kruss, Hamburg, Germany) by the DuNouy Ring method at room temperature (25°C). The morphology and particle sizes of dried samples of the pigment dispersions were viewed by transmission electron microscopy (TEM) (JEOL, JEM-2100, Tokyo, Japan). The ink samples, after one year of storage, were diluted and applied to a glass substrate. The solvent was removed by evaporation and the resultant dried ink samples were then observed by scanning electron microscopy (SEM) (JSM 6400, JEOL, Tokyo, Japan) and TEM. The inks were diluted using deionised water and their zeta-potential was measured by nanosizing Zetasizer (Nano Series, Malvern Instruments Ltd, UK). The charge on pigment surface was evaluated at 25°C.

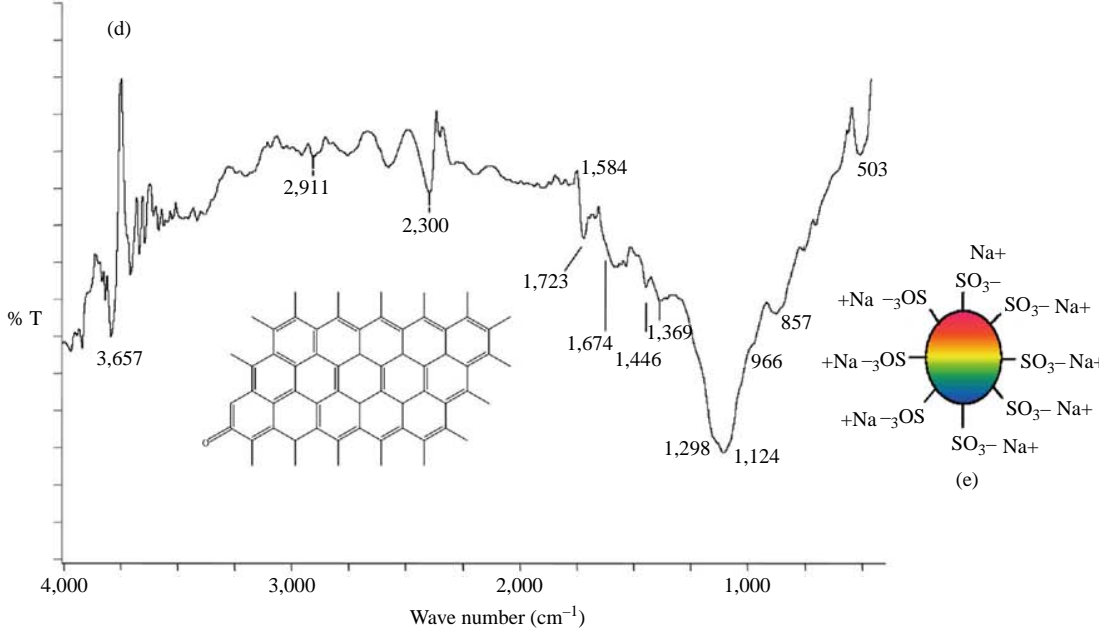
Table I Properties of ink ingredients from the surface-modified pigment dispersions

Chemicals	Colour index of pigments used	Chemical class	Average particle size (nm)	Solid content (%(w/w))	Viscosity ^a (mPa s)	Zeta-potential (mV)
Cyan: C (IJX 253 C)	Pigment Blue 15:3	Phthalocyanine	91	9.45	1.37	- 55
Magenta: M (IJX 266D)	Pigment Red 122	Dimethyl quinacridone	105	9.96	1.70	– 57
Yellow: Y (IJX 273B)	Pigment Yellow 74	Monoazo; acetoacetyl	105	9.66	1.43	- 52
Black: K (CAB-O-JET200)	Pigment Black 7	Carbon black	69	18.65	3.10	-64
Vanatex S-711-Polyacrylate emulsion			116	50.7	1,000	- 38
Note: ^a The viscosity was measured at sh	ear-strain rate of 33	0 s ⁻¹ at 25°C				

Volume 39 · Number 6 · 2010 · 327-341

Figure 1 FTIR spectra of the surface-modified pigments





Notes: Spectrum (a) a cyan colour modified from C.I. Pigment Blue 15:4; spectrum (b) a magenta colour modified from C.I. Pigment Red 122; spectrum (c) a yellow colour modified from C.I. Pigment Yellow 74; spectrum (d) a carbon black modified from C.I. Pigment Black 7; and scheme (e) a surface-modified pigment in an electrical double layer for the above pigment

Preparation of the silk fabrics

A plain weave silk fabric, constructed with 73 ends per inch \times 62 picks per inch, with a basic weight of 0.11 kg m⁻², was used. The fabric was cut into rectangles of 22 cm \times 31 cm. Then, the samples were bleached using dilute (0.2 per cent w/v) hydrogen peroxide, at pH 10.5 and a temperature of 100°C, for 1 h.

The bleaching formulation was composed of hydrogen peroxide ($2g\ l^{-1}$, reagent grade, ≥ 98 per cent, anhydrous Sigma-Aldrich, Pte. Ltd, Singapore), sodium carbonate ($10g\ l^{-1}$, American Chemical Society (ACS) reagent, anhydrous, 99.95-100.05 per cent dry basis, Sigma-Aldrich, Pte. Ltd, Singapore) and deionised water and then used at

Volume 39 · Number 6 · 2010 · 327-341

a 1:50 (v/v) ratio of silk fabric: bleaching solution. The bleached fabrics were washed with deionised water several times to remove the remaining oxidizing agent and then dried at 50° C for $4\,h$.

Preparation of the chitosan-containing pre-treatment solutions

The three chitosan powders, FL-80, FM-80 and FM-40, had an average molar mass of 120, 370 and 850 kg mol $^{-1}$, respectively, with an N-deacetylation degree of 88, 87 and 88 per cent, respectively, and were obtained from the Koyo Chemical Co. Ltd (Japan). Each of the three chitosan types were prepared at 0.25, 0.5, 1 and 2 per cent w/v in a 1 per cent w/v aqueous solution of acetic acid (ACS reagent, \geq 99.7 per cent, Sigma-Aldrich, Singapore) by heating at 60°C until a homogeneous solution was obtained, except that 2 per cent w/v solution could not be made for FM-40 because it could not dissolve at room temperature. The highest concentration of the pre-treatment solution gave difficulty to apply on the fabric because of both the limited solubility capacity and the stickiness of the chitosan solution when it was used for padding on the fabric.

Pretreatment of the fabrics

The bleached silk fabrics were each padded with the pretreating solutions at 100 per cent pick up in a padding machine (Tsuji Dyeing Machine Mfg, Osaka, Japan). The fabrics were later steamed, pre-treated at 80°C for 5 min and fixed at 110°C for 2 min in an oven (Rapid Labortex Corporation, Taiwan). After the pre-treatment, the silk fabrics were characterised by FTIR-attenuated total reflectance (ATR) spectroscopy (Spectrum One, Perkin Elmer, UK), to confirm the existence of the pre-treatments on the silk fabrics. Likewise, all of the ink colours printed on the silk fabrics were characterised by FTIR spectroscopy to observe the functional groups of the inks and the fabrics.

Printing on the fabric

Each silk fabric was supported on a flat plastic sheet using double-sided adhesive tape to give stable dimensions to the fabric in the media-feeding path for the ink jet printer. The samples were printed with the in-house formulated ink jet inks using an Epson Stylus $^{\rm TM}$ C65 printer (Epson (Thailand), Bangkok, Thailand), at a resolution of $5,760 \times 1,440$ optimised dpi. After printing, each printed silk sample was steamed at 100° C for 5 min to fix the printed inks.

Evaluation of the printed fabric

Colour gamut

The colour test chart of each of the printed fabrics was evaluated according to CIE $L^*a^*b^*$ colour space (Commission International I'Eclairage), determined using a spectrophotometer (GretagMacbeth Spectrolino, 45/0, X-rite, Incorporated, Regensdorf, Switzerland), with an illuminant D50 and the 2° observer, based on the CIE 1931 system (Berns, 2000). The L^* axis runs from top to bottom with a maximum of 100 representing a perfect reflecting diffuser. The minimum value for L^* is zero, which represents black. The a^* and b^* axes have no specific numerical limits. Positive and negative values for a^* represent a red and green colours, respectively, whilst the same for b^* represents a yellow and blue colours, respectively. The equations for CIE 1976 L^* a^* b^* (CIELAB) colour space are presented elsewhere (Berns, 2000).

Wash fastness

The treatment of the fabric before and after the printing process is an important aspect of the ability to ensure a good fastness property. Thus, the printed silk fabrics (non-treated and chitosan pre-treated) were soaked in 5 per cent w/v NaCl (ACS reagent, ≥99.7 per cent, Sigma-Aldrich, Singapore) and then steamed for 5 min to fix and stabilise the inks on the fabrics. Wash fastness evaluations were carried out according to ISO 105-C06 (1994). Thus, in each case, a sample (100 × 40 mm) in contact with the specified adjacent fabric was washed, rinsed and dried. Each printed fabric, together with its attached multifibre strip, was washed at 40°C for 30 min in liquor containing 4 g of standard detergent (SDC, ISO 105, without optical brightener) per 11 of water at a liquor volume of 150 ml. The adjacent multifibre fabric (DW) contained wool, acrylic, polyester, polyamide, bleached cotton and cellulose diacetate fabrics. Any change in the colour of the adjacent fabric was compared using the grey scale for staining in accordance with ISO 105-A03 (1993). The colour difference in the printed fabrics, from before and after washings, was also reported in terms of the colour strength (K/S) and the relative colour strength, as derived in equations (1) and (2), from which the K/S ratio and the relative colour strength were calculated:

Colour strength,
$$K/S = \frac{(1-R)^2}{2R}$$
 (1)

Relative colour strength =
$$\frac{(K/S)_{after washing}}{(K/S)_{before washing}}$$
 (2)

Here, R = the reflectance of printed silk fabric in the range of the highest absorption, based on ISO 105-C06 (1994). The fabrics were printed as a solid pattern in the four colours (cyan, magenta, yellow and black). The printed fabrics, before and after the washing treatment, were evaluated using a spectrophotometer (X-rite, SP62, d/8, X – Rite Asia Pacific Ltd, Quarry Bay, Hong Kong). The reflectance of samples was measured five times in different areas to determine the K/S-values. An averaged value was then calculated.

Crock fastness

The crock fastness of the printed fabric was evaluated using the AATCC Crockmeter (Atlas Electric Devices Corporation, Chicago, Illinois, USA) and AATCC Test Method 8-2001 (2002). The amount of colour that was transferred from the printed surface to the other tested surfaces, during a controlled rubbing process, was judged using a grey-scale chart (Grey Scale for Staining or the Chromatic Transference Scale). Each printed sample was rubbed with a standard white cotton fabric in ten back-and-forth motions, under both dry and wet conditions. The amount of colour transferred to the cotton fabrics was graded in a range from 1 to 5, in an increasing order of rub fastness.

Results and discussion

Quality of the pigmented ink jet inks

Figure 1 shows the IR spectra of the surface-modified organic pigments: C.I. Pigment Blue 15:4 (spectrum (a)), C.I. Pigment Yellow 74 (spectrum (b)), C.I. Pigment Red 122 (spectrum (c)) and C.I. Pigment Black 7 (spectrum (d)), which all have strongly electrolytic sulphonate groups on their pigment surface, whilst the black pigment (spectrum (d)) has in

Volume 39 · Number 6 · 2010 · 327-341

addition the weakly electrolytic carboxylic acid, hydroxyl and ketonic carbonyl groups on its surface which did not influence the behaviour of the sulphonic acid group. These weakly electrolytic groups were generated during the production of carbon black. For the four pigments, the IR peaks give evidence for the presence of the sulphonate groups as follows: the peaks at around 1,369-1,288 cm⁻¹ are assigned to the asymmetrical stretching of -S-O, 1,124-1,090 cm⁻¹ for the S=O stretching, and 1,023-809 cm⁻¹ for -S-O symmetric stretching of the $-SO_3^-$ group. The peaks at 1,610, 1,607, 1,594-1,592, and 1,486 cm⁻¹ are the -C=C- stretching of the aromatic rings in the pigments. The peak at 1,508 cm spectrum (a) of Figure 1 relates to the C=N stretching of the phthalocyanine blue pigment. That at 3,274 cm⁻¹ in spectrum (b) of Figure 1 relates to the N=H stretching of the quinacridone red pigment, whilst that at 1,576 cm⁻¹ in spectrum (c) of Figure 1 relates to the N=N stretching of the monoazo yellow pigment. The peaks at 1,636 and $1,675\,\mathrm{cm}^{-1}$ relate to the C=O stretching of the magenta pigment in spectrum (b) of Figure 1, and the yellow pigment in spectrum (c) of Figure 1, respectively. More peaks are seen in the spectrum of the carbon black pigment in spectrum (d) of Figure 1, where the sharp peak at 1,723 cm⁻¹ indicates the C=O stretching from the carboxylic acid group and the peaks at 1,674 cm indicate the presence of the ketone carbonyl group, that at 1,446 cm⁻¹ the presence of the anionic carboxylate groups, COO⁻, and finally the small peak at 3,657 cm⁻¹ relates to the O-H stretching of carbon black. A schematic drawing of Figure 1(e) represents the pigment surface that was modified by Cabot's diazonium attachment chemistry (Belmont, 1994) to give the sulphonate groups. Here, the sphere is the CI pigment having the attached functional groups on the surface which are surrounded by the positive counter ions.

Zeta-potential measurements were used to confirm the nature of the negatively charged, surface-modified pigments in all of the pigment dispersions and pigmented inks. The black pigment dispersion had the highest zeta-potential (-64 mV, Table I), as did the black ink (-50.9 mV, Table II). It should be noted that all of the four pigments were surface modified with sulphonate groups. However, only the black ink pigment systems contained the OH and COOH groups, albeit it at only a relatively low density. We deduce that the attached functional groups on the surface, surrounded by the positive counter ions, are in a suitable continuous medium, for example, in a colloidal state with one electrical double layer, as shown schematically in schematic drawing of Figure 1(e). The negatively charged pigment surface, together with the components of the continuous aqueous medium, stabilises the inks in a colloidal state.

The presence of the sulphonate and/or carboxylate groups gives an electrostatic repulsive force between the particles, fulfilling the so-called self-dispersing property in a water-based vehicle, without the need for additional dispersing agents because all the pigment concentrates contained a 4.85 per cent final concentration of non-ionic surfactant.

The sulphonate group-containing pigments, as stronger electrolytes, have a better water solubility than that of the carboxylate anion-containing pigments. It has been reported that the print performance of the black inks having —COOH groups (Cab-O-jet 300), as defined by their optical density and water fastness, was superior to those containing —SO₃H groups (Cab-O-jet 200) (Belmont, 1994; Johnson and Belmont, 1997).

Particle size and stability

The prepared inks (cyan, magenta, yellow and black colours) had pH values in the range of 8-9. The particle sizes of the inks were measured after filtration to check for the presence of oversized ink particles. This was because larger particles could clog the orifice of the printer during ink jet printing. The four inks had different average particle sizes with the black ink having the smallest average particle size at 60 nm and the cyan ink the largest size at 105 nm. The pigments in the magenta and yellow inks were in-between with average particle sizes within the range of 79 nm (Figure 2).

The pigmentary species that were present in the formulated inks had very narrow particle size distributions. Figure 2 shows the stability of the inks in terms of the particle size distributions of the inks following ten months and one year of storage. The particle sizes of the cyan and yellow inks remained fairly constant over the year, whilst the magenta and black inks contained a minute fraction of larger particles in the size range of $100-120 \,\mu\mathrm{m}$ and $8-100 \,\mu\mathrm{m}$, respectively, after ten months to one year of storage. Analysis of the ink particles by TEM and SEM (Figure 3) revealed that the particle sizes of the pigments in the dried cyan and yellow inks were still less than 120 nm. However, the majority of the pigments in the magenta and black inks had larger particles, at around 300 and 200 nm, respectively. The smaller the primary particle size is the greater is the tendency towards aggregation or agglomeration. The oversized particles were created by the low level of aggregation that involved only a small amount of polymer binder. All of the oversized pigments were removed by filtration, causing the inks to become suitable for ink jet application as shown by the fact that the particle size remained unchanged over ten months. The jetting of these inks was smooth during printing and, in addition, very little, if any cleaning of the print head nozzles was required.

The zeta-potential gives a useful guide to the strength of the repulsive force that operates between the colloidal particles of the ink, and the strongly negative charges (-43 to -51 mV) observed for all the inks (Table II) suggest that they are likely to be stable in solution and not aggregate. This strong

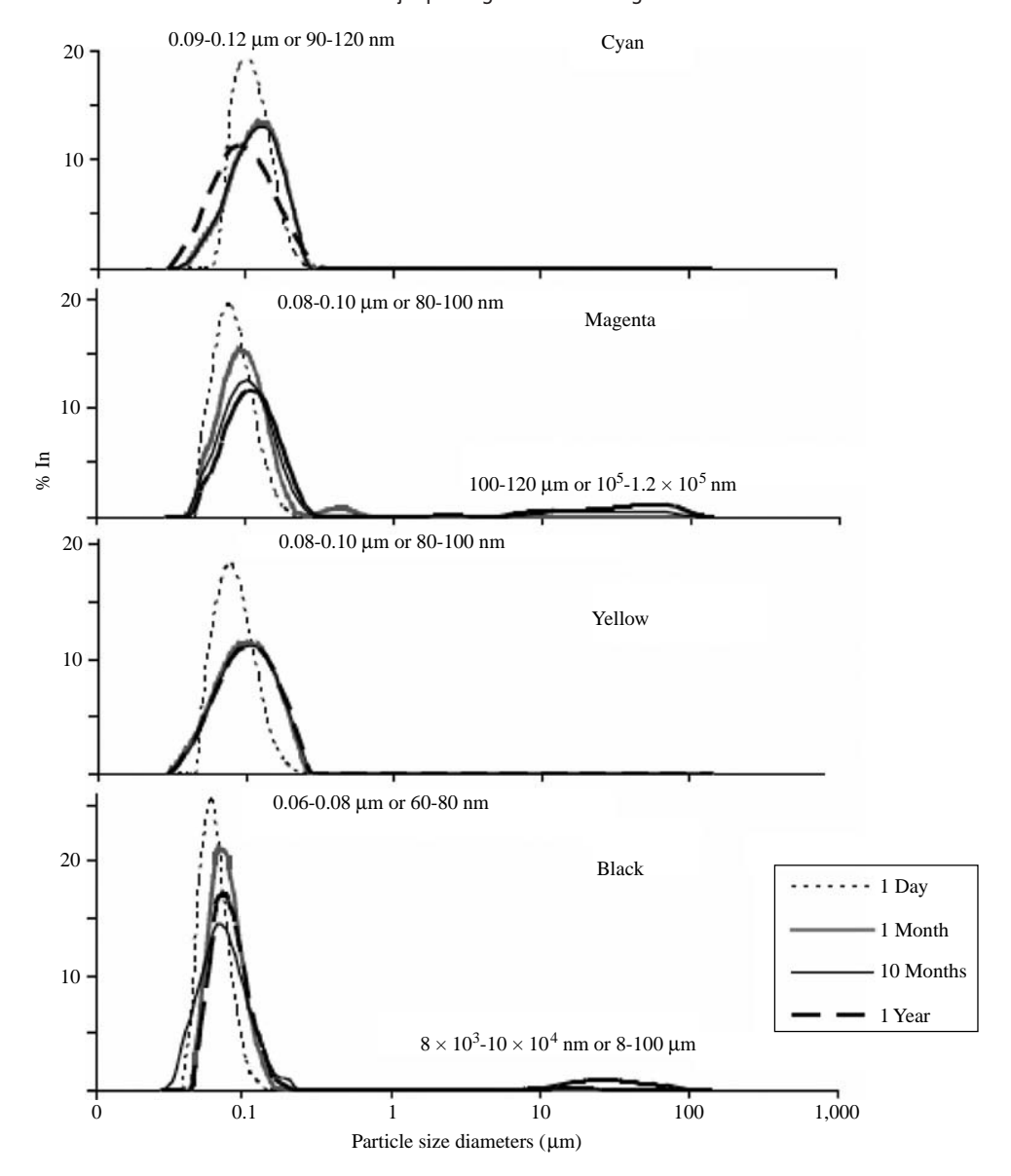
Table II Ink properties of the four pigmented inkjet ink colours

Inks	Viscosity (mPa s)	Surface tension (mN m ⁻¹)	Density (g cm ⁻³)	Zeta-potential (mV)	Solid content (%)
Cyan	2.4	44 ± 2	1.04	-48	28
Magenta	2.5	44 ± 1	1.05	-43	28
Yellow	2.5	45 ± 1	1.05	-43	28
Black	2.5	43 ± 0	1.05	-51	29

Note: Data are shown as the mean ± 1 (SD) and are derived from three replicates

Volume 39 · Number 6 · 2010 · 327-341

Figure 2 The particle size and their distributions for the ink jet printing inks after storage for the indicated times



negative zeta-potential is due to the sulphonate or carboxylate groups on the pigment surface (Jason, 2004). Indeed, the other ink properties (Table II) are not contrary to the notion that these inks are suitable for use in a textile ink jet printing system.

Rheological features

Typically, the viscosity of an ink jet ink is approximately 1-5 mPas. Above this range, the ink becomes too viscous to flow through the nozzle or pass through the orifice, resulting in a clogging problem during drop ejection. The viscosity of all of the prepared inks was measured at room temperature (25°C), where typical Newtonian flow behaviour was observed at the appropriate shear-strain rate, giving viscosity values of approximately 2.5 mPas for all the inks. Thus, these low-viscosity inks could be printed by the ink jet printing

method, using piezo technology, since the piezo print head uses a high shear force in jetting the ink.

When the inks were deposited on the silk surface, the ink bulk fluid (non-coloured medium) was absorbed by the wetting, spreading, penetration and evaporation processes that all took place simultaneously, allowing penetration into the medium. The non-volatile ink components in the medium provided the basis for many cohesive networks to be developed resulting in adhesion or mechanical entrapment on the silk surface.

Characterisation of the pre-treated fabrics and the printed silk fabrics

Chitosan has amino groups that are similar to those on the silk fabrics. Viscosity of the padding of chitosan solutions in Figure 4(a) increases with molecular mass at the fixed concentration, 0.5 per cent w/v and increasing the chitosan